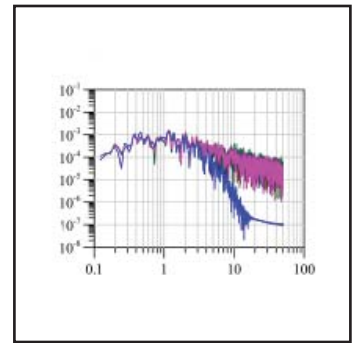
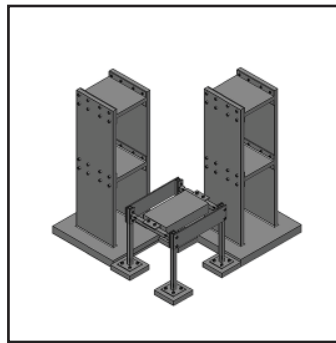
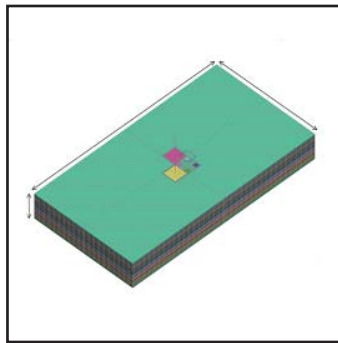
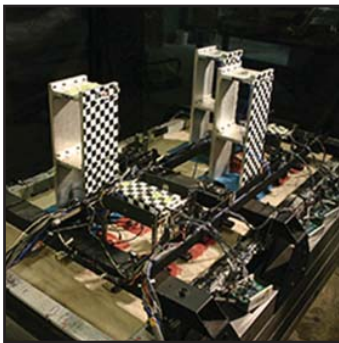


Site Response, Soil-Structure Interaction and Structure-Soil-Structure Interaction for Performance Assessment of Buildings and Nuclear Structures

by
Chandrakanth Bolisetti and Andrew S. Whittaker



Technical Report MCEER-15-0002

June 15, 2015

NOTICE

This report was prepared by the University at Buffalo, State University of New York, as a result of research sponsored by MCEER through a grant from the National Science Foundation under grant number CMMI-0830331 and other sponsors. Neither MCEER, associates of MCEER, its sponsors, University at Buffalo, State University of New York, nor any person acting on their behalf:

- a. makes any warranty, express or implied, with respect to the use of any information, apparatus, method, or process disclosed in this report or that such use may not infringe upon privately owned rights; or
- b. assumes any liabilities of whatsoever kind with respect to the use of, or the damage resulting from the use of, any information, apparatus, method, or process disclosed in this report.

Any opinions, findings, and conclusions or recommendations expressed in this publication are those of the author(s) and do not necessarily reflect the views of MCEER, the National Science Foundation or other sponsors.

**Site Response, Soil-Structure Interaction and
Structure-Soil-Structure Interaction for
Performance Assessment of Buildings and Nuclear Structures**

by

Chandrakanth Bolisetti¹ and Andrew S. Whittaker²

Publication Date: June 15, 2015

Submittal Date: December 15, 2014

Technical Report MCEER-15-0002

National Science Foundation Grant Number: CMMI-0830331

- 1 Postdoctoral Associate, Idaho National Laboratory; former Graduate Student, Department of Civil, Structural and Environmental Engineering, University at Buffalo, State University of New York
- 2 Professor, Chair, and MCEER Director, Department of Civil, Structural and Environmental Engineering, University at Buffalo, State University of New York

MCEER

University at Buffalo, State University of New York

212 Ketter Hall, Buffalo, NY 14260

E-mail: mceer@buffalo.edu; Website: <http://mceer.buffalo.edu>

Preface

MCEER is a national center of excellence dedicated to the discovery and development of new knowledge, tools and technologies that equip communities to become more disaster resilient in the face of earthquakes and other extreme events. MCEER accomplishes this through a system of multidisciplinary, multi-hazard research, in tandem with complimentary education and outreach initiatives.

Headquartered at the University at Buffalo, The State University of New York, MCEER was originally established by the National Science Foundation in 1986, as the first National Center for Earthquake Engineering Research (NCEER). In 1998, it became known as the Multidisciplinary Center for Earthquake Engineering Research (MCEER), from which the current name, MCEER, evolved.

Comprising a consortium of researchers and industry partners from numerous disciplines and institutions throughout the United States, MCEER's mission has expanded from its original focus on earthquake engineering to one which addresses the technical and socio-economic impacts of a variety of hazards, both natural and man-made, on critical infrastructure, facilities, and society.

The Center derives support from several Federal agencies, including the National Science Foundation, Federal Highway Administration, National Institute of Standards and Technology, Department of Homeland Security/Federal Emergency Management Agency, and the State of New York, other state governments, academic institutions, foreign governments and private industry.

The studies presented in this report are a part of the NSF funded project titled, 'Seismic Performance Assessment of Buildings in Dense Urban Regions,' and referred to in this report as the City Block project. The goal of this project is to understand the significance of structure-soil-structure interaction in buildings through a series of centrifuge experiments and numerical simulations, and develop guidelines for analysts and engineers in accounting for structure-soil-structure interaction in the design and performance assessment of buildings. A total of six centrifuge experiments were performed at the NEES@UCDavis geotechnical centrifuge facility. These experiments tested small-scale building models placed on dry sand (Test 1 to Test 4) and liquefiable soil (Test 5 and Test 6). The City Block project involved a team of six universities including the University of California, Berkeley, University of California, Davis, University of California, San Diego, University at Buffalo, and the California Polytechnic State University.

This report presents three studies that share the common goal of better understanding the phenomena of site response, soil-structure interaction and structure-soil-structure interaction, and advancing the numerical tools that simulate these phenomena. The first two studies involve an assessment of the industry-standard frequency-domain and time-domain programs used for site-response and soil-structure interaction analyses. The more recently developed nonlinear time-domain methods are benchmarked against the traditionally used frequency-domain methods for low-intensity ground shaking, and their predictions are compared for higher intensity shaking. The results are used to provide practical guidelines for the usage of these programs. The third study involves the examination of structure-soil-structure interaction effects in two of the City Block centrifuge experiments through analysis of experimental data and numerical simulations. The numerical simulations are performed using the frequency- and time-domain programs assessed in the first two studies and supplement the experimental data by providing a better insight into the phenomenon of structure-soil-structure interaction.

ABSTRACT

During an earthquake, the flexibility of the near-surface soil affects the dynamic response of the supported structure. This dynamic interaction is termed soil-structure interaction (SSI). Soil-structure interaction is important for performance-based design, which has seen increasing use in earthquake engineering in the United States in the last decade. Soil-structure interaction analysis is preceded by site-response analysis, which is the process of calculating the response of a soil profile to rock motion at depth. Soil flexibility also results in the interaction of adjacent structures through intermediate soil. This interaction is termed structure-soil-structure interaction (SSSI), which can be important for the performance assessment of buildings, especially those constructed in dense, urban areas. The studies presented herein share the common goal of a better understanding of the phenomena of site response, SSI and SSSI, and advancing the numerical tools that simulate these phenomena.

The state-of-the-art in site-response and SSI analysis of buildings and nuclear structures involves the use of linear or equivalent-linear numerical methods that function in the frequency domain. However, nonlinear time-domain methods may be more appropriate for cases involving intense earthquakes that result in highly nonlinear soil and foundation response. Such nonlinear methods are available but rarely used due to the higher computational requirements and lack of experience with analysts and regulators. This report assesses industry-standard equivalent linear and nonlinear site-response and SSI analysis programs, and provides practical guidelines on their usage. The assessment includes benchmarking the time-domain programs against frequency-domain programs for analyses involving almost linear soil response, and a comparison of the predictions of these programs for analyses involving highly nonlinear soil and foundation response. The assessment also identifies the various pitfalls that can be expected when using these programs and suggests workarounds.

Structure-soil-structure interaction has been rarely studied, mainly due to the lack of experimental or field-based case-studies that demonstrate its effects on structural response. The US National Science Foundation funded a research project titled ‘Seismic Performance Assessment of Buildings in Dense Urban Environments’ to understand the significance of SSSI in buildings through a series of centrifuge experiments and numerical simulations. The experiments involve small-scale building models with commonly-found superstructure and foundation configurations. This report describes some of these centrifuge experiments, and their numerical simulations, which are comprehensive and performed using both equivalent-linear and nonlinear SSI analysis programs. The numerical and experimental results show that wave-based SSSI does not significantly affect the global response of the buildings considered in this study.

ACKNOWLEDGEMENTS

The research presented in this report is funded by the US National Science Foundation under Grant CMMI-0830331, ‘Seismic Performance Assessment of Dense Urban Environments’ (the City Block project), and MCEER. The financial support is gratefully acknowledged.

The authors would like to thank the other Principal Investigators of the City Block project, Prof. Jonathan Bray, Prof. Bruce Kutter, Prof. Greg Feigel and Prof. Tara Hutchinson, and involved graduate students, Dr. Zhiqiang Chen, Dr. H. Benjamin Mason and Dr. Nicholas W. Trombetta.

Various professionals in the industry practice and in academia have provided valuable assistance over the course of this research project. Ibbi Almufti, Dr. Michael Willford, Dr. Yuli Huang and Dr. Armin Masroor of Arup, San Francisco provided much guidance on performing site-response and soil-structure interaction analysis in LS-DYNA. Dr. Farhang Ostadan of Bechtel, San Francisco provided counsel on the use of SASSI. Dr. Irfan Baig and Dr. Said Bolourchi of Simpson Gumpertz and Heger, Boston provided guidance on and identified challenges with the use of SHAKE. Prof. Youssef Hashash at University of Illinois at Urbana-Champaign provided guidance with DEEPSOIL. Prof. Boris Jeremic at University of California at Davis, Prof. Jacobo Bielak at Carnegie Mellon University and Dr. Ushnish Basu at Livermore Software Technology Corporation provided guidance in understanding the domain reduction method and performing soil-structure interaction analysis using this method in LS-DYNA. The authors are grateful for this support.

TABLE OF CONTENTS

SECTION 1 INTRODUCTION.....	1
1.1 Background.....	1
1.2 Motivation	2
1.2.1 Assessment of numerical methods in site-response and soil-structure interaction analysis	2
1.2.2 Seismic structure-soil-structure interaction in dense urban environments.....	4
1.3 Report organization	5
SECTION 2 SITE-RESPONSE ANALYSIS: A REVIEW	7
2.1 Dynamic behavior of soils during earthquakes	7
2.1.1 Experimental response of cyclically loaded soils	7
2.1.2 Numerical material models for dynamic soil behavior	8
2.1.2.1 Equivalent-linear models.....	8
2.1.2.2 Nonlinear hysteretic models	10
2.2 Site-response analysis.....	11
2.2.1 The nature of site response.....	12
2.2.2 One-dimensional methods of site-response analysis.....	12
2.2.2.1 Evolution of one-dimensional site-response analysis methods	13
2.2.2.2 Equivalent-linear methods.....	14
2.2.2.2.1 SHAKE.....	15
2.2.2.3 Nonlinear methods.....	16
2.2.2.3.1 DEEPSOIL	17
2.2.2.3.2 LS-DYNA	19
2.2.2.4 Validation of one-dimensional site-response analysis programs.....	20
2.2.2.5 Comparison and limitations of various one-dimensional methods.....	26
2.2.3 Multi-dimensional analyses	27

SECTION 3 SOIL-STRUCTURE INTERACTION: A REVIEW.....29

3.1 Introduction 29

3.2 Numerical methods in soil-structure interaction analysis..... 31

 3.2.1 Substructuring method 32

 3.2.2 Direct method..... 34

 3.2.3 Domain reduction method..... 36

3.3 Soil-structure interaction analysis using industry-standard numerical programs 38

 3.3.1 SASSI..... 38

 3.3.1.1 Theory and implementation..... 39

 3.3.1.2 Modeling and analysis procedure 42

 3.3.2 LS-DYNA 44

 3.3.2.1 Direct method 44

 3.3.2.2 The effective seismic input method..... 45

 3.3.3 The US NRC ESSI Simulator 47

 3.3.4 Assessment of numerical soil-structure interaction analysis methods 47

3.4 Structure-soil-structure interaction 48

SECTION 4 AN ASSESSMENT OF SITE-RESPONSE ANALYSIS PROGRAMS51

4.1 Introduction 51

4.2 Soil profiles used for site-response analysis..... 51

4.3 Selection of input ground motions..... 52

4.4 Numerical modeling 58

 4.4.1 Material modeling..... 59

 4.4.2 Site layering 61

4.5 Numerical analyses..... 63

 4.5.1 Modal analyses..... 63

 4.5.2 Site-response analyses for sites E1 and E2 64

 4.5.3 Site-response analyses for site W1..... 64

 4.5.4 Site-response analyses for site W2..... 64

4.6	Observations.....	65
4.6.1	Site E1.....	66
4.6.2	Site E2.....	67
4.6.3	Site W1.....	69
4.6.3.1	Response to ordinary ground motions.....	69
4.6.3.2	Response to pulse-like ground motions.....	70
4.6.3.3	Effect of pressure-dependence of soil properties.....	73
4.6.4	Site W2.....	73
4.6.4.1	Response to ordinary ground motions.....	73
4.6.4.2	Response to pulse-like ground motions.....	75
4.6.4.3	Effect of pressure-dependence of soil properties.....	77
4.7	Summary and conclusions.....	78
4.7.1	General conclusions regarding nonlinear site response.....	78
4.7.2	Comparison of equivalent-linear and nonlinear responses.....	79
4.7.3	Comparison between the responses from DEEPSOIL and LS-DYNA.....	80
4.7.4	Key issues faced during site-response analysis.....	81
4.7.4.1	SHAKE.....	81
4.7.4.2	DEEPSOIL.....	83
4.7.4.3	LS-DYNA.....	85
4.7.4.4	Sensitivity of high-frequency response.....	86
4.7.5	Calculation and specification of input for site-response analysis.....	87
4.8	Site-response analysis for biaxial horizontal shaking.....	89
4.9	Recommendations for future research.....	91

SECTION 5 AN ASSESSMENT OF SOIL-STRUCTURE INTERACTION ANALYSIS

PROGRAMS	93
-----------------------	-----------

5.1	Overview.....	93
5.2	Calculation of linear elastic SSI response using SASSI and LS-DYNA.....	93
5.2.1	Model description.....	93
5.2.2	Modeling in SASSI.....	95
5.2.3	Modeling in LS-DYNA using the direct method and the effective seismic input method....	96

5.2.4	Analysis results and comparison between SASSI and LS-DYNA.....	99
5.2.4.1	Free-field response	99
5.2.4.2	Fixed-base responses	100
5.2.4.3	Response of the basemat alone.....	101
5.2.4.4	Response of LM1 with SSI effects.....	102
5.2.4.5	Response of LM2 with SSI effects.....	104
5.2.5	Observations.....	106
5.3	Calculation of nonlinear SSI responses using SASSI and LS-DYNA	108
5.3.1	Superstructure and soil modeling.....	108
5.3.2	Analysis results and comparison.....	109
5.3.2.1	MS1F_2	110
5.3.2.2	MS1F_2 equipped with rigid grade beams.....	114
5.3.2.3	MS2F	117
5.3.3	Observations.....	120
5.4	Practical considerations for SSI analysis using SASSI and LS-DYNA.....	121
5.4.1	Selection of analysis frequencies in SASSI	122
5.4.2	Foundation meshing in SASSI.....	123
5.4.3	Column-basemat connection properties in SASSI.....	124
5.4.4	Sensitivity of rocking response to site layering in SASSI and LS-DYNA	126
5.4.5	Hourglass effects in LS-DYNA response	127
5.5	Summary and conclusions.....	129
5.6	Recommendations	130

SECTION 6 THE NEES CITY BLOCK CENTRIFUGE EXPERIMENTS: TEST 3 AND

TEST 4 131

6.1	Introduction	131
6.2	Geotechnical centrifuge testing.....	131
6.2.1	Background	131
6.2.2	Advantages and limitations.....	136
6.2.3	The NEES@UC Davis centrifuge facility	137

6.3	Test 2: Two adjacent structures on dense, dry sand	139
6.3.1	Test description	139
6.3.2	Soil profile.....	140
6.3.3	Model design and instrumentation	140
6.3.3.1	Selection of prototype building parameters.....	141
6.3.3.2	Design of experimental model structures	141
6.3.3.3	Instrumentation.....	146
6.3.4	Input ground motions and test chronology.....	147
6.4	Test 3: An in-plane SSSI configuration on dense, dry sand	149
6.4.1	Test description	149
6.4.1.1	The ‘transmitter-receiver’ configuration	151
6.4.2	Soil profile.....	151
6.4.3	Model design and instrumentation	151
6.4.3.1	Design of two-story model, MS2F_iSSSI	152
6.4.3.2	Design of the one-story models, MS1F_2_Baseline and MS1F_2_iSSSI.....	154
6.4.3.3	Instrumentation.....	156
6.4.4	Input ground motions and test chronology.....	157
6.5	Test 4: Anti-plane, and combined in-plane anti-plane SSSI configurations on dense, dry sand....	159
6.5.1	Test description	159
6.5.2	Soil profile.....	164
6.5.3	Model design and instrumentation	164
6.5.3.1	Differences in model designs from Test 3	164
6.5.3.2	Instrumentation.....	165
6.5.4	Input ground motions and test chronology.....	166

SECTION 7 EXPERIMENTAL RESULTS AND COMPARISON WITH NUMERICAL SIMULATIONS 169

7.1	Introduction	169
7.2	Scope of experimental data analysis and numerical simulations.....	169
7.3	Examination of site response.....	174
7.3.1	Calculation of the material properties	174

7.3.2	Site-response analysis in SHAKE	176
7.3.3	Site-response analysis in DEEPSOIL	176
7.3.4	Site-response analysis in LS-DYNA.....	177
7.3.5	Variability in the input ground motion and soil properties during the experiments	178
7.3.6	Comparison of experimental and numerical site responses	180
7.4	Examination of SSI and SSSI effects	182
7.4.1	Modeling in SASSI	183
7.4.2	Modeling in LS-DYNA	189
7.4.3	Calibration of fixed-base models	194
7.4.4	Comparison of experimental and numerical results	195
7.4.4.1	MS1F_2	196
7.4.4.2	Footing response in MS1F_2.....	199
7.4.4.2.1	Moment-rotation response.....	200
7.4.4.2.2	Vertical force-displacement response.....	202
7.4.4.3	MS2F	206
7.4.5	Effect of basement restraint on the response of MS1F_2	208
7.4.5.1	Pseudo-static analyses	210
7.4.5.2	Dynamic analyses.....	212
7.4.6	Effect of basement restraint on the response of MS1F_1	215
7.5	Summary and conclusions	217
SECTION 8 SUMMARY, CONCLUSIONS AND RECOMMENDATIONS.....		221
8.1	Summary.....	221
8.2	Conclusions	223
8.2.1	Assessment of industry-standard site-response analysis programs.....	223
8.2.2	Assessment of industry-standard SSI analysis programs.....	225
8.2.3	Centrifuge experiments and numerical simulations of the NEES City Block project	227
8.3	Future research	228
REFERENCES.....		231

APPENDIX A RESULTS OF SITE-RESPONSE ANALYSES.....	245
APPENDIX B THE ORMSBY WAVELET.....	325

LIST OF FIGURES

Figure 2-1: Calculation of equivalent-linear parameters: secant shear modulus and effective damping ratio	8
Figure 2-2: Upper bound modulus reduction and damping curves for sand [from Seed and Idriss (1970)].	9
Figure 2-3: Nonlinear hysteretic model with a hyperbolic backbone curve and extended Masing rules (Hashash and Park, 2001)	11
Figure 2-4: One-dimensional site-response analysis.....	13
Figure 2-5: The lumped-mass and finite element models for site-response analysis [figure adopted from Hashash <i>et al.</i> (2010) and modified].....	16
Figure 2-6: Ground motion input in time-domain one-dimensional site-response analysis	17
Figure 2-7: The hysteresis loop for the MAT_HYSTERETIC model for a given input strain, and the corresponding backbone curve.....	20
Figure 2-8: Sample comparisons between the numerical and observed site response from Dickenson (1994).....	22
Figure 2-9: Sample comparisons between the numerical and observed site response from Chang (1996)	22
Figure 2-10: Sample comparisons of numerical and experimental data from Borja <i>et al.</i> (1999).....	23
Figure 2-11: Section view and instrumentation of the Turkey Flat site (Kwok <i>et al.</i> , 2008)	24
Figure 2-12: Blind predictions at locations V1 and D2 using different numerical programs and the corresponding residuals (Kwok <i>et al.</i> , 2008)	25
Figure 3-1: Decrease in seismic demand due to SSI effects in idealized design response spectra [adopted from Mylonakis and Gazetas (2000) and modified]	30
Figure 3-2: A typical code design spectrum and response spectra from some recorded strong ground motions (Mylonakis and Gazetas, 2000).....	31
Figure 3-3: Steps in a substructuring analysis (Kramer and Stewart, 2004).....	33
Figure 3-4: Substructure methods of SSI analysis (Ostadan, 2006a).....	34
Figure 3-5: Finite element model for soil-structure interaction analysis using the direct method.....	35
Figure 3-6: Illustration of the domain reduction method (Jeremic <i>et al.</i> , 2013).....	38
Figure 3-7: Substructuring in the flexible-volume method in SASSI (Ostadan, 2006a)	40
Figure 3-8: Sample model for SSI analysis using the effective seismic input in LS-DYNA	46
Figure 3-9: Layout of the buildings considered by Çelebi (1993a) and Çelebi (1993b) for examining SSSI	50
Figure 4-1: Soil profiles used for site-response analyses.....	52

Figure 4-2: Acceleration time series of the input ground motions used for WUS soil profiles.....	55
Figure 4-3: Acceleration response spectra and Fourier amplitude spectra of the input ground motions used for WUS soil profiles.....	56
Figure 4-4: Acceleration time series of the input ground motions used for CEUS soil profiles.....	57
Figure 4-5: Acceleration response spectra and Fourier amplitude spectra of the input ground motions used for CEUS soil profiles.....	58
Figure 4-6: Backbone and damping curves of the materials used in site-response analysis.....	61
Figure 4-7: Fourier transforms of the surface accelerations for site W1 subjected to ground motion WP2 (left) and site W2 subjected to ground motion WO2 (right).....	81
Figure 4-8. Peak acceleration and peak strain profiles (left) and acceleration response spectra at the surface (right) for site W2 subjected to ground motion WP1	83
Figure 4-9: Hysteresis loops of three layers in site W2 showing an abrupt change in the peak strains when subjected to ground motion WP2.....	84
Figure 4-10: Examination of the hysteresis loops of layers involved in abrupt changes in the peak strains in site W2 subjected to ground motion WP2	85
Figure 4-11: Acceleration time series at 50m depth (left) and the peak acceleration profile (right) for site W1 subjected to ground motion WP2	86
Figure 4-12: Outcrop and within ground motions.....	88
Figure 4-13: Surface acceleration response spectra in the X direction for uniaxial and biaxial analysis performed for sites W1 and W2.....	90
Figure 5-1: Lumped mass structures, LM1 and LM2, used for the verification analyses of SASSI and LS-DYNA.....	94
Figure 5-2: SASSI finite element models of LM1 and LM2	96
Figure 5-3: LS-DYNA finite element models of LM1 (left) and LM2 (right)	97
Figure 5-4: LS-DYNA finite element model for SSI analysis of LM2 using the direct method.....	97
Figure 5-5: LS-DYNA finite element models for the effective seismic input method: site-response analysis (left) and SSI analysis (right).....	99
Figure 5-6: 1% damped acceleration response spectra (left) and Fourier transforms of the surface free-field accelerations computed using site-response analysis and the SSI analysis for LM2.....	100
Figure 5-7: Response spectra for 1% damping of the roof accelerations of the fixed-base models of LM1 (left) and LM2 (right) calculated using SASSI and LS-DYNA.....	101
Figure 5-8: Response spectra for 1% damping of the horizontal acceleration at center of the basemat (left) and the vertical acceleration at the edge of the basemat (right) for SSI analysis of the rigid basemat alone	101

Figure 5-9: Acceleration amplification spectra from the surface free field of the soil to the roof of LM1	102
Figure 5-10: Deconstruction of the horizontal roof accelerations of LM1 subjected to the Ormsby wavelet	103
Figure 5-11: Acceleration amplification spectra from the surface free field of the soil to the roof of LM2	105
Figure 5-12: Deconstruction of the horizontal roof accelerations of LM2 subjected to the Ormsby wavelet	106
Figure 5-13: Acceleration response spectra at the roof of MS1F_2 subjected to the JOS_L ground motion for the preliminary linear analysis	110
Figure 5-14: Acceleration response spectra at the roof of MS1F_2 calculated using strain-compatible soil properties in SASSI, and nonlinear soil properties in LS-DYNA.....	112
Figure 5-15: 5% damped acceleration response spectra at the roof of MS1F_2 subjected to the JOS_L ground motion calculated using strain compatible soil properties in SASSI and nonlinear soil properties in LS-DYNA but ignoring nonlinear soil behavior at the vicinity of the footings	113
Figure 5-16: Acceleration response spectra at the roof of MS1F_2 equipped with grade beams, calculated using strain-compatible soil properties in SASSI, and nonlinear soil properties in LS-DYNA	115
Figure 5-17: Time series of the horizontal displacement of two adjacent footings (along the X direction) of MS1F_2 for the PRI_H ground motion.....	116
Figure 5-18: Screenshots of the deformation at the footings of the MS1F_2 for the PRI_H ground motion at about 7 sec.....	117
Figure 5-19: Acceleration response spectra at the roof of MS2F subjected to the JOS_L ground motion calculated using strain-compatible moduli and 2% damping ratio for the soil.....	117
Figure 5-20: Acceleration response spectra at the roof of MS2F calculated using strain-compatible soil properties in SASSI, and nonlinear soil properties in LS-DYNA.....	119
Figure 5-21: Response spectra of the accelerations from structural deformations calculated for MS2F using strain-compatible properties in SASSI and nonlinear properties in LS-DYNA.....	120
Figure 5-22: Acceleration response spectra calculated at the roof of LM2 using SASSI for two sets of analysis frequencies, and using LS-DYNA	122
Figure 5-23: Sensitivity of the rocking response of MS2F calculated using SASSI to the number of nodes in the basemat	124
Figure 5-24: Description of the column-basemat connection of LM2 as modeled in SASSI and the beam cross-section properties used to model the three different connections employed in Section 5.4.3	125

Figure 5-25: SASSI response of the LM2 structure for various structure-basemat connections considered in Section 5.4.3, and the LS-DYNA response	125
Figure 5-26: Sensitivity of the rocking accelerations of MS2F to site layering in the equivalent-linear method	127
Figure 5-27: Sensitivity of the LS-DYNA response of LM2 to hourglass effects.....	128
Figure 5-28: Screenshots of the LS-DYNA response (500 times amplified) of LM2 with and without hourglass control.....	129
Figure 6-1: The UC Davis centrifuge	133
Figure 6-2: Photographs of the experimental model building process. Courtesy of the City Block team	135
Figure 6-3: Rendering of the horizontal uniaxial shake table used at the UC Davis centrifuge facility (courtesy of the staff at the Center for Geotechnical Modeling, UC Davis).....	138
Figure 6-4: FSB-2 container used in the City Block experiments (courtesy of the staff at the Center for Geotechnical Modeling, UC Davis).....	138
Figure 6-5: Photograph of the building models in the laminar box during Test 1	139
Figure 6-6: Photograph of the building models in the laminar box during Test 2.....	140
Figure 6-7: Models used in Test 1 and Test 2.....	143
Figure 6-8: Elevations of experimental models in the shaking direction, with dimensions in model scale (Chen <i>et al.</i> , 2010)	144
Figure 6-9: Designs of the three ‘fuses’ used in MS1F_1 and MS3F, dimensions in model scale (Chen <i>et al.</i> , 2010).....	145
Figure 6-10: Photograph of the building models in the laminar box during Test 3.....	149
Figure 6-11: Plan view of the experimental models in the laminar box during Test 3 (dimensions in model scale) (Mason <i>et al.</i> , 2010c).....	150
Figure 6-12: Elevation view of the experimental models in the laminar box during Test 3 (dimensions in model scale) (Mason <i>et al.</i> , 2010c).....	150
Figure 6-13: Final design of model MS2F_iSSSI (Mason <i>et al.</i> , 2010c).....	154
Figure 6-14: Dimensions of the one-story model in Test 3 (Mason <i>et al.</i> , 2010c)	155
Figure 6-15: Photographs of fully constructed one-story model in Test 3.....	156
Figure 6-16: SASSI numerical models of individual buildings considered during the planning of Test 4 (arrows indicate direction of shaking)	160
Figure 6-17: SASSI numerical models of the building arrangements, CBL-1 and CBL-2, considered during the planning phase of Test 4 (arrows indicate direction of shaking).....	160
Figure 6-18: Numerical models of building arrangements, CBL-3 to CBL-5, considered during the planning phase of Test 4 (arrows indicate direction of shaking)	161

Figure 6-19: Photograph of the building models in the laminar box during Test 4.....	162
Figure 6-20: Locations of the models in the laminar box during Test 4 (dimensions in model scale) (Trombetta <i>et al.</i> , 2011)	163
Figure 6-21: Differences between the Test 3 and Test 4 beam fuses (Trombetta <i>et al.</i> , 2011)	165
Figure 6-22: Photograph of the first centrifuge model on the arm shortly after the accidental oil leak ...	167
Figure 7-1: Ground motions selected, and the nomenclature used for the experimental models during data analysis and numerical simulations performed for Tests 3 and 4 [arrows indicate direction of shaking; renderings adopted from Trombetta (2013) and modified].....	171
Figure 7-2: Five percent damped acceleration response spectra of the ground motions selected for data analysis and numerical simulations.....	172
Figure 7-3: Acceleration time series of the ground motions selected for data analysis and numerical simulations.....	172
Figure 7-4: Modulus reduction and damping curves for sand calculated by Seed and Idriss (1970)	176
Figure 7-5: LS-DYNA finite element model for the site-response analysis of the City Block soil profile	178
Figure 7-6: Acceleration response spectra of the considered input ground motions (recorded at the base of the laminar box) in Tests 1 through 4	179
Figure 7-7: Acceleration response spectra of the input at the base of the laminar box (left) and surface-free-field-to-base transfer functions (right) calculated for six applications of the JOS_L ground motion during Test 3	180
Figure 7-8: Free-field surface acceleration response spectra calculated from experimental data and numerical simulations for the considered ground motions in Tests 3 and 4	182
Figure 7-9: Small-strain and strain-compatible shear moduli and damping ratios used for SSI analyses using SASSI for simulation of Tests 3 and 4	184
Figure 7-10: SASSI numerical models of the baseline models of MS1F_2 and MS2F.....	186
Figure 7-11: SASSI numerical model of the in-plane SSSI arrangement in Test 3	186
Figure 7-12: SASSI numerical model of the anti-plane SSSI arrangement in Test 4	187
Figure 7-13: SASSI numerical model of the in-plane SSSI arrangement in Test 3	187
Figure 7-14: LS-DYNA finite element model for soil-structure interaction analysis of the cSSSI arrangement during Test 4	190
Figure 7-15: Preliminary model of MS1F_2 in LS-DYNA with explicit modeling of the beam fuses using shell elements (left) and the close-up of one of the beam fuses (right)	191
Figure 7-16: Close-up isometric views of the SSI models of MS1F_2 (left) and MS2F (right) in LS-DYNA (soil elements far away from the structure are not shown for clarity).....	192

Figure 7-17: Close-up isometric view of the SSI model for the in-plane SSSI case of Test 3 in LS-DYNA (soil elements far away from the structures are not shown for clarity).....	193
Figure 7-18: Close-up isometric view of the SSI model for the anti-plane SSSI case of Test 4 in LS-DYNA (soil elements far away from the structures are not shown for clarity)	193
Figure 7-19: Close-up isometric view of the SSI model for the combined SSSI case of Test 4 in LS-DYNA (soil elements far away from the structures are not shown for clarity)	194
Figure 7-20: Response spectra of the roof acceleration of MS1F_2 from numerical simulations using SASSI and LS-DYNA, and experimental observations for JOS_L and LCN ground motions	198
Figure 7-21: Response spectra of the roof acceleration of MS1F_2 from numerical simulations using SASSI and LS-DYNA, and experimental observations for SCS_H and PRI_H ground motions	199
Figure 7-22: Moment-rotation response of the footings of MS1F_2 in various SSSI arrangements, calculated using LS-DYNA (separation allowed) analyses for the JOS_L ground motion	201
Figure 7-23: Moment rotation-response of the footings of MS1F_2 in various SSSI arrangements, calculated using LS-DYNA (separation allowed) analyses for the LCN ground motion	201
Figure 7-24: Moment-rotation response of the footings of MS1F_2 in various SSSI arrangements, calculated using LS-DYNA (separation allowed) analyses for the SCS_H ground motion	202
Figure 7-25: Moment-rotation response of the footings of MS1F_2 in various SSSI arrangements, calculated using LS-DYNA (separation allowed) analyses for the PRI_H ground motion	202
Figure 7-26: Vertical force-displacement response of the footings of MS1F_2 in various SSSI arrangements, calculated using LS-DYNA (separation allowed) analyses for JOS_L ground motion	204
Figure 7-27: Vertical force-displacement response of the footings of MS1F_2 in various SSSI arrangements, calculated using LS-DYNA (separation allowed) analyses for LCN ground motion	204
Figure 7-28: Vertical force-displacement response of the footings of MS1F_2 in various SSSI arrangements, calculated using LS-DYNA (separation allowed) analyses for SCS_H ground motion ...	205
Figure 7-29: Vertical force-displacement response of the footings of MS1F_2 in various SSSI arrangements, calculated using LS-DYNA (separation allowed) analyses for PRI_H ground motion	205
Figure 7-30: Response spectra of the roof acceleration of MS2F from numerical simulations using SASSI and LS-DYNA, and experimental observations for JOS_L and LCN ground motions	207
Figure 7-31: Response spectra of the roof acceleration of MS2F from numerical simulations using SASSI and LS-DYNA, and experimental observations for SCS_H and PRI_H ground motions	208
Figure 7-32: LS-DYNA numerical model of the iSSSI_B case with MS1F_2 on the left and MS2F_B on the right (soil elements are not shown for clarity)	209
Figure 7-33: Isometric view of the LS-DYNA numerical model used for pseudo-static analysis of the iSSSI_B case.....	210

Figure 7-34: Moment-rotation response and the vertical force-displacement response of the restrained MS1F_2 footings in the baseline and iSSSI_B cases	211
Figure 7-35: Lateral force-displacement response of the MS1F_2 superstructure in the baseline case and the iSSSI_B case	212
Figure 7-36: Response spectra of the roof acceleration of MS1F_2 from numerical simulations using LS-DYNA for four ground motions.....	214
Figure 7-37: Moment-rotation responses of the restrained footings of MS1F_2 in the baseline and iSSSI_B cases calculated for the four ground motions.....	215
Figure 7-38: Response spectra of the roof acceleration of MS1F_1 calculated using numerical simulations in LS-DYNA for four ground motions	216
Figure A-1: Stress-strain loops at three different depths for site E1 subjected to ground motion EO1.....	246
Figure A-2: Stress-strain loops at three different depths for site E1 subjected to ground motion EO2....	247
Figure A-3: Stress-strain loops at three different depths for site E1 subjected to ground motion EO3....	248
Figure A-4: Peak acceleration and peak strain profiles for site E1 subjected to ground motion EO1	249
Figure A-5: Peak acceleration and peak strain profiles for site E1 subjected to ground motion EO2	250
Figure A-6: Peak acceleration and peak strain profiles for site E1 subjected to ground motion EO3	251
Figure A-7: Acceleration response spectra of the base outcrop motion, and accelerations at three different depths for site E1 subjected to ground motion EO1	252
Figure A-8: Acceleration response spectra of the base outcrop motion, and accelerations at three different depths for site E1 subjected to ground motion EO2	253
Figure A-9: Acceleration response spectra of the base outcrop motion, and accelerations at three different depths for site E1 subjected to ground motion EO3	254
Figure A-10: Acceleration response histories at three different depths for site E1 subjected to ground motion EO1.....	255
Figure A-11: Acceleration response histories at three different depths for site E1 subjected to ground motion EO2.....	256
Figure A-12: Acceleration response histories at three different depths for site E1 subjected to ground motion EO3.....	257
Figure A-13: Spectral amplification of accelerations from the base to the surface of site E1 for ground motions EO1, EO2 and EO3	258
Figure A-14: Stress-strain loops at three different depths for site E2 subjected to ground motion EO1..	259
Figure A-15: Stress-strain loops at three different depths for site E2 subjected to ground motion EO2..	260
Figure A-16: Stress-strain loops at three different depths for site E2 subjected to ground motion EO3..	261

Figure A-17: Peak acceleration and peak strain profiles for site E2 subjected to ground motion EO1....	262
Figure A-18: Peak acceleration and peak strain profiles for site E2 subjected to ground motion EO2....	263
Figure A-19: Peak acceleration and peak strain profiles for site E2 subjected to ground motion EO3....	264
Figure A-20: Acceleration response spectra of the base outcrop motion, and accelerations at three different depths for site E2 subjected to ground motion EO1.....	265
Figure A-21: Acceleration response spectra of the base outcrop motion, and accelerations at three different depths for site E2 subjected to ground motion EO2.....	266
Figure A-22: Acceleration response spectra of the base outcrop motion, and accelerations at three different depths for site E2 subjected to ground motion EO3.....	267
Figure A-23: Acceleration response histories at three different depths for site E2 subjected to ground motion EO1.....	268
Figure A-24: Acceleration response histories at three different depths for site E2 subjected to ground motion EO2.....	269
Figure A-25: Acceleration response histories at three different depths for site E2 subjected to ground motion EO3.....	270
Figure A-26: Spectral amplification of accelerations in site E2 from the base to the surface for ground motions EO1, EO2 and EO3.....	271
Figure A-27: Stress-strain loops at three different depths for site W1 subjected to ground motion WO1.....	272
Figure A-28: Stress-strain loops at three different depths for site W1 subjected to ground motion WO2.....	273
Figure A-29: Stress-strain loops at three different depths for site W1 subjected to ground motion WO3.....	274
Figure A-30: Peak acceleration and peak strain profiles for site W1 subjected to ground motion WO1.....	275
Figure A-31: Peak acceleration and peak strain profiles for site W1 subjected to ground motion WO2.....	276
Figure A-32: Peak acceleration and peak strain profiles for site W1 subjected to ground motion WO3.....	277
Figure A-33: Acceleration response spectra of the base outcrop motion, and accelerations at three different depths for site W1 subjected to ground motion WO1.....	278
Figure A-34: Acceleration response spectra of the base outcrop motion, and accelerations at three different depths for site W1 subjected to ground motion WO2.....	279

Figure A-35: Acceleration response spectra of the base outcrop motion, and accelerations at three different depths for site W1 subjected to ground motion WO3	280
Figure A-36: Acceleration response histories at three different depths for site W1 subjected to ground motion WO1.....	281
Figure A-37: Acceleration response histories at three different depths for site W1 subjected to ground motion WO2.....	282
Figure A-38: Acceleration response histories at three different depths for site W1 subjected to ground motion WO3.....	283
Figure A-39: Spectral amplification of accelerations in site W1 from the base to the surface for ground motions WO1, WO2 and WO3	284
Figure A-40: Stress-strain loops at three different depths for site W1 subjected to ground motion WP1	285
Figure A-41: Stress-strain loops at three different depths for site W1 subjected to ground motion WP2	286
Figure A-42: Stress-strain loops at three different depths for site W1 subjected to ground motion WP3	287
Figure A-43: Peak acceleration and peak strain profiles for site W1 subjected to ground motion WP1	288
Figure A-44: Peak acceleration and peak strain profiles for site W1 subjected to ground motion WP2	289
Figure A-45: Peak acceleration and peak strain profiles for site W1 subjected to ground motion WP3	290
Figure A-46: Acceleration response spectra of the base outcrop motion, and accelerations at three different depths for site W1 subjected to ground motion WP1.....	291
Figure A-47: Acceleration response spectra of the base outcrop motion, and accelerations at three different depths for site W1 subjected to ground motion WP2.....	292
Figure A-48: Acceleration response spectra of the base outcrop motion, and accelerations at three different depths for site W1 subjected to ground motion WP3.....	293
Figure A-49: Acceleration response histories at three different depths for site W1 subjected to ground motion WP1	294
Figure A-50: Acceleration response histories at three different depths for site W1 subjected to ground motion WP2.....	295
Figure A-51: Acceleration response histories at three different depths for site W1 subjected to ground motion WP3	296

Figure A-52: Spectral amplification of accelerations in site W1 from the base to the surface for ground motions WP1, WP2 and WP3	297
Figure A-53: Stress-strain loops at three different depths for site W2 subjected to ground motion WO1.....	298
Figure A-54: Stress-strain loops at three different depths for site W2 subjected to ground motion WO2.....	299
Figure A-55: Stress-strain loops at three different depths for site W2 subjected to ground motion WO3.....	300
Figure A-56: Peak acceleration and peak strain profiles for site W2 subjected to ground motion WO1.....	301
Figure A-57: Peak acceleration and peak strain profiles for site W2 subjected to ground motion WO2.....	302
Figure A-58: Peak acceleration and peak strain profiles for site W2 subjected to ground motion WO3.....	303
Figure A-59: Acceleration response spectra of the base outcrop motion, and accelerations at three different depths for site W2 subjected to ground motion WO1	304
Figure A-60: Acceleration response spectra of the base outcrop motion, and accelerations at three different depths for site W2 subjected to ground motion WO2.....	305
Figure A-61: Acceleration response spectra of the base outcrop motion, and accelerations at three different depths for site W2 subjected to ground motion WO3	306
Figure A-62: Acceleration response histories at three different depths for site W2 subjected to ground motion WO1.....	307
Figure A-63: Acceleration response histories at three different depths for site W2 subjected to ground motion WO2.....	308
Figure A-64: Acceleration response histories at three different depths for site W2 subjected to ground motion WO3.....	309
Figure A-65: Spectral amplification of accelerations in site W2 from the base to the surface for ground motions WO1, WO2 and WO3	310
Figure A-66: Stress-strain loops at three different depths for site W2 subjected to ground motion WP1	311
Figure A-67: Stress-strain loops at three different depths for site W2 subjected to ground motion WP2	312
Figure A-68: Stress-strain loops at three different depths for site W2 subjected to ground motion WP3	313

Figure A-69: Peak acceleration and peak strain profiles for site W2 subjected to ground motion WP1	314
Figure A-70: Peak acceleration and peak strain profiles for site W2 subjected to ground motion WP2	315
Figure A-71: Peak acceleration and peak strain profiles for site W2 subjected to ground motion WP3	316
Figure A-72: Acceleration response spectra of the input motion, and accelerations at three different depths for site W2 subjected to ground motion WP1	317
Figure A-73: Acceleration response spectra of the input motion, and accelerations at three different depths for site W2 subjected to ground motion WP2	318
Figure A-74: Acceleration response spectra of the input motion, and accelerations at three different depths for site W2 subjected to ground motion WP3	319
Figure A-75: Acceleration response histories at three different depths for site W2 subjected to ground motion WP1 (unequal scales used for clarity)	320
Figure A-76: Acceleration response histories at three different depths for site W2 subjected to ground motion WP2 (unequal scales used for clarity)	321
Figure A-77: Acceleration response histories at three different depths for site W2 subjected to ground motion WP3	322
Figure A-78: Spectral amplification of accelerations in site W2 from the base to the surface for ground motions WP1, WP2 and WP3	323
Figure B-1: Time series of an Ormsby wavelet	326
Figure B-2: Fourier transform of an Ormsby wavelet	326
Figure B-3: 1% damped response spectrum of an Ormsby wavelet.....	326

LIST OF TABLES

Table 4-1: Input ground motions used for site-response analysis	54
Table 4-2: Model parameters used to define the soil materials in DEEPSOIL.....	61
Table 4-3: Layer thicknesses and captured maximum frequencies in each material	63
Table 4-4: Time periods of the soil profiles from modal analysis	64
Table 5-1: Lumped masses and beam cross section properties of the structural models used for analyses using SASSI and LS-DYNA.....	94
Table 5-2: Analysis time in minutes for elastic SSI analyses of LM2 subjected to the Ormsby wavelet.	107
Table 6-1: Scale factors used in centrifuge testing ^a (Kutter, 1995)	132
Table 6-2: Target design parameters for model structures at prototype scale (Chen <i>et al.</i> , 2010)	141
Table 6-3: Specifications of superstructures at the model scale (Chen <i>et al.</i> , 2010)	142
Table 6-4: Specifications of foundations at the model scale (Chen <i>et al.</i> , 2010).....	142
Table 6-5: Prototype-scale properties of the designed experimental models calculated using the numerical models in OpenSees and hammer tests (Chen <i>et al.</i> , 2010).....	145
Table 6-6: Test 2 ground motions and their sequence (only 55g ground motions included).....	148
Table 6-7: Dimensionless parameters governing the design of the two-story shear wall model, MS2F_iSSSI (Mason <i>et al.</i> , 2011).....	153
Table 6-8: Test 3 ground motions and their sequence (55g earthquake ground motions only) (Mason <i>et al.</i> , 2010c)	158
Table 6-9: Test 4 ground motions and their sequence (only 55g ground motions applied to models with original floor masses are included) (Trombetta <i>et al.</i> , 2011).....	168
Table 7-1: Soil layer properties used for site-response analysis in Tests 3 and 4.....	175
Table 7-2: DEEPSOIL curve parameters used for the Test 4 site-response analysis.....	177
Table 7-3: Material properties used in the SASSI analyses	188
Table 7-4: Description of the numerical model of MS1F_2 ^a (dimensions in prototype scale).....	188
Table 7-5: Description of the numerical model of MS2F ^a (dimensions in prototype scale).....	189
Table 7-6: Comparison of the prototype scale fixed-base time periods calculated from SASSI and hammer tests for all the models	195

SECTION 1

INTRODUCTION

1.1 Background

Traditional structural design involves the assumption that structures are founded on rigid ground. This assumption is reasonable in many cases, such as flexible buildings constructed on stiff soil sites. Accounting for soil flexibility in the analysis of such buildings does not generally affect the response in a significant way. For stiff, heavy buildings (and other structures), soil flexibility can change the response due to soil-foundation-structure interaction (SFSI) or, as it is more commonly known, soil-structure interaction (SSI). Soil-structure interaction effects comprise 1) changes in the dynamic behavior of the structure, namely, an increase in the time period and damping, and 2) modification of the input ground motion with respect to a free soil surface, or free field. The former is known as inertial interaction, and the latter as kinematic interaction. Ignoring SSI effects in building design has traditionally been assumed to be conservative. However, studies [e.g., Mylonakis and Gazetas (2000)] have shown that this may not always be the case. Accounting for SSI effects in buildings is not mandatory in the United States, although ASCE Standard 7 (ASCE, 2010) and FEMA 440 (FEMA, 2005) provide guidelines to include SSI effects in design. Although SSI effects may not be significant for most buildings, and the cost of SSI analysis may not be recovered by reducing the sizes of beams, columns and walls in buildings, they are of great importance for the design of safety-related nuclear structures, including nuclear power plants. Nuclear structures tend to have large plan dimensions, be stiff and be heavy—attributes that can lead to significant SSI. Soil-structure interaction analysis of nuclear structures is routine and generally follows the procedures set forth in ASCE Standard 4, Seismic Analysis of Safety-Related Nuclear Structures (ASCE, 1998; ASCE, forthcoming).

An extension of SSI is interaction of adjacent structures. During an earthquake, the presence of one structure may affect the dynamic response of another, resulting in structure-soil-structure interaction (SSSI). Structure-soil-structure interaction may be important for the performance assessment of buildings in dense urban areas but little is known since there are well-documented field and/or experimental data. Structure-soil-structure interaction is not implemented in practice and there are no related provisions in building codes.

Site-response analysis typically involves one-dimensional analysis of a soil column composed of multiple layers, spanning from the rock horizon at depth up to the ground surface. Site-response analysis is a precursor to SSI analysis. It is also used to propagate rock motions at depth through soil columns to establish free-field surface motions for analysis of surface- or near-surface-mounted structures. Site-

response analysis is often bypassed for building design in the United States by using ground motion prediction (or attenuation) relationships for seismic hazard calculations that include an empirical component associated with shear wave velocity in the upper 30m of the soil column—the part of the column thought to most influence free-field surface response.

1.2 Motivation

The earthquake engineering profession in the United States is embracing performance-based earthquake engineering. The FEMA P-58 products (FEMA, 2012) provide the background knowledge, implementation advice and calculation tools to enable calculations of loss in individual buildings either for an earthquake of a specific intensity or over a period of time (based on annualized calculations of loss). The knowledge, advice and tools rely on the correct calculation of the earthquake shaking input to the building. Although SSI effects will likely reduce losses in buildings during earthquakes in most cases, the percentage reduction is unknown, and indeed, in certain cases that are yet to be identified, losses may increase due to SSI effects. An accurate calculation of loss will likely require explicit consideration of SSI and structure-soil-structure interaction (SSSI) effects.

Seismic probabilistic risk assessment is now being routinely used to assess the adequacy of new and existing nuclear power plants in the United States. Soil-structure interaction (and perhaps SSSI) analysis is a key component of the risk assessment calculations because it influences demands on structural components and floor spectra with which equipment vulnerability is judged.

This report has the goal of advancing the profession's knowledge of SSI and SSSI effects in both buildings in dense urban regions and in safety-related nuclear structures. The following sections present the motivation and objectives of the studies presented in this report.

1.2.1 Assessment of numerical methods in site-response and soil-structure interaction analysis

Site response and SSI are complex nonlinear phenomena involving three-dimensional wave propagation in soils. Site-response analyses have been traditionally performed in the linear domain assuming one-dimensional vertically propagating shear waves in soil profiles with infinitely horizontal soil layers. The most widely used site-response analysis program is the equivalent-linear, frequency-domain program, SHAKE (Schnabel et al., 2012).

Soil-structure interaction analysis of buildings is often performed by modeling the soil beneath the foundations with a set of springs that simulate the flexibility of the soil. The properties of these springs are either calculated using established analytical solutions, or calibrated using experimental data. SSI analyses of nuclear structures are performed using more sophisticated, yet linear, three-dimensional

methods. Of the several methods developed, the most widely used is the numerical program, SASSI (Lysmer et al., 1999), which performs a linear analysis in the frequency domain. These linear methods of site-response and SSI analyses have been used for several decades due to their simplicity and computational efficiency. Although the use of these methods will likely result in accurate predictions for low intensity earthquakes, where the soil behavior is essentially linear, their utility for intense ground motions resulting in large soil strains is unproven.

Significant developments in finite-element methods as well as the availability of computational resources have led to the development of nonlinear methods for site-response and soil-structure interaction analyses. Comprehensive simulations of nonlinear site response and SSI, including foundation gapping and sliding, are now possible on personal computers with commercially available programs such as ABAQUS (Dassault Systèmes, 2005) and LS-DYNA (LSTC, 2013). However, these methods are not yet well established and require much greater computational resources than the frequency-domain programs. Severe earthquake shaking can produce highly nonlinear responses in soils, for which verified and validated nonlinear analysis codes should be better suited for calculating responses than the traditional linear codes.

Nuclear power plant structures are designed for earthquake shaking with return periods between 10,000 and 50,000 years, which result in significant ground accelerations across much of the United States, and significant strains in soils at the sites of many plants. The accuracy of the traditional equivalent-linear methods of site-response and SSI analysis at soil sites experiencing significant bedrock shaking is not known. This leaves the analyst in a conundrum for SSI analysis at sites involving significant shaking and substantially nonlinear soil behavior, namely, either 1) use traditional equivalent-linear tools that are likely incapable of capturing the response of highly nonlinear soils or foundation gapping and sliding that may accompany intense ground motions, or 2) use nonlinear material models and computer codes that can capture explicitly nonlinear soil behavior and foundation gapping and sliding, but which have seen very little use in the past and with which regulators have no substantial experience.

To improve the knowledge and advance practice in site-response and SSI analysis, a series of studies are performed with the following objectives:

1. Benchmark nonlinear site-response and SSI analysis programs against linear programs for elastic soils, and nonlinear soils at small strains.
2. Compare the results of linear and nonlinear site-response analysis programs for a range of soil profiles and ground motion intensities commonly encountered in nuclear construction.
3. Compare the results of linear and nonlinear SSI analysis programs for buildings with different foundation configurations on very soft soil, subjected to a range of ground motion intensities.

4. Examine the differences between the predictions of linear and nonlinear programs, and provide guidance for practicing engineers on the use of these programs.
5. Identify the various challenges and pitfalls that can be encountered performing site-response and SSI analysis, and provide guidance in dealing with or avoiding these challenges and pitfalls.

1.2.2 Seismic structure-soil-structure interaction in dense urban environments

The US National Science Foundation (NSF) funded a research project titled ‘Seismic Performance Assessment in Dense Urban Areas’ to study the effects of SSI and SSSI in dense urban regions. This project, also known as the NEES City Block project or the City Block project, involved a series of six centrifuge experiments of small-scale model buildings at the NEES@UCDavis geotechnical centrifuge facility. The first two experiments involved low- to mid-rise buildings designed to have realistic, code-conforming, dynamic properties with nonlinear behavior at the global level. These buildings were placed far apart in Test 1 and adjacent to each other in Test 2, and comparisons of the structural responses from these tests are expected to provide insight into SSSI in such structures. Test 3 and Test 4 involved buildings that were much stiffer than those in Test 1 and Test 2, and carefully designed to exacerbate SSSI effects. Different structural arrangements (in-plane, anti-plane and combined in-plane anti-plane) are tested to investigate the mechanisms of interaction between these structures. Test 5 and Test 6 involved idealized linear structures founded on liquefiable soil, and the effect of interaction on these structures is examined during liquefaction. The models in each test are subjected to several ground motions of different intensities. These ground motions include both ordinary and pulse motions with forward directivity. The data gathered from these tests has been carefully curated (Mason et al., 2010b; Mason et al., 2010a; Mason et al., 2011; Trombetta et al., 2011) and analyzed by the City Block team (Jones, 2013; Mason, 2011; Trombetta, 2013). The study presented in this report only deals with Test 3 and Test 4 to avoid duplication of prior efforts by other researchers in the City Block project. The objectives of this study are:

1. Analyze the experimental data from Test 3 and Test 4 to examine the site response and SSSI in the model buildings.
2. Numerically simulate the experiments of Test 3 and Test 4 using linear, frequency-domain and nonlinear, time-domain programs, and examine the numerical results.
3. Make qualitative comparisons of the experimental and numerical results and assess the predictions of the numerical programs.

1.3 Report organization

This report is organized into nine sections with contents as follows:

- Section 2 describes the commonly used numerical models that simulate the shear behavior of soils, presents the evolution, state-of-the-art, and limitations of one-dimensional site-response analysis, and describes some studies of three-dimensional site response.
- Section 3 presents a similar review of SSI analysis, emphasizes the latest methods developed for SSI analyses including nonlinear time-domain methods such as the direct method and the domain reduction method, and reviews previous studies on SSSI.
- Section 4 assesses the current, industry-standard, site-response analysis programs for a range of soil profiles and ground motion characteristics. It provides a description of the selection of the soil profiles and ground motions, and numerical modeling, discusses the results, makes statements on the practical issues faced using each of the programs, provides guidelines for the input of ground motion to site-response analysis, and studies biaxial site-response analysis.
- Section 5 presents an assessment of the current, industry-standard, SSI programs, benchmarks time-domain programs against frequency-domain programs for linear elastic analyses, compares results from linear, frequency-domain analyses with strain-compatible soil properties and nonlinear time-domain analyses, describes results, and makes statements on the various practical issues encountered using these programs.
- Section 6 presents a brief description of centrifuge testing including its advantages and disadvantages, an introduction to the NEES@UC Davis centrifuge facility, the experimental procedures of Tests 2, 3 and 4, including the design and construction of models, and the input ground motion sequence for each test.
- Section 7 presents experimental results from Test 3 and Test 4 and makes comparisons with numerical simulations performed using linear frequency-domain and nonlinear time-domain programs. The section provides a description of the numerical models, examines the experimental and numerical results, presents an exploratory study on local SSSI effects between two particular types of foundation systems, and draws conclusions on the effect of SSSI on the global and local structural response.
- Section 8 presents the overarching conclusions for each of the studies performed in this report. The section presents recommendations for future research in the domains of site-response, SSI and SSSI analysis.

SECTION 2

SITE-RESPONSE ANALYSIS: A REVIEW

2.1 Dynamic behavior of soils during earthquakes

Earthquakes induce an irregular cyclic loading in soil that results in a range of stresses and strains. Soils close to the ground surface and sufficiently far away from built structures are known to deform predominantly in shear during an earthquake (Kramer, 1996), and a substantial amount of analytical and experimental research has therefore been performed to characterize the cyclic shear behavior of soils. Studies have also been performed to understand the three-dimensional behavior of soils for more complex situations involving three-dimensional stress fields. Numerical material models have been developed from these studies and implemented in computer programs that are used in seismic analyses. A few of these material models, especially those used in site-response and soil-structure interaction analyses, are described in this section.

2.1.1 Experimental response of cyclically loaded soils

Soils are known to exhibit a nonlinear hysteretic behavior when cyclically loaded in shear. For monotonically increasing loads, they exhibit nonlinear behavior with gradual softening, which manifests as a decrease in shear modulus with strain (Hardin and Drnevich, 1972). Several field and laboratory testing methods have been developed to characterize this behavior, which are classified into low-strain tests and high-strain tests. Low-strain tests are performed at strain levels that are low enough so that no nonlinear behavior is induced in the soil. The shear strain in these tests is typically below 0.001% (Kramer, 1996). Many of these tests involve calculation of the wave velocities through low-amplitude wave propagation to calculate the elastic properties (moduli and wave velocities). High-strain tests, such as the cone penetration test (CPT), are also used to calculate elastic properties. The CPT involves a steady penetration of the standard cone penetrometer into the soil, which has a cylindrical body with a conical tip equipped with a load cell measuring the tip resistance. The observed tip resistance, along with established empirical relationships, is used to calculate the shear modulus and relative density of the soil. The CPT is a quick and inexpensive procedure that can be performed both in the field and in the laboratory, making it one of the most widely used methods in geotechnical engineering practice (Kramer, 1996). Cyclic nonlinear behavior of the soil is characterized through high-strain tests. The most widely used tests for this purpose are the cyclic triaxial test and the cyclic direct simple shear test, which involve a pseudo-static stress-controlled or strain-controlled cyclic loading of a vertically loaded soil specimen. Model tests

at a larger scale are also possible, and can be performed using a laminar box excited on a shaking table. Further details regarding these tests and more testing procedures can be found in Kramer (1996).

2.1.2 Numerical material models for dynamic soil behavior

Soil materials exhibit a diverse range of complex constitutive behaviors, which makes the development of numerical models quite challenging. Several models of varying complexity have been developed in earthquake engineering, which are categorized by (Kramer, 1996) as: 1) equivalent-linear models; 2) cyclic nonlinear models; and 3) advanced constitutive models. Equivalent-linear models and cyclic nonlinear models are based on shear behavior only, and are employed for one-dimensional site-response analyses. Advanced constitutive models incorporate the three-dimensional nonlinear behavior of the soil, and are used for more comprehensive site-response analyses and soil-structure interaction analyses.

2.1.2.1 Equivalent-linear models

Hardin and Drnevich (1972) observed that soils subjected to cycles of symmetrical shear loads of constant amplitude show a hysteretic stress-strain behavior as illustrated in Figure 2-1.

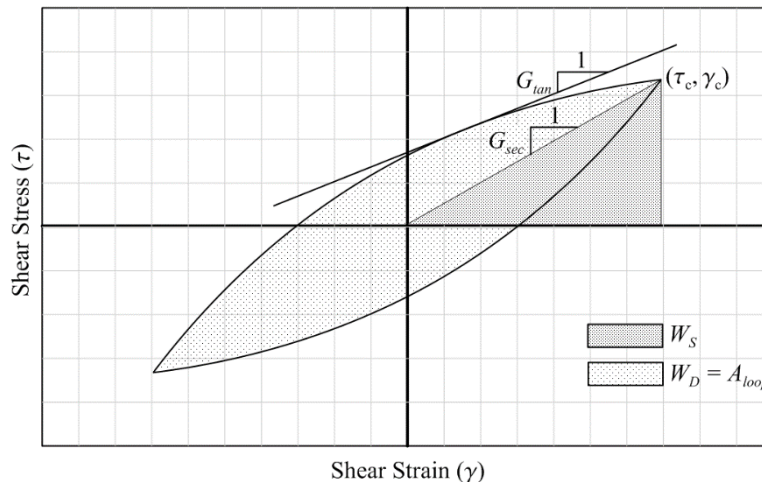


Figure 2-1: Calculation of equivalent-linear parameters: secant shear modulus and effective damping ratio

The instantaneous slope of the stress-strain curve (or the tangent shear modulus, G_{tan}) decreases with the increase in strain, indicating softening in the soil. Also a closed loop indicates the dissipation of energy that is equal to the area of the loop for each loading cycle. The equivalent-linear model simplifies

this behavior by characterizing the hysteresis loop by 1) an equivalent stiffness or secant modulus (G_{sec}), and 2) an equivalent damping ratio that is directly proportional to the hysteretic energy dissipated (Figure 2-1). The secant modulus is calculated as

$$G_{sec} = \frac{\tau_c}{\gamma_c} \quad (2-1)$$

where τ_c and γ_c are the amplitudes of shear stress and shear strain respectively, and the equivalent damping ratio ξ is given by

$$\xi = \frac{W_D}{4\pi W_S} = \frac{1}{2\pi} \frac{A_{loop}}{G_{sec} \gamma_c^2} \quad (2-2)$$

where W_D is the energy dissipated in each load cycle, W_S is the maximum strain energy during loading, A_{loop} is the area enclosed in the loop (Kramer, 1996), and other terms are defined above. As the maximum strain of the loading cycles is increased, the secant shear modulus decreases and the effective damping increases. The largest value of shear modulus corresponds to zero strain and is termed the initial shear modulus, G_0 . The variation of the shear modulus and damping with strain are represented by the modulus reduction curve and the damping curve respectively (Figure 2-2).

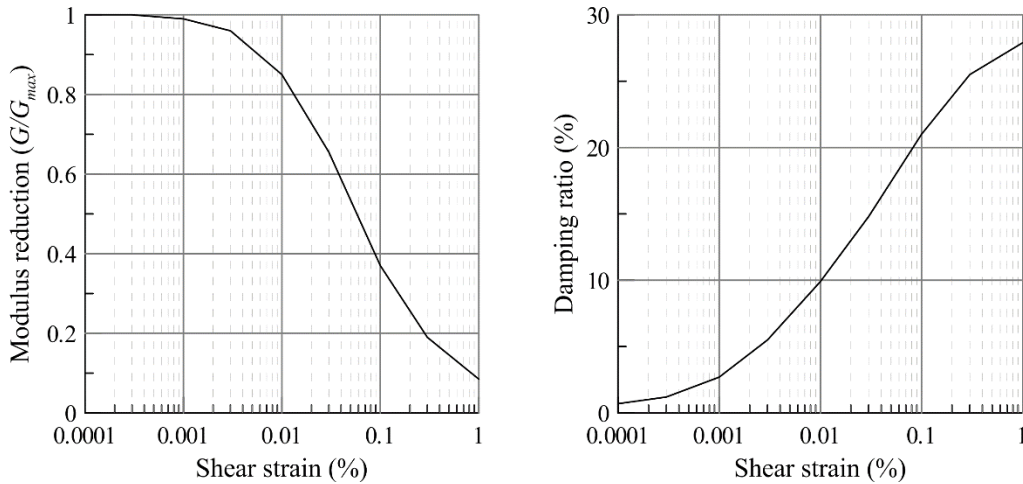


Figure 2-2: Upper bound modulus reduction and damping curves for sand [from Seed and Idriss (1970)]

The modulus reduction curve, when represented as a stress-strain curve, is called as a *backbone* curve. These curves, including the equivalent shear modulus and damping, constitute the equivalent-linear soil model, which is used in a class of site-response analysis methods known as equivalent-linear methods

(Section 2.2.2.2). These parameters depend on the effective mean principal stress for a given soil, and are known to remain almost constant in the frequency range of loading considered in traditional seismic analyses (i.e., 0-25 Hz). Given their simplicity and the ease in experimental calibration, significant efforts have been made to characterize these parameters for various soils.

2.1.2.2 Nonlinear hysteretic models

Nonlinear hysteretic models use the actual hysteresis path during the analysis and enable a more realistic modeling of the soil shear behavior. The hysteresis path is characterized by 1) the backbone curve, and 2) a set of rules that govern the hysteresis path during under an irregular cyclic loading. Various expressions have been proposed for the backbone curve [e.g. the Ramberg-Osgood model (Ramberg and Osgood, 1943), the hyperbolic model or the Kodner-Zelasko model (Lee and Finn, 1978), the modified hyperbolic model or the modified Kodner-Zelasko (MKZ) model (Matasovic, 1993)], each developed to better reproduce the experimental stress-strain data. The most well-known set of hysteresis rules are based on the Masing rules [proposed by Masing (1926), as per Kramer (1996)] and are called as the *extended Masing rules*. These rules are as follows (Kramer, 1996):

1. For initial loading, the stress-strain curve follows the backbone curve [given by $F_{bb}(\tau, \gamma)$]
2. When a stress reversal occurs at a point (γ_r, τ_r) , the path of the stress-strain curve changes to

$$\frac{\tau - \tau_r}{2} = F_{bb}\left(\frac{\gamma - \gamma_r}{2}\right)$$

which implies that the new curve has the same shape as the backbone curve (with the origin shifted to the reversal point), but is twice enlarged. The first two rules describe the Masing behavior (Masing, 1926), which were later extended to better describe the soil behavior under general cyclic loading and called the extended Masing rules.

3. If an unloading or reloading curve exceeds the past maximum strain and intersects the backbone curve, it follows the backbone curve until the next reversal.
4. If an unloading or reloading curve crosses another curve from the previous cycle, it follows the stress-strain curve of the previous cycle.

Since they define the shape of the loops the hysteresis rules significantly affect the nonlinear response, specifically hysteretic damping. Other sets of rules have also been proposed to better match the hysteretic damping calculated from laboratory tests than the extended Masing rules [e.g. Pyke (2000) Muravskii (2005)]. Modifications to the extended Masing rules have also been developed to include pore

water pressure effects, such as modulus degradation (decrease in the secant shear modulus in subsequent cycles) due to excess pore water pressure [e.g. (Matasovic, 1993)].

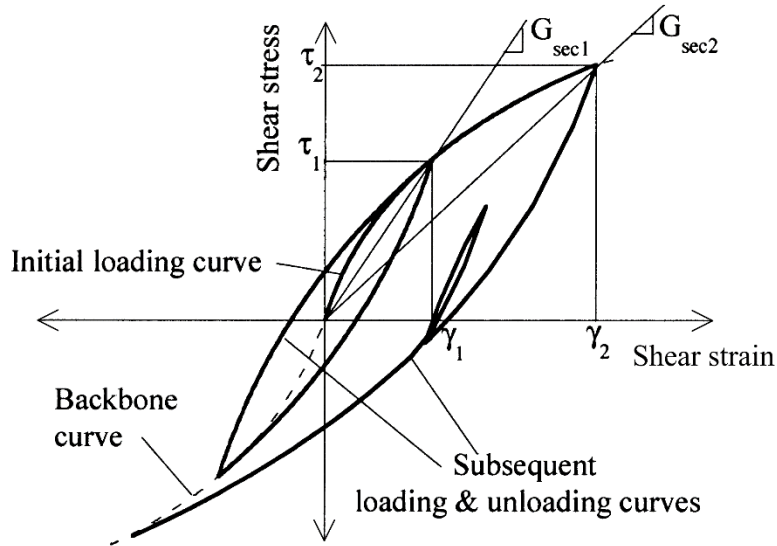


Figure 2-3: Nonlinear hysteretic model with a hyperbolic backbone curve and extended Masing rules (Hashash and Park, 2001)

2.2 Site-response analysis

Site-response analysis (SRA) is the process of calculating the response of a soil deposit to an earthquake ground motion in the absence of structures (called as the free-field response). It is a nonlinear three-dimensional wave-propagation problem that involves the excitation of a soil deposit by a wave-field comprising body and surface waves. Seminal site-response analyses were motivated by field observations indicating higher accelerations on the surface of a soil deposit, as compared to a rock outcrop in the vicinity (Kanai, 1952). This suggested that the type of soil deposit (or, in general, the local characteristics of the site) influenced the magnitude of surface acceleration. Presently the main purpose of site-response analysis is to characterize the effects of the local site conditions such as 1) material properties of the underlying soil layers, and 2) surface topographies such as cliffs and ridges on the surface free-field ground motion. Site-response analysis is also a precursor to soil-structure interaction analysis, in which the free-field site response needs to be calculated before an interaction analysis (Bolisetti, 2010; Kramer, 1996; Wolf, 1985). The present study only deals with the calculation of site response for application in soil-structure interaction analysis without considering topographic effects.

2.2.1 The nature of site response

After the early site-response analysis studies such as Kanai (1952) it was well-understood that the surface free-field acceleration during an earthquake is affected by the properties of the underlying soil deposit. As the earthquake waves propagate upwards in the soil profile, selected frequencies in the input motion are amplified resulting in new peaks in the surface acceleration response spectrum. For weak ground motions that induce small soil strains (and therefore a nearly linear site response), these frequencies correspond to the resonant frequencies of the soil deposit. Therefore a proper assessment of the seismic hazard at a site requires a reasonable estimation of these amplifications, and the frequencies at which these amplifications occur. As the ground motions become more intense, larger soil strains are induced in the soil deposit, introducing nonlinear site effects. These effects include 1) decrease in the resonant frequencies (or lengthening of the time period) of amplification due to the softening of the soil, and 2) decrease in magnitude of amplification (or sometimes de-amplification) due to hysteretic damping. Studies investigating the nonlinear effects in site response have also noted a spike-like waveform in the surface acceleration indicating a high frequency response (Archuleta *et al.*, 2000; Iai *et al.*, 1995; Porcella, 1980). This was later attributed to the dilatancy of sand, in which the accelerations were recorded (Iai *et al.*, 1995). While the preceding site-response effects are limited to simple sites resulting in one-dimensional response, more complex soil deposits result in three-dimensional effects, which are discussed in Section 2.2.3.

2.2.2 One-dimensional methods of site-response analysis

Most site-response analyses are performed using the one-dimensional methods, which are based on the following assumptions: a) soil profiles comprise of horizontal layers stacked atop of each other, b) the soil layers are homogeneous along the horizontal plane, and c) the ground motion incident on the soil deposit is in the form of vertically propagating shear waves. These assumptions simplify the site-response phenomenon and enable the use of simplified numerical models for numerical analysis. However the soil deposits that do not conform to these assumptions need to be analyzed using multi-dimensional methods. The one-dimensional method is considered reasonable for many civil engineering applications (Kramer, 1996), and is presently the most-widely used in practice. One-dimensional site-response analysis involves the excitation of a soil profile using the horizontal component of a ground motion, and calculating the response of the individual soil layers (Figure 2-4). An upward wave propagation analysis typically involves the input of a *rock outcrop motion* (ground motion recorded at a nearby, outcropping bedrock) at the soil-bedrock interface, while the bedrock is replaced by a transmitting boundary to enable the radiation of outgoing waves. If the ground motion at depth is available from recorded data (termed as a

within-profile ground motion), it is directly input at the base of the soil profile while assuming rigid properties for the bedrock. In a downward wave propagation analysis, the surface free-field motion is input at the topmost layer of the soil, and the response of underlying layers is calculated. This process termed as *deconvolution* (Figure 2-4).

The response of a soil deposit with linear viscoelastic properties can be computed using available closed-form solutions (Kramer, 1996). Since these solutions are in the form of frequency-dependent transfer functions, the computations are typically performed in the frequency domain. Nonlinear one-dimensional site-response analyses are performed using either 1) the equivalent-linear method, or 2) the nonlinear method. The equivalent-linear method can be employed both in the frequency as well as the time domains, whereas the nonlinear method can only be implemented in the time domain. A description of each of these methods is presented in Sections 2.2.2.2 and 2.2.2.3.

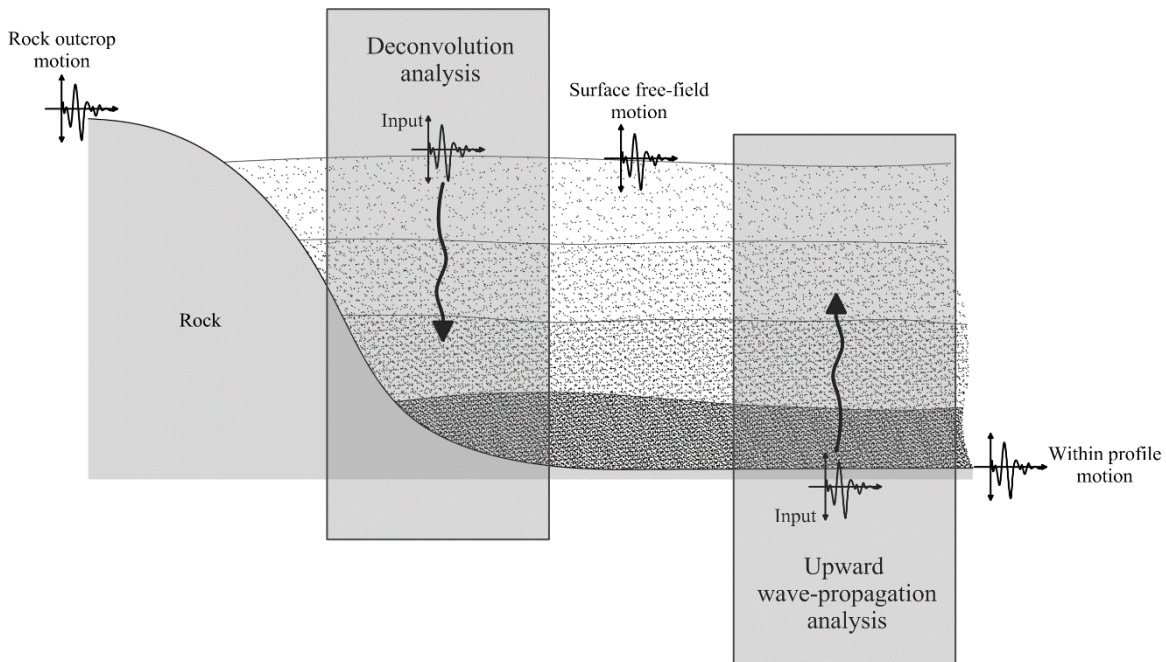


Figure 2-4: One-dimensional site-response analysis

2.2.2.1 Evolution of one-dimensional site-response analysis methods

Early site-response studies involved linear one-dimensional simulations to calculate the ground motion amplification from the bedrock to the soil surface [e.g. Kanai (1952), Idriss and Seed (1967a)]. Subsequent field observations indicating nonlinear soil response led to the development nonlinear site-response analysis methods. Idriss and Seed (1967a) proposed the use of the equivalent-linear approach, which involves the approximation of the nonlinear response by a linear analysis with modified material

properties. They performed the computations in the time domain and assumed bilinear properties for the soil. A subsequent work by Hardin and Drnevich (1972) provided substantial insight into the nonlinear shear behavior of soil, enabling several researchers to develop more nonlinear soil models. Schnabel *et al.* (1972) later implemented the equivalent-linear method in the frequency domain and developed the numerical program SHAKE, which is now widely used in practice. Chen and Joyner (1974) performed time-domain analyses using a multi-linear model, and in a later study (Joyner and Chen, 1975) modeled the soil using a rheological model based on the family of material models developed by Iwan (1967). Several other nonlinear material models, such as the Kodner-Zelasko model (Lee and Finn, 1978), and the hyperbolic (MKZ) model (Matasovic, 1993), were later developed and incorporated into nonlinear time-domain programs, which use different numerical integration techniques to calculate the site response. Some of the well-known nonlinear time-domain programs include DESRA-2 (Lee and Finn, 1978), D-MOD (Matasovic, 1993), TESS (Pyke, 2000) and DEEPSOIL (Hashash *et al.*, 2011). DESRA-2 uses the hyperbolic model (or the Kodner-Zelasko model) for the soil, and simulates the soil hysteretic behavior using extended Masing rules. Matasovic (1993) improved the hyperbolic model by introducing additional parameters and implemented it in D-MOD along with a pore-water pressure model to simulate modulus degradation. Hashash and Park (2001) further modified this model to account for pressure dependence of the soil properties before implementation in DEEPSOIL, and also improved the low-strain damping behavior using various viscous damping formulations. Yang *et al.*, (2004) developed a web-based platform for site-response and liquefaction analysis, which uses the open-source finite element program, OpenSees (Mazzoni *et al.*, 2009; McKenna and Fenves, 2001), along with a plasticity-based soil constitutive model developed by Elgamal *et al.* (2002). Commercial finite element programs such as LS-DYNA (LSTC, 2013) and ABAQUS (Dassault Systèmes, 2005) can also be used to perform site-response analysis in the time domain by using appropriate constitutive models for the soil. The numerical programs SHAKE, DEEPSOIL and LS-DYNA are considered in this study, and are described in more detail in Sections 2.2.2.2.1, 2.2.2.3.1, and 2.2.2.3.2, respectively.

2.2.2.2 Equivalent-linear methods

The equivalent-linear method involves the calculation of an approximate nonlinear response using a linear analysis with the soil layer properties adjusted accordingly. These layer properties are calculated by an iterative procedure involving a series of linear analyses that can be performed either in the frequency or the time domains. A linear analysis is first performed using the initial values of shear modulus and damping ratio, and the peak strains in the soil layers are computed. An effective shear strain is calculated for each layer by multiplying the peak shear strain by an *effective shear strain ratio*. This

strain value, along with the modulus reduction and damping curves, is used to update the shear modulus and damping of each layer. The new values are used to perform another iteration of linear analysis, and the iterations are continued until the shear strains from consecutive analyses match within a pre-defined tolerance. The effective shear strain ratio is a key parameter that relates the loading conditions occurring during the earthquake to those in the laboratory tests that are used to calculate the modulus reduction and damping curves (Kramer, 1996). A value less than 1 is typically chosen, and Idriss and Sun (1992) suggest the following expression to calculate the effective shear strain ratio.

$$\alpha = \frac{M - 1}{10} \quad (2-3)$$

where α is the effective shear strain ratio, and M is the magnitude of the earthquake. The SHAKE user's manual (Schnabel *et al.*, 2012) recommends a value of 0.65, which has traditionally been used in practice. However these recommendations are not validated by published empirical or analytical results as to the knowledge of the author and are only based on experience matching numerical response with recorded data. Idriss and Sun (1992) have found this value to vary between 0.4 and 0.75, while Yoshida *et al.*, (2002) note a much larger range between 0.2 and 1. Dickenson (1994) suggested that the response obtained using the traditional value of 0.65 for the effective shear strain ratio can be slightly improved by using a value between 0.35 and 0.55 for $M_s = 6$ to 7 events, and between 0.55 and 0.7 for $M_s = 7$ to 8 events, where M_s is the surface-wave magnitude. These studies indicate that an appropriate value of α depends largely on the characteristics of the input earthquake and not only on the model. Modifications to the equivalent-linear model have been proposed by researchers [e.g., Assimaki *et al.* (2000); Yoshida *et al.* (2002)], which involve frequency-dependent formulations for the effective shear strain ratio, shear modulus and damping. However these modified versions are rarely used in practice.

2.2.2.2.1 SHAKE

SHAKE performs one-dimensional equivalent-linear site-response analysis in the frequency domain. Site-response analysis in SHAKE requires defining 1) the soil layer properties (thickness, mass density, initial shear modulus and damping ratio), 2) the modulus reduction and damping curves for each material, 3) the ground motion input including the input location, 4) the analysis parameters (number of iterations and the effective shear strain ratio), and 5) the output requests. The dynamic material properties include the modulus reduction (backbone curve) and damping curves that are defined for each material. The stress-strain behavior of the soil is assumed to be Kelvin-Voigt type, which follows the equation

$$\tau = G\gamma + \eta\dot{\gamma} \quad (2-4)$$

where τ is the shear stress, γ is the shear strain, G is the tangential shear modulus, and η is the coefficient of viscosity (Schnabel *et al.*, 1972), and the dot denotes the derivative. The input ground motion can be defined at any layer interface as a rock-outcrop or within motion. The response of the soil profile to the input ground motion can be obtained in the form of acceleration response histories and frequency-domain transfer functions at the layer interfaces, as well as stress and strain response histories within the layers. The iterated values of shear modulus and damping ratio can also be obtained for each layer, and are indicative of the degree of nonlinearity induced by the earthquake.

2.2.2.3 Nonlinear methods

Nonlinear site-response analysis is performed by modeling the soil profile in two approaches: 1) the lumped-mass approach, and 2) the finite element approach. In the lumped-mass approach the soil layers are lumped into adjacent nodal masses, which are connected by springs that model the soil stress-strain behavior in shear. The input ground motion is applied at the base of the soil column, and the dynamic equations of motion are integrated to calculate the response of the soil layers. In the finite element approach, the soil layers are modeled using solid elements stacked on top of each other, and constrained to only move in shear (Figure 2-5).

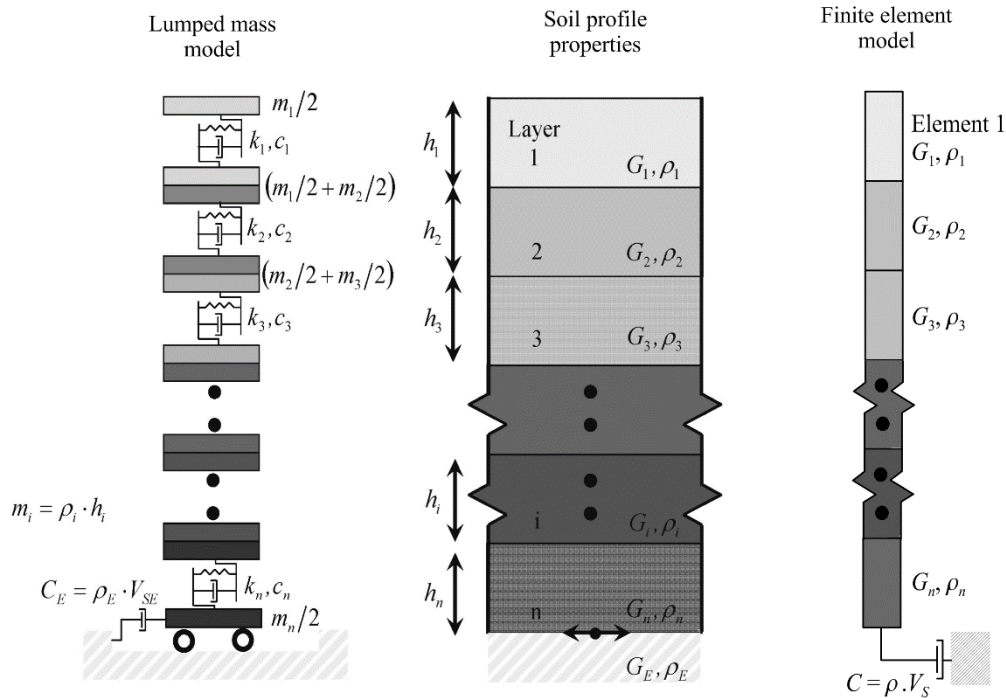


Figure 2-5: The lumped-mass and finite element models for site-response analysis [figure adopted from Hashash *et al.* (2010) and modified]

In these models the bedrock is modeled either as 1) a rigid material (also called as the fixed-base condition), preventing the radiation of the waves reflected from the surface, or 2) linear viscous material (also called as the flexible-base condition), which allows the radiation of reflected waves and is modeled as a transmitting boundary. For the rigid bedrock assumption, the ground motion (acceleration, velocity, or displacement time-series) is directly prescribed at the base of the soil profile. For the linear viscous bedrock assumption, the transmitting boundary is modeled using viscous dashpots at the base of the soil profile, and the input ground motion is prescribed at the soil-bedrock interface in the form of shear stresses (Figure 2-6). The properties of these dashpots and the input shear stresses are calculated as follows:

$$C = \rho V_s \quad (2-5)$$

$$\tau(t) = \rho V_s \cdot \dot{y}(t) \quad (2-6)$$

where C is the damping coefficient of the viscous dashpots, ρ and V_s are the unit mass and elastic shear wave velocity of the bedrock material, $\tau(t)$ is the input shear stress as a function of time, and $\dot{y}(t)$ is the velocity history of the outcrop ground motion (Lysmer, 1978). Joyner and Chen (1975) first used this approach, which was adopted from a transmitting boundary model proposed by Lysmer and Kuhlemeyer (1969) for three-dimensional infinite media.

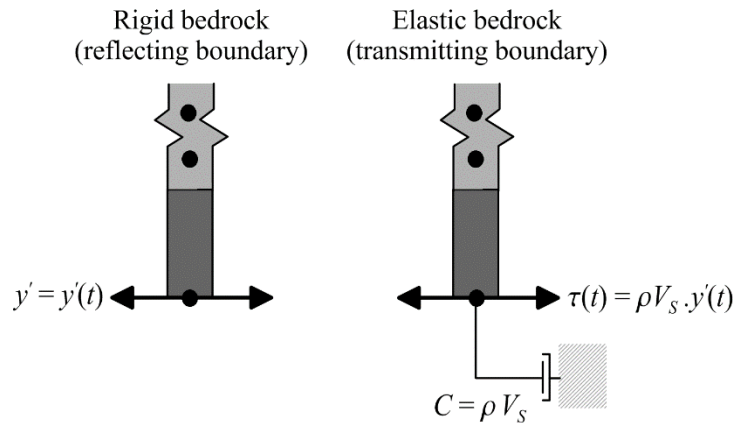


Figure 2-6: Ground motion input in time-domain one-dimensional site-response analysis

2.2.2.3.1 DEEPSOIL

DEEPSOIL is a one-dimensional site-response analysis program developed primarily for time-domain nonlinear analysis of deep soil sites (Hashash and Park, 2001). Frequency-domain equivalent-linear analysis is also incorporated into this program, and is performed using the same method as followed in SHAKE. DEEPSOIL uses the lumped-mass approach for the nonlinear time-domain analysis

(Figure 2-5). It employs the modified hyperbolic or MKZ model (Matasovic, 1993) for the soil, which simulates pressure-dependent soil properties and uses a modified version of the extended Masing rules to model the hysteretic behavior. The backbone curve for this model is defined by the following equation:

$$\tau = \frac{G_0 \gamma}{1 + \beta (\gamma / \gamma_r)^s} \quad (2-7)$$

where τ is the shear stress, γ is the shear strain, G_0 is the maximum shear modulus, β and s are dimensionless parameters, and γ_r is a reference shear strain. Pressure dependence is introduced in the model through the following equation, which defines the variation of the reference shear strain with pressure:

$$\gamma_r = a \left(\frac{\sigma'}{\sigma_{ref}} \right)^b \quad (2-8)$$

where σ' is the effective confining pressure, a and b are the curve fitting parameters, and σ_{ref} is the reference confining pressure. DEEPSOIL is also capable of performing an effective stress analysis and uses the pore water pressure model developed by Matasovic (1993) for this purpose. This model captures the pore water pressure build-up as well as the resulting modulus degradation effect.

The backbone curve of the hyperbolic model and its variants (such as the modified hyperbolic model) are almost linear at strains smaller than 10⁻⁴% and result in negligible hysteretic damping, unlike real soils that exhibit a finite amount of damping (Hashash and Park, 2001). This is compensated in DEEPSOIL by incorporating a frequency-independent viscous damping formulation. It is also referred to as low-strain damping and depends on the confining pressure as follows:

$$\xi = \xi_{ref} \left(\frac{1}{\sigma'_v} \right)^d \quad (2-9)$$

where ξ_{ref} is the low-strain damping at a reference effective vertical stress σ_{ref} , σ'_v is the effective vertical stress, and d is a curve fitting parameter (Phillips and Hashash, 2009). Phillips and Hashash (2009) also note that using the extended Masing rules to calculate the hysteresis loops leads to an overestimation of the hysteretic damping in high strains. DEEPSOIL provides two approaches to circumvent this problem. The first approach involves using the experimental data to determine a best fit either only for the modulus reduction curve (which results in a poor match in hysteretic damping), only for the damping curve (which results in a poor match for the modulus reduction), or a fit that matches both the curves simultaneously (which results in an optimum between both). The second approach (termed as the MRDF-UIUC approach) introduces a damping reduction factor, $F(\gamma_m)$, which is

multiplied to the damping curve that is calculated using extended Masing rules. The damping reduction factor is given by the equation

$$F(\gamma_m) = p_1 - p_2 \left(1 - \frac{G_{\gamma_m}}{G_0} \right)^{p_3} \quad (2-10)$$

where p_1 , p_2 , and p_3 are dimensionless parameters to best fit the experimental damping curve, γ_m is the strain from the damping curve, G_{γ_m} is the value of reduced shear modulus at the corresponding strain, and G_0 is the maximum shear modulus. In order to accommodate the damping reduction factor while maintaining the compatibility between the modulus reduction and hysteretic damping curves, the extended Masing rules are modified by changing the equations for unloading-reloading behavior. Further details regarding the damping reduction factor and the modified unloading-reloading behavior are presented in Phillips and Hashash (2009). DEEPSOIL also enables the inclusion of pore water pressure effects by performing an effective stress analysis using the models developed by Matasovic (1993). Numerical integration of the dynamic equations of motion is carried out using the implicit Newmark- β method (Chopra, 1995).

2.2.2.3.2 LS-DYNA

LS-DYNA is a commercial finite element program that primarily uses the explicit method for numerical integration (LSTC, 2013). It provides a large collection of material models including several soil models that can be used in seismic analyses (e.g. Ramberg-Osgood model, Drucker-Prager model, Mohr-Coulomb model). Analyses in this research are performed using the MAT_HYSTERETIC model (*MAT_079 in LS-DYNA), which was developed by Arup specifically for site-response and soil-structure interaction analyses. The MAT_HYSTERETIC model is capable of three-dimensional constitutive behavior and can be used only with eight-node solid elements. Hysteretic behavior is generated in this model by superposing multiple layers having elastic-perfectly plastic properties in parallel. The value of stress at any instant is equal to the sum of the stresses in the individual elastic-perfectly plastic layers, which results in a piecewise-linear backbone curve. Figure 2-7 below illustrates the hysteretic behavior of the MAT_HYSTERETIC model for a given loading.

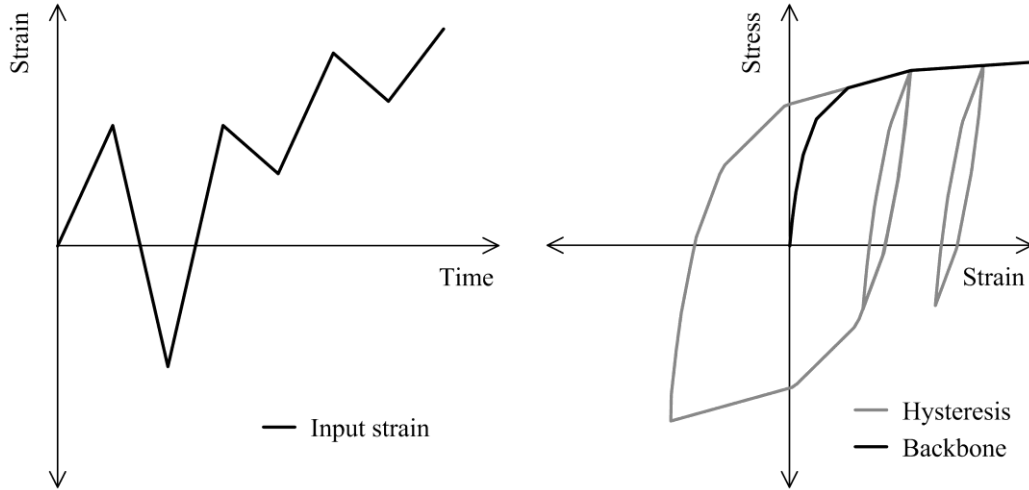


Figure 2-7: The hysteresis loop for the MAT_HYSTERETIC model for a given input strain, and the corresponding backbone curve

The backbone curve is directly input by the user as a set of ten shear stress and shear strain values. This curve is subsequently broken down into ten layers of elastic-perfectly plastic properties, each having a value of shear modulus and yield stress. These properties are pressure dependent as described by the following equations:

$$G(p) = \frac{G_0(p - p_0)^b}{(p_{ref} - p_0)^b} \quad (2-11)$$

$$\frac{\tau(p)}{\tau(p_{ref})} = \sqrt{\frac{a_0 + a_1(p - p_0) + a_2(p - p_0)^2}{a_0 + a_1(p_{ref} - p_0) + a_2(p_{ref} - p_0)^2}} \quad (2-12)$$

where p is the current pressure, p_0 is the cut-off or datum pressure, p_{ref} is the reference pressure at which input values are calculated, G_0 is the shear modulus of the layer at the reference pressure, $G(p)$ is the shear modulus of the layer at pressure p , $\tau(p_{ref})$ is the yield stress of the layer at the reference pressure, $\tau(p)$ is the yield stress of the layer at pressure p , b is the exponent for pressure sensitive moduli, and a_0 , a_1 , and a_2 are the yield function constants. Additional effects such as dilatancy and strain rate effects are also included in the material model, which are illustrated in the LS-DYNA keyword manual (LSTC, 2013).

2.2.2.4 Validation of one-dimensional site-response analysis programs

One-dimensional site-response analysis programs are typically validated by comparing the numerical response of a real soil profile to recorded field data. The soil profile is modeled using the

material properties calculated from site investigations or laboratory testing. The input motion for the numerical analysis is either 1) taken from a ground motion recorded at a nearby rock outcrop and specified as an outcrop motion, or 2) taken from a ground motion recorded at the bottom of the soil profile in a down-hole array and specified as a within motion. Idriss and Seed (1968a) and Seed and Idriss (1969) first compared the numerical site responses with field data recorded during the 1957 San Francisco earthquake, the 1962 Mexico earthquake, and the 1964 Alaskan earthquake, and noted that the site response was captured fairly well. Although the ground motions used were of low intensity, with peak input accelerations not more than 0.07g, the observations made in these studies further motivated the use of one-dimensional site-response analyses. The strong ground motion data recorded during the 1989 Loma Prieta earthquake led to more such studies, such as Idriss (1990), Dickenson (1994), and Chang (1996), which involved the validation of different numerical site-response analysis programs. Idriss (1990) used this data to assess the accuracy of the numerical program SHAKE and found that it offers a reasonable accuracy in estimating the peak acceleration responses for low-intensity motions, but only a fair accuracy in estimating the spectral shapes. They suggested the use of nonlinear methods for more intense ground motions with input rock accelerations greater than 0.2g. Dickenson (1994) conducted a similar study for the programs SHAKE04 (Youngs, 2004), which is a slightly modified version of SHAKE, and also the nonlinear program MAR-DESRA, which is a modified version of the program DESRA-2 (Lee and Finn, 1978). They considered a total of ten deep, soft clay sites in the Bay Area, and found good agreements only for a few sites (Figure 2-8). They also found that the accuracy of the numerical response was sensitive to the choice of the outcrop ground motion, in cases where multiple rock outcrop recordings were available for a single site. Chang (1996) performed similar validation studies for the programs SHAKE and D-MOD using the recorded data from deep, stiff clay sites during the 1989 Loma Prieta earthquake as well as the 1994 Northridge earthquake (Figure 2-9). While the above studies conclude that the corresponding numerical programs make reasonably good predictions of site response, Kwok (2007) indicated that some of the studies might have involved the modification of model parameters to arrive at a better match.

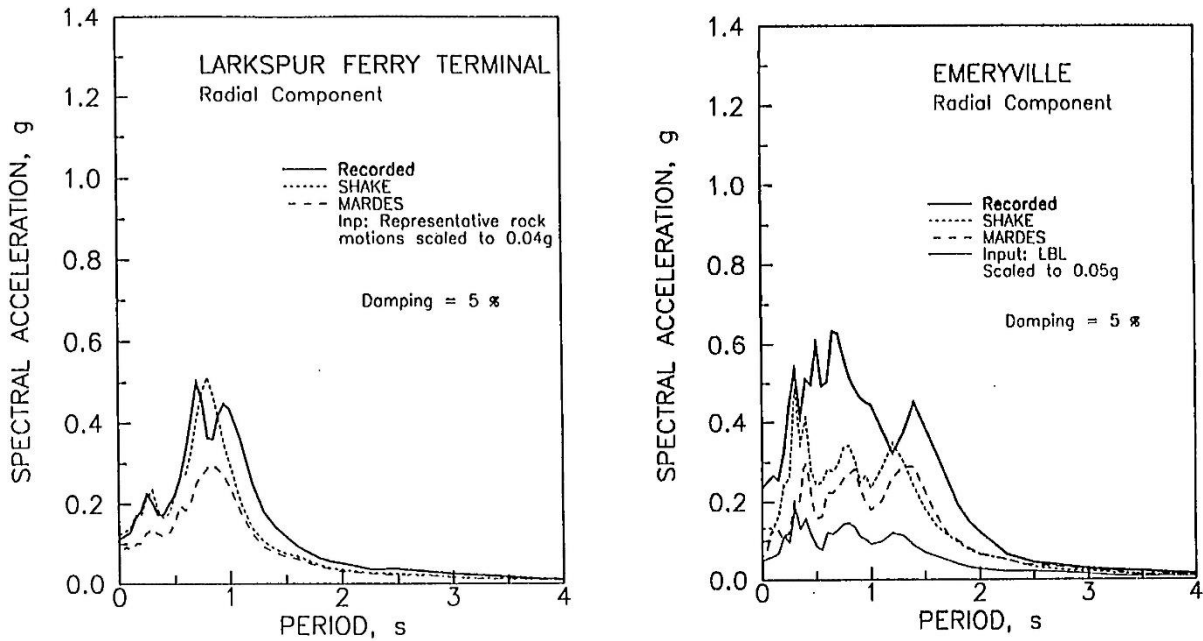


Figure 2-8: Sample comparisons between the numerical and observed site response from Dickenson (1994)

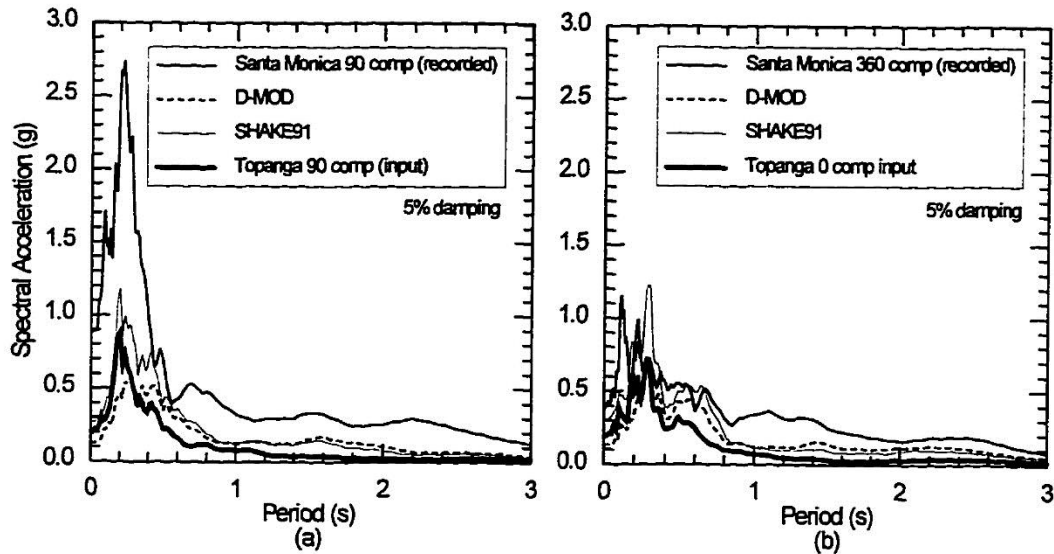


Figure 2-9: Sample comparisons between the numerical and observed site response from Chang (1996)

Unlike in the above studies that used data from a nearby rock outcrop, data from vertical down-hole accelerometer arrays enable a more reliable validation of one-dimensional site-response analysis programs. The Lotung Large-Scale Seismic Test (LSST) in Taiwan, which included two down-hole

arrays and three surface arrays for a soil-structure interaction experiment, facilitated the recordings from a total of 11 earthquakes with peak surface accelerations ranging from 0.03g to 0.21g for the horizontal component, and from 0.01g to 0.20g for the vertical component (Chang *et al.*, 1991). Chang *et al.* (1991) found that the body waves propagated at an angle of 6 degrees to the vertical, indicating almost one-dimensional propagation and that the data is suitable for the validation of one-dimensional methods. Chang *et al.* (1990) used this data to validate the program SHAKE, for both upward wave-propagation analyses (convolution) as well as deconvolution analyses. The results showed that SHAKE overestimated the high-frequency response in the deconvolution analysis as well as the resonant frequency response in the upward wave-propagation analysis. They also used a modified version of the nonlinear program DESRA-2 (Lee and Finn, 1978) and found that the nonlinear site-response analysis resulted in better agreement with recorded data. Borja *et al.* (1999) performed a similar study using the Lotung data to assess the programs SHAKE and SPECTRA. SPECTRA is a fully nonlinear program that employs a constitutive model based on three-dimensional bounding-surface plasticity theory (Borja and Amies, 1994). Both the programs showed reasonable matches with the experimental data, but the nonlinear numerical response was better (Figure 2-10).

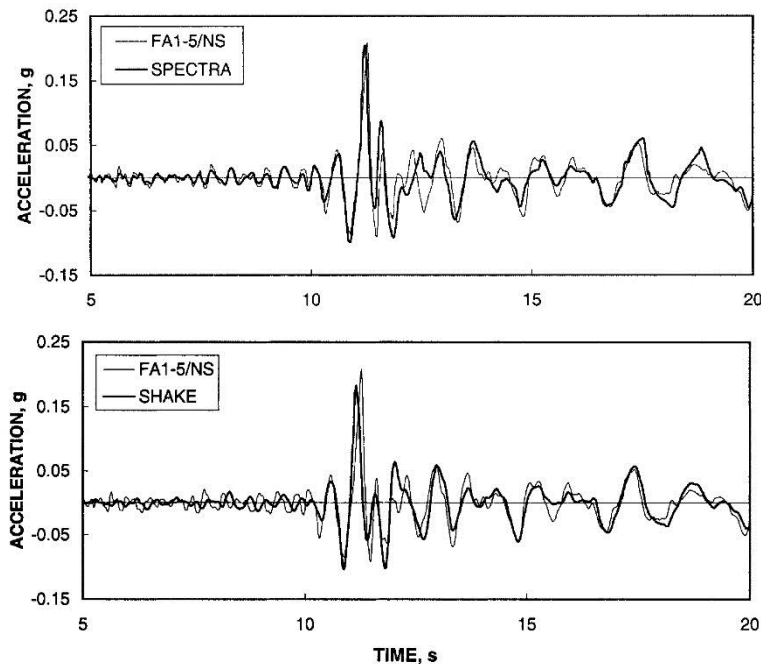


Figure 2-10: Sample comparisons of numerical and experimental data from Borja *et al.* (1999)

Kwok *et al.* (2008) investigated the results of a blind-prediction study that required the site-response prediction of the Turkey-Flat site before the surface acceleration data was available. Turkey-Flat

is a shallow stiff soil site with recording instruments available in a vertical down-hole array and also at a nearby rock outcrop (Figure 2-11).

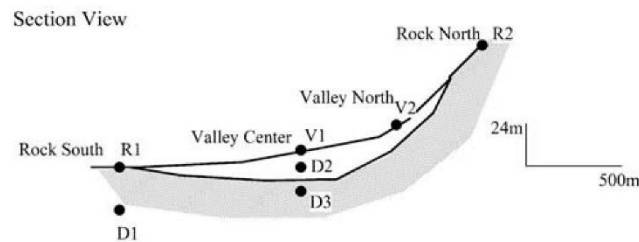


Figure 2-11: Section view and instrumentation of the Turkey Flat site (Kwok *et al.*, 2008)

Their study considered six different site-response analysis programs [SHAKE04 (Youngs, 2004), which is a modified version of SHAKE, D-MOD_2 (Matasovic, 2006), DEEPSOIL (Hashash *et al.*, 2011), OPENSEES (Mazzoni *et al.*, 2009; McKenna and Fenves, 2001), TESS (Pyke, 2000), and SUMDES (Li *et al.*, 1992)] for the blind prediction and used a within profile ground motion for input, which was recorded from the 2004 Parkfield earthquake and had a peak acceleration of about 0.1g. They observed that most of the programs captured the shape of the acceleration time series reasonably well, but significantly underestimated the measured amplitude at certain time instants. A comparison of the acceleration response spectra calculated from different programs indicated that the responses were similar at the elongated period of the soil profile, but they were all significantly lower than the measured response at this period. Additionally they found a large disparity between the responses from different programs at short periods (Figure 2-12).

After further investigations they attributed the poor prediction to a bias in the measurement of near-surface soil properties, and identified the one-dimensional approximation of a three-dimensional phenomenon as another possible reason. Validation of a one-dimensional site-response analysis program ideally requires data recorded from a true one-dimensional wave field, which is not produced by real earthquakes. Nevertheless the above studies used data from real earthquakes and, with the exception of the studies using LSST data, it is unclear if they verified the validity of the one-dimensional method for the sites considered.

Validation can also be performed through laboratory experiments using a laminar box for the soil. Elgamal *et al.* (2005) performed a series of centrifuge tests, and used the data to calibrate the parameters of a nonlinear finite element site-response analysis program. Simulations using the calibrated parameters showed good agreements with the experimental data. Similar experiments are possible at a larger scale while using a shaking table, but such tests are yet to be performed.

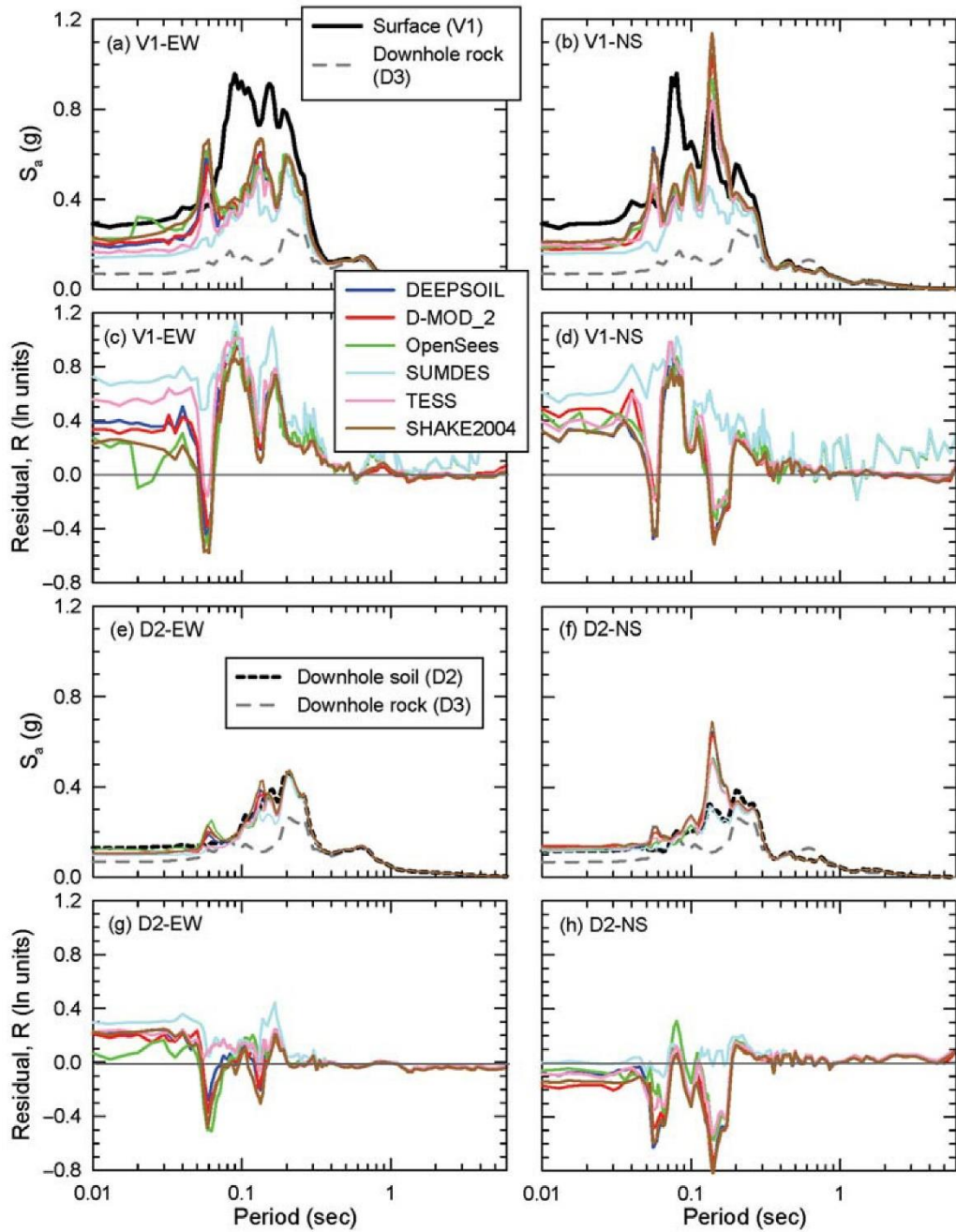


Figure 2-12: Blind predictions at locations V1 and D2 using different numerical programs and the corresponding residuals¹ (Kwok *et al.*, 2008)

¹ Residual is defined as $R(T) = \ln \left[S_a(T) \right]_{\text{data}} - \ln \left[S_a(T) \right]_{\text{predicted}}$

2.2.2.5 Comparison and limitations of various one-dimensional methods

The equivalent-linear method was developed as a computationally simpler alternative to the nonlinear method, although the latter involves a more realistic simulation of soil behavior. The equivalent-linear method is constrained to only elastic deformations and therefore cannot simulate soil failure and related effects such as permanent displacements and liquefaction. Furthermore the ambiguity in the selection of the effective strain ratio makes this method even less credible compared to the nonlinear method (Yoshida *et al.*, 2002). Idriss and Seed (1968b) performed a nonlinear site-response analysis assuming bilinear properties for the soil, and used the computed hysteretic stress-strain loops to calculate the equivalent-linear properties (reduced shear modulus and equivalent damping) for each layer. They performed a linear analysis using these properties and found that the responses of the soil layers match reasonably well with the nonlinear responses. Although this was not a direct equivalent-linear analysis (involving iterations to calculate the equivalent-linear properties), they demonstrated that the results of a nonlinear analysis can be captured reasonably well by a linear analysis. Constantopoulos *et al.* (1974) made detailed comparisons between the results of a nonlinear (using the Ramberg-Osgood model) and an equivalent-linear analysis using a few hypothetical soil profile models. Their study showed that 1) the equivalent-linear method underestimates the peak displacements and overestimates the peak accelerations, 2) the resonant period of the soil profile calculated from the two methods match reasonably well, and 3) the differences between the solutions from the two methods increase with the intensity of the excitation. Joyner and Chen (1975) performed another comparison involving a deep soil profile subjected to an intense excitation, and found that they match reasonably well for longer periods but the equivalent-linear method does not reproduce the short-period components present in the nonlinear solution. Also the peak accelerations were underestimated, contrary to Constantopoulos *et al.* (1974). Finn and Martin (1978), in a study comparing prominent site-response analysis programs, found that SHAKE overestimated the peak shear stresses in the soil layers, and also the acceleration amplitude at the resonant time period of the soil profile. While Finn and Martin (1978) attributed this to resonance in a linear analysis, Yoshida *et al.*, (2002) contended that it is due to the mechanism of the equivalent-linear method itself, specifically the definition of the effective shear strain ratio as a fraction of the effective shear strain. By reexamining the work by previous researchers, Yoshida *et al.*, (2002) summarized that the equivalent-linear method results in 1) the overestimation of the shear stress as compared to the nonlinear method, which leads to an overestimation of the peak accelerations under strong shaking, and 2) underestimation of high-frequency amplifications, which sometimes leads to the underestimation of the peak accelerations. They attributed these drawbacks to the concept of a constant value of effective shear strain ratio, and also proposed a frequency-dependent formulation for this parameter that resulted in a better agreement between the equivalent-linear and nonlinear analyses.

Despite the drawbacks the equivalent-linear method is still preferred over the nonlinear method in practice, often due to poor understanding of nonlinear soil parameters that may not be clearly associated with measurable soil properties (Kwok, 2007). Nonlinear methods also occasionally result in abnormal high-frequency components in the acceleration response. This is either due to the soil material model used in the analysis [e.g., the multi-linear material model used by Chen and Joyner (1974)], or the type of integration technique used for solving the dynamic equations (Joyner and Chen, 1975). Chen and Joyner (1974) investigated this issue and confirmed that these frequencies occur due to the resonance of the individual layers of the numerical model, and suggested that the noise be removed using digital filtering.

The one-dimensional method was developed specifically for horizontally layered soil deposits subjected to vertically propagating waves, but no definite guidelines are yet proposed that assist in deciding the validity of this method for given site conditions. Additionally most of the numerical programs require a uni-directional horizontal input, which entails an assumption that the horizontal components of ground motion are uncorrelated. As this is not true, the correlation between the horizontal components needs to be accounted for by applying them simultaneously in the input. This requires multidimensional plasticity based material models [such as the one described in Borja *et al.* (1999)] that model the correlation between the stress components. However the author is not aware of studies that have investigated the effects of ignoring the correlation between horizontal components.

2.2.3 Multi-dimensional analyses

The assumption of vertical wave propagation does not hold in many cases that involve significant contribution of two- or three-dimensional wave fields and require multi-dimensional site-response analysis simulations. Some of these cases have been thoroughly investigated, which include 1) sites with uneven surface topographies such as earth banks, cliffs and ridges, and 2) heterogeneous basins, where the soil-bedrock interface is not horizontal. Early studies addressing these effects used discrete numerical methods (such as the finite element, or finite difference methods) and performed two-dimensional linear elastic analyses [e.g. Idriss and Seed (1967b) and Boore (1972)]. Although they did not account for soil nonlinearity, these studies were notable in pointing out that the site amplifications in the presence of topographical features were considerably different from those calculated from one-dimensional analyses. Nonlinear two-dimensional analyses were also performed at that time: Joyner (1975), for example, investigated the multi-dimensional effects of the presence of soft basins and earth dams using a rheological model from the family of models developed by Iwan (1967). In more recent work, Assimaki and Gazetas (2004) performed parametric studies involving two-dimensional site-response analyses to investigate the contribution of site properties and the input ground motion characteristics on topographic effects.

Three-dimensional linear and nonlinear site-response simulations have also been performed, primarily in the field of computational seismology. The main application of these simulations is the characterization of seismic hazard while accounting for large scale three-dimensional effects such as of basins and directivity (Taborda, 2010). Xu *et al.* (2003) noted that the three dimensional basin effects 1) significantly increase the amplitude of the surface acceleration response, and 2) extend the duration of the strong phase of the ground motion, as compared to a one-dimensional analysis. Despite the significant computational challenges involved, several such studies have been attempted, including Xu (1998), Xu *et al.* (2003), Day *et al.* (2006), and Restrepo *et al.* (2011). Each of these studies has indicated the importance of three-dimensional effects, especially basin effects, which cannot be reproduced by one-dimensional simulations.

SECTION 3

SOIL-STRUCTURE INTERACTION: A REVIEW

3.1 Introduction

Earthquake waves originate from a fault rupture and propagate in the earth's crust. In the absence of structures at a site of interest, the resulting ground motion is called the *free-field* ground motion. When a structure, or a set of structures, is present at a site of interest, the ground motion results in structural shaking. Traditionally the response of structures to ground motion is calculated by disregarding the flexibility of the soil below, assuming the structure is fixed to the ground, and subjecting the structure to a free-field ground motion. This is called fixed-base analysis. In reality, soil is flexible and the dynamic response of the soil affects the dynamic response of the structure, and vice versa. This interaction between soil and structure is called soil-foundation-structure interaction (SFSI) or soil-structure interaction (SSI). There are two aspects of SSI: 1) the modification of the free-field ground motion due to the presence of a stiff foundation in the soil, and 2) modification of the structural response due to the flexibility of the soil (flexible-base). The former is called *kinematic* interaction, and results in a deviation of the ground motion input to the structure from the free-field ground motion. The latter is called *inertial* interaction and results in a deviation of the response of the structure from the fixed-base response. Inertial interaction results in 1) an increase in the natural time period of the structure due to soil flexibility (period elongation), and 2) an increase in the structural damping due to energy dissipation from the hysteretic behavior of the soil at the foundation (hysteretic damping) and the radiation of the reflected wave-field away from the structure (radiation damping). An accurate estimation of structural response when accounting for SSI (SSI analysis) requires the simulation of kinematic interaction and inertial interaction, including period elongation, hysteretic damping and radiation damping.

SSI is often neglected in the design of non-nuclear structures. The most common argument for neglecting SSI is that it results in a negligible change in the response of the structure. Indeed, SSI effects are small for many conventional structures such as light, flexible buildings founded on stiff soil. For these cases, the response of the structure is very close to the fixed-base response. Another reason for ignoring SSI is a common misconception that SSI effects are always beneficial and result in a net decrease in structural demand. The provisions for incorporating SSI in structural design in ASCE Standard 7 (ASCE, 2010) include a reduction in the design base shear. This reduction in seismic demand is illustrated in

Figure 3-1, which shows the change in the design spectral acceleration S_a , when the structural time period² increases from T to \bar{T} , and the damping ratio increases from β to $\bar{\beta}$ due to SSI effects.

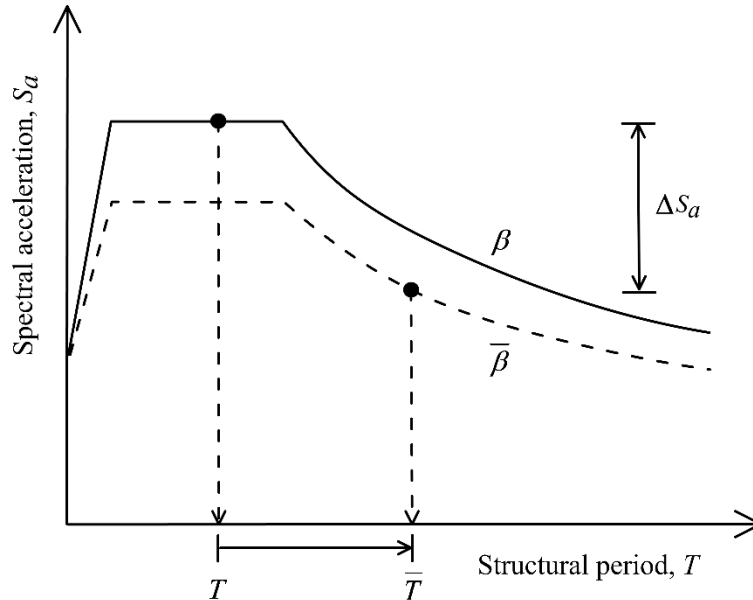


Figure 3-1: Decrease in seismic demand due to SSI effects in idealized design response spectra [adopted from Mylonakis and Gazetas (2000) and modified]

However this decrease is due to the idealized shape of the design response spectrum, in which the spectral acceleration decreases with the structural period in the intermediate- and long-period ranges. In reality, spectral accelerations calculated from recorded ground motions may also increase with period in the long-period range due to 1) amplification of the rock motion at the site period of deep soil sites, or 2) forward fault-rupture directivity (Somerville *et al.*, 1997), which results in a long period pulse in the ground motion that manifests as large spectral accelerations at periods greater than 0.5 sec. Response spectra for some such ground motions are presented in Figure 3-2, which also enables a comparison between the response spectra with a sample design response spectrum. In addition to the increase in spectral accelerations, Mylonakis and Gazetas (2000) also demonstrated that the increase in structural period can result in an increase in the ductility demands for structures founded on soft soils. However, irrespective of its beneficial or detrimental effects, there is growing consensus that SSI should still be considered for performance assessment of buildings (FEMA, 2012; Mylonakis and Gazetas, 2000;

² It should be noted that time periods of most buildings are in the range for which, the design spectral acceleration is either constant or decreasing with structural period.

Stewart et al., 1999b). Guidelines for including SSI in the design and performance assessment of buildings are provided in ASCE Standard 7 (ASCE, 2010), FEMA 440 (FEMA, 2005) and NIST GCR 12-917-2 (NIST, 2012).

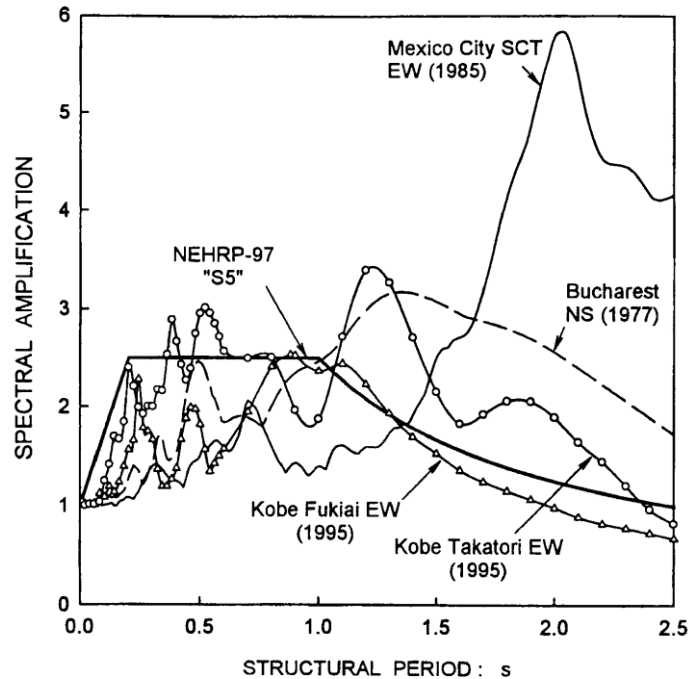


Figure 3-2: A typical code design spectrum and response spectra from some recorded strong ground motions (Mylonakis and Gazetas, 2000)

Unlike buildings, SSI can significantly affect the response of nuclear power plant structures. Nuclear power plants are stiff and heavy, which are characteristics that facilitate SSI. Indeed most of the early research in numerical SSI analyses was motivated by its significance in the design of nuclear power plants (Kausel, 2010). Design and performance assessment of nuclear power plants in the United States account for SSI, and guidelines for performing SSI analyses for these structures are presented in ASCE Standard 4 (ASCE, 1998; ASCE, forthcoming).

3.2 Numerical methods in soil-structure interaction analysis

Early SSI analyses involved analytical calculations of the response of footings resting on a semi-infinite half-space. Most of these studies [e.g., Veletsos and Wei (1971), Luco and Westman (1971), Veletsos and Verbic (1973), Veletsos and Verbic (1974)] calculated frequency-dependent impedance functions for rigid foundations that were limited to rectangular or circular shapes, and lay atop of elastic

or viscoelastic halfspaces. Amongst the studies that involved seismic analysis of buildings, a study by Jennings and Bielak (1973) showed that the SSI response of a building with n resonant frequencies can be found by the superposition of $n + 2$ damped, linear oscillators subjected to modified excitations, with the two additional oscillators corresponding to translation and rotation of the foundation. Veletsos and Meek (1974), in an influential paper, used this result to obtain the properties of an equivalent single-degree-of-freedom (SDOF) oscillator that had the same time period and damping ratio as an SDOF system founded on linear elastic soil. By comprehensive numerical studies on the equivalent oscillator, their study was also extended into identifying various system parameters that could be used to assess the significance of SSI effects. These studies also led to the development of early guidelines in FEMA 274 (FEMA, 1997) to account for SSI effects in structural design. The advent of numerical tools such as the finite element and boundary element methods in the 1970's enabled researchers to take up more complicated foundation configurations (such as embedded foundations and foundations on layered media) to calculate impedance functions [e.g., Elsabee *et al.* (1977), Kausel and Roesset (1975)]. Gazetas (1991) summarized frequency-dependent impedance functions for different foundation shapes and configurations (including embedded foundations and arbitrarily shaped foundations), which were calculated over the years using various analytical and numerical techniques.

Early SSI analysis involved modeling the flexibility of the soil at the foundation through equivalent springs and dashpots, with pre-calculated impedance functions. This method of SSI analysis is also called the spring method. The spring method had several limitations: the foundation stiffness and damping functions calculated in the studies described above were frequency-dependent, and were only applicable to a narrow range of frequencies (Roesset, 1998). Additionally, problems in practice involved more complicated foundations with non-rectangular or circular shapes, deeply embedded foundations, and soil profiles with non-uniform variation of shear modulus with depth. These problems required more sophisticated methods, which were later developed mainly for the nuclear industry (Kausel, 2010; Roesset, 1998). As such, the pursuit of more sophisticated SSI analyses methods resulted in two main approaches: the substructuring method, and the direct method. These methods are also used in the SSI analyses presented in this report, and therefore are described in the following sections.

3.2.1 Substructuring method

In the substructuring method of SSI analysis, the soil-structure system is divided into different components (or substructures), and the response of each substructure is calculated independently (Figure 3-3). The substructures are 'connected' by applying equal and opposite interaction forces to each of the substructure models. The responses of all the substructures are later combined by superposition to

calculate the final response of the system. The substructure technique therefore provides an advantage of the choice of a suitable analysis method for calculating the response of each substructure. Since the individual responses of the substructures are added by superposition, the substructure method is limited to linear analyses. Two of the widely-used software programs that use the substructuring technique are SASSI (A System of Analysis of Soil-Structure Interaction) (Lysmer *et al.*, 1999) and CLASSI (Continuum Linear Analysis of Soil-Structure Interaction), both of which, function in the frequency domain.

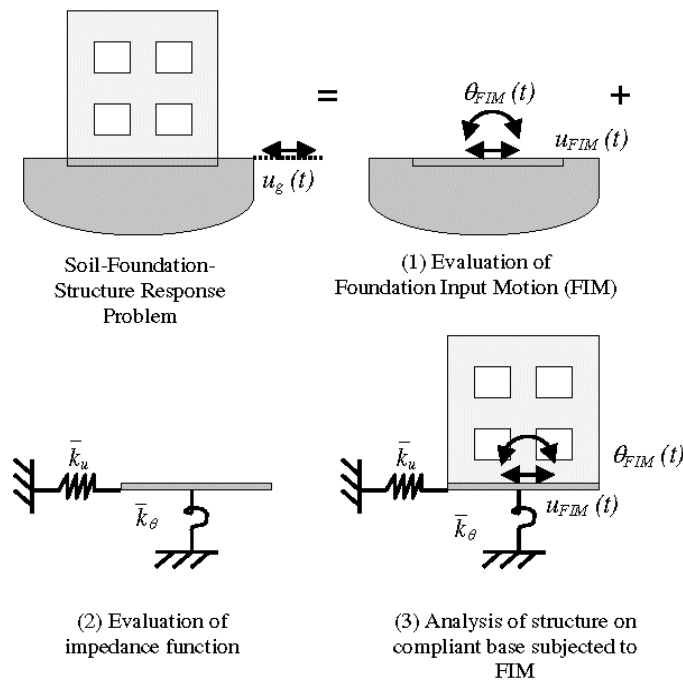


Figure 3-3: Steps in a substructuring analysis (Kramer and Stewart, 2004)

Most often, the soil-structure system is subdivided into a soil medium and a structure, as illustrated in Figure 3-3, and the responses of these substructures are calculated through site-response analysis and structural analysis, respectively. Structural analysis can be conveniently performed by finite element methods, once the seismic input and impedance at the foundation are calculated. The calculation of the seismic input should account for kinematic interaction, and is called a scattering analysis. The calculation of foundation impedance (which is the complex stiffness that includes both stiffness and damping functions) should include radiation damping and is called the interaction analysis or the impedance analysis. Substructuring methods can be classified into four types based on the way the scattering problem and interaction problem are solved (Ostadan, 2006a), 1) the rigid boundary method, 2) the flexible boundary method, 3) the flexible volume method, and 4) the subtraction method. All four

methods involve site-response analysis to calculate the free field ground motion, impedance analysis to calculate the foundation impedance and the structural response analysis to calculate the structural response. The first two methods also involve scattering analysis, which involves the calculation of foundation input motion (motion at the foundation in the presence of a rigid, massless structure). Figure 3-4 presents a summary of these methods.

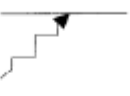
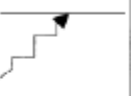
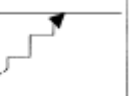
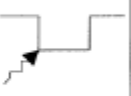
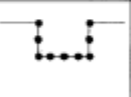
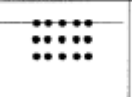
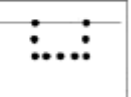
Method Analysis	Rigid Boundary	Flexible Boundary	Flexible Volume	Subtraction
Site Response Analysis (a)				
Scattering Analysis (b)			None	None
Impedance Analysis (c)				
Structural Response Analysis (d)	Standard	Standard +	Standard +	Standard +

Figure 3-4: Substructure methods of SSI analysis (Ostadan, 2006a)

3.2.2 Direct method

The substructuring method is advantageous in terms of computational requirements and the flexibility of using different analysis methods for different substructures, but it is limited to linear analysis. A more realistic simulation of the nonlinear response of the soil-structure system is possible through the direct approach, in which, the entire soil-structure system is analyzed in a single step, circumventing the use of superposition. Soil-structure interaction using the direct method can be performed in commercial finite element programs such as ABAQUS (Dassault Systèmes, 2005), ANSYS (ANSYS Inc., 2013) and LS-DYNA (LSTC, 2013), or the open source finite element program, OpenSees (Mazzoni *et al.*, 2009). Figure 3-5 presents an illustration of a finite element model for SSI analysis using the direct method. Soil-structure interaction analysis using the direct method requires significant computational resources in comparison with the substructuring method, and has therefore been rarely performed in practice. Consequently, nonlinear SSI analysis using the direct method is not yet well established, and some challenges still exist including, 1) specifying the ground motion input, 2)

simulating an infinite domain, and 3) developing reliable three-dimensional nonlinear constitutive models for soil.

The direct method is currently performed only for cases involving vertically propagating shear or compressive waves. Ground motion input for these cases is applied either as a force input (for viscoelastic bedrock) or an acceleration input (for rigid bedrock) to the nodes at the bottom of the soil profile, similar to the specification of input in a nonlinear site-response analysis (see Section 2.2.2.3). Inclined waves and other wave-fields cannot yet be specified as input in the direct method.

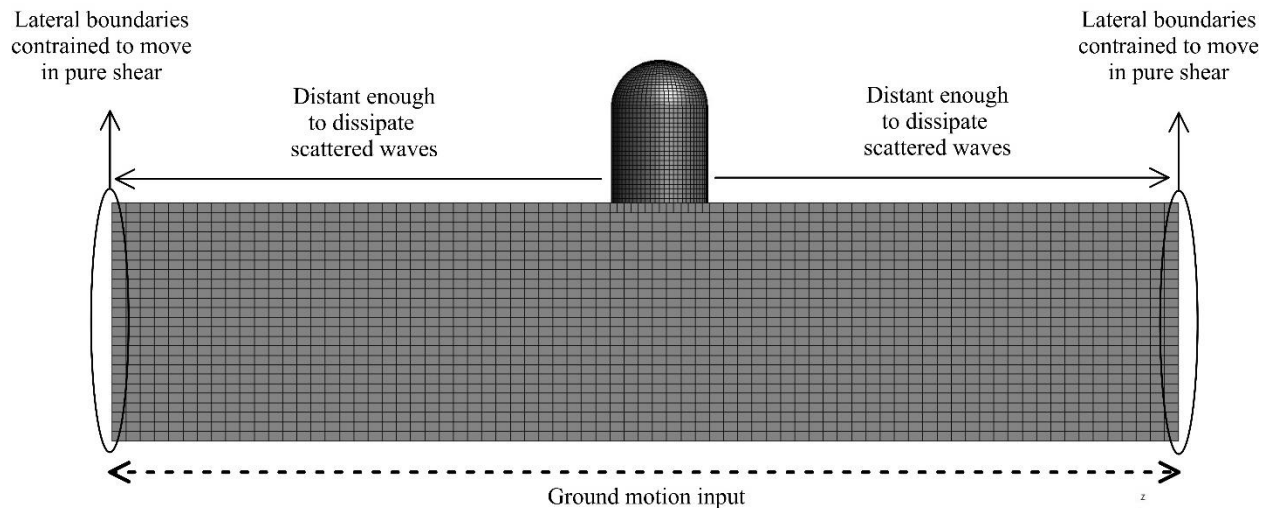


Figure 3-5: Finite element model for soil-structure interaction analysis using the direct method

Simulating an infinite domain is another major challenge in performing nonlinear SSI analysis using the direct method. An infinite soil domain can be simulated by building a finite domain that satisfies the following conditions: 1) effective damping of the waves radiating away from the structure so that they do not reflect back into the soil domain from the lateral boundaries, and 2) stress equilibrium at the lateral boundaries to account for the rest of the soil domain that is not included in the finite domain model. The former can be achieved by using absorbing boundary models at the lateral boundaries that absorb the incoming waves and minimize reflections. Absorbing boundary models have been developed and implemented in commercial finite element programs. Examples include the viscous boundary model by Lysmer and Kuhlemeyer (1969) and, a more recent, Perfectly Matched Layer (PML) model introduced to the SSI analysis domain by Basu (2009), both of which, have been implemented in LS-DYNA. However these boundary models are limited to waves propagating in linear elastic materials. No absorbing boundaries have yet been developed for nonlinear materials, to the knowledge of the author.

Another approach to simulate radiation damping is to build a very large soil domain with sufficient plan dimensions to dissipate the radiating waves before they reach the lateral boundaries. In this approach, the radiating waves are dissipated completely by soil hysteresis and viscous damping in the soil domain. Therefore a reasonable amount of viscous damping should be provided. The plan dimensions can be determined by a trial-and-error procedure, and ensuring that the acceleration responses at the boundaries of the soil domain are equal to the free-field acceleration, which is calculated from a separate site-response analysis. The stress equilibrium at the lateral boundaries can be obtained by constraining the elements at the boundaries to move in pure shear, thus simulating the free-field condition (assuming that the input comprises vertically propagating shear waves).

3.2.3 Domain reduction method

The domain reduction method (DRM), proposed by Bielak *et al.* (2003), is a two-step approach to input a complex three-dimensional wave field for the seismic analysis of a soil-structure system. This soil-structure system could be a geological feature, a structure with neighboring soil, or even a large landmass with numerous structures, such as an entire city. Although the DRM was primarily developed for application in large-scale models involving earthquake simulations from fault rupture to surface shaking at the site of interest (Taborda, 2010; Taborda and Bielak, 2011; Xu *et al.*, 2003; Yoshimura *et al.*, 2003), it is also useful for SSI analyses performed at a smaller scale. Large-scale earthquake simulations involve modeling a large soil domain including the seismic source (e.g., a ruptured region in a fault), and the local feature of interest, at which the response needs to be calculated. The DRM provides a way to model only the local feature with equivalent loads, which represent the loading from the seismic source, applied at its boundaries. This method effectively circumvents the modeling of a large soil domain, thus significantly reducing the computational requirements of the problem.

Consider a large-scale domain, with a local feature of interest, illustrated in Figure 3-6a. In this figure, Ω denotes the internal region of the domain, Ω^+ denotes the external region, Γ denotes the boundary between the internal and external region, u_e denotes the displacements of the nodes in the external region, u_b denotes the displacement of the nodes at the boundary, u_i denotes the displacements of the nodes in the internal region, and $P_e(t)$ denotes the external force history from a seismic source. Figure 3-6b illustrates an auxiliary model of the large-scale domain, in which, Ω^0 denotes the free-field internal region that is free of the local feature, u_e^0 , u_b^0 and u_i^0 denote the free-field displacements of the nodes in the external region, the boundary, and the internal region, respectively.

The DRM involves two steps: 1) analysis of the auxiliary model subjected to external loads, and 2) analysis of the internal region Ω with the local feature of interest, with effective forces representing

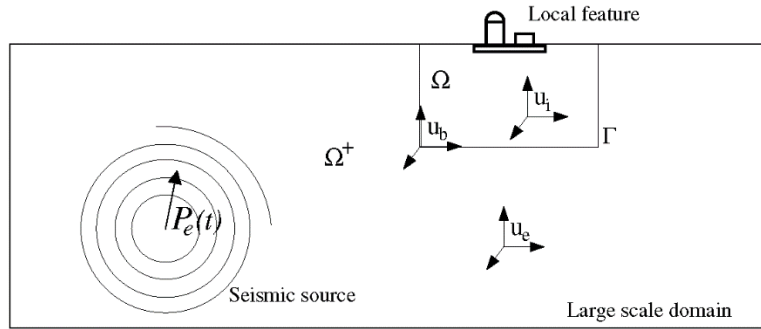
the seismic source. The effective forces are calculated from the free-field results calculated in the first step. These loads are given by the equation

$$\begin{bmatrix} P_i^{eff} \\ P_b^{eff} \\ P_e^{eff} \end{bmatrix} = \begin{bmatrix} 0 \\ -M_{be}^{\Omega+} \ddot{u}_e^0 - K_{be}^{\Omega+} u_e^0 \\ M_{eb}^{\Omega+} \ddot{u}_b^0 + K_{eb}^{\Omega+} u_b^0 \end{bmatrix} \quad (3-1)$$

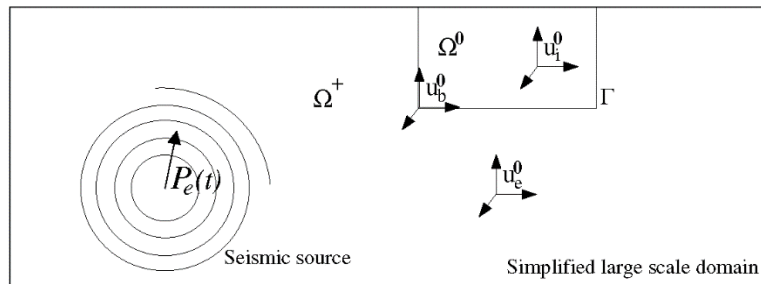
where $\begin{bmatrix} P_i^{eff} \\ P_b^{eff} \\ P_e^{eff} \end{bmatrix}$ is the effective force and M and K are the mass and stiffness matrices, respectively, of the regions described by the subscripts e, b and i, referring to the external domain, boundary and internal domain, respectively. The superscript 0 for the displacements and accelerations (e.g., u_e^0 and \ddot{u}_e^0) indicates free-field; these displacements and accelerations are provided by the auxiliary analysis. The derivation is presented in Bielak *et al.* (2003) and is not described here. The subscripts of the mass and stiffness matrices in equation (3-1) indicate that the effective forces have non-zero values only at the intersection of e and b nodes, namely, at the boundary Γ . Therefore, analysis of the internal domain can be performed by applying the effective forces only at the boundary, and the external soil domain need not be modeled completely. This analysis also results in scattered waves reflected from the structure and travelling back into the halfspace. An absorbing boundary is therefore required outside Γ , and can be modeled using one of the absorbing boundary models presented in the previous section.

It should be noted that although the DRM formulation requires that the external domain be linearly elastic, the internal domain can be fully nonlinear. Therefore, the auxiliary analysis that provides the free-field result, namely the site-response analysis, can only be performed in the linear domain. Nonlinear site response can be accounted for by using strain-compatible properties for the external soil domain (Bielak, 2013).

The DRM provides a computationally economical alternative to the direct method for nonlinear SSI analysis. However, unlike in the direct method, the primary nonlinearities in the DRM can only be accounted for using the equivalent linear approach. The DRM has been used in some studies for large-scale simulations (Taborda, 2010; Taborda and Bielak, 2011; Yoshimura *et al.*, 2003) but has rarely been used for SSI analyses. It has been implemented in the US NRC ESSI simulator (Jeremic *et al.*, 2011), which is currently being developed for high-performance, high-fidelity SSI analyses of nuclear structures. The DRM has not yet been implemented in commercial finite element programs. However, the effective seismic input method, which is a predecessor of the DRM and developed by Bielak and Christiano (1984), has been implemented in LS-DYNA, specifically for SSI analyses. The effective seismic input method and DRM are essentially equivalent in theory, but the DRM is easier to implement in a finite element formulation (Bielak, 2013).



a. A large-scale domain containing a local feature of interest



b. Auxiliary model of the large-scale domain

Figure 3-6: Illustration of the domain reduction method (Jeremic *et al.*, 2013)

3.3 Soil-structure interaction analysis using industry-standard numerical programs

3.3.1 SASSI

SASSI is currently the most widely used numerical program in the nuclear industry of the United States for seismic SSI analysis. Although developed by a single team, headed by Professor John Lysmer at the University of California at Berkeley, several modified versions of the program with varying capabilities now exist. The version SASSI2000 distributed by University of California, Berkeley and Ostadan (2010) is used to perform the analyses presented in this report.

SASSI uses the substructuring method in the frequency domain and is capable of performing two- and three-dimensional analyses for any foundation shape and any superstructure. Substructuring method allows the SSI problem to be solved in parts, with each part solved using a different method of analysis. The SASSI solution to the SSI problem is solved in three parts: 1) the site-response problem, which involves the calculation of the free-field input to the structure and is solved using analytical methods, 2) the impedance problem, which involves calculating the impedance functions at the foundation and solved using the axisymmetric finite element method, and 3) the structural analysis problem, which involves the calculation of the structural response from the impedance functions and the site-response input and solved using the regular finite element method. Two types of substructuring techniques are available in SASSI:

1) the flexible-volume method, and 2) the subtraction method. Although the subtraction method requires a smaller number of interaction nodes and is more computationally efficient, recent studies have shown that it may not result in accurate solutions in some cases (Mertz *et al.*, 2010). Therefore, the SSI analyses of the studies presented in this report are performed using the flexible-volume method. The following sections briefly describe the theory and implementation of the flexible-volume method, and the procedure for modeling and analysis in SASSI. These descriptions are largely adopted from the SASSI user manual (Ostadan, 2006b) and the theoretical manual (Ostadan, 2006a).

3.3.1.1 Theory and implementation

Substructuring for the flexible-volume method is performed as illustrated in Figure 3-7. The total system is shown in panel a of the figure, and is divided into three substructures shown in panels b, c, and d. These substructures are: 1) the free-field, labeled as substructure I and shown in panel b, 2) the excavated soil volume, labeled as substructure II and shown in panel c, and 3) the structure-foundation system, labeled as substructure III and shown in panel d. From Figure 3-7 it can be seen that the total system is a combination of the substructure I and substructure III, with substructure II excluded. If the total system, including the substructures, are discretized into nodes and elements as shown in the figure, the equation of motion for the system can be written as follows.

$$[M](\hat{U}) + [K](\hat{U}) = (\hat{Q}) \quad (3-2)$$

where,

$[M]$ = mass matrix of the total system

$[K]$ = complex stiffness matrix of the total system

(\hat{U}) = displacement vector of the total system

(\hat{Q}) = external load vector

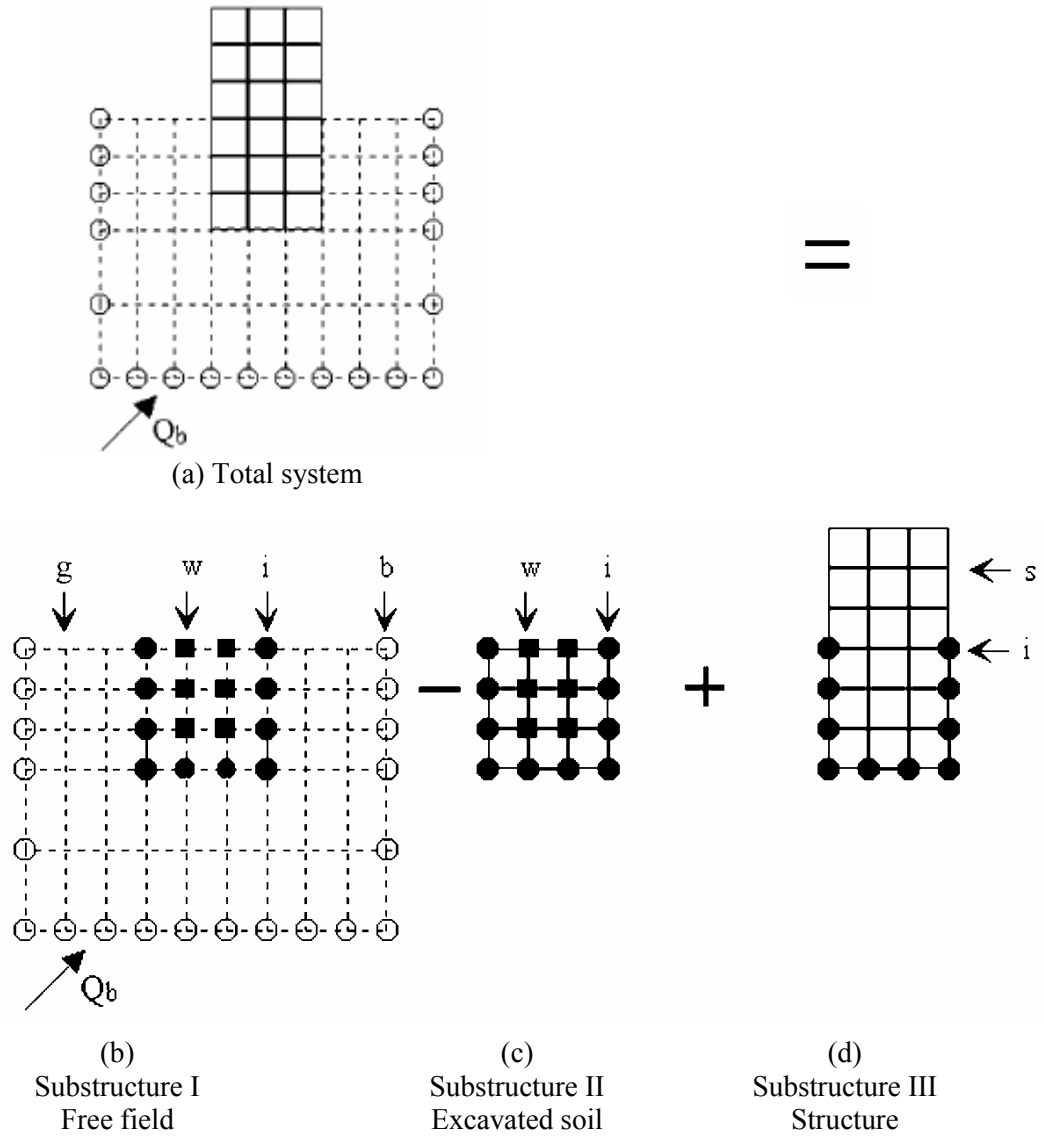


Figure 3-7: Substructuring in the flexible-volume method in SASSI (Ostadan, 2006a)

If the external load is a harmonic excitation $(\hat{Q}) = (Q)e^{i\omega t}$, where ω is the excitation frequency, the displacement response of the system would be $(\hat{U}) = (U)e^{i\omega t}$. Therefore, by substituting the expressions for the displacement response and external loads, the equation of motion can be written as

$$[C](U) = (Q) \quad (3-3)$$

where matrix $[C]$ is the complex, frequency-dependent, dynamic stiffness matrix given by

$$[C]=[K]-\omega^2[M] \quad (3-4)$$

The nodes in each substructure shown in the figure are referred to as follows:

- b - boundary of the total system
- i - boundary between the soil and the structure
- w - within the excavated volume
- g - remaining part of the free-field
- s - remaining part of the structure
- f - combination of 'i' and 'w' nodes (the interaction nodes)

Additionally each substructure has its own dynamic stiffness matrix $[C]$ and displacement vector (U) .

For example, the stiffness matrix $[C^{III}]$, and the displacement vector (U^{III}) for substructure III can be written as,

$$[C^{III}] = \begin{bmatrix} C_{ii}^{III} & C_{is}^{III} \\ C_{si}^{III} & C_{ss}^{III} \end{bmatrix} \text{ and } (U^{III}) = \begin{pmatrix} U_i \\ U_s \end{pmatrix} \quad (3-5)$$

The stiffness of the soil medium (substructure I) can be represented by a matrix of impedance functions at all the interaction nodes (f nodes). The flexible-volume method requires that the impedance functions be calculated at all the nodes in the excavated soil (unlike the subtraction method, which involves the calculation of impedance functions only at the nodes on the boundary of the excavated soil). Therefore, if the impedance functions are denoted by X , the impedance matrix for the foundation nodes can be written as

$$[X_{fr}] = \begin{bmatrix} X_{ii} & X_{iw} \\ X_{wi} & X_{ww} \end{bmatrix} \quad (3-6)$$

Following the substructuring in Figure 3-7, and using appropriate dynamic stiffness matrices and displacement vectors for each substructure, the equation of motion can be written as (Ostadan, 2006a)

$$\begin{bmatrix} C_{ii}^{III} - C_{ii}^{II} + X_{ii} & -C_{iw}^{II} + X_{iw} & C_{is}^{III} \\ -C_{wi}^{II} + X_{wi} & -C_{ww}^{II} + X_{ww} & 0 \\ C_{si}^{III} & 0 & C_{ss}^{III} \end{bmatrix} \begin{pmatrix} U_i \\ U_w \\ U_s \end{pmatrix} = \begin{pmatrix} X_{ii} U_i' + X_{iw} U_w' \\ X_{wi} U_i' + X_{ww} U_w' \\ 0 \end{pmatrix} \quad (3-7)$$

where U_i' and U_w' are the free-field displacements at i and w nodes imposed by the free-field ground motion and calculated from the site-response analysis. It can be seen that the right-hand side of equation (3-7) denotes the external forces on the total system (there are no external forces on the s nodes) and the

left-hand denotes the internal forces. After the dynamic stiffness matrices, impedance matrices, and the free-field ground motions are obtained, equation (3-7) can be used to calculate the responses of the structure-foundation system, U_s and U_i . These responses are calculated separately for each frequency in a set of frequencies input by the user. The responses for other frequencies calculated by interpolation, using an interpolation function that is similar to the frequency-domain response of a two-degree-of-freedom system. A more detailed description of this interpolation technique is provided in the SASSI theoretical manual (Ostadan, 2006a).

The following steps briefly describe the algorithm for SSI analysis in SASSI. These steps are used for both the flexible-volume method, and the subtraction method:

- Step 1 - Solving the site-response problem: SASSI performs site-response analysis to calculate the response of the soil profile. Displacements imposed at the interaction nodes by the free-field ground motion are calculated in this step.
- Step 2 - Solving the impedance problem: The impedance matrix $[X_{ff}]$, which includes the impedance functions at the interaction nodes, is calculated in this step. In the flexible-volume method, impedance is calculated at the i and w nodes, whereas in the subtraction method, it is calculated only at the i nodes.
- Step 3 - Forming the load vector: The load vector [right-hand side in equation (3-7)] is calculated by multiplying the impedance matrix calculated in Step 2 with the free-field displacement calculated in Step 1.
- Step 4 - Forming the complex stiffness matrix: Using material properties and nodal masses supplied by the user, the mass matrix $[M]$ and the complex stiffness matrix $[K]$ are calculated. The complex dynamic stiffness matrix is then calculated for each substructure using equation (3-4). The matrices are then assembled as shown in the left-hand side of equation (3-7) to calculate the dynamic stiffness matrix of the soil-structure system.
- Step 5 - Solving the equations of motion: After forming the load vector in Step 3 and the dynamic stiffness matrix in Step 4, they are substituted in the equation of motion (3-7) to calculate the response of the system.

3.3.1.2 Modeling and analysis procedure

Since the substructuring method can be used only with linear models, the soil and structure are assumed to have linear viscoelastic properties. Nonlinear response can be approximately calculated using equivalent linear, strain-compatible properties for the soil. These properties are typically calculated using

SHAKE, but can be calculated using other equivalent linear site-response analysis programs. The soil layers in SASSI are assumed to be horizontally infinite, and parallel to each other. Unlike the one-dimensional site-response analysis programs, SASSI is capable of simulating three-dimensional wave propagation, including surface waves. The input ground motion is defined as a wave-field composed of body and surface waves, and as either an outcrop or a within motion in any layer of the soil profile. The bedrock underlying the soil profile can be modeled either as rigid or a viscoelastic halfspace. The lateral transmitting boundaries are intrinsically modeled in the program, and do not have to be modeled by the user. The structure-foundation system in SASSI is modeled using two-dimensional or three-dimensional finite elements. The element library includes two-noded beam elements, eight-noded solid elements, four-noded thin shell elements, and two-noded spring elements, and lumped masses can be provided at the nodes as required. SASSI also requires modeling the excavated soil elements, which are a part of the substructuring equation (Ostadan, 2006a), when an embedded foundation is involved.

The SASSI program consists of 13 modules, of which, only five are relevant to the SSI analyses of this report. These modules are, SITE, POINT, HOUSE, ANALYS and MOTION. Each of the SASSI modules is an independent executable file, and the modules are run consecutively. The role of each module and some of its main input parameters are briefly described below in an order in which, the modules are run for an SSI analysis.

- SITE: This module performs the site-response analysis, the results of which, are used to calculate the free-field input at the interaction nodes. The input to the SITE module includes the soil profile model (thickness and material properties of each layer), location of the input ground motion, and the composition of the input wave field. The analyses of this report only involve vertically propagating shear waves, and therefore a vertically propagating SV wave field is specified in this module. The analysis frequencies, for which the SSI analysis is performed, are also input in the SITE module. The SASSI user manual (Ostadan, 2006b) recommends about 10 to 20 frequencies, chosen based on the fixed-base frequencies of the superstructure.
- POINT: This module performs a point load analysis for the soil halfspace, namely, the response of halfspace to the application of a unit point load. This analysis is performed in each co-ordinate direction for each of the frequencies input in the SITE module. The input to the POINT module includes the maximum number of soil layers into which, the foundation is embedded. The point load solution is calculated for all the layers into which the structure is embedded.

- HOUSE: This module calculates the mass matrix $[M]$, and stiffness matrix $[K]$ (and therefore the dynamic stiffness matrix $[C]$), of the structure and the excavated soil. The input to the HOUSE module is the finite element model of the structure-foundation system and of the excavated soil.
- ANALYS: This is the main module in SASSI, which assembles the impedance matrix of the interaction nodes, and the dynamic stiffness matrix of the total system, and calculates the final acceleration transfer functions of the response at the structural nodes relative to the input location.
- MOTION: This module reads the input acceleration (from a separate file named ‘SASSI. T14’) and uses the transfer functions output by the ANALYS module to calculate the output accelerations. The input to this module includes the nodes at which, the output accelerations are requested.

3.3.2 LS-DYNA

The commercial finite element program, LS-DYNA, is equipped with a large number of material models that can be used to model soil and structure, and several contact models that can be used to simulate the foundation-soil interface. LS-DYNA is therefore a suitable choice for comprehensive nonlinear SSI analyses, and is employed for the SSI analyses presented in this report. Soil-structure interaction analyses in LS-DYNA can be performed by 1) the direct method or 2) the effective seismic input method. The procedures for these methods are briefly described in the following sections.

3.3.2.1 Direct method

The direct method is described in Section 3.2.2. The procedures for performing an SSI analysis using the direct method in LS-DYNA are presented in this section.

The absorbing boundaries implemented in LS-DYNA do not facilitate the application of equilibrating stresses at the lateral boundaries. Therefore the direct method in LS-DYNA can be most efficiently performed by modeling a soil domain large enough to dissipate the scattered waves before they reach the lateral boundaries. The soil domain can be modeled using eight-noded brick elements. Although several soil material models are available, the analyses presented in this report use the MAT_HYSTERETIC material, which is also used for site-response analyses and described in Section 2.2.2.3.2. The nodes on the lateral boundaries at each elevation can be constrained using the *CONSTRAINED_NODE_SET option, which enables the nodes to move together in the horizontal and vertical directions. For a sufficiently large soil domain, this constraint imitates the free-field condition at the lateral boundary

by providing the necessary stresses for simulating an infinite soil domain. The input ground motion can be specified as described in Section 2.2.2.3.

Secondary nonlinearities such as gapping and sliding can be simulated in LS-DYNA. These nonlinearities involve separation at the soil-foundation interface, which can be simulated using *CONTACT_AUTOMATIC_SURFACE_TO_SURFACE. A soil-foundation interface that does not allow separation can be modeled using *CONTACT_TIED_SURFACE_TO_SURFACE for a flexible foundation, or *CONSTRAINED_EXTRA_NODES for a rigid foundation. Correct simulation of separation at the soil-foundation requires gravity loading on the structure. For the analyses (using the direct method) presented in this report, gravity loads are applied by performing a preliminary analysis using dynamic relaxation. A description of the dynamic relaxation method is provided in the LS-DYNA keyword user manual (LSTC, 2013).

LS-DYNA has the option of modeling viscous damping (for both soil and structural elements) that is independent of the frequency, unlike Rayleigh damping. This frequency-independent damping was developed by Arup, and can be provided using the *DAMPING_FREQUENCY_RANGE option. A small value of damping (< 2%) should be used as recommended in the LS-DYNA keyword user manual (LSTC, 2013).

3.3.2.2 The effective seismic input method

Soil-structure interaction analysis can be performed in LS-DYNA using the effective seismic input method through a series of steps described in the keyword user manual, as well as on the LSTC website: http://www.lstc.com/applications/soil_structure. A brief description of these steps, adapted to the SSI analyses presented in this report, follows:

1. For cases involving vertically propagating shear wave input, perform an auxiliary site-response analysis with the boundary Γ (see Figure 3-6) between the internal domain and external domain, modeled using the *INTERFACE_SSI_AUX_EMBEDDED option. Other approaches need to be adopted for cases involving inclined wave input, and are not discussed here. In case the free-field internal domain Ω^0 is not included in the site-response analysis model (namely, if the site-response analysis model contains an excavation), the *INTERFACE_SSI_AUX should be used (Basu, 2014). The site-response analysis results in a ground motion file named gmbin, which contains the free-field ground motion at the interface (u_b^0) that is to be used as input in a transient analysis. Note that the external domain in the site-response analysis should be linearly elastic and modeled using the MAT_ELASTIC material model.

2. Build the soil-structure model for transient analysis. This model includes the internal domain Ω (with the structure) surrounded by a few layers of elements corresponding to the external domain, which is again surrounded by a few layers of elements of the PML material acting as an absorbing boundary. Figure 3-8 illustrates the cross-section and isometric views of a sample LS-DYNA model for transient analysis in the effective seismic input method. The red elements in the figure correspond to the structure, the green elements correspond to the soil in the internal domain, the blue elements correspond to the external domain, and the gray elements correspond to the PML boundary. The boundary Γ between the internal and external domains should be modeled using *INTERFACE_SSI for the transient analysis. This interface model reads the free-field ground motions from the gmbin file, and applies equivalent forces calculated using equation (3-1) at the Γ boundary.

3. For cases that require gravity loading on the structure, a preliminary static analysis is needed. The model for static analysis is similar to that of the transient analysis, except that PML boundary is not included. The boundary Γ is modeled using the *INTERFACE_SSI_STATIC with the same interface ID that will be used in the transient analysis. This interface model records the gravity deformations on the boundary and applies them in the transient analysis. The static analysis with gravity loads can be performed using dynamic relaxation, described in the keyword user manual (LSTC, 2013).

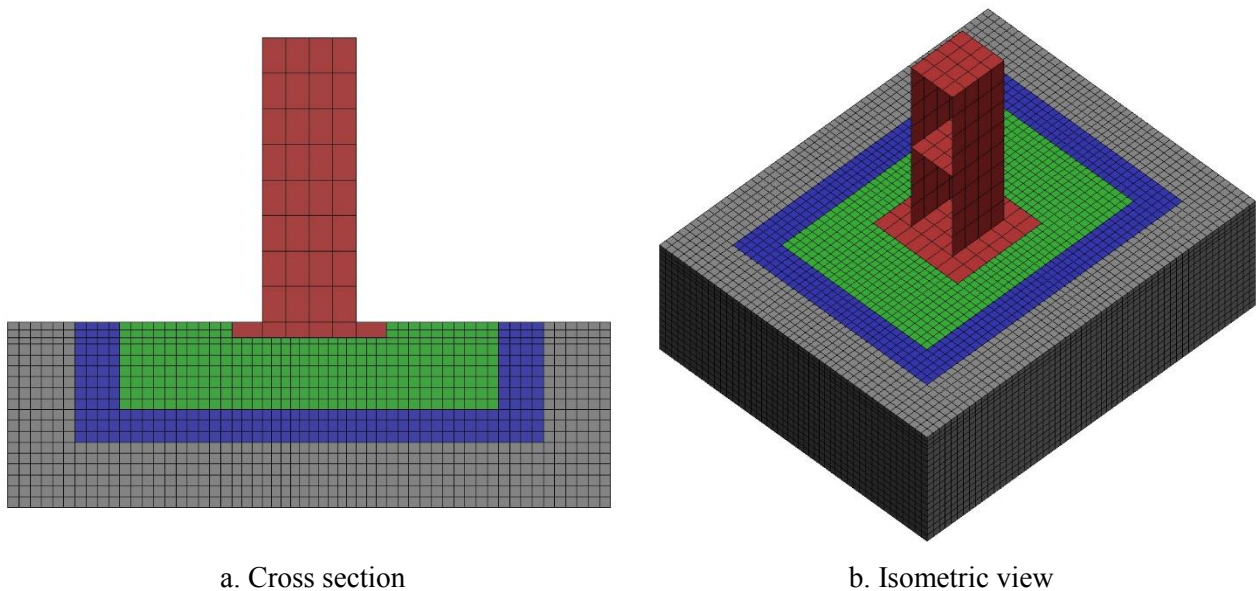


Figure 3-8: Sample model for SSI analysis using the effective seismic input in LS-DYNA

As mentioned in Section 3.2.3, the external domain (blue in Figure 3-8) can be modeled using a linear elastic material (*MAT_ELASTIC in LS-DYNA). The internal domain (green in Figure 3-8) can be modeled with any of the soil models available in LS-DYNA. The soil-foundation interface and damping can be modeled as in the direct method described in the previous section.

3.3.3 The US NRC ESSI Simulator

The US Nuclear Regulatory Commission Earthquake Soil-Structure Interaction Simulator (US NRC ESSI Simulator) is a collection of hardware, software, and related documentation, specifically developed for soil-structure interaction simulations of nuclear structures. It is under development by Jeremic *et al.* (2011) through funding from the US Nuclear Regulatory Commission and the Lawrence Berkeley National Laboratory. The primary motivation for the ESSI simulator is to perform high-performance soil-structure interaction simulations with high fidelity that reduces modeling uncertainties in the response³. The ESSI simulator program can perform time-domain nonlinear finite element analysis and is equipped with various element types, material models and contact algorithms. Soil-structure interaction analysis in the ESSI Simulator is performed using the domain reduction method described in Section 3.2.3. The theory and application procedures are described in the accompanying documentation (Jeremic *et al.*, 2013), which also includes the details of verification and validation of the program. The ESSI simulator computer uses a parallel processing framework for efficient computation, with the hardware being under constant development. Further details regarding the ESSI simulator can be found on the website: http://sokocalo.engr.ucdavis.edu/~jeremic/ESSI_Simulator/.

3.3.4 Assessment of numerical soil-structure interaction analysis methods

The state-of-the-art of SSI analysis in the nuclear industry of the United States involves performing SSI analysis using the linear, frequency-domain program, SASSI with equivalent linear, strain-compatible properties for the soil. Indeed, the linear frequency-domain programs should accurately predict responses for low-intensity ground motions involving almost linear response in the soil. However, for intense earthquake shaking involving large soil strains, nonlinear, time-domain methods using hysteretic soil models are theoretically more appropriate than the frequency-domain methods. However nonlinear time-domain methods of SSI analysis have been developed only recently, and are not yet well understood or established.

³ Modeling uncertainties are the uncertainties in response that are a consequence of numerical modeling. These can include uncertainties due to simplifying assumptions such as modeling a nonlinear system using equivalent linear properties and ignoring secondary nonlinearities such as gapping and sliding of the foundation.

Advancement of the usage of nonlinear time-domain programs requires detailed assessments that compare the predictions of time-domain and frequency-domain programs for a range of ground motions, soil profiles and structural characteristics. The first step of this assessment is to benchmark the time-domain programs against the frequency-domain programs for low-intensity ground motions, or with linear soil properties, and affirm that they result in similar predictions for cases involving linear soil and structural response. The predictions of these programs for cases involving nonlinear material models and larger strains are expected to differ. For these cases the assessment studies should examine the differences and provide guidelines to practicing engineers on the usage of these programs.

To the knowledge of the author, very few studies assessing numerical SSI programs have so far been performed, mainly due to the contemporariness of the time-domain, nonlinear methods. In one such study Xu *et al.* (2006) compared the predictions made using SASSI and LS-DYNA from the SSI analyses of deeply embedded nuclear structures. They found that the results calculated using SASSI and LS-DYNA differed considerably for both linear and nonlinear analyses. While the differences are expected for nonlinear analyses, they stipulated that the results from linear analyses performed in the two programs diverged due to the differences in the corresponding damping formulations. However similar studies performed by Anderson *et al.* (2013b) and Coronado *et al.* (2013) showed that the linear SSI analyses of deeply embedded nuclear structures using time-domain and frequency-domain programs resulted in very similar structural responses. In these studies, Anderson *et al.* (2013b) compared the results from SAP2000 (Computers and Structures Inc., 2011) to those from SASSI2010 (Ostadan and Deng, 2011), while Coronado *et al.* (2013) compared the results from the extended subtraction method in SASSI2010 to those calculated using the commercial finite element program ANSYS (ANSYS Inc., 2013).

3.4 Structure-soil-structure interaction

A direct consequence of soil-structure interaction is the interaction of adjacent structures through the soil around them, namely, structure-soil-structure interaction (SSSI). Although SSI has been studied extensively, very few studies of SSSI have been attempted. These studies are mostly limited to analytical calculations of highly simplified structures founded on idealized soil profiles. For example, the seminal study by Luco and Contesse (1973) examined anti-plane interaction between two infinitely long shear walls subjected to vertically incident SH waves of harmonic time-dependence. Wong and Trifunac (1975) extended this study to an array of several structures with varying size and stiffness subjected to a shear wave incident at an arbitrary angle. Both of these analytical studies investigated the significance of parameters such as separation distance, foundation size, and stiffness of the structures on SSSI. Luco and Contesse (1973) identified the factors that determine the degree of interaction between structures as a) relative foundation sizes, b) distance between the structures, c) mass of the superstructure relative to the

mass of the soil excavated for the foundation, d) mass of the foundation relative to the mass of excavated soil, and e) relative stiffness of the structures and the soil. Parametric analyses were performed and it was concluded that SSSI effects are especially important for smaller and lighter structures situated close to heavier structures. A similar conclusion was drawn by Wong and Trifunac (1975). Both studies noted that the degree of interaction depends mainly on the type of wave interference (constructive or destructive) occurring between the scattered waves from the foundations, which is a function of the spacing and arrangement of the foundations. Some studies [e.g., Matthees and Magiera (1982), Lin *et al.* (1987), Qian and Beskos (1996), Padron *et al.* (2009), Anderson *et al.* (2013a), Bolisetti and Whittaker (2011)] have investigated SSSI between adjacent structures (buildings and nuclear power plants) using more rigorous three-dimensional numerical methods, and most of these studies concluded that SSSI could considerably affect structural response. A more comprehensive list of SSSI studies can be found in Menglin *et al.* (2011).

A primary reason for the lack of studies of SSSI is the unavailability of case studies either from field data or laboratory experiments. The only case study, to the knowledge of the author, was performed by Çelebi (1993b), who analyzed data recorded from two well-instrumented neighboring buildings to examine SSSI. The layout of these buildings and the instrumentation is presented in Figure 3-9. Çelebi (1993b) employed spectral analysis techniques to find correlations between the responses of the buildings to the 1987 Whittier-Narrows earthquake. The study examined the roof response, basement response, and free-field response of the buildings, and concluded that 1) the dynamic response of the building affected the basement response and the free-field response, and 2) there was considerable SSSI between the structures at specific frequencies. The latter conclusion also corroborates the findings of the study by Murakami and Luco (1977) who performed an analytical investigation of the interaction between an array of idealized shear-wall-like structures, and found that the interaction between these structures was the most prominent at the, so called, Rayleigh frequencies, which are determined by the properties of the soil and sizes of the foundation (Murakami and Luco, 1977).

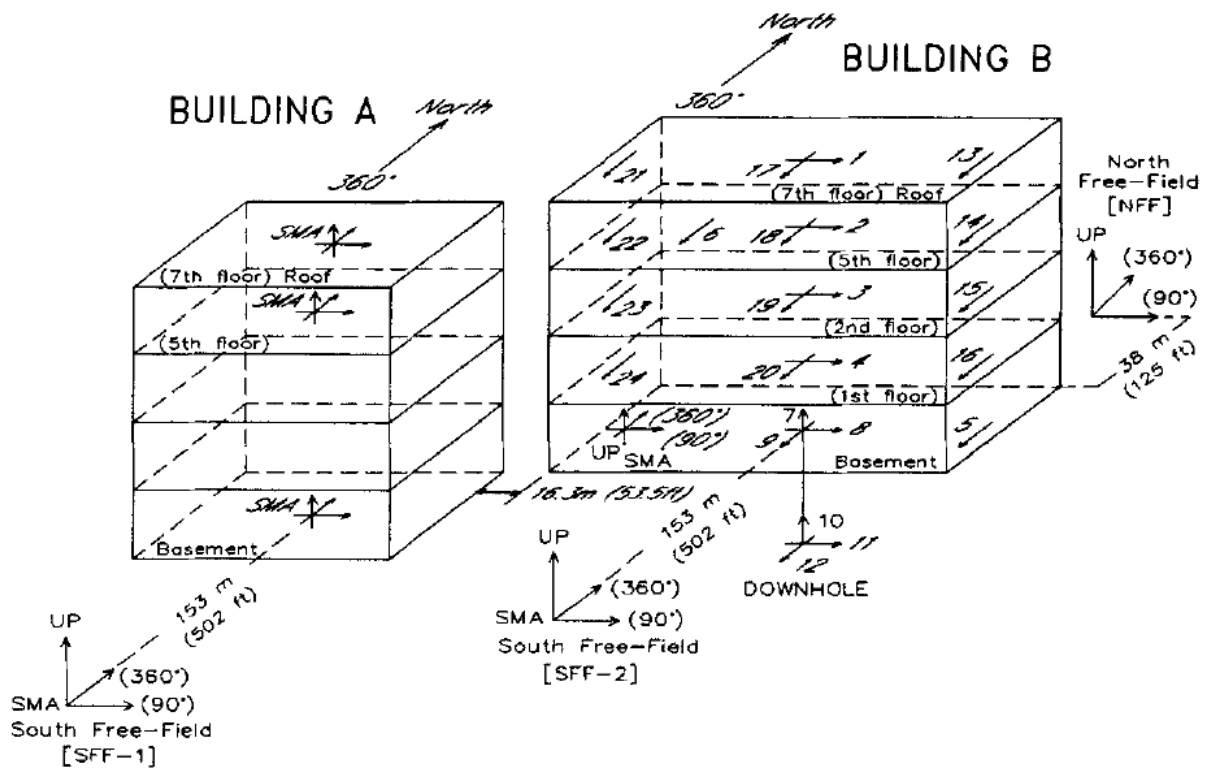


Figure 3-9: Layout of the buildings considered by Çelebi (1993a) and Çelebi (1993b) for examining SSSI

SECTION 4

AN ASSESSMENT OF SITE-RESPONSE ANALYSIS PROGRAMS

4.1 Introduction

This section presents an assessment of the state-of-the-art one-dimensional site-response analysis programs that are widely used in practice. These programs are: 1) SHAKE, which performs an equivalent-linear site-response analysis in the frequency domain, 2) DEEPSOIL, which performs a nonlinear site-response analysis in the time domain, and 3) LS-DYNA, which is a commercial finite element analysis program that is capable of time-domain nonlinear analysis. A description of one-dimensional site-response analysis using these programs is presented in Section 2. This section includes a comparison of site responses calculated using these programs while accounting for different site conditions and earthquake ground motions encountered in the United States. The results of these analyses and their comparisons are used to evaluate the efficiency of these programs and also identify the issues encountered while performing site-response analysis.

4.2 Soil profiles used for site-response analysis

Four hypothetical soil profiles are considered in this study and their properties are chosen to reflect the site conditions encountered in the United States. Figure 4-1 presents the soil profiles in which, sites W1, and W2 are representative of the Western United States (WUS), and sites E1, and E2 are representative of the Central and Eastern United States (CEUS).

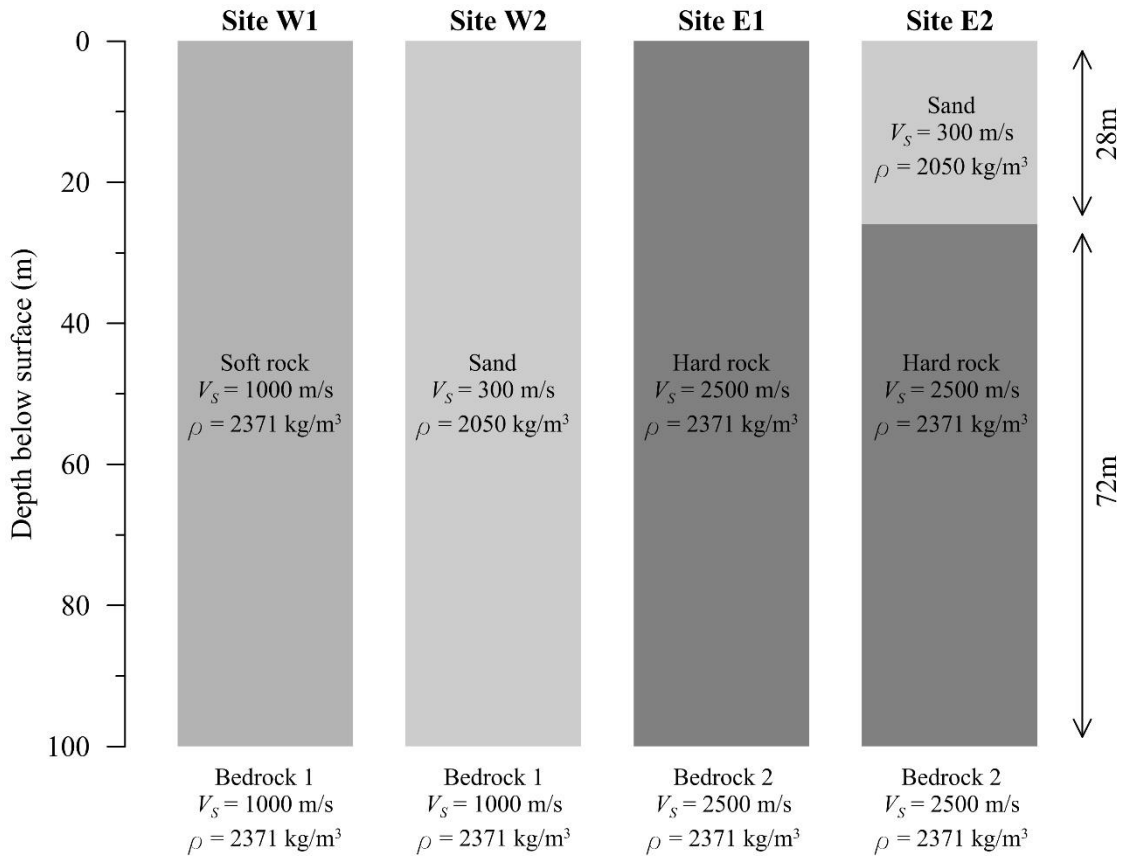


Figure 4-1: Soil profiles used for site-response analyses

Although more sites are required for a comprehensive representation, these four sites are deemed sufficient for a high-level assessment. Each site is 100 m deep and is underlain by linear viscous bedrock. Figure 4-1 also presents the linear material properties (small-strain shear modulus, v_s , and mass density, ρ) of the different soil layers and the bedrock, and the nonlinear properties (modulus reduction and damping curves) are presented in Section 4.4. Since the present study only involves comparisons between the solutions of different analysis programs and does not involve recorded data, the choice of idealized, hypothetical soil profiles (as opposed to real soil profiles) is reasonable.

4.3 Selection of input ground motions

Single component ground motions are used for input in one-dimensional site-response analyses. A total of nine ground motions are used: six motions for the WUS soil profiles (three ordinary motions and three near-fault pulse motions with forward directivity), and three motions for the CEUS soil profiles. Details of these ground motions are presented in Table 4-1. The ordinary WUS motions and the CEUS motions are chosen to cover a range of frequency contents and peak accelerations. The pulse motions for the WUS

soil profiles are chosen to cover a range of pulse periods. Figure 4-2 presents the acceleration time series and Figure 4-3 presents the acceleration response spectra and Fourier response spectra of the WUS ground motions. The amplitude of the pulse motion WP3 is significantly less than the other pulse motions, and is presented along with the ordinary ground motions in Figure 4-3. The acceleration time series, acceleration response spectra and the Fourier amplitude spectra of the CEUS motions are presented in Figure 4-4 and Figure 4-5. The WUS ordinary motions and the CEUS motions are picked from a database of ground motions assembled by Huang *et al.* (2009), which includes a set of ground motions for a WUS site (Diablo Canyon Nuclear Generating Station, California) and another set for a CEUS site (North Anna Power Station, Virginia). Two of the pulse motions (WP1 and WP2) are chosen from the suite of ground motions used in the CityBlock project, and one pulse motion (WP3) is chosen from the database of pulse motions created by Baker (2007). The input ground motions are applied at the base of the soil profile through a transmitting boundary (outcrop input⁴) for all analyses except for those involving site W2 subjected to pulse motion, which are performed using a reflecting boundary. The reason for choosing a reflecting boundary for these cases is described in Section 4.7.4.3.

⁴ The *outcrop* ground motion at a particular layer is the ground motion that would be recorded if there were no layers above. The actual ground motion recorded in a particular layer is termed a *within* ground motion. An *outcrop input* is the method of ground motion input that is used when the base of the soil profile is assumed to be a transmitting boundary (also referred to as flexible bedrock). A *within input* is the method of input that is used when the base is assumed to be a rigid boundary (also referred to as rigid bedrock). For specifying an outcrop input, the bedrock is modeled using a set of dampers that absorb the waves reflected from the surface, which in reality, radiate into the halfspace. The ground motion input is specified at the base of the soil profile as a shear force history that is proportional to the velocity history of the *outcrop ground motion* at this depth. For a within input the soil profile is assumed to have a fixed base and the *within ground motion* at this depth is directly applied as an acceleration (or velocity or displacement) history. Therefore an outcrop ground motion is used to specify an outcrop input, and a within ground motion is used to specify a within input. These procedures for providing the earthquake input to a soil profile are presented in more detail in Section 2.2.2.3.

Table 4-1: Input ground motions used for site-response analysis

CEUS ground motions					
Ground motion ID	Earthquake (Year)	Station	Component	Peak acc. (g)^a	
EO1	Mineral, VA (2011)	Charlottesville	090	0.101	
EO2	New Hampshire (1982)	Franklin Falls Dam	315	0.313	
EO3	Saguenay, Canada (1988)	Dickey	090	0.092	
WUS ordinary ground motions					
WO1	Northridge (1994)	Vasquez Rock Park	000	0.151	
WO2	Northridge (1994)	Wonderland Ave	185	0.172	
WO3	San Fernando (1971)	Lake Hughes	111	0.192	
WUS pulse motions					
Ground motion ID	Earthquake (Year)	Station	Component	Peak acc. (g)^a	T_p (sec)^b
WP1	Landers (1992)	Lucerne	260	0.727	5.1
WP2	Northridge (1994)	Rinaldi	228	0.825	1.5
WP3	Chi Chi (1999)	TCU128	128	0.187	9.0

^a Peak ground acceleration of the recorded ground motions

^b Pulse period as specified in the PEER NGA ground motion database (PEER, 2011) for WP1 and WP2, and as calculated by Baker (2007) for WP3

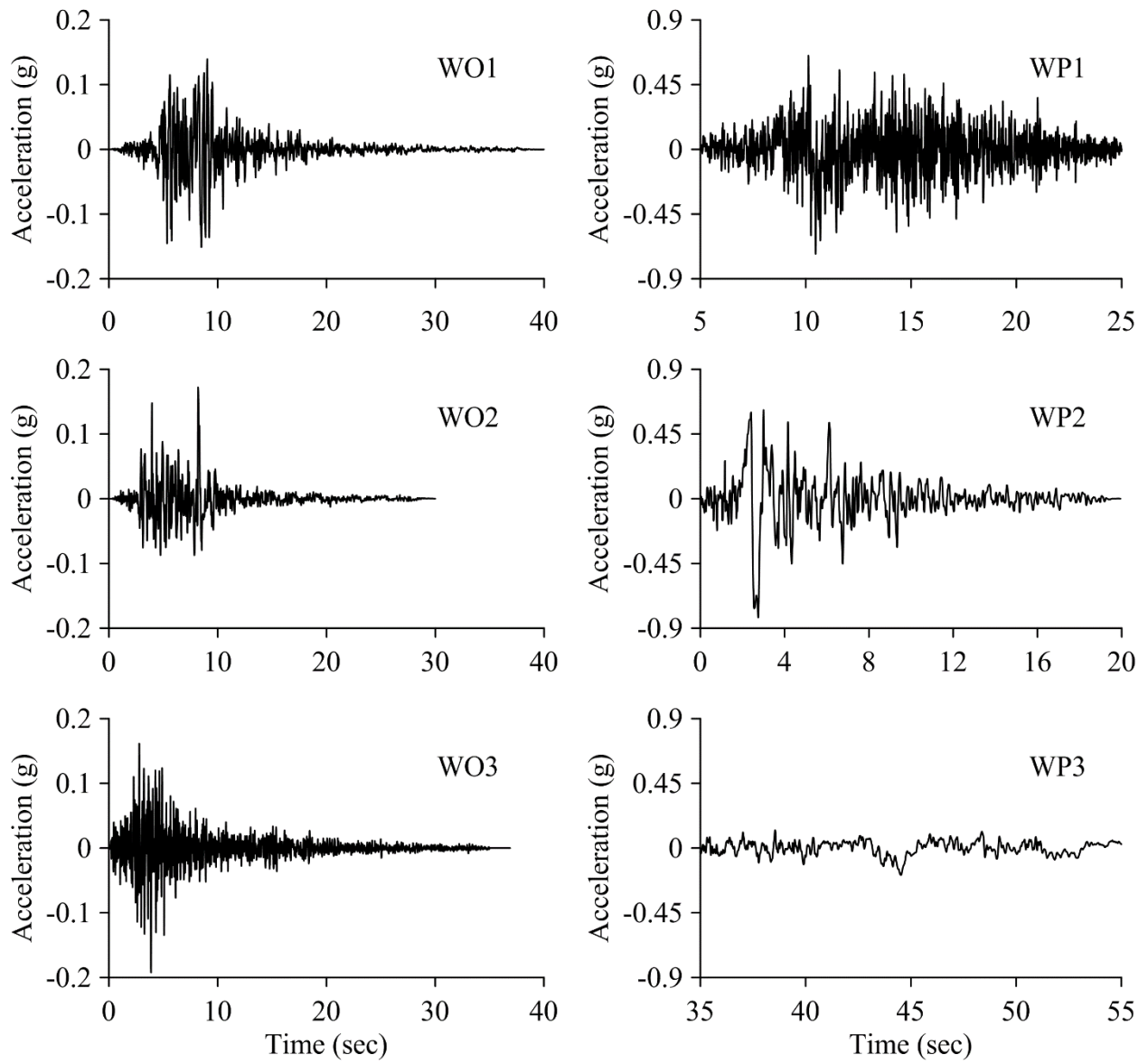
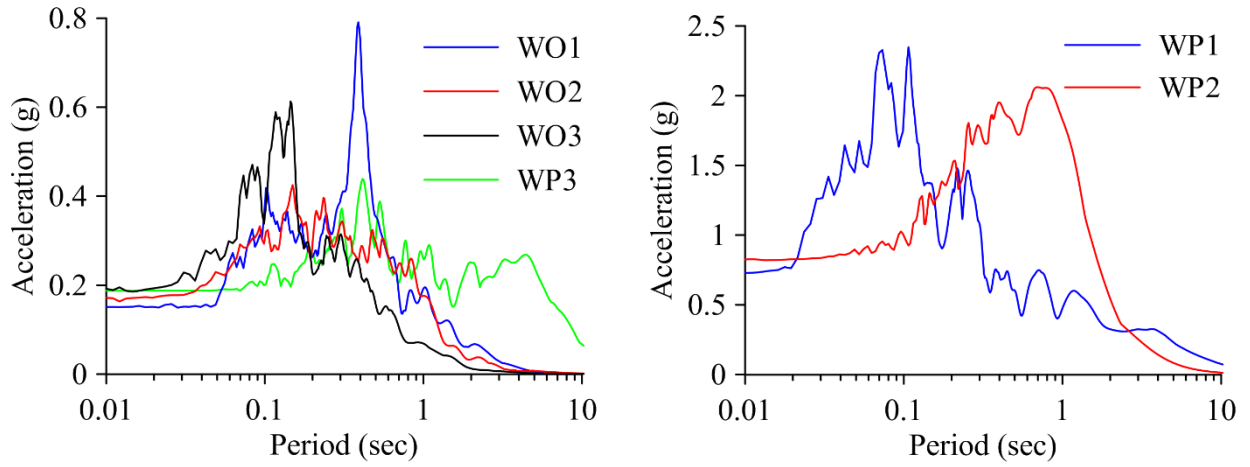
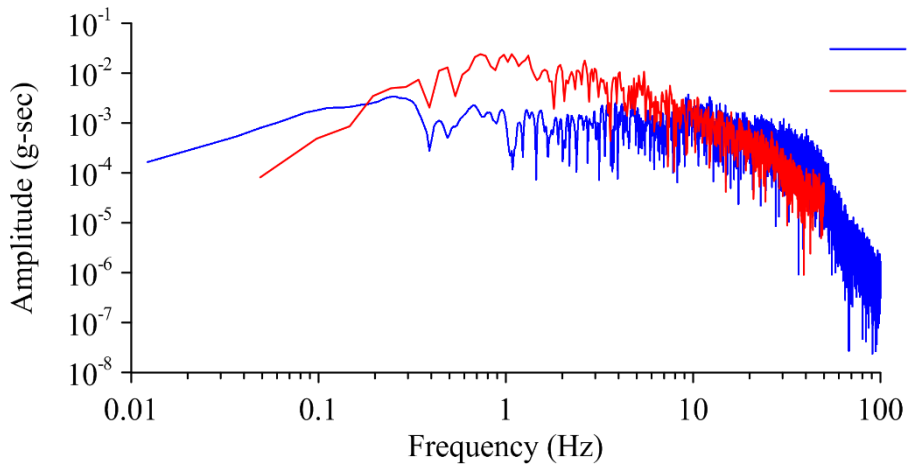
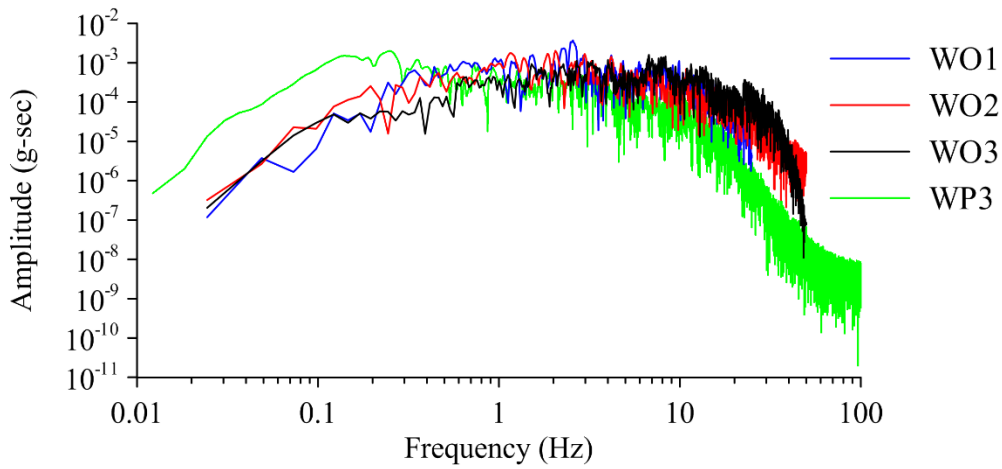


Figure 4-2: Acceleration time series of the input ground motions used for WUS soil profiles



a. Acceleration response spectra



b. Fourier transforms

Figure 4-3: Acceleration response spectra and Fourier amplitude spectra of the input ground motions used for WUS soil profiles

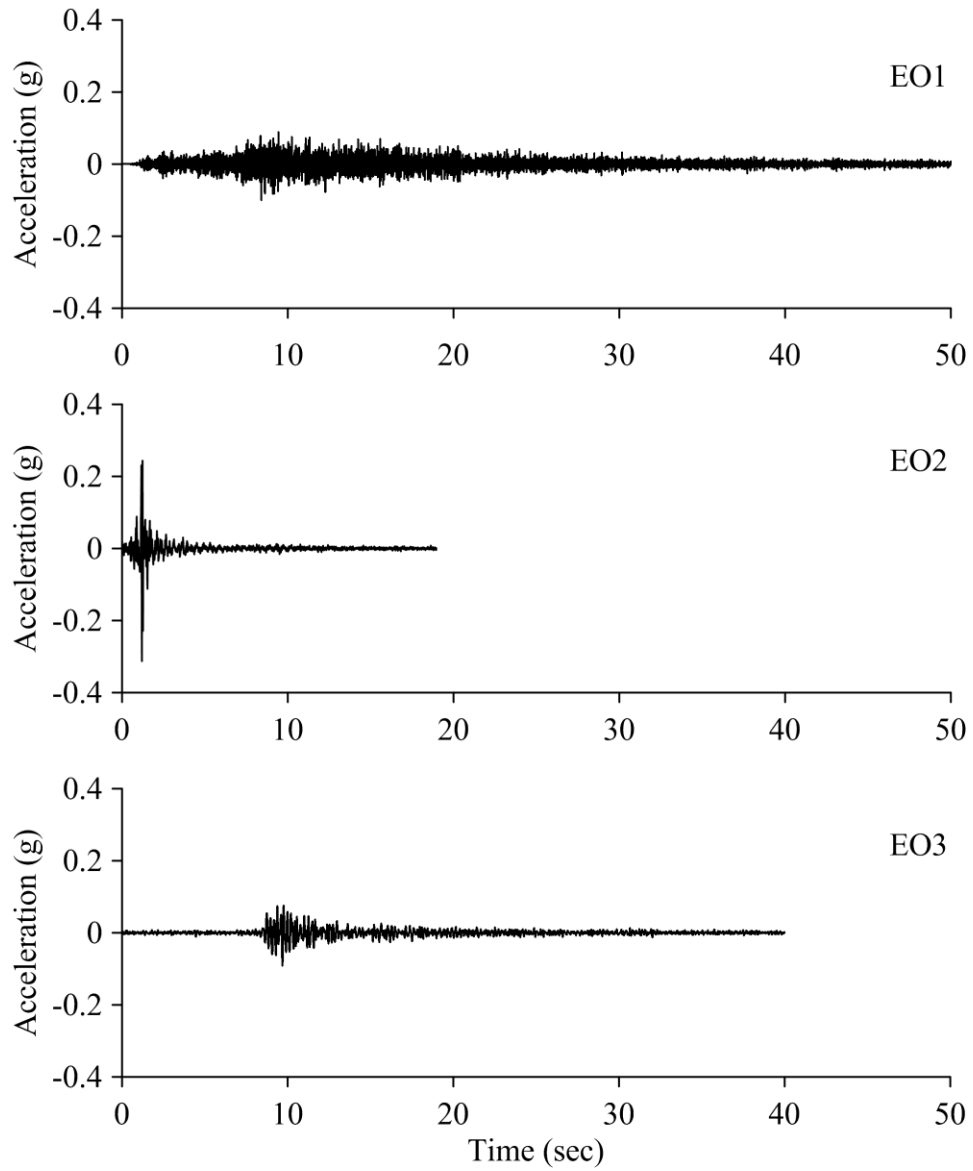
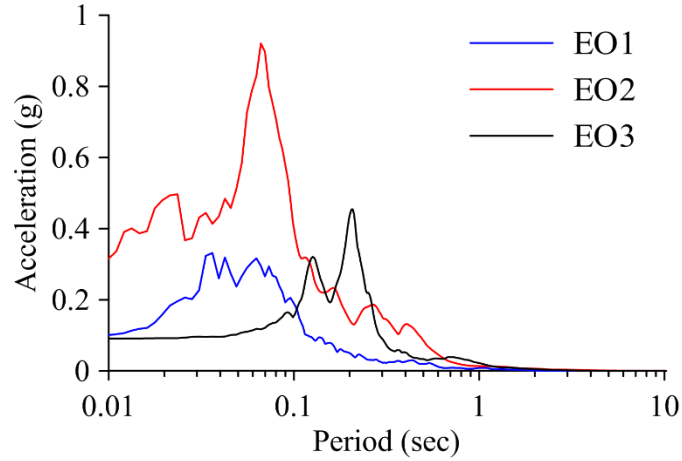
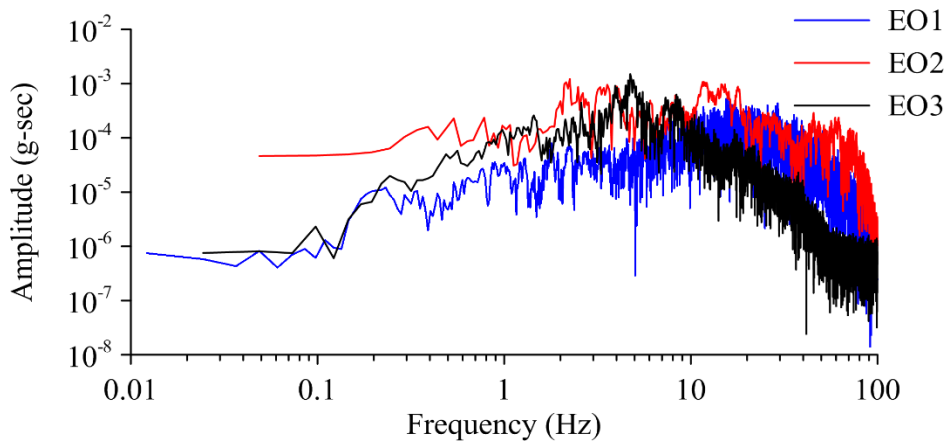


Figure 4-4: Acceleration time series of the input ground motions used for CEUS soil profiles



a. Acceleration response spectra



b. Fourier transforms

Figure 4-5: Acceleration response spectra and Fourier amplitude spectra of the input ground motions used for CEUS soil profiles

4.4 Numerical modeling

General procedures for one-dimensional site-response analysis in SHAKE, DEEPSOIL and LS-DYNA are described in Section 2 along with the corresponding soil material models. This section presents the numerical modeling of the soil profiles and the associated material properties. To enable a comparison of results from different programs, efforts are made to maintain the consistency between their numerical models and material properties. Although the material models employed in the programs are different, the corresponding model parameters are chosen such that the resultant dynamic soil properties (modulus reduction and damping curves) are similar.

4.4.1 Material modeling

Three types of materials are used for the soil: Sand ($V_s = 300$ m/sec), Soft rock ($V_s = 1000$ m/sec) and Hard rock ($V_s = 2500$ m/sec). Linear viscous properties are assumed for the bedrock of the CEUS and WUS sites along with shear wave velocities of 2500 m/s and 1000 m/s, respectively. The mass densities and small-strain shear-wave velocities of all the materials are shown in Figure 4-1 and are input “as is”. The dynamic soil properties are defined differently in each program based on the material model, but the parameters of these models are chosen such that the resultant properties are similar. The backbone curves and damping curves calculated from these parameters are presented in Figure 4-6 below. The backbone curves used for the different programs match very closely, but small differences exist between the damping curves.

The three numerical programs, SHAKE, DEEPSOIL and LS-DYNA employ different numerical models to simulate the stress-strain response of the soil. These numerical models are described in Sections 2.2.2.2.1, 2.2.2.3.1 and 2.2.2.3.2, respectively. SHAKE requires a direct input of the modulus reduction and damping curves as a set of discrete points. DEEPSOIL provides the choice of two nonlinear material models: the ‘MRDF Pressure-Dependent Hyperbolic Model’, and the ‘Pressure-Dependent Hyperbolic model’ (Hashash *et al.*, 2011). The Pressure-Dependent Hyperbolic Model is used for site-response analysis in this study and is referred to as the ‘hyperbolic model’ hereafter. Modeling in LS-DYNA is performed using the MAT_HYSTERETIC_SOIL model. The backbone curves presented in Figure 4-6 are taken from a collection of material property data provided by Arup. Identical modulus reduction curves are assumed for soft rock and hard rock, which is an acceptable assumption because neither rock type experiences significant strain softening compared to the soil layers. DEEPSOIL hyperbolic curves are fit into these data and the corresponding model parameters are calculated for each material as shown in Table 4-2. Discrete points are then taken from the DEEPSOIL curves and are used as input for SHAKE and LS-DYNA to maintain equivalence between the material properties used in different programs and enable a fair comparison of the corresponding responses. DEEPSOIL also calculates and provides the damping curves for each material, which are directly input in SHAKE. The LS-DYNA damping curves shown in Figure 4-6 are independently calculated by integrating the stress-strain loops for each strain amplitude. Preliminary analyses using the MAT_HYSTERETIC_SOIL model revealed an unrealistically large contribution of higher frequencies in the acceleration response, especially in cases involving large strains. To examine this issue an alternative approach was adopted that involved increasing the number of points in the backbone curve to 120. This was performed by modeling each layer by superimposing 12 solid elements (12 elements sharing the same eight nodes) as opposed to using a single element in the usual approach (see Section 2.2.2.3.2 for the description of site-response analysis using finite element

programs such as LS-DYNA). Each of these elements has 10 points in the backbone curve, and these curves are chosen such that their sum equals the DEEPSOIL backbone curve of the corresponding material. The superposition causes the elements to act in parallel, and the resultant stress value at a particular strain equals the sum of the stresses in each element. Thus each 12-element set acts as a single element with 120 points in the backbone curve. This approach is only adopted for the WUS sites since very small strains are expected in the CEUS sites for the chosen ground motions. The 120-point backbone curves for Sand and Soft rock are presented in Figure 4-6 along with the backbone curves and damping curves. In this figure LS-DYNA 10pt represents the 10-point backbone curve, while LS-DYNA 120pt represents the 120-point backbone curve. As seen in the figure, the curves from each program match closely, except for slight differences in the damping curves in LS-DYNA 10pt, which is due to the multi-linear shape of its stress-strain curve.

The analyses for WUS soil profiles are also performed with pressure-dependent properties for the soil, to model a more realistic variation of the shear strength with confining pressure. This variation is modeled in the MAT_HYSTERETIC_SOIL model in LS-DYNA by using the values 0, 0, 0 and 1 for the parameters b , a_0 , a_1 and a_2 , respectively, and a reference pressure equal to the confining pressure at a depth of 20m [refer to equations (2-11) and (2-12) or the LS-DYNA keyword manual (LSTC, 2013) for a description of these parameters]. The backbone curve at the reference pressure is taken as the curve shown in Figure 4-6. From equation (2-12), incorporating pressure dependence increases the shear strength of the layers below the reference point and decreases the shear strength of the layers above the reference depth. An equivalent pressure-dependence of the soil properties is achieved in DEEPSOIL by using a value of 1 for b , which results in a linear variation of γ_r [refer to equations (2-7) and (2-8) for the parameters b and γ_r] with confining pressure. These parameters used in the DEEPSOIL and LS-DYNA material models simulate a linear increase in strength with the confining pressure. The material curves calculated by DEEPSOIL using these parameters are also used in the SHAKE input.

DEEPSOIL also calculates the small-strain damping for each material from the stress-strain data. From the stress-strain data used in this study DEEPSOIL calculates a small-strain damping ratio of about 1.1%, which used along with the ‘frequency-independent’ damping option. This damping ratio is also incorporated into LS-DYNA using the *DAMPING_FREQUENCY_RANGE option, which provides frequency-independent damping in the specified frequency range (2 to 50 Hz for this study). A maximum strain increment of 0.005 for ordinary motions, and 0.001 for pulse motions, is used for the DEEPSOIL analyses. The widely adopted effective shear strain ratio of 0.65 is used for all SHAKE analyses.

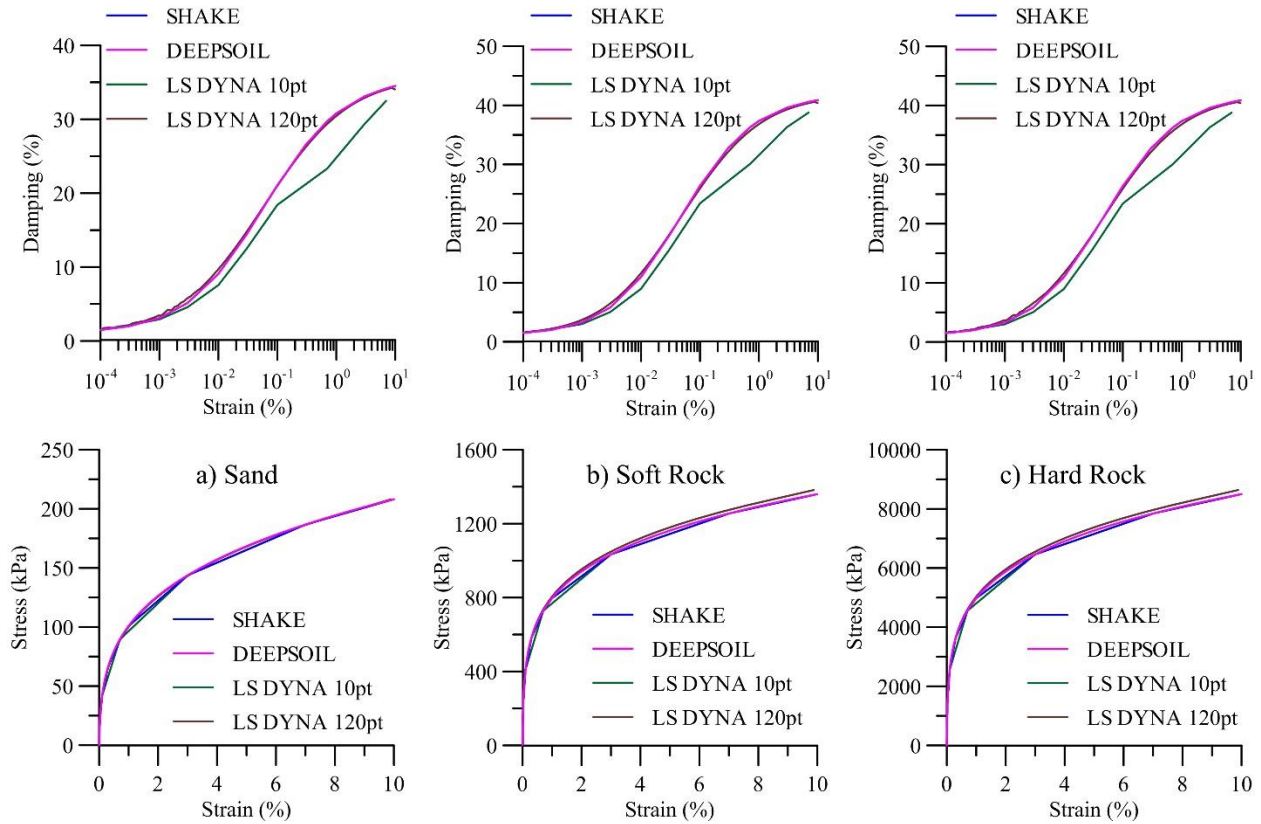


Figure 4-6: Backbone and damping curves of the materials used in site-response analysis

Table 4-2: Model parameters used to define the soil materials in DEEPSOIL

	Sand	Soft rock	Hard rock
Small-strain damping ratio ¹ , ξ (%)	1.09	1.13	1.13
Reference strain ² , γ_r (%)	0.0188	0.0218	0.0218
Stress-strain curve parameter, β	1.050	1.455	1.455
Stress-strain curve parameter, δ	0.705	0.780	0.780

¹Pressure dependence of damping is ignored by setting the parameter d to 0

²Pressure dependence of the stress-strain curve is ignored (included) by setting the parameter b to 0 (1)

4.4.2 Site layering

The thickness of the soil layers in a numerical model governs the shortest wavelength (which corresponds to the highest frequency) of the shear waves that can be captured through the simulations.

Softer materials require a smaller layer thickness compared to stiffer materials to capture the same maximum frequency. The maximum layer thickness is given by the equation:

$$t_{\max} \leq \frac{\lambda_{\min}}{n} = \frac{V_s}{n \cdot f_{\max}} \quad (4-1)$$

where t_{\max} is the maximum thickness of the soil layers, λ_{\min} is the minimum wavelength of the shear waves, V_s is the shear wave velocity, f_{\max} is the maximum frequency of the shear waves, and n is the desired number of layers per shortest wave length. The inequality in equation 3-1 governs the ‘resolution’ with which the shortest wavelength is captured during wave propagation in the soil layers. For example, when a value of 10 is used for n , the shortest wavelength is captured by at least 10 soil layers, namely 10 values of displacement. Therefore a larger value of n results in a higher resolution of the wave propagation in the soil profile as well as higher computational requirements. The second part of equation 3-1 is the standard equation that relates wavelength and frequency. Equation (4-1) gives an accurate maximum thickness for a linear analysis, where the shear modulus (and therefore the shear wave velocity) remains constant through time. Nonlinear analyses involve softening of the layers in time and therefore require a smaller maximum thickness (larger number of layers) to capture a certain maximum frequency throughout the analysis.

Site-response analysis for traditional structures is typically performed using a maximum frequency of 15 Hz, but a considerably higher frequency is generally needed for safety-related nuclear applications. Therefore the layer thicknesses for this study are chosen to accommodate a maximum frequency of at least 30 Hz (in a linear analysis), while maintaining a reasonable computing time. The SHAKE user manual (Schnabel *et al.*, 2009) recommends a value of five for n , but a value of 10 is chosen for this study, to account for the higher frequencies as well as for the softening in nonlinear analyses. The layer thicknesses calculated using this value and their corresponding maximum frequencies (captured in a fully linear analysis) are presented in Table 4-3 for each of the three materials.

Considering the thicknesses presented in the table above, site W1 is modeled using 50 layers of soft rock, site W2 is modeled using 100 layers of sand, site E1 is modeled using 25 layers of hard rock, and site E2 is modeled using 28 layers of sand and 18 layers of hard rock.

Table 4-3: Layer thicknesses and captured maximum frequencies in each material

Material	Shear wave velocity (m/s)	Layer thickness (m)	Maximum frequency (Hz) assuming $n=10$
Sand	300	1	30
Soft Rock	1000	2	50
Hard Rock	2500	4	62.5

4.5 Numerical analyses

4.5.1 Modal analyses

Prior to performing site-response analyses, modal analysis is performed for each soil profile model. LS-DYNA is used for this purpose and a viscous damping ratio of 1.1% is assumed for all models. The resonant time periods of a uniform soil profile (such as site E1, site W1 and site W2) can also be calculated analytically using the equation

$$T_n = \frac{4H}{(2n-1) \cdot V_s} \quad (4-2)$$

where, T_n is the natural frequency of the n^{th} mode, V_s is the shear-wave velocity of the soil material, and H is the height of the soil profile (Kramer, 1996). The numerically and analytically calculated time periods of the soil profiles are presented in Table 4-4 below, for the first two translational modes. The time periods calculated from the LS DYNA analyses match well with the analytical calculations for the uniform soil profiles, site E1, site W1 and site W2.

Table 4-4: Time periods of the soil profiles from modal analysis

Soil profile	Modal time periods calculated using LS-DYNA (sec)		Modal time periods from analytical calculations (sec)	
	1 st mode	2 nd mode	1 st mode	2 nd mode
Site E1	0.16	0.05	0.16	0.05
Site E2	0.39	0.14	-	-
Site W1	0.40	0.13	0.40	0.13
Site W2	1.32	0.44	1.33	0.44

4.5.2 Site-response analyses for sites E1 and E2

The analyses for sites E1 and E2 are performed using SHAKE, DEEPSOIL and LS-DYNA (using the MAT_HYSTERETIC_SOIL model with 10-point backbone curve) for each of the ground motions EO1, EO2 and EO3. Ground motions are input at the base of the soil profile with a transmitting boundary. An effective shear-strain ratio of 0.65 is used for the SHAKE analyses, and a maximum strain increment of 0.005 is used for the DEEPSOIL analyses.

4.5.3 Site-response analyses for site W1

Site-response analyses for site W1 are performed using four numerical methods: SHAKE, DEEPSOIL, LS-DYNA using the 10 point backbone curve (referred to as LS-DYNA 10pt) and LS-DYNA using the 120 point backbone curve (referred to as LS-DYNA 120pt). Analyses are performed for each of the ordinary ground motions WO1, WO2 and WO3, and the pulse motions WP1, WP2 and WP3. Both pressure-independent (PI) and pressure-dependent (PD) properties are considered. Ground motions are input at the base of the soil profile as an outcrop. An effective shear-strain ratio of 0.65 is used for the SHAKE analyses. For the DEEPSOIL analyses, a maximum strain increment of 0.005 is used for the ordinary ground motions and 0.001 for the pulse motions.

4.5.4 Site-response analyses for site W2

Site-response analyses for site W2 are performed using SHAKE, DEEPSOIL, LS-DYNA 10pt and LS-DYNA 120pt for each of the ordinary ground motions WO1, WO2 and WO3, and the pulse

motions WP1, WP2 and WP3. Both pressure-independent (PI) and pressure-dependent (PD) properties are considered. The ordinary ground motions are input at the base of siteW2 as an outcrop (force input) and the pulse motions are input directly as within motions (acceleration input). An effective shear strain ratio of 0.65 is used for the SHAKE analyses and a maximum strain increment of 0.001 is used for the DEEPSOIL analyses for all ground motions.

4.6 Observations

Figure A-1 to Figure A-78 present the results of site-response analyses of all the soil profiles. The results calculated from different numerical programs are presented together in each figure to enable a comparison. Observations gathered from these results are presented in this section. Further insights into some of these observations are presented in Section 4.7.

The results of each site-response analysis are presented in terms of 1) stress-strain loops, acceleration response spectra and acceleration response histories at three different depths in the soil profile (depths are indicated in each figure), 2) the peak acceleration and peak shear strain profiles and 3) acceleration amplification spectra at the surface. The acceleration amplification spectrum at the surface is calculated for each analysis as the ratio of the spectral acceleration at the surface to the spectral acceleration at the base of the soil profile. For sites E1, W1 and W2, the acceleration response spectra, acceleration response histories and the stress-strain loops are calculated at 1) the surface, 2) mid-depth, and 3) the base. For site E2, which is the site composed of 28m of sand lying atop of 72m of hard rock, the acceleration response spectra and response histories are calculated at 1) the surface, 2) sand-hard rock interface, and 3) at the base. The stress-strain loops for site E2 are calculated at 1) the lowest layer of sand, 2) the topmost layer of hard rock and 3) the base layer. While the accelerations in a particular layer are measured at the top of the layer, the stresses and strains are calculated at the midpoint. Therefore small differences exist between the depths at which the accelerations and the corresponding stress-strain loops are calculated. Additionally due to some constraints in calculating the acceleration output in DEEPSOIL, the base acceleration response spectra and response histories from all programs are calculated one layer above the bottom of the soil profile. Since the soil profiles have different layer thicknesses small differences exist between the depths at which the base accelerations are calculated (96m for sites E1 and E2, 98m for site W1 and 100m for siteW2). The figures presenting the acceleration response spectra also include the input ground motion at the base. The acceleration response spectra, acceleration amplification spectra, peak acceleration profiles and peak strain profiles for sites W1 and W2 also include the results calculated with pressure-dependent properties for the soil. For the corresponding figures, the pressure-independent results are indicated by PI and the pressure-dependent results are indicated by PD.

4.6.1 Site E1

Site E1 is a uniform site composed of hard rock and is the stiffest of the four sites. Figure A-1 to Figure A-13 present the site-response results of site E1 subjected to ground motions EO1, EO2 and EO3 (peak accelerations of 0.10g, 0.31g and 0.09g). Figure A-1 to Figure A-3 present the stress-strain loops for the three ground motions, and are followed by the peak acceleration and peak shear strain profiles (Figure A-4 to Figure A-6), acceleration response spectra (Figure A-7 to Figure A-9), acceleration response histories (Figure A-10 to Figure A-12), and the spectral amplifications (Figure A-13). Each of these figures includes the responses calculated using SHAKE, DEEPSOIL and LS-DYNA 10pt.

- a. *Hysteretic behavior and the extent of nonlinear response:* The stress-strain loops presented in Figure A-1, Figure A-2 and Figure A-3 indicate that the soil layers in site E1 remain almost linear for the three ground motions. The peak strain profiles (Figure A-4, Figure A-5 and Figure A-6) calculated from SHAKE, DEEPSOIL and LS-DYNA 10pt are quite similar for all the ground motions. The maximum peak shear strain is close to 0.0003% for ground motion EO1, 0.0012% for ground motion EO2, and 0.001% for EO3. At these strain levels the modulus reduction ratios in hard rock are approximately 0.95, 0.89 and 0.90, respectively, which indicate slight nonlinearity. The equivalent viscous damping ratios for these strain levels lie between 2% and 4% of critical for the three ground motions.
- b. *Acceleration response:* The acceleration response spectra (Figure A-7, Figure A-8 and Figure A-9) calculated using SHAKE, DEEPSOIL and LS-DYNA 10pt are very similar for the three ground motions. There are small differences at short periods (< 0.05 sec) that are more apparent in the amplification spectra in Figure A-13. However the acceleration response histories (Figure A-10 to Figure A-12) and the peak acceleration profiles (Figure A-4 to Figure A-6) are in good agreement for the three ground motions. Although differences between the responses of SHAKE and the time-domain programs are expected for nonlinear soils, the minor differences between DEEPSOIL and LS-DYNA 10pt at these strain levels can be attributed to the differences in the backbone curves and the viscous damping formulations of the two programs.
- c. *Site amplification:* Site E1 has the first two translational modes at 0.16 sec and 0.05 sec. The acceleration amplification spectra in Figure A-13 clearly show the peaks around the first modal period. The amplification spectra for ground motion EO1 show another peak between 0.05 and 0.06 sec, which corresponds to the second mode. The strongest ground motion, EO2, results in the smallest maximum amplification at the elongated site period (see Figure A-13), which is due to the greater energy dissipation provided by the nonlinear hysteretic behavior of the soil. Additionally the amplifications calculated from different programs match quite well, except for slight differences at periods less than 0.05 sec.

- d. *Variation of outcrop motion through depth*: The acceleration response spectrum computed at the surface of site E1 is very close to the acceleration response spectrum of the outcrop motion at the base for all the ground motions. This similarity of the outcrop motions at the surface and the base indicates that the outcrop motion in site E1 does not change significantly with depth. Therefore if site E1 was an outcropping rock, the rock outcrop motion at the surface of this site can be directly used as an outcrop input for a nearby soil site, without performing a deconvolution analysis. However the outcrop motion and the within motion at the base are quite different, indicating that the presence of the hard rock soil profile significantly affects the response at the base. This observation and its significance are discussed further in Section 4.7.5.

4.6.2 Site E2

Site E2 is non-uniform and is comprised of a 28m deep layer of sand atop of 72m of hard rock. Figure A-14 to Figure A-26 present the site-response results of site E2 subjected to ground motions EO1, EO2 and EO3 (peak accelerations of 0.10g, 0.31g and 0.09g). Figure A-14 to Figure A-16 present the stress-strain loops for the three ground motions, and are followed by the peak acceleration and peak shear strain profiles (Figure A-17 to Figure A-19), acceleration response spectra (Figure A-20 to Figure A-22), acceleration response histories (Figure A-23 to Figure A-25), and the spectral amplifications (Figure A-26). Each of these figures includes the responses calculated using SHAKE, DEEPSOIL and LS-DYNA 10pt.

- a. *Hysteretic behavior and the extent of nonlinear response*: The peak strain profiles presented in Figure A-17 to Figure A-19 show that the highest peak strains induced by the three ground motions in site E2 are about 0.007% for EO1 and 0.025% for EO2. For ground motion EO3, the highest peak strains calculated by the three programs vary between 0.01% and 0.018%. Given that the largest strains always occur in the sand layers, these strain levels correspond to modulus reduction ratios of about 0.65 and 0.44 for EO1 and EO2, respectively, and lie between 0.5 and 0.6 for EO3. The corresponding equivalent viscous damping ratios are about 8%, 13% and 10%, respectively for the three ground motions. At these strain levels, the stress-strain loops presented in Figure A-14 to Figure A-16 indicate that the hard rock layers remain almost linear, while the sand layers show considerable nonlinear behavior. The peak strain profiles calculated using SHAKE, DEEPSOIL and LS-DYNA 10pt are similar for EO1 and EO2, but differ significantly in the sand layers for EO3. SHAKE results in the lowest values for peak strains, followed by LS-DYNA 10pt and DEEPSOIL.
- b. *Acceleration response*: Examination of the acceleration response spectra in Figure A-20, Figure A-21 and Figure A-22 indicates that the responses calculated by SHAKE, DEEPSOIL and LS-

DYNA 10pt match well for periods above 0.1 sec. The differences at shorter periods are considerable, and are greater than those seen in site E1 for the same ground motions. Additionally these differences are significantly greater in the surface response than in the response at 28m depth and at the base, which are in the hard rock layers, indicating that the differences in the acceleration responses increase with strain. SHAKE underestimates the short-period accelerations on the surface as compared to DEEPSOIL and LS-DYNA. Additionally the SHAKE response spectra in these periods tend to ‘flatten out’ indicating the absence of the corresponding frequencies in the acceleration response. This is also evident from the SHAKE acceleration response history, which is smooth compared to that of DEEPSOIL and LS-DYNA (Figure A-23 to Figure A-25) indicating a smaller contribution of higher frequencies in the response. Additional discussion on the high-frequency response issue in SHAKE is presented in bullet 2 of Section 4.7.2. The peak acceleration profiles (Figure A-17 to Figure A-19) calculated from the three programs match reasonably well for all ground motions in the hard rock layers, but are significantly different in the sand layers for ground motion EO3. SHAKE underestimates the peak accelerations in the sand layers for this ground motion, which is a consequence of underestimating the short period accelerations. The differences between the peak accelerations calculated by DEEPSOIL and LS-DYNA 10pt are also considerable, which is a result of the differences in the hysteretic models employed in the two programs.

- c. *Site amplification:* Site E2 has the first two translational modes at 0.39 sec and 0.14 sec. The amplification spectra in Figure A-26 show peaks corresponding to the elongated site period, which lies between 0.4 and 0.5 sec for ground motions EO1 and EO3, and between 0.5 and 0.6 sec for EO2. However the peaks corresponding to the second mode are seen only for ground motions EO1 and EO2. The elongated second mode period is slightly less than 0.15 sec for EO1 and lies between 0.15 and 0.2 sec for EO2. As observed for site E1, the spectral amplification at the site period of E2 is the smallest for the strongest ground motion, EO2. Additionally SHAKE overestimates this amplification compared to the time-domain programs, which suggests that the equivalent viscous damping is underestimated. This is consistent with the observation that SHAKE underestimates the peak strains in the soil layers, which results in the underestimation of the equivalent viscous damping.
- d. *Variation of outcrop motion through depth:* In contrast with site E1, the outcrop motion at the surface of site E2 is different from the outcrop at the base, with the largest differences seen in ground motion EO2 (Figure A-21). However the acceleration response at 28m depth, which corresponds to the sand-hard rock interface, approaches the base outcrop ground motion. This suggests that the presence of the sand layer above the relatively stiff hard rock does not affect the

ground motion at the interface significantly and therefore the outcrop and within motions are similar at this depth. This observation and its significance are discussed further in Section 4.7.5.

4.6.3 Site W1

4.6.3.1 Response to ordinary ground motions

Site W1 is uniform site composed of soft rock. Figure A-27 to Figure A-39 present the site-response results of site W1 subjected to ground motions WO1, WO2 and WO3 (peak accelerations of 0.15g, 0.17g and 0.19g). Figure A-27 to Figure A-29 present the stress-strain loops for the three ground motions, and are followed by the peak acceleration and peak shear strain profiles (Figure A-30 to Figure A-32), acceleration response spectra (Figure A-33 to Figure A-35), acceleration response histories (Figure A-36 to Figure A-38), and the spectral amplifications (Figure A-39). Each of these figures includes the responses calculated using SHAKE, DEEPSOIL, LS-DYNA 10pt and LS-DYNA 120pt. Only the results of the analyses performed using pressure-independent (PI) properties are discussed in this section. Results of the analyses performed using pressure-dependent (PD) properties are discussed in Section 4.6.3.3.

- a. *Hysteretic behavior and the extent of nonlinear response:* The peak strain profiles in Figure A-30, Figure A-31 and Figure A-32 show that the largest strains calculated by different numerical programs vary between 0.018% and 0.024% for WO1, 0.018% and 0.026% for WO2, and 0.006% and 0.008% for WO3. These strain ranges correspond to modulus reduction ratios that lie between 0.38 and 0.44 for WO1, 0.37 and 0.44 for WO2, and 0.60 and 0.65 for WO3. The equivalent viscous damping ratios corresponding to these ranges are approximately 15%, 15% and 9% for WO1, WO2 and WO3, respectively. At these strain levels the stress-strain loops in Figure A-27, Figure A-28 and Figure A-29 indicate that the lower layers of the soil profile show considerable nonlinear behavior for the three ground motions. The stress-strain loops of LS-DYNA 10pt and LS-DYNA 120pt match closely for all the ground motions indicating that increasing the number of points in the backbone curve results in negligible changes in the hysteretic response. The peak strain profiles show that SHAKE underestimates the peak strains compared to the time-domain programs. Although the peak strains from LS-DYNA 10pt and LS-DYNA 120pt match closely for all the ground motions, DEEPSOIL comparatively underestimates the peak strains for ground motions WO2 and WO3. This can be attributed to the differences in the hysteretic models employed in DEEPSOIL and LS-DYNA.
- b. *Acceleration response:* The acceleration response spectra in Figure A-33, Figure A-34 and Figure A-35 show differences in the responses calculated from SHAKE, DEEPSOIL, LS-DYNA 10pt and LS-DYNA 120pt. These differences are greater in the short period range, especially for

periods less than 0.1 sec. The acceleration response spectrum calculated using SHAKE has near constant amplitude at short periods, indicating the absence of the corresponding frequencies in the response. This observation is consistent with the acceleration response histories presented in Figure A-36, Figure A-37 and Figure A-38, which show that the responses calculated from SHAKE are smoother compared to those calculated from the time-domain programs (see bullet 2 in Section 4.7.2 for additional discussion on this issue). The acceleration response spectra calculated from the time-domain programs are similar except for periods less than 0.1 sec. The response spectra calculated from LS-DYNA 120pt show smaller short-period accelerations compared to LS-DYNA 10pt and DEEPSOIL, especially for ground motions WO1 and WO2. Considerable differences exist between the peak accelerations computed by the different programs, and these differences vary along the depth of the soil profile. A notable trend is that LS-DYNA 120pt calculates smaller peak accelerations than LS-DYNA 10pt and DEEPSOIL in most layers, especially for ground motions WO1 and WO2, which is consistent with the underestimation of the short period accelerations by LS-DYNA 120pt for these ground motions.

- c. *Site amplification:* Site W1 has the first two translational modes at 0.40 sec and 0.13 sec. From the amplification spectra presented in Figure A-39, the elongated site period lies between 0.4 and 0.6 sec for ground motions WO1 and WO2, and between 0.4 and 0.5 sec for ground motion WO3. The amplification spectra for ground motion WO3 also show a peak corresponding to the second mode at about 0.15 sec. The amplifications calculated from the different programs are fairly close at the site periods, but considerable differences arise for periods less than 0.1 sec. LS-DYNA 10pt significantly overestimates the amplifications at periods greater than 5 sec compared to the other programs, which is reduced in LS-DYNA 120pt.
- d. *Variation of outcrop motion through depth:* Despite being a uniform soil profile, the acceleration response spectrum computed at the surface of site W1 is considerably different from the acceleration response spectrum of the outcrop motion at the base, unlike site E1. This indicates that when larger strains are induced in the soil profile, the rock outcrop motion changes considerably through the depth. Therefore if site W1 was an outcropping rock, the outcrop motion calculated at the surface of this site cannot be directly used as an outcrop input at the base of a nearby soil site. Instead, a deconvolution analysis would be required to calculate the outcrop ground motion at depth. Detailed explanation of this observation is presented in Section 4.7.5.

4.6.3.2 Response to pulse-like ground motions

Figure A-40 to Figure A-52 present the site-response results of site W1 subjected to ground motions WP1, WP2 and WP3. These ground motions have peak accelerations of 0.73g, 0.83g and 0.19g,

and pulse periods of 5.1 sec, 1.5 sec, and 9.0 sec respectively (see Table 4-1). Figure A-40 to Figure A-42 present the stress-strain loops for the three ground motions, and are followed by the peak acceleration and peak shear strain profiles (Figure A-43 to Figure A-45), acceleration response spectra (Figure A-46 to Figure A-48), acceleration response histories (Figure A-49 to Figure A-51), and the spectral amplifications (Figure A-52). Each of these figures includes the responses calculated using SHAKE, DEEPSOIL, LS-DYNA 10pt and LS-DYNA 120pt. Only the results of the analyses performed using pressure-independent (PI) properties are discussed in this section. Results of the analyses performed using pressure-dependent (PD) properties are discussed in Section 4.6.3.3.

- a. *Hysteretic behavior and the extent of nonlinear response:* The peak strain profiles in Figure A-43, Figure A-44 and Figure A-45 show that the largest strains calculated by the numerical programs vary between 0.12% and 0.45% for WP1, 0.6% and 1.5% for WP2, and 0.05% and 0.09% for WP3, which are an order of magnitude greater than the strains calculated for the ordinary ground motions. These strain levels in soft rock correspond to modulus reduction ratios that lie between 0.06 and 0.15 for WP1, 0.03 and 0.05 for WP2, and 0.18 and 0.27 for WP3, which indicates significant softening in the soil layers. The equivalent viscous damping ratios corresponding to these ranges are between 22% and 28% for WP1, 30% and 35% for WP2, and 15% and 20% for WP3. The stress-strain loops in Figure A-40, Figure A-41 and Figure A-42 also indicate significant nonlinear behavior in the soil profile. The peak strain profiles show significant differences between the peak strains calculated by SHAKE and the time-domain programs for the three pulse motions. SHAKE underestimates the peak strains in the soil profile as compared to the time-domain programs and the underestimation is much greater than that observed for the ordinary motions. Of the time-domain programs, DEEPSOIL calculates the smallest peak strains; the LS-DYNA 10pt and LS-DYNA 120pt results are similar. Additionally, Figure A-43 and Figure A-44, which present the peak strain profiles for WP1 and WP2 respectively, show that DEEPSOIL predicts large changes in the peak strains between consecutive layers, unlike LS-DYNA 10pt and LS-DYNA 120pt, which predict a smoother strain profile. This DEEPSOIL result is considered unrealistic and is examined more closely in Section 4.7.4.2.
- b. *Acceleration response:* A comparison of the acceleration response spectra (Figure A-46 to Figure A-48) calculated by the different programs shows larger differences for the pulse motions than the ordinary ground motions, especially in the short period range. The acceleration response spectra calculated by SHAKE are significantly different from those calculated by the time-domain programs, especially for ground motion WP2. As seen for the ordinary ground motions, the SHAKE acceleration spectra show near constant amplitude at periods less than 0.1 sec, indicating the absence of the corresponding frequencies in the response (see bullet 2 in Section

4.7.2 for additional discussion on this issue). However the SHAKE response at longer periods achieves a better match with the time-domain programs, except for WP2, where the response is significantly overestimated. The responses calculated from the time-domain programs have greater differences than those observed for the ordinary ground motions. The LS-DYNA 10pt response to WP2 ground motion, which results in the largest strains, shows very high amplification in the acceleration response for periods less than 0.3 sec, compared to the other time-domain programs. This is also evident from the acceleration response history in Figure A-50, which shows unrealistic spikes in the LS-DYNA 10pt response. This is resolved in LS DYNA 120pt, which results in smoother and more realistic acceleration response histories as well as smaller short period amplifications. This suggests that increasing the number of points in the backbone curve circumvents the high-frequency issues associated with LS-DYNA 10pt. The acceleration response spectra calculated by the time-domain programs are considerably different in the long period range for ground motion WP2, which is due to the differences in hysteresis rules followed in DEEPSOIL and LS-DYNA. The peak acceleration profiles differ significantly for ground motions WP1 and WP2 (see Figure A-43 and Figure A-44), but have match better for the less intense ground motion, WP3 (see Figure A-45). The peak accelerations calculated using SHAKE match closely with those using DEEPSOIL and LS-DYNA 120pt for ground motions WP1 and WP3. For WP2, SHAKE underestimates the accelerations at the lower layers, and overestimates the accelerations in the upper layers. LS-DYNA 10pt results in larger peak accelerations, especially in the middle and lower layers for ground motions WP1 and WP2, due to the high-frequency response, which is evident from the acceleration response spectra presented in middle panel of Figure A-47. The peak accelerations calculated by DEEPSOIL and LS-DYNA 120pt match reasonably well for all three ground motions, except for the slight overestimation by DEEPSOIL for ground motion WP3, in layers below 60m .

- c. *Site amplification:* The amplification spectra in Figure A-52 show that the elongated site period lies between 0.6 and 0.8 sec for WP1, between 1.5 and 2.5 sec for WP2, and between 0.5 sec and 0.6 sec for WP3, which are significantly greater than the elongated site periods calculated for the ordinary ground motions. The peak amplification is greatest for the weakest ground motion, WP3, and smallest for the strongest ground motion, WP2. These observations indicate that the intensity of the ground motion increases the elongated site period, and also the hysteretic damping, which leads to smaller peak amplifications. The amplification spectra calculated using SHAKE are considerably different from those calculated from the time-domain programs. SHAKE overestimates the amplifications at the site period for all ground motions and underestimates the elongated site period for WP1 and WP2, which are the consequences of a significant

underestimation of peak strains. Although amplifications calculated using the time-domain programs are comparatively closer to each other, there are differences, especially for periods less than 0.3 sec.

- d. *Variation of outcrop motion through depth*: The acceleration response spectra calculated at the surface differ significantly from the base outcrop for ground motions WP1 and WP2, and the differences are significantly greater than those observed for ground motion WP3 and the ordinary ground motions. This indicates that for the stronger ground motions the outcrop motion in soft rock varies significantly through the depth. This further suggests that for stronger ground motions that induce larger strains, the rock outcrop motion at the surface needs to be deconvolved to calculate the outcrop motion at a depth, before using it as an input for a nearby soil site. Further insight into this observation is presented in Section 4.7.5.

4.6.3.3 Effect of pressure-dependence of soil properties

Incorporating pressure-dependence in the soil properties changes the response of site W1 to both ordinary as well as pulse ground motions. Since the shear strength of the soil increases when pressure-dependence is introduced, the peak strain in the soil layers decreases. This decrease is more prominent for the pulse motions (e.g., Figure A-43) than ordinary ground motions (e.g., Figure A-30). However the acceleration response spectra show larger surface spectral accelerations at the site period for all the ground motions. Consequently the spectral amplifications (Figure A-39 and Figure A-52) are considerably larger when pressure-dependent properties are used for the soil. The peak accelerations are also slightly larger when pressure-dependent properties are used, especially for the layers closer to the surface. Incorporating pressure-dependence also decreases the differences between the responses calculated from the different numerical programs. This is a consequence of the significant decrease in the peak strains when pressure-dependence is included.

4.6.4 Site W2

4.6.4.1 Response to ordinary ground motions

Site W2 is uniform site composed of sand. Figure A-53 to Figure A-65 present the site-response results of site W2 subjected to ground motions WO1, WO2 and WO3 (peak accelerations of 0.15g, 0.17g and 0.19g). Figure A-53 to Figure A-55 present the stress-strain loops for the three ground motions, and are followed by the peak acceleration and peak shear strain profiles (Figure A-56 to Figure A-58), acceleration response spectra (Figure A-59 to Figure A-61), acceleration response histories (Figure A-62 to Figure A-64), and the spectral amplifications (Figure A-65). Each of these figures includes the

responses calculated using SHAKE, DEEPSOIL, LS-DYNA 10pt and LS-DYNA 120pt. Only the results of the analyses performed using pressure-independent (PI) properties are discussed in this section. Results of the analyses performed using pressure-dependent (PD) properties are discussed in Section 4.6.4.3.

- a. *Hysteretic behavior and the extent of nonlinear response:* The peak strain profiles in Figure A-56, Figure A-57 and Figure A-58 show that the largest peak strains calculated by different numerical programs vary between 0.12% and 0.18% for WO1, 0.06% to 0.09% for WO2, and 0.03% to 0.04% for WO3. These strain ranges correspond to modulus reduction ratios that lie between 0.49 and 0.57 for WO1, 0.24 and 0.29 for WO2, and 0.36 and 0.41 for WO3. The equivalent viscous damping ratios corresponding to these ranges are 23%, 19% and 15% for WO1, WO2 and WO3, respectively. These strain levels and modulus reduction ratios indicate significant softening in the soil layers due to nonlinear behavior. Nonlinear response is also evident from the stress-strain loops presented in Figure A-53, Figure A-54 and Figure A-55. The stress-strain hysteresis of LS-DYNA 10pt and LS-DYNA 120pt are quite similar, but differ considerably from that of DEEPSOIL. The peak strain profiles calculated using LS-DYNA 10pt and LS-DYNA 120pt are also very similar. SHAKE overestimates the strains in the upper layers and underestimates the strains in the lower layers compared to the time-domain programs. Analysis using DEEPSOIL again results in large changes in the peak strains in consecutive layers. However the peak strains in most layers are only slightly different from those calculated using LS-DYNA. The large changes in the peak strains are investigated in more detail in Section 4.7.4.2.
- b. *Acceleration response:* The acceleration response spectra presented in Figure A-59, Figure A-60 and Figure A-61 show considerable differences between the responses calculated by SHAKE, DEEPSOIL, LS-DYNA 10pt and LS-DYNA 120pt for periods less than 0.3 sec. The acceleration response spectra calculated using SHAKE have near constant amplitudes for periods less than about 0.1 sec. This is similar to the observations made from the responses of site W1, and indicates the absence of high-frequency content in the response – also evident from the relatively smooth acceleration response histories computed by SHAKE (see Figure A-62, Figure A-63 and Figure A-64 for acceleration response histories; see bullet 2 in Section 4.7.2 for additional discussion on this issue). Of the time-domain programs, LS-DYNA 10pt calculates the largest responses in the short period range, followed by DEEPSOIL and LS-DYNA 120pt. Similar to the response of site W1 to ground motion WP2, analysis using LS-DYNA 10pt results in significant overestimations of the short period accelerations for ground motion WO2, and unrealistic spikes in the corresponding acceleration response histories (seen in Figure A-63). The acceleration response spectra calculated using the time-domain programs match well in the long period range, and slightly differ from those calculated using SHAKE. The differences between the response

spectra calculated using DEEPSOIL and LS-DYNA 120pt can be attributed to the difference in the corresponding hysteretic models. Figure A-56, Figure A-57 and Figure A-58 show significant differences between the peak acceleration profiles calculated using the different programs. Analyses using DEEPSOIL and LS-DYNA 10pt result in larger peak accelerations than LS-DYNA 120pt and SHAKE. Large overestimation of the peak accelerations by LS-DYNA 10pt is a consequence of the high-frequency noise in the response.

- c. *Site amplification*: Site W2 has first two translational modes at 1.3 sec and 0.4 sec. The acceleration amplification spectra in Figure A-65 show that the elongated site periods are about 3 sec for WO1, 2.5 sec for WO2 and 2 sec for WO3. Additionally the surface response is de-amplified for periods less than 1 sec for all the ordinary WUS motions. Differences between the amplifications calculated by different programs are considerable, especially for short periods. Large differences are also seen for periods greater than 4 sec for ground motion WO1. SHAKE overestimates the amplifications near the elongated site period, especially for WO2 and WO3, which is a consequence of the underestimation of strains.
- d. *Variation of outcrop motion through depth*: The acceleration response spectra at the surface (see top panels in Figure A-59, Figure A-60 and Figure A-61) are significantly different from the base outcrop for all ground motions and the differences are larger than those observed for site W1. However, unlike for site W1, the acceleration response spectra at the base approach the base outcrop, indicating that the presence of the sand layer atop the bedrock does not significantly affect the ground motion at the sand bedrock interface. This is consistent with results of site E2, which show that the acceleration at the interface of sand and hard rock is similar to the outcrop input ground motion. Further insight into this observation and its significance is provided in Section 4.7.5.

4.6.4.2 Response to pulse-like ground motions

Figure A-66 to Figure A-78 present the site-response results of site W2 subjected to ground motions WP1, WP2 and WP3. These ground motions have peak accelerations of 0.73g, 0.83g and 0.19g, and pulse periods of 5.1 sec, 1.5 sec, and 9.0 sec, respectively (see Table 4-1). Figure A-66 to Figure A-68 present the stress-strain loops for the three ground motions, and are followed by the peak acceleration and peak shear strain profiles (Figure A-69 to Figure A-71), acceleration response spectra (Figure A-72 to Figure A-74), acceleration response histories (Figure A-75 to Figure A-77), and the spectral amplifications (Figure A-78). Each of these figures includes the responses calculated using SHAKE, DEEPSOIL, LS-DYNA 10pt and LS-DYNA 120pt. Only the results of the analyses performed

using pressure-independent properties are discussed in this section. Results of the analyses performed using pressure-dependent properties are discussed in Section 4.6.4.3.

- a. *Hysteretic behavior and the extent of nonlinear response*: The peak strain profiles in Figure A-69, Figure A-70 and Figure A-71 show that the largest peak strains calculated by different numerical programs vary between 1.5% and 4% for WP1, 2.5% and 5% for WP2, and 1.2% to 3.5% for WO3. These strain ranges correspond to modulus reduction ratios that lie between 0.02 and 0.04 for WP1, 0.02 and 0.03 for WP2, and 0.02 and 0.05 for WP3. The equivalent viscous damping ratios for these ranges lie between 30% and 35% for all the ground motions. Significant differences are observed in the peak strain profiles calculated by different programs at these strain levels, except for LS-DYNA 10pt and LS-DYNA 120pt, which produce similar stress-strain loops (see Figure A-66 to Figure A-68) and peak strain profiles. As seen in the responses of site W2 for ordinary ground motions, analysis using DEEPSOIL results in large changes in the peak strains in consecutive layers and these changes are significantly greater than those observed for the ordinary ground motions. Apart from the layers involved in these changes, the DEEPSOIL peak strains in most layers match fairly well with LS-DYNA 10pt and LS-DYNA 120pt. Similar to the observations made for ordinary ground motions, SHAKE results in a significant underestimation of the peak strains as compared to the time-domain programs, especially for ground motion WP1 and WP3, which leads to the underestimation of elongated site period as well as the overestimation of corresponding spectral amplifications.
- b. *Acceleration response*: The acceleration response spectra in Figure A-72, Figure A-73 and Figure A-74 are significantly different for the three programs, and the differences are greater than those observed for the ordinary ground motions. Also, as observed for ordinary ground motions, SHAKE predicts a near constant spectral acceleration at shorter periods (less than 0.2 sec) indicating the absence of high-frequency components in the response (see bullet 2 in Section 4.7.2 for additional discussion on this issue). Additionally the spectral accelerations calculated using SHAKE are significantly overestimated as compared to the time-domain programs in the long period range, which is a consequence of underestimating the peak strains. Analyses using LS-DYNA 10pt result in very large short period accelerations, which is also evident from the large unrealistic spikes in the corresponding acceleration response histories (see Figure A-75, Figure A-76 and Figure A-77). As observed from the results for ordinary ground motions, LS-DYNA 120pt circumvents this issue and predicts smaller spectral accelerations in the short period range, and also more realistic acceleration response histories. As a result LS-DYNA 120pt predicts spectral accelerations that are closer to LS-DYNA 10pt at longer periods and to DEEPSOIL at shorter periods. Significant differences are also observed in the peak acceleration

profiles calculated from SHAKE and the time-domain programs as seen from Figure A-69 and Figure A-71. Amongst the time-domain programs, the peak accelerations are the greatest for LS-DYNA 10pt, which is primarily due to the short period (high-frequency) response observed in the corresponding acceleration response spectra. The peak accelerations obtained using LS-DYNA 120pt and DEEPSOIL match reasonably well for all the ground motions.

- c. *Site amplification:* The acceleration amplification spectra presented in Figure A-78 show very large elongations in the site period compared to the ordinary ground motions. Although significant differences exist between their amplification spectra, the time-domain programs predict an elongated site period of greater than 6 sec for all the pulse motions. This indicates highly nonlinear behavior, given that the linear elastic time period of this site is 1.3 sec. Very large differences exist between the amplification spectra calculated using SHAKE and the time-domain programs, with SHAKE underestimating the elongated site period and overestimating the amplifications at this site period. This is a consequence of the significant underestimation of the shear strain, which is a result of using a lower value for the effective shear strain ratio (0.22) than the traditional value of 0.65. Additionally the spectral amplification at the elongated site period is the smallest for the strongest ground motion, WP2.
- d. *Effect of pulse period:* A notable observation to be made is that the ground motion WP3 results in peak strains that are in the same range as WP1 and WP2, in spite of having substantially smaller peak accelerations (see left panel of Figure A-71). This does not happen for site W1, for which ground motion WP3 results in significantly smaller strains than WP1 and WP2. This suggests that subjecting site W2 to a ground motion with a pulse period close to the elongated site period results in very large strains in the soil profile, compared to an ordinary ground motion with similar peak ground acceleration.
- e. *Variation of outcrop motion through depth:* The acceleration response spectra in Figure A-72, Figure A-73 and Figure A-74 show that the base outcrop is significantly different from the surface level acceleration response spectrum for all ground motions, but is similar to the within motion calculated at the base. This is consistent with the observations made for the ordinary ground motions, and suggests that the presence of the sand layer does not significantly affect the ground motion at the sand-bedrock interface. Further insight into this observation and its significance is provided in Section 4.7.5.

4.6.4.3 Effect of pressure-dependence of soil properties

Similar to site W1, the response of site W2 changes considerably when pressure-dependence is incorporated in the soil properties. The peak strains in the lower layers of the site are lower while the peak

strains in the mid and upper layers are higher as compared with the pressure-independent (PI) case (e.g. Figure A-56, Figure A-57). The increase in the peak strain in the upper layers is due to the weakening of the soil layers above the reference depth as compared to the pressure-independent properties (see Section 4.4.1). However the trends in the acceleration response are similar to those seen for site W1: using pressure-dependent properties results in larger spectral accelerations (and consequently higher spectral amplifications) at the surface compared with the pressure-independent case (e.g., Figure A-59 and Figure A-73). Additionally the variability in the site response is also generally smaller when pressure-dependent properties are used. This is a consequence of the significantly smaller strains in the lower layers of the soil profile.

4.7 Summary and conclusions

Site-response analysis is performed for four different soil profiles using industry-standard numerical programs, SHAKE, DEEPSOIL and LS-DYNA. Results of site-response analyses from all the programs are presented in Appendix A and the observations gathered from all analyses are presented in Section 4.6. These observations are summarized in this section, and are used to explain some of the practical issues faced in site-response analysis. Section 4.7.1 presents conclusions regarding nonlinear site response in general, and Sections 4.7.2 and 4.7.3 present conclusions derived from the comparisons between equivalent-linear and nonlinear site responses, and nonlinear site responses calculated from different time-domain programs, respectively. Section 4.7.4 presents the key issues faced while performing site-response analysis in different programs, along with their implications in practice and some possible solutions. The observations made in Section 4.6 are used to make recommendations for calculation and specification of input for one-dimensional site-response analysis. These recommendations are presented in Section 4.7.5, followed by a description of some prospects for future research in Section 4.9.

4.7.1 General conclusions regarding nonlinear site response

The following conclusions can be made regarding site-response analysis using the soil profiles and ground motions considered in this study:

1. As the intensity of the ground motion increases, the elongation in the site period (period of maximum spectral amplification) increases, and the amplification at this period decreases. This is due to the nonlinear behavior of the soil, which involves reduction of the shear modulus (which increases the elongation) and increase in hysteretic damping (which decreases the amplification).

The spectral amplification here refers to the amplification of the acceleration from the within motion at the base (and not the outcrop input) to the surface of the soil profile at each period.

2. Pulse motions with long pulse periods can induce very large strains in deep, soft soil profiles compared to ordinary ground motions of similar peak ground acceleration. This is observed when the pulse period of the input is close to the elongated period of the soil profile, such as site W2 subjected to ground motion WP3, which resulted in strains similar to those calculated for significantly more intense pulse motions, WP1 and WP2.

4.7.2 Comparison of equivalent-linear and nonlinear responses

The difference in responses calculated using SHAKE and the time-domain programs, DEEPSOIL and LS-DYNA, varies by the soil profile and ground motion. The WUS soil profiles, site W1 and site W2, show larger differences than the CEUS profiles site E1 and site E2. For the CEUS profiles, the responses are the closest in the hard rock layers of site E1 and site E2 since they are subject to very small strains, but are considerably different in the sand layers of site E2. For the WUS soil profiles the responses are closer for site W1 than site W2, and for ordinary ground motions than pulse-like ground motions. The following conclusions can be drawn from the observations made in Section 4.6:

1. The difference between the equivalent-linear and nonlinear response increases with strain in the soil layers and thus with the nonlinearity induced in the soil profile.
2. The elongated site periods calculated by SHAKE and the nonlinear analyses match fairly well in most cases.
3. The surface spectral accelerations calculated using SHAKE and the nonlinear programs are increasingly different at shorter periods. Additionally the short-period spectral accelerations calculated using SHAKE are almost constant, especially for sites W1 and W2, which undergo larger strains. This observation is further explained in Section 4.7.4.1.
4. SHAKE underestimates the peak shear strains as compared with the nonlinear programs for intense ground motions, especially in the lower layers of the soil profile where the strains are the largest. This is because the equivalent-linear method accounts for nonlinear behavior in an ‘averaged’ sense by decreasing the shear modulus based on the effective shear strain, which can be seen as a measure of the extent of nonlinearity induced by the earthquake. In contrast, nonlinear analysis accounts explicitly for softening and load-history effects.
5. SHAKE overestimates the acceleration amplifications at the site period compared with the nonlinear programs, especially for intense ground motions. This is a result of underestimating the damping ratio in the soil layers, which stems from the underestimation of the peak shear strains.

6. Results of the analyses with pressure-dependent properties for sites W1 and W2 show similar trends to those with pressure-independent properties. However, the differences between the equivalent-linear and nonlinear responses for the pressure-dependent analyses are smaller, because the soil layers sustain much lower strains.

4.7.3 Comparison between the responses from DEEPSOIL and LS-DYNA

Despite using very similar backbone curves and damping curves to model the soil materials in DEEPSOIL and LS-DYNA, the site responses calculated using these programs can be significantly different for analyses involving large strains. The following conclusions can be made from the observations made in Section 4.6:

1. The peak strain profiles as well as the acceleration response spectra match well for site E1. However, differences in responses increase for softer soil profiles, sites W1 and W2, and also in the sand layer of site E2. This indicates that the responses calculated using the nonlinear programs are increasingly different for larger strains induced in the soil layers.
2. The peak strain profiles calculated from LS-DYNA 10pt and LS-DYNA 120pt are similar for most cases indicating that the increase in the number of points in the backbone curve causes negligible changes in the hysteretic behavior. However, significant differences arise between the peak strains calculated using DEEPSOIL and LS-DYNA, which is a result of using different hysteresis rules in the two programs.
3. Analyses using DEEPSOIL sometimes predict abrupt changes in the peak strains of consecutive layers. This observation is further examined in Section 4.7.4.2.
4. The differences between the acceleration response spectra at the surface are more prominent at shorter periods, especially for sites W1 and W2. LS-DYNA 10pt sometimes overestimates the short period response compared with DEEPSOIL and LS-DYNA 120pt.
5. The acceleration response spectra calculated using DEEPSOIL and LS-DYNA 120pt are reasonably close for most cases. In some cases DEEPSOIL overestimates the short period response compared with LS-DYNA 120pt. This is attributed to the abrupt changes in the peak strains of consecutive layers.
6. The differences between the calculated nonlinear responses are smaller when pressure-dependence is introduced, because smaller strains are induced in the layers.

4.7.4 Key issues faced during site-response analysis

4.7.4.1 SHAKE

Analysis using SHAKE results in near constant spectral accelerations in the short period range for sites W1 and W2. This observation is also reported in the study by Stewart and Kwok (2008). The spectral acceleration for site W1 (PI) subjected to ground motion WP2 is effectively constant at periods less (frequencies greater) than 0.15 sec (6.7 Hz). Similarly the spectral accelerations for site W2 (PI) subjected to ground motion WO2 remain constant at periods less than 0.1 sec. A comparison of the Fourier transforms for these cases (Figure 4-7) indicates that these short-period spectral accelerations correspond to very small amplitudes in the frequency domain, indicating that the equivalent-linear procedure is unable to reproduce the higher frequency response.

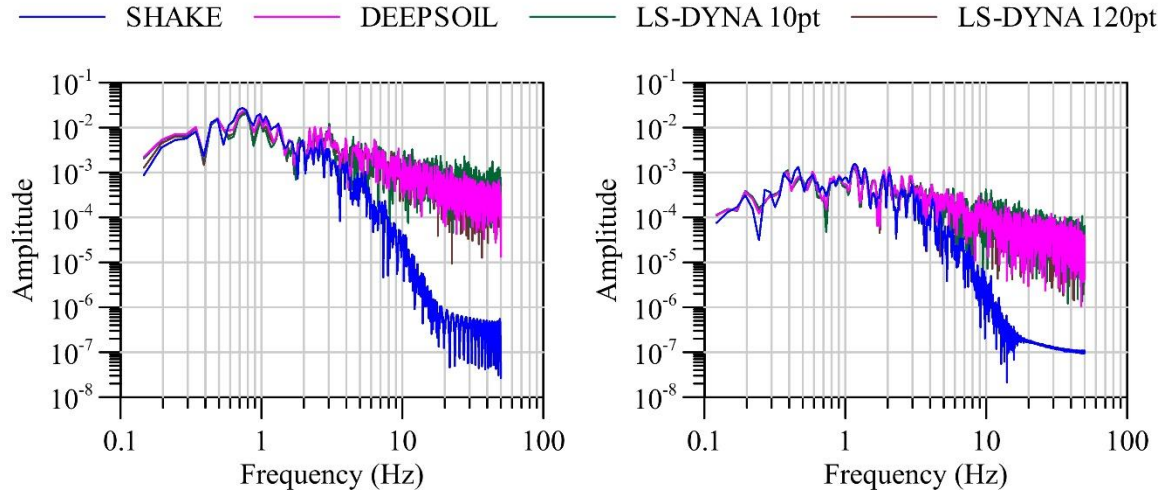


Figure 4-7: Fourier transforms of the surface accelerations for site W1 subjected to ground motion WP2 (left) and site W2 subjected to ground motion WO2 (right)

This is because the equivalent-linear procedure cannot capture some of the higher modes of vibration of the soil profile that are excited due to the continuous changes in the soil material properties through time. Nonlinear procedures can capture these higher modes of vibration, since they simulate the changes in material properties in through time. However, the nonlinear procedures are also susceptible to numerical noise based on the material model and the integration algorithms used (Chen and Joyner, 1974; Joyner and Chen, 1975). It should also be noted that the equivalent-linear method does not consistently overestimate or underestimate the short period (high frequency) response as compared with the nonlinear methods, although the corresponding Fourier amplitude is always underestimated. This can be seen in Figure A-60 and Figure A-46, where SHAKE overestimates the short period response as compared with

DEEPSOIL and LS-DYNA 120pt (LS-DYNA 10pt results in relatively higher responses due to numerical noise at these periods) for site W2 subjected to ground motion WO2, while it underestimates the response for site W1 subjected to ground motion WP1.

Analysis using SHAKE does not converge for site W2 subjected to pulse motions in spite of using the numerical models and analysis parameters that are identical to those used for the ordinary ground motions. The nonlinear procedures estimate peak strains close to 4% for the W2 site subjected to pulse motions, which substantially larger than the 1% peak shear strain that is universally accepted as SHAKE's limit. Modifications to the SHAKE analysis, namely, extrapolation of the modulus reduction curves to a peak strain greater than 10% and decreasing the layer thickness, do not enable convergence. Notably, analysis for the same soil profile and ground motions converges when the equivalent-linear option of the program DEEPSOIL (referred to as DEEPSOIL-EL hereafter) is used. The SHAKE analysis converges when the effective shear strain ratio is reduced to 0.22 from a traditionally recommended value of 0.65, but the resultant responses are very different from the corresponding DEEPSOIL-EL responses. Specifically, when compared with the nonlinear analyses (Figure 4-8), the SHAKE analysis with an effective shear strain ratio of 0.22 significantly underestimates the peak strains and overestimates the spectral acceleration at the site period. The SHAKE analysis also converges for an effective shear strain ratio at 0.65 if the maximum analysis frequency is reduced to 45Hz from the value of 100Hz used for ordinary ground motions⁵. The resultant responses after this modification match exactly with the corresponding DEEPSOIL-EL results [note that the DEEPSOIL-EL and SHAKE ($\alpha = 0.65$) results overlap in Figure 4-8], and show smaller differences from the nonlinear results.

⁵ Issues with convergence are not encountered with a different version of SHAKE (Baig and Bolourchi, 2013), suggesting that the problem is intrinsic to the source code.

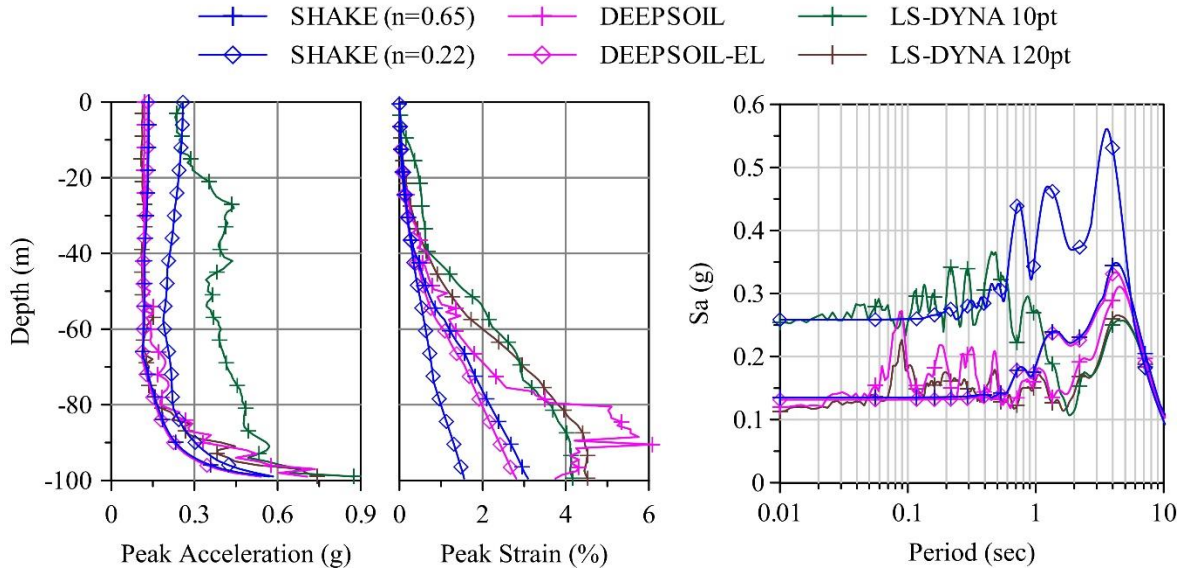


Figure 4-8. Peak acceleration and peak strain profiles (left) and acceleration response spectra at the surface (right) for site W2 subjected to ground motion WP1

4.7.4.2 DEEPSOIL

Analysis using DEEPSOIL occasionally resulted in abrupt changes in the peak strains of consecutive layers, despite the layers having the same material properties. These changes were associated with the peak strains in the soil profile greater than 0.1%. SHAKE and LS-DYNA resulted in relatively smooth peak strain profiles for the corresponding analyses. An example of this behavior is site W2 subjected to ground motion WP2. The DEEPSOIL peak strain profile for this case is presented in Figure A-70, which shows many “spikes” through the depth of the soil profile. The largest spike in this peak strain profile is formed by the strains in three consecutive layers at depths 94.5m, 95.5m and 96.5m, where the peak strains are 2.3%, 7% and 2.6%, respectively. A comparison of the hysteresis loops calculated by DEEPSOIL for these layers is presented in Figure 4-9 below. Arrows in this figure indicate the path of hysteresis. The large cycle in this figure corresponds to the pulse of the ground motion, and the smaller cycles correspond to the rest of the ground motion.

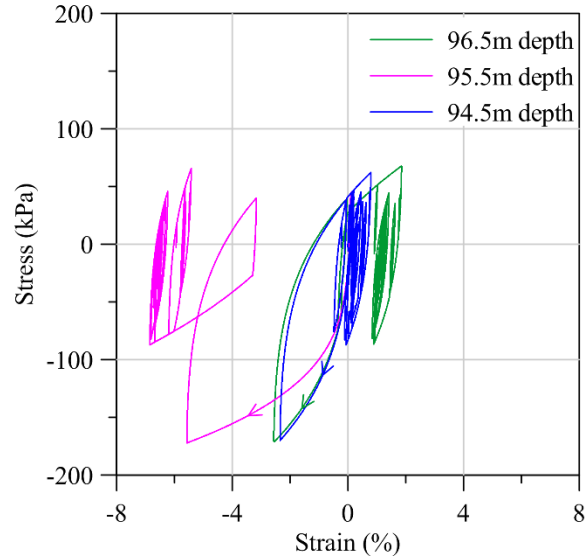


Figure 4-9: Hysteresis loops of three layers in site W2 showing an abrupt change in the peak strains when subjected to ground motion WP2

In this figure, the hysteresis loops of the three layers match closely in the smaller cycles in the initial part of the earthquake, while the second layer at 95.5m diverges significantly from the other two adjacent layers in the large cycle. This divergence results in a large difference between the peak strains of the consecutive layers and thus a spike in the peak strain profile. The large cycle in Figure 4-9 is isolated and more clearly reproduced in Figure 4-10, with panel a and panel b representing the hysteresis loops of the three layers from 0 to 2.05 sec, and 0 to 2.3 sec respectively. Panel a shows that the initial parts of the hysteresis paths (before 2.05 sec) are close to each other, with the path of the layer at 95.5m depth approaching the backbone curve (dotted line). This hysteresis path then follows the backbone curve according to rule 3 of the extended Masing rules (see Section 2.1.2.2 for a description of the extended Masing rules). However, the other two layers miss the backbone curve and then trace a completely different path resulting in large differences in the final peak strains. This indicates that small changes in the initial paths of the hysteresis loops might lead to very large differences in the final peak strains, which is unrealistic. This behavior is not seen in LS-DYNA since the MAT_HYSTERETIC_SOIL model is not governed by the extended Masing rules. Although DEEPSOIL results in unrealistic peak strain profiles, the corresponding acceleration responses are reasonably close to those calculated from LS-DYNA 120pt indicating that this behavior does not affect the acceleration response. However caution has to be exercised for applications where the peak strain is important, such as predicting permanent displacements in the soil profile.

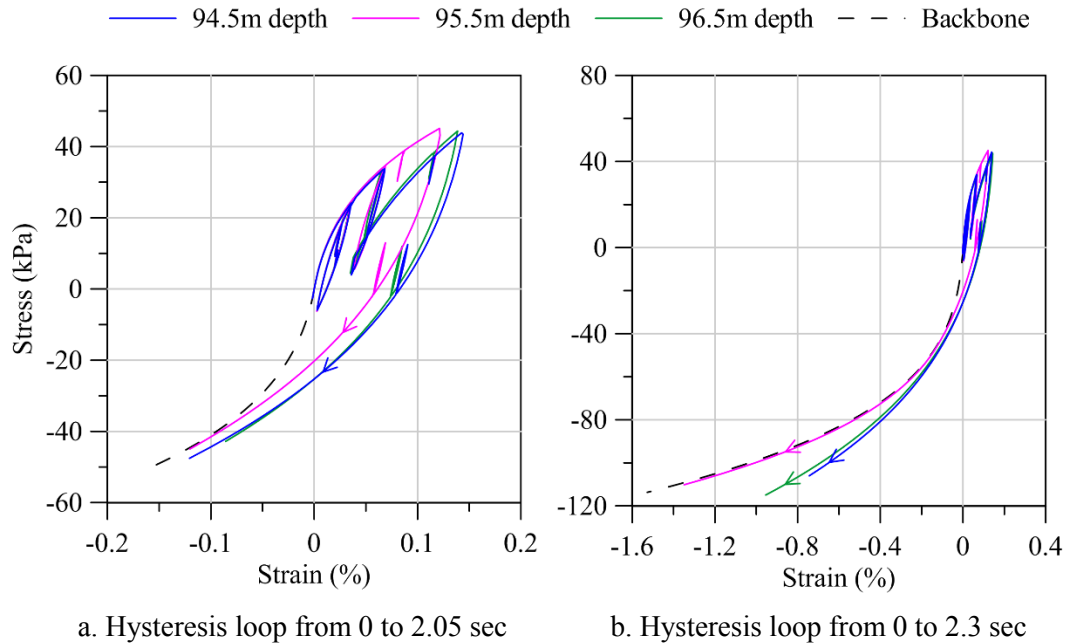


Figure 4-10: Examination of the hysteresis loops of layers involved in abrupt changes in the peak strains in site W2 subjected to ground motion WP2

4.7.4.3 LS-DYNA

Significant high-frequency content was seen in the LS-DYNA response when the 10 point backbone curve was used. Examination of the corresponding acceleration response histories (e.g. Figure A-76) indicated that these components were unrealistic and were a consequence of the 10-point model. This hypothesis is substantiated by the significant reduction in the high-frequency content when the 120-point backbone curve was used (compare acceleration response histories in Figure A-76). This indicates that the high-frequency noise in the LS-DYNA 10pt response is primarily due to the significant changes in stiffness in its multilinear backbone curve. Increasing the number of points in the backbone curve significantly decreases the stiffness increments and therefore results in smoother accelerations. An alternative approach (Huang, 2013) to achieve a smoother acceleration response is to incorporate strain-rate effects in LS-DYNA 10pt. Figure 4-11 also presents the results when strain-rate effects⁶ are included in the model. This observation could play a critical role in estimating the seismic demands for stiff structures such as nuclear power plants since higher frequencies are most important in these structures.

⁶ Strain-rate effects are included in the MAT_HYSTERETIC_SOIL model by defining the curve, LCSR, which specifies the scale factor for the yield strength as a function of strain-rate (LSTC, 2013)

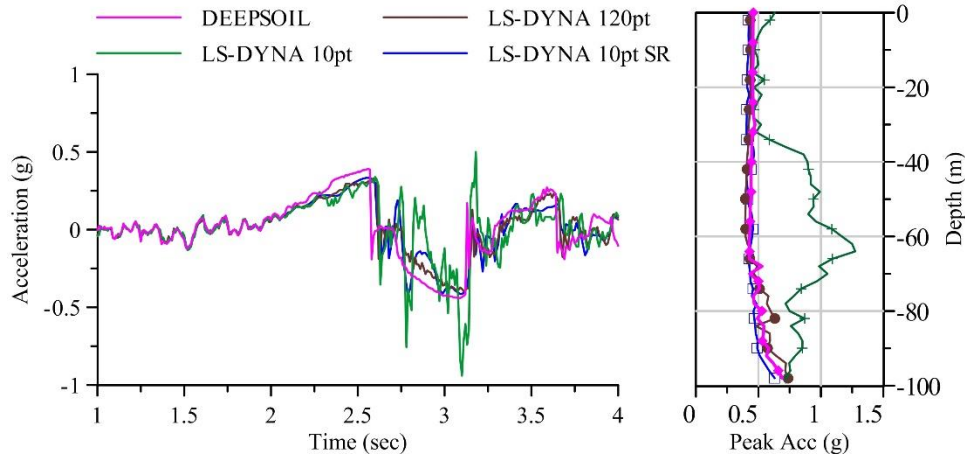


Figure 4-11: Acceleration time series at 50m depth (left) and the peak acceleration profile (right) for site W1 subjected to ground motion WP2

LS-DYNA 120pt results in numerical instabilities for analyses involving site W2 subjected to pulse motions, when the transmitting boundary is employed. However these numerical instabilities are not encountered when a reflecting boundary is employed for the same cases. Using a transmitting boundary involves the application of an input force (a ‘natural’ boundary condition⁷) at the bedrock, while the reflecting boundary involves the application of an acceleration input (an ‘essential’ boundary condition⁷). Instabilities with the transmitting boundary condition arise because finite element methods directly comply with the essential boundary conditions but only indirectly comply with the natural boundary conditions. It is theorized that the errors due to the natural boundary condition at the base, where the strains are very large for the pulse motions, lead to numerical instabilities. Further investigation is required to fully understand this problem.

4.7.4.4 Sensitivity of high-frequency response

The site responses calculated from various numerical programs were most different in the short period (high frequency) range, which is critical for stiff structures such as nuclear power plants. Analyses using SHAKE resulted in a near constant response, while the responses calculated using the time-domain programs showed considerable variability, in the short periods. Noticeable differences in the short period spectral accelerations were observed even in the analyses for site E1 (see Figure A-8), in which the soil

⁷ In the terminology used in finite element methods, the boundary conditions involving displacements, accelerations, etc., are termed ‘essential’ boundary conditions, and the boundary conditions involving tractions, forces, etc., are termed ‘natural’ boundary conditions (Bathe, 1996)

layers remained almost linear. However the range of periods at which these variations occur was different for each site: for example, the spectral accelerations calculated by the different programs at the surface of site E1 (with a first mode period of 0.16 sec) when subjected to ground motion EO2 deviated from each other at periods less than 0.04 sec (see Figure A-8), whereas for site W1 (first mode period of 0.40 sec) subjected to ground motion WO2 the deviations occurred at periods less than 0.20 sec. The site-dependence of these period ranges indicates that the variability in the short period responses might be due to a poor match in the higher mode responses calculated from the different programs. Kwok *et al.* (2008) observed the variability in the short period responses calculated by different time-domain programs and attributed it to differences in the corresponding viscous damping formulations. However the DEEPSOIL and LS-DYNA analyses performed in this study consider almost similar viscous damping formulations (frequency-independent damping; damping ratio of 1.1%). While viscous damping could be an issue, the variability also arises from the differences in the hysteretic material models (such as differences in the hysteresis rules). Furthermore these observations indicate that the high frequency response is more sensitive to the changes in the viscous damping and hysteretic material models than the response at lower frequencies, which are typically focused on in traditional civil engineering structures. Validation efforts therefore require much more attention to the high frequency response in order to improve the credibility of site-response analysis programs for nuclear applications.

4.7.5 Calculation and specification of input for site-response analysis

Earthquake ground motions are most often recorded at the surface of an outcropping rock (rock outcrop motion), but not at depth (within profile motion). However the concept of ‘outcrop input’ allows the usage of a nearby recorded rock outcrop ground motion as the input for site-response analysis (see Section 2.2.2) when a transmitting boundary is assumed for the base of the soil profile. Consider the illustration in Figure 4-12 with a hypothetical soil profile (right) and outcropping bedrock (left). In this figure, V_B is the low-strain shear wave velocity of the bedrock and V_A is the low-strain shear wave velocity of the material in the soil profile. Let O_{RS} be the ground motion recorded at the surface of the outcropping rock, O_{RB} and W_{RB} be the outcrop and within motions at the base of the soil profile (calculated using a deconvolution analysis), and O_{SS} be the surface response of the soil profile. Assume that the soil profile and bedrock are horizontally infinite and do not interact with each other.

Most often in practice, site-response analysis is performed by using the ground motion O_{RS} to calculate the outcrop input forces at the base, and not O_{RB} , which is the outcrop ground motion at the base. The analyses of site E1 showed that the response at the surface of the hard rock profile is very close to the

outcrop motion at the base, indicating that the outcrop motion does not change significantly through the depth for very stiff sites. Therefore it can be said that the recorded ground motion, O_{RS} , is close to the base outcrop, O_{RB} , and can be used as an outcrop input at the base of the soil profile, avoiding the need for a deconvolution analysis. However this is not true for the analysis of site W1, which involves considerably larger strains. The outcrop ground motion in this case differs through the depth soil profile, which is evident from the surface response of site W1 differing considerably from the input outcrop even for ordinary ground motions. In these cases the base outcrop ground motion O_{RB} should be calculated by a deconvolution analysis, and this ground motion can be specified as outcrop input to the soil profile under consideration.

From the results of site E2 and site W2 it can be seen that the presence of a very soft soil layer on the top of a relatively hard rock does not influence the ground motion at the soil-rock interface significantly. Namely, if V_A is significantly smaller than V_B , the outcrop ground motion at the base, O_{RB} , is almost equal to the within motion, W_{RB} , indicating that the bedrock behaves like a rigid base to the soil profile. Therefore the rigid base assumption can be used in these cases and the calculated base outcrop motion, O_{RB} , can be input to the soil profile as a within motion, which is conveniently provided as direct acceleration input (as opposed to the outcrop input, which is provided as a series of shear forces).

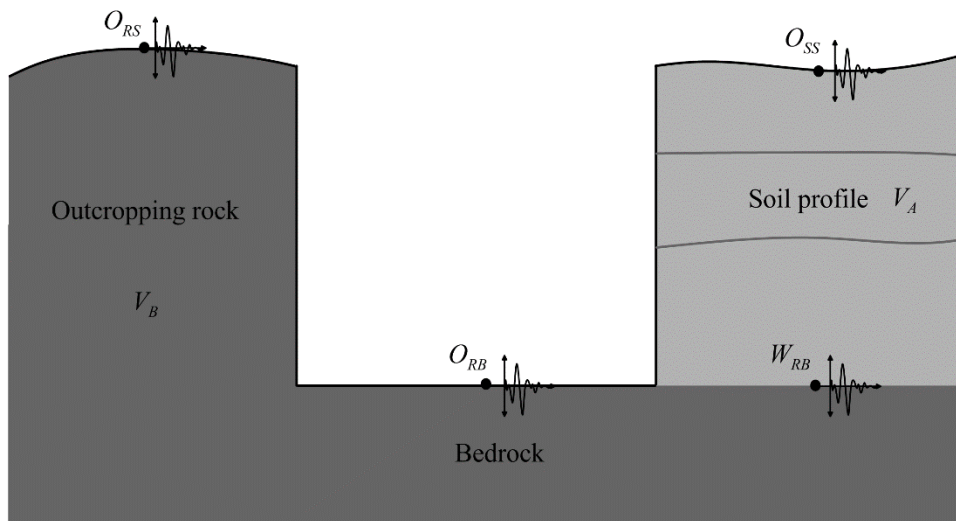


Figure 4-12: Outcrop and within ground motions

The following statements can be made regarding the *calculation of input from a recorded rock outcrop* for the site-response analysis of a nearby soil profile:

1. If a ground motion is recorded on a very stiff outcropping rock (such as site E1 with a low-strain shear wave velocity of 2500 m/s) where mostly linear strains are expected, the recorded ground motion can be directly used as an input at the base of a nearby soil site.
2. If some nonlinearity is expected in the response of the outcropping rock, the recorded acceleration should be deconvolved to calculate the ground motion at the base level of the nearby soil site. This ground motion should be used as the input for site-response analysis.

The following statements can be made regarding the *specification of input and the boundary condition at the base* for the site-response analysis for a soil profile, when the ground motion at the base of the soil profile is available:

1. For soil sites that are very soft compared to the underlying bedrock, the bedrock can be assumed as rigid and ground motion calculated in bullets 1 or 2 can be directly input as a within motion, namely, in the form of accelerations (rigid boundary assumption).
2. If the stiffness of the soil site is comparable to the underlying bedrock, the ground motion calculated in bullets 1 or 2 should be specified as an outcrop input at the base of the soil site (transmitting boundary assumption).

4.8 Site-response analysis for biaxial horizontal shaking

One-dimensional site-response analysis is traditionally performed independently for the two horizontal components of the ground motion, with the assumption that site response in orthogonal directions is uncorrelated. However, since soil is a nonlinear material, the shear stresses in the principal directions are generally correlated (Hadjian, 1981). The MAT_HYSTERETIC_SOIL material model accounts for this correlation by defining the failure surface of each of the nested surface layers by the equation

$$J_{2i} < \frac{4}{3} \tau_{\max i}^2 \quad (4-3)$$

where, J_{2i} is the second invariant of the stress tensor in layer i , and $\tau_{\max i}$ is its yield stress. The material models in SHAKE and DEEPSOIL only account for one-dimensional shear behavior and therefore cannot simulate biaxial site response. To investigate the interaction between the horizontal components of the site response, biaxial analyses are performed for sites W1 and W2 using LS-DYNA 120pt. These sites are subjected to simultaneous excitation in two horizontal directions (X and Y); ground motion WP2 is used in the X direction and the corresponding perpendicular component (WP2y) is used in the Y direction. The correlation coefficient for the two horizontal components is 0.32 (Hadjian, 1981). These ground motions are applied at three different intensities: 50%, 100% and 150% of the recorded motion. Figure 4-13 below presents the acceleration response spectra calculated from these analyses at the surface of site W1. To

enable a comparison between the results of uniaxial and biaxial shaking, the responses are presented for site W1 subjected to ground motions WP2 and WP2y simultaneously (biaxial), as well as ground motion WP2 alone (uniaxial). The spectra are calculated for the responses in the X direction, and only the pressure-independent (PI) cases are considered.

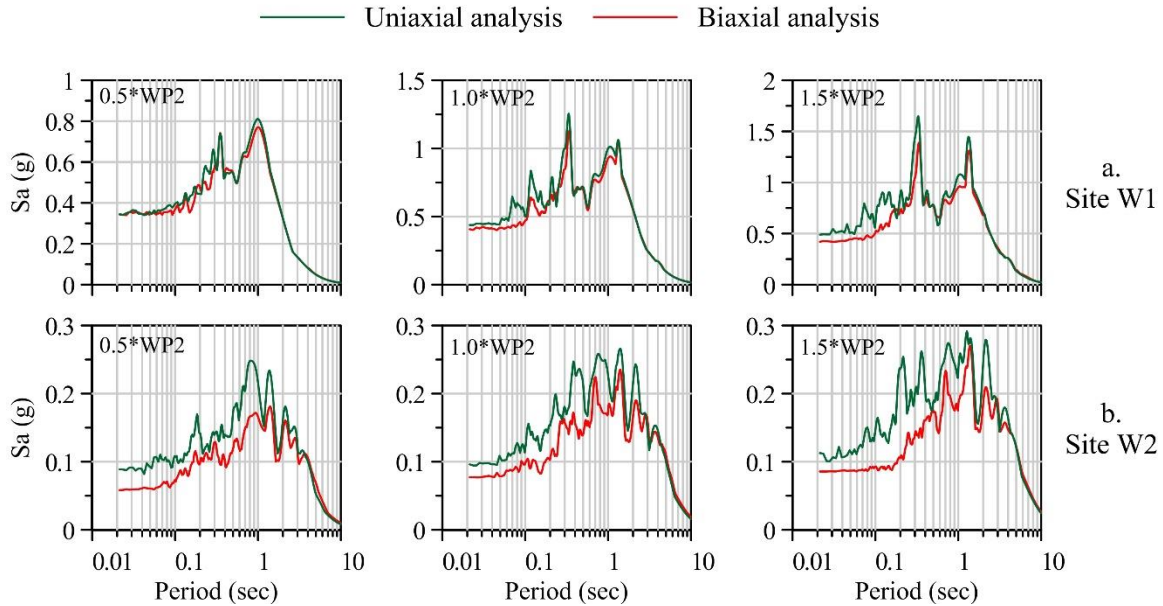


Figure 4-13: Surface acceleration response spectra in the X direction for uniaxial and biaxial analysis performed for sites W1 and W2

Slight differences are seen between the responses of site W1, with the uniaxial analysis predicting higher spectral accelerations than the biaxial analysis, especially in the short period range. The differences between the uniaxial and biaxial results are greater for site W2 and increase with the ground motion intensity. The response sensitivity to ground motion intensity is expected because each nested surface of the MAT_HYSTERETIC_SOIL material undergoes yielding earlier in a biaxial analysis (recall that both of the stress components are included in the stress invariant; see equation 4). Larger strains are induced in the biaxial analysis, leading to higher hysteretic damping and smaller accelerations. From a practical perspective, the differences between the uniaxial and biaxial site responses are minor for site W1 (as compared with those observed between the results from different numerical programs) but are significant for site W2. Further study using other material models is needed to more completely characterize the differences between uniaxial and biaxial site response.

4.9 Recommendations for future research

Although a number of studies have been performed to develop numerical models for one-dimensional site-response analysis, significant differences still exist in the responses calculated from the industry-standard numerical programs especially 1) in the short period range, and 2) for the cases involving large strains. Robust validation of these programs is therefore needed to increase the credibility of these programs, especially for soft soil profiles subjected to intense ground motions. These validations need to be in the form of large-scale laboratory experiments since the one-dimensional wave field is not produced by a real earthquake. Particular attention needs to be paid to the short-period (high-frequency) response of the soil profiles since it is critical for calculating the seismic demands in stiff structures such as nuclear power plants. Additionally, the present material models need to be extended and validated for very large strains (greater than 1%) in order to accommodate site-response analyses for nuclear applications, which involve the calculation of seismic demands for ground motions with very long return periods.

SECTION 5

AN ASSESSMENT OF SOIL-STRUCTURE INTERACTION ANALYSIS PROGRAMS

5.1 Overview

This section presents an assessment of the industry-standard soil-structure interaction (SSI) analysis programs, SASSI (Lysmer *et al.*, 1999) and LS-DYNA (LSTC, 2013). SASSI is a frequency-domain program for linear analyses, and LS-DYNA is a time-domain program capable of linear and nonlinear analyses. The assessment involves comparisons of the SSI responses calculated using the two programs for 1) simple models involving uniform elastic soil profiles and lumped mass structures on a surface basemat (Section 5.2), and 2) nonlinear models involving the soil profile and experimental model structures used in the City Block project (Section 5.3). The model structures MS1F_2 and MS2F used in Tests 3 and 4 are considered for the nonlinear analyses. Nonlinearities in the soil, foundation-soil interface, and the structure (only MS1F_2) are modeled. The process of performing these comparisons reveal some practical challenges in performing SSI analysis, and these challenges are identified in Section 5.4.

5.2 Calculation of linear elastic SSI response using SASSI and LS-DYNA

Soil-structure interaction analysis using SASSI and LS-DYNA can be a complicated task prone to modeling errors. Before assessing these programs for the solution of nonlinear problems, they are compared and assessed for linear elastic problems. The SASSI analyses are performed using the flexible-volume method (Ostadan, 2006a) and the LS-DYNA analyses are performed using both the direct method and the effective seismic input method, which is a predecessor of the domain reduction method (DRM). These methods are described in Section 3.2.

5.2.1 Model description

A uniform soil profile with a depth of 29.47m (equal to the depth of the soil profile used in the City Block project) is chosen for the elastic analyses presented in this section. The soil material is assumed to be linear viscoelastic with a mass density of 1700 kg/m^3 , shear wave velocity of 164.59 m/s, Poisson's ratio of 0.3, and a damping ratio of 0.02. Two lumped mass structures are considered for analysis: 1) a 10m tall structure (LM1) with one lumped mass at the top, and 2) a 25.6m tall structure (LM2) with lumped masses at the top, mid-height and the bottom. Both the structures are founded on a basemat identical to that of the experimental model MS2F (Section 6.4.3.1), designed for the centrifuge experiments of the City Block project. This basemat has a plan area of $13.8\text{m} \times 13.8\text{m}$ with a thickness of

1.4m, and embedded with an embedment depth equal to the mat thickness. Both structures are assumed to be made of Aluminum, with a mass density of 2700 kg/m³, elastic modulus of 69 GPa, and a Poisson's ratio of 0.3. The lumped masses and beam cross section properties of the structures are presented in Table 5-1. The structures are shown in Figure 5-1. LM1 is designed to produce minimal SSI effects, and LM2 is designed as a lumped-mass representation of MS2F, which shows significant SSI effects.

Table 5-1: Lumped masses and beam cross section properties of the structural models used for analyses using SASSI and LS-DYNA

Structure	Lumped mass (Metric tons)		Beam cross section properties		
			A (m ²) ^a	SA (m ²) ^b	I _{yy} (m ⁴) ^c
LM1	166		0.213	0.114	1.06
LM2	Top	311.35	0.213	10.02	70.63
	Mid-height	518.92			
	Base	207.57			

^a Area of cross section

^b Shear area

^c Moment of inertia for bending in the Y direction (ground motion is along the X direction)

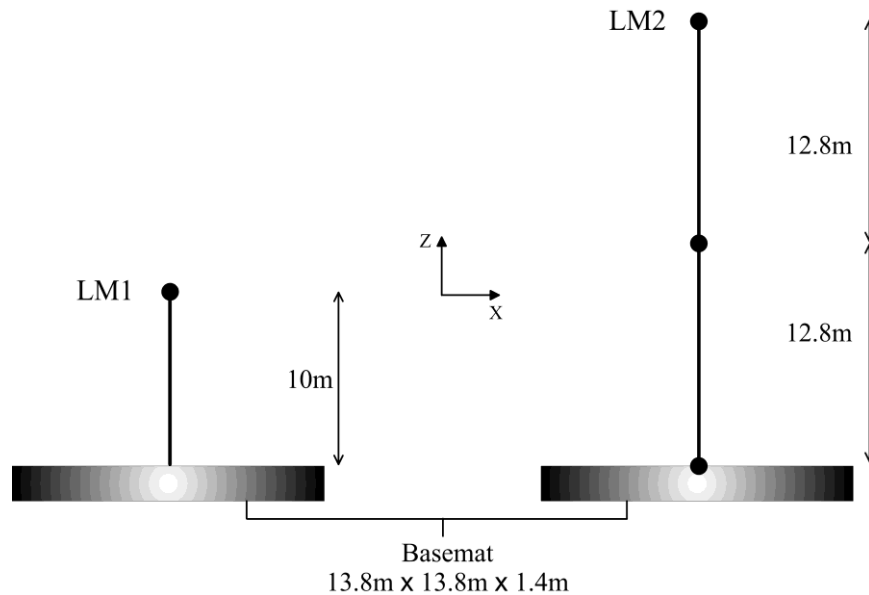


Figure 5-1: Lumped mass structures, LM1 and LM2, used for the verification analyses of SASSI and LS-DYNA

Prior to performing SSI analyses, the fixed-base models of the structures are analyzed using SASSI and LS-DYNA and results are compared to ensure that the structural models in the two programs are equivalent. SSI analyses are then performed with the rigid basemat alone and the responses are compared. Following these preliminary analyses, each of the structures, LM1 and LM2, is analyzed for 1) rigid superstructure on a rigid basemat, and 2) flexible superstructure on a rigid basemat, and 3) flexible superstructure on a flexible basemat. The analyses are performed using SASSI and LS-DYNA and the results are compared in Section 5.2.4. A single ground motion is used for the comparisons made in this section. This ground motion is an Ormsby wavelet with a peak acceleration of 0.5g, and frequency parameters, 0Hz, 0.2Hz, 20Hz, and 25Hz (refer to Appendix B for information on the Ormsby wavelet). The ground motion is applied at the base of the soil profile assuming rigid bedrock beneath the soil.

5.2.2 Modeling in SASSI

General modeling procedures in SASSI are described in Section 3.3.1 and the modeling details corresponding to the SSI analysis of LM1 and LM2 are presented in this section.

The soil profile in SASSI is modeled with 15 layers, all with the same shear wave velocity (164.59 m/s), compressive wave velocity (307.91 m/s) and damping ratio (0.02). The analysis is performed for 44 frequencies, ranging from 0.02Hz to 25Hz. Although the SASSI user manual recommends only 10 to 20 frequencies for analysis, a larger number of frequencies are used for reasons described in Section 5.4.1. The basemat and excavated soil elements are modeled using eight-noded brick elements, and the superstructure is modeled using beam elements with the properties specified in Table 5-1. Lumped masses specified in Table 5-1 are assigned to the superstructure nodes. The basemat is just embedded below the soil surface, with an embedment depth equal to its thickness. The superstructure is connected to the basemat with rigid beam elements. Since SASSI does not have a rigid material model, rigid elements are usually modeled by using a very large elastic modulus or large cross-section properties. A damping ratio of 0.02 is used for the soil, the basemat, and the superstructure. The control motion is applied at the base of the soil profile as a vertically propagating shear wave. A reflecting boundary is modeled at the base since the bedrock is assumed to be rigid. The SASSI models of LM1 and LM2 are presented in Figure 5-2. The lumped masses in this figure are indicated by red solid circles, and the ground surface is indicated by a shaded brown area.

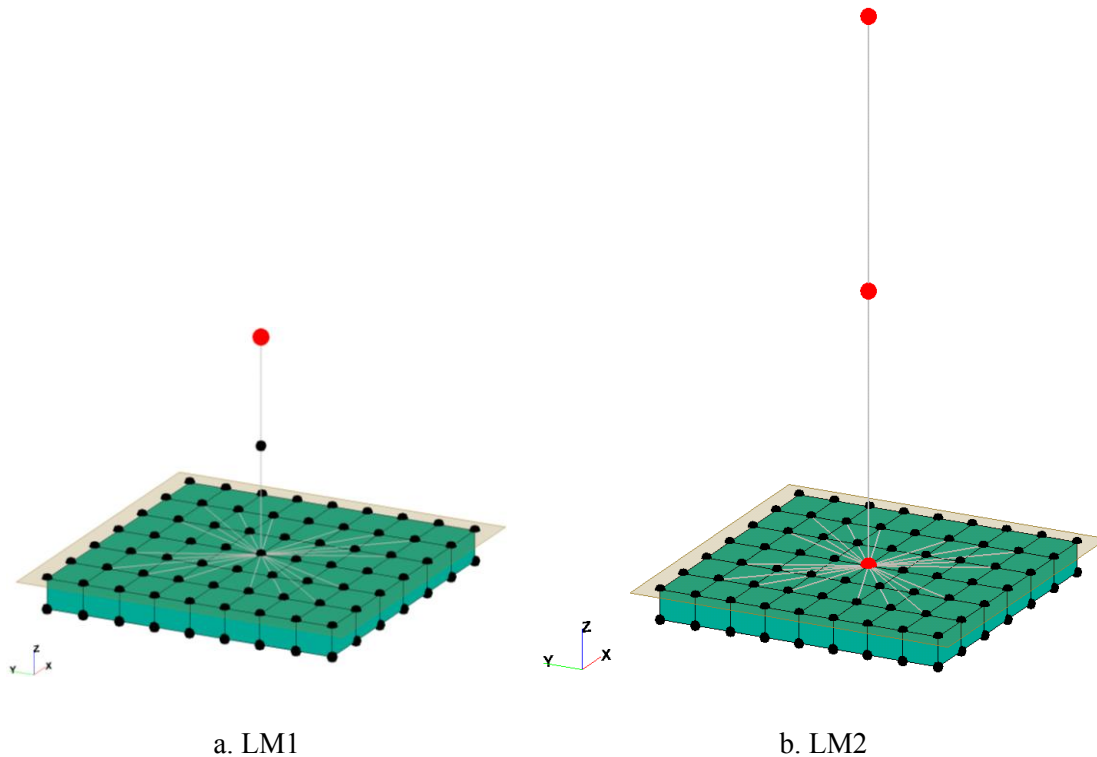


Figure 5-2: SASSI finite element models of LM1 and LM2

5.2.3 Modeling in LS-DYNA using the direct method and the effective seismic input method

General modeling procedures for the LS-DYNA direct method as well as the effective seismic input method are explained in Section 3.2 and the details corresponding to the SSI modeling of LM1 and LM2 are presented in this section.

The basemat and the superstructure in LS-DYNA are modeled using eight-noded brick elements and two-noded beam elements, respectively. The beams elements are of the Belytschko-Schwer resultant type (LSTC, 2013), with the input properties presented in Table 5-1. Lumped masses specified in Table 5-1 are assigned to the superstructure beam element nodes. A rigid connection between the superstructure and the basemat is modeled using the `*CONSTRAINED_NODAL_RIGID_BODY` option, which creates a rigid connection between a specified set of nodes. Figure 5-3 presents the finite element models of LM1 and LM2. The contact interface between the soil and the basemat is modeled differently for the rigid basemat and the flexible basemat cases. When the basemat is flexible, the time-step of the analysis is controlled by the solid elements of the basemat. This time-step can be much smaller than the time-step corresponding to the soil elements and can therefore significantly increase the analysis time. In order to have a larger time-step (and a smaller analysis time) the basemat is meshed to be considerably coarser

than the surrounding soil. Therefore, the basemat-soil interface in this case is created using the *CONTACT_TIED_SURFACE_TO_SURFACE option available in LS-DYNA. This ties the soil to the basemat allowing no separation at the basemat-soil interface. For the rigid basemat, the rigid elements are not included in the time-step calculation, and therefore the basemat is meshed identically to the surrounding soil to avoid the use of contact elements.

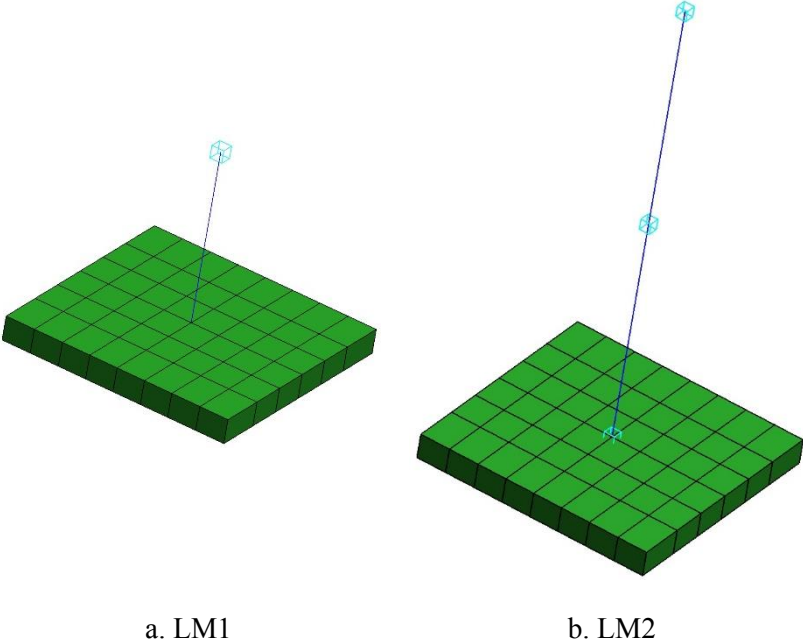


Figure 5-3: LS-DYNA finite element models of LM1 (left) and LM2 (right)

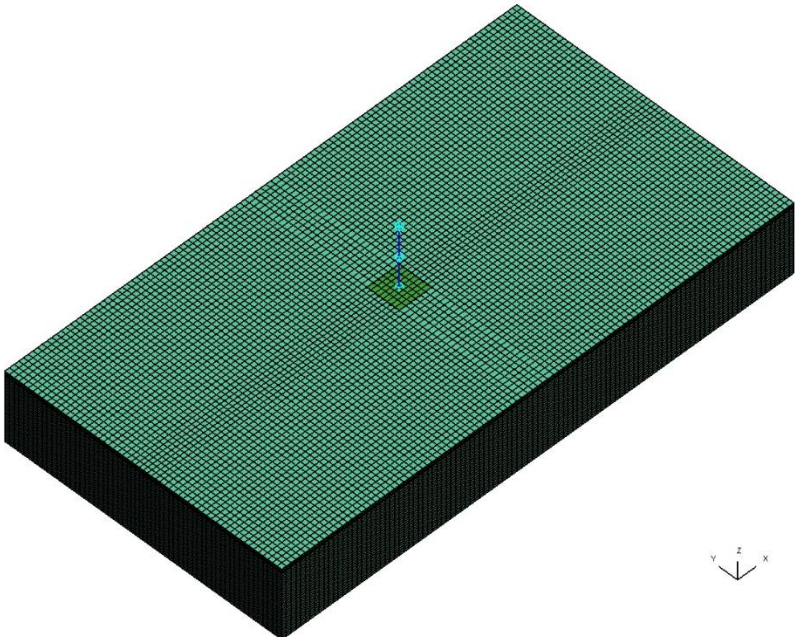


Figure 5-4: LS-DYNA finite element model for SSI analysis of LM2 using the direct method

A soil domain of size 219m × 118m (219m in the shaking direction, X) in plan and 29.47m deep, comprising eight-noded solid elements, is built for analysis using the direct method in LS-DYNA. No transmitting boundary is employed at the boundaries of the soil domain. Instead, the soil domain is made large enough such that the scattered waves are almost damped before reaching the boundaries. The lateral boundaries are constrained in such a way that the perimeter nodes at each elevation move together in the horizontal direction (see Section 3.2.2), creating a ‘free-field’ condition at the boundaries. The adequacy of the soil domain size is checked by comparing the surface free-field ground motion in a soil-structure interaction analysis to the free-field surface ground motion calculated using a separate one-dimensional site-response analysis performed in LS-DYNA. Section 5.2.4.1 presents the results for these analyses and demonstrates that the soil domain is large enough for linear elastic SSI analyses. The input ground motion is applied directly at the base of the soil profile as an acceleration input. This method of input is consistent with the rigid bedrock assumption made for the analyses in this section. Elastic material is modeled using the *MAT_ELASTIC material model with an elastic modulus of 1.085×10^8 Pa, which is equivalent⁸ to the shear wave velocity and Poisson’s ratio specified in Section 5.2.1. Damping is modeled using the *DAMPING_FREQUENCY_RANGE_DEFORM option, which provides an approximately frequency-independent damping in a given frequency range. A damping ratio of 0.02 is specified in the frequency range of 1 to 25 Hz, which is adequate for the analyses presented in this section.

The effective seismic input method involves an initial site-response analysis that calculates the input forces for a subsequent SSI analysis. These forces are input at boundary of the near-field soil (refer to Section 3.3.2.2 for description of the effective seismic input method in LS-DYNA) for an SSI analysis. The site-response model and the SSI model used in the effective seismic input method are presented in Figure 5-5. In the SSI model, the basemat is indicated in green, the near-field soil is indicated in light green, the far-field soil is indicated navy blue, and the PML material at the boundaries is indicated in orange. The basemat-soil interface is modeled as in the direct method. A damping ratio of 0.02 is also applied to the soil and the structure as in the direct method.

⁸ The elastic modulus is slightly decreased to account for the stiffening by the *DAMPING_FREQUENCY_RANGE_DEFORM.

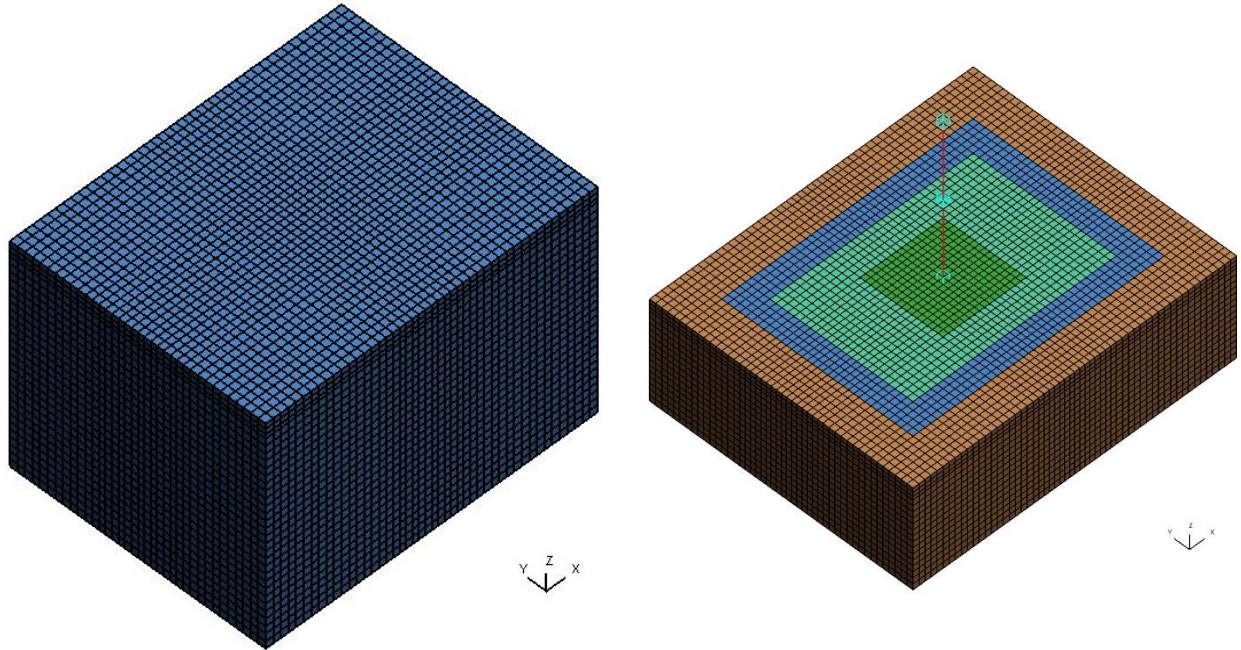


Figure 5-5: LS-DYNA finite element models for the effective seismic input method: site-response analysis (left) and SSI analysis (right)

In the vertical direction the element sizes in the soil domain of the direct method and the effective seismic input method are identical. This element size is limited to 1m, which allows the propagation of frequencies up to 15Hz for the shear wave velocity of 164.59 m/s when a value 10 is used for n in equation (4-1) (refer to Section 4.4.2 for a description of the site layering procedure). This maximum frequency of propagation is adequate for the analyses presented in this section.

5.2.4 Analysis results and comparison between SASSI and LS-DYNA

5.2.4.1 Free-field response

The free-field response of the soil domain to the Ormsby wavelet, calculated using SASSI, LS-DYNA one-dimensional site-response analysis, and the LS-DYNA SSI analysis, is presented in Figure 5-6. The left panel presents 1% damped response spectra, and the right panel presents the Fourier transforms of the acceleration at the surface of the soil domain. The figure clearly shows that the free-field responses calculated from the two programs are almost identical. Small differences in the peak amplitudes exist due to the differences in the damping formulations adopted in the two programs. While SASSI uses a formulation that models a truly frequency-independent damping ratio, the damping formulation used in LS-DYNA only models an approximately frequency-independent damping ratio. Additionally the LS-DYNA formulation results in a small increase the stiffness of the model, which is

compensated by a reduction in the elastic stiffness of the materials as recommended in the LS-DYNA keyword manual (LSTC, 2013). This compensation can also result in the differences in the SASSI and LS-DYNA responses. A notable feature of these results, however, is the peaks in the response spectra and the Fourier transforms. These peaks correspond to the natural frequencies of the soil profile, which can be calculated using the expression, $(2n-1)V_s/4H$, where n is the vibration mode number, V_s is the shear wave velocity of the material, and H is the total depth of the soil profile (Kramer, 1996). The peaks in the Fourier transforms presented in Figure 5-6 show that the vibration modes occur at 1.4Hz, 4.2Hz, 7Hz, 9.8Hz, and so on. These frequencies are identical to those calculated analytically using the above expression.

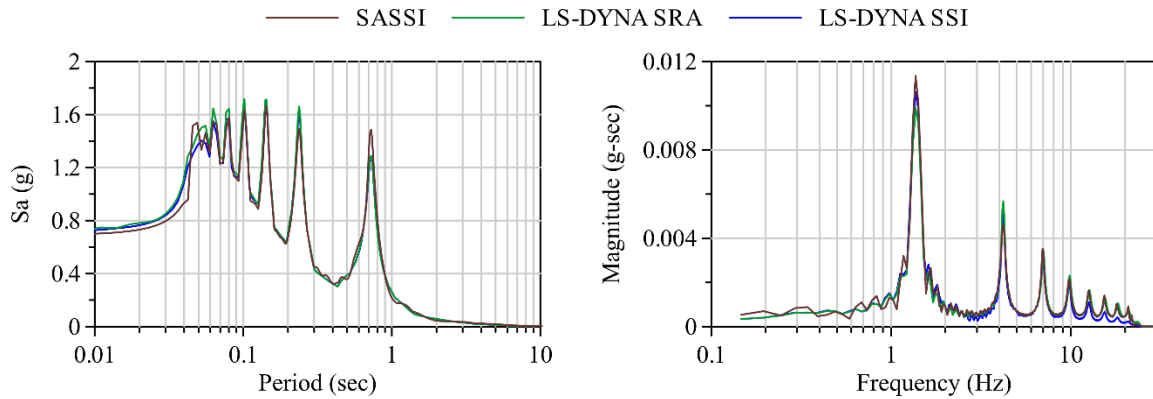


Figure 5-6: 1% damped acceleration response spectra (left) and Fourier transforms of the surface free-field accelerations computed using site-response analysis and the SSI analysis for LM2

5.2.4.2 Fixed-base responses

Figure 5-7 presents 1% damped response spectra of the horizontal acceleration at the roof of the fixed-base models of LM1 and LM2 calculated using SASSI and LS-DYNA. These response spectra are almost identical, indicating that the fixed-base models of the structures in SASSI and LS-DYNA are equivalent. Slight differences in the peak spectral accelerations exist, and are unavoidable given the difference in the damping formulations used in the programs as explained in Section 5.2.4.1. The figure shows that LM1 and LM2 have fixed base time periods of 0.23 sec and 0.14 sec, respectively.

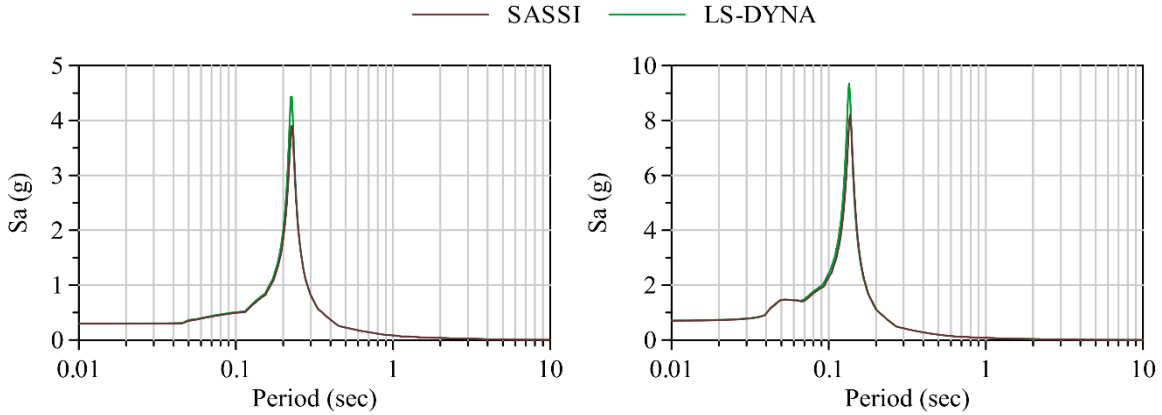


Figure 5-7: Response spectra for 1% damping of the roof accelerations of the fixed-base models of LM1 (left) and LM2 (right) calculated using SASSI and LS-DYNA

5.2.4.3 Response of the basemat alone

Figure 5-8 below presents the 1% damped response spectra of the horizontal and vertical accelerations of the basemat. The figure shows that the horizontal acceleration responses calculated from the different programs are almost identical, but small differences exist between the vertical acceleration spectra. The differences between the vertical accelerations can be attributed to the damping formulations as described in 5.2.4.1. The peaks in the response spectra and the Fourier transforms correspond to the vibration modes of the soil profile.

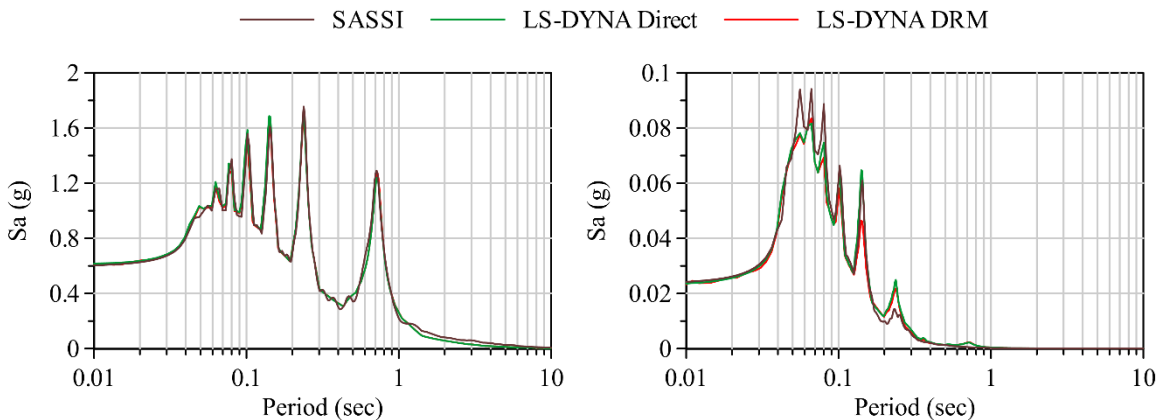


Figure 5-8: Response spectra for 1% damping of the horizontal acceleration at center of the basemat (left) and the vertical acceleration at the edge of the basemat (right) for SSI analysis of the rigid basemat alone

5.2.4.4 Response of LM1 with SSI effects

Figure 5-9 presents 1% damped amplification spectra of the horizontal acceleration at the roof of LM1 from the surface free field of the soil for three cases: rigid structure on a rigid basemat, flexible structure on a rigid basemat, and flexible structure on a flexible basemat. For each case, the amplification is calculated using SASSI, LS-DYNA direct method and LS-DYNA DRM.

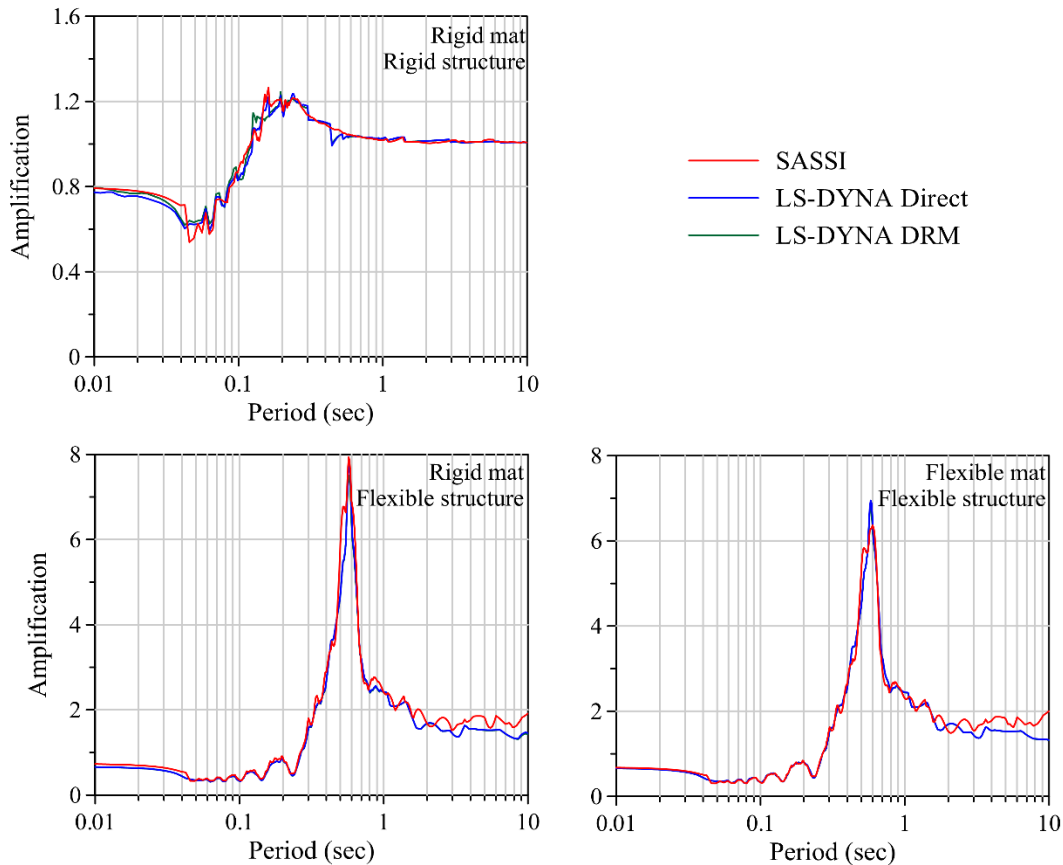


Figure 5-9: Acceleration amplification spectra from the surface free field of the soil to the roof of LM1

The figure shows that the amplification spectra calculated using the three methods are almost identical for all cases. Notably, the responses calculated using the direct method and DRM in LS-DYNA overlap, indicating that the methods are equivalent for LM1. A comparison of the responses in the lower two panels of the figure indicates that including the flexibility of the basemat decreases the peak structural amplification for LM1. Figure 5-9 also shows that the flexible-base period of LM1 is about 0.6 sec, which is much greater than the fixed-base period of 0.23 sec, indicating period lengthening due to SSI effects.

Figure 5-10 presents a deconstruction of the roof accelerations of LM1 for each analysis case into 1) acceleration relative to the basemat, 2) acceleration due to rocking of the basemat, and 3) acceleration due to structural deformations. One percent damped response spectra for these components are presented. Since the direct method and DRM produce identical results, the deconstruction is presented only for SASSI and the LS-DYNA direct method. The three rows in Figure 5-10 correspond to the three analysis cases.

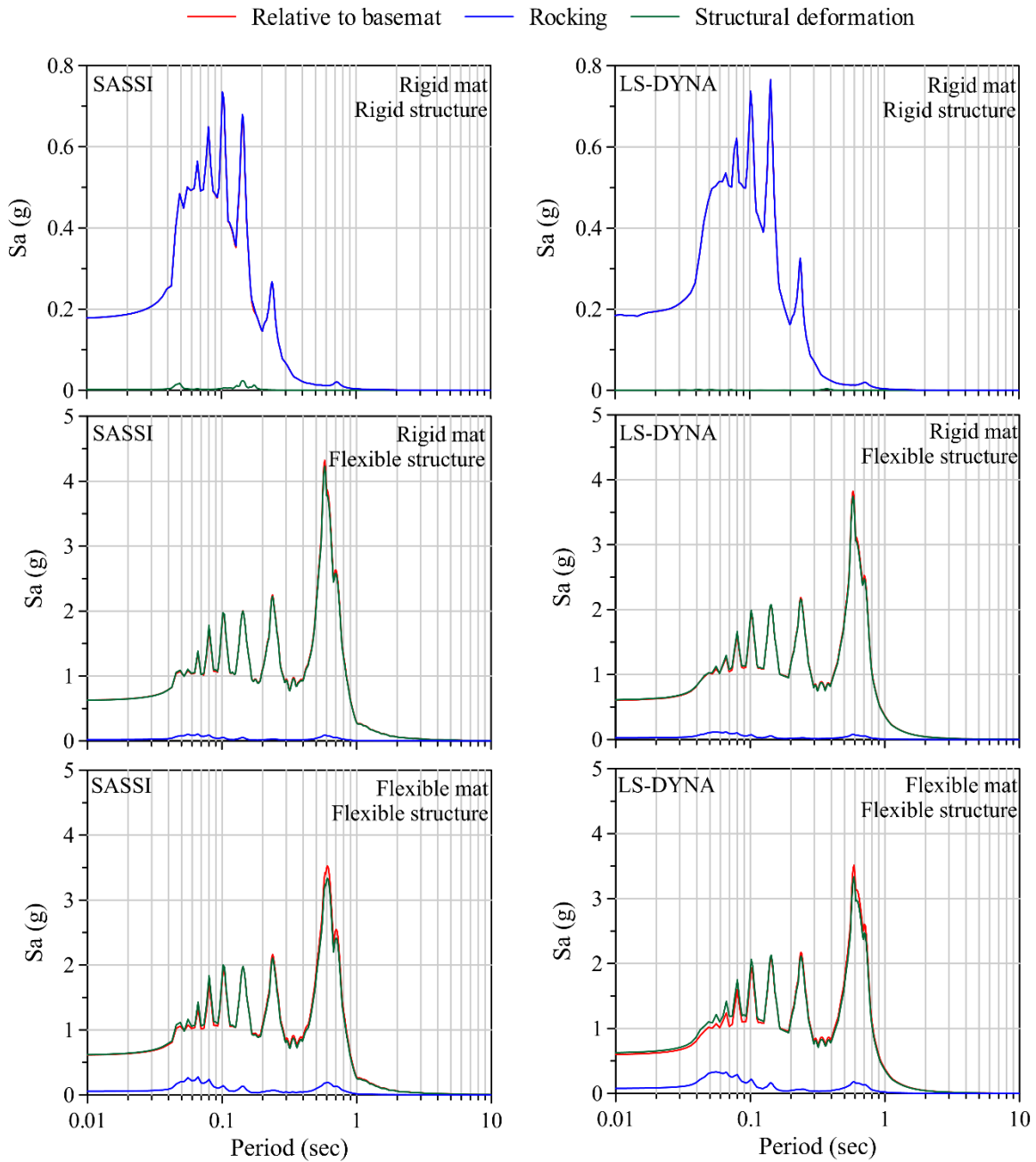


Figure 5-10: Deconstruction of the horizontal roof accelerations of LM1 subjected to the Ormsby wavelet

The figure shows that the rocking component clearly dominates the response when the superstructure is rigid (top row), and the structural deformations are negligible. In contrast, for the flexible structure cases (middle and bottom rows), the structural deformations dominate the response of LM1 and the rocking response is negligible, indicating that the SSI effects in LM1 are minimal. A comparison of the responses in the middle panel and the bottom panel shows that the flexibility of the basemat has a small, but measurable, effect on the rocking accelerations and structural deformations. It can be seen that the flexibility of the basemat slightly increases the rocking acceleration and decreases the accelerations from structural deformations in the first mode. A comparison of the SASSI (left panels) and LS-DYNA (right panels) results shows minor differences in the peak spectral accelerations in all cases. These differences can be attributed to the material damping formulations in the programs, as discussed in Section 5.2.4.1.

5.2.4.5 Response of LM2 with SSI effects

Figure 5-11 presents 1% damped amplification spectra of the horizontal acceleration at the roof of structure LM2 from the surface free field of the soil for the three analysis cases. For each case, the acceleration is calculated using SASSI, LS-DYNA direct method and LS-DYNA DRM. The top panel of the figure shows that spectral amplifications are almost identical for the analysis case with a rigid structure on a rigid basemat. However the bottom two panels show that the peak amplifications calculated using SASSI are considerably larger than those calculated using LS-DYNA. These differences are larger than those seen for LM1. This, again, can be attributed to the damping formulations of the two programs, and specifically to the fact that the damping ratio in LS-DYNA is not truly frequency-independent. The responses calculated using the LS-DYNA direct and DRM are almost identical for all cases, which is also observed in LM1. This indicates that the methods are equivalent for the structures considered in this section. In contrast with LM1, accounting for the basemat flexibility slightly increases the peak structural amplifications, indicating that the impact of basemat flexibility on the structural response depends on the flexible-base period of the structure. Figure 5-11 also shows that the flexible-base period of LM2 is about 0.42 sec, which is much longer than the fixed-base period of 0.14 sec indicating significant period lengthening due to SSI effects.

Figure 5-12 presents a similar deconstruction of the roof accelerations as in Figure 5-10, but for the responses of LM2. The three rows in Figure 5-12 correspond to the three analysis cases. Similar to LM1, the rocking component dominates the response when the structure is rigid, and the structural accelerations are almost zero. The absence of structural deformations in this case verifies the rigidity of the structure-basemat connection. Unlike the response of LM1, the rocking component dominates the

response of LM2 even when the superstructure is flexible, as seen from the middle and bottom rows of Figure 5-12. This is due to the much higher stiffness of LM2 in the shaking direction. Additionally a comparison of the responses in the second and third rows shows that the basemat flexibility has only a minor effect on the rocking as well as the structural deformation components. A comparison of the SASSI (left panels) and LS-DYNA (right panels) results shows minor differences in the peak spectral accelerations in all cases. These differences can be attributed to the material damping formulations in the programs, as discussed in Section 5.2.4.1.

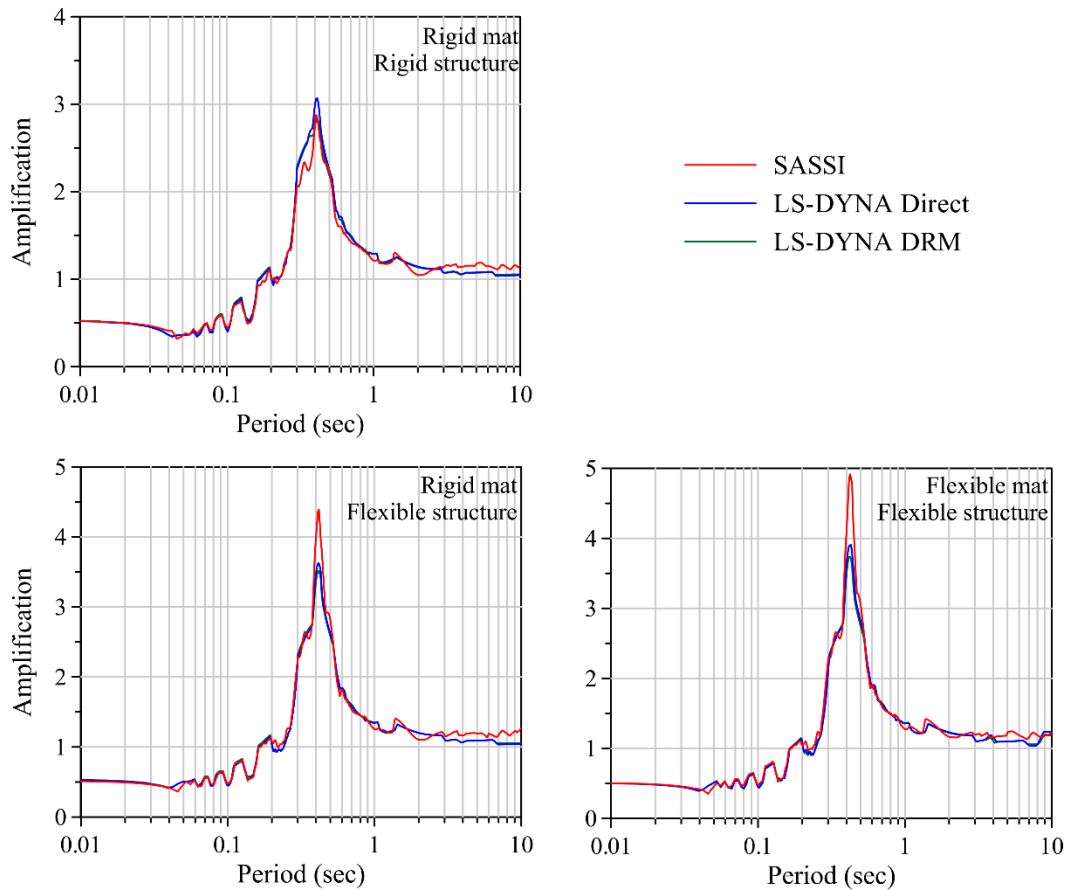


Figure 5-11: Acceleration amplification spectra from the surface free field of the soil to the roof of LM2

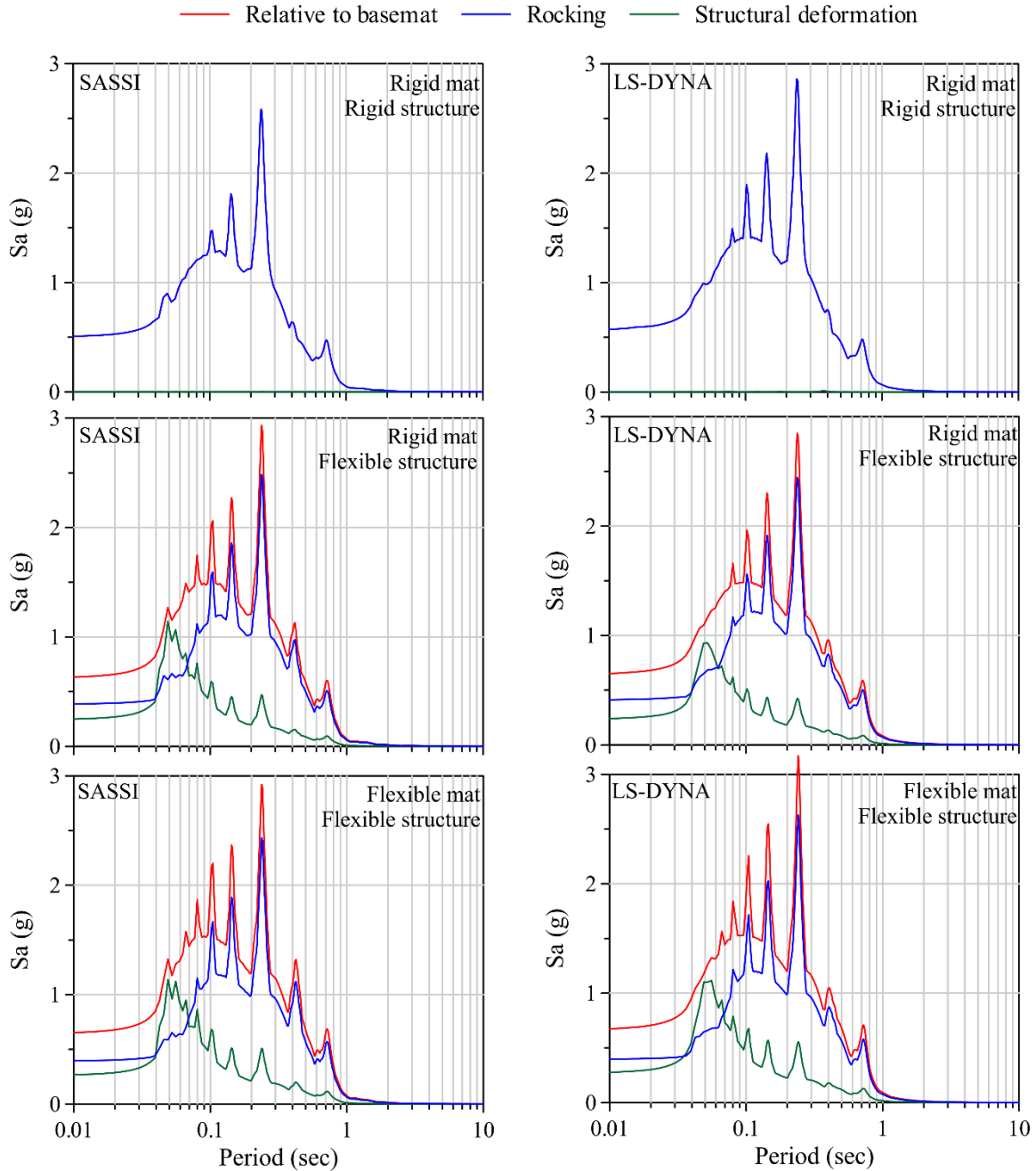


Figure 5-12: Deconstruction of the horizontal roof accelerations of LM2 subjected to the Ormsby wavelet

5.2.5 Observations

The following observations can be made from the linear elastic analyses presented in this section:

1. The free-field soil responses calculated using SASSI and LS-DYNA are almost identical, with small differences in the peak spectral accelerations. This is due to the difference in the damping

formulations of the two programs, as well as errors in the adjustment of the elastic modulus in LS-DYNA, which is required for the *DAMPING_FREQUENCY_RANGE_DEFORM option.

2. Analysis of the fixed-base models in SASSI and LS-DYNA result in almost identical responses indicating that the models are equivalent. Small differences in the responses result from the difference in the damping formulations.
3. The structural responses calculated from the LS-DYNA direct method and DRM are essentially identical for both LM1 and LM2 in all cases. The methods are equivalent for elastic SSI analyses.
4. Basemat flexibility has a small but measurable effect on the overall response of LM1 and LM2. For LM1, accounting for basemat flexibility decreases the peak spectral amplification at the roof, whereas it increases for LM2. This indicates that the effect of basemat flexibility depends on the flexible-base time period of the structure.
5. SASSI and LS-DYNA produce very similar responses for both structures for the cases considered in this section. Small differences in the peak spectral amplifications at the roof are attributed to differences in the damping formulations in the programs. The programs also produce almost identical responses for the rocking, and structural deformation components of the response. This verifies that the SSI analysis programs SASSI and LS-DYNA are equivalent in the linear elastic range.
6. The analysis times for SASSI, LS-DYNA direct method, and LS-DYNA DRM are summarized in Table 5-2. SSI analysis in SASSI is faster than both the LS-DYNA direct method and the DRM.
7. The LS-DYNA DRM uses a smaller soil domain than the direct method and so is faster for all the analysis cases. The DRM and the direct method results are identical.

Table 5-2: Analysis time in minutes for elastic SSI analyses of LM2 subjected to the Ormsby wavelet

	Analysis case		
	Rigid basemat Rigid structure	Rigid basemat Flexible structure	Flexible basemat Flexible structure
SASSI	0.5	0.5	1.0
LS-DYNA Direct	6.5	31.5	127.1
LS-DYNA DRM	6.1	27.5	29

5.3 Calculation of nonlinear SSI responses using SASSI and LS-DYNA

Nonlinear SSI responses calculated using SASSI and LS-DYNA are compared in this section. The comparisons are made for the building models, MS1F_2 and MS2F, considered in the City Block project. The soil profile used in the City Block project is adopted for the analyses of this section. The numerical models of the soil profile and the buildings are presented in Section 7.3 and Section 7.4, respectively. MS1F_2 is a one-story moment-frame structure based on spread footings, and MS2F is a two-story shear wall structure founded on a basemat. The design of the models MS1F_2 and MS2F are based on realistic superstructure and foundation designs, and using these models for the numerical analyses presented in this will provide an insight into nonlinear SSI effects in buildings commonly encountered in practice. This section only considers SSI effects in the standalone structures (no SSSI). No comparison is made with experimental results in this section. The ground motions used for the SSI analyses of the City Block project are also used for the analyses of this section. These ground motions, identified as JOS_L, LCN, SCS_H and PRI_H, are presented in Figure 7-2 and Figure 7-3 using 5% damped acceleration response spectra and acceleration time series, respectively.

The SASSI and LS-DYNA responses of MS1F_2 and MS2F are compared for two cases: 1) linear elastic analyses in both SASSI and LS-DYNA using strain-compatible shear moduli and 2% damping ratio for the soil, and 2) equivalent-linear analyses in SASSI using strain-compatible shear moduli and damping for the soil, and nonlinear analyses in LS-DYNA. Analyses for the former case are performed for the low-intensity ground motion, JOS_L. Analyses for the latter case are performed for all four ground motions. The analyses in the latter case are also performed for MS1F_2 equipped with rigid grade beams to demonstrate the effect of restraining the rocking of footings.

5.3.1 Superstructure and soil modeling

The numerical models of the soil profile, as well as of the structures MS1F_2 and MS2F, in SASSI and LS-DYNA are described in detail in Sections 7.3 and 7.4, and are briefly described here. Since SASSI is a linear analysis program, the soil profile in SASSI is modeled using strain-compatible properties that approximate the nonlinear soil response. These properties are dependent on the ground motion input and are calculated using the site-response analysis program, SHAKE, for each ground motion. The strain-compatible properties for the ground motions considered in this section are presented in Figure 7-9. The process of calculating the strain-compatible properties in SHAKE, and the soil profile modeling in SASSI are presented in Section 7.3.2 and Section 7.4.1, respectively. The SASSI numerical models of MS1F_2 and MS2F are presented in Section 7.4.1. For the equivalent-linear case, the soil material in LS-DYNA is modeled using the *MAT_ELASTIC model with strain-compatible moduli. For

the nonlinear analyses, the soil is modeled using the *MAT_HYSTERETIC material model. Damping is modeled using the *DAMPING_FREQUENCY_RANGE_DEFORM option for both the equivalent-linear and nonlinear analyses. This option is used in nonlinear analyses to model only the low-strain damping in the soil domain and structural damping. Soil damping in a nonlinear analysis is primarily achieved through the hysteretic response of the soil. The footings of MS1F_2, and the basemat of MS2F are modeled as rigid, for the reasons given in Section 7.4.2. The foundation-soil interface in LS-DYNA is modeled as 1) a ‘tied’ interface with no loss of contact between the soil and the foundation, and 2) a more realistic interface that allows for loss of contact between the soil and the foundation, resulting in sliding and gapping. The tied interface is modeled using the *CONSTRAINED_EXTRA_NODES option, which constrains the soil nodes at the soil-foundation interface to move along with the rigid foundation. If the foundation is flexible, the contact model, *CONTACT_TIED_SURFACE_TO_SURFACE, should be employed. To allow separation at the foundation-soil interface, the *CONTACT_AUTOMATIC_SURFACE_TO_SURFACE option, which is also used in the City Block simulations described in Section 7.4. Further details regarding the LS-DYNA numerical models of the soil profile, and the structures MS1F_2 and MS2F, are presented in Section 7.4.

5.3.2 Analysis results and comparison

Nonlinear behavior in a soil-structure system can be classified into 1) nonlinear site response (primary nonlinearities), which results in differences in the free-field soil response and therefore the foundation-level input to the structures, and 2) nonlinear behavior at the foundation (soil hysteresis, gapping, sliding) and nonlinear structural behavior (secondary nonlinearities). Although SASSI can approximately account for the primary nonlinearities when strain-compatible soil properties are used, it cannot directly account for secondary nonlinearities. LS-DYNA can directly account for all the nonlinear behavior in the soil-structure system. For a linear model, the responses calculated using SASSI and LS-DYNA should be very close, as seen in Section 5.2. However, differences can be expected between the nonlinear responses calculated using SASSI and LS-DYNA, even when identical material properties are used. These differences primarily arise from the extent of nonlinear behavior captured by the two programs. As seen in the site-response comparisons presented in Section 4, it is expected that the SASSI and LS-DYNA responses are increasingly different as the response of the system is more nonlinear.

The differences in the total acceleration at the roof of a structure calculated using SASSI and LS-DYNA reflect both the primary and secondary nonlinearities in the soil-structure system. Primary nonlinearities are investigated in Section 4 through an assessment of site-response analysis programs. To address secondary nonlinearities, which is the focus of this section, the roof accelerations relative to base are considered, which do not include the free-field acceleration. Therefore the roof acceleration of

MS1F_2 is calculated in terms of 1) acceleration relative to the base (one of the footings), and 2) total acceleration. Similarly, since MS2F predominantly responds in the rocking mode, the roof acceleration of this structure is calculated in terms of 1) acceleration due to rocking, and 2) total acceleration. The former component in the roof acceleration in both the structures is assumed to be primarily influenced by secondary nonlinearities. The usage of contact models in LS-DYNA introduces high-frequency noise in the acceleration response of the structures. Therefore all the LS-DYNA acceleration responses are filtered using a low-pass filter with a cut-off frequency of 10 Hz. Since the anticipated flexible-base frequencies of the structures, and the fundamental frequency of the soil profile (all around 1.7 Hz) are much smaller than 10 Hz, this cut-off frequency is deemed appropriate for the analyses presented in this section. The following sections present the responses of MS1F_2 and MS2F for various cases and compare the responses calculated using SASSI and LS-DYNA.

5.3.2.1 MS1F_2

Before comparing the equivalent-linear response in SASSI and the nonlinear response in LS-DYNA, a linear elastic analysis is performed using strain-compatible moduli and 2% damping ratio in both the programs, and for the JOS_L ground motion input. Figure 5-13 presents the 5% damped response spectra of the accelerations relative to the base, and the total accelerations at the roof of MS1F_2 for this linear elastic analysis. The figure shows that the results are almost identical, demonstrating the equivalency of the SASSI and LS-DYNA SSI models of MS1F_2 in the linear domain.

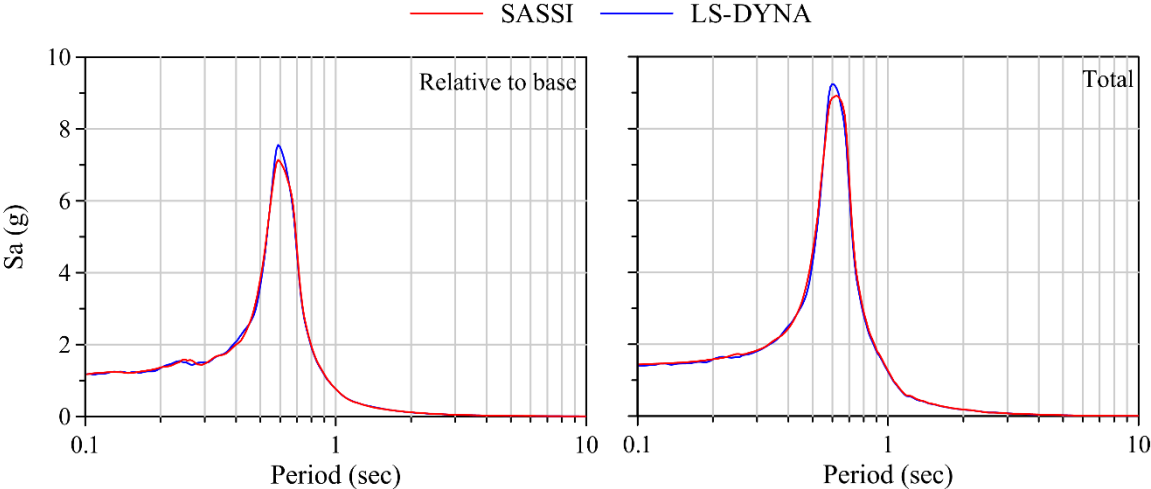


Figure 5-13: Acceleration response spectra at the roof of MS1F_2 subjected to the JOS_L ground motion for the preliminary linear analysis

Nonlinear SSI response of MS1F_2 is calculated by changing the material properties in the linear models of SASSI and LS-DYNA, and modeling the foundation-soil interface in LS-DYNA using the appropriate contact models. The equivalent-linear, strain-compatible moduli and damping ratios are used in SASSI, and the nonlinear hysteretic material model, *MAT_HYSTERETIC, is used in LS-DYNA to model the soil.

The analysis results for the four ground motions are presented in Figure 5-14. In this figure 'LS-DYNA (tied)' and 'LS-DYNA (separation allowed)' represent the two foundation-soil interface conditions mentioned previously. Contrary to the results of the linear analysis in Figure 5-13, this figure shows significant differences in the SASSI and LS-DYNA results for both relative and total acceleration responses. The differences are significant even for the JOS_L ground motion, which results in similar free-field accelerations in SASSI and LS-DYNA (see Section 7.3.4 for free-field responses). The peaks in the relative acceleration spectra calculated using LS-DYNA (separation allowed) occur at longer periods than those calculated using SASSI, indicating that the differences arise from increased flexibility either at the foundation or in the superstructure, due to nonlinear behavior. Since the fuses of MS1F_2 did not yield for the first three ground motions, the differences in the structural responses are attributed to nonlinear behavior in the soil near the footings. This hypothesis is confirmed by performing a separate nonlinear analysis in LS-DYNA, with the soil in the vicinity of the footings modeled with linear elastic material, and with a tied foundation condition. Figure 5-15 presents the results of this analysis as well as the results for the SASSI analysis for the JOS_L ground motion.

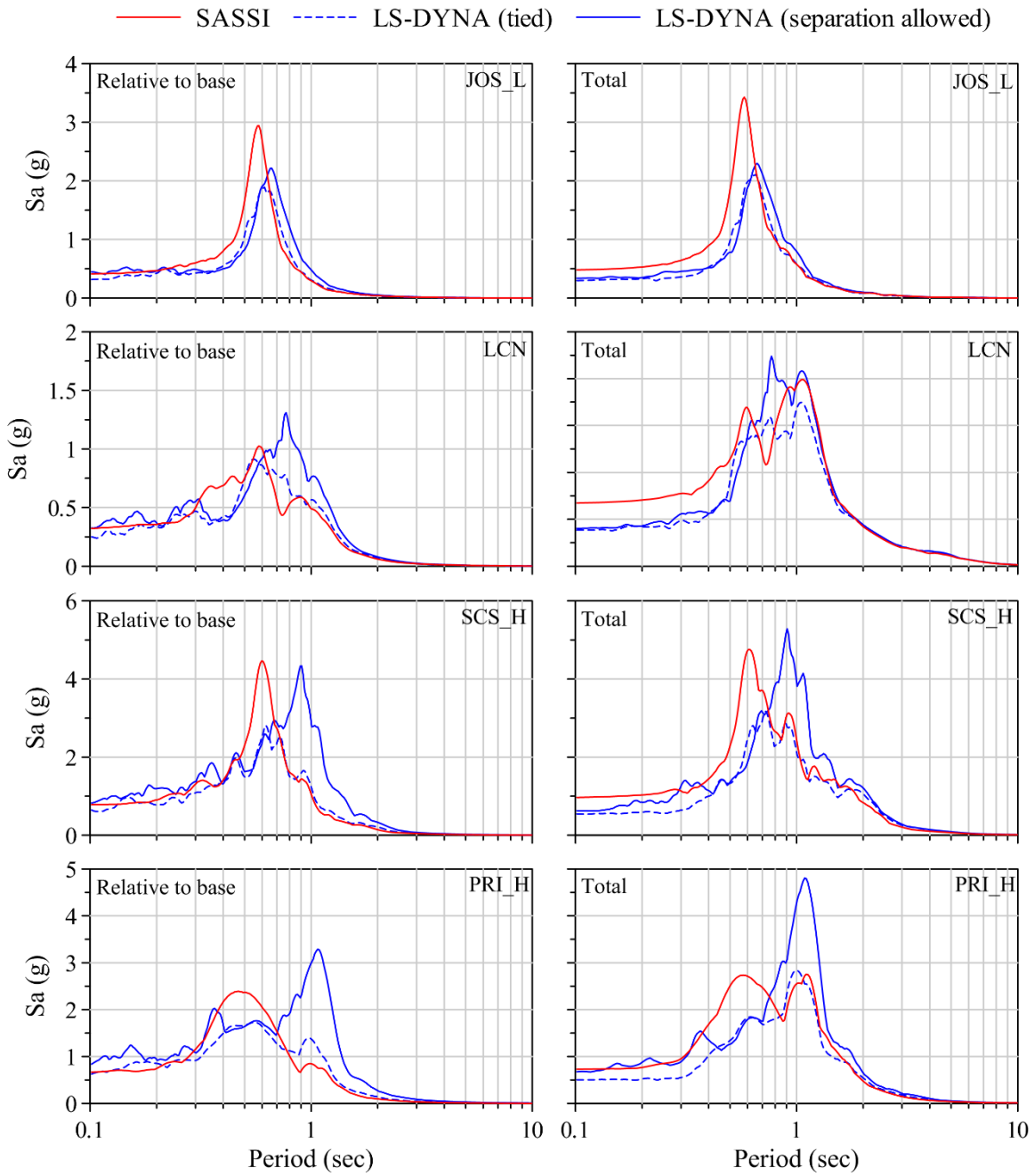


Figure 5-14: Acceleration response spectra at the roof of MS1F_2 calculated using strain-compatible soil properties in SASSI, and nonlinear soil properties in LS-DYNA

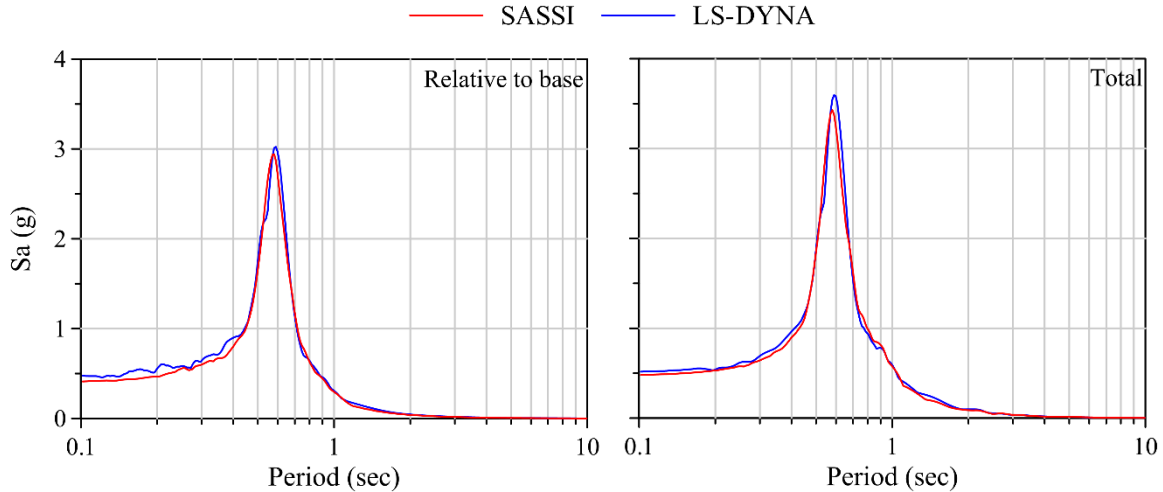


Figure 5-15: 5% damped acceleration response spectra at the roof of MS1F_2 subjected to the JOS_L ground motion calculated using strain compatible soil properties in SASSI and nonlinear soil properties in LS-DYNA but ignoring nonlinear soil behavior at the vicinity of the footings

The SASSI and LS-DYNA responses shown in this figure virtually identical, and confirm that differences in the structural responses for the JOS_L ground motion in Figure 5-14 are due to nonlinear soil behavior in the vicinity of the footings. Figure 5-14 also shows that preventing separation at the foundation-soil interface in the LS-DYNA model by using a tied foundation condition significantly changes the response. Specifically, the peaks of the relative acceleration spectra occur at a shorter period (which is still longer than the period corresponding to the SASSI responses), and the amplitude of these peaks is smaller as compared with the LS-DYNA case that allows separation at the foundation. This indicates that a significant amount of nonlinear behavior at the foundation is due to the gapping and sliding of footings, and partly due to the hysteretic behavior of the soil. However, difference between the LS-DYNA results for the tied interface and the SASSI results indicates that the nonlinear response due to soil hysteresis is still significant. In summary, the results presented in Figure 5-14 show the significant impact of secondary nonlinearities, including sliding and gapping of the footings and hysteretic behavior of soil at the footing vicinity, on the MS1F_2 response. These nonlinearities result in larger peak spectral accelerations that occur at longer periods as compared with the equivalent-linear response.

Yielding of the beam fuses is observed in the LS-DYNA response to the PRI_H ground motion when separation at the foundation-soil interface is allowed. However, no yielding is observed in the corresponding LS-DYNA response for the tied foundation case, indicating that gapping and sliding of the footings result in increased ductility demands in the roof beams. No yielding is observed in the beams for

the other ground motions for both the LS-DYNA cases. SASSI cannot directly capture yielding in a superstructure.

5.3.2.2 MS1F_2 equipped with rigid grade beams

Considering the observed significance of footing displacement in the response of MS1F_2, the impact on the response of restraining the footings through grade beams is investigated in this section. Grade beams that connect the footings are used in practice to prevent the differential horizontal displacement of footings. Grade beams can also restrain the independent rocking of footings. Rigid grade beams are simulated in LS-DYNA by constraining all the rigid footings to move together, acting as a single rigid body. Rigid grade beams in SASSI are explicitly modeled as very stiff beams connecting the bases of the columns. Figure 5-16 presents the SASSI and LS-DYNA responses of MS1F_2 equipped with rigid grade beams. The LS-DYNA response accounts for separation at the foundation-soil interface. The results presented in this figure are markedly different from the responses of MS1F_2 without grade beams. Firstly, the responses calculated from SASSI and LS-DYNA for the modified structure with grade beams are much closer than those calculated for the original structure (Figure 5-14). This observation holds for both the relative accelerations and the total accelerations at the roof, and indicates that using grade beams reduces nonlinear behavior at the footings. Secondly, although the period of maximum spectral acceleration (relative to the base) remains almost unchanged for the SASSI responses, it decreases significantly for the LS-DYNA responses. Thirdly, the peak spectral accelerations of modified MS1F_2 are slightly smaller than those calculated for the original structure for all but the JOS_L ground motion. These differences are all primarily due to the reduced gapping and sliding of the footings when grade beams are used, which also leads to lesser hysteretic behavior in the soil at the vicinity of the footings. Figure 5-16 also shows a significant reduction in the peak spectral acceleration at the roof of the modified structure for the PRI_H ground motion. The SSI period of the original structure (about 1.2 sec) coincides with the spectral peak in the free-field response for this ground motion. Using grade beams reduces the SSI period to about 0.45 sec, and therefore reduces the peak spectral acceleration at the roof of the modified structure. No yielding is observed in the beams of MS1F_2 equipped with grade beams, even for the PRI_H ground motion. The grade beams prevent differential horizontal movement of the footings: footing spreading. The footings in the original structure slide and rock independently, resulting in footing spreading, which increases the bending moment in the beam fuses at the roof level. Grade beams restrict the footing spreading and result in smaller moment demands in the beams.

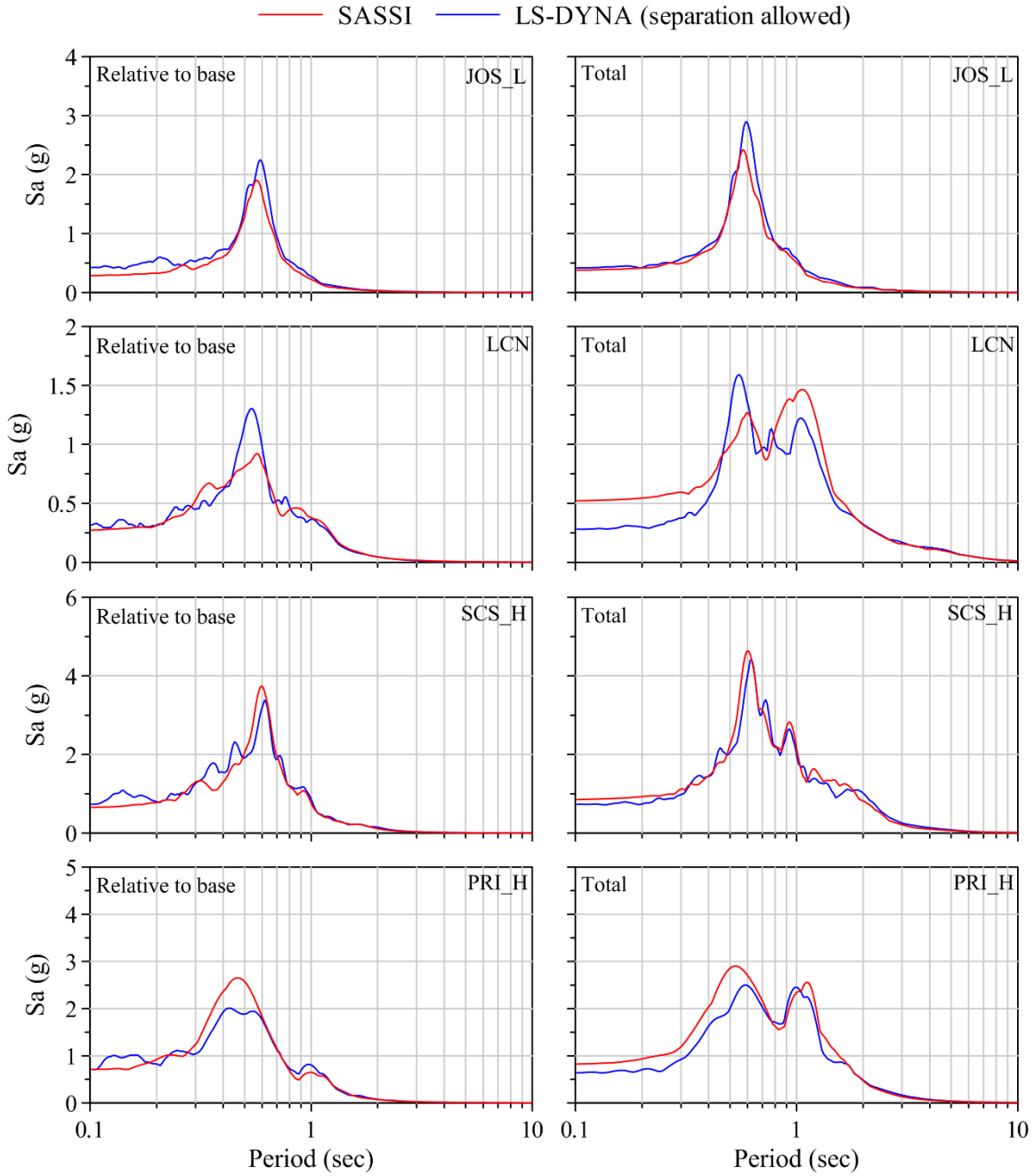


Figure 5-16: Acceleration response spectra at the roof of MS1F_2 equipped with grade beams, calculated using strain-compatible soil properties in SASSI, and nonlinear soil properties in LS-DYNA

Figure 5-17 presents the displacement of two adjacent footings along the X-direction for both the original and modified MS1F_2 subjected to the PRI_H ground motion. Footings 1 and 2 in the figure correspond to the left-hand side and right-hand side footings of the structure, when facing in the positive Y-direction. Footing 2 shows larger residual displacements than footing 1 for the original structure, indicating lateral spreading. The footings in modified MS1F_2 have identical displacements. Figure 5-18 presents screenshots of the deformed LS-DYNA models of the original and modified structures. The figure clearly shows the reduction in footing displacements when grade beams are used.

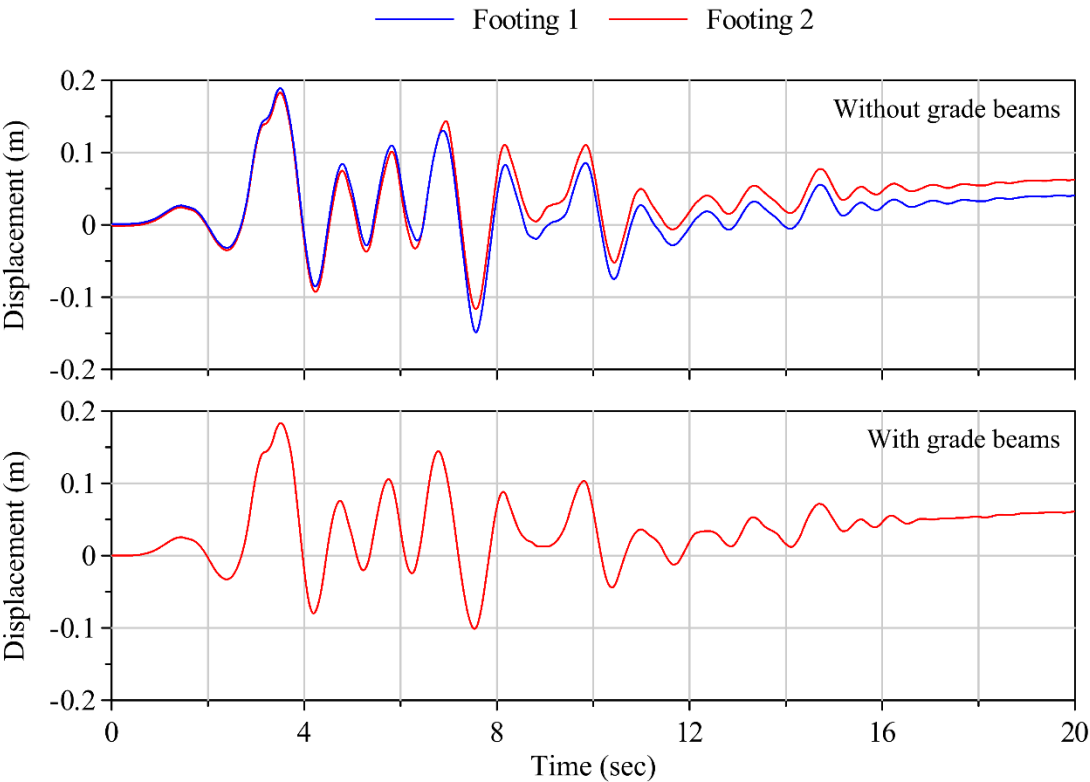
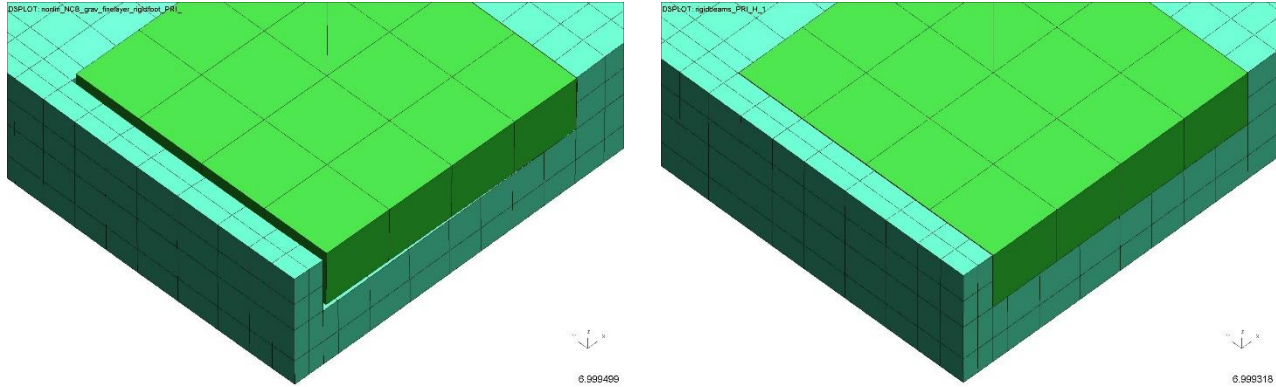


Figure 5-17: Time series of the horizontal displacement of two adjacent footings (along the X direction) of MS1F_2 for the PRI_H ground motion



a. original MS1F_2

b. MS1F_2 with grade beams

Figure 5-18: Screenshots of the deformation at the footings of the MS1F_2 for the PRI_H ground motion at about 7 sec

5.3.2.3 MS2F

Similar to MS1F_2, a linear elastic analysis is first performed for MS2F using strain-compatible moduli and 2% damping ratio for the soil in both SASSI and LS-DYNA. This linear elastic analysis is performed for the JOS_L ground motion only. Results for this analysis are presented in Figure 5-19.

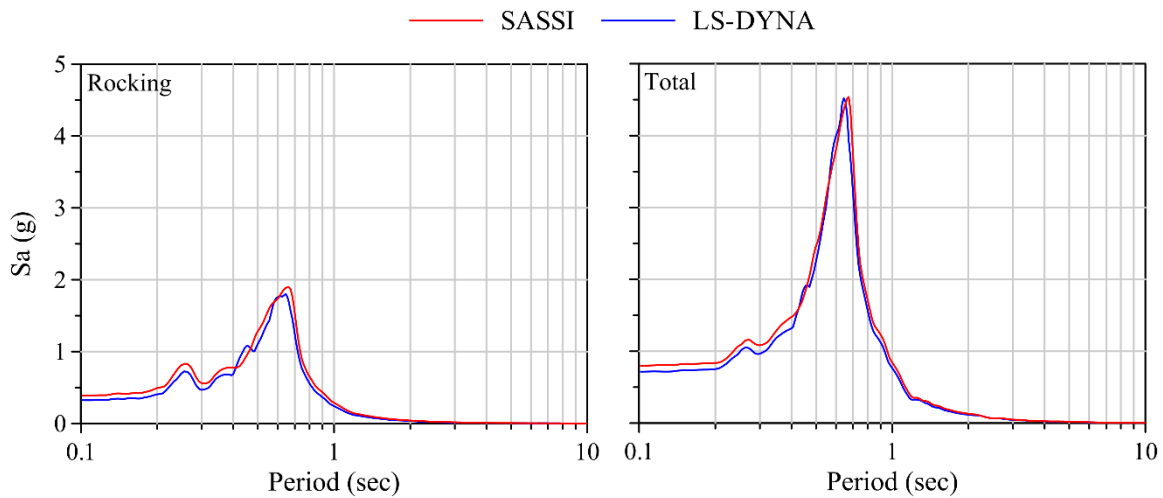


Figure 5-19: Acceleration response spectra at the roof of MS2F subjected to the JOS_L ground motion calculated using strain-compatible moduli and 2% damping ratio for the soil

The figure shows that the SASSI and LS-DYNA responses are very close, but not as close as the responses calculated for MS1F_2. This is because the rocking response of MS2F is particularly sensitive

to the layer thickness and properties in the vicinity of the foundation. Small differences exist between the thicknesses of the soil layers near the surface of the SASSI and LS-DYNA models. The LS-DYNA structural model is founded on a finely-meshed soil to account for the large strains expected in the nonlinear analysis. However the SASSI structural model is founded directly on the soil layers, which are not meshed with brick elements, unlike in LS-DYNA. The sensitivity of the MS2F response to the soil layer thicknesses and material properties is further examined in Section 5.4.4. The close match of the SASSI and LS-DYNA responses in Figure 5-19 still confirms that the corresponding numerical models are equivalent in the linear domain.

Following the verification of the numerical models for linear analysis, nonlinear analyses in LS-DYNA and equivalent-linear analyses in SASSI are performed for MS2F subjected to the four ground motions. Similar to MS1F_2, two contact models (tied and separation-allowed) are employed for the foundation-soil interface. Figure 5-20 presents the 5% damped response spectra of the roof accelerations (rocking accelerations in the left panels and total accelerations in the right panels) calculated using SASSI and LS-DYNA. The figure shows that the SASSI and LS-DYNA responses are closer than those calculated for MS1F_2 without grade beams. The LS-DYNA responses for the two contact conditions are also closer than those calculated for MS1F_2. There is a small increase in the peak spectral accelerations calculated using LS-DYNA when the foundation-soil interface enables separation. This increase is due to the sliding of the basemat from loss of contact with the surrounding soil. This increase is much smaller than that observed for MS1F_2 (without grade beams), indicating that the degree of sliding and gapping in MS2F is smaller. Figure 5-20 shows that although the SASSI and LS-DYNA responses are close for the JOS_L ground motion, the peak spectral responses of the total acceleration are smaller than those calculated using SASSI for the other three ground motions. This is primarily because of the underestimation of the free-field response by LS-DYNA as compared with SASSI as seen in Figure 7-8 (this figure presents the free-field responses calculated from SHAKE, which are generally identical to those calculated using SASSI). The peak spectral acceleration of the rocking response calculated using LS-DYNA is also slightly smaller than the corresponding SASSI response for the SCS_H and the PRI_H ground motions. This is because of the hysteretic response of the soil in the vicinity of the basemat (secondary nonlinearities) that involves softening of the soil and damping of the rocking response of MS2F. However the comparatively small difference between the SASSI and LS-DYNA responses for MS2F, as compared with MS1F_2, indicates that the secondary nonlinearities for the basemat are smaller than those observed for the footings.

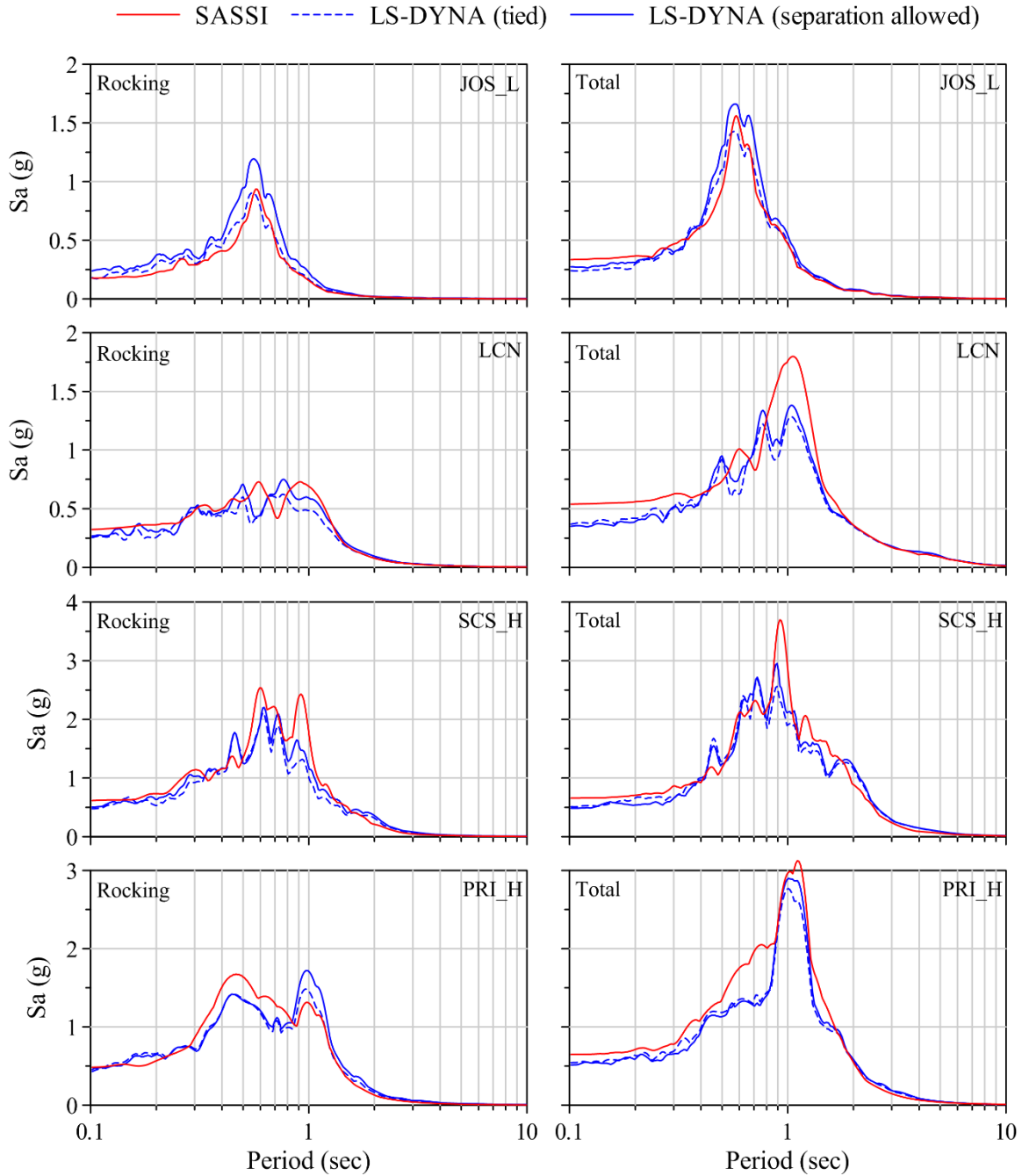


Figure 5-20: Acceleration response spectra at the roof of MS2F calculated using strain-compatible soil properties in SASSI, and nonlinear soil properties in LS-DYNA

Figure 5-21 presents the 5% damped spectral responses of the roof accelerations from structural deformation in MS2F. These accelerations are calculated by subtracting the rocking acceleration at the roof from the basemat input acceleration (horizontal acceleration at the center of the basemat). A comparison of the magnitude of spectral accelerations in this figure with those in Figure 5-20 shows that

the acceleration component from structural deformation is significantly smaller than the rocking acceleration for all ground motions. This is expected since MS2F is designed to primarily respond in the rocking mode. The figure also shows that the spectral accelerations calculated using LS-DYNA are much larger than those calculated using SASSI at periods shorter than the rocking period (~ 0.6 sec for JOS_L, and ~ 1 sec for the other ground motions). This is mainly due to the high-frequency (short period) noise introduced by the contact elements used in LS-DYNA. Since the fixed-base time period of MS2F (0.14 sec) is in the range of the frequencies corresponding to the noise, this high-frequency response is amplified in the structure. The difference between the amplitude of the short-period response calculated using the two contact models in LS-DYNA also indicates that this response might be a result of using contact elements. However since this component of the acceleration is negligible as compared with the rocking accelerations, the effects of these short-period components can be ignored for this structure.

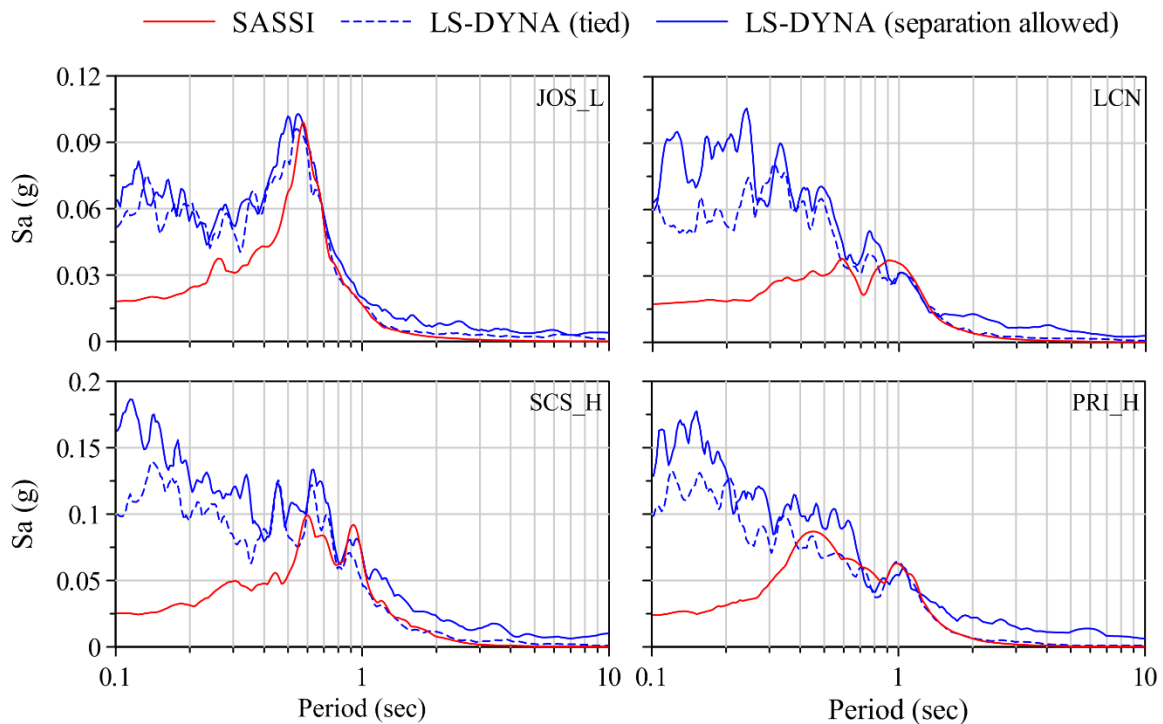


Figure 5-21: Response spectra of the accelerations from structural deformations calculated for MS2F using strain-compatible properties in SASSI and nonlinear properties in LS-DYNA

5.3.3 Observations

The following observations can be made from the equivalent-linear and nonlinear analyses presented in Section 5.3.2:

1. The responses calculated using SASSI and LS-DYNA for the linear analyses match very closely for both MS1F_2 and MS2F, indicating that the soil and structural models built in SASSI and LS-DYNA are equivalent in the linear domain.
2. Significant differences are seen in the equivalent-linear (SASSI) and nonlinear (LS-DYNA) responses of MS1F_2 even for the low-intensity ground motion, JOS_L. This is due to the highly nonlinear behavior of the soil in the vicinity of the footings (secondary nonlinearities).
3. Accounting for separation at the foundation-soil interface significantly increases the response of MS1F_2 due to the contribution from sliding and gapping of the footings. Neglecting footing sliding and gapping can result in unconservative estimates of demands for MS1F_2.
4. Restraining the rocking of the footings using rigid grade beams in MS1F_2 leads to a marked difference in response. The SASSI and LS-DYNA responses of modified MS1F_2 are much closer due to the significant reduction in the secondary nonlinearities.
5. Retrofitting MS1F_2 with rigid grade beams affects the yielding of the roof beams for the PRI_H ground motion. The grade beams compel the footings to respond together, preventing lateral spreading of the footings and reducing the moment demand in the beams.
6. The equivalent-linear (SASSI) and nonlinear (LS-DYNA) responses of MS2F are much less different than the responses calculated for MS1F_2 without grade beams. Most of the differences in the total response are attributed to the difference in the free-field input to the structure. Differences in the rocking responses are smaller, and are due to the nonlinear response of the soil in the vicinity of the basemat.
7. Accounting for sliding and gapping of the basemat slightly increases the peak spectral accelerations of MS2F. However this increase is much smaller than that observed for MS1F_2.
8. The secondary nonlinearities in MS2F are much less pronounced than those in MS1F_2 without grade beams.
9. The roof accelerations from structural deformation of MS2F calculated using LS-DYNA contains a significant contribution of short-period accelerations as compared with SASSI. This is due to the amplification of high-frequency noise (introduced by the contact models) by the superstructure.

5.4 Practical considerations for SSI analysis using SASSI and LS-DYNA

The process of comparing the SASSI and LS-DYNA responses in the linear and nonlinear domain revealed several challenges that could be faced by analysts performing SSI analyses using these programs. These challenges are unlikely to be identified if only one of the programs is used for the

analysis. To avoid these challenges some practical considerations are to be made while performing the SSI analyses. This section outlines these considerations for both SASSI and LS-DYNA.

5.4.1 Selection of analysis frequencies in SASSI

The SASSI input includes a set of frequencies at which the analysis is performed. The SASSI user manual (Ostadan, 2006b) mentions that a reasonable response can usually be achieved when 10 to 20 frequencies are used. Additionally, the manual recommends that these frequencies be chosen based on the peaks in the transfer functions observed in the fixed-base response of the structure. Figure 5-22 presents the spectral accelerations at the roof of the LM2 structure calculated using SASSI for a set of 28 frequencies and a set of 44 frequencies. The LS-DYNA response is also presented in the plots for comparison. The frequencies used in the analysis are indicated with solid black circles on the SASSI responses. Both the frequency sets have an adequate number of frequencies around the fixed-base period (0.14 sec).

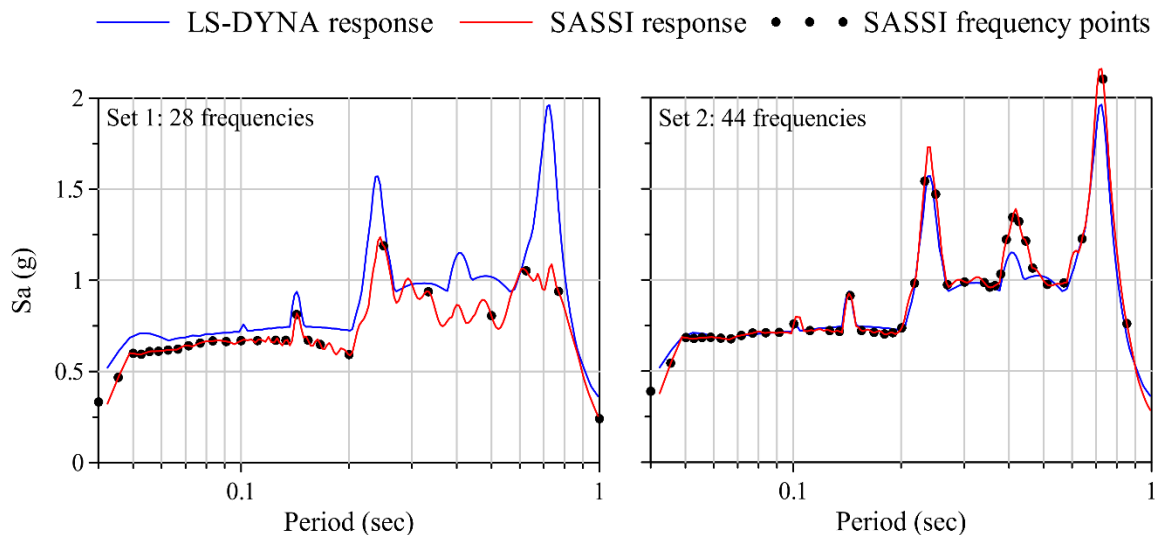


Figure 5-22: Acceleration response spectra calculated at the roof of LM2 using SASSI for two sets of analysis frequencies, and using LS-DYNA

However, the significant difference in the SASSI response resulting from the use of more frequencies between 0.2 sec and 1 sec is clear in the figure. It appears that this improvement primarily comes from including more frequencies at the three peaks occurring at about 0.25 sec, 0.4 sec, and 0.7 sec. The peak at 0.4 sec corresponds to the flexible-base period of the structure, and the other two peaks correspond to the natural periods of the soil profile. This indicates that the input set of frequencies should

be complete enough to characterize the peaks in the transfer function corresponding to 1) flexible-base period of the structure, and 2) the natural periods of the site. Additionally, the frequency set should also include the dominant frequencies of the input ground motion. Although the site periods can be estimated by a separate site-response analysis, the flexible-base period of the structure can be difficult to identify before the analysis, especially for complex structures. This makes it difficult to choose the analysis frequencies a priori.

5.4.2 Foundation meshing in SASSI

The SSI analysis in SASSI involves calculation of the foundation impedance functions at the interaction nodes. For the analysis of MS2F presented in this section, the interaction nodes include all of the nodes in the basemat. SASSI calculates the impedance functions only for these nodes and forms the impedance matrix, which is used to calculate the transfer functions. Therefore the meshing of the basemat (which determines the number of nodes in the basemat) affects the foundation impedance matrix, and therefore the overall foundation impedance. This is unlike the finite element method, in which the foundation impedance is sensitive to the meshing of the soil around the basemat, and not the meshing of the basemat itself, which is modeled as a rigid body. Figure 5-23 presents the rocking response of MS2F calculated using SASSI for the two different basemat meshes shown in the figure. The corresponding LS-DYNA response is also provided for comparison. The figure shows significant differences between the SASSI responses calculated for the two basemat meshes, and that the response for basemat 2, which has a finer mesh, is almost identical to the LS-DYNA response⁹. Therefore care must be taken when meshing the foundation for a SASSI analysis.

⁹ The structure-basemat connections employed in the two basemat models are also different. However since the basemat is modeled to be much stiffer than the surrounding soil, the structure-basemat connection is assumed to have no effect on the structural response.

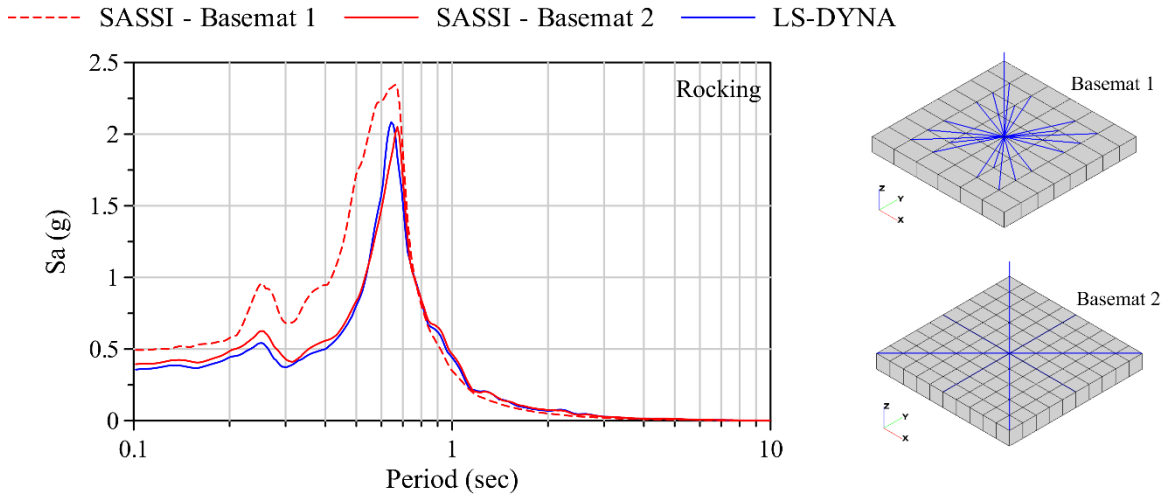


Figure 5-23: Sensitivity of the rocking response of MS2F calculated using SASSI to the number of nodes in the basemat

5.4.3 Column-basemat connection properties in SASSI

SASSI does not have a provision to directly model a rigid connection between the beam elements of the structure and the solid elements of the foundation. These connections can be modeled using beam elements with a stiffness much larger than the stiffness of the beams elements in the superstructure (see Figure 5-24). However, if the stiffness of these connection beams is too large, SASSI produces anomalous results, as shown in Figure 5-25. The figure shows the SASSI responses (1% damped acceleration amplification spectra from the surface free-field), calculated at the roof of the LM2 structure when subjected to the Ormsby wavelet, for three different values of stiffness of the beams constituting the column-basemat connection. The column-basemat connection in LS-DYNA is modeled using the *CONSTRAINED_NODAL_RIGID_BODY option, which provides a fully rigid connection. Figure 5-25 also includes the corresponding LS-DYNA response. There are large differences between the SASSI responses calculated using the different value of stiffness for the column-basemat connection beams. Only the SASSI response with connection 3 matches closely with the LS-DYNA response.

- Connection 1: $EI = 6.9 \times 10^{22} \text{ kN-m}^2$
- Connection 2: $EI = 6.9 \times 10^{18} \text{ kN-m}^2$
- Connection 3: $EI = 6.9 \times 10^{15} \text{ kN-m}^2$

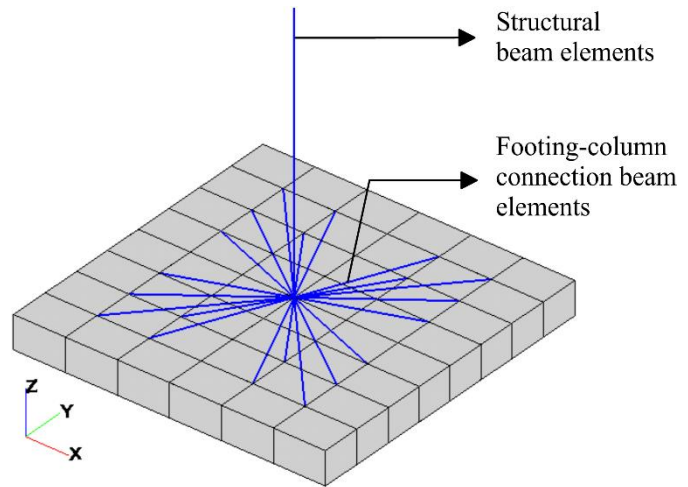


Figure 5-24: Description of the column-basemat connection of LM2 as modeled in SASSI and the beam cross-section properties used to model the three different connections employed in Section 5.4.3

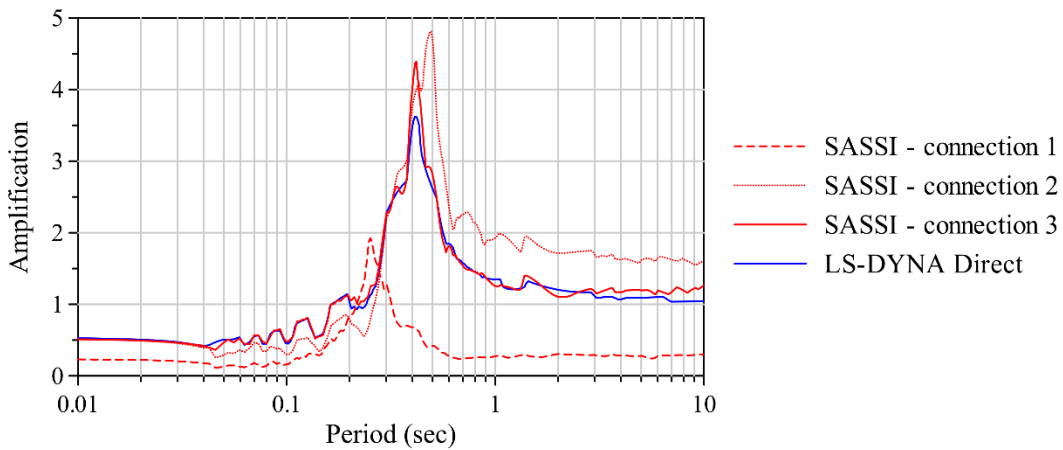


Figure 5-25: SASSI response of the LM2 structure for various structure-basemat connections considered in Section 5.4.3, and the LS-DYNA response

It is difficult to pinpoint the exact reason for the anomalous responses in SASSI without access to the source code. On the basis of this limited study, the rigid beams should be modeled using a stiffness that is at most 10^4 times greater than that of the superstructure beam elements. Using a stiffness that is too large can result in anomalous responses, which can be taken as a true response without a benchmark solution such as the one provided by LS-DYNA in this case.

5.4.4 Sensitivity of rocking response to site layering in SASSI and LS-DYNA

The soil layer thicknesses in a soil profile model (for both site-response and soil-structure interaction analyses) are chosen based on the maximum frequency (minimum wavelength) that propagates through the soil profile. The SHAKE and the SASSI user manuals recommend at least five soil layers per minimum wavelength [$n = 5$ in equation (4-1)], whereas Jeremić *et al.* (2009) recommend 10 layers per minimum wavelength for time-domain nonlinear analyses. However these recommendations are primarily intended for site-response predictions, and do not consider the impact on SSI response of a structure. Figure 5-26, for example, presents the SSI response of MS2F subjected to the JOS_L ground motion, calculated using SASSI and LS-DYNA for two site layering procedures. Layering scheme 1 corresponds to a soil profile with layer thicknesses calculated using $n = 5$, and layering scheme 2 corresponds to the layer thicknesses calculated using $n = 10$. The figure also includes the corresponding strain compatible shear wave velocities calculated using SHAKE, and the site responses calculated using SASSI and LS-DYNA. Although the site responses for these profiles are identical, the corresponding rocking responses vary considerably. The variation in the rocking response is significantly greater for SASSI than for LS-DYNA. This is because the strain-compatible properties in SASSI are calculated from a site-response analysis, and do not account for the stresses imposed by a structure. LS-DYNA, however, performs a fully nonlinear analysis and accounts for the soil stresses imposed by the structure. The small variation in the LS-DYNA response indicates that the thickness of the soil layers near the foundation have a minor effect on the rocking response of MS2F.

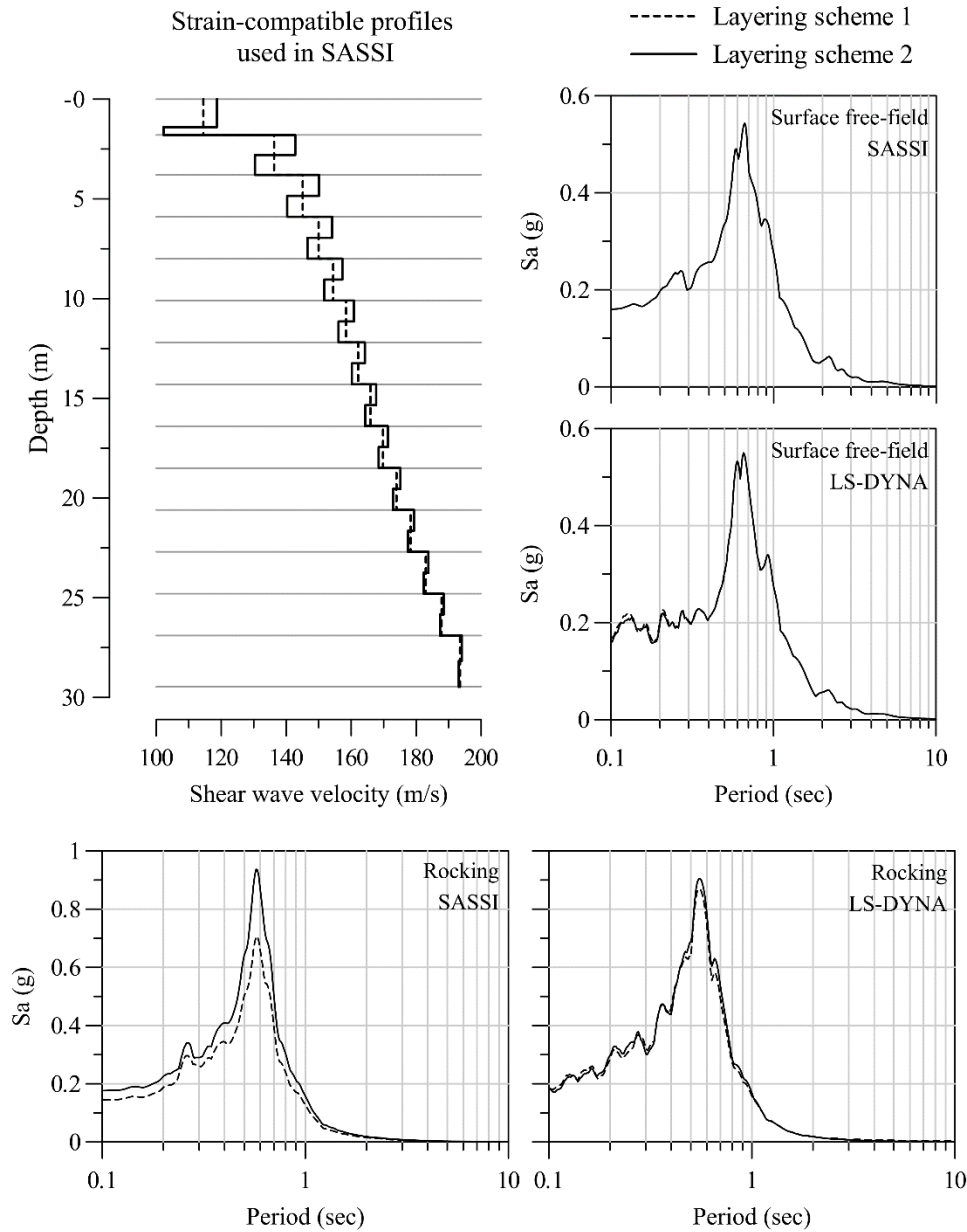


Figure 5-26: Sensitivity of the rocking accelerations of MS2F to site layering in the equivalent-linear method

5.4.5 Hourglass effects in LS-DYNA response

Preliminary analyses of LM2 with a flexible basemat and a flexible superstructure revealed large differences between the SASSI and LS-DYNA responses. Figure 5-27 presents the 1% damped acceleration amplification spectra at the roof of LM2. The dotted blue line in this figure presents the LS-DYNA response of LM2 in this analysis. This figure clearly shows that the SASSI and LS-DYNA responses are very different. The peak amplification in the LS-DYNA response occurs at a longer period

and is smaller than that of the SASSI response, indicating significant softening in either the structure or the foundation of the LS-DYNA model. An examination of the deformed shape calculated using LS-DYNA (panel a in Figure 5-28) reveals that the deformation in the solid elements at the perimeter of the basemat is comparable to the deformation in the adjacent soil elements. This result is unrealistic, given that the basemat is significantly stiffer than the soil, and is likely a result of hourglass effects. To further investigate this result the LS-DYNA analysis is performed again using hourglass control [IHQ = 5 in *CONTROL_HOURLASS; refer to the LS-DYNA keyword manual (LSTC, 2013)], that prevents the formation of hourglass modes. The solid blue line in Figure 5-27 presents the amplification spectra for the LS-DYNA analysis with hourglass control. The SASSI and LS-DYNA results are now much closer, indicating that the softening in the LS-DYNA model is due to hourglass effects. The corresponding deformed shape (panel b in Figure 5-28) also shows a significant smaller deformation in the basemat elements than the adjacent soil elements. Hourglass control should therefore be used for SSI analyses in LS-DYNA. An alternative method to avoid hourglass effects is to use full integration in the solid elements. However this requires much longer computation times.

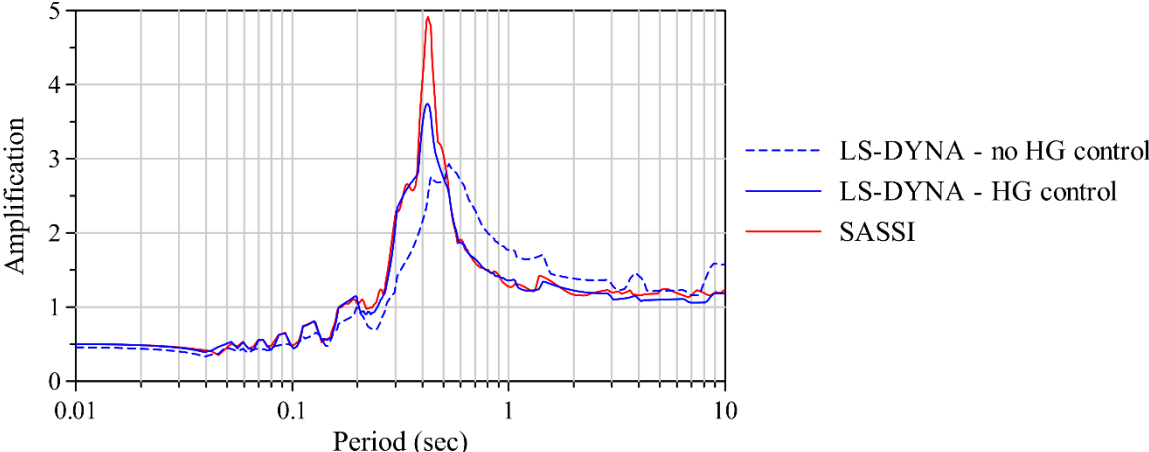


Figure 5-27: Sensitivity of the LS-DYNA response of LM2 to hourglass effects

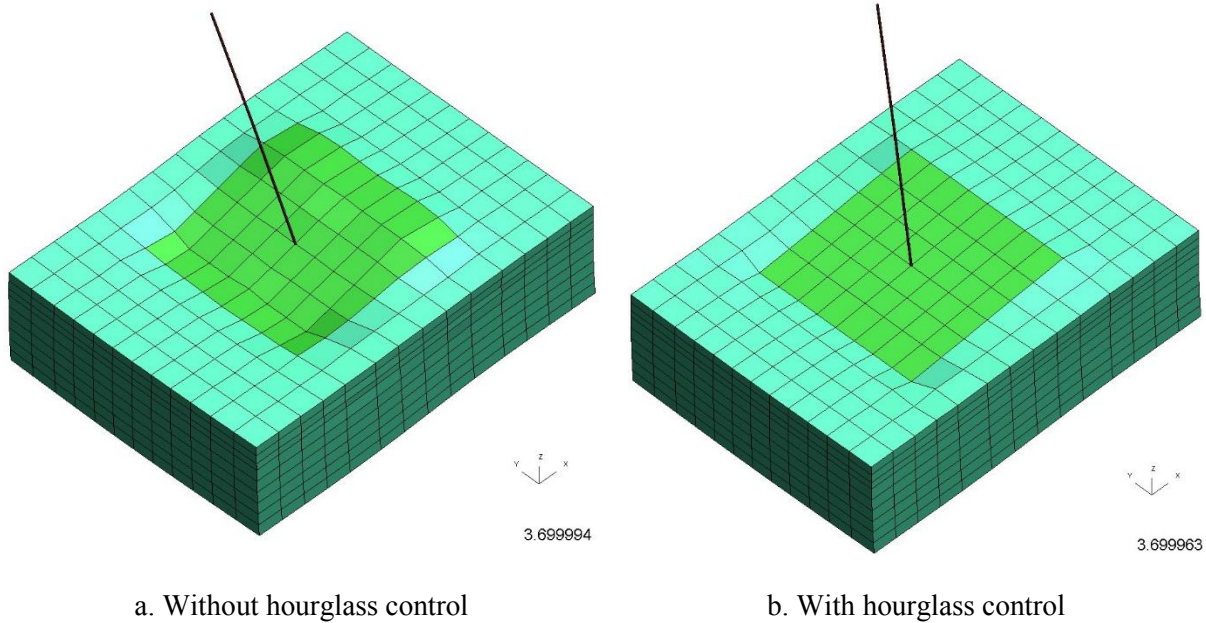


Figure 5-28: Screenshots of the LS-DYNA response (500 times amplified) of LM2 with and without hourglass control

5.5 Summary and conclusions

Linear elastic and fully nonlinear SSI analyses are performed in SASSI and LS-DYNA. The process of the performing these analyses and a comparison of results revealed some potential challenges for SSI analysts. The following conclusions can be drawn from the studies presented in this section:

1. SASSI and LS-DYNA produce almost identical responses for SSI analysis of linear elastic models. Small differences in peak spectral accelerations can be expected, which arise from the differences in the damping formulations.
2. The nonlinear response predictions of SASSI and LS-DYNA for MS1F_2 are very different even for low-intensity ground motions, due to nonlinear soil behavior in the immediate vicinity of the footings. Restraining footing rocking using grade beams reduces this nonlinear behavior and brings the SASSI and LS-DYNA responses much closer. Equipping a structure with grade beams also reduces ductility demands in the floor beams of moment frames by eliminating relative horizontal displacement in the footings (footing spreading).
3. The nonlinear response predictions of SASSI and LS-DYNA are closer for the two-story shear wall structure on a basemat (MS2F) than those of the one-story moment frame structure on spread footings (MS1F_2) because the secondary nonlinearities are much smaller. The response predictions from the two programs become increasingly different for more intense ground

motions due to 1) the differences in the site response, and 2) increasing nonlinear behavior of the soil near the foundation.

4. The responses of both the structures can be significantly affected by foundation sliding and gapping caused by separation at the foundation-soil interface. Neglecting these effects can result in unconservative acceleration demands in the superstructure.

5.6 Recommendations

SSI effects in buildings are typically evaluated using simplified methods such as those prescribed in ASCE 7-10 (ASCE, 2010) and FEMA 440 (FEMA, 2005), which are based on linear analytical solutions. The study presented in this section shows that nonlinear SSI effects can be significant in buildings, especially for structures founded on spread footings. Ignoring these effects can result in unconservative estimates of demand in the superstructure. In the context of performance-based design, nonlinear soil-structure interaction effects should be considered if accurate estimates of loss are required.

Soil-structure interaction analysis using either SASSI or LS-DYNA can be complicated, both in terms of execution and interpretation of the results. The possible anomalous results presented in Section 5.4 could be interpreted as the correct response. Indeed the issues presented in this section may not have been identified if only one of the programs had been used for analysis. For example, the SASSI response with an inadequate number of frequencies presented in Figure 5-22 could be assumed to be the exact result, if not compared with a reference result calculated using LS-DYNA. The use of both programs and preliminary analyses with simplified models may be the only practical way to ensure that the results are accurate.

SECTION 6

THE NEES CITY BLOCK CENTRIFUGE EXPERIMENTS: TEST 3 AND TEST 4

6.1 Introduction

The experimental program of the NEES City Block project included six centrifuge tests, titled Test 1 through Test 6, that examined the phenomena of soil-structure interaction (SSI) and structure-soil-structure interaction (SSSI). A preliminary test, Test 0, was performed on the soil alone to calibrate the ground motions to be input to the centrifuge shake table during Tests 1 through 6. Test 1 is a baseline test that involves two building models (a one-story model supported on footings, and a three-story model on an embedded basement), representing a low-rise and a mid-rise SMRF building at the prototype scale, placed sufficiently far away from each other to eliminate significant interaction. These structures are placed directly adjacent to each other in Test 2 to observe SSSI effects between the structures. Test 3 and Test 4 involve stiffer, heavier structures (a one-story model supported on footings and a two story shear wall model) designed to exacerbate the interaction between the structures in such a way that the dynamic behavior of one structure affects the behavior of the other structure. These structures are placed in different arrangements to understand the effects of their relative location on SSSI. The study presented in this report is only confined to Test 3 and Test 4. Descriptions of the plan and execution of Test 3 and Test 4 are presented in Sections 6.4, and 6.5, respectively. Experimental results are presented in the next section, along with the description of the comprehensive numerical simulations of Test 3 and Test 4. Test 6 and Test 7 examine liquefaction effects, along with SSSI, and are not presented in this report. Data and documentation for all the NEES City Block experiments are available for open access in the project website in the NEEShub Project Warehouse ([https://nees.org/warehouse /project/639](https://nees.org/warehouse/project/639)).

6.2 Geotechnical centrifuge testing

6.2.1 Background

Physical phenomena such as site effects and soil-structure interaction (SSI) occur at a very large dimensional scale and are almost impossible to physically simulate in the laboratory at a full scale. Scale models can be built, but owing to the complicated material behavior of soil it is desirable that these models have an identical strength and stiffness as the prototype. To maintain identical strength and stiffness in the model and prototype, similitude laws are used to establish scale factors for all the other parameters in the model, given the factor with which the model is scaled down from the prototype. These scale factors are listed in Table 6-1 below. Derivations for these scale factors are presented in Kutter (1995) and Bolisetti (2010). The acceleration scale factor in the table indicates that the model acceleration

is scaled up the same amount as the model dimensions are scaled down. This indicates that for a model that is smaller than the prototype by a factor of 50, the accelerations should be scaled up 50 times, including acceleration due to gravity, which is only possible in a centrifuge.

Table 6-1: Scale factors used in centrifuge testing^a (Kutter, 1995)

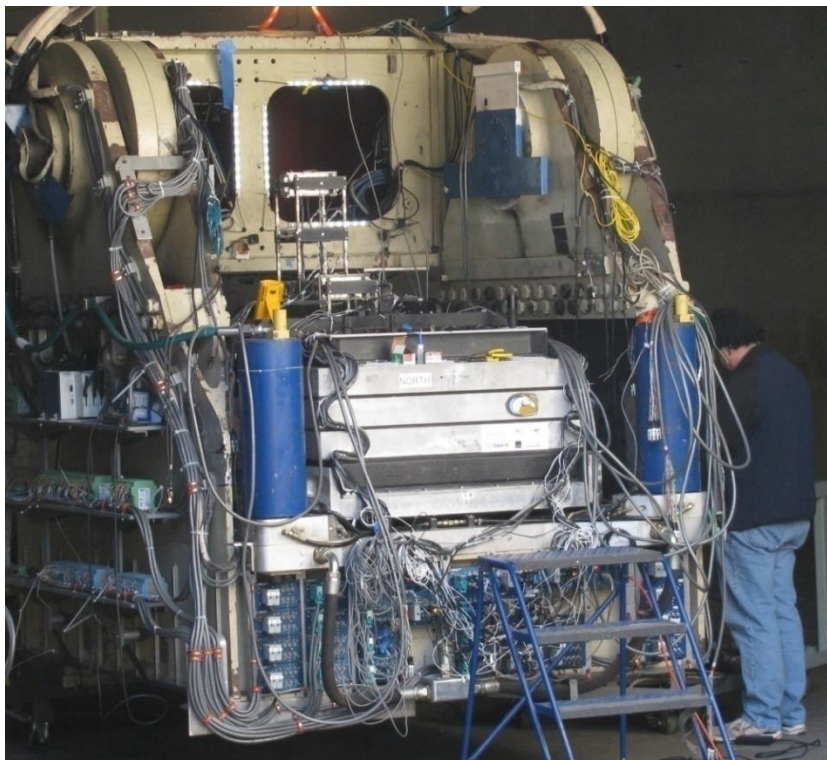
Quantity	Scaling Factor
Stress	1
Strain	1
Length	$1/N$
Acceleration	N
Dynamic Time	$1/N$
Period	$1/N$
Frequency	N
Mass	$1/N^3$
Force	$1/N^2$

^a N is the centrifuge scale factor, and a value of 55 is used for the City Block project

A geotechnical centrifuge consists of a swing bucket that hangs freely on one end of a horizontal arm, which is attached to a vertical axle that supports the rotation of the arm-bucket assembly (see Figure 6-1). The swing bucket contains a laminar box mounted on a shake table that simulates earthquake shaking. The swing bucket is equipped with a data acquisition system. The laminar box contains the instrumented experimental model including the soil and structures. The role of the laminar box is to simulate a transmitting boundary that absorbs the waves radiating from the soil surface and the structures (if any) thus simulating an infinite soil halfspace. When the centrifuge arm rotates around the vertical axle, it creates a centrifugal force acting in the vertical direction relative to the soil-structure model in the laminar box. By maintaining a pre-determined angular velocity, a vertical force equivalent to the required gravitational force in the model can be simulated.



a. Photograph of the UC Davis Geotechnical Centrifuge showing the horizontal arm, the swing bucket, and the laminar box



b. Photograph of the centrifuge swing bucket when fully equipped showing the laminar box in the bucket and the data acquisition system attached to the outside walls of the bucket

Figure 6-1: The UC Davis centrifuge

A centrifuge test is conceived by choosing the prototype structures and soil site characteristics such as topography and soil profile. The centrifuge scale factor is the most crucial parameter in the test plan and is determined by the size of the laminar box, size of the prototype structures, and the level of detail desired in the experimental models. For the City Block project, a scale factor of 55 was chosen. Once the scale factor is chosen the model structures are designed and the test ground motions are selected. Model structures are then fabricated and instrumented with strain gages, accelerometers, etc. The laminar box is filled with the soil using a technique that maintains a desired in-situ relative density. This technique is known as pluviation, and the device used for this purpose is known as the pluviator (Figure 6-2). The pluviator is an elevated soil container that gradually pours the soil into the laminar box placed below. It is moved back and forth along the length of the laminar box at a specific speed, so as to maintain uniformity in the soil profile. The relative density of the soil in the laminar box is determined by the rate at which the soil is discharged from the pluviator. This rate depends on the speed of the pluviator and its elevation, which are pre-calibrated in order to achieve the intended relative density in the laminar box. The instruments used to record soil responses (e.g., accelerometers, pore pressure transducers) are placed in the soil during pluviation. Instrumented structural models are also carefully placed in the soil during pluviation (or after pluviation in case of surface mounted structures). The laminar box containing the soil-structure model is then carefully transferred onto the swing bucket on the centrifuge arm (Figure 6-2). The soil and structural instruments are then connected to the data acquisition system before the centrifuge is spun for testing.



a. A building model before instrumentation



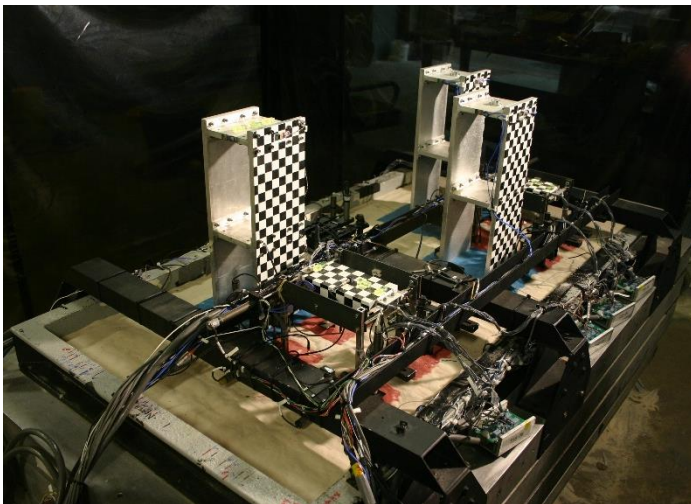
b. Laminar box before pluviation



c. Pluviation



d. Laminar box right after pluviation



e. Laminar box and building models after instrumentation



f. Laminar box in the swing bucket

Figure 6-2: Photographs of the experimental model building process. Courtesy of the City Block team

6.2.2 Advantages and limitations

Centrifuge testing can be a very useful tool for gaining insight into several geotechnical phenomena. Field observations from reconnaissance missions and data analysis from instrumented structures can be helpful but are limited in terms of the types of structures and ground motions. Centrifuge testing is therefore an economical alternative that can physically simulate complex geotechnical phenomena in a laboratory. By the nature of laboratory testing, these phenomena can be repeatedly simulated for a wide range of situations. The repeatability also enables the analysis of simpler problems at first and the gradual increase of complexity (e.g., by adding additional structures) thereby allowing complex problems to be broken down and understood incrementally.

Centrifuge testing has several limitations that must be considered before interpreting test data. Predictably most of these limitations arise from the fact that centrifuge tests are 1) scaled down by large factors (scale effects), and 2) performed in the finite domain of a laminar box as opposed to an infinite soil halfspace (boundary effects). Soil in a centrifuge model, being a much smaller specimen than the corresponding prototype, may exhibit different stress-strain behavior from that expected in the prototype. This is called the ‘particle size’ effect (Kutter, 1995), which is also observed with other geotechnical testing techniques such as triaxial tests, where specimens of different sizes may exhibit different strain softening rates. A similar argument can be made for structural models, which are typically tested at near full scale unlike centrifuge models. Although soil models exhibit particle size effects, it is incorrect to employ the simplistic assumption that a ‘sand specimen in the centrifuge represents gravel in the prototype’ (Kutter, 1995). An important consequence of particle size effects lies in the shear behavior at the soil-structure interface. Soil shear behavior is localized to a ‘shear band’ of soil particles and its thickness depends on the soil properties (Kutter, 1995). Since the soil properties in centrifuge testing are independent of scale, the shear band thickness at the soil-structure interface is the same in the model and in the prototype. This leads to a scaling inconsistency in the shear behavior at the contact interface since the foundations of the prototype and the (much smaller) model experience the shear band of the same thickness. Time scaling also results in rate effects in the centrifuge. Since the centrifuge model experiences the same dynamic stresses and strains as the prototype in a much smaller time span, strain rate effects can be significant.

One of the goals of using a laminar box is to produce a one-dimensional wave field in the soil comprising of vertically propagating shear waves. An ideal laminar box needs to have the same stiffness and damping ratio as the contained soil profile, and should have a mechanism to create the correct shear stresses at the sides of the soil to reproduce a one-dimensional wave field. Such a laminar box is almost impossible to build given the complexity of nonlinear stress-strain behavior of the soil. Several laminar boxes have been developed to better address this problem but none creates a perfect one-dimensional

wave field (Kutter, 1995). Boundary effects are therefore expected in centrifuge tests and are partly avoided by placing the structures away from the walls of the laminar box.

The mass of the centrifuge model, including the soil, structures and the laminar box, is usually of the same order as that of the shake table and the swing bucket itself. Centrifuge models are therefore susceptible to soil-container-shaker interaction, which leads to an interaction between the soil response and the input to the laminar box. This interaction also acts as an energy dissipation mechanism at the base of the laminar box. Ilankatharan and Kutter (2010) found that the soil-container-shaker interaction considerably affects the model response and should be accounted for in numerical simulations.

Given the above limitations, centrifuge testing may not be suitable for directly modeling a specific prototype event, but is useful in discovering mechanisms of behavior, or comparing the performance of similar structures under different geotechnical conditions (Kutter, 1995). Centrifuge test data can also be used to validate numerical tools, provided the above stated effects are carefully accounted for in the numerical simulations.

6.2.3 The NEES@UC Davis centrifuge facility

The NEES City Block (NCB) project involves a series of centrifuge experiments that aim to understand and characterize the effects of structure-soil-structure interaction on buildings (also called as ‘city block effects’ or ‘site-city effects’) in the context of performance assessment of buildings in dense urban environments. These experiments are performed on scale models of buildings placed on soil, and the recorded data is used to understand the mechanisms and consequences of SSSI effects on the corresponding prototype buildings. The City Block experiments require a sufficiently large centrifuge to accommodate 6 building models and a robust data acquisition system capable of recording the response of these structures in significant detail. The Center for Geotechnical Modeling (CGM) at UC Davis, an equipment site of the George E. Brown, Jr. Network for Earthquake Engineering Simulation (NEES), operates the largest geotechnical centrifuge in the United States and was used for the NEES City Block experiments. The UC Davis centrifuge (Figure 6-1) has a 9m radius arm and can accommodate payloads of 4.5 tons at a rotational speed of 90 rpm, which corresponds to a centrifugal acceleration of 75g.

The centrifuge facility owns both uniaxial (horizontal only) and biaxial (horizontal and vertical) shake tables. Only the uniaxial shake table is used for the City Block project. This shake table is capable of producing peak accelerations of up to 30g and a velocity of up to 0.8m/s, depending upon the mass and stiffness of the experimental model. It is approximately 6.6ft × 3.3ft in plan and holds containers of 5.8ft × 2.3ft × 2.0ft in size. Figure 6-3 below is a 3D rendering of the uniaxial shake table. The CGM is equipped with 1) two Flexible Shear Beam containers (FSB-1 and FSB-2) designed to move along with the soil profile, 2) a Rigid Container (RC-1) with transparent side walls providing a clear view of below

grade soil behavior, and 3) a Hinged Plate Container (HPC-1), which is also flexible but retains the residual lateral deformation of the soil profile. The FSB-2 container is used in the first two City Block experiments. This container has the inner dimensions 65in \times 31in \times 23in (65in in the shaking direction) and is built from aluminum rings separated by thin strips of neoprene as shown in Figure 6-4. Further information regarding the specifications of the centrifuge can be found at the NEES at UC Davis website (www.nees.ucdavis.edu).

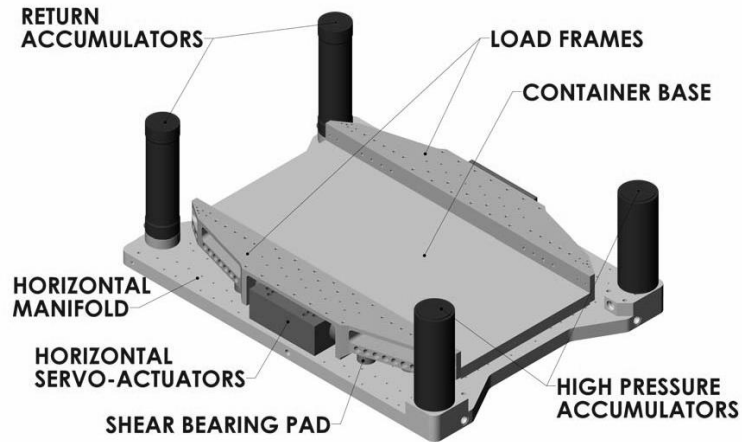


Figure 6-3: Rendering of the horizontal uniaxial shake table used at the UC Davis centrifuge facility (courtesy of the staff at the Center for Geotechnical Modeling, UC Davis)

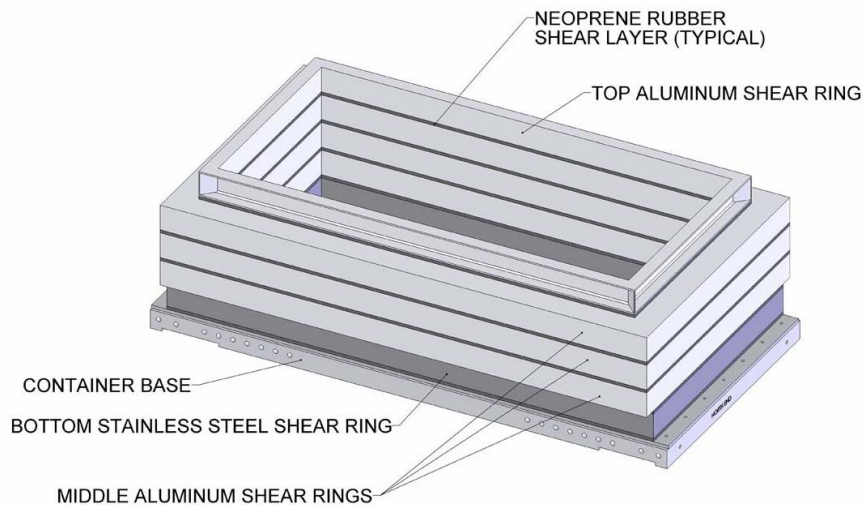


Figure 6-4: FSB-2 container used in the City Block experiments (courtesy of the staff at the Center for Geotechnical Modeling, UC Davis)

6.3 Test 2: Two adjacent structures on dense, dry sand

6.3.1 Test description

Test 2 was the second of the two baseline tests (Test 1 being the first) that involved two steel moment resisting frame (SMRF) model structures placed on dense, dry Nevada sand. The main goal of Test 1 was to examine the soil-structure interaction (SSI) effects on a one-story building model supported on spread footings and a three-story building model supported on a basement (Bolisetti, 2010). Test 2 was performed to examine the structure-soil-structure interaction (SSSI) between these models by placing them adjacent to each other in a line parallel to the shaking direction (termed as in-plane SSSI or iSSSI) and comparing their seismic responses to those observed during Test 1. The Test 1 models therefore serve as baseline to the Test 2 models. Figure 6-5 and Figure 6-6 present photographs of the arrangement of the models in the laminar box during Test 1 and Test 2, respectively.

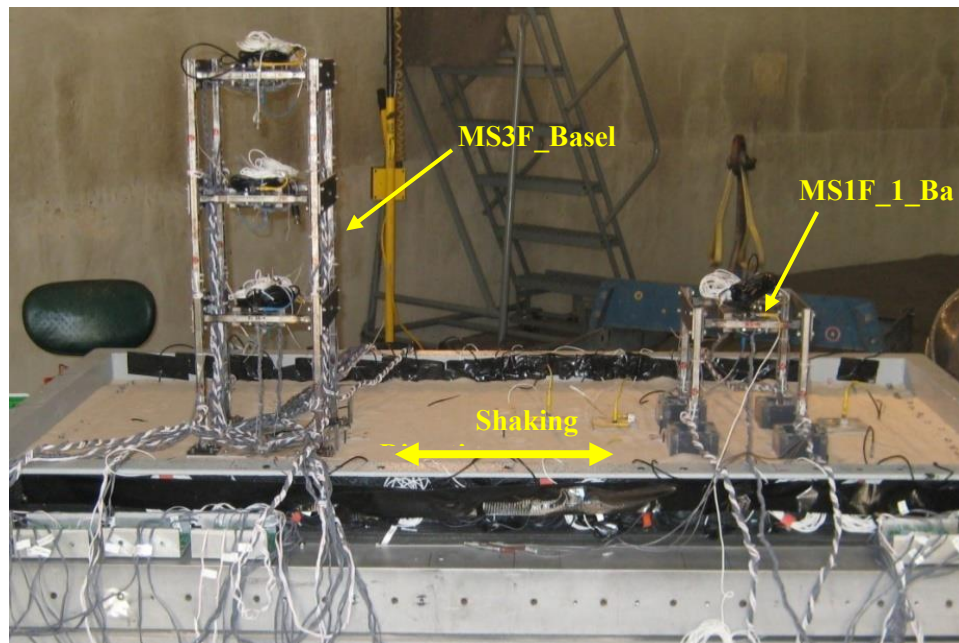


Figure 6-5: Photograph of the building models in the laminar box during Test 1

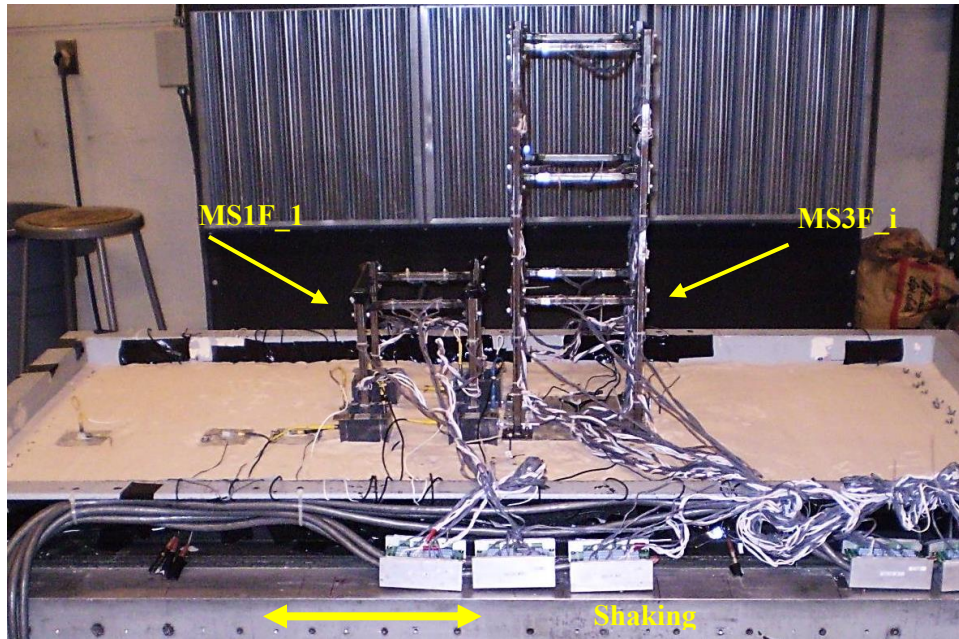


Figure 6-6: Photograph of the building models in the laminar box during Test 2

6.3.2 Soil profile

Dense, dry Nevada sand was used in Test2 (and Test 0 and Test 1). This sand was fine and uniformly graded, with a coefficient of uniformity (C_u) equal to 1.06 and a mean grain diameter (D_{50}) of 0.15mm. Nevada sand was delivered to the UC Davis centrifuge facility in batches. The soil has a specific gravity (G_s) of 2.65 and void ratios, e_{min} and e_{max} , of 0.510 and 0.748 respectively, based on the laboratory tests performed on the batch of sand used in Test 0 and Test 1. No material tests were performed on batches that arrived after Test 1 because the differences between material properties of different batches of Nevada sand were assumed to be small. The laminar box was filled to a depth of 21.1in during Test 2 [identical to Test 0 and Test 1; see Bolisetti (2010)], which corresponds to a depth of 97ft at the prototype scale. A relative density of 80% was maintained during pluviation.

6.3.3 Model design and instrumentation

Chen *et al.* (2010) designed and developed the model buildings used in Test 1 and Test 2. The one-story model (herein referred to as MS1F_1) represents a three-story steel moment resisting frame (SMRF) building at the prototype scale, and the three-story model (herein referred to as MS3F) represents a nine-story SMRF building at the prototype scale. The designs procedures for the models are presented

in Bolisetti (2010) as a part of the description of Test 1, and are reproduced here¹⁰. Slight modifications were made to the one-story model for Test 2 as explained in Section 6.3.3.2.

6.3.3.1 Selection of prototype building parameters

The prototype building designs were developed by Ganuza (2006). These designs assumed a fixed-base, and were developed for a class D site in Los Angeles. As such, they were deemed suitable for the City Block project. After consultation with the project practice committee, Chen *et al.* (2010) adopted a three-story SMRF building, *lam123*, and a nine-story SMRF building, *lam19*, as prototypes to develop models for centrifuge testing. Key design parameters for the buildings at the prototype scale are presented in Table 6-2 below. In this table, T_n is the time period of the n^{th} mode of vibration, V_y/W is the strength (base shear at yield) to weight ratio, and γ_y is the yield drift ratio in the uppermost story.

Table 6-2: Target design parameters for model structures at prototype scale (Chen *et al.*, 2010)

Prototype structure	Description	T_n (sec)	V_y/W	γ_y (%)
<i>lam19</i>	SMRF, 9-story	2.6, 0.8, 0.5 ^a	0.2	1.4
<i>lam123</i>	SMRF, 3-story	1.1 ^a	0.3	1.2

^aThe rationale for targeting only the lower modes is provided in Section 6.3.3.2 below

6.3.3.2 Design of experimental model structures

The dimensions of a centrifuge model are generally determined by geometrically scaling down the prototype dimensions by a scale factor N [equal to 55 in this project; refer to Section 3.2 in Bolisetti (2010)]. This was not practical for the prototype buildings since it would have resulted in a model with numerous beams and columns. As such, the models were designed to capture only the first few modes of corresponding prototype buildings. Model MS1F_1 was designed to capture the first mode of the prototype building, *lam123*, and model MS3F was designed to capture the first three modes of the prototype building, *lam19*. These modes contributed almost 95% of the total reactive masses (Chen *et al.*, 2010). Additionally, the models targeted the yield base shear ratio (V_y/W) and yield drift ratio (γ_y) of the prototypes. The experimental models were also equipped with foundations. The one-story model, MS1F_1, was built atop spread footings, whereas the three-story model, MS3F, was built atop an

¹⁰ The one-story and three story models are referred to as MS1F_SF80 and MS3F_B in the description of Test 1 in Bolisetti (2010).

embedded one-story (in model scale, and three-story in prototype scale) basement. The models were symmetric in plan and very stiff in the direction orthogonal to the uniaxial shaking. Figure 6-7 presents photographs of the models equipped with strain gages, prior to testing. Unlike Test 1, these models were placed adjacent to each other with a gap of 5 mm between the foundations (Figure 6-6). Sketches detailing the frame elevations along the shaking direction are presented in Figure 6-8. Each model structure consisted of two parallel frames connected to each other using stiff steel plates. Further information on the models is presented in Table 6-3 and Table 6-4.

Table 6-3: Specifications of superstructures at the model scale (Chen *et al.*, 2010)

Structure	Plan dimensions ^a (in) $L \times B$	Elevation ^{a,b} (in) $L \times (H_1, H_2, H_3)$	Floor Mass (lb)
MS3F	7.9 × 7.9	7.9 × (9.1, 7.9, 7.9)	8.75 (M2), 6.88 (M1)
MS1F_1	7.1 × 7.9	7.1 × 9.1	9.26 (M3)

^a L is the length in the shaking direction, and B is the length in the orthogonal direction

^b H_n is the height of the n^{th} story

Table 6-4: Specifications of foundations at the model scale (Chen *et al.*, 2010)

Structure	Foundation type	Dimensions ^a (in) $L_f \times B_f \times H_f$	Depth (in)	Foundation mass (lb)
MS3F	Basement below mat	8.4 × 8.4 × 7.9 ^b	7.9	18.74 ^d
MS1F_1	Isolated spread footings	11/8 × 11/8 × 7/8 ^c	0.8	6.92 ^e

^a L_f is the length in shaking direction, H_f is the height and B_f is the length in orthogonal direction

^b Dimensions of the basement

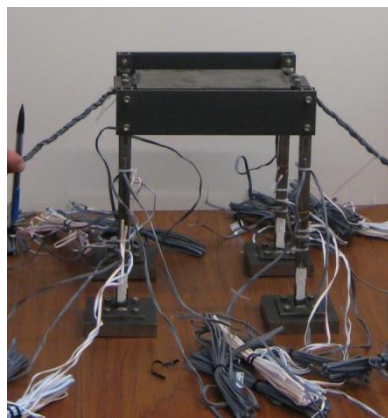
^c Dimensions of each individual footing

^d Combined mass of basement and mat

^e Combined mass of all footings

The beams and columns in the models were constructed using 1/2" × 1/2" × 1/16" steel tubing. The beams spanning in the direction orthogonal to the shaking direction were replaced by 'rigid plates' made of steel having a rectangular cross section of 1/8" wide and 2" deep. These plates provided high stiffness in the orthogonal-to-shaking direction so that the drift response in that direction was minimal. Rigid connections were provided at the beam-column joints. Steel plates of known mass (denoted by M1, M2 and M3) were supported between the beams at each story of both structures to provide the required

reactive masses. Table 6-3 presents the values of these masses and Figure 6-8 shows their locations in the superstructure. Columns of both the structures were rigidly connected to the foundations. The spread footings of MS1F_1 were constructed of steel and placed just below the soil surface. The basement walls of MS3F_iSSSI were made of 1/2" thick aluminum and the basement was completely embedded in the soil. Table 6-3 and Table 6-4 present the configurations and important dimensions of the models and Figure 6-8 provides their elevations.



a) MS1F_1



b) MS3F

Figure 6-7: Models used in Test 1 and Test 2

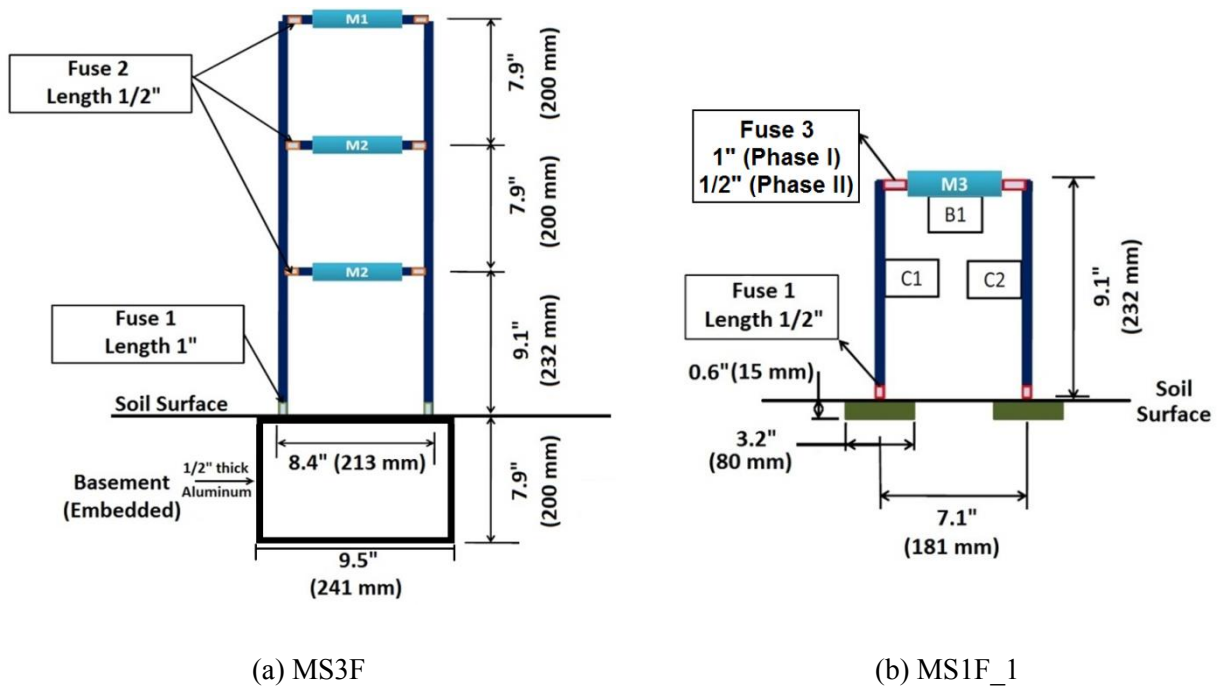


Figure 6-8: Elevations of experimental models in the shaking direction, with dimensions in model scale (Chen *et al.*, 2010)

Nonlinearity in these structures was introduced by constructing ‘fuses’ at locations of potential plastic hinges; see Figure 6-8 and Figure 6-9. This was achieved by reducing the cross-section area of the member for a certain length, thereby decreasing the plastic moment at that location and promoting the formation of a plastic hinge. Three types of fuses (shown in Figure 6-9) were designed and detailed with different lengths in the structures to achieve the required design of the models.

The Phase I beams used in MS1F_1 (see panel b of Figure 6-8) for Test 1 responded in an unexpected way, namely, plastic hinges were formed at the two ends of each of the 1-inch long fuses. Details regarding this failure mechanism are presented in the Test 1 data report (Mason *et al.*, 2010a). This mode of failure was avoided in later tests by reducing the size of Fuse 3 to 0.5 in (Phase II beams) from 1 in (Phase I beams). Model MS1F_1 of Test 2 was tested using both the Phase I and Phase II beams to maintain consistency with Test 1. Section 6.3.4 presents the test sequence showing the ground motions for which the Phase I and Phase II beams were used.

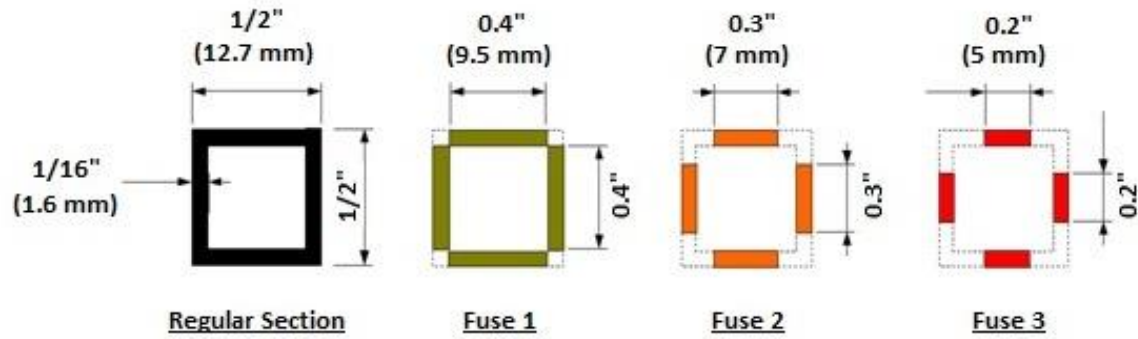


Figure 6-9: Designs of the three ‘fuses’ used in MS1F_1 and MS3F, dimensions in model scale (Chen *et al.*, 2010)

Chen *et al.*,(2010) also developed numerical models of these models to predict their behavior during Test 1. Two-dimensional models were developed in the finite element program, OpenSees [e.g., Mazzoni *et al.* (2009)]. The nonlinear beams and columns were modeled using *beam with hinges* elements, and foundation flexibility was modeled using the beam-on-nonlinear-Winkler-foundation (BNWF) model available in OpenSees. Details regarding these simulations can be found in Chen *et al.*,(2010). However this procedure cannot be used to simulate the SSSI effects that were expected during Test 2, and no pre-test numerical simulations were carried out to predict these effects. Hammer tests were conducted to calculate the fixed base time period of the experimental models. The dynamic properties of the models calculated by OpenSees analyses and calculated by analysis of hammer test data are summarized in Table 6-5.

Table 6-5: Prototype-scale properties of the designed experimental models calculated using the numerical models in OpenSees and hammer tests (Chen *et al.*, 2010)

Structure	OpenSees Analysis				Hammer Test
	Fixed-base time period T_{fix} (sec)	Drift ratio γ_y (fixed-base)	Base shear ratio V_y/W (fixed-base)	Flexible-base time period T_{ssi} (sec)	Fixed-base time period T_{fix} (sec)
MS3F	2.26, 0.67, 0.35	1.66	0.21	2.36, 0.71, 0.39	2.14, 0.66, 0.35
MS1F_1	1.06	1.72	0.59	1.14	0.93

6.3.3.3 Instrumentation

A total of 164 transducers were used in Test 2. One hundred and thirteen of these transducers were used in the structure-foundation system, which included 14 linear displacement potentiometers, 32 uniaxial accelerometers, and 67 strain-gages. An additional 41 transducers were used to capture the soil response, and three accelerometers were used to monitor the rack accelerations. Seven accelerometers were used in unloaded foundations placed in the soil to track the attenuation of surface acceleration away from the structures. Only details regarding the instrumentation of the structure-foundation system are included in this report. Information regarding the instrumentation used in the soil, rack and the unloaded foundations is presented in the Test 2 data report (Mason *et al.*, 2010b).

Standard elongation uniaxial strain gages were used at the top and bottom ends of the columns to measure the bending moments and axial loads. Triaxial shear rosettes were used at the mid-height of each column in each story to calculate shear forces. High elongation strain gages were used on the top and bottom flanges of the beam fuses.

Three accelerometers on each floor mass measured the floor acceleration in the three principal directions: shaking direction (north-south); orthogonal-to-shaking direction (east-west); and vertical direction. To check the (unintended) torsional response of the superstructure, a fourth accelerometer was placed at the mid-span of one beam that measured horizontal acceleration of the floor eccentric to the shaking direction. Horizontal and vertical accelerometers were placed on each of the spread footings of MS1F_1 to measure the acceleration input to the superstructure and the rocking response of the foundations. Nine accelerometers were placed on the basement-mat system of MS3F to capture its translational and rotational response.

Displacement transducers were placed throughout the structure-foundation system and attached to a specially designed rack, which also served as a reference frame for the displacement measurements. The horizontal displacement of each floor was measured by a linear potentiometer. One horizontal potentiometer was installed for each footing of the one-story structure to measure the transient and residual sliding displacements in the shaking direction. Two horizontal potentiometers at the soil surface level measured the translational response of the basement-mat foundation. Settlement and rocking response were recorded by vertically-installed potentiometers on each of two footings of the one-story structure and the basement of the three-story structure. Additional details and sketches of instrumentation plans can be found in Mason *et al.* (2010b).

6.3.4 Input ground motions and test chronology

The main goal of Test 2 was to calculate SSSI effects by benchmarking the model responses against those observed in Test 1, where the model structures were isolated from each other. To maintain consistency between the tests, the ground motions used for Test1 were also used in Test 2, and were input in the same order. Details regarding the selection of ground motions for Test 1 are presented in Bolisetti (2010). Test 2 was performed over three days involving three spins (each spin consisting of a spin-up of the centrifuge, shaking of the models at a desired g-level, and spin-down) with a total of 25 ground motions and 10 step-waves. Step-waves are very low amplitude ground motions (0.01 g) that were applied at the beginning and end of each spin to ‘heat-up’ the shaker, ensure that all the sensors were functioning, and check the elastic time period of the soil profile. Of the 25 ground motions, 21 were applied at 55g, and two each were applied at 40g and 20g. Only the first 21 ground motions are relevant to this study. Table 6-6 below presents the final schedule of ground motions for Test2, excluding the step-waves. The peak ground accelerations (PGA) observed at the container base and soil surface (measured at free-field) are provided in the table at the prototype scale. Additional details regarding the test sequence can be found in the Test 2 data report (Mason *et al.*, 2010b).

Table 6-6: Test 2 ground motions and their sequence (only 55g ground motions included)

Spin # -- Date -- MSIF_1 beam design	GM #	ID	Earthquake	Station	Amp. factor^a	PGA^b
Spin 1 -- 12-09-2009 -- Phase I beam Fuse 3 1" length	1	JOS_L_1	92 Landers	Joshua Tree 090	0.22	0.05
	2	TCU_L_1	99 Chi Chi	TCU078 270 (E)	0.55	0.10
	3	RRS_1	94 Northridge	Rinaldi R Sta 228	0.42	0.37
	4	PTS_1	87 Sup Hills	Parachute T S 315	0.49	0.13
	5	SCS_L_1	94 Northridge	Sylmar Conv Sta 052	0.20	0.18
	6	LCN_1	92 Landers	Lucerne 260	0.70	0.25
Spin 2 -- 12-09-2009 -- Phase II beam Fuse 3 0.5" length	7	JOS_L_2	92 Landers	Joshua Tree 090	0.22	0.05
	8	TCU_L_2	99 Chi Chi	TCU078 270 (E)	0.55	0.11
	9	RRS_2	94 Northridge	Rinaldi R Sta 228	0.42	0.36
	10	PTS_2	87 Sup Hills	Parachute T S 315	0.47	0.12
	11	SCS_L_2	94 Northridge	Sylmar Conv Sta 052	0.20	0.19
	12	LCN_2	92 Landers	Lucerne 260	0.70	0.26
Spin 3 -- 12-10-2009 -- Phase II beam Fuse 3 0.5" length	13	JOS_L_3	92 Landers	Joshua Tree 090	0.22	0.05
	14	WVC_L	89 Loma Prieta	Saratoga WV Col 270	0.80	0.28
	15	SCS_H	94 Northridge	Sylmar Conv Sta 052	1.00	0.57
	16	JOS_H	92 Landers	Joshua Tree 090	1.00	0.35
	17	WPI	94 Northridge	Newhall W Pico C046	0.80	0.42
	18	PRI_mod	95 Kobe	Port Island-Mod-79m	5.10	0.64
	19	TCU_H	99 Chi Chi	TCU078 270 (E)	1.00	0.30
	20	WVC_H	89 Loma Prieta	Saratoga WV Col 270	1.50	0.35
	21	JOS_L_4	92 Landers	Joshua Tree 090	0.22	0.06

^a Factor applied to the input ground motion

^b Measured at the base of the laminar box

6.4 Test 3: An in-plane SSSI configuration on dense, dry sand

6.4.1 Test description

The results of Test 1 and Test 2 showed some kinematic SSI effects in the response of the models but little inertial SSI and SSSI effects (Jones, 2013; Mason, 2011; Trombetta, 2013). In view of the lack of SSI and SSSI in Test 1 and Test 2, the main goals of Test 3 were to 1) promote significant inertial SSI and 2) generate interaction between adjacent structures (SSSI). Two structural models were designed for Test 3: 1) a one-story SMRF model on footings, which is a modified version of MS1F_1 used in Test 1 and Test 2, and herein termed as MS1F_2 and 2) a two-story shear wall model on basemat herein termed as MS2F. These models were designed to have significant inertial SSI, and to act as a ‘transmitter-receiver’ couple (described in Section 6.4.1.1) when placed adjacent to each other. Test 3 included two cases: 1) MS1F_2 placed far enough from other structures so that there is no SSSI, and 2) MS1F_2 and MS2F placed adjacent to each other along the direction of shaking causing in-plane SSSI (iSSSI). The former is intended to serve as a baseline case for MS1F_2 in the calculation of SSSI effects in the latter case. To avoid confusion between the one-story models of the two cases the models in the baseline and iSSSI cases are named as MS1F_2_Baseline and MS1F_2_iSSSI, respectively. Accordingly, the two-story structure is named as MS2F_iSSSI. Figure 6-10 shows a photograph of the fully instrumented models placed in the laminar box, along with the nomenclature of the models used in this section. Figure 6-11 and Figure 6-12 present sketches of the plan view and the elevation view, respectively, showing the locations of these models in the laminar box.

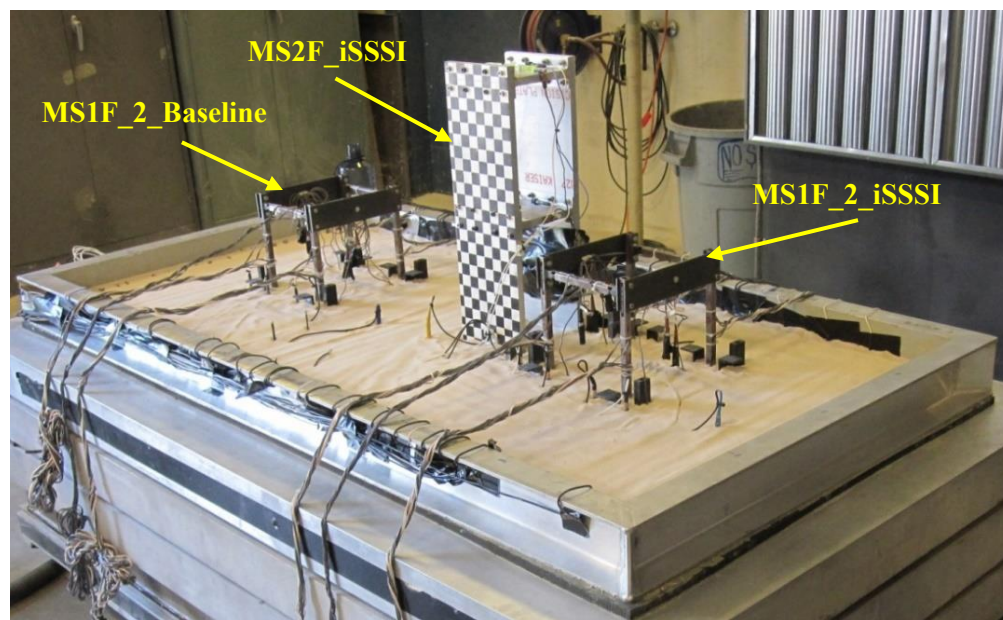


Figure 6-10: Photograph of the building models in the laminar box during Test 3

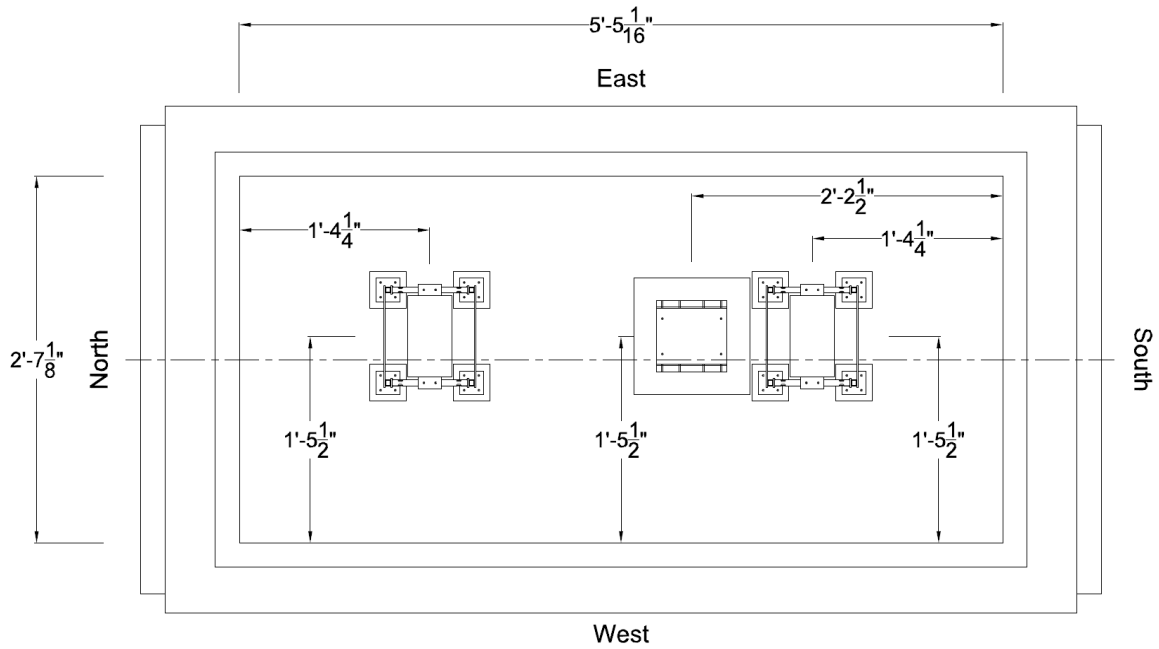


Figure 6-11: Plan view of the experimental models in the laminar box during Test 3 (dimensions in model scale) (Mason *et al.*, 2010c)

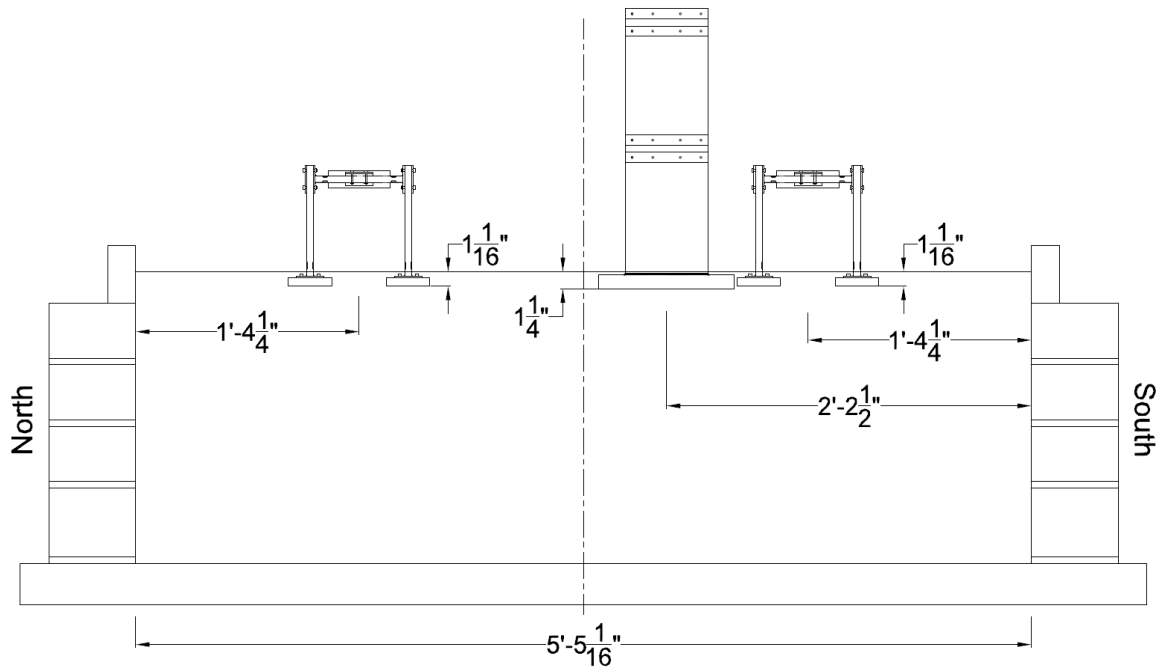


Figure 6-12: Elevation view of the experimental models in the laminar box during Test 3 (dimensions in model scale) (Mason *et al.*, 2010c)

6.4.1.1 The ‘transmitter-receiver’ configuration

The basic hypothesis of Test 3 was that placing a heavy, stiff structure against a light, flexible structure having equal flexible-base time periods would amplify the SSSI effects due to resonance between these structures. The heavier structure, termed here as the ‘transmitter’, was expected to transmit energy by driving the lighter structure, which is termed here as the ‘receiver’. Due to the transmitted energy the response of the receiver structure was expected to be amplified compared to a control structure, which was identical to the receiver but was isolated from the other structures. During Test 3 the two-story shear wall model, MS2F_iSSSI and the one-story SMRF model, MS1F_2_iSSSI, were placed adjacent to each other and were expected to behave as transmitter and receiver structures, respectively, by exhibiting in-plane SSSI. The baseline one-story model, MS1F_2_Baseline, was placed away from these two models and the laminar box boundary, thereby serving as a control structure for observing SSSI effects in the seismic response of MS1F_2_iSSSI.

6.4.2 Soil profile

The soil profile in Test 3 was identical to that in the previous tests (see Section 6.3.2 for the description of Test 2 soil profile). Dry, dense Nevada sand was used at a relative density of 80%, and the laminar box was filled to a depth of 21.1 in corresponding to a prototype depth of 96.7 ft.

6.4.3 Model design and instrumentation

The experimental models of Test 3 were designed to maximize the SSSI effects between the transmitter and receiver structures, especially during strong shaking events. Unlike Test 1 and Test 2, no specific prototype structures were used in this test to calculate the target design properties. The model MS2F_iSSSI was designed to be stiff and heavy to exhibit significant inertial interaction, and also have a flexible-base time period close to that of the soil profile. The design of MS1F_2_Baseline (and the identical model, MS1F_2_iSSSI) was based on the one-story model of Test 1 and Test 2, but was modified to match the flexible-base time period of MS2F_iSSSI. Brief descriptions of the designs of the two-story model and the one-story model are presented in Sections 6.4.3.1 and 6.4.3.2 respectively.

Numerical models of both model structures were developed in OpenSees. However no pre-test numerical simulations were performed on the complete experimental model to predict the SSSI effects. Complete details of the design, construction and numerical modeling can be found in the Test 3 data report (Mason *et al.*, 2010c).

6.4.3.1 Design of two-story model, MS2F_iSSSI

The degree of inertial interaction in the seismic response of an elastic structure can be evaluated using dimensionless parameters that are functions of the properties of the soil and structure. Some of these parameters that have been widely used by previous researchers (Bielak, 1975; Stewart *et al.*, 1999a; Stewart *et al.*, 1999b; Veletsos and Meek, 1974) are: 1) the soil-to-structure stiffness ratio (σ); 2) structure-to-soil mass ratio (δ); 3) ratio of effective structural height to the effective foundation radius (h_{eff}/r_{θ}). Assuming that the model remains elastic, these parameters, including a few others, were used to guide the design of MS2F_iSSSI. Table 6-7 lists all the predictive parameters and the corresponding ranges that were targeted to make the model more susceptible to inertial interaction. Also indicated in the table are the values that were achieved with the final design. Based on these predictive parameters and the need to keep the model elastic throughout testing, a tall rocking shear wall structure was considered the ideal choice for the transmitter structure. A prototype scale rocking time period of 0.6 sec was targeted, which was the approximate natural time period of the soil profile. This was expected to induce resonance between the structure and the soil profile and further increase inertial interaction. A macro-level numerical model of MS2F_iSSSI was developed in OpenSees. Base flexibility was modeled using Beam on Nonlinear Winkler Foundations (BNWF), which has been implemented in the program. Specific details regarding the numerical modeling are provided in Mason *et al.* (2010c) and are not discussed here. The dimensions of the model were selected so the predictive parameters were in the target ranges, and the required rocking time period was achieved. The final model (in the stiffer direction) had a fixed-base 1st mode time period of 0.13 sec and a flexible-base 1st mode time period of 0.60 sec at the prototype scale. The dimensions of the designed model are illustrated in panels a and b of Figure 6-13. A photograph of the fully constructed model is shown in panel c of the figure.

Table 6-7: Dimensionless parameters governing the design of the two-story shear wall model, MS2F_iSSSI (Mason *et al.*, 2011)

Parameter	Definition	Range to maximize SSI	Values calculated for final design
$\frac{1}{\sigma}$	$\frac{V_s}{T_{fb} \cdot h_{eff}}$	>0.2	0.775
$\frac{h_{eff}}{r_{\theta}}$	-	>1.0 <4.0	2.597
δ	$\frac{m_{structure}}{(\rho_{soil} \pi r_{eff}^2 h_{eff})}$	>0.15	0.272
$\frac{D_f}{r_{eff}}$	-	<0.25	0.224
$\frac{m_{fnd}}{m_{structure}}$	-	minimize	0.644
$\frac{L}{2h_{eff}}$	-	minimize	0.337

V_s = Shear wave velocity of the soil

ρ_{soil} = Mass density of the soil

T_{fb} = Fixed-base time period of the structure

h_{eff} = Effective height of the structure calculated using the 1st flexible-base mode shape

$m_{structure}$ = Total superstructure mass

m_{fnd} = Total foundation mass

r_{eff} = Effective foundation radius (translation)

r_{θ} = Effective foundation radius (rocking)

L = Foundation length in direction of translation

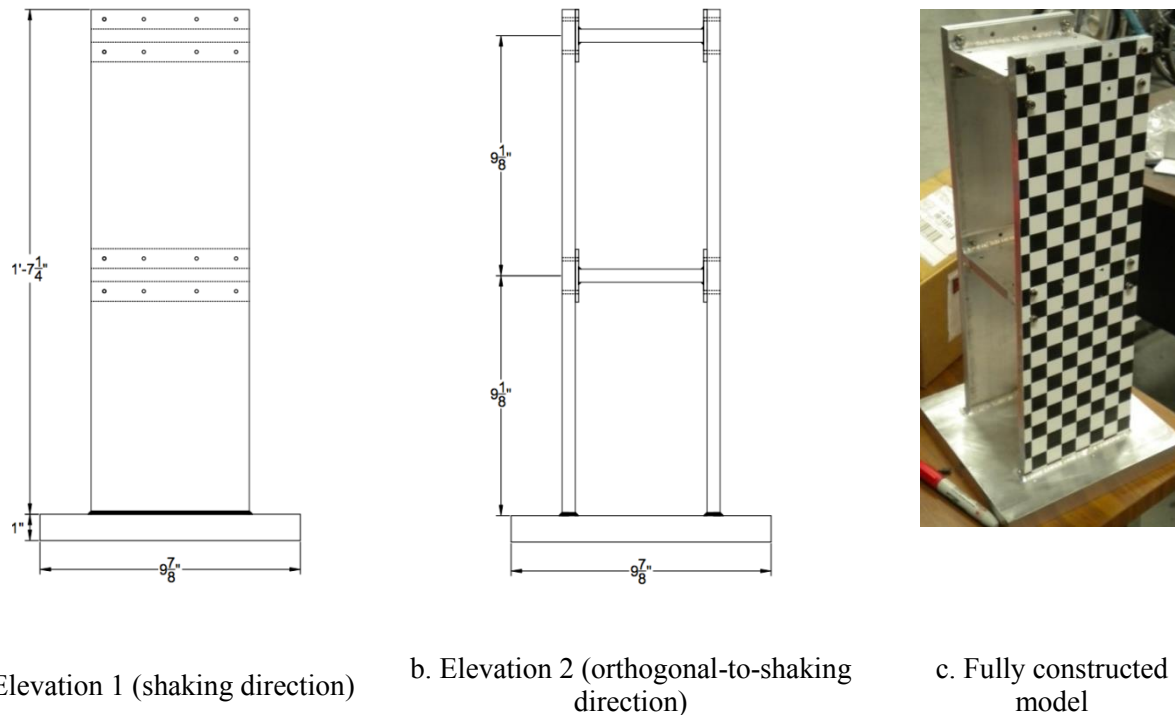


Figure 6-13: Final design of model MS2F_iSSSI (Mason *et al.*, 2010c)

The entire model (walls, floor masses and foundation) was constructed using Aluminum 6061 plate stock of various thicknesses. The superstructure shear walls were continuous through the two floors and were welded to a mat foundation. Each shear wall was 19.25 in tall, 6 in wide and 0.5 in thick. The floor masses were welded to a connection plate that was bolted to the shear walls at the floor levels (Figure 6-13). The story height was 9.125 in. The floor masses measured 6 in \times 5 in in plan (6 in along the shaking direction) and were 0.5 in thick. Each floor mass weighed 2 lb, including the weight of the connection plates. The mat foundation was square in plan, measured 9.875 in on side, and had a thickness of 1 in. A foundation embedment of 1.25 in below the soil surface was assumed in the numerical modeling, and this embedment was targeted during the experiment.

6.4.3.2 Design of the one-story models, MS1F_2_Baseline and MS1F_2_iSSSI

The basic design concept for the one-story model of Test 3 was adopted from the MS1F_1 used in Tests 1 and 2. Design specifications and construction procedures of this model are provided in Section 6.3.3.2 as well as Mason *et al.* (2010a) and Bolisetti (2010). The target flexible-base time period of the one-story model was 0.6 sec unlike the original model, which had a time period of 1 sec. To meet this target, the story height and the floor mass of the original model were decreased until the required flexible-base time period was achieved. To avoid the ‘shear-like’ failure observed during Test 1 [see Test 1 data

report by Mason *et al.* (2010a)], a shorter fuse length (3/8") was used with the Fuse 3 design (see Figure 6-9).

Grade 6061 Aluminum was used for the construction of the floor mass and footings, thereby making them lighter than the original model, which used steel. Lighter floor mass resulted in a shorter time period, whereas lighter footings were expected to exacerbate SSI effects in the response. The floor mass in the modified model was 3.86 lb whereas the original model had a floor mass of 9.06 lb (see Table 6-3 and Table 6-4 for specifications of the original model). The column height was also reduced to 7.125 inches from 9.125 inches in the original model. Eigen analysis of the modified model in OpenSees showed a flexible-base 1st mode time period of 0.65 sec, which was considered sufficiently close to the target time period of 0.60 sec. The fixed-base 1st mode time period was 0.471 sec, and the flexible-base 2nd mode time period was 0.151 sec (Mason *et al.*, 2010c). Beam and column members in the models were constructed using 1/2" × 1/2" × 1/16" A513 steel tubing as in the original model, MS1F_1. The foundation dimensions, beam lengths and column fuse design of this model were not changed. Figure 6-14 presents the dimensions of the model in elevation and plan views, and Figure 6-15 presents photographs of the fully constructed model equipped with strain gages.

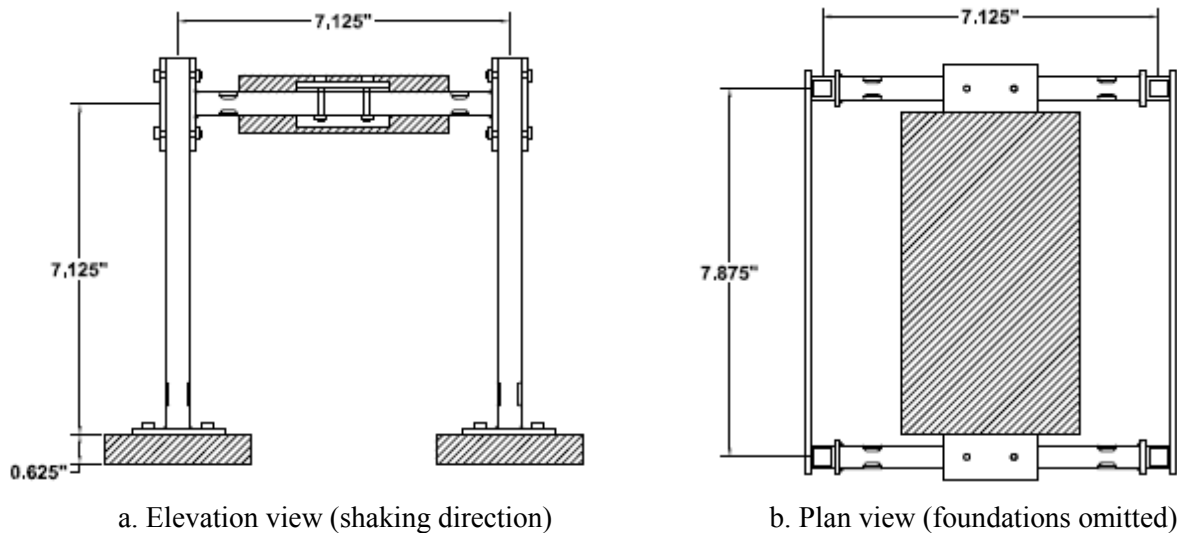
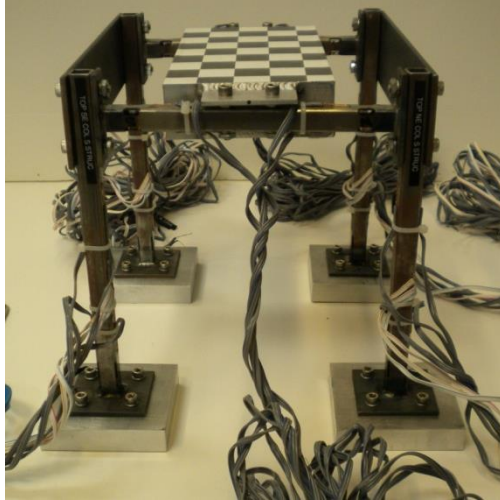
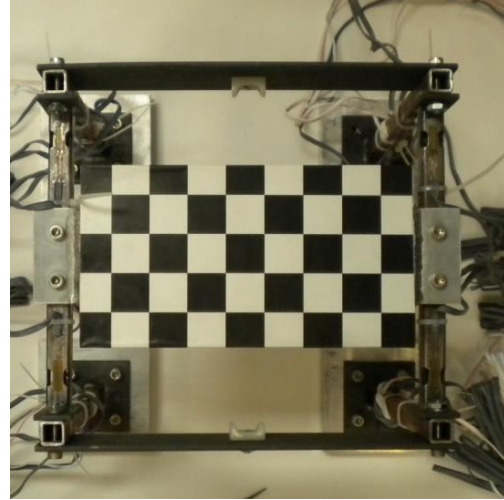


Figure 6-14: Dimensions of the one-story model in Test 3 (Mason *et al.*, 2010c)



a. Elevation view (shaking direction)



b. Plan view

Figure 6-15: Photographs of fully constructed one-story model in Test 3

6.4.3.3 Instrumentation

A total of 176 transducers were used in Test 3 to instrument the experimental setup. One hundred and thirty six of these transducers were used in the structure-foundation system, which included 26 linear displacement potentiometers, 46 uniaxial accelerometers, and 64 strain-gages. Various sensors failed during different spins and were either discarded or replaced. The instrumentation list for all of the spins are documented in the Test 3 data report (Mason *et al.*, 2010c), along with a chronological list of sensors that failed throughout the experiment.

Standard elongation uniaxial strain gages were used at the top and bottom ends of the columns in the one-story models to measure bending moments and axial loads. Triaxial shear rosettes were used at the mid-height of each column to calculate shear forces. High elongation strain gages were used on the top and bottom flanges of the beams in the fuses. The strains in model MS2F_iSSSI were not measured.

Two accelerometers on each floor mass measured the story acceleration in the shaking direction (north-south) direction. One of these accelerometers was placed at the mid-point of a beam to measure unintended story acceleration eccentric to the shaking direction. Two additional vertical accelerometers were placed at the edges of each floor mass to monitor the rocking in the structures. Horizontal and vertical accelerometers were placed on each of the spread footings of one-story models to measure the acceleration input to the superstructure, and the rocking response of the footings. Six accelerometers were placed on the mat foundation of the MS2F_iSSSI model that measured three translational accelerations, acceleration in the torsional direction, and rocking.

Displacement transducers were placed throughout the structure-foundation system and attached to a specially designed rack, which also served as a reference frame for the displacement measurements. The horizontal displacement of each floor was measured by a linear potentiometer. One horizontal potentiometer was installed for each footing of the one-story models to measure the transient and residual sliding displacements in the shaking direction. One horizontal potentiometer at the soil surface level measured the translational response of the mat foundation of model MS2F_iSSSI. Settlement and rocking responses were recorded by vertically-installed potentiometers on the footings of the one-story models and the mat foundation of model MS2F_iSSSI. An additional 40 transducers were used to measure the acceleration and displacement responses of the soil and the container. Accelerometers were installed through the depth of the soil profile and on the surface. An accelerometer placed at the soil surface between the models MS2F_iSSSI and MS1F_Baseline was assumed to measure the free field surface acceleration. Further details regarding the Test 3 instrumentation are documented by (Mason *et al.*, 2010c).

6.4.4 Input ground motions and test chronology

The ground motions used in Test 3 were identical to those used in the previous tests. A total of eight spins were conducted to perform the ground motion simulations and the cone penetration tests (CPT). The CPTs were performed during the first and last spins to evaluate in-flight soil properties, and ground motions were applied during the other spins. During spin-down after the seventh spin, ground motions were again applied at 42.8g to collect data at a different centrifuge scaling factor. Various problems occurred in a few of these spins and the centrifuge had to be spun down before applying the scheduled number of ground motions (Mason *et al.*, 2010c).

A total of 40 shaking events were completed through these eight spins, which included 13 step waves at 55g, two step waves at 42.8g, 23 earthquake ground motions at 55g, and two earthquake ground motions at 42.8g. After spin 5 it was determined that the beams of the one-story model had accumulated significant plastic strains and they were replaced with a new set of beams for the next spin. A list of ground motions completed during each spin is presented in Table 6-8, excluding step waves and the 42.8g earthquake ground motions. Only the spins consisting of earthquake ground motions are included. A complete list of ground motions and a detailed test chronology is presented in the Test 3 data report (Mason *et al.*, 2010c).

Table 6-8: Test 3 ground motions and their sequence (55g earthquake ground motions only)
(Mason *et al.*, 2010c)

Spin # Date	GM #	Ground Motion ID	Earthquake	Station	Amp. Factor^a	PGA^b
Spin 2 7-12-2010	1	JOS_L_1	92 Landers	Joshua Tree 090	0.22	0.07
Spin 3 7-15-2010	2	JOS_L_2	92 Landers	Joshua Tree 090	0.22	0.06
	3	TCU_L_1	99 Chi Chi	TCU078 270 (E)	0.55	0.13
Spin 4 7-16-2010	4	JOS_L_3	92 Landers	Joshua Tree 090	0.22	0.07
Spin 5 7-16-2010	5	JOS_L_4	92 Landers	Joshua Tree 090	0.22	0.06
	6	TCU_L_2	99 Chi Chi	TCU078 270 (E)	0.55	0.12
	7	RRS	94 Northridge	Rinaldi R Sta 228	0.42	0.40
	8	PTS	87 Sup Hills	Parachute T S 315	0.49	0.10
	9	SCS_L_1	94 Northridge	Sylmar Conv Sta 052	0.20	0.15
	10	LCN_1	92 Landers	Lucerne 260	0.70	0.26
	11	WVC_L	89 Loma Prieta	Saratoga WV Col 270	0.80	0.24
	12	SCS_H_1	94 Northridge	Sylmar Conv Sta 052	1.00	0.58
	13	PRI_H_1	95 Kobe	Port Island-Mod-79m	5.10	0.64
14	JOS_L_5	92 Landers	Joshua Tree 090	0.22	0.06	
Damaged one-story model beams replaced with new beams						
Spin 7 7-21-2010	15	JOS_L_6	92 Landers	Joshua Tree 090	0.22	0.06
	16	JOS_H	92 Landers	Joshua Tree 090	1.00	0.36
	17	WPI	94 Northridge	Newhall W Pico C 046	0.80	0.42
	18	TCU_H	99 Chi Chi	TCU078 270 (E)	1.00	0.33
	19	WVC_H	89 Loma Prieta	Saratoga WV Col 270	1.50	0.35
	20	SCS_H_2	94 Northridge	Sylmar Conv Sta 052	1.00	0.60
	21	PRI_2	95 Kobe	Port Island-Mod-79m	5.10	0.60
	22	SCS_H_3	94 Northridge	Newhall W Pico C 046	1.00	0.63
	23	JOS_L_7	92 Landers	Joshua Tree 090	0.22	0.07

^a Factor applied to the input ground motion

^b Measured at the base of the laminar box

6.5 Test 4: Anti-plane, and combined in-plane anti-plane SSSI configurations on dense, dry sand

6.5.1 Test description

After Test 3, which examined the effects of in-plane SSSI (or iSSSI) between two structures arranged in a line parallel to the direction of shaking, the preliminary goal for Test 4 was to simulate a ‘complete city block’ by including five structures on dry, dense sand. A series of numerical SSSI simulations were performed in the program SASSI (Lysmer *et al.*, 1999) considering various combinations of buildings, two of them with five buildings clustered together. These arrangements included the building models used in the prior tests, as well as their modified versions such as 1) one-story model in Test 3 on mat foundations instead of spread footings (MS1F_mat), and 2) the three-story model with a reduced (shallower) basement (MS3F_reduced). Numerical simulations were performed at the prototype scale for eight arrangements (CBL-1 to CBL-8) of building models (city blocks), with two of the arrangements consisting of five buildings clustered together. The SASSI numerical models of the individual structures are presented in Figure 6-16, and the numerical models of the arrangements are presented in Figure 6-17 and Figure 6-18. Global responses of the structures were calculated for each arrangement and compared to examine the effect of the surrounding buildings. Results from the larger arrangements, CBL-1 and CBL-2 showed some SSSI effects, but these arrangements were too complicated to draw definitive conclusions. Results from the smaller arrangements, CBL-3, CBL-4 and CBL-5, also showed some SSSI effects and prompted the need to first examine smaller arrangements with two or three buildings before considering the larger city blocks. This experience revealed the complicated nature of SSSI in practice and guided the City Block team to adopt a bottom-up approach to investigating this phenomenon. Test 4 was thus configured as a direct extension of Test 3, and examined two aspects of SSSI: 1) the effects of anti-plane SSSI (or aSSSI) between two structures arranged in a line perpendicular to the direction of shaking, and 2) the effects of SSSI in an ‘L’ shaped configuration achieved by combining the in-plane and anti-plane configurations (herein referred to as cSSSI).

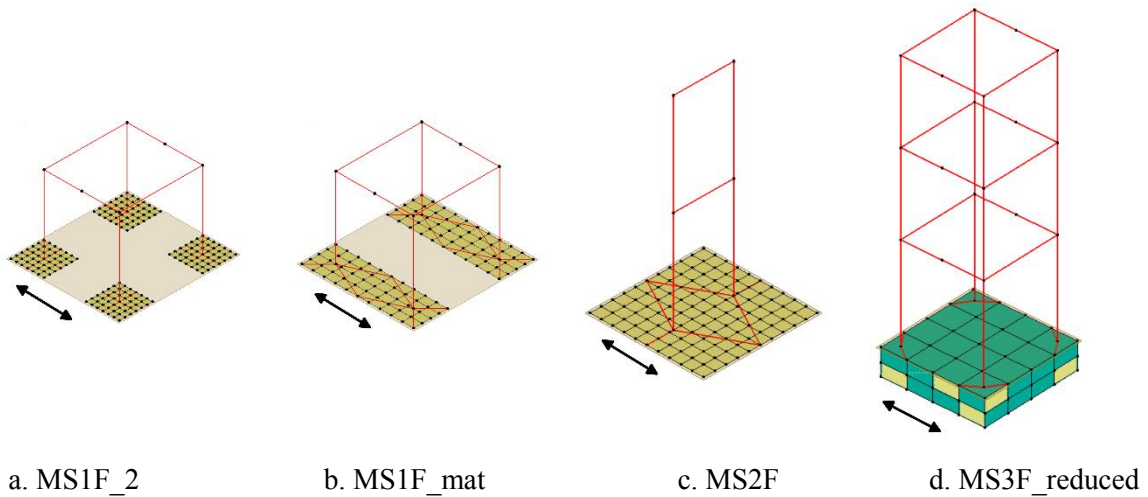


Figure 6-16: SASSI numerical models of individual buildings considered during the planning of Test 4 (arrows indicate direction of shaking)

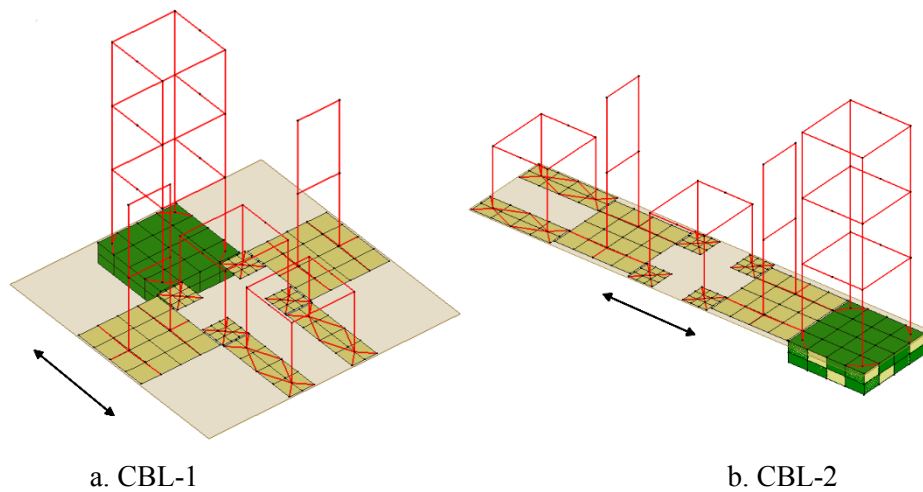


Figure 6-17: SASSI numerical models of the building arrangements, CBL-1 and CBL-2, considered during the planning phase of Test 4 (arrows indicate direction of shaking)

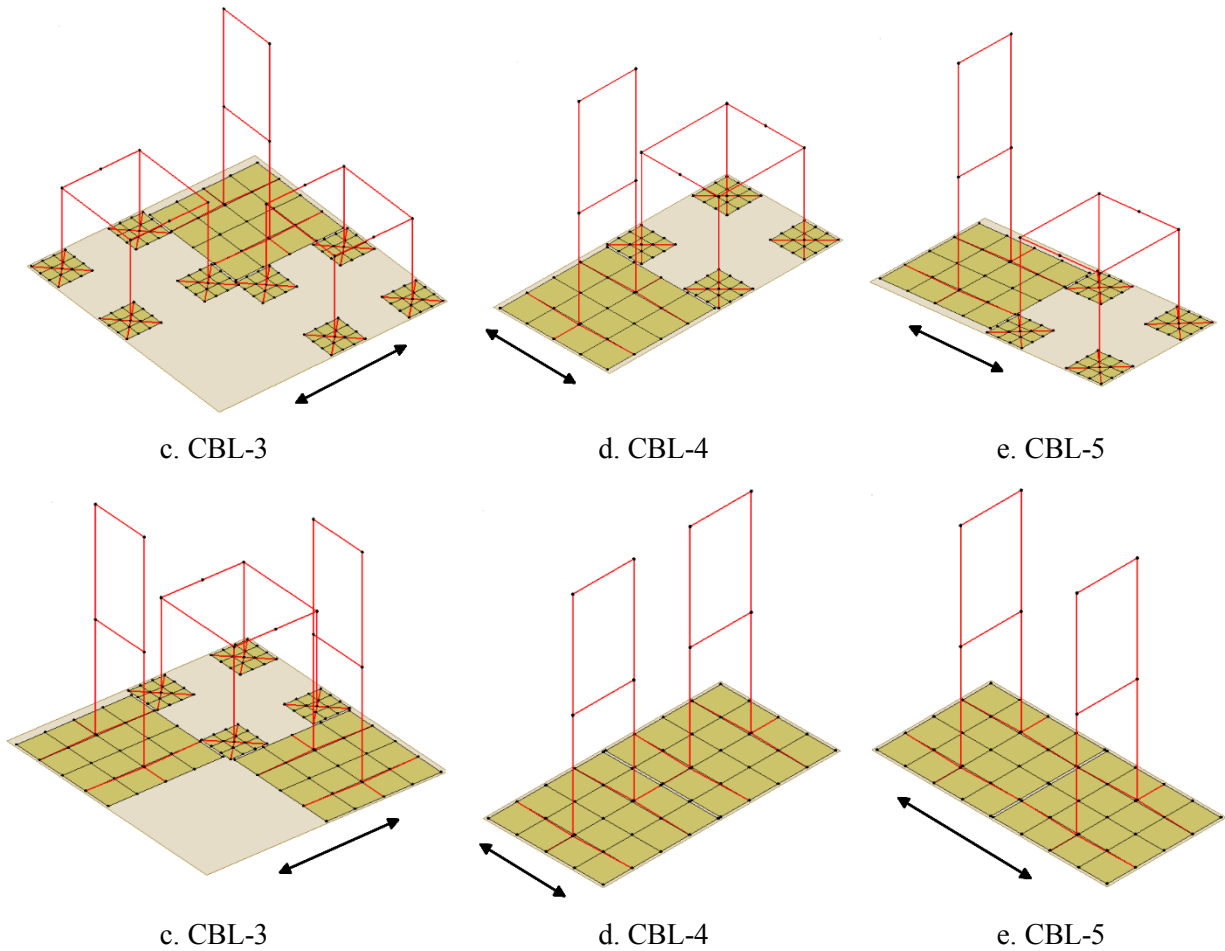


Figure 6-18: Numerical models of building arrangements, CBL-3 to CBL-5, considered during the planning phase of Test 4 (arrows indicate direction of shaking)

To maintain continuity with Test 3, the Test 4 models were designed to be as similar as possible to the Test 3 models (see Section 6.5.3.1 for the changes in model design from Test 3). No new models were designed for Test 4. The first configuration examining anti-plane SSSI consisted of two models placed at the north end of the laminar box arranged in a line perpendicular to the shaking direction (see Figure 6-19 and Figure 6-20): a one-story SMRF model and a two-story shear wall model, which are herein termed as MS1F_2_aSSSI, and MS2F_aSSSI respectively. The second configuration was placed at the south end of the box, and consisted of a one-story SMRF model with two adjacent two-story shear-wall models. This resulted in an ‘L’ shaped configuration with the one-story model at its corner (see Figure 6-19 and Figure 6-20). The one-story model of the second configuration is termed herein as MS1F_2_cSSSI, and the two-story models are termed as MS2F_ciSSSI and MS1F_caSSSI. Figure 6-19 presents a photograph of the Test 4 experimental models when fully instrumented and arranged in the

laminar box. Figure 6-20 presents sketches showing the exact locations of these models in the laminar box.

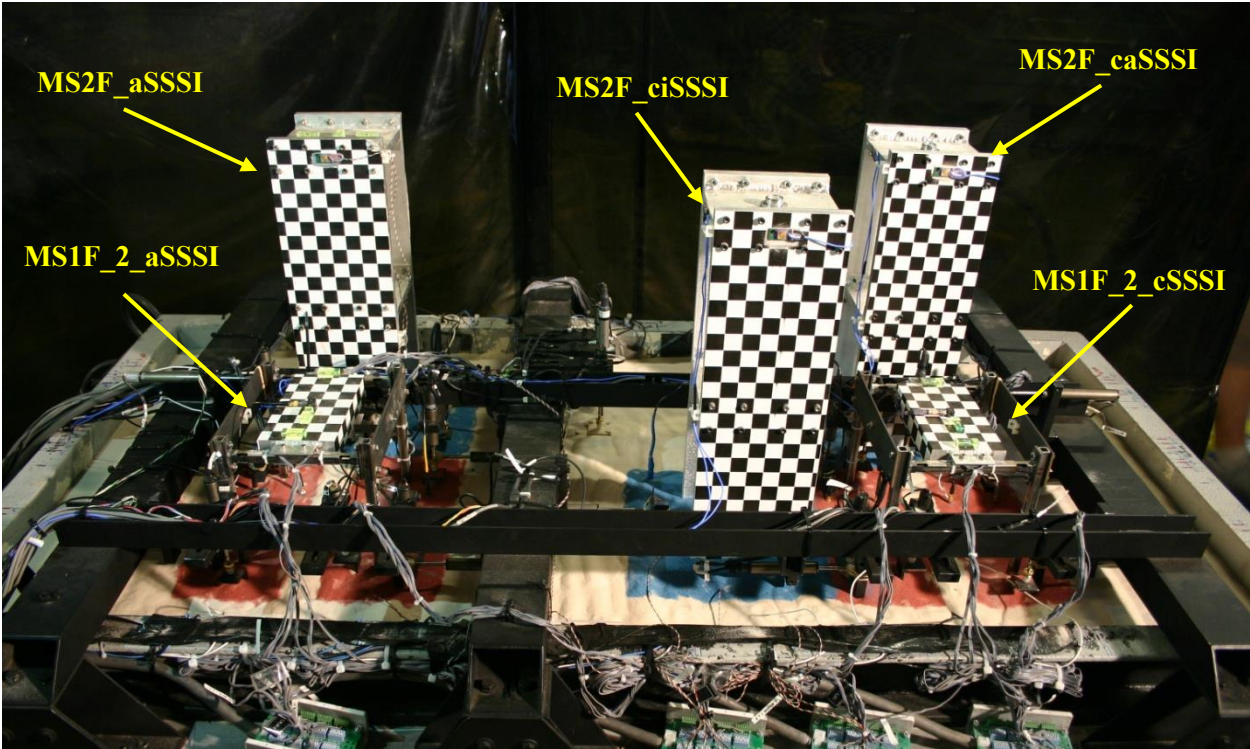
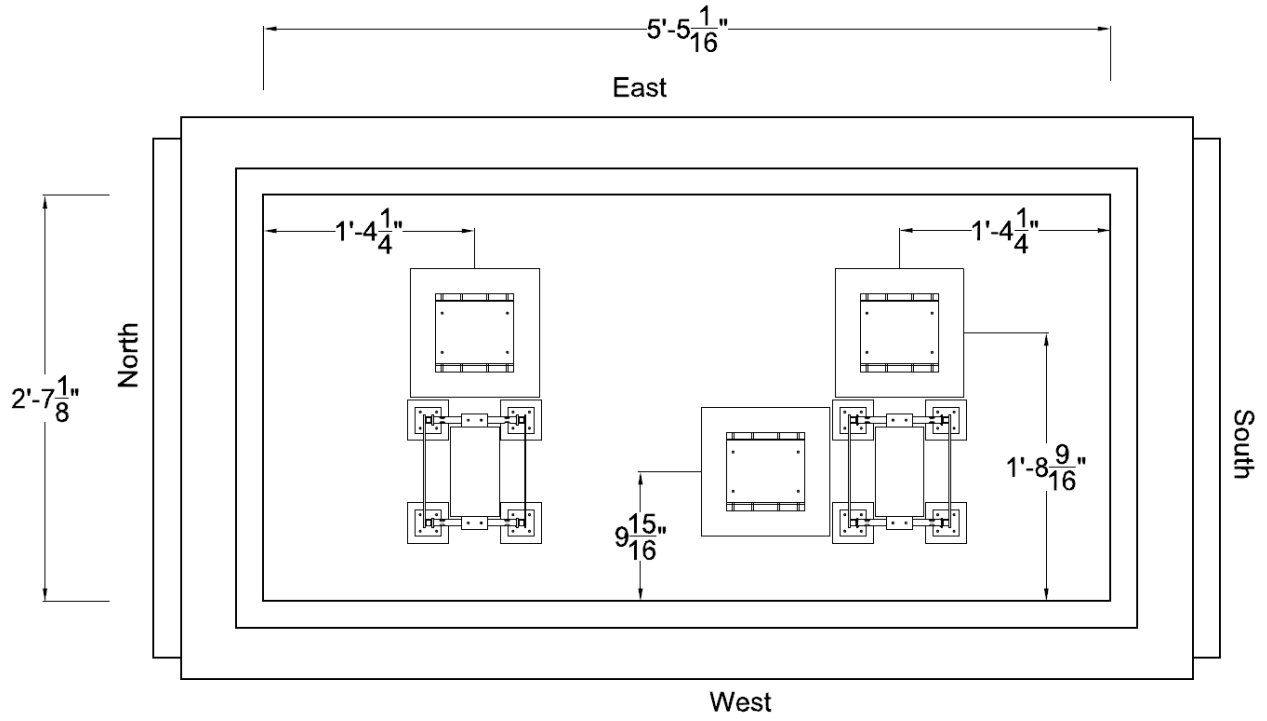
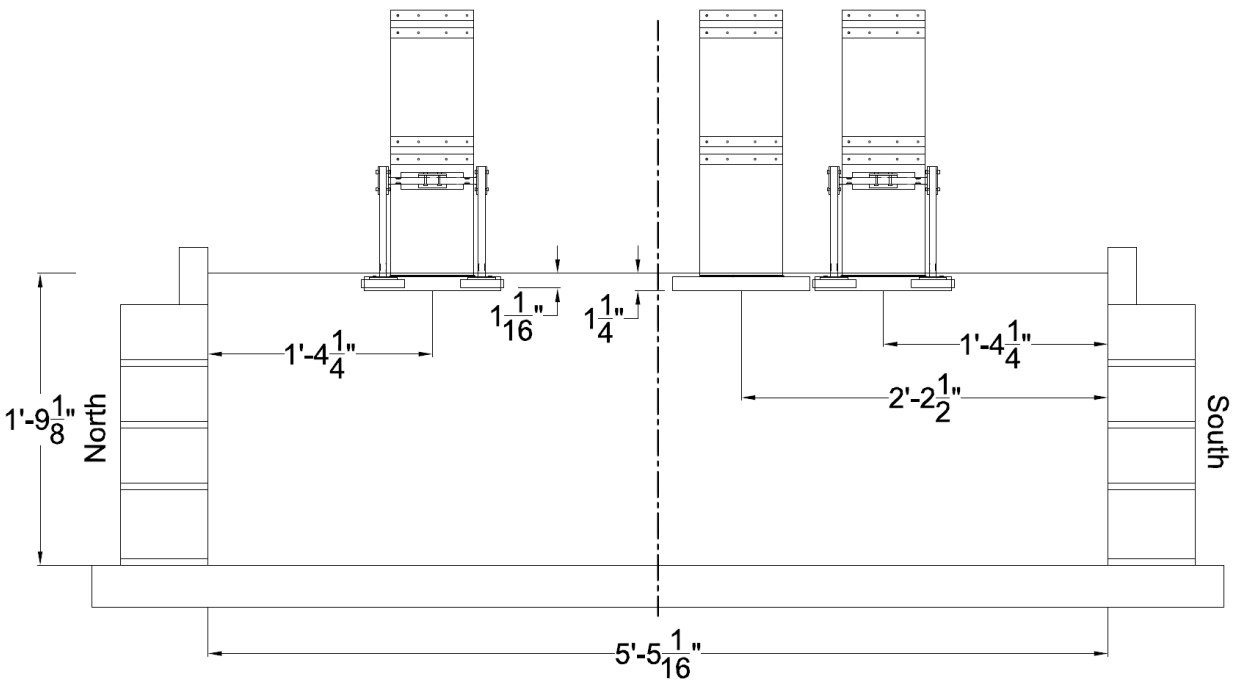


Figure 6-19: Photograph of the building models in the laminar box during Test 4



a. Plan view



b. Elevation view

**Figure 6-20: Locations of the models in the laminar box during Test 4 (dimensions in model scale)
(Trombetta *et al.*, 2011)**

Seminal analytical studies that examined SSSI (Luco and Contesse, 1973; Wong and Trifunac, 1975) dealt with anti-plane configurations. Specifically, they examined the interaction effects between infinitely long elastic shear wall structures with semi-circular foundations subjected to SH-waves exhibiting particle motions parallel to the length of the shear walls. Although the structures used in Test 4 are different from these analytical counterparts, it was expected that the results from the first portion of this test examining anti-plane SSSI serve to corroborate analytical observations. A comparison of the responses of this configuration in Test 4 with those of the in-plane configuration in Test 3 was expected to provide insight into the relative effects of iSSSI and aSSSI.

Observations made by Bray (2011) during earthquake reconnaissance visits suggest that corner buildings in dense urban areas undergo the most severe damage when struck by strong earthquakes. The second portion of Test 4 therefore attempts to simulate SSSI effects in a corner building of a City Block by superposing the in-plane and anti-plane configurations. This was also a progression towards the overarching goal of the project, which is to simulate a City Block with a two-dimensional array of structures clustered together.

6.5.2 Soil profile

Since Test 4 was an extension of Test 3, the soil profile in Test 4 was identical to that of Test 3. Dense, dry Nevada sand was used at a relative density of 80%, and the laminar box was filled to a depth of 21.1 in, which corresponds to a prototype depth of 96.7 ft. Details of the soil material are presented in Section 6.3.2, as well as the Test 4 data report (Trombetta *et al.*, 2011).

6.5.3 Model design and instrumentation

Two types of structural models were used during Test 4: the one-story SMRF model with shallow embedded footings and the two-story rocking shear wall model with a shallow embedded mat foundation. These models, designed for Test 3, acted as receiver and transmitter structures respectively, and were expected to exacerbate the in-plane SSSI effects. Therefore the same designs were used during Test 4. The design procedures and specifications of these models are presented in Section 6.4.3 and in the Test 3 data report (Mason *et al.*, 2010c). Only the modifications made to these designs for Test 4 are presented below.

6.5.3.1 Differences in model designs from Test 3

The two-story model used in Test 4 is identical to that in Test 3 and is not presented here. Slight differences in the one-story models arose due to unexpected problems (Trombetta *et al.*, 2011) in the

manufacturing of the beams and columns. After their delivery from the machine shop, it was noticed that the beams and columns had longer fuses than specified. While this difference was negligible for the columns, the beam fuses were 1.5 times longer than planned (Figure 6-21). The OpenSees numerical analysis of the model with the longer beam fuses showed a flexible-base 1st mode time period of 0.62 sec, rather than the period of 0.61 sec in Test 3 model. The yield drift ratios and the base shear ratios were similar to the Test 3 model. These differences were deemed insignificant and models were assumed to be sufficiently similar to enable a comparison of the results of Test 3 and Test 4.

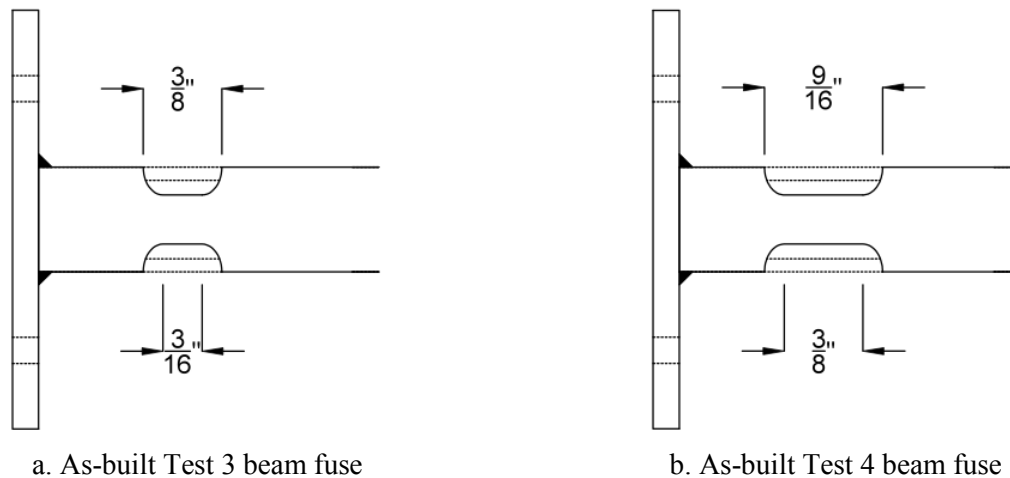


Figure 6-21: Differences between the Test 3 and Test 4 beam fuses (Trombetta *et al.*, 2011)

6.5.3.2 Instrumentation

The instrumentation strategy for Test 4 was quite similar to Test 3 since the models were almost identical. Since Test 4 involved five structures (unlike Test 3, which had three structures) the redundancy in the instrumentation had to be reduced for this test owing to the limited number of channels available for use. A total of 165 transducers were used during Test 4, which included uniaxial accelerometers, linear displacement potentiometers, and regular and high elongation strain gages. One hundred and twenty six of these transducers were used in the structure-foundation system, which consisted of 48 strain gages, 49 accelerometers, and 29 linear displacement potentiometers.

Similar to Test 3, standard elongation uniaxial strain gages were used at the top and bottom ends of the columns in the one-story models to measure bending moments and axial loads. The shear strains in the columns of the one-story models were not measured in this test, and no strains were measured in the two-story models.

The accelerometers in the structures were also placed in a similar manner to Test 3. Accelerometers placed on the floor masses and beams measured the translational acceleration in the two

horizontal directions, as well as the torsional acceleration. Since the two-story models were expected to respond mostly in a rocking mode, only the second story accelerations were measured. Three footings in each one-story structure were instrumented with horizontal and vertical accelerometers to measure the acceleration input to the superstructure, and the translational, vertical and rocking accelerations of the individual footings. The mat foundations were also similarly instrumented to measure the acceleration input to the superstructure, and the translational, torsional and rocking responses of the foundation.

Displacement transducers were placed throughout the structure-foundation system and attached to a specially designed rack, which also served as a reference frame for the displacement measurements. The horizontal displacement of each floor was measured by a linear potentiometer. Only the second floor displacements were measured in the two-story models. One horizontal potentiometer was installed for each footing of the one-story models to measure the transient and residual sliding displacements in the shaking direction. Settlement and rocking responses were recorded by vertically-installed potentiometers on the footings of the one-story models. Although translational displacements were measured for the foundations of all the three two-story models, rocking was only measured in the MS2F_aSSSI mat foundation.

The soil and laminar box were instrumented with 36 accelerometers and three displacement potentiometers. Accelerometers were installed through the depth of the soil profile and on the surface. An accelerometer placed at the soil surface exactly in between the two configurations was assumed to measure the free field surface acceleration. Further details regarding the Test 4 instrumentation are documented in the data report (Trombetta *et al.*, 2011).

6.5.4 Input ground motions and test chronology

During the first attempt at testing of the experimental model, the set up was damaged due to an accidental oil leak while the centrifuge was spinning up. A significant portion of the oil in the hydraulic system of the shake table was spilled onto the laminar box and its surroundings. It was later noticed that the oil had seeped into as much as 3 inches into the soil, and also under the foundations (Figure 6-22). This led to the test being abandoned and the model was rebuilt, starting from pluviation of the soil. The model that was tested during Test 4 was therefore the second centrifuge model.

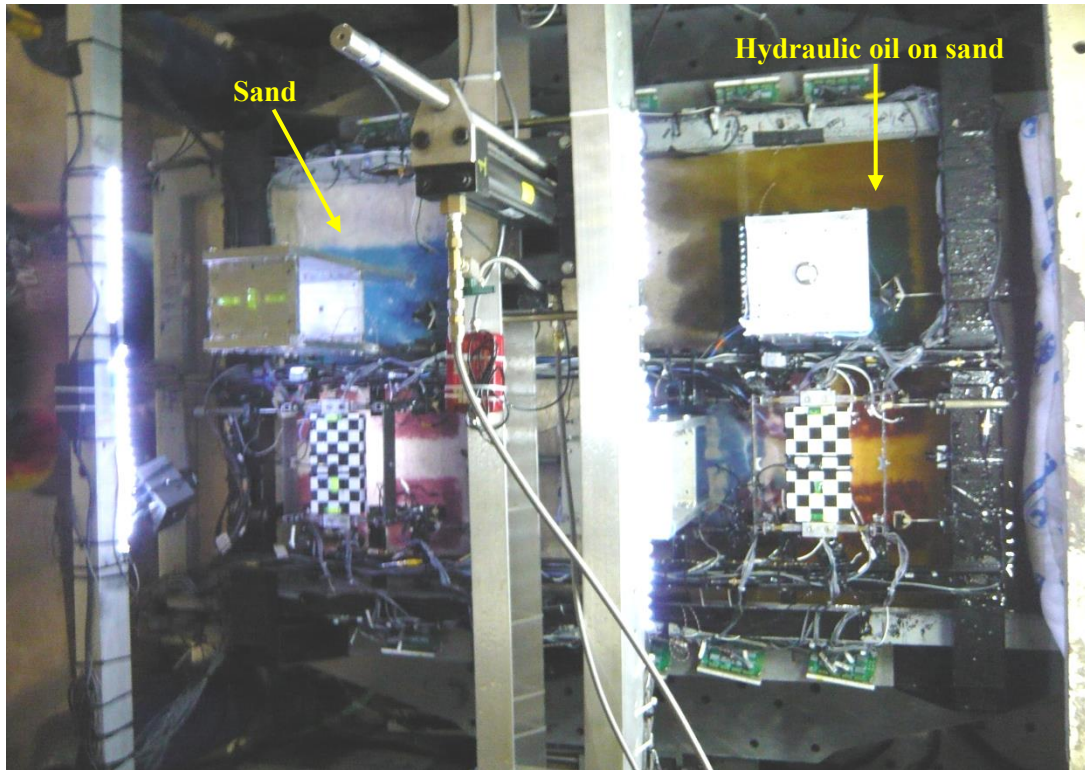


Figure 6-22: Photograph of the first centrifuge model on the arm shortly after the accidental oil leak

The rebuilt centrifuge model was spun for a total of five times and involved five CPTs, four bender element tests, and 47 shaking events. The goals of the original test plan were achieved after 26 shaking events in a span of four spins. However the in-test data processing results showed that the one-story model beams did not accumulate residual strains to the same extent as observed during Test 3 for the same ground motions. Despite the elastic strains being close to the Test 3 values, the differences in the residual strains of the beams were large enough that it was deemed to be due to an increase in the yield strength of the steel material, since a different batch of steel tubes was used after Test 3 (Trombetta *et al.*, 2011). Due to these differences, the ground motions were repeated after increasing the floor mass of the one-story models by 2.2 lb each, with an intention to further yield the beams and capture some nonlinear response. This part of the test is not relevant to this thesis and is not presented here. Complete details regarding this modification can be found in the Test 4 data report (Trombetta *et al.*, 2011).

The first 26 shaking events included eight step waves and 18 earthquake ground motions at 55g. The last 21 shaking events with increased one-story model floor masses included two step waves and 15 earthquake ground motions at 55g, and two step waves and two earthquake ground motions at 43g. Table 6-9 lists the 18 earthquake ground motions applied to the original model (with smaller floor masses) at

55g with their respective spin numbers. A detailed test chronology and a complete list of shaking events is presented in the Test 4 data report (Trombetta *et al.*, 2011).

Table 6-9: Test 4 ground motions and their sequence (only 55g ground motions applied to models with original floor masses are included) (Trombetta *et al.*, 2011)

Spin # Date	GM #	GM ID	Earthquake	Station	Amp. Factor ^a	PGA ^b
Spin 1 6-16-2011	1	JOS_L_1	92 Landers	Joshua Tree 090	0.22	0.06
	2	TCU	99 Chi Chi	TCU078 270 (E)	0.55	0.13
	3	RRS	94 Northridge	Rinaldi R Sta 228	0.42	0.37
Spin 3 6-17-2011	4	JOS_L_2	92 Landers	Joshua Tree 090	0.22	0.06
	5	PTS	87 Sup Hills	Parachute T S 315	0.49	0.12
	6	SCS_L	94 Northridge	Sylmar Conv Sta 052	0.20	0.19
	7	LCN	92 Landers	Lucerne 260	0.70	0.26
	8	WVC_L	89 Loma Prieta	Saratoga WV Col 270	0.80	0.24
	9	SCS_H	94 Northridge	Sylmar Conv Sta 052	1.00	0.58
	10	PRI_mod	95 Kobe	Port Island-Mod-79m	5.10	0.64
	11	PRI_mod_55	95 Kobe	Port Island-Mod-79m	7.00	0.58
Spin 4 6-20-2011	12	JOS_L_3	92 Landers	Joshua Tree 090	0.22	0.07
	13	JOS_L_4	92 Landers	Joshua Tree 090	0.22	0.06
	14	JOS_H	92 Landers	Joshua Tree 090	1.00	0.34
	15	WPI	94 Northridge	Newhall WPico C046	0.80	0.39
	16	TCU_H	99 Chi Chi	TCU078 270 (E)	1.00	0.31
	17	WVC_H	89 Loma Prieta	Saratoga WV Col 270	1.50	0.35
	18	JOS_L_5	92 Landers	Joshua Tree 090	0.22	0.07

^a Factor multiplied to the input ground motion

^b Peak acceleration measured at the base of the laminar box

SECTION 7

EXPERIMENTAL RESULTS AND COMPARISON WITH NUMERICAL SIMULATIONS

7.1 Introduction

This section presents an analysis of the data recorded in the centrifuge experiments described in Section 6, and a qualitative comparison of this data with responses calculated using numerical simulations. The site response of the soil profile, soil-structure interaction (SSI) and structure-soil-structure interaction (SSSI) effects in the building models are examined. Numerical site-response analyses are performed using SHAKE, DEEPSOIL and LS-DYNA. Soil-structure interaction analyses are performed using SASSI and LS-DYNA. The data analysis and numerical simulations are only performed for a subset of the ground motions used during the experiments. Section 7.2 presents the scope of experimental data analysis and numerical simulations performed in this section. Section 7.3 describes the numerical simulations of site response using the three programs, and compares the experimental and numerical site responses. Section 7.4 presents a description of the soil-structure interaction simulations of the experiments of Tests 3 and 4, and examines SSI and SSSI effects observed in the experiments and numerical simulations.

7.2 Scope of experimental data analysis and numerical simulations

A large amount of data was recorded during the NEES City Block centrifuge experiments from strain gages, accelerometers and displacement transducers placed on, in and around the experimental models. These data are used to gain insight into the effects of SSI and SSSI on both global and local structural behavior. From the City Block project team, Trombetta *et al.* (2013a) and Mason *et al.* (2013) used data from Test 1 and Test 2 to study the effects of SSSI on the nonlinear response of superstructures and foundations. Importantly, they showed that the footings of the one-story model showed a stiffer moment-rotation response when placed against the basement of the three-story model, resulting in larger demands in the columns of the superstructure. Chen *et al.* (2013) developed a seismic system-identification framework to estimate SSI parameters from centrifuge test data, and successfully applied this framework to data recorded during Test 1 and Test 2. In a separate study, Trombetta *et al.* (2013b) utilized data from Tests 3 and 4 and examined SSSI effects on structural response through spectral analysis. They also studied the effects of SSSI on footing response and hysteretic damping of the one-story structure.

The studies presented in the following sections examine SSSI effects on the structures in Tests 3 and 4, which involved the two building models, MS1F_2 and MS2F, being tested in various arrangements. These arrangements included, 1) in-plane SSSI (or iSSSI)¹¹ between MS1F_2 and MS2F during Test 3, 2) anti-plane SSSI (or aSSSI)¹¹ between MS1F_2 and MS2F during Test 4, and 3) combined in-plane anti-plane SSSI or (cSSSI)¹¹ between two MS2F models and MS1F_2 in an ‘L’ shaped arrangement, as shown in Figure 7-1. MS1F_2 was also tested alone with no SSSI effects. This case of MS1F_2 provides a baseline to examine SSSI effects in other configurations. However the baseline case for MS2F was not established by testing. Numerical simulations are performed for all the cases considered in Tests 3 and 4. Additionally, the baseline case for MS2F is simulated for completeness. The different arrangements used in Tests 3 and 4, and the nomenclature used for the individual models in these arrangements is summarized in Figure 7-1.

The soil and structural specimens used in the different experiments were built from different batches of the same materials. There are minor differences in the construction of MS1F_2 across different tests, as explained in Section 6.5.3.1. Sequential testing in the centrifuge results in variations in the structural and soil properties over the course of each test as a consequence of nonlinear behavior and accumulation of permanent strains in the soil and the structure. For these reasons, only a few of the ground motions used in the experiments are selected for the comparison of structural and soil responses across different tests. These ground motions are selected such that 1) the specifications of MS1F_2 used in Tests 3 and 4 are almost identical, 2) they follow the same order in the different tests, thus maintaining similar initial conditions, and 3) the structures are almost elastic and have little or no damage at the beginning of the first ground motion in each test. The selected ground motions are listed in Figure 7-1, and their response spectra and acceleration time series are presented in Figure 7-2 and Figure 7-3, respectively.

¹¹ In-plane interaction refers to the interaction between structures arranged along the axis of ground shaking. Anti-plane interaction refers to the interaction between structure arranged in a direction perpendicular to the direction of shaking. Combined in-plane anti-plane interaction refers to the interaction between structures placed in an ‘L’ shaped arrangement as shown in Figure 6-19.

Chosen ground motions

1. JOS_L
2. LCN
3. SCS_H
4. PRI_H

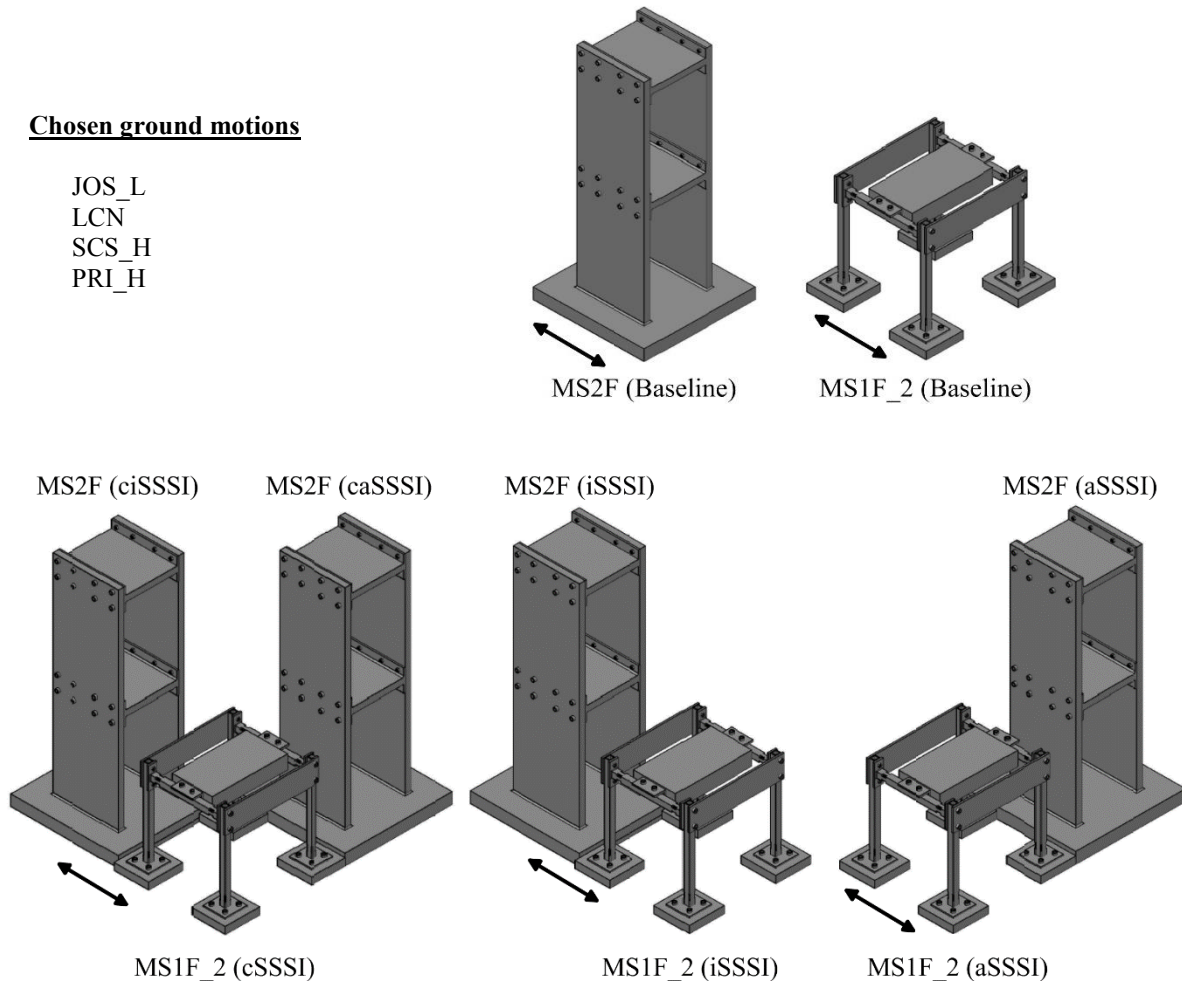


Figure 7-1: Ground motions selected, and the nomenclature used for the experimental models during data analysis and numerical simulations performed for Tests 3 and 4 [arrows indicate direction of shaking; renderings adopted from Trombetta (2013) and modified]

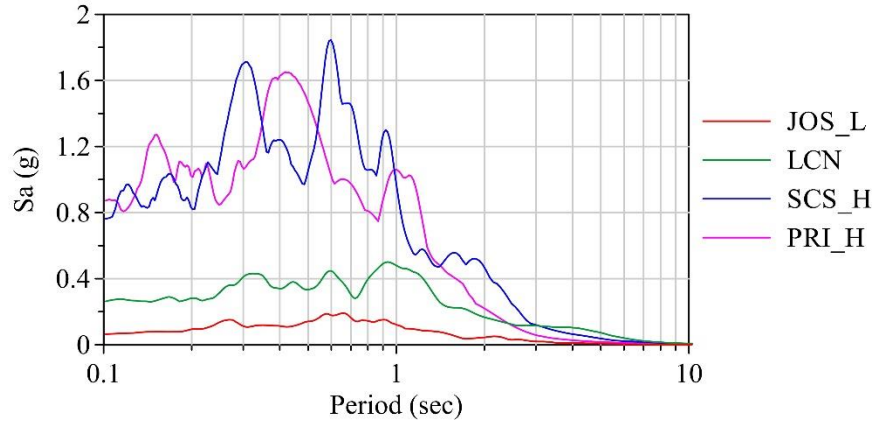


Figure 7-2: Five percent damped acceleration response spectra of the ground motions selected for data analysis and numerical simulations

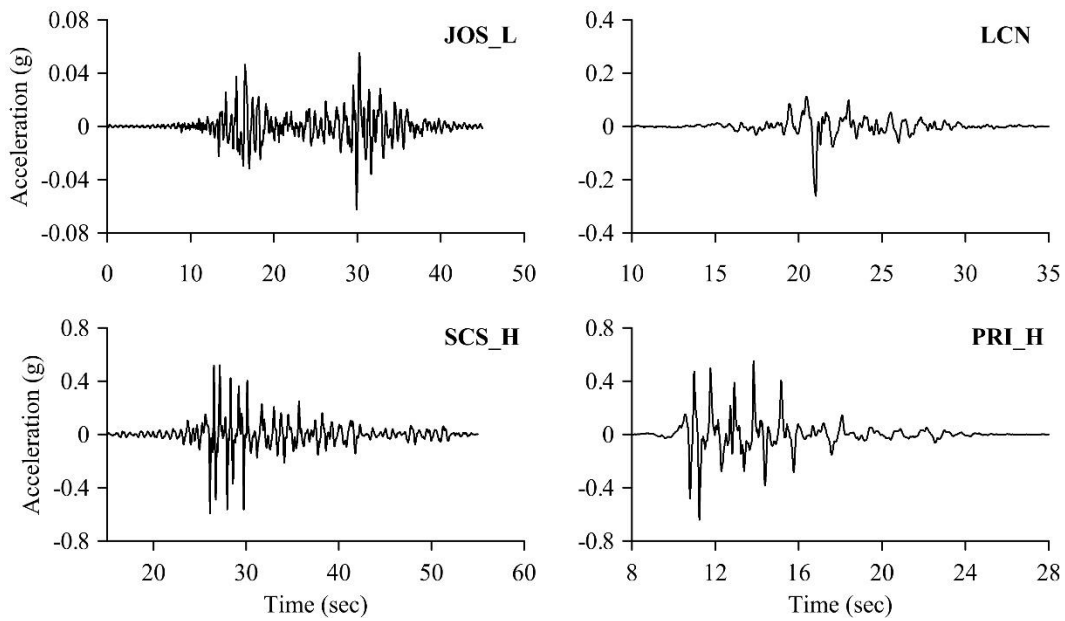


Figure 7-3: Acceleration time series of the ground motions selected for data analysis and numerical simulations

Centrifuge models do not exactly represent a real soil-structure system due to boundary effects and box-shaker-container interaction (Ilankatharan, 2008; Ilankatharan and Kutter, 2010; Kutter, 1995), as described in Section 6.2.2. Numerical simulation of a centrifuge experiment for validation purposes should ideally address all of these limitations (Oberkampff and Trucano, 2008) to enable a robust comparison of experimental and numerical results. Addressing these limitations in numerical simulations

is a challenging task and requires a good understanding of the underlying mechanisms (e.g., shaker-container interaction) and the involved physical properties (e.g., the friction coefficient between the soil and the walls of the container). Additionally numerical programs such as SHAKE and SASSI are limited to linear analyses and therefore cannot explicitly capture nonlinear aspects of the soil-structure system such as nonlinear site response, yielding of the beam fuses, sliding, gapping and uplift of the foundations, and softening of the soil in the immediate vicinity of the foundation. Aside from these challenges, the City Block project did not involve comprehensive soil testing, requiring the use of calibration and empirical relations and databases from the literature to calculate soil properties for the numerical simulations. Accordingly, direct numerical simulations of the centrifuge tests are not performed in the study presented in this section. Instead, numerical models are built as follows:

1. The numerical models are built at the prototype scale and not at the centrifuge model scale.
2. The numerical models are built assuming almost complete dissipation of the radiated waves, thus neglecting lateral boundary effects in the laminar box.
3. The numerical models are built with a fixed base, assuming no energy dissipation at the base of the soil profile, as opposed to the energy dissipation that occurs at the base of the laminar box due to shaker-container interaction (Section 6.2.2).
4. The foundation embedment in the numerical models is slightly smaller than those adopted in the experiments, for both structures. The foundations in the numerical model are embedded to a depth equal to the thickness of the foundation, simplifying the finite element meshing of the foundations and the surrounding soil.
5. The numerical simulations are performed separately for each ground motion and not consecutively as in the experiments, setting aside cumulative soil strain, cumulative structural damage, and changing soil properties due to consolidation.

These modifications might lead to a considerable deviation of the numerical response of the models from the experimental response, but they are required given the aforementioned limitations. It is assumed that they do not considerably affect the interaction between the structures (i.e., the comparison of structural responses when it is tested alone and in the presence of neighboring structures). As a consequence of these modifications, it is more appropriate to make only qualitative comparisons between the numerical and experimental results and not a direct comparison. The following sections describe the numerical simulations of site response and SSI, and compare experimental and numerical results. Section 7.3 presents a description and results of site-response simulations, and Section 7.4 presents a description and results of SSI and SSSI simulations.

7.3 Examination of site response

Site-response analysis is performed at the prototype scale using SHAKE (Schnabel *et al.*, 1972) and DEEPSOIL (Hashash *et al.*, 2011) for the ground motions listed in Figure 7-1. Numerical modeling in these programs includes layering the soil profile and specifying the material properties, input ground motion, and analysis parameters. The ground motion recorded at the base of the laminar box during the experiments is used as the input at the base of the soil profile model assuming rigid bedrock. Since the same set of input ground motions were used in all the City Block experiments, site-response analyses are only performed for the input ground motions recorded during Test 3. Slight differences exist between the same input ground motions recorded in the different tests, but it is assumed that these differences have only a minor effect on the strain-compatible shear moduli and damping ratios of the soil. The inter-test and intra-test variability in the ground motions recorded at the base of the laminar box are investigated in Section 7.3.4.

7.3.1 Calculation of the material properties

For Tests 1 through 4, the laminar box was filled with dry Nevada sand filled to a depth of 21.1 inches (equivalent to 29.5 m at the prototype scale using the scale factor $N = 55$). This soil profile is modeled at the prototype scale with 14 layers lying atop a bedrock halfspace. An initial damping ratio of 0.05, and a density of 16.66 kN/m^3 is assumed for all the layers in the soil profile. The small-strain shear modulus, G_{\max} , is evaluated for each layer using the following empirical relationship developed for sands (Kramer, 1996; Seed and Idriss, 1970):

$$G_{\max} = 1000K_{2,\max}(\sigma'_m)^{0.5} \quad (7-1)$$

In this equation, $K_{2,\max}$ is a parameter determined from the void ratio or relative density of the sand, and σ'_m is the mean principal effective stress at the corresponding depth. The depth of a layer is taken as the distance from the soil surface to the center of that layer. A value of 50 is chosen for $K_{2,\max}$, based on a calibration analysis¹² performed using the JOS_L_1 motion of Test 4. The mean principal effective stress, σ'_m , is calculated as

¹² The maximum shear moduli calculated using equation (7-1) are only estimates and not based on laboratory testing. Due to a lack of reliable test data to calculate the small-strain shear modulus, the SHAKE numerical model is calibrated to reproduce the response of the soil profile measured during the experiment. This is done by modifying the parameter $K_{2,\max}$ (and therefore the input shear moduli) so that the response calculated at the surface of the soil profile for the ground motion JOS_L_1 matches the surface free-field response recorded during the experiment.

$$\sigma'_m = \sigma'_v \left(\frac{1+2K_0}{3} \right) \quad (7-2)$$

where σ'_v is the effective vertical pressure, and K_0 is the coefficient of earth pressure at rest. Since the sand used in the experiment is completely dry, σ'_v at a particular depth in the soil profile is calculated as the vertical pressure at that point. A constant value of 0.35, which is suitable for dense sands, is chosen for K_0 following Craig (1997). Using these parameters, the mean principal effective stress and therefore G_{\max} is calculated for each layer. These values are presented in Table 7-1. The individual layer thicknesses are chosen such that a maximum frequency of 8 Hz can pass through the soil column according to equation (4-1). The layer thicknesses are also presented in Table 7-1.

Table 7-1: Soil layer properties used for site-response analysis in Tests 3 and 4

Layer	Thickness (m)	Unit Weight (kN/m ³)	G_{\max} (MPa)
1	1.80	16.66	31.9
2	2.00	16.66	56.3
3	2.10	16.66	74.0
4	2.10	16.66	88.6
5	2.10	16.66	101.1
6	2.10	16.66	112.2
7	2.10	16.66	122.3
8	2.10	16.66	131.7
9	2.10	16.66	140.4
10	2.10	16.66	148.6
11	2.10	16.66	156.4
12	2.10	16.66	163.8
13	2.10	16.66	170.9
14	2.57	16.66	178.4

7.3.2 Site-response analysis in SHAKE

The following properties are input for each layer for a SHAKE analysis: 1) layer thickness, 2) mass density, ρ , 3) small-strain shear modulus, G , 4) small-strain damping ratio, β , and 5) dynamic material properties (modulus reduction and damping curves). The values presented in Table 7-1 are directly input into SHAKE, along with a small-strain damping ratio of 5% for all the layers. The modulus reduction and damping curves developed by Seed and Idriss (1970) for sands are used in the analyses. The lower bound modulus reduction curve (panel a, Figure 7-4) and the upper bound damping ratio curve (panel b, Figure 7-4), both of which are available in the SHAKE database, are employed. The bedrock is modeled using a linear elastic material with no modulus reduction and a constant damping ratio of 1%. The traditionally recommended value of 0.65 is used for the effective shear strain ratio. Analyses are performed for the four ground motions of Figure 7-1. The free-field site responses are presented in Section 7.3.4.

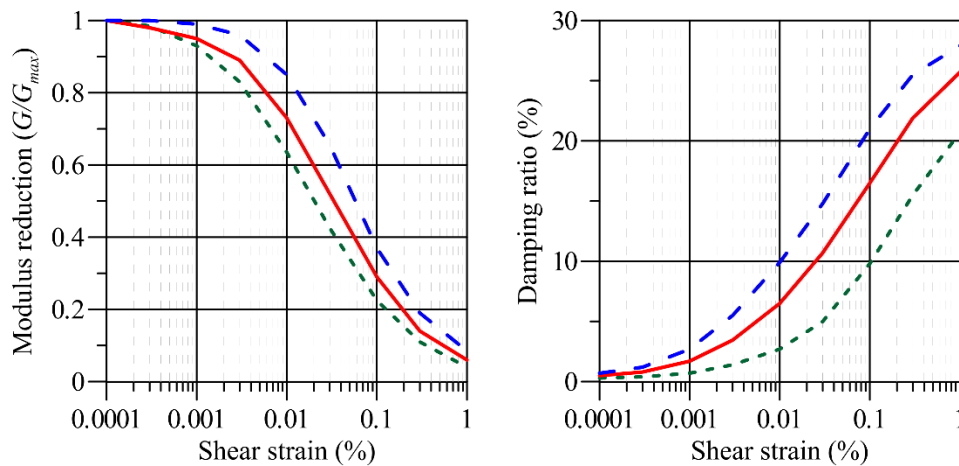


Figure 7-4: Modulus reduction and damping curves for sand calculated by Seed and Idriss (1970)

7.3.3 Site-response analysis in DEEPSOIL

DEEPSOIL performs time-domain nonlinear site-response analysis using the modified hyperbolic model, or the Modified Kodner-Zelasko (MKZ) model (Matasovic, 1993), to simulate the shear behavior of soil. This model is described in detail in Section 2.2.2.3.1. Each layer in the DEEPSOIL is defined by same properties as in SHAKE. However DEEPSOIL uses the MKZ model instead of modulus reduction and damping curves. The layer thickness, unit weight and the small strain shear modulus of the soil layers are listed in Table 7-1. The model parameters that define the MKZ model are listed in Table 7-2. These parameters are chosen such that the resulting modulus reduction and strain compatible damping curves

are almost equal to those specified in the SHAKE analysis, thus maintaining equivalence between the material properties. The MKZ model parameters are calculated using a curve-fitting tool included in DEEPSOIL that calculates the appropriate values for the parameters for a given pair of shear modulus and damping curves. A detailed description of the calculation of the model parameters corresponding to a given set of modulus reduction and damping curves is presented in Phillips and Hashash (2009) and the DEEPSOIL user manual (Hashash *et al.*, 2011). Additionally, a value of 0.001 is used for the maximum strain increment for all ground motions. This parameter affects the time-step calculation in the Newmark- β method (Hashash and Park, 2001; Hashash *et al.*, 2011).

Table 7-2: DEEPSOIL curve parameters used for the Test 4 site-response analysis

Small-strain damping ratio ¹ , ξ (%)	0.42
Reference strain ² , γ_r (%)	0.0378
Stress-strain curve parameter, β	1.56
Stress-strain curve parameter, s	0.765

¹ Pressure dependence of damping is ignored by setting the parameter d to 0

² Pressure dependence of the stress-strain curve is ignored by setting the parameter b to 0

7.3.4 Site-response analysis in LS-DYNA

Site-response analyses for the City Block soil profile are also performed using the nonlinear finite element program, LS-DYNA, for the ground motions listed in Figure 7-1. Section 2.2.2.3.2 presents a description of nonlinear site-response analysis using LS-DYNA. Only the details specific to the analyses of the City Block soil profile are presented in this section. The layering of the soil profile in LS-DYNA is identical to SHAKE and DEEPSOIL. Each of the 14 soil layers, with properties presented in Table 7-1, is modeled using a single eight-noded solid element in LS-DYNA. All these elements are constrained to move in pure lateral shear. The acceleration input is applied directly at the base of the soil column, which is consistent with a rigid bedrock assumption beneath the soil profile. Figure 7-5 presents the LS-DYNA model of the soil profile used for site-response analysis.

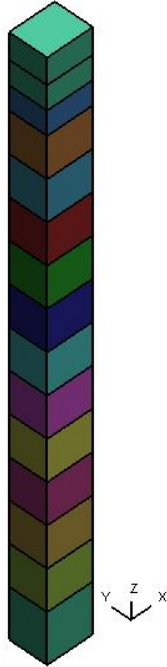


Figure 7-5: LS-DYNA finite element model for the site-response analysis of the City Block soil profile

The soil material is modeled using the MAT_HYSTERETIC model (LSTC, 2013), described in Section 2.2.2.3.2. This model simulates the shear behavior of soil with a piece-wise linear stress-strain curve such as that shown in Figure 2-7. These stress-strain curves are calculated from the modulus reduction curves using the following equation,

$$\tau(\gamma) = \frac{G}{G_{\max}}(\gamma) \cdot G_{\max} \cdot \gamma \quad (7-3)$$

where τ and γ are the instantaneous shear stress, and shear strain, respectively, and G/G_{\max} is the modulus reduction ratio. The modulus reduction curve used for SHAKE is used for the calculation of the stress-strain curves of all the layers.

7.3.5 Variability in the input ground motion and soil properties during the experiments

The primary goal of this section is the examination of SSSI effects, which involves comparison of the responses of MS1F_2 and MS2F recorded in the various arrangements of Tests 3 and 4. Factors such as variability in the soil properties in different tests and the variability in the input ground motions contribute to the differences between the structural responses across the tests. Therefore, it is important to examine these factors before making observations on the effects of SSSI on structural response in Section

7.4.4. Two factors are examined in this section: 1) the inter-test and intra-test variability in the input ground motion, and 2) the inter-test and intra-test variability in site response, which identifies the variability in soil properties.

Figure 7-6 presents the acceleration response spectra of the input ground motions achieved by the centrifuge shaker during Tests 1 through 4 for nine ground motions, including the four ground motions considered in this section. The figure shows significant inter-test variability in the input for four ground motions: JOS_L, TCU_L, PTS and SCS_L. However the inputs achieved during Tests 3 and 4 are similar for all the ground motions: even more so for the ground motions, JOS_L, LCN, SCS_H and PRI_H, which are the ground motions selected for analysis in this section. The reasons for the inter-test variability in the ground motions is not relevant to this discussion. However, to objectively examine the SSSI effects during the experiment for these ground motions, the variability in inputs must be considered.

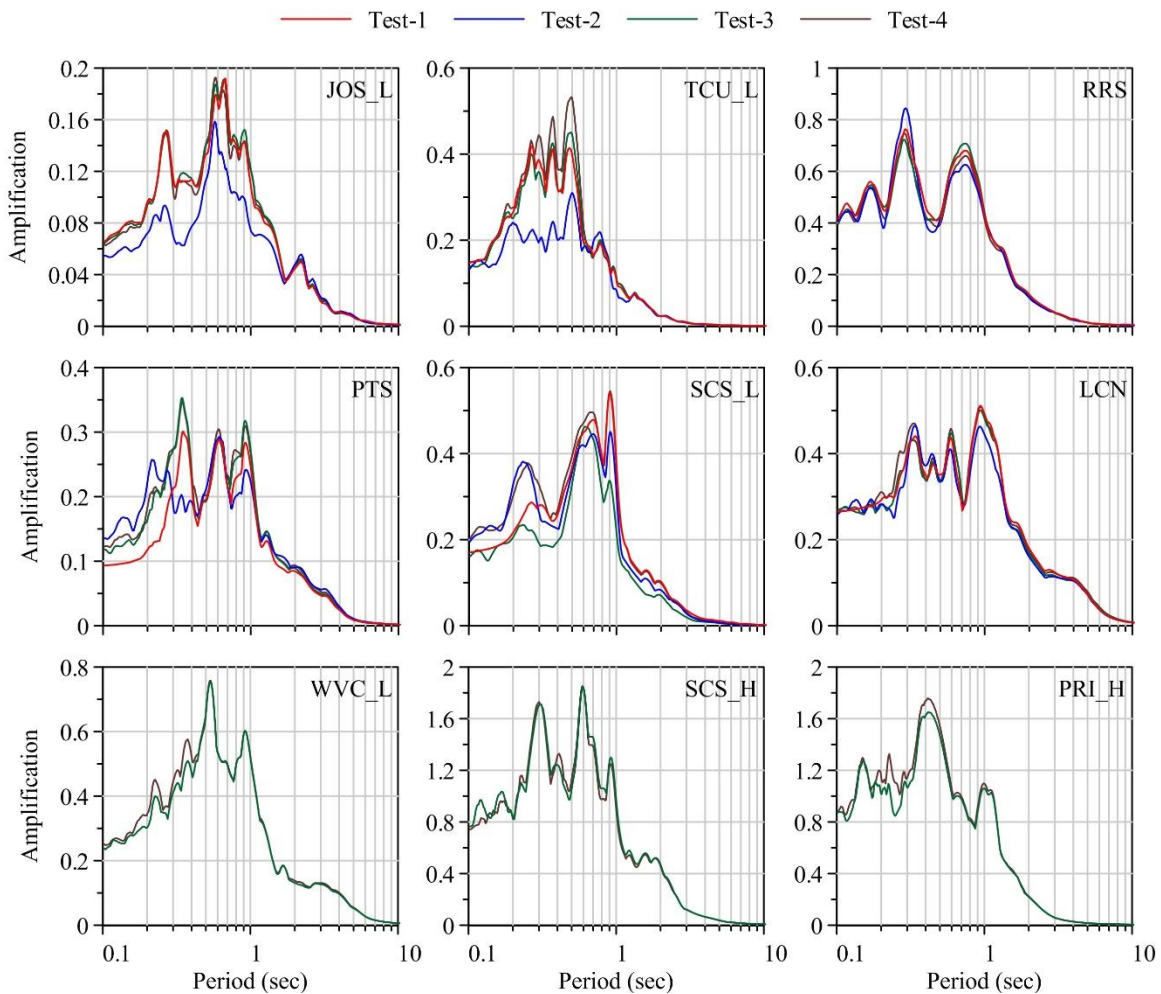


Figure 7-6: Acceleration response spectra of the considered input ground motions (recorded at the base of the laminar box) in Tests 1 through 4

The ground motion JOS_L was input seven times at various instances during Test 3. Data from six inputs are used to examine the variability in site response during the test: intra-test variability. Figure 7-7 presents the acceleration response spectra of the input at the base of the laminar box, and the spectral amplifications of the free-field acceleration at the surface of the soil. Small differences are evident in the input acceleration, but the variability in the amplifications is considerable. The intra-test variability in site response, although not significant, shows that progressive changes in soil properties will result in a change in site response and therefore adds to the variability in the acceleration input to the structure. This variability must be considered in the analysis of data from a centrifuge test.

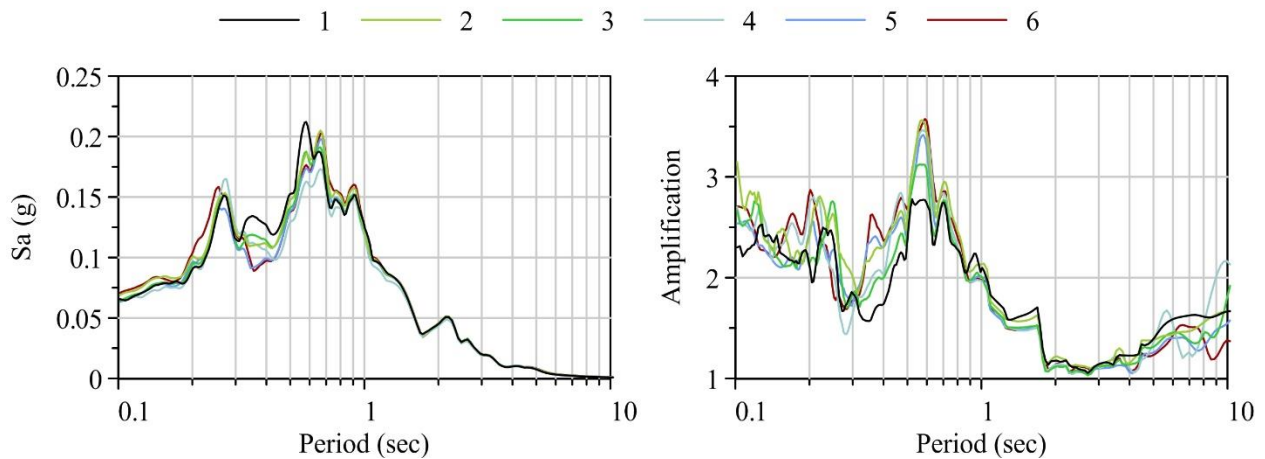


Figure 7-7: Acceleration response spectra of the input at the base of the laminar box (left) and surface-free-field-to-base transfer functions (right) calculated for six applications of the JOS_L ground motion during Test 3

7.3.6 Comparison of experimental and numerical site responses

The experimental and numerical site responses for the ground motions considered for data analysis (see Figure 7-1) are presented in this section. Comparisons are made between the experimental site responses and the numerical site responses calculated using SHAKE, DEEPSOIL and LS-DYNA. Figure 7-8 presents the response spectra of the free-field surface accelerations for the ground motions selected for detailed analysis in this section. The plots in the left column present spectra calculated from experimental recordings in Tests 3 and 4; the plots in the right column present spectra calculated from numerical simulations in SHAKE, DEEPSOIL and LS-DYNA. The figure shows differences between the response spectra of each ground motion recorded in Tests 3 and 4. These differences are a result of the variation in the input ground motion, as discussed earlier, and different mechanical properties for the soil specimens used for Tests 3 and 4. However, these differences are smaller than those in the results of the

numerical simulations, which show that the nonlinear programs, DEEPSOIL and LS-DYNA, yield similar results, but that these are significantly different from the equivalent-linear results produced by SHAKE. In particular, SHAKE predicts larger spectral accelerations than the nonlinear programs for all ground motions, especially at the site period (period of maximum spectral acceleration). This overprediction is a consequence of the equivalent-linear method accounting for nonlinear behavior in an ‘averaged’ sense¹³.

Figure 7-8 also shows significant differences between the experimental and numerical results for all ground motions, except the JOS_L ground motion. The results for the JOS_L ground motion match better since the soil profile properties input to the numerical models are calculated through calibration using data from this ground motion. For the other ground motions, the shapes of the experimental and numerical response spectra are qualitatively similar, albeit having different magnitudes, especially at periods smaller than the site period. In addition, the numerical simulations also reasonably predict the site period for the JOS_L, LCN and PRI_H ground motions. Figure 7-8 shows that the site period is about 0.6 sec during the JOS_L ground motion, and about 1 sec during the LCN and PRI_H ground motions. The site period is not clear from the surface response spectra for the SCS_H ground motion. The numerical programs reasonably capture the elongation of the site period for increasing intensity of ground motions (JOS_L < LCN < SCS_H < PRI_H). The primary reason for the large differences between the experimental and numerical results is the lack of measured material properties. Whereas the numerical programs reasonably predict the almost linear response during the low-intensity JOS_L ground motion, the predictions of the measured responses for the more intense ground motions are poor, reinforcing the need for estimates of nonlinear properties (or modulus reduction and damping curves) for validation of soil models and computer codes.

¹³ The variability in the results of the numerical programs was examined in more detail in Section 4.

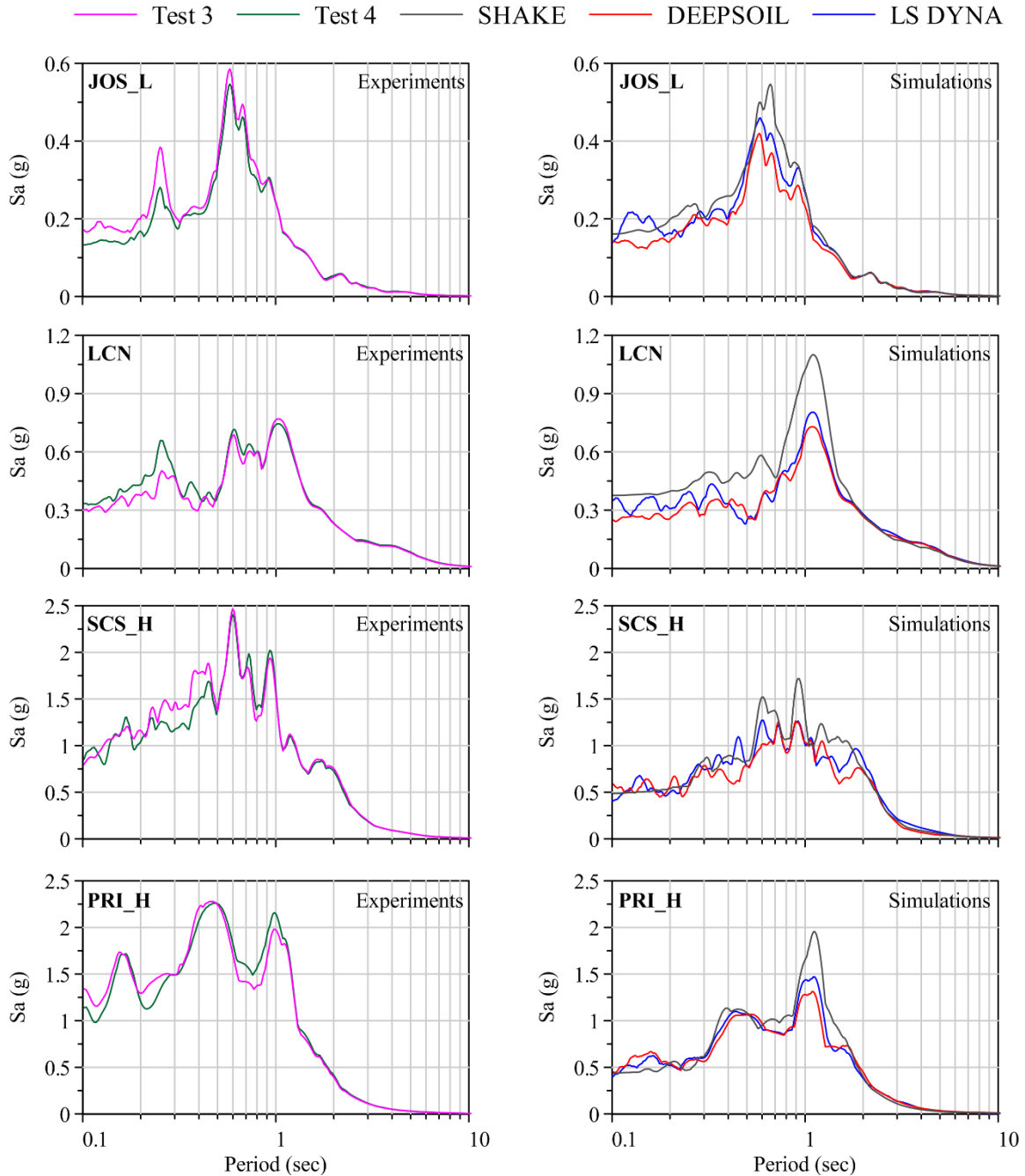


Figure 7-8: Free-field surface acceleration response spectra calculated from experimental data and numerical simulations for the considered ground motions in Tests 3 and 4

7.4 Examination of SSI and SSSI effects

The experimental data is analyzed in this section to examine the soil-structure interaction and structure-soil-structure interaction effects observed in Tests 3 and 4. Numerical simulations of the

centrifuge tests are also performed at the prototype scale. Linear analyses are performed using SASSI and nonlinear analyses are performed using LS-DYNA, for all structural arrangements for the ground motions listed in Figure 7-1. Numerical modeling in these programs is described in the next sections, and qualitative comparisons between the experimental and numerical results are made in Section 7.4.4.

7.4.1 Modeling in SASSI

SASSI modeling for the simulation of Tests 3 and 4 is described in this section. A more detailed description of SSI analysis in SASSI is presented in Section 3.3.1 as well as in Bolisetti (2010). The SASSI numerical model comprises 1) the soil profile model, 2) the structural model, and 3) the excavated soil model for embedded foundations. Since SASSI performs a linear analysis, strain-compatible properties are used for the soil. The properties are usually calculated using SHAKE, which, apart from equivalent-linear site response, outputs strain-compatible shear moduli and damping ratios of the soil layers for each ground motion. The SASSI soil profile is therefore different for each ground motion input. Although the strain-compatible properties from the SHAKE analyses presented in Section 7.3.2 could be used in this section, the properties are calculated through separate SHAKE analyses because the soil profile developed for the SSI analyses of this section is discretized with 29 layers (as opposed to 14 for the site-response analyses) for reasons given in Section 5.4.4. However, the layer properties at each depth remain the same as in Table 7-1. The small-strain shear modulus and damping ratio through the depth of the soil column for the more finely discretized soil profile are presented in Figure 7-9. This figure also includes the strain-compatible shear modulus and damping ratio profiles calculated for each ground motion using SHAKE and input in the SASSI analyses of this section. A Poisson's ratio of 0.3 (Kulhawy and Mayne, 1990; Mason, 2014) is used for the soil in the analyses described in this section.

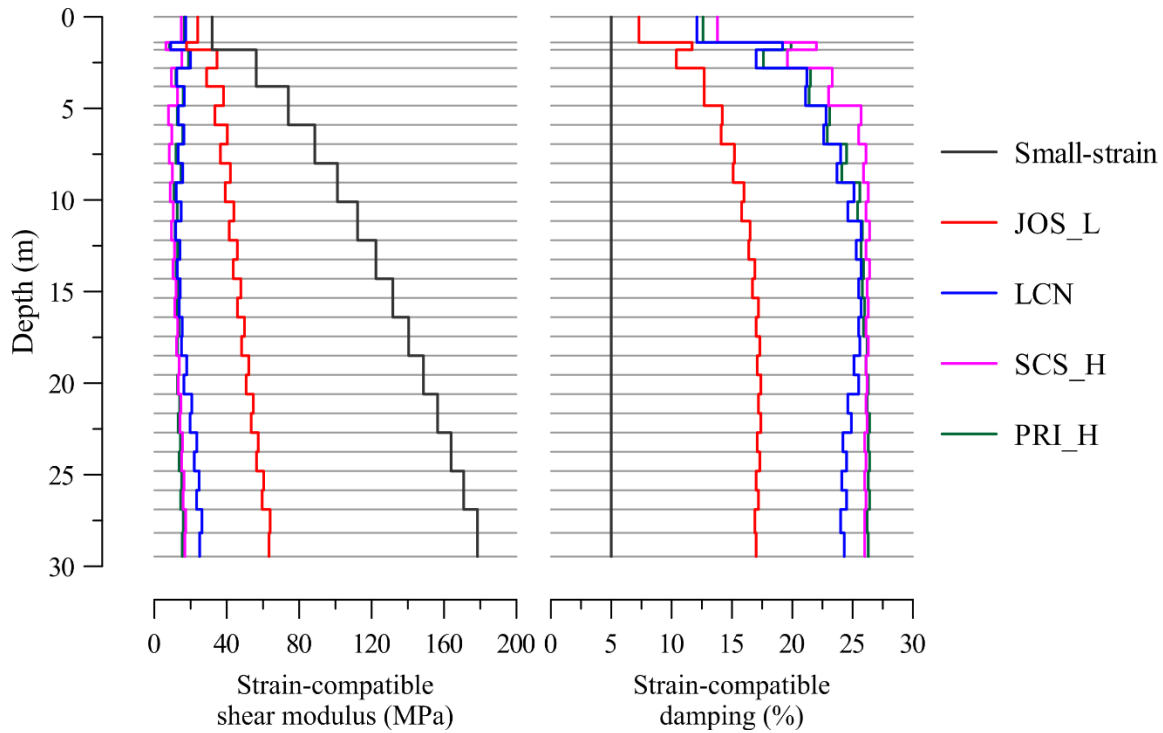


Figure 7-9: Small-strain and strain-compatible shear moduli and damping ratios used for SSI analyses using SASSI for simulation of Tests 3 and 4

SASSI only models horizontally infinite soil layers, and therefore the boundary effects from the laminar box must be neglected in the numerical analyses. The earthquake input is modeled as a vertically propagating shear wave-field to be consistent with the experiments. Additionally, the base of the soil profile is fixed, consistent with the rigid bedrock assumption. The structure-foundation system is modeled using two-dimensional or three-dimensional finite elements in SASSI. For the numerical simulation of the City Block experiments, three-dimensional finite element models of the experimental model buildings are developed at the prototype scale. The model parameters are scaled to the prototype level by multiplication using the scale factors presented in Table 6-1. Each beam and column of MS1F_2 is modeled using a beam element with the corresponding material and cross-section properties. The coordinates of the nodes of the beam elements are taken as the centers of the cross-sections of the beams and columns in the experimental model. The floor mass is simulated by assigning appropriate lumped masses on the floor beams. MS2F is modeled using two beam elements as a two-story lumped mass structure, with each beam modeled as the aggregate of two shear walls. The masses of the shear walls and the floors are lumped at the floor levels. Miscellaneous additions to the floor mass, such as bolts, instrumentation wires, etc., are included in the lumped masses. The SASSI numerical models of MS1F_2 and MS2F are presented in Figure 7-10. The lumped masses in this figure are indicated as red dots in the beam elements, and the

ground surface is indicated in brown. Since SASSI does not allow for explicit modeling of the beam cross-sections, the beam and column fuses cannot be modeled explicitly. The fuses are therefore modeled in an averaged sense by decreasing the moment of inertia of the beam element cross-section through a calibration of the fixed-base numerical models to the data from hammer tests on the experimental models. This calibration process is described in Section 7.4.3. Details of the numerical models of MS1F_2 and MS2F are presented in Table 7-4 and Table 7-5, respectively.

The footings of MS1F_2 and the mat foundation of MS2F are modeled using eight-noded solid elements. The foundations are embedded to a depth equal to their thickness, namely, the top of the foundation is at the same elevation as the ground surface. This embedment depth is slightly smaller than that used in the experiments for both structures. The column-foundation connections of both buildings are modeled using stiff beam elements as shown in Figure 7-10. The stiff beams are modeled with a negligible mass and a very large stiffness compared to the rest of the structure. These beams ensure that the column-foundation connections are almost rigid. The excavated soil, for the embedded footings and the basemat, is modeled using eight-noded solid elements and has the same dimensions as the corresponding foundations. The solid elements of the excavated soil have the same material properties as the corresponding layers in the soil profile, as required by SASSI.

SASSI analyses are performed for the arrangements listed in Figure 7-1. The numerical models for these arrangements are built by combining the numerical models of the individual buildings, and changing their co-ordinates according to their new position in the box. A 0.5m gap is maintained between the foundations of the adjacent buildings, which is equal to the gap used in the experiment, at the prototype scale. The numerical models for these building arrangements are presented in Figure 7-10. Each of the building arrangements is subjected to the ground motions of Figure 7-1.

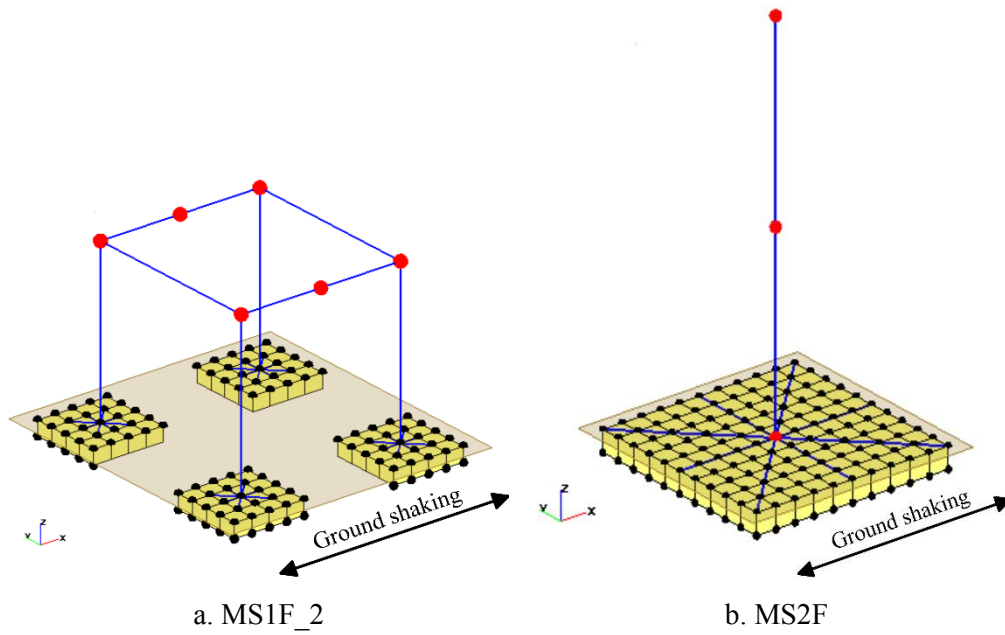


Figure 7-10: SASSI numerical models of the baseline models of MS1F_2 and MS2F

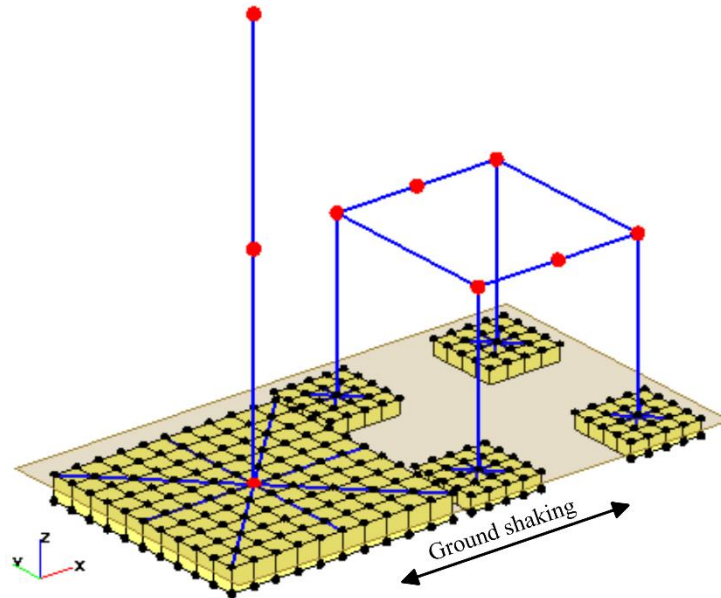


Figure 7-11: SASSI numerical model of the in-plane SSSI arrangement in Test 3

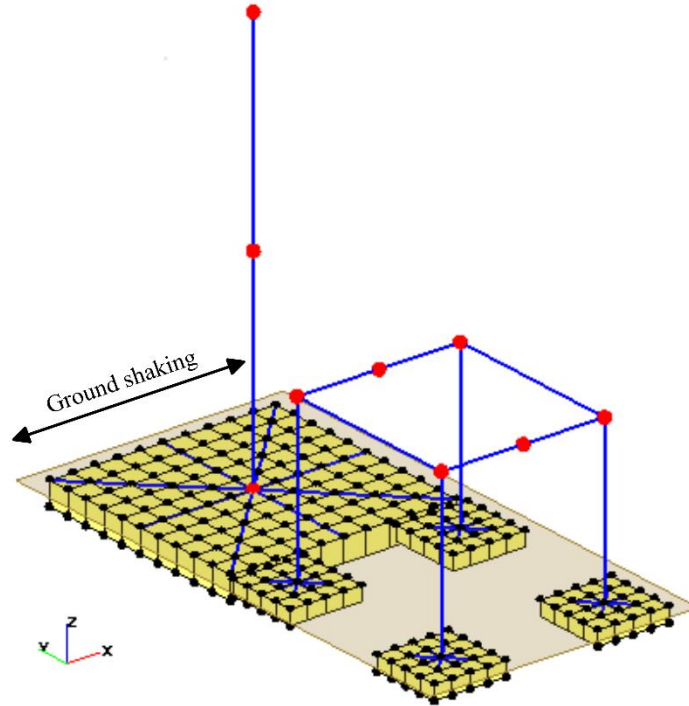


Figure 7-12: SASSI numerical model of the anti-plane SSSI arrangement in Test 4

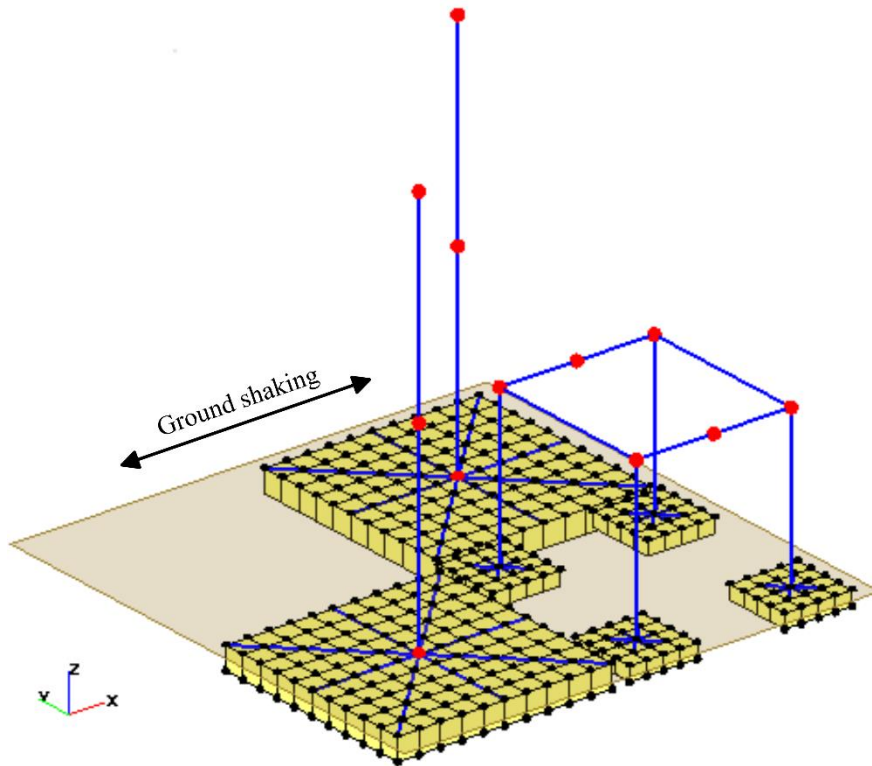


Figure 7-13: SASSI numerical model of the in-plane SSSI arrangement in Test 3

Table 7-3: Material properties used in the SASSI analyses

Property	Steel	Aluminum
Elastic modulus (GPa)	200	69
Poisson's ratio	0.3	0.3
Unit weight (kN/m ³)	76.84	26.48
Damping ratio (%)	2	2

Table 7-4: Description of the numerical model of MS1F_2^a (dimensions in prototype scale)

Plan dimensions ^b $L \times B$ (m)	Height (m)	Nodal masses on each beam ^c (kg)		Moment of Inertia (m ⁴)	
		Center	End	Beams ^c	Columns
9.96 × 11.00	12.76	145578	1820	0.0106	0.0141
Footing dimensions (m)		4.37 × 4.37			
Footing thickness (m)		0.875			

^a The area of the cross section, shear area, and torsional inertia are the same for all elements, and are calculated from the cross section of the experimental model

^b L is along the direction of shaking; see Figure 7-10

^c Only for the beams parallel to the direction of shaking

Table 7-5: Description of the numerical model of MS2F^a (dimensions in prototype scale)

Floor height ^b (m)	Moment of Inertia ^{a,c} (m ⁴)	
	Y-bending	X-bending
12.58	70.63	0.51
Mat dimensions (m)	13.80 × 13.80	
Mat thickness (m)	1.34	

^a The area of the cross section, shear area, and torsional inertia are the same for all elements, and are calculated from the cross section of the experimental model

^b Story heights are equal

^c X is the direction of shaking; Z is the vertical direction; see Figure 7-10

7.4.2 Modeling in LS-DYNA

Nonlinear soil-structure interaction analysis for Tests 3 and 4 using LS-DYNA is described in this section. General modeling procedures for soil-structure interaction analysis in LS-DYNA are presented in Section 3.3.2. Only the details corresponding to the simulations of Tests 3 and 4 are presented here.

The LS-DYNA numerical analyses are performed using the direct method (see Section 3.2 for the description of the direct method and the domain reduction method), which involves modeling a large soil domain to simulate an infinite soil halfspace. The soil domain in the current analyses is modeled using eight-noded solid elements. The linear soil properties (small-strain shear modulus, small-strain damping, unit weight and Poisson's ratio) for these analyses are the same as used in SHAKE and presented in Figure 7-9. The soil layer thicknesses are the same as in SASSI. Each soil layer in SASSI corresponds to one solid element layer in LS-DYNA. The soil material is modeled using the MAT_HYSTERETIC material with the same material properties as used for the site-response analyses in Section 7.3.4. For the simulations in this section, a soil domain of size 219m × 118m in plan (219m in the shaking direction, X) and 29.47m deep is built, which is about 15 times the width of the basemat of MS2F. This soil domain is equal in size to that used in the verification analyses of Section 5.2. The lateral boundaries for this soil domain are modeled as described in Section 5.2.3. Figure 7-14 presents a sample LS-DYNA model used for the analysis of the combined SSSI arrangement in Test 4. The large dimensions of the soil domain relative to the plan dimensions of the structures are apparent in this figure. The soil layers, indicated by different colors, are also seen in the figure. The input ground motion for all the analyses is applied

directly at the base as an acceleration input, which is consistent with the fixed-base assumption for the soil profile.

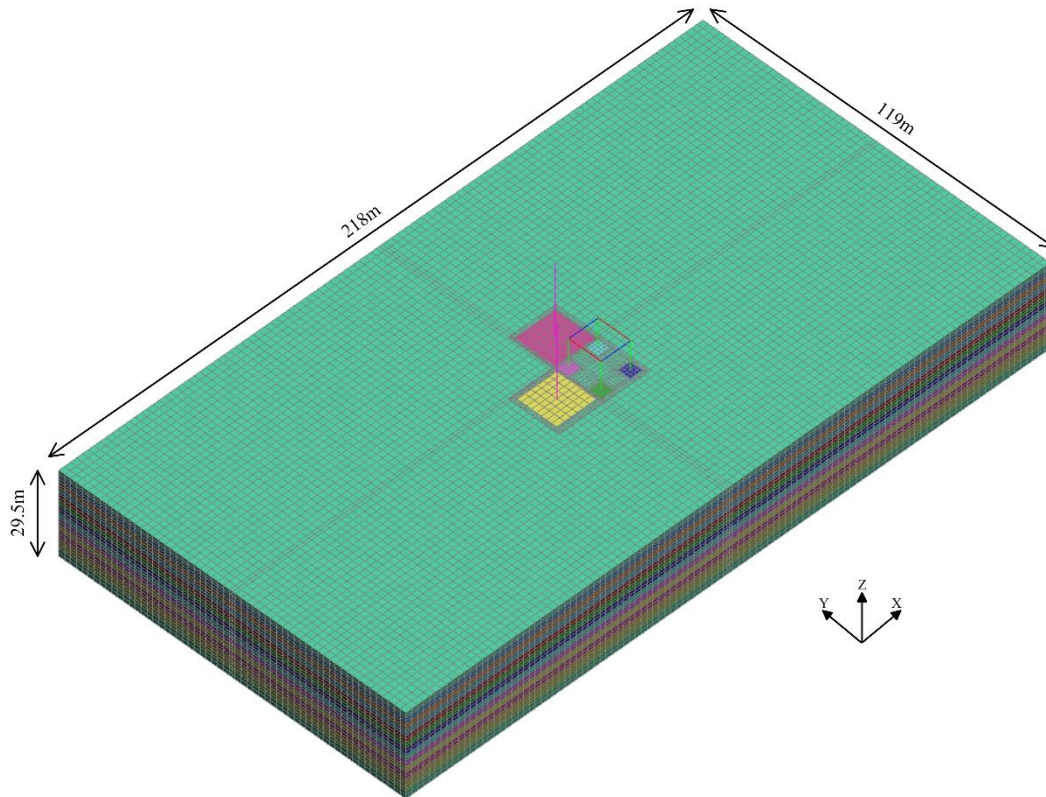


Figure 7-14: LS-DYNA finite element model for soil-structure interaction analysis of the cSSSI arrangement during Test 4

The building models MS1F_2 and MS2F are modeled as described previously for the SASSI analyses: Table 7-4 for MS1F_2, and Table 7-5 for MS2F. Nonlinear behavior in MS1F_2 can be simulated in LS-DYNA. Although the beam fuses in the experimental models can be modeled explicitly in LS-DYNA, preliminary analyses using one such model (in which the fuses were modeled using shell elements; see Figure 7-15) required very long runtimes. Since only qualitative comparisons are made between the experimental and numerical results, the beam fuses are not modeled explicitly and lumped plastic hinges are used instead. Nonlinearity in the beams is modeled using the material model, *MAT_SEISMIC_BEAM, available in the LS-DYNA material database (LSTC, 2013). This material model simulates nonlinear behavior at one of the nodes of the beam element in the form of a plastic hinge, which follows a plastic moment-rotation curve input by the user. The plastic moment-rotation curve is calculated from a pseudo-static analysis of one of the beam fuses shown in Figure 7-15. To account for the interaction between the shear force in the fuse and the moment-rotation behavior, a shear force equal

to a quarter of the roof mass is applied on the fuse during the pseudo-static analysis. The effects of axial force, and changes in the shear force during the earthquake on the moment-rotation behavior are neglected. Additionally, the fuses in the columns are not modeled since no yielding of the column fuses was observed in the experiments.

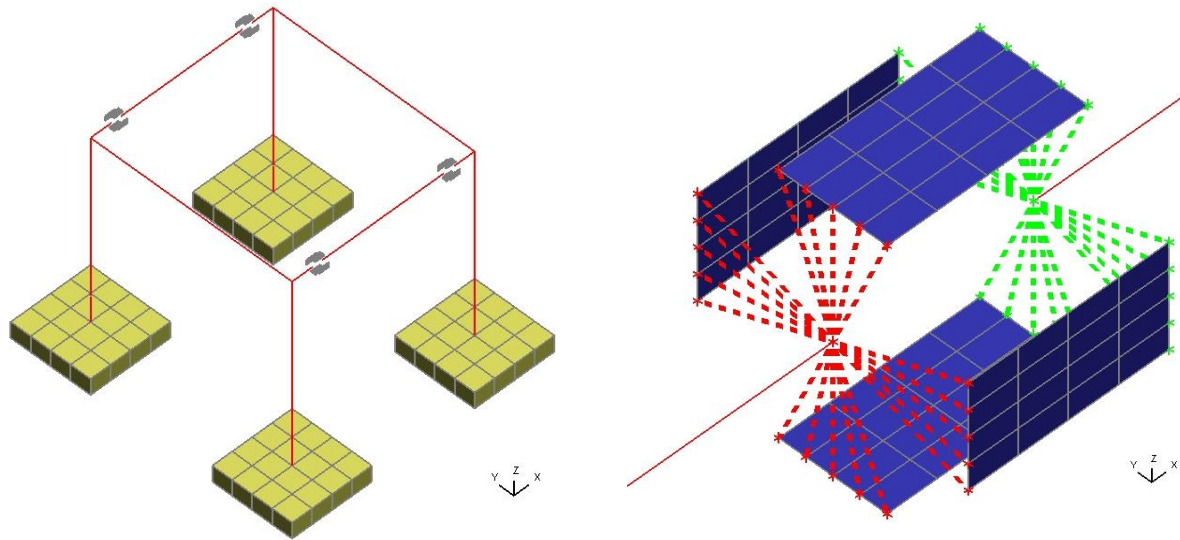


Figure 7-15: Preliminary model of MS1F_2 in LS-DYNA with explicit modeling of the beam fuses using shell elements (left) and the close-up of one of the beam fuses (right)

The footings of MS1F_2 and the basemat of MS2F are modeled using solid elements. Both foundations are embedded such that the top of the foundation is at grade. The dimensions of the foundations are the same as used in SASSI, and are presented in Table 7-4 and Table 7-5. Both the footings and the basemat are modeled using the rigid material model available in LS-DYNA, which uses rigid body dynamics to simulate a completely rigid material. Preliminary analyses using an elastic material for the foundations revealed that the solid elements of the footing or those of the basemat (for the analysis case of stand-alone MS2F model) control the analysis time-step. Using the rigid material model avoids including the footing and basemat elements in the time-step calculations, resulting in an increase in the time step and a reduction in the analysis time. For these analyses, the use of a rigid material model for the foundations reduced the analysis time by about two-thirds.

The LS-DYNA models used for the various analyses cases are presented in Figure 7-16 (baseline cases of MS1F_2 and MS2F), Figure 7-17 (in-plane SSSI case), Figure 7-18 (anti-plane SSSI case), and Figure 7-19 (combined SSSI case). The figures only present the superstructures, foundations, and soil elements close to the foundations. The rest of the soil domain is shown in Figure 7-14 and is not shown in these figures for clarity. The figures also show that a much finer mesh is used for the soil close to the

foundations as compared with the rest of the soil domain. This is to accommodate the large soil strains that are expected near the foundations. The interface between the finer mesh and the coarser mesh is modeled using the contact model, `*CONTACT_TIED_SURFACE_TO_SURFACE`. This model simulates a fully tied contact at the interface and does not allow separation. The foundation-soil interface for both the footings and the basemat can be modeled as either 1) a ‘tied’ interface with no loss of contact between the soil and the foundation, or 2) a more realistic interface that allows for loss of contact between the soil and the foundation, resulting in sliding, gapping and uplift. The analyses in this section are performed for both the interface conditions. The tied interface is modeled using the `*CONSTRAINED_EXTRA_NODES` option, which constrains the soil nodes at the interface to move along with the rigid footing or basemat. The second type of interface is modeled using the contact model, `*CONTACT_AUTOMATIC_SURFACE_TO_SURFACE`, that allows sliding and separation. This contact model adopts the Coulomb friction model to simulate sliding, and a friction coefficient of 0.84 is used for the analyses presented in this section. This friction coefficient is calculated as $\tan \phi$, where ϕ is the friction angle of Nevada sand, which is estimated to be between 37 and 42 degrees (Mason *et al.*, 2011). A friction angle of 40 degrees is used for the analyses presented in this section.

Structural damping is modeled using the `*DAMPING_FREQUENCY_RANGE` option, which simulates an approximately frequency-independent damping in a given frequency range. This damping option is also used to simulate the low-strain damping in the soil. A 2% damping ratio is used for the structures, and a 0.4% damping is used for the soil in the frequencies between 1 Hz and 25 Hz. The 0.4% ratio for the soil is the same as used in DEEPSOIL, as described in Section 7.3.3.

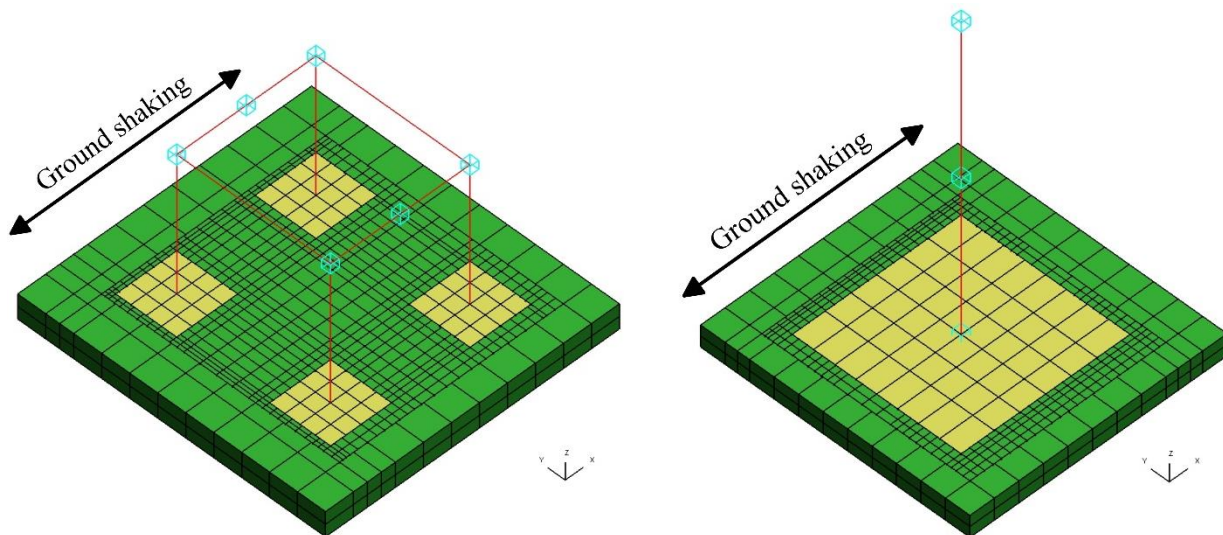


Figure 7-16: Close-up isometric views of the SSI models of MS1F_2 (left) and MS2F (right) in LS-DYNA (soil elements far away from the structure are not shown for clarity)

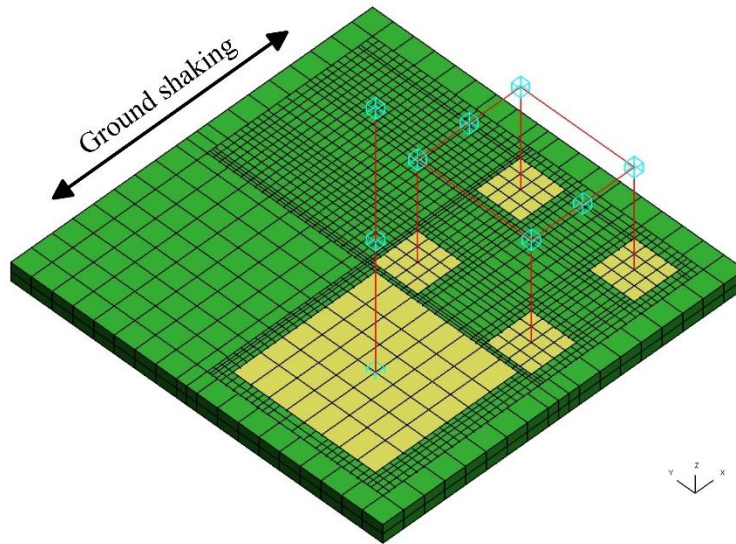


Figure 7-17: Close-up isometric view of the SSI model for the in-plane SSSI case of Test 3 in LS-DYNA (soil elements far away from the structures are not shown for clarity)

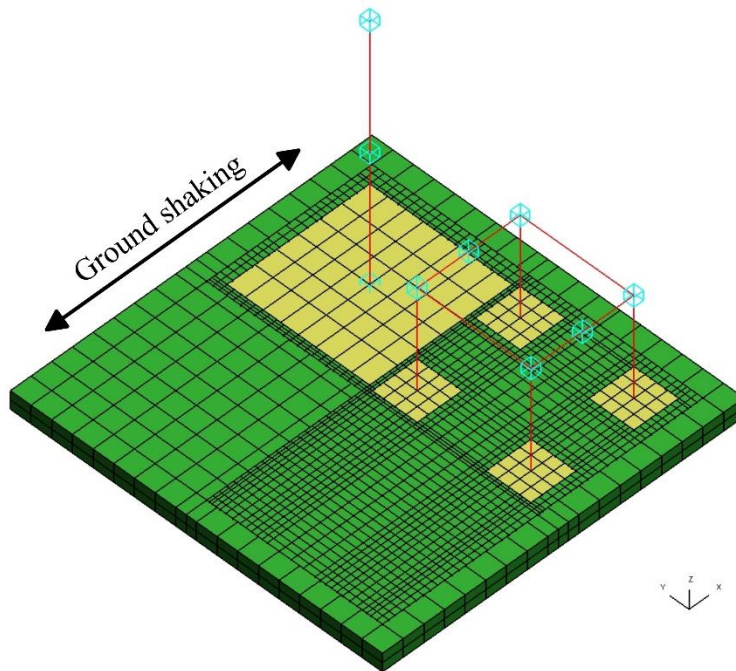


Figure 7-18: Close-up isometric view of the SSI model for the anti-plane SSSI case of Test 4 in LS-DYNA (soil elements far away from the structures are not shown for clarity)

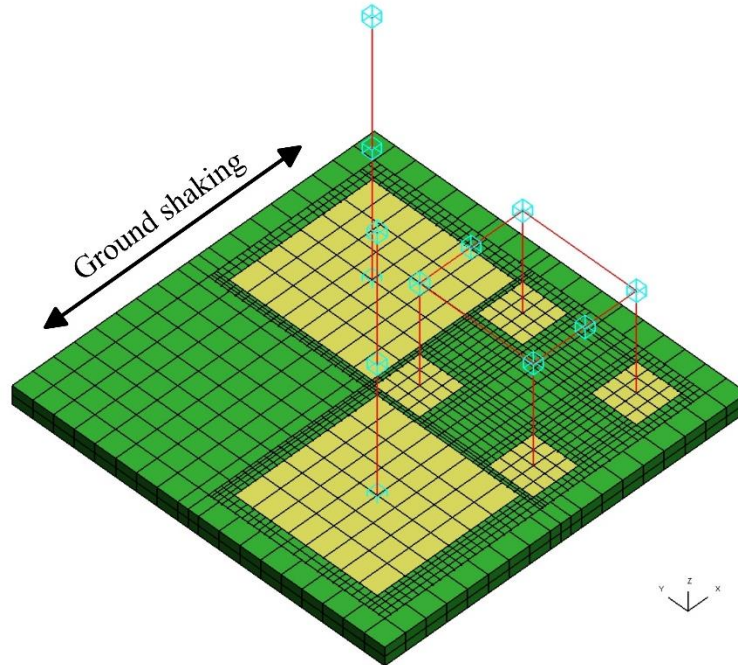


Figure 7-19: Close-up isometric view of the SSI model for the combined SSSI case of Test 4 in LS-DYNA (soil elements far away from the structures are not shown for clarity)

7.4.3 Calibration of fixed-base models

Prior to performing the soil-structure interaction analyses, the structural models of MS1F_2 and MS2F in SASSI and LS-DYNA are calibrated to achieve their target dynamic properties, which are the fixed-base time periods of the experimental model structures in the prototype scale. Calibration of the numerical models is required to account for the miscellaneous masses such as nuts, bolts and instrumentation, and also the reduction in structural stiffness due to the beam and column fuses. These factors cannot be directly accounted for in the numerical models. Therefore the moment of inertia of the beam elements and the lumped masses are adjusted until the target time period is achieved, and these adjusted values are used in the SSI analysis.

The SASSI fixed-base model of each experimental model is built by modeling the superstructure on a very stiff soil profile. This soil profile is modeled using very thin layers having a shear modulus much greater than the shear modulus of steel used in the superstructure model. This ensures that the soil profile is very stiff compared to the structure, imitating an almost fixed-base condition. The soil profile consists of three horizontal layers, each with a thickness of 0.003 m. A shear wave velocity of 3.06×10^7 m/s, and a unit weight of 0.48 kN/m^3 are specified for each layer including the bedrock. Seismic excitation is applied to this model at the base of the soil profile. Excitation for the LS-DYNA model is applied by specifying an acceleration input at the base of the structure. The time period of the structure is

calculated from the acceleration amplification spectrum at the roof of the structure. The calibrated values of moments of inertia are presented in Table 7-4 and Table 7-5. The fixed-base time periods calculated from the SASSI and LS-DYNA analyses are presented in Table 7-6, together with the time periods of the individual structures calculated from hammer tests.

Table 7-6: Comparison of the prototype scale fixed-base time periods calculated from SASSI and hammer tests for all the models

Superstructure	Time period(s) (sec)		
	SASSI	LS-DYNA	Hammer test
MS1F_2	0.49	0.48	0.47
MS2F	0.13	0.14	0.13

7.4.4 Comparison of experimental and numerical results

The experimental and numerical responses of MS1F_2 and MS2F are presented in this section for the baseline cases and the SSSI configurations illustrated in Figure 7-1. SSSI effects are examined by comparing the structural response in the baseline case with the responses in various SSSI configurations. Structural response is measured using acceleration response spectra at the roof of the structures.

Figure 7-20 and Figure 7-21 present the experimental and numerical responses of MS1F_2 for the baseline case and the SSSI cases illustrated in Figure 7-1. Figure 7-20 presents the responses for the JOS_L and LCN ground motions. Figure 7-21 presents the responses for the SCS_H and PRI_H ground motions. Similarly, the experimental and numerical responses of MS2F for the baseline and SSSI cases are presented in Figure 7-30 (JOS_L and LCN ground motions) and Figure 7-31 (SCS_H and PRI_H ground motions). The numerical responses of MS2F also include the baseline case. The numerical responses for each case are calculated using SASSI, LS-DYNA with a tied soil-foundation interface, and LS-DYNA with separation allowed at the soil-foundation interface. Observations made from the experimental and numerical results regarding SSSI effects on the response of each building model are presented in Sections 7.4.4.1 and 7.4.4.2. Qualitative comparisons between the experimental and numerical results with regards to SSSI are also presented.

7.4.4.1 MS1F_2

After the completion of Test 4, and during the dismantling of the experimental setup, it was noticed that MS1F_2 in the anti-plane SSSI arrangement (aSSSI model of MS1F_2) was inadequately assembled. Consequently, the experimental results presented in Figure 7-20 and Figure 7-21 (indicated in light blue) show that the response of this structure is erratic and very different from the responses of MS1F_2 in other SSSI arrangements. The MS1F_2 response in the aSSSI arrangement is therefore ignored in this study.

The experimental results in Figure 7-20 and Figure 7-21 show that the response of MS1F_2 for a given ground motion is similar in all the arrangements illustrated in Figure 7-1. The one exception is the peak spectral acceleration in the combined SSSI case for the JOS_L ground motion. However this reduction in response is not seen in the experimental results from the other ground motions, and does not indicate a general trend. Small differences are evident in the experimental responses for the more intense ground motions, SCS_H and PRI_H, but these could be attributed to changes in material properties and variability in input ground motion, as described in Section 7.3.5. The global response of MS1F_2 in these experiments is not affected by SSSI. The same observation is made from examination of the numerical results calculated using SASSI and LS-DYNA. Figure 7-20 and Figure 7-21 show that the variability in the numerical responses of MS1F_2 for a given ground motion for different arrangements is minor. Given that the variabilities in input ground motion and the material properties can be ruled out for the numerical simulations, these minor differences can be attributed to the interaction between the structures. The interaction between the structures that are in the arrangements illustrated in Figure 7-1 do not affect the global response of MS1F_2 sufficiently to warrant consideration of SSSI effects.

The results show that the numerical predictions from SASSI and LS-DYNA agree reasonably well with the experimental results, with regards to the magnitude of SSSI effects in MS1F_2. However the numerical and experimental responses are quite different for all ground motions, especially in terms of the spectral accelerations. Although some differences are expected for the reasons given in Section 7.2, the differences seen in the results are particularly large and warrant investigation. A similar magnitude of differences between experimental and numerical results is seen in the results calculated by another City Block researcher (Jones, 2013) who performed numerical simulations of Tests 3 and 4 using the program FLAC (Itasca Consulting Group, 2005). Jones (2013) found that the peak spectral accelerations calculated using the numerical programs were much smaller than those from the experiments. To explain the differences between the experimental and numerical results, Jones (2013) conducted a series of sensitivity analyses in FLAC to understand the effect of parameters such as the shear-wave velocity profile of the soil, fixed-base time period of the structure, and modulus reduction and damping and curves, on the response of the structure. These sensitivity analyses did not adequately explain the under-prediction of the

numerical simulations and Jones (2013) speculated that the differences might be due to the combined resonance of the soil profile and the structure. However the nonlinear systems (soil, structure) considered here do not resonate. Further studies are required to understand the differences between the experimental and numerical results, which is not the focus of this study.

In spite of the differences in the magnitude of the spectral accelerations, the shape of the response spectra from the numerical simulations and the experimental data are qualitatively similar for the JOS_L ground motion. Both SASSI and LS-DYNA result in reasonable predictions of the flexible-base time period for this ground motion. However the response spectra calculated by SASSI and LS-DYNA (with the tied interface) have a very different shape from the experimental response spectra for the other three, more intense ground motions, especially LCN. For these ground motions, SASSI and LS-DYNA (tied) result in rather poor predictions of the period of maximum spectral acceleration. The other LS-DYNA (separation allowing interface) analyses, on the other hand, result in response spectra that look similar in shape to the experimental responses for the SCS_H and PRI_H ground motion, and a reasonable prediction of the period of maximum spectral acceleration. This indicates that the LS-DYNA analyses that allow gapping and sliding of the footings result in more reasonable predictions than SASSI and LS-DYNA (tied). This result is expected given that the soil around the footings undergoes highly nonlinear response as described in Section 5.3.2.1. All the numerical programs result in poor predictions of the period of the spectral peaks in the LCN ground motion, which is a consequence of the poor prediction of site response around the flexible-base time period of MS1F_2, which is about 0.6 to 0.8 sec (see Figure 7-8). The experimental site response for this ground motion shows a peak at 0.6 sec, which being close to the flexible-base time period of MS1F_2, results in a dominant peak in the structural response. The site response calculated from the numerical simulations only show a peak at 1 sec.

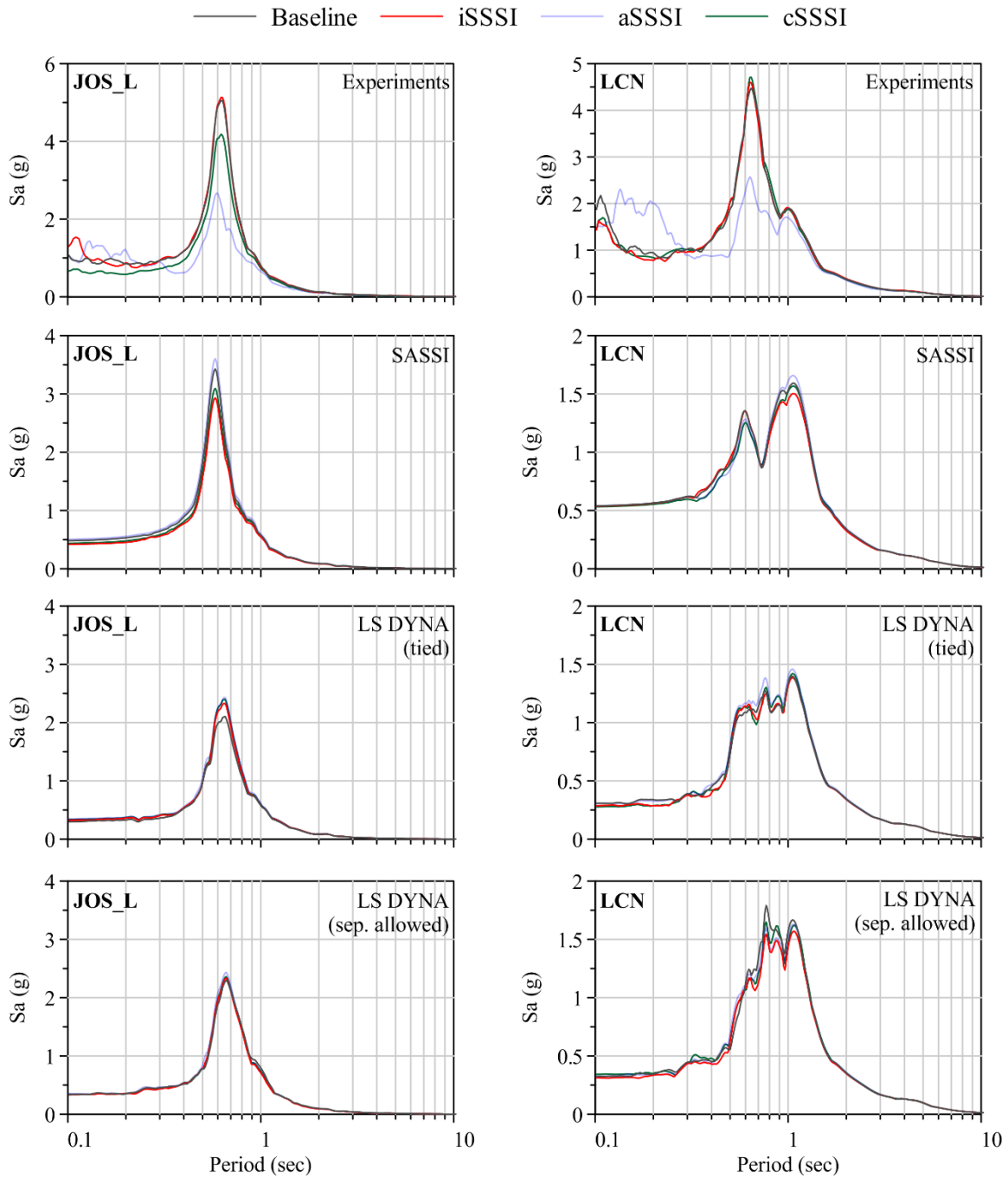


Figure 7-20: Response spectra of the roof acceleration of MS1F_2 from numerical simulations using SASSI and LS-DYNA, and experimental observations for JOS_L and LCN ground motions

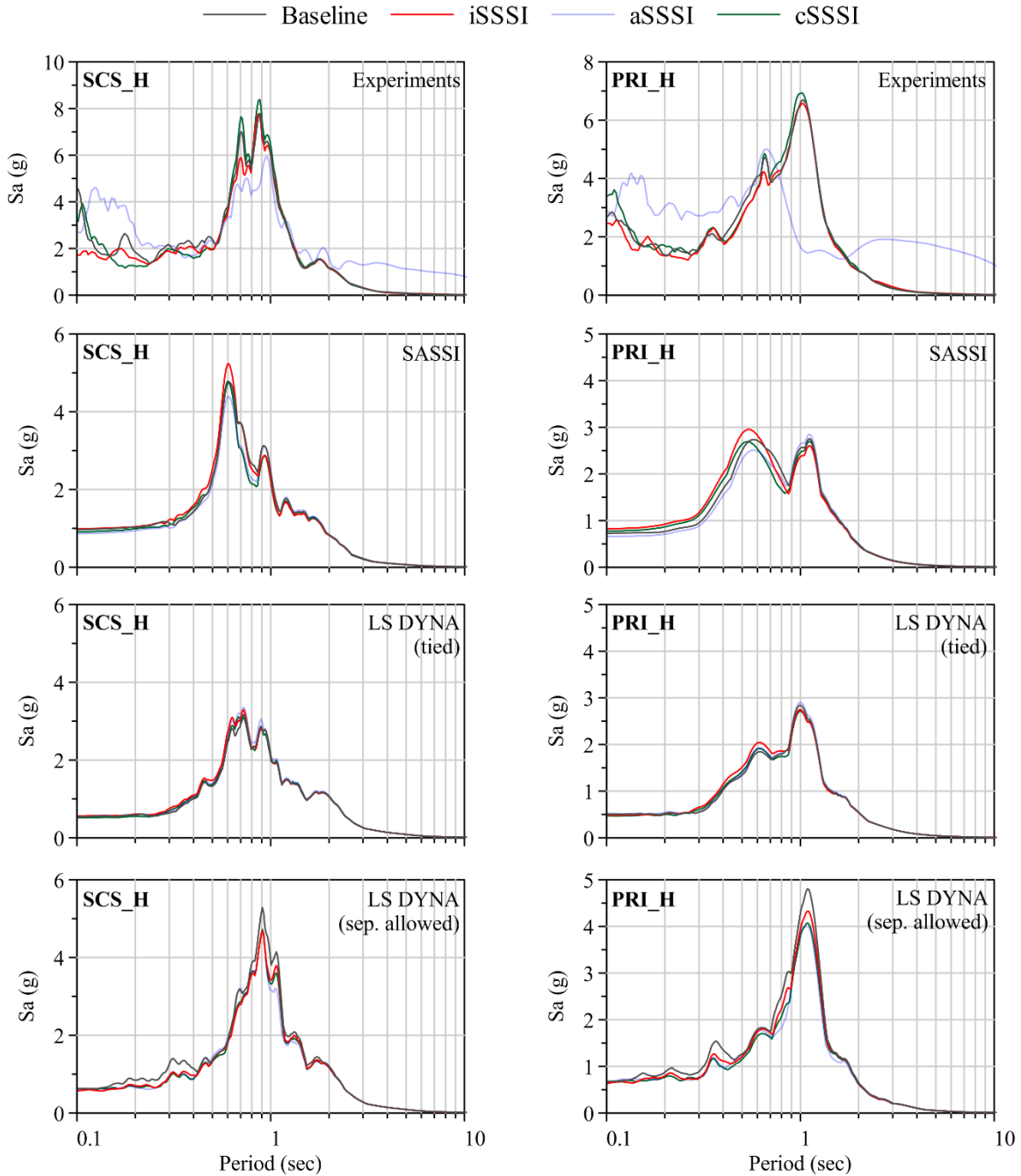


Figure 7-21: Response spectra of the roof acceleration of MS1F_2 from numerical simulations using SASSI and LS-DYNA, and experimental observations for SCS_H and PRI_H ground motions

7.4.4.2 Footing response in MS1F_2

The results presented in Section 7.4.3 show that SSSI in Tests 3 and 4 has no meaningful effect on the global response of MS1F_2. However SSSI effects can still affect the local response of the

footings due to restraint provided by adjacent substructures. Analysis of data from Tests 1 and 2 by Mason (2011) and Trombetta (2013) showed that the footings of MS1F_1 underwent smaller displacements and rotations, when restrained by the basement of MS3F. Mason (2011) concluded from Tests 3 and 4 that SSSI did not have a significant effect on the displacements of the footings closest to the basemat, except that they had residual upward displacements due to the rocking of the adjacent basemat. Trombetta (2013) examined the data from Tests 3 and 4 and found that the demands on the columns of MS1F_2 supported on restrained footings (footings closest to the basemat) increased for most of the ground motions. In this section, the numerical results from the nonlinear LS-DYNA analyses (with separation-allowing interface) are examined to understand the local SSSI effects on the footings of MS1F_2 adjacent to the MS2F basemat. Specifically, the moment-rotation response in rocking and the force-displacement response in the vertical direction are examined. The same four ground motions considered in the previous sections are used in this section. The footing responses calculated from numerical results are not compared with the experimental data.

7.4.4.2.1 Moment-rotation response

Figure 7-22, Figure 7-23, Figure 7-24 and Figure 7-25 present the moment-rotation responses of two footings in MS1F_2 during the ground motions, JOS_L, LCN, SCS_H and PRI_H, respectively, for the baseline case as well as the SSSI arrangements considered in this section. The top row in each figure presents the responses of the footing that is always the farthest from the adjacent structures (termed ‘far’ footing hereafter), and the bottom row presents the responses of the footing that is always closest to the adjacent structures (termed called ‘near’ footing hereafter). The location of the footing in the plan view of each arrangement is identified by a solid black square in an inset in the top left corner of each plot.

The plots presented in the first row of each figure show that the moment-rotation behavior of the far footing is barely affected by the presence of the adjacent structures. However, the moment-rotation behavior of the near footing is affected, although not considerably, for all the ground motions. Notice that the plots corresponding to the iSSSI and cSSSI cases (second and fourth in each row) of the near footing show larger negative rotations on average (the plots are skewed slightly to the left), than the baseline and aSSSI cases, for all four ground motions. For the co-ordinate system used in these analyses, negative rotation denotes that the footing rotates towards basemat (i.e., the side of the footing closest to the basemat is moving downwards) in the iSSSI arrangement. This indicates that the footing, when close to the basemat of the iSSSI and ciSSSI models of MS2F, undergoes more negative, asymmetric, rotation and rotates towards the basemat when compared with its response in the baseline and aSSSI cases. This is expected since the soil between the basemat and the footing experiences rocking from two foundations resulting and larger strains and consequent softening, compared with the baseline case in which the soil

experiences rocking only from the footing. However, this softening is not significant enough to result in a consistent change in the peak footing moment or rotation in the near footing in comparison with the far footing.

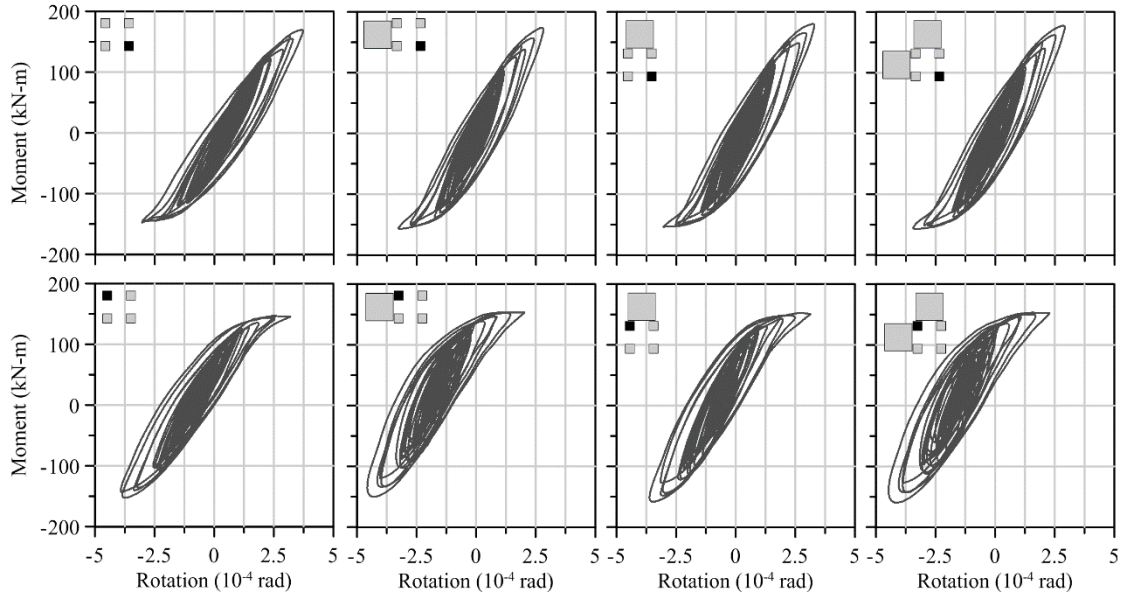


Figure 7-22: Moment-rotation response of the footings of MS1F_2 in various SSSI arrangements, calculated using LS-DYNA (separation allowed) analyses for the JOS_L ground motion

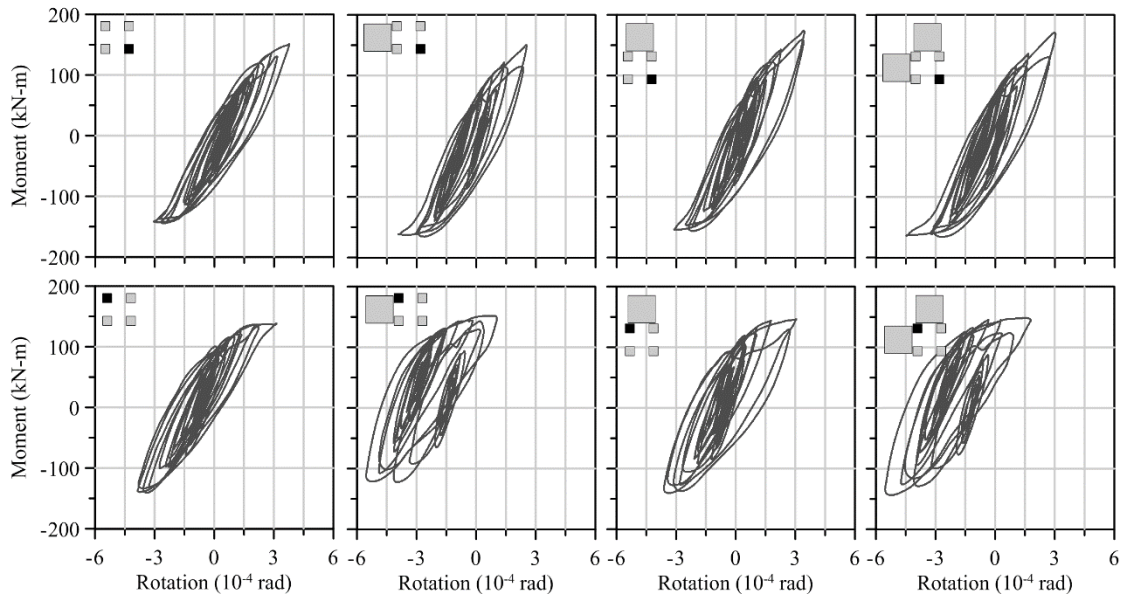


Figure 7-23: Moment rotation-response of the footings of MS1F_2 in various SSSI arrangements, calculated using LS-DYNA (separation allowed) analyses for the LCN ground motion

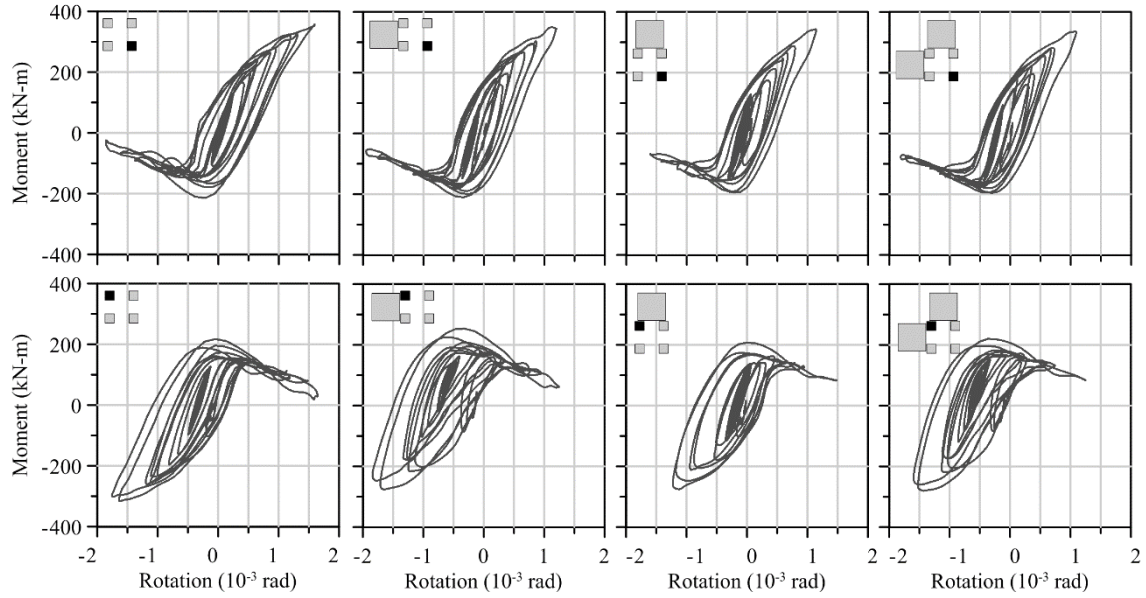


Figure 7-24: Moment-rotation response of the footings of MS1F_2 in various SSSI arrangements, calculated using LS-DYNA (separation allowed) analyses for the SCS_H ground motion

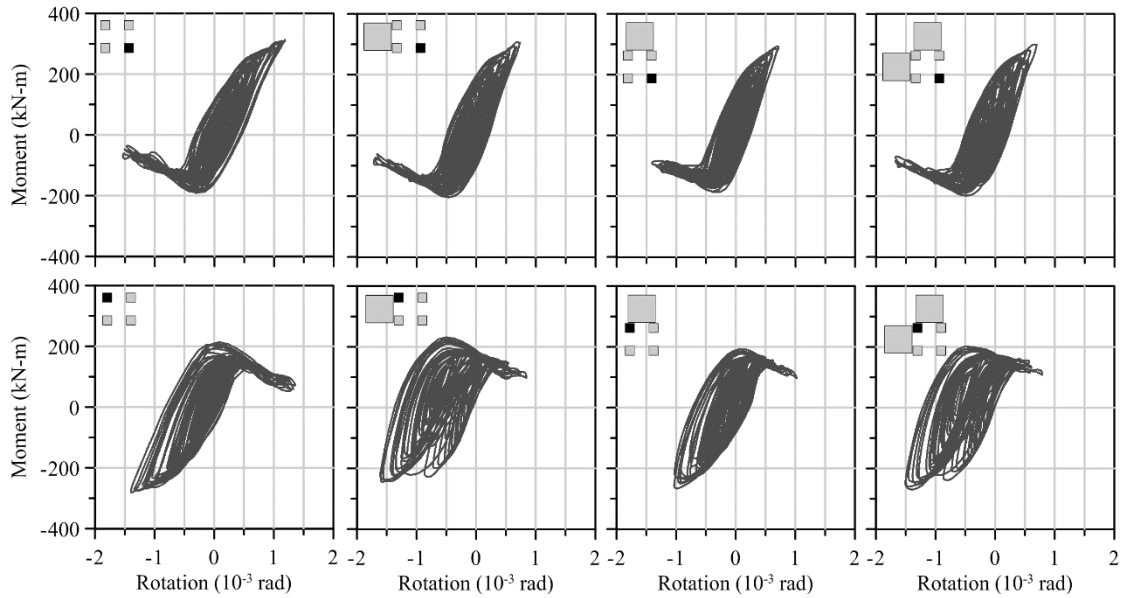


Figure 7-25: Moment-rotation response of the footings of MS1F_2 in various SSSI arrangements, calculated using LS-DYNA (separation allowed) analyses for the PRI_H ground motion

7.4.4.2.2 Vertical force-displacement response

Figure 7-26, Figure 7-27, Figure 7-28 and Figure 7-29 present the vertical force-displacement responses for the ground motions JOS_L, LCN, SCS_H, and PRI_H, respectively, for the far footing and the near footing. The first row in each figure presents the responses of the far footing, and the second row

presents the responses of the near footing. The location of the footings relative to the adjacent structures is indicated by a black solid square at the top left corner of each plot. The vertical forces in these results are calculated as the axial earthquake-induced compressive forces in the columns above each footing. The vertical displacement of each footing is calculated as the downward displacement of the center of the footing. The results do not include the vertical forces and displacements from gravity loading, and the earthquake-induced forces are calculated by subtracting the gravity loadings from the corresponding transient results.

The first row in each figure shows that the vertical forces and displacements in the far footing are virtually identical for the baseline and SSSI cases, indicating that the response of the far footing is unaffected by the presence of an adjacent structure. The vertical displacement of the near footing is significantly greater for the SSSI cases. Specifically, the displacements are the greatest for the cSSSI case, for which the peak displacement of the near footing is almost twice that of the baseline case, for the LCN, SCS_H and PRI_H ground motions. This is due to softening of the soil between the adjacent structures due to the presence of two foundations. Rocking of both the basemat and the footings deforms the soil more than in the baseline case, resulting in larger plastic strains and softer response of the soil. This observation is different from that by Mason (2011) who noted that the footings adjacent to the MS2F basemat had residual upward displacements, likely from the upheaval of the soil around MS2F due to the rocking of the basemat. The main reason for the difference between the experimental and numerical observations could be the inability of the soil material model to capture residual displacements, which is challenging and requires the use of sophisticated material models. Note that the numerical models were built with the objective of simulating the transient responses of the soil-structure system and not necessarily to predict the residual displacements.

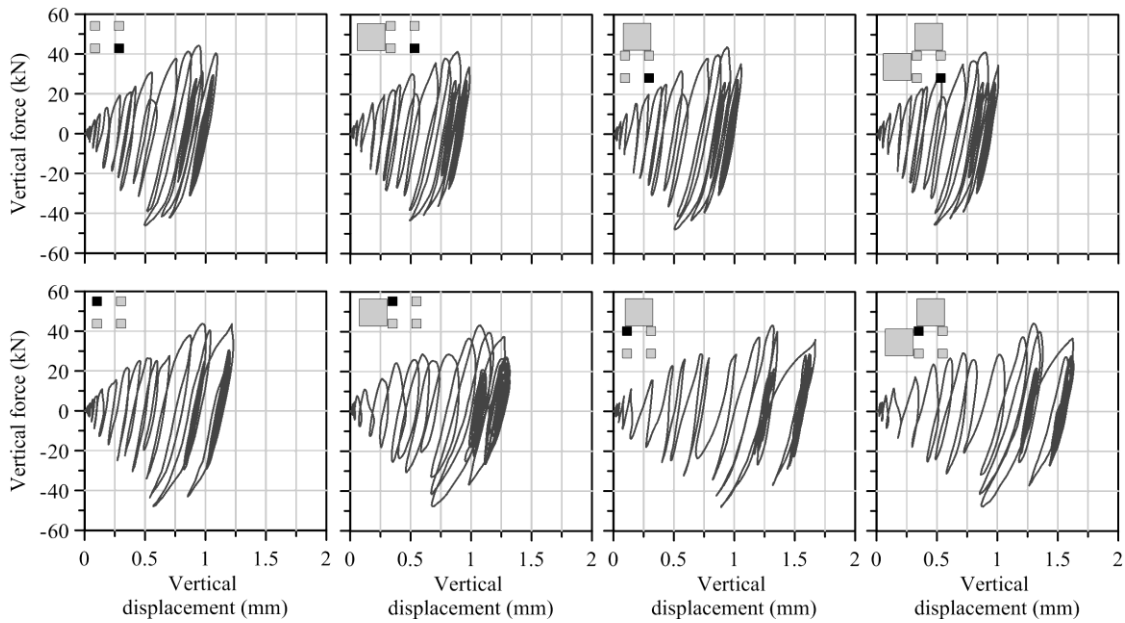


Figure 7-26: Vertical force-displacement response of the footings of MS1F_2 in various SSSI arrangements, calculated using LS-DYNA (separation allowed) analyses for JOS_L ground motion

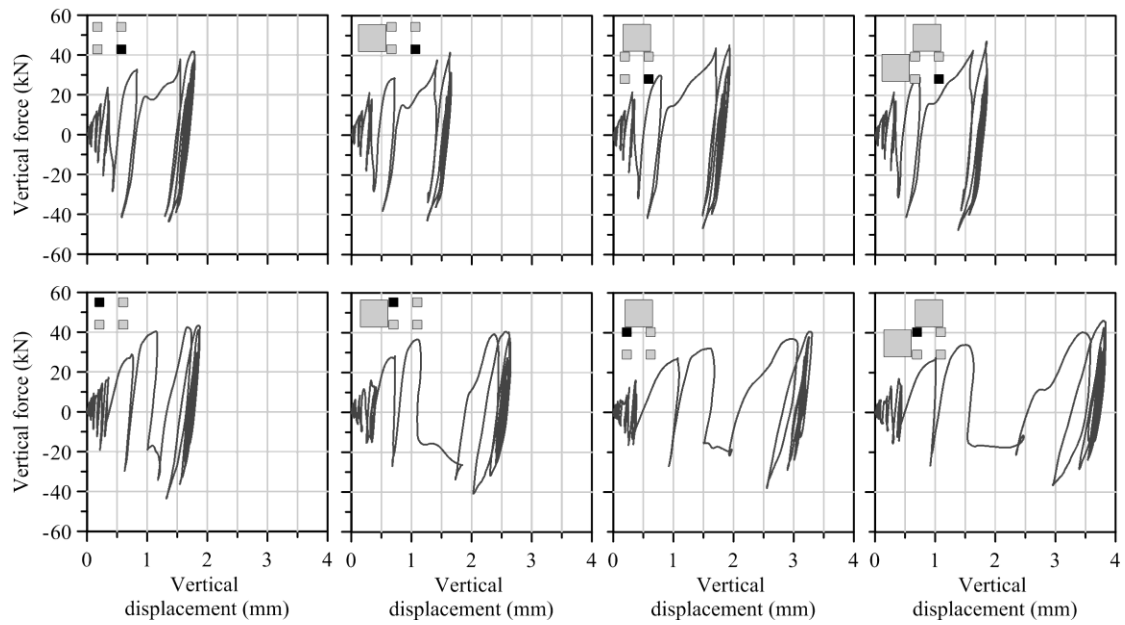


Figure 7-27: Vertical force-displacement response of the footings of MS1F_2 in various SSSI arrangements, calculated using LS-DYNA (separation allowed) analyses for LCN ground motion

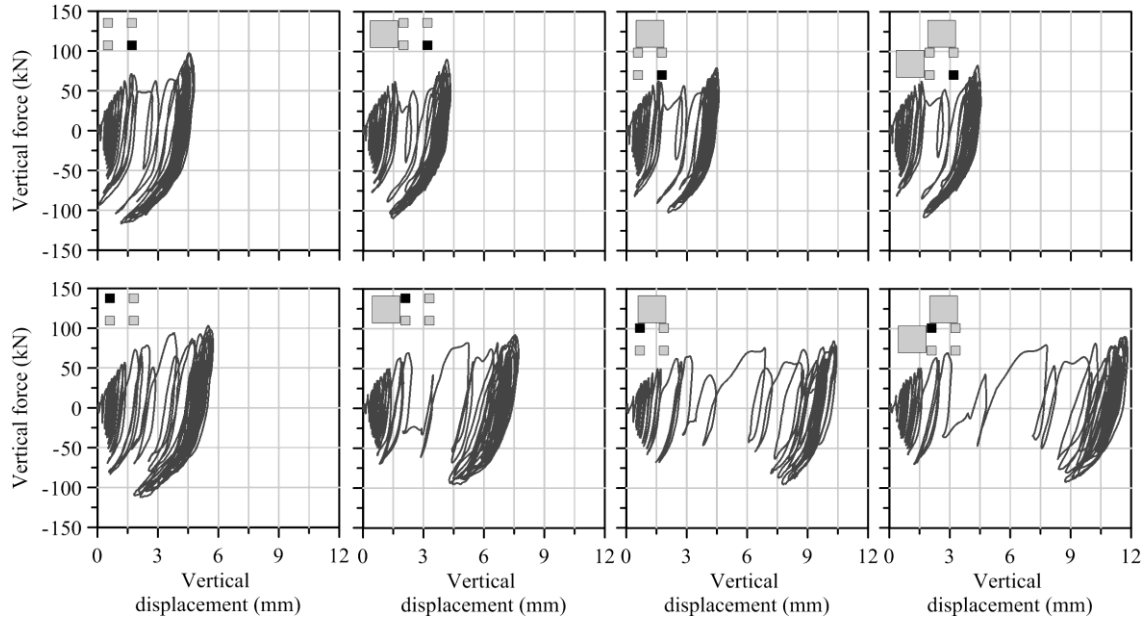


Figure 7-28: Vertical force-displacement response of the footings of MS1F_2 in various SSSI arrangements, calculated using LS-DYNA (separation allowed) analyses for SCS_H ground motion

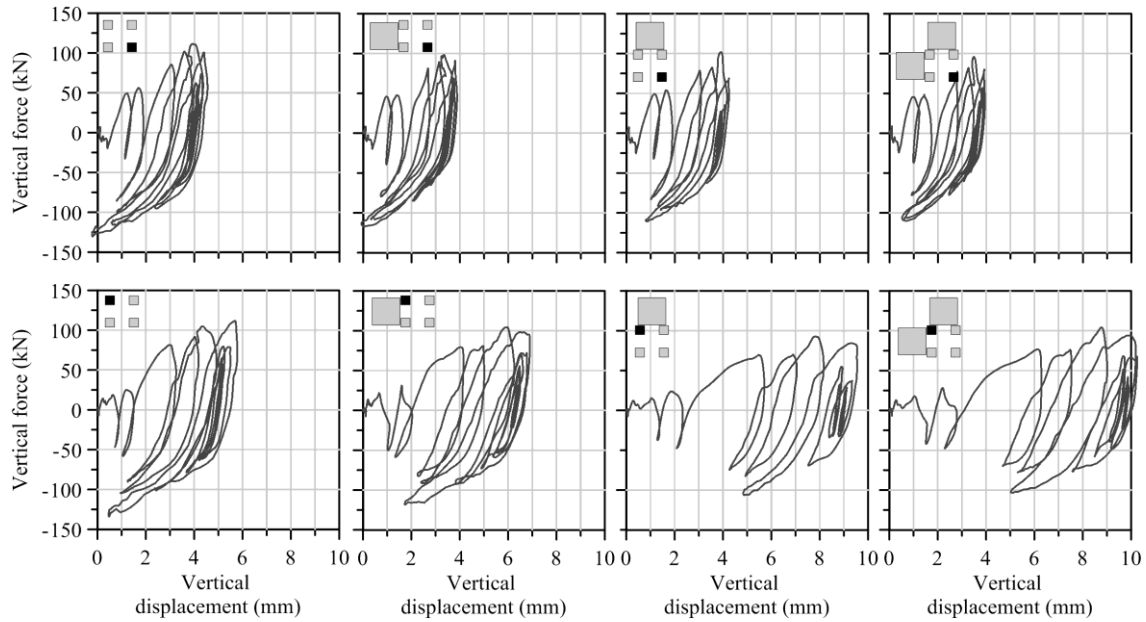


Figure 7-29: Vertical force-displacement response of the footings of MS1F_2 in various SSSI arrangements, calculated using LS-DYNA (separation allowed) analyses for PRI_H ground motion

The results show no considerable change due in the vertical forces on the footings due to SSSI: the peak vertical forces in the SSSI cases are similar to the peak vertical forces in the baseline case. This observation is contrary to that made by Trombetta (2013) who noted that restraining the footings of

MS1F_2 led to an increase in the peak demands in the columns above these footings for a majority of the input ground motions.

7.4.4.3 MS2F

The shear wall structure, MS2F, was designed to act as a ‘transmitter’ structure that affects the adjacent MS1F_2 response by transmitting energy through the soil. However, the numerical and experimental responses of MS1F_2 show negligible SSSI effects, even for the combined SSSI arrangement, which comprised two MS2F models adjacent to the MS1F_2, indicating that MS2F did not perform the expected ‘transmitting’ function.

Unlike MS1F_2, Figure 7-30 shows significant variability in the experimental responses of MS2F in different arrangements for the JOS_L and LCN ground motions. Specifically, the response of the model in the anti-plane combined SSSI arrangement (caSSSI) is different from response of the other models, which are similar for the JOS_L ground motion. For the LCN ground motion, the ciSSSI and caSSSI models of MS2F respond differently from the other two models. This indicates that MS2F is more sensitive to the presence of the adjacent MS1F_2 in the ciSSSI and caSSSI arrangements, than in the ciSSSI and caSSSI arrangements during the JOS_L and LCN ground motions. However this behavior of the ciSSSI and caSSSI models of MS2F is not apparent from Figure 7-31, which shows that the experimental responses of MS2F in various arrangements are very similar during the SCS_H and PRI_H ground motions. This shows that the SSSI effects seen in the ciSSSI and caSSSI arrangements for the first two ground motions may be a result of erratic behavior and not interaction between the structures. The results of the numerical simulations presented in Figure 7-30 and Figure 7-31 also show that the responses of MS2F in the different arrangements are very similar for each ground motion. There are small differences in the responses for a given ground motion, but these are too small to warrant consideration. Identical to MS1F_2, the SSSI arrangements illustrated in Figure 7-1 have little to no effect on the global structural response of MS2F.

Figure 7-30 also shows that the numerical simulations result in reasonable predictions of the spectral accelerations for the JOS_L ground motion, in terms of the peak spectral acceleration as well as the corresponding period, with the exception of the caSSSI model. The predictions are not as good for the LCN ground motion, which is due to the inaccurate prediction of the site response at the flexible-base time period of the structures (around 0.6 to 0.8 sec). For the more intense ground motions, SCS_H and PRI_H, the nonlinear analyses in LS-DYNA result in spectral shapes that are closer to those observed in the experiments, than the linear analyses in SASSI. However the magnitude of the numerically calculated spectral accelerations are much smaller than those calculated from experimental results for these ground motions.

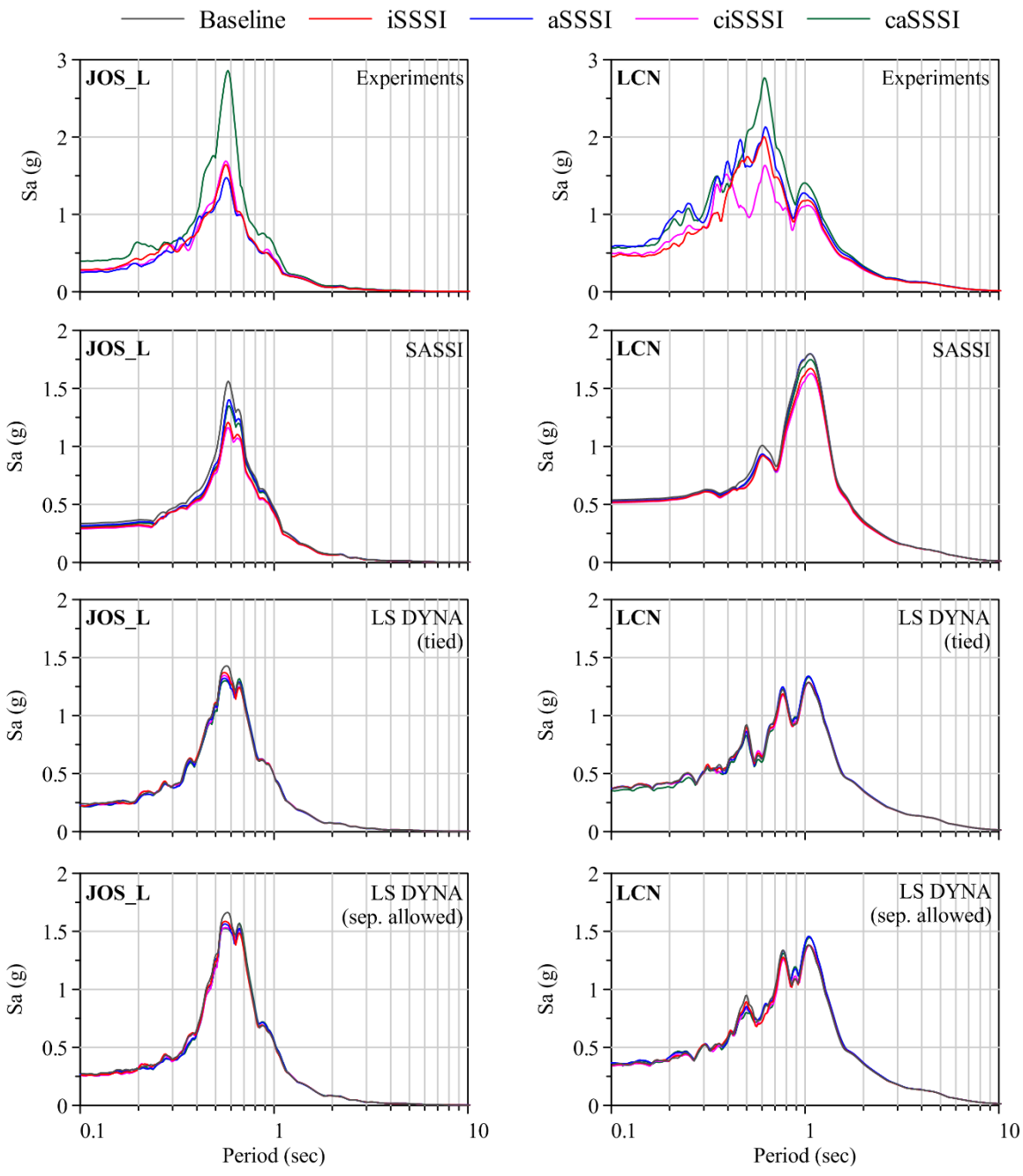


Figure 7-30: Response spectra of the roof acceleration of MS2F from numerical simulations using SASSI and LS-DYNA, and experimental observations for JOS_L and LCN ground motions

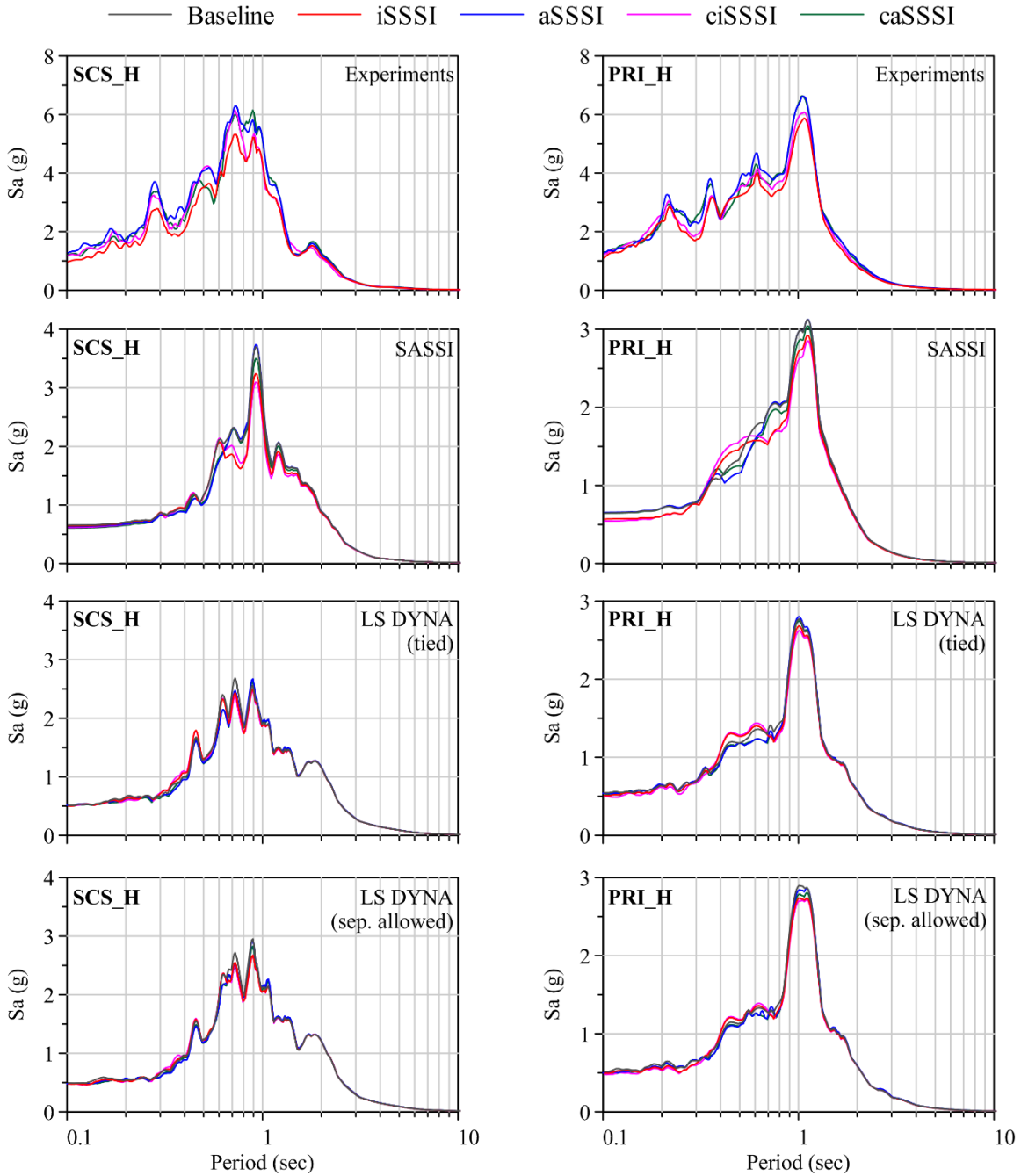


Figure 7-31: Response spectra of the roof acceleration of MS2F from numerical simulations using SASSI and LS-DYNA, and experimental observations for SCS_H and PRI_H ground motions

7.4.5 Effect of basement restraint on the response of MS1F_2

The footing responses calculated using numerical simulations and presented in Section 7.4.4.2 showed that footing restraint by the adjacent basemat did not result in considerable changes in column demands. However it is possible that a larger neighboring foundation, such as a deeply embedded

basement, provides more restraint resulting in a considerable change in near footing response and near column demands, as observed by Mason (2011) and Trombetta (2013). The effects of such a restraint, between spread footings and a deep basement, is investigated numerically in this section using nonlinear SSI analyses in LS-DYNA. The two superstructure models, MS1F_2 and MS2F, are used for this purpose. However the basemat of MS2F is replaced with a basement of plan dimensions 15m × 17m, and is fully embedded to a depth of 10.1m. The basement walls are 0.5m thick and are numerically modeled using shell elements and a rigid material model with the unit weight of aluminum, which was used in the construction of the MS3F basement in Tests 1 and 2 (see Table 7-3). However the unit weight of the basement is not likely to affect the restraint on adjacent footings, which is the focus of this study. The interface between the basement and soil is modeled using the contact properties used for the foundation-soil interfaces of MS2F and MS1F_2. No changes are made in the footings of MS1F_2. The effect of basement restraint is investigated using 1) a pseudo-static analysis involving horizontal forces proportional to roof masses applied at roof levels, and 2) a dynamic analysis with the four ground motions used in the previous sections. These analyses are performed for two cases: 1) a baseline case with MS1F_2 alone, and 2) an in-plane SSSI case with MS1F_2 placed adjacent to MS2F with a deep basement (hereafter referred to as MS2F_B): the iSSSI_B case. The baseline case is the same as in the previous sections, with its LS-DYNA numerical model presented in Figure 7-16. The LS-DYNA numerical model of the iSSSI_B case is presented in Figure 7-32.

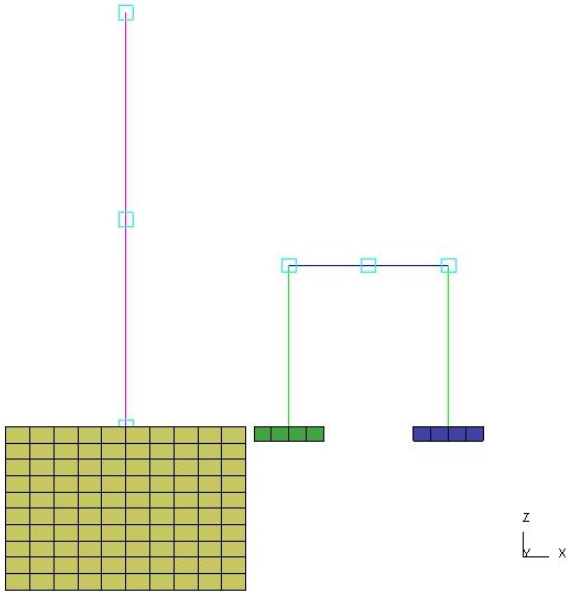


Figure 7-32: LS-DYNA numerical model of the iSSSI_B case with MS1F_2 on the left and MS2F_B on the right (soil elements are not shown for clarity)

7.4.5.1 Pseudo-static analyses

Pseudo-static analyses are performed for the baseline and iSSSI_B cases to investigate SSSI effects on MS1F_2 due to an adjacent basement. Global SSSI effects are examined from the lateral force-displacement response at the roof. Local SSSI effects due to footing restraint are examined using 1) the moment-rotation response, and 2) the vertical force-displacement response of the restrained footings. Given that dynamic effects in this analysis are negligible, a much smaller soil domain is built, significantly reducing the computational cost. The numerical model used for the pseudo-static analysis is presented in Figure 7-33. The lateral force is applied to the roof nodes of MS1F_2 and the forces are proportional to the values of the corresponding lumped masses. No lateral forces are applied to the MS2F superstructure and the peak value of each lateral force at each roof mass is equal to the corresponding mass times acceleration due to gravity. Additionally the forces are applied in the negative X direction, pushing the superstructure and footings of MS1F_2 towards MS2F. This is assumed to provide more restraint to the footings, compared with that when the force is applied in the direction away from MS2F, resulting in more SSSI. The foundation-soil interface for both the structures is modeled to allow for separation. Details of these contact models are presented in Section 7.4.2.

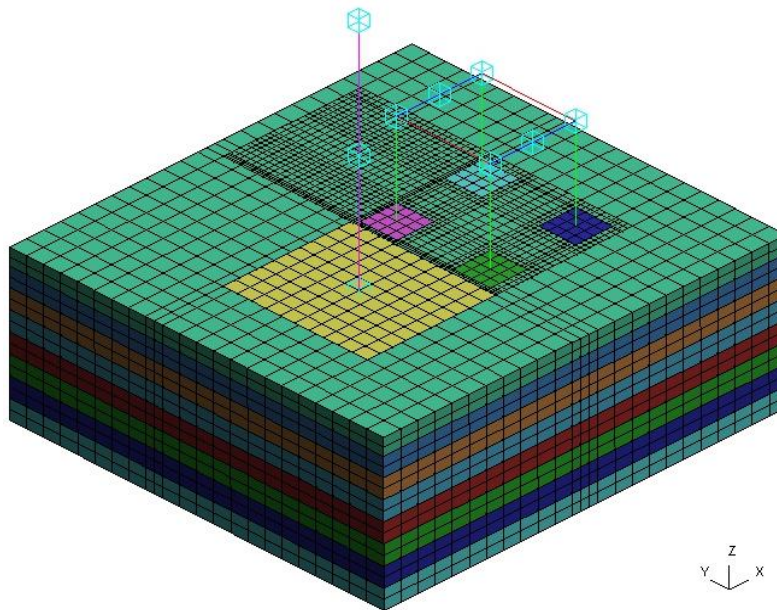


Figure 7-33: Isometric view of the LS-DYNA numerical model used for pseudo-static analysis of the iSSSI_B case

Figure 7-34 presents the moment-rotation response, and the vertical force-vertical displacement response of one of the two MS1F_2 footings closest to the basement. The responses are presented for the

baseline and iSSSI cases. The figure shows that the slope of the moment-rotation and vertical force-displacement responses are considerably larger for the iSSSI_B case, for which the footing is restrained by a rigid basement. The difference in the slopes is significant in the vertical force-displacement response, indicating that this response is more sensitive to footing restraint than the moment-rotation response. The results of the pseudo-static analyses therefore show a considerable increase in both the rocking stiffness and vertical stiffness of the restrained footings due to SSSI. As a result of the increased footing stiffness, the global lateral stiffness of MS1F_2 is also greater for the iSSSI_B case. This is evident from Figure 7-35, which presents the lateral force-displacement response of MS1F_2 for the baseline and iSSSI_B cases. The increase in the lateral stiffness of MS1F_2 for the iSSSI_B case is clear from this figure. Foundation restraint due to adjacent basement(s) may result in a meaningful change in global structural response.

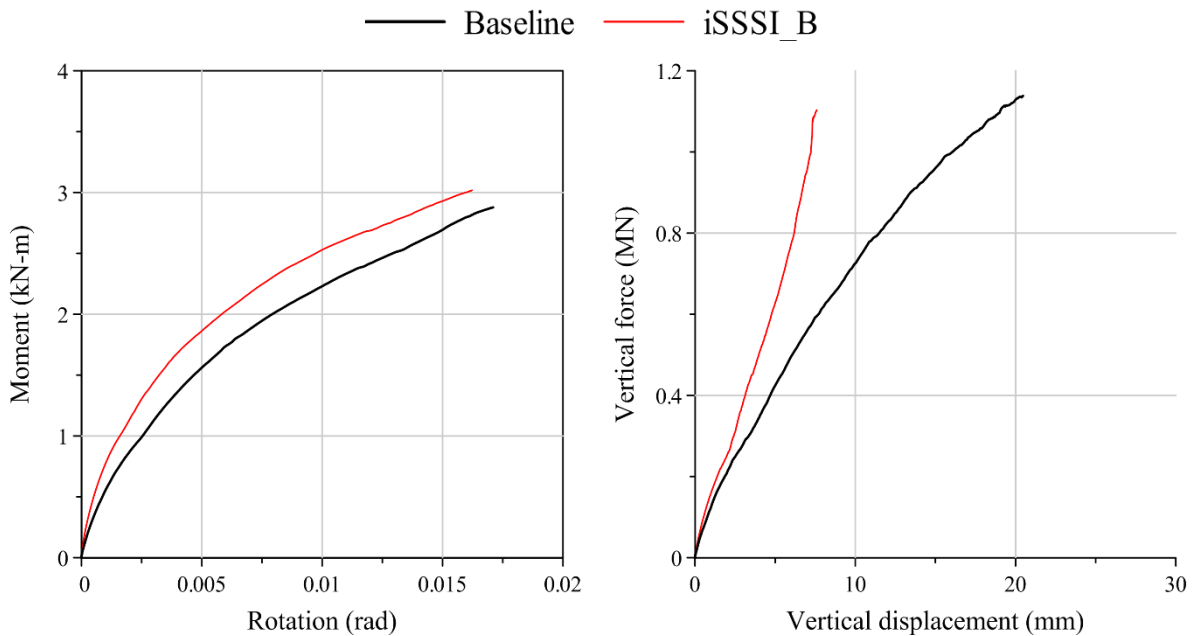


Figure 7-34: Moment-rotation response and the vertical force-displacement response of the restrained MS1F_2 footings in the baseline and iSSSI_B cases

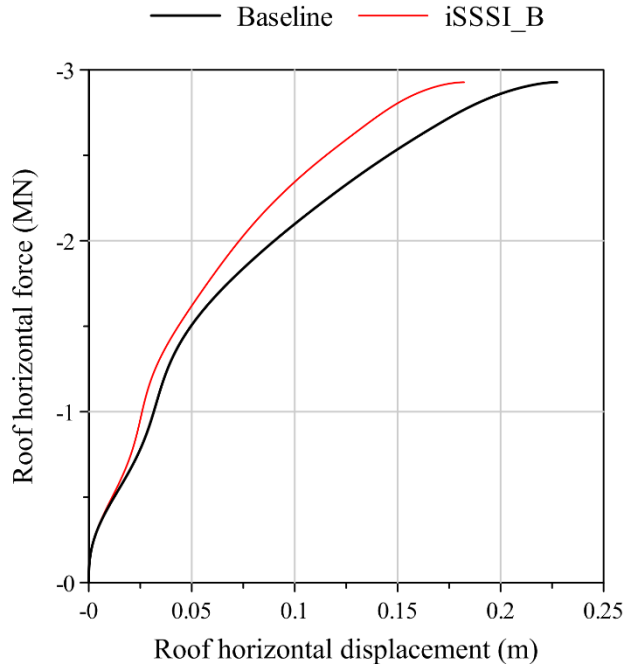


Figure 7-35: Lateral force-displacement response of the MS1F_2 superstructure in the baseline case and the iSSSI_B case

7.4.5.2 Dynamic analyses

The pseudo-static analyses showed an increase in the rocking and vertical stiffnesses of the near footings of MS1F_2 when they are restrained by a deep basement. This also led to an increase in the global lateral stiffness of the superstructure. This section investigates the effects of this interaction on the seismic response of MS1F_2. Since MS2F_B is founded on a deep basement, it is assumed that the SSSI effects on this structure are negligible and the response of MS2F_B is not examined. The dynamic analyses are performed for the four ground motions, JOS_L, LCN, SCS_H and PRI_H, used previously in this section. The structural response is measured using roof acceleration response spectra in MS1F_2. The SSSI effects are examined by comparing the response of the structure in the baseline case to that in the iSSSI_B case. The moment-rotation response and the vertical force-displacement responses of the footings closest to the basement are also examined.

Figure 7-36 presents the responses of MS1F_2 calculated using LS-DYNA for the baseline and iSSSI_B cases for the four ground motions. The panels in the left column in the figure present the response calculated using a tied soil-foundation interface; the panels in the right column present the response calculated using an interface that allows separation. The figure shows that the responses in the baseline and iSSSI_B cases are similar when simulated with a tied interface, indicating that the SSSI effects are negligible. However there are significant differences in the baseline and iSSSI responses

calculated using the separation-allowing interface for the LCN, SCS_H and PRI_H ground motions. The differences are primarily in the peak spectral accelerations, which are much smaller for the iSSSI_B case than in the baseline case. Additionally, the period of peak spectral acceleration is slightly smaller in the iSSSI_B case indicating stiffening in the response. To further investigate the reason for these differences, the moment-rotation responses of the restrained footing are calculated for the baseline and iSSSI_B cases from the results of the analyses performed with separation-allowing interface. These responses are presented in Figure 7-37. Two important observations can be made from this figure: 1) the average slope of the moment-rotation curves is higher for the iSSSI_B case than in the baseline case, and 2) the moment-rotation response of the iSSSI_B case shows only a small negative slope portion (at large positive rotations) unlike for the baseline case where the slope of the moment-rotation curve is negative beyond a rotation of $+0.0004$ radians. The former is consistent with the findings of the pseudo-static analyses, which showed stiffening in the moment-rotation behavior of the restrained footing. The negative slope portion in the moment-rotation response corresponds to partial uplift (or gapping) of the footing, which results in a sudden drop in the moment with gradual increase in the rotation. The moment-rotation responses show that gapping in the restrained footings is almost completely absent in the iSSSI_B case, while there is significant gapping in the footings in the baseline case. This explains the large differences between the roof response of the baseline and iSSSI_B cases: since secondary nonlinearities such as sliding and gapping, contribute significantly to the response of MS1F_2 (see Section 5.3.2.1 for a detailed description of the SSI response of MS1F_2), reduction of gapping in the iSSSI_B case reduces the superstructure response as seen in Figure 7-36. The reduction of gapping in this case is due to the increase in the rocking stiffness, which results in smaller footing rotations. In the case of the restrained footings of MS1F_2 the rotations are smaller than the threshold required for gapping between the soil and the footings. Additionally the absence of SSSI effects in the results calculated using a tied soil-foundation interface supports the conclusion that the significant SSSI in the iSSSI_B case in Figure 7-36 is due to a reduction in gapping.

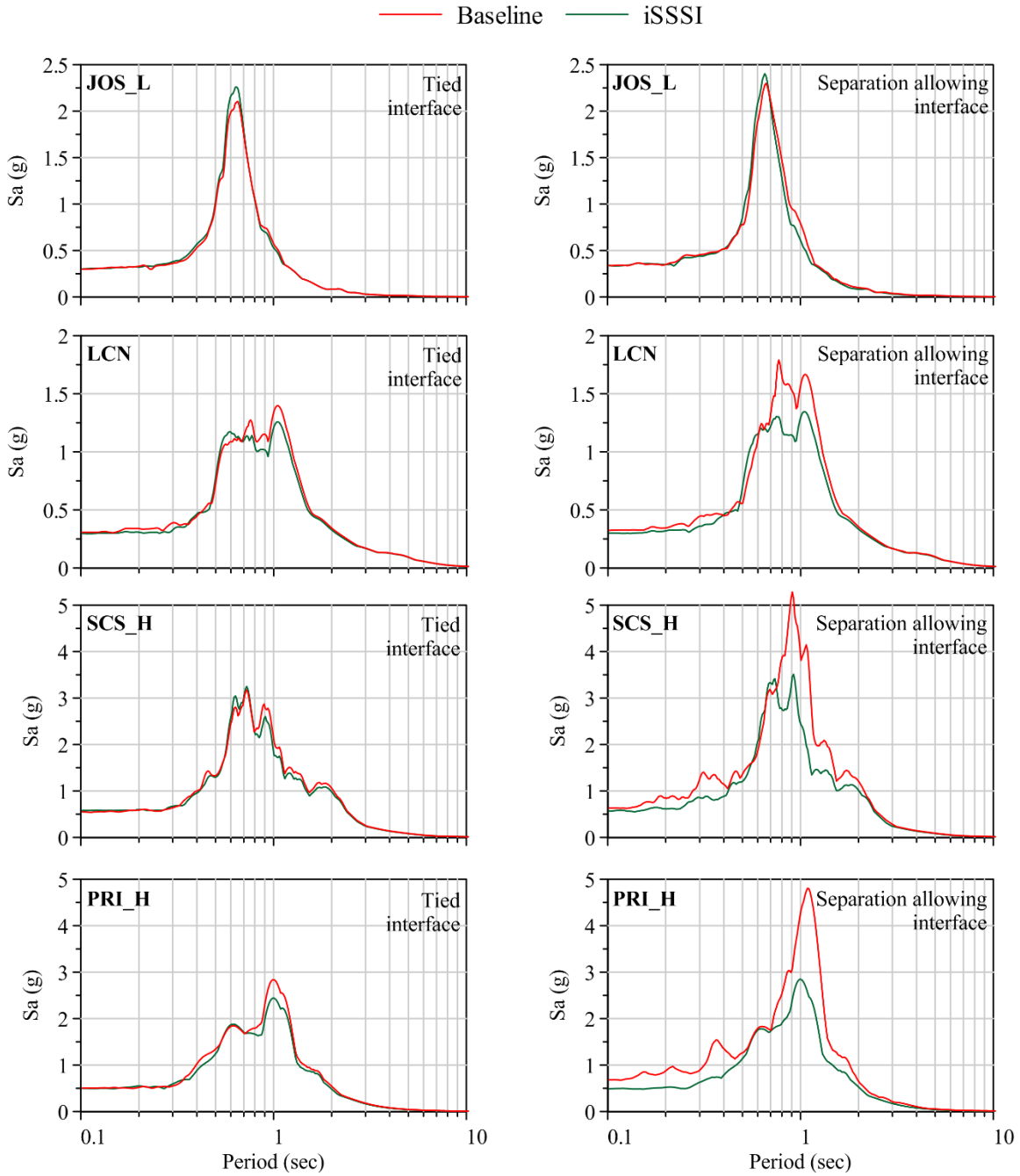


Figure 7-36: Response spectra of the roof acceleration of MS1F_2 from numerical simulations using LS-DYNA for four ground motions

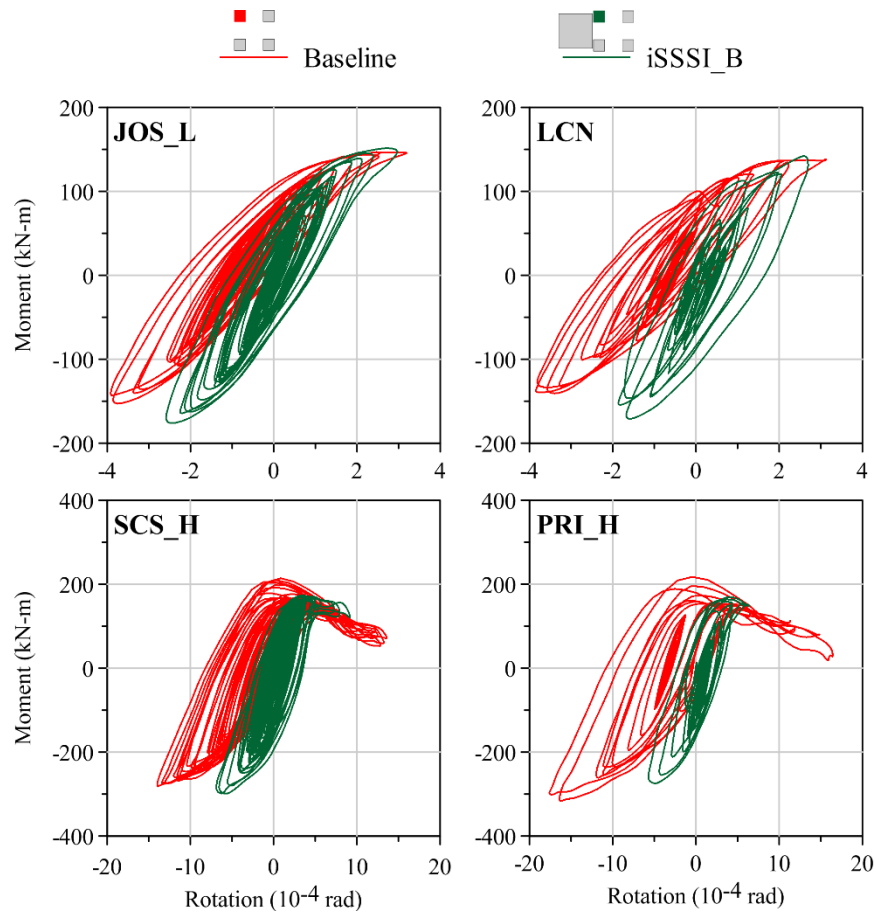


Figure 7-37: Moment-rotation responses of the restrained footings of MS1F_2 in the baseline and iSSSI_B cases calculated for the four ground motions

7.4.6 Effect of basement restraint on the response of MS1F_1

The analyses presented in Section 7.4.5 showed that the presence of a basement significantly affects the response of MS1F_2. However, MS1F_2 is founded on light footings, designed to intensify the SSI effects comprising rocking and sliding of the footings, unlike MS1F_1, which is designed to have realistic, code-conforming dynamic properties. This section investigates the effect of an adjacent basement on the response of a more realistic footing structure, MS1F_1.

MS1F_1 is a heavier and more flexible model than MS1F_2 and is described in Section 6.3.3. Specifically, MS1F_1 is taller, and has heavier roof masses and heavier footings that are made of steel (as opposed to aluminum used for MS1F_2). The numerical models of the baseline and iSSSI_B cases of MS1F_1 are built by making modifications to the numerical models used in the previous section for MS1F_2. No changes are made to the superstructure or the basement of MS2F_B. The foundation-soil interfaces of both the structures are modeled to allow separation, and analyses with tied interfaces are not

performed. The ground motions used previously, JOS_L, LCN, SCS_H and PRI_H, are used for the analyses in this section. Structure-soil-structure interaction effects in MS1F_1 are examined by comparing acceleration response spectra at the roof for the baseline case and the iSSSI_B cases. Figure 7-38 presents these acceleration response spectra and enables such a comparison. The figure shows that roof responses of MS1F_1 are virtually identical for the baseline and iSSSI_B cases. This observation is different from that of the responses of MS1F_2, which show significant SSSI effects when a separation-allowing interface is used. The smaller SSSI effects in MS1F_1 are due to the flexible superstructure, which results in less rocking in the footings and consequently no gapping for both the baseline and the iSSSI_B cases. Additionally, the footings in MS1F_1 are much heavier and have a larger moment of inertia than those of MS1F_2 and require larger moments to produce the same rotation. This further decreases the footing rotations and avoids gapping under the footings. Figure 7-38 also shows slightly greater peak spectral accelerations for the iSSSI_B case than in the baseline case. This is because restraining the footings in the iSSSI_B case decreases the footing rotations from those observed in the baseline case, resulting in smaller hysteretic energy dissipation in the soil at the vicinity of the footings. Therefore the hysteretic damping is slightly smaller, causing an increase in the peak spectral accelerations.

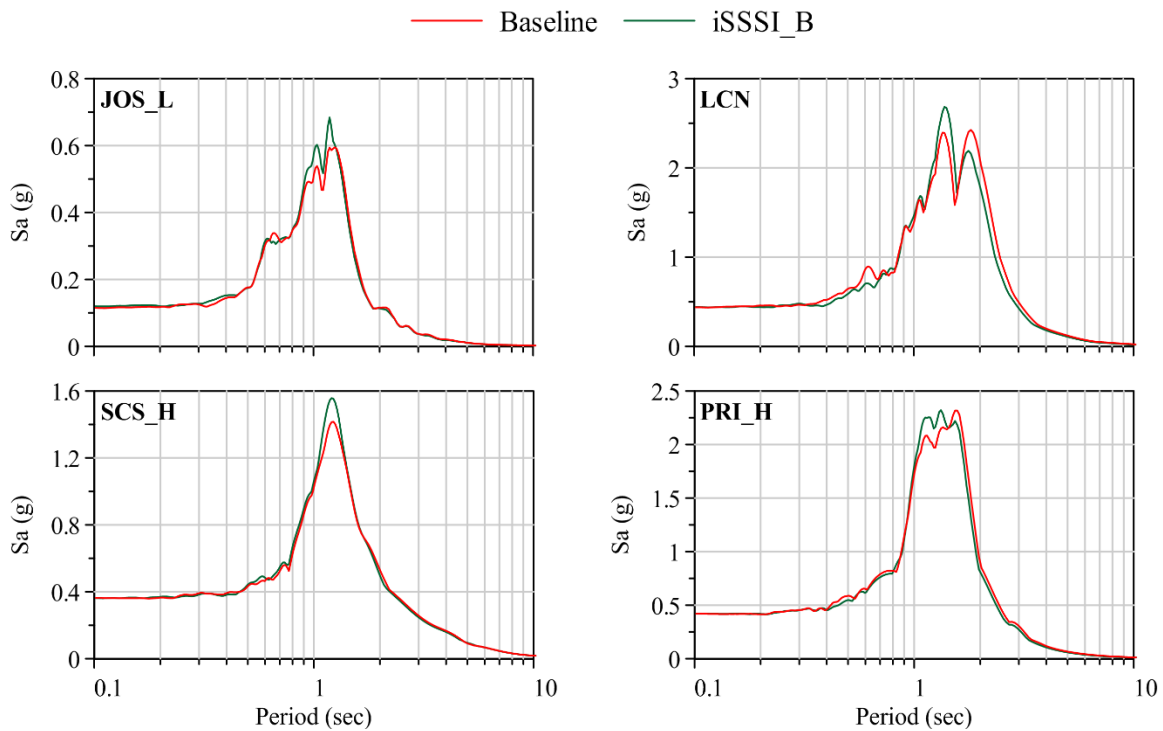


Figure 7-38: Response spectra of the roof acceleration of MS1F_1 calculated using numerical simulations in LS-DYNA for four ground motions

7.5 Summary and conclusions

Four centrifuge experiments were conducted at the NEES@UCDavis centrifuge facility to understand the effects of SSSI on buildings in dense urban environments. Test 1 involved two baseline SMRF structures (MS1F_1 and MS3F) placed sufficiently far away from each to not introduce any SSSI effects. These structures were placed directly adjacent to each other in Test 2 to isolate and understand the impact of SSSI. Tests 3 and 4 involved a two-story shear wall structure (MS2F) and a one-story SMRF structure (MS1F_2) designed to act as a ‘transmitter-receiver’ couple. The baseline model of MS1F_2 and an in-plane SSSI configuration were studied in Test 3, and an anti-plane SSSI and a combined in-plane anti-plane SSSI configuration were studied in Test 4. Numerical simulations were performed to calculate the site response and SSI response. The frequency-domain equivalent-linear program, SHAKE, and the nonlinear time-domain programs, DEEPSOIL and LS-DYNA, were used for site-response analysis. The SSI analyses were performed using frequency-domain linear program SASSI, and the direct method in LS-DYNA. The LS-DYNA analyses were performed for two cases: using the tied interface, and a separation-allowing interface. In addition to the SSSI arrangements considered in the City Block experiments and illustrated in Figure 7-1, numerical simulations were performed to investigate the SSSI effects in MS1F_2 due to the presence of an adjacent structure with a basement (MS2F_B). This investigation was performed through pseudo-static and dynamic analyses of the SSI models. To understand the effects of an adjacent basement on the response of a structure with more realistic footings, the dynamic analyses were rerun after replacing MS1F_2 with MS1F_1. The following conclusions can be drawn from the experimental and numerical results:

1. Considerable inter-test variability and intra-test variability exist in the input ground motion and the site response. This variability needs to be taken into account when assessing SSSI effects, so as to not overstate the effects, if any.
2. The site period elongates and hysteretic damping increases as the ground motion intensity increases due to nonlinear behavior in the soil. The numerical programs capture this period elongation reasonably well.
3. The equivalent-linear program, SHAKE, overpredicts spectral accelerations at the site period in comparison with the nonlinear programs, which result in predictions that are similar to each other. All programs predict smaller spectral accelerations at periods less than the elongated site period than those calculated from the experimental results.
4. The experimental results show that the interaction between MS1F_2 and MS2F in the SSSI arrangements considered in the City Block experiments have no considerable effect on global structural responses. Some variability in the response of MS2F in different arrangements is

observed for the JOS_L and LCN ground motions but this is deemed erratic because the variability is not seen in either the remaining experiments or the numerical simulations.

5. The numerical results agree with the experimental results in terms of the (small) magnitude of SSSI effects. The global structural responses calculated in different SSSI arrangements are virtually identical for a given ground motion, indicating that the interaction between MS1F_2 and MS2F in these arrangements is insignificant.
6. There are large differences between the numerical and experimental results in terms of the magnitude of spectral accelerations, especially for MS1F_2. Similar differences were also observed by another City Block researcher (Jones, 2013), who performed numerical simulations using FLAC. The reason for these differences warrants further investigation, which is outside the purview of this study.
7. Of the different numerical analysis methods, only LS-DYNA (with a separation-allowing interface) reasonably captures the shape of the roof response spectra of MS1F_2 for the more intense ground motions, SCS_H and PRI_H. This indicates that simulating foundation nonlinearities, such as footing sliding and gapping, are important to accurately predict structural response for surface- or near-surface-mounted structures subjected to intense ground motions.
8. Large differences between the experimental and numerical predictions of spectral accelerations are seen for MS2F during the more intense ground motions, SCS_H and PRI_H, which were also observed by Jones (2013). However all of the numerical programs make reasonable predictions of spectral shape and the flexible-base time period of MS2F.
9. The ‘transmitter-receiver’ hypothesis, which was presumed for the design of Tests 3 and 4, was negated because MS1F_2 and MS2F responded almost independently of each other.
10. The response of the footing close to the basemat of the adjacent MS2F (in the iSSSI and ciSSSI positions) showed more asymmetric behavior than the footings away from the basemat. This asymmetric behavior could be addressed when modeling the footings by spring-based methods of SSI analysis.
11. The experimental and numerical results from Tests 3 and 4 showed that the structure-soil-structure interaction due to the dynamic behavior of the structures (which can also be referred to as wave-based SSSI) is not significant for the SSSI arrangements considered in the City Block project. Since these structures are rather generic, it can be said that wave-based SSSI effects are not important for calculating the global response of low- to medium-rise structures.
12. Pseudo-static analysis provides a convenient and computationally economical alternative to dynamic analysis to investigate SSSI effects resulting from foundation restraints. Such an investigation of the interaction between MS1F_2 and MS2F_B (MS2F with a deep basement)

showed that the rocking and vertical stiffnesses of the footings restrained by an adjacent basement increased considerably. Additionally, the vertical stiffness of the footings was more sensitive to restraint by the adjacent basement than the rocking stiffness. The increase in the footing stiffness also increased the global lateral stiffness of the MS1F_2.

13. Dynamic analyses showed that the presence of an adjacent deep basement considerably changes the global structural response of MS1F_2, when the soil-footing interface was modeled to allow separation. This is primarily due to the reduction in gapping between the soil and the footings, which contributes significantly to the MS1F_2 response as shown in Section 5, by increasing the rocking stiffness of the restrained footings. The SSSI effects in MS1F_2 involving a tied footing-soil interface were much smaller since gapping was not simulated.
14. The response of MS1F_2 exhibits a situation where local SSSI effects due to footing restraint from an adjacent basement results in considerable changes in the global structural response. SSSI effects from local foundation restraint should therefore be accounted for in stiff structures founded on spread footings where considerable gapping, or uplift, is expected in design basis shaking.
15. The heavier, more flexible MS1F_1 showed much smaller SSSI effects when placed adjacent to a structure with a deep basement than MS1F_2. This is because the superstructure of MS1F_1 is more flexible, and its footings are heavier than those of MS1F_2; thus, gapping is less likely to occur beneath the footings of MS1F_1.
16. The numerical analyses do not show any consistent changes in the column demands due to restraints provided by an adjacent basement. Rather, the results of the numerical analyses show that an increase in footing stiffness due to restraint reduces the transient rotations.
17. SSSI is a complicated phenomenon that needs to be investigated with ‘bottom-up’ approach by starting with very simple, elastic, experimental models. Experimental data must be supplemented by comprehensive nonlinear numerical simulations to gain insight into the underlying physical mechanisms.

SECTION 8

SUMMARY, CONCLUSIONS AND RECOMMENDATIONS

8.1 Summary

Soil-structure interaction (SSI) analysis is the process of calculating structural response accounting for the flexibility of the underlying soil. Site-response analysis is a precursor to SSI analysis and involves the calculation of the response of a soil deposit to a bedrock motion. Site-response analysis is also used to calculate free-field surface ground motion for input to surface or near-surface mounted structures. Structure-soil-structure interaction (SSSI) is an extension of SSI, and refers to the interaction of neighboring structures through the soil surrounding them. The larger goal of this report is to improve the current understanding of site response, SSI and SSSI, and to advance the numerical tools that simulate these phenomena for deployment in performance assessment of buildings and nuclear structures.

Section 2 reviews the numerical methods for site-response analysis, including their evolution, and the state-of-the-art. It describes site-response analysis using the equivalent-linear frequency-domain program SHAKE (Schnabel *et al.*, 2012), and the nonlinear time-domain programs DEEPSOIL (Hashash *et al.*, 2011) and LS-DYNA (LSTC, 2013). Section 3 presents a similarly structured review of numerical methods in SSI analyses and describes SSI analysis using the linear frequency-domain program SASSI (Lysmer *et al.*, 1999), and LS-DYNA. It presents a review of past studies of SSSI in buildings and nuclear structures.

Site response, SSI and SSSI are complex nonlinear problems involving three-dimensional wave propagation and sometimes, very large strains in the soil. Traditionally, site-response analysis is bypassed for most buildings in lieu of using attenuation relationships that empirically account for the influence of the underlying soil deposit on the surface ground motion. Soil-structure interaction is usually ignored for buildings that are flexible and constructed on stiff soil sites, but when important, is accounted for using simplified methods that model the underlying soil using equivalent springs and dashpots. Nuclear structures, generally being stiff and heavy, elicit significant SSI, and are analyzed with more rigorous methods. Site-response analysis for nuclear applications is performed using one-dimensional equivalent-linear methods in the frequency domain, typically using SHAKE. Soil-structure interaction analysis for these applications is typically performed using SASSI, which is a linear, frequency-domain program that is capable of three-dimensional SSI analyses. These frequency-domain methods, developed several decades ago, are now very well established and are used extensively in both the civil and nuclear industry because of their simplicity and computational efficiency. There is consensus that the linear frequency-domain methods will likely result in accurate predictions for low intensity earthquakes, where soil strains

are small and the behavior is essentially linear. However the utility of these methods for intense earthquakes, resulting in large soil strains, is unproven. Nonlinear time-domain methods, which have been developed more recently, potentially enable a more realistic modeling of soil-structure systems, and can capture nonlinearities near the foundation such as gapping and sliding that are much more likely with intense earthquake shaking. Well-known nonlinear time-domain programs are DEEPSOIL, used for site-response analysis, FLAC (Itasca Consulting Group, 2005), used for site-response and SSI analysis, and the commercial finite element programs, ABAQUS (Dassault Systèmes, 2005) and LS-DYNA, used for site-response and SSI analyses. The nonlinear methods are computationally more expensive than the linear frequency-domain methods and their use has been limited to high-value buildings, bridges and petrochemical facilities.

Sections 4 and 5 of this report present detailed assessments of current, industry-standard site-response and SSI analysis programs, respectively, and provide guidelines to practicing engineers on the usage of these programs. Section 4 presents an assessment of the site-response analysis programs, SHAKE, DEEPSOIL and LS-DYNA. The assessment includes calculation of responses of four idealized, but representative, soil sites (two sites representing Central and Eastern United States, and two sites representing Western United States) subjected to various bedrock ground motions of different intensities and frequency contents. The responses calculated using the different programs are compared for all sites and ground motions, and challenges and pitfalls with the use of each of these programs are identified. Biaxial site-response analysis is also studied to understand the effect on site response of simultaneously applying two horizontal ground motion components on site response. Guidelines are provided on the use of site-response analysis programs for different levels of expected peak shear strains in the soil profile. Section 5 presents an assessment of industry-standard SSI analysis programs, SASSI and LS-DYNA. The first step in the assessment is to benchmark the time-domain program LS-DYNA (using the domain reduction method as well as the direct method) against the frequency-domain program SASSI, for linear SSI analyses. This is done by performing linear SSI analyses of two idealized, lumped mass structures using SASSI and LS-DYNA, and verifying that the responses calculated using the two programs are similar. The second part of the assessment involves calculating nonlinear SSI responses of a one-story structure founded on spread footings and a two-story structure founded on a basemat for four input ground motions of different intensities. Nonlinear responses are calculated in SASSI using strain-compatible moduli and damping ratios for the soils. LS-DYNA analyses are performed using two soil-foundation interfaces: 1) an interface that is tied and does not allow separation (gapping and sliding) between the soil and the foundation, and 2) an interface that allows separation between the soil and the foundation. The responses calculated using SASSI and LS-DYNA are compared for all the ground motions, and challenges and pitfalls in performing SSI analyses using these programs are identified.

Unlike for SSI, which has been studied for many decades and is currently well understood, studies of SSSI are small in number and mostly limited to analytical studies involving highly idealized structures, foundations and soil profiles. A better understanding of SSSI is important for performance assessment of buildings in dense urban areas, which are often constructed in ‘city blocks’ and may interact with each other during an earthquake. The US NSF funded project titled ‘Seismic Performance Assessment in Dense Urban Environments’, and called the ‘City Block project’ in this report, attempts to remedy the lack of SSSI research through a series of centrifuge experiments and numerical simulations. Six centrifuge experiments were conducted as a part of this project at the NEES@UC Davis centrifuge facility, on scaled-down models of buildings. The first two experiments, Tests 1 and 2, examined SSI and SSSI in buildings designed with code-conforming properties. Test 3 and 4 involved stiffer buildings that were designed to experience more SSI and SSSI. Tests 5 and 6 examined SSI and SSSI in idealized structures founded on liquefiable soils. Section 6 describes Tests 2, 3 and 4 of the City Block centrifuge experiments. It includes descriptions of the test plan, design and construction of the model structures, and the chronology of the input ground motions used during the tests. Section 7 presents numerical simulations of site response in Tests 3 and 4 using SHAKE, DEEPSOIL and LS-DYNA, and numerical simulations of SSI and SSSI using SASSI and LS-DYNA. The results of the simulations are qualitatively compared to the experimental results to make observations regarding the effects of SSSI on the global responses of the model structures. Section 7 also presents an exploratory study on the effects of SSSI through foundation restraint from adjacent substructures.

8.2 Conclusions

The overarching conclusions of each study in this report are presented in the sections that follow.

8.2.1 Assessment of industry-standard site-response analysis programs

The following conclusions are drawn from the assessment of the site-response analysis programs, SHAKE, DEEPSOIL and LS-DYNA, in Section 4:

- Equivalent-linear and nonlinear programs result in very similar predictions of response for stiff sites subjected to low intensity ground motions. The predictions become increasingly different for analyses involving higher strains, and at higher frequencies. The predictions from equivalent-linear programs start diverging from those of the nonlinear programs when the equivalent-linear peak shear strains in the soil are greater than about 0.1%. The predictions of the equivalent-linear and nonlinear programs are very different at peak shear strains greater than 1%.

- The differences between the predictions of the equivalent-linear and nonlinear programs for cases involving large shear strains are as follows :
 - The spectral accelerations calculated using the equivalent-linear and nonlinear programs are increasingly different at shorter periods (periods smaller than the elongated site period). The equivalent-linear programs tend to result in almost constant spectral accelerations at these periods, which is a manifestation of near-zero frequency content in the response at the corresponding frequencies. This is a direct consequence of modeling the soil response using a secant shear modulus, as opposed to modeling the changes in the shear modulus with time, as in a nonlinear analysis. Modeling cyclic changes in shear modulus results in high-frequency response when the shear modulus is high, and low-frequency response when the shear modulus is low. Equivalent-linear programs do not capture the high-frequency content since they simulate the soil response with a constant shear modulus, which is equal to the iterated modulus.
 - The equivalent-linear programs tend to underestimate the peak strains in the soil layers in comparison with the nonlinear programs.
 - The equivalent-linear programs tend to overestimate the acceleration amplifications at the site period in comparison with the nonlinear programs.
 - The equivalent-linear and nonlinear programs predict almost the same elongated site periods for rock and firm soil sites. For others, involving very soft soil sites subjected to intense ground motions, the equivalent-linear programs predict slightly smaller site periods than the nonlinear programs.
- The site responses calculated using all three programs contain anomalous responses for peak strains greater than 1%. Of particular importance is the response at higher frequencies ($> 15\text{Hz}$), which is important for nuclear structures: SHAKE tends to underestimate the site response at these frequencies when compared with the responses calculated using the nonlinear programs due to reasons given earlier. LS-DYNA analysis using the MAT_HYSTERETIC material model tends to result in an unusual number of spikes in the acceleration response when compared with the other programs. These spikes result in short-period spectral accelerations that are larger than those calculated using DEEPSOIL. This anomalous response from LS-DYNA is due to sudden changes in the slope of the backbone curve used in the MAT_HYSTERETIC material model, which currently accepts a maximum of 10 stress strain points as input. Increasing the number of points significantly (such as 120, in the study presented in this report) will ‘smoothen’ the backbone curve, reduce the spikes in the acceleration response, and result in a response that is much closer to that calculated using DEEPSOIL. DEEPSOIL also results in anomalous responses for analyses involving large strains: there are large differences in the peak strains of consecutive layers, despite the layers having identical

material properties. An investigation into this anomalous response revealed that it is due to the usage of extended Masing rules of soil hysteresis (see Section 2.1.2.2 for a description of extended Masing rules).

- There is significant variability in the site-response predictions from different programs for high-intensity ground motions, despite using almost identical input material properties, and very simple soil profiles. Greater deviations between the predictions are expected for the more complex soil profiles encountered in practice.
- Equivalent-linear methods should provide a reasonable solution if soil strains are small and can be used with high confidence if the peak soil shear strains are expected to be less than 0.1%. Nonlinear analysis should be performed and its results substantially weighted for design, when peak shear strains are significantly greater than 0.1%.
- Site-response analysis is typically performed using only one component of ground motion. Performing a biaxial analysis by simultaneously using two horizontal components of ground motion can considerably affect the site response for intense ground motions resulting in large shear strains.

8.2.2 Assessment of industry-standard SSI analysis programs

The following conclusions are drawn from the assessment of the SSI analysis programs, SASSI and LS-DYNA, in Section 5:

- The frequency-domain program, SASSI and the time-domain program, LS-DYNA, result in almost identical responses for SSI analyses of linear models. This is an important result in the benchmarking of time-domain programs against the frequency-domain programs for linear analyses. However the frequency-domain programs are much more computationally efficient: for one analysis case considered in this study, SASSI was about 120+ times faster than the direct method in LS-DYNA. The domain reduction method in LS-DYNA also offers a computationally efficient alternative to the direct method, while producing almost identical results: for one analysis case, the domain reduction method was about four times faster than the direct method.
- Nonlinear SSI predictions can be significantly different from those made using linear frequency-domain programs. The differences are greatest for cases with significant nonlinearities, such as nonlinear site response (primary nonlinearities) and nonlinear behavior at the foundation (secondary nonlinearities), namely, soil hysteresis, and gapping and sliding underneath the foundation. In the study presented in this report, the responses of a one-story footing structure calculated using SASSI and LS-DYNA differed considerably, even for a very low intensity ground motion due to nonlinear soil behavior at the vicinity of the footings.

- Soil-structure interaction analyses in both the frequency domain in SASSI and time domain in LS-DYNA can produce anomalous responses, which can go unnoticed if only one of the programs is used. Some practical considerations should be made to avoid these anomalous responses. Some of these considerations include:
 - Structural response calculated using SASSI can be particularly sensitive to the number of analysis frequencies at which the transfer functions are calculated. Although the SASSI user manual (Ostadan, 2006b) recommends 10 to 20 frequencies, which are to be selected based on the fixed-base natural frequencies of the structure, it was found that a larger number of frequencies is required, and that the input frequency set should be sufficient enough to characterize the peaks in the transfer function corresponding to 1) the flexible-base (and not the fixed-base) frequency of the structure, and 2) the natural frequencies of the soil profile. However since the flexible-base frequencies of the structure may not be available before the analysis, it is difficult to choose the analysis frequencies a priori.
 - Structural response calculated using SASSI can be sensitive to the number of elements (i.e., the meshing) of the foundation, in spite of the foundation being significantly stiffer than the surrounding soil. The number of elements in the foundation governs the number of interaction nodes: the nodes for which SASSI calculates the foundation impedance functions. However, it is difficult to identify the adequacy of the number of foundation elements unless an analysis result from a different program, such as LS-DYNA, is available for comparison.
 - The rocking response of a structure calculated using SASSI can be considerably different for two different site layering schemes, although these schemes result in identical site responses at the surface. Smaller layer thicknesses are required near the foundation of the structure to produce a structural response that is similar to that calculated using LS-DYNA. The site layering scheme used for site-response analysis (see Section 4.4.2 for description of site layering for site-response analysis), may not be adequate for SSI analysis in SASSI.
 - The responses of linear or nonlinear models calculated using LS-DYNA can be affected by hourglass modes in the elements of the foundation, and of the soil. These modes can be mitigated using hourglass control in LS-DYNA.
- Nonlinear response at the vicinity of the foundations (secondary nonlinearities) can be significant in buildings. This nonlinear response can lead to an increase in superstructure demands. A considerable increase in the roof accelerations of the one-story structure with footings is observed when it is modeled with a soil-footing interface that simulates gapping and sliding, as opposed to an interface that does not allow separation between the soil and the footing. Ignoring secondary nonlinearities

such as gapping and sliding can therefore result in an unconservative prediction of superstructure response.

- Structures with spread footings are susceptible to an increase in framing ductility demands due to footing spreading: residual displacements of the footings away from each other. Connecting the footings with grade beams will eliminate footing spreading and reduce ductility demands in the superstructure.

8.2.3 Centrifuge experiments and numerical simulations of the NEES City Block project

The following conclusions are drawn from the centrifuge experiments examining SSSI and the corresponding numerical simulations presented in Sections 6 and 7:

- Accurate numerical modeling of centrifuge experiments is very difficult. It requires modeling of the centrifuge itself, and careful determination of the soil properties when the centrifuge is in flight.
- Analysis of the data recorded from a centrifuge test to examine SSSI involves the comparison of the data from two different models: usually a baseline model involving a single structure sufficiently far away from neighboring structures, and an SSSI model involving multiple structures that interact with each other during an earthquake. For an accurate assessment of SSSI effects through this comparison, inherent variabilities in input ground motion and material properties should be accounted for. The variability in the input ground motion and soil properties for the City Block experiments are considerable.
- The site-response predictions calculated using SHAKE, DEEPSOIL and LS-DYNA are very different from the experimental results, especially in the short period range, but capture the elongated time period reasonably well.
- Structure-soil-structure interaction analyses can be performed in the frequency domain using SASSI and the time domain using LS-DYNA, with explicit modeling of the soil and structures, and without using soil springs. However some practical considerations for SSI analysis, noted in the previous section, should be made to avoid anomalous responses and produce reasonable predictions.
- Structure-soil-structure interaction does not result in any significant change in the global structural responses of the structures considered in Tests 3 and 4 of the City Block project. There is reasonable agreement between the experimental and numerical results in this regard.
- There are significant differences between the roof responses calculated from numerical simulations and those from experiments. Numerical simulations by another City Block researcher (Jones, 2013) using FLAC (Itasca Consulting Group, 2005) also showed similar differences. The causes of the

differences between numerical and experimental responses is beyond the scope of this research project.

- Structure-soil-structure interaction effects due to dynamic response of the structures, namely, wave-based effects, have a negligible effect on the responses of low- to medium-rise structures such as those considered in Tests 3 and 4 of the City Block project.
- Structure-soil-structure interaction through foundation restraint by an adjacent substructure or foundation may affect the local response of the foundation, such as its moment-rotation response or its vertical force-vertical displacement response. Such effects of SSSI, which do not involve dynamic effects, can be conveniently examined through pseudo-static analyses. The pseudo static analyses performed in this study revealed that the presence of an adjacent basement increases the rocking stiffness and vertical stiffness of footings, with the vertical stiffness being more sensitive to the restraint provided by the basement. For the structure considered in this study, the increase in footing stiffness also resulted in an increase in the global lateral stiffness of the structure.
- The dynamic SSSI analyses presented in Section 7 showed that restraint on footings by an adjacent basement considerably reduced the transient rotations and transient vertical displacement of the footings. In one case, involving a stiff superstructure and very light footings prone to gapping and uplift, the effects of footing restraint by the adjacent basement resulted in significant changes in the global response of the superstructure. Further investigation revealed that this change was due smaller footing rotations, which resulted in a reduction in gapping beneath the footings.
- The numerical investigations presented in Section 7 revealed no significant changes in the demands on the columns above the restrained footings due to the presence of an adjacent substructure or foundation.
- Structure-soil-structure interaction due to restraint from an adjacent foundation can affect global superstructure response in some cases, and nonlinear analysis that simulates separation at the foundation-soil interface is needed to accurately compute the response. Accurate simulation of SSSI requires nonlinear analysis with robust contact models.

8.3 Future research

- *Investigation of the mechanisms of structure-soil-structure interaction:* The study performed in this research project, as well as by other City Block researchers, showed that wave-based SSSI, namely, the effect of the dynamic response of one structure on the dynamic response of an adjacent structure, is negligible for the low- to medium-rise buildings considered in Test 1 through Test 4 of the City Block project. Interaction between neighboring structures can result from 1) foundation restraint due

to the presence of an adjacent foundation, 2) modification of the ground motion due to kinematic interaction, and 3) shielding of ground motion by adjacent structures. The first mechanism was observed in the spread footings of a one-story structure considered in this study, when placed against a basement. The second mechanism can be important in cases involving significant kinematic interaction, such as very deep basements or buildings adjacent to underground tunnels. Shielding will be important for buildings in dense urban regions involving deeply embedded foundations or underground tunnels, subjected to horizontal and inclined wave-fields. These mechanisms should be explored as a part of an investigation of SSSI in dense urban areas.

- *Effect of SSI and SSSI in performance assessment of buildings using the second generation performance-based earthquake engineering (FEMA-P58) procedures:* The effects of SSI and SSSI can be interpreted in terms of acceleration response spectra, spectral amplifications, or engineering demand parameters such as peak roof acceleration, peak story drift and residual story drift. Although these are valid interpretations of interaction effects, they are not sufficiently tangible to make objective decisions regarding the significance of SSI and SSSI in the overall design of a structure. An alternate way to judge the importance of SSI and SSSI is to estimate the change in earthquake loss with its explicit considerations, where losses can be expressed in terms of repair cost, downtime, and casualties, and calculated for intensities of ground motion or on an annualized basis. The FEMA-P58 methodology (FEMA, 2012) could be used for these calculations.
- *Improvement of the numerical predictions of site response and SSI:* The numerical methods for site-response and SSI analysis can be improved by:
 - *Validation:* Validation of the industry-standard numerical programs is a critical challenge for site-response and SSI analysis. The validation exercises should be performed with an emphasis on large strains ($> 1\%$) and high frequencies (> 10 Hz).
 - *Accounting for three-dimensional effects:* Earthquakes produce complex three-dimensional wave-fields involving body and surface waves. Three-dimensional effects are typically ignored, and further studies are required to evaluate their significance.
- *Soil-structure interaction effects in base-isolated nuclear power plants:* Base isolation can significantly reduce mean seismic demands in structures, systems and components of fixed base nuclear power plants. Base-isolation may also reduce SSI effects in nuclear power plants but it is unknown whether this reduction is sufficient to warrant neglecting the effects altogether when calculating distributions of seismic demand, as is required by ASCE Standard 4 (ASCE, 1998; ASCE, forthcoming). Further study is required to examine the influence of base isolation on SSI effects in nuclear structures. This study should investigate whether a) a fixed-base analysis using a free-field ground motion (ignoring SSI effects) can be performed in lieu of an SSI analysis, to calculate

distributions of seismic demands in base isolated nuclear structures, and b) rocking effects are significant on sites considered appropriate for use of horizontal base isolation.

SECTION 9

REFERENCES

- Anderson, L. M., Carey, S., Amin, J., and Ostadan, F. (2013a). "Effect of Separation Distance and Soil Parameters on the Structure-Soil-Structure Interaction Response of Adjacent Deeply Embedded Structures." *22nd International Conference in Structural Mechanics in Reactor Technology (SMiRT-22)*, San Francisco, California.
- Anderson, L. M., Elkhoraibi, T., and Ostadan, F. (2013b). "Validation of SASSI2010 Solution Methods through Independent Verification Using SAP2000 for Deeply Embedded Structures with Large Footprints." *22nd International Conference in Structural Mechanics in Reactor Technology - SMiRT 22*, August 2013, San Francisco, California.
- ANSYS Inc. (2013). Computer Program ANSYS 13.0, ANSYS Inc., Canonsburg, Pennsylvania.
- Archuleta, R. J., Bonilla, L. F., and Lavallée, D. (2000). "Nonlinearity in Observed and Computed Accelerograms." *Proceedings: 12th World Conference in Earthquake Engineering*, Auckland, New Zealand.
- American Society of Civil Engineers (ASCE). (1998). "Seismic Analysis of Safety-Related Nuclear Structures and Commentary." *ASCE 4-98*, American Society of Civil Engineers, Reston, Virginia.
- American Society of Civil Engineers (ASCE). (2010). "Minimum Design Loads for Buildings and Other Structures." *ASCE/SEI 7-10*, American Society of Civil Engineers, Reston, Virginia.
- American Society of Civil Engineers (ASCE). (forthcoming). "Seismic Analysis of Safety-Related Nuclear Structures and Commentary." *ASCE 4-**, American Society of Civil Engineers, Reston, Virginia.
- Assimaki, D., Kausel, E., and Whittle, A. (2000). "Model for Dynamic Shear Modulus and Damping for Granular Soils." *ASCE Journal for Geotechnical and Geoenvironmental Engineering*, 126, 859-869.
- Assimaki, D., and Gazetas, G. (2004). "Soil and Topographic Amplification on Canyon Banks and the 1999 Athens Earthquake." *Journal of Earthquake Engineering*, 8(1), 1-43.
- Baig, I., and Bolourchi, S. (2013). *Personal Communication*
- Baker, J. W. (2007). "Quantitative Classification of Near-Fault Ground Motions Using Wavelet Analysis." *Bulletin of the Seismological Society of America*, 97(5), 1486-1501.

- Basu, U. (2009). "Explicit Finite Element Perfectly Matched Layer for Transient Three-Dimensional Elastic Waves." *International Journal for Numerical Methods in Engineering*, 77, 151-176.
- Basu, U. (2014). *Personal Communication*
- Bathe, K.-J. (1996). "Finite Element Procedures." Prentice Hall, Upper Saddle River, New Jersey.
- Bielak, J. (1975). "Dynamic Behaviour of Structures with Embedded Foundations." *Earthquake Engineering & Structural Dynamics*, 3, 259-274.
- Bielak, J., and Christiano, P. (1984). "On the Effective Seismic Input for Nonlinear Soil-Structure Interaction Systems." *Earthquake Engineering & Structural Dynamics*, 12(1), 107-119.
- Bielak, J., Loukakis, K., Hisada, Y., and Yoshimura, C. (2003). "Domain Reduction Method for Three-Dimensional Earthquake Modeling in Localized Regions, Part-I: Theory." *Bulletin of the Seismological Society of America*, 93(2), 817-824.
- Bielak, J. (2013). *Personal Communication*
- Bolisetti, C. (2010). "Numerical and Physical Simulations of Soil-Structure Interaction." M.S. Thesis, University at Buffalo, The State University of New York, Buffalo, New York.
- Bolisetti, C., and Whittaker, A. S. (2011). "Seismic Structure-Soil-Structure Interaction in Nuclear Power Plant Structures." *21st International Conference in Structural Mechanics in Reactor Technology (SMiRT-21)*, New Delhi, India.
- Boore, D. M. (1972). "A Note on the Effect of Simple Topography on Seismic SH Waves." *Bulletin of the Seismological Society of America*, 62(1), 275-284.
- Borja, R., and Amies, A. (1994). "Multiaxial Cyclic Plasticity Model for Clays." *Journal of Geotechnical Engineering*, 120(6), 1051-1070.
- Borja, R. I., Chao, H. Y., Montáns, F. J., and Lin, C. H. (1999). "Nonlinear Ground Response at Lotung LSST Site." *Journal of Geotechnical and Geoenvironmental Engineering*, 125(3), 187-197.
- Bray, J. (2011). *Personal Communication*
- Çelebi, M. (1993a). "Seismic Responses of Two Adjacent Buildings. I: Data and Analyses." *Journal of Structural Engineering*, 119(8), 2461-2476.
- Çelebi, M. (1993b). "Seismic Responses of Two Adjacent Buildings. II: Interaction." *Journal of Structural Engineering*, 119(8), 2477-2492.

- Chang, C.-Y., Mok, C. M., Power, M. S., Tang, Y. K., Tang, H. T., and Stepp, J. C. (1990). "Equivalent Linear and Nonlinear Ground Response Analyses at Lotung Seismic Experiment Site." *Proceedings: Fourth U.S. National Conference on Earthquake Engineering* Earthquake Engineering Research Institute, Palm Springs, California.
- Chang, C.-Y., Mok, C. M., and Power, M. S. (1991). "Analysis of Ground Response Data at Lotung Large-Scale Soil-Structure Interaction Experiment Site." Report NP-7306-M, Electric Power Research Institute, Palo Alto, California.
- Chang, S. W. (1996). "Seismic Response of Deep Stiff Soil Deposits." Ph.D. Dissertation, University of California, Berkeley, California.
- Chen, A. T. F., and Joyner, W. B. (1974). "Multi-linear Analysis for Ground Motion Studies of Layered Systems." Report USGS-GD-74-020, United States Department of the Interior Geological Survey, Menlo Park, California.
- Chen, Z., Hutchinson, T. C., Trombetta, N. W., Mason, H. B., Bray, J. D., Jones, K. C., Bolisetti, C., Whittaker, A. S., Choy, B. Y., Kutter, B. L., Feigel, G. L., Montgomery, J., Patel, R. J., and Reitherman, R. D. (2010). "Seismic Performance Assessment in Dense Urban Areas: Evaluation of Nonlinear Building-Foundation Systems using Centrifuge Tests." *Proceedings: Fifth International Conference on Recent Advances in Geotechnical Earthquake Engineering and Soil Dynamics*, May 24-29, 2010, San Diego, California.
- Chen, Z., Trombetta, N. W., Hutchinson, T. C., Mason, H. B., Bray, J. D., and Kutter, B. L. (2013). "Seismic System Identification Using Centrifuge-Based Soil-Structure Interaction Test Data." *Journal of Earthquake Engineering*, 17(4), 469-496.
- Chopra, A. K. (1995). "Dynamics of Structures." Prentice Hall.
- Computers and Structures Inc. (2011). Computer Program SAP2000 - Structural Analysis Program, Version 11.0.0, Computers and Structures, Inc., Berkeley, California.
- Constantopoulos, I. V., Roesset, J. M., and Christian, J. T. (1974). "A Comparison of Linear and Exact Nonlinear Analyses of Soil Amplification." *Proceedings: The Fifth World Conference in Earthquake Engineering*, Rome.
- Coronado, C., Anderson, L. M., and Ostadan, F. (2013). "Verification of SASSI Extended Subtraction Method for Computing the Seismic Response of Deeply Embedded Structures." *22nd International Conference in Structural Mechanics in Reactor Technology - SMiRT 22*, August 2013, San Francisco, California.

- Craig, R. F. (1997). "Soil Mechanics." E & FN Spon, New York.
- Dassault Systèmes (2005). Computer Program ABAQUS - Finite Element Analysis Software, Dassault Systèmes, Providence, Rhode Island.
- Day, S. M., Bielak, J., Dreger, D., Graves, R., Larsen, S., Olsen, K. B., Pitarka, A., and Guzman, L. R. (2006). "Numerical Simulation of Basin Effects on Long Period Ground Motion." *Proceedings: Proceedings of the 8th U.S. National Conference on Earthquake Engineering*, San Francisco, California.
- Dickenson, S. E. (1994). "Dynamic Response of Soft and Deep Cohesive Soils During the Loma Prieta Earthquake of October 17, 1989." Ph.D. Dissertation, University of California, Berkeley, California.
- Elgamal, A., Yang, Z., and Parra, E. (2002). "Computational Modeling of Cyclic Mobility and Post-Liquefaction Site Response." *Soil Dynamics and Earthquake Engineering*, 22, 259-271.
- Elgamal, A., Yang, Z., Lai, T., Kutter, B. L., and Wilson, D. W. (2005). "Dynamic Response of Saturated Dense Sand in Laminated Centrifuge Container." *Journal of Geotechnical and Geoenvironmental Engineering*, 131(5), 598-609.
- Elsabee, F., Kausel, E., and Roesset, J. M. (1977). "Dynamic Stiffness of Embedded Foundations." *Proceedings: Second Annual Engineering Mechanics Division Specialty Conference*, ASCE, North Carolina State University, Raleigh, North Carolina, 40-43.
- Federal Emergency Management Agency (FEMA). (1997). "NEHRP Commentary on the Guidelines for Seismic Rehabilitation of Buildings." *FEMA 274*, Federal Emergency Management Agency, Washington, District of Columbia.
- Federal Emergency Management Agency (FEMA). (2005). "Improvement of Nonlinear Static Seismic Analysis Procedures." *FEMA 440*, Federal Emergency Management Agency, Washington, District of Columbia.
- Federal Emergency Management Agency (FEMA). (2012). "Seismic Performance Assessment of Buildings." *FEMA P-58*, Federal Emergency Management Agency, Washington, District of Columbia.
- Finn, W. D. L., and Martin, G. R. (1978). "Comparison of Dynamic Analyses for Saturated Sand." *Proceedings: Earthquake Engineering and Soil Dynamics: Proceedings of the ASCE Geotechnical Engineering Division Specialty Conference*, Pasadena, California, 472-491.
- Ganuza, E. A. B. (2006). "Seismic Behavior of Hybrid Lateral-Force-Resisting Systems." M.S. Dissertation, University at Buffalo, The State University of New York, Buffalo, New York.

- Gazetas, G. (1991). "Foundation Vibrations." *Foundation Engineering Handbook*, Ed. H. Fang, Kluwer Academic Publishers, Norwell, Massachusetts.
- Hadjian, A. H. (1981). "On the Correlation of the Components of Strong Ground Motion - Part 2." *Bulletin of the Seismological Society of America*, 71(4), 1323-1331.
- Hardin, B. O., and Drnevich, V. P. (1972). "Shear Modulus and Damping in Soils: Measurement and Parameter Effects." *Journal of the Soil Mechanics and Foundations Division, ASCE*, 98(8), 473-496.
- Hashash, Y. M. A., and Park, D. (2001). "Nonlinear One-Dimensional Seismic Ground Motion Propagation in the Mississippi Embayment." *Engineering Geology*, 62, 185-206.
- Hashash, Y. M. A., Phillips, C., and Groholski, D. R. (2010). "Recent Advances in Nonlinear Site Response Analysis." *Fifth International Conference on Recent Advances in Geotechnical Earthquake Engineering and Soil Dynamics*, May 24-29, San Diego, California.
- Hashash, Y. M. A., Groholski, D. R., Phillips, C. A., Park, D., and Musgrove, M. (2011). "DEEPSOIL 5.0 User Manual and Tutorial." 107 p.
- Huang, Y.-N., Whittaker, A. S., Kennedy, R. P., and Mayes, R. L. (2009). "Assessment of Base-Isolated Nuclear Structures for Design and Beyond-Design Basis Earthquake Shaking." Multidisciplinary Center for Earthquake Engineering (MCEER), Buffalo, New York.
- Huang, Y. (2013). *Personal Communication*
- Iai, S., Morita, T., Kameoka, T., Matsunaga, Y., and Abiko, K. (1995). "Response of a Dense Sand Deposit During 1993 Kushiro-Oki Earthquake." *Soils and Foundations, Japanese Society of Soil Mechanics and Foundation Engineering*, 35(1), 115-131.
- Idriss, I. M., and Seed, H. B. (1967a). "Response of Horizontal Soil Layers During Earthquakes." Soil Mechanics and Bituminous Materials Research Laboratory, University of California, Berkeley, Berkeley, California.
- Idriss, I. M., and Seed, H. B. (1967b). "Response of Earth Banks During Earthquakes." *Journal of the Soil Mechanics and Foundations Division, ASCE*, 93(SM3), 61-82.
- Idriss, I. M., and Seed, H. B. (1968a). "An Analysis of Ground Motions During the 1957 San Francisco Earthquake." *Bulletin of the Seismological Society of America*, 58(6), 2013-2032.
- Idriss, I. M., and Seed, H. B. (1968b). "Seismic Response of Horizontal Soil Layers." *Proceedings of ASCE, Journal of Soil Mechanics and Foundations Division*, 94, 1003-1031.

- Idriss, I. M. (1990). "Response of Soft Soil Sites During Earthquakes." *Proceedings: Proceedings Memorial Symposium to Honor Professor Harry Bolton Seed*, Berkeley, California.
- Idriss, I. M., and Sun, J. I. (1992). "User's Manual for SHAKE91: A Computer Program for Conducting Equivalent Linear Seismic Response Analyses of Horizontally Layered Soil Deposits."
- Ilankatharan, M. (2008). "Centrifuge Modeling for Soil-Pile-Bridge Systems with Numerical Simulations Accounting for Soil-Container-Shaker Interaction." Ph.D. Dissertation, University of California, Davis, California.
- Ilankatharan, M., and Kutter, B. (2010). "Modeling Input Motion Boundary Conditions for Simulations of Geotechnical Shaking Table Tests." *Earthquake Spectra*, 26(2), 349-369.
- Itasca Consulting Group (2005). Computer Program FLAC: Advanced, Two Dimensional Continuum Modeling for Geotechnical Analysis of Rock, Soil, and Structural Support, Itasca Consulting Group, Inc., Minneapolis, Minnesota.
- Iwan, W. D. (1967). "On a Class of Models for the Yielding Behavior of Continuous and Composite Systems." *Journal of Applied Mechanics*, 34, 612-617.
- Jennings, P. C., and Bielak, J. (1973). "Dynamics of Building-Soil Interaction." *Bulletin of the Seismological Society of America*, 63(1), 9-48.
- Jeremic, B., Kammerer, A., Tafazzoli, N., and Kamrani, B. (2011). "The NRC ESSI Simulator." *21st International Conference in Structural Mechanics and Reactor Technology: SMiRT 21*, New Delhi, India.
- Jeremic, B., Jie, G., Preisig, M., and Tafazzoli, N. (2013). "The NRC ESSI Simulator Notes." *Technical Report*, University of California at Davis, and Lawrence Berkeley National Laboratory, Davis, California.
- Jeremić, B., Jie, G., Preisig, M., and Tafazzoli, N. (2009). "Time Domain Simulation of Soil-Foundation-Structure Interaction in Non-Uniform Soils." *Earthquake Engineering & Structural Dynamics*, 38(5), 699-718.
- Jones, K. C. (2013). "Dynamic Soil-Structure Interaction Analysis of Structures in Dense Urban Environments." Ph.D. Dissertation, University of California, Berkeley, California.
- Joyner, W. B. (1975). "A Method for Calculating Nonlinear Seismic Response in Two Dimensions." *Bulletin of the Seismological Society of America*, 65(5), 1337-1357.
- Joyner, W. B., and Chen, A. T. F. (1975). "Calculation of Nonlinear Ground Response in Earthquakes." *Bulletin of the Seismological Society of America*, 65(5), 1315-1336.

- Kanai, K. (1952). "Relation between the Nature of Surface Layer and the Amplitudes of Earthquake Motions." *Bulletin of Earthquake Research Institute*, 30, 31-37.
- Kausel, E., and Roesset, J. M. (1975). "Dynamic Stiffness of Circular Foundations." *Journal of the Engineering Mechanics Division*, 101, EM6, 771-748.
- Kausel, E. (2010). "Early History of Soil-Structure Interaction." *Soil Dynamics and Earthquake Engineering*, 30, 822-832.
- Kramer, S. L. (1996). "Geotechnical Earthquake Engineering." Prentice Hall, Upper Saddle River, New Jersey.
- Kramer, S. L., and Stewart, J. P. (2004). "Geotechnical Aspects of Seismic Hazards." *Earthquake Engineering From Engineering Seismology to Performance-Based Engineering*, eds. Y. Bozorgnia, and V. V. Bertero, CRC Press.
- Kulhawy, F. H., and Mayne, P. W. (1990). "Manual on Estimating the Soil Properties for Foundation Design." Report EL-6800, Electric Power Research Institute, Palo Alto, California.
- Kutter, B. L. (1995). "Recent Advances in Centrifuge Modeling of Seismic Shaking." *Proceedings: Third International Conference on Recent Advances in Geotechnical Earthquake Engineering and Soil Dynamics*, April 2-7, St. Louis, Missouri.
- Kwok, A. O. L., Stewart, J. P., and Hashash, Y. M. A. (2008). "Nonlinear Ground-Response Analysis of Turkey Flat Shallow Stiff-Soil Site to Strong Ground Motion." *Bulletin of the Seismological Society of America*, 98(1), 331-343.
- Kwok, O. L. (2007). "Application of One-Dimensional Geotechnical Modeling for Site Response Predictions." Ph.D. Dissertation, University of California, Los Angeles, California.
- Lee, M. K. W., and Finn, W. (1978). "DESRA-2: Dynamic Effective Stress Response Analysis of Soil Deposits with Energy Transmitting Boundary Including Assessment of Liquefaction Potential." The University of British Columbia, Faculty of Applied Science, Vancouver, British Columbia.
- Li, X. S., Z., W., and Shen, C. K. (1992). "SUMDES: A Nonlinear Procedure for Response Analysis of Horizontally-Layered Sites Subjected to Multi-Directional Earthquake Loading, Manual." Department of Civil Engineering, University of California, Davis, California.
- Lin, H., -T., Roesset, J. M., and Tassoulas, J. L. (1987). "Dynamic Interaction Between Adjacent Foundations." *Earthquake Engineering and Structural Dynamics*, 15, 323-343.

- Livermore Software Technology Corporation (LSTC). (2013). "LS-DYNA Keyword User's Manual - Version R 7.0." Livermore Software Technology Corporation, Livermore, California.
- Luco, J. E., and Westman, R. A. (1971). "Dynamic Response of Circular Footings." *Journal of the Engineering Mechanics Division*, 97, EM5, 1381-1395.
- Luco, J. E., and Contesse, L. (1973). "Dynamic Structure-Soil-Structure Interaction." *Bulletin of the Seismological Society of America*, 63(4), 1289-1303.
- Lysmer, J., and Kuhlemeyer, R. L. (1969). "Finite Dynamic Model for Infinite Media." *Journal of Engineering Mechanics Division, ASCE*, 95, EM4, 859-877.
- Lysmer, J. (1978). "Analytical Procedures in Soil Dynamics." Report UCB/EERC-78/29, Earthquake Engineering Research Center, University of California, Berkeley, California.
- Lysmer, J., Ostadan, F., and Chin, C. (1999). Computer Program SASSI2000 - A System for Analysis of Soil-Structure Interaction, University of California, Berkeley, California.
- Masing, G. (1926). "Eigenspannungen und Verfestigung beim Messing." *Proceedings: 2nd International Congress on Applied Mechanics*, Zurich, Switzerland, 332-335.
- Mason, H. B., Trombetta, N. W., Gille, S., Lund, J., Zupan, J., Jones, K. C., Puangnak, H., Bolisetti, C., Bray, J., Hutchinson, T., Fiegel, G., Kutter, B. L., and Whittaker, A. S. (2010a). "Seismic Performance Assessment in Dense Urban Environments: Centrifuge Data Report for HBM02 (Test 1)." University of California at Davis Center for Geotechnical Modeling, Davis, California.
- Mason, H. B., Trombetta, N. W., Gille, S., Lund, J., Zupan, J., Jones, K. C., Puangnak, H., Bolisetti, C., Bray, J., Hutchinson, T., Fiegel, G., Kutter, B. L., and Whittaker, A. S. (2010b). "Seismic Performance Assessment in Dense Urban Environments: Centrifuge Data Report for HBM03 (Test 2)." University of California at Davis Center for Geotechnical Modeling, Davis, California.
- Mason, H. B., Trombetta, N. W., Gille, S., Lund, J., Zupan, J., Jones, K. C., Puangnak, H., Bolisetti, C., Bray, J., Hutchinson, T., Fiegel, G., Kutter, B. L., and Whittaker, A. S. (2010c). "Seismic Performance Assessment in Dense Urban Environments: Centrifuge data report for HBM04 (Test 3)." Report in preparation, University of California at Davis Center for Geotechnical Modeling, Davis, California.
- Mason, H. B. (2011). "Seismic Performance Assessment in Dense Urban Environments." Ph.D. Dissertation, University of California, Berkeley, California.
- Mason, H. B., Trombetta, N. W., Gille, S., Lund, J., Zupan, J., Jones, K. C., Puangnak, H., Bolisetti, C., Bray, J., Hutchinson, T., Fiegel, G., Kutter, B. L., and Whittaker, A. S. (2011). "Seismic Performance

Assessment in Dense Urban Environments: Centrifuge Data Report for HBM04 (Test 3)." Report No. UCD/CGMDR-03/11, University of California at Davis Center for Geotechnical Modeling, Davis, California.

Mason, H. B., Trombetta, N. W., Chen, Z., Bray, J. D., Hutchinson, T. C., and Kutter, B. L. (2013). "Seismic Soil–Foundation–Structure Interaction Observed in Geotechnical Centrifuge Experiments." *Soil Dynamics and Earthquake Engineering*, 48, 162-174.

Mason, H. B. (2014). *Personal Communication*

Matasovic, N. (1993). "Seismic Response of Composite Horizontally-Layered Soil Deposits." Ph. D. Dissertation, University of California, Los Angeles, California.

Matasovic, N. (2006). "D-MOD_2: A Computer Program for Seismic Response Analysis of Horizontally Layered Soil Deposits, Earthfill Dams and Solid Waste Landfills." Geomotions, LLC, Lacey, WA.

Mathees, W., and Magiera, G. (1982). "A Sensitivity Study of Seismic Structure-Soil-Structure Interaction Problems for Nuclear Power Plants." *Nuclear Engineering and Design*, 73, 343-363.

Mazzoni, S., McKenna, F., Scott, M. H., and Fenves, G. L. (2009). Computer Program OpenSees: Open System for Earthquake Engineering Simulation, Pacific Earthquake Engineering Research Center (PEER), University of California, Berkeley, California.

McKenna, F., and Fenves, G. L. (2001). "The OpenSees Command Language Manual: Version 1.2." Pacific Earthquake Engineering Research (PEER) Center, University of California, Berkeley, California.

Menglin, L., Huaifeng, W., Xi, C., and Yongmei, Z. (2011). "Structure-Soil-Structure Interaction: Literature Review." *Soil Dynamics and Earthquake Engineering*, 31, 1724-1731.

Mertz, G., Cuesta, I., Maham, A., and Costantino, M. (2010). "Seismic Response of Embedded Facilities Using the SASSI Subtraction Method." Los Alamos National Laboratory, Los Alamos, New Mexico.

Murakami, H., and Luco, J. E. (1977). "Seismic Response of a Periodic Array of Structures." *Journal of the Engineering Mechanics Division, ASCE SM5*, 103, 965-976.

Muravskii, G. (2005). "On Description of Hysteretic Behaviour of Materials." *International Journal of Solids and Structures*, 42(9–10), 2625-2644.

Mylonakis, G., and Gazetas, G. (2000). "Seismic Soil-Structure Interaction: Beneficial or Detrimental?." *Journal of Earthquake Engineering*, 4(3), 277-301.

National Institute of Standards and Technology (NIST). (2012). "Soil-Structure Interaction for Building Structures." *NIST GCR 12-917-21*, National Institute of Standards and Technology, Gaithersburg, Maryland.

Oberkampf, W. L., and Trucano, T. G. (2008). "Verification and Validation Benchmarks." *Nuclear Engineering and Design*, 238(3), 716-743.

Ostadan, F. (2006a). "SASSI2000: A System for Analysis of Soil Structure Interaction - Theoretical Manual." University of California, Berkeley, California.

Ostadan, F. (2006b). "SASSI2000: A System for Analysis of Soil Structure Interaction - User's Manual." University of California, Berkeley, California.

Ostadan, F. (2010). *Personal Communication*

Ostadan, F., and Deng, N. (2011). Computer Program SASSI2010 - A System for Analysis of Soil-Structure Interaction, Version 1.1, Geotechnical and Hydraulic Engineering Services, Bechtel National Inc., San Francisco, California.

Padron, L. A., Aznarez, J. J., and Maeso, O. (2009). "Dynamic Structure-Soil-Structure Interaction between Nearby Piled Buildings under Seismic Excitation by BEM-FEM Model." *Soil Dynamics and Earthquake Engineering*, 29, 1084-1096.

PEER (2011). "PEER Ground Motion Database." <http://peer.berkeley.edu/peer_ground_motion_database>. (25th November, 2012).

Phillips, C., and Hashash, Y. M. A. (2009). "Damping Formulation for Nonlinear 1D Site Response Analyses." *Soil Dynamics & Earthquake Engineering*, 29, 1143-1158.

Porcella, R. L. (1980). "Atypical Accelerograms Recorded During Recent Earthquakes." *Geological Survey Circular*, Report 854-B, United States Department of the Interior, Menlo Park, California, 1-7.

Pyke, R. M. (2000). "TESS Users' Manual." TAGA Engineering Software Services, Lafayette, California.

Qian, J., and Beskos, D. E. (1996). "Harmonic Wave Response of Two 3-D Rigid Surface Foundations." *Soil Dynamics and Earthquake Engineering*, 15, 95-110.

Ramberg, W., and Osgood, W. (1943). "Description of Stress-Strain Curves by Three Parameters." *Technical Note No. 902*, National Advisory Committee of Aeronautics, Washington, District of Columbia.

Restrepo, D., Taborda, R., and Bielak, J. (2011). "Effects of Soil Nonlinearity on Ground Response in 3D Simulations - An Application to the Salt Lake City Basin." *Proceedings: 4th IASPEI / IAEE International Symposium*, University of California, Santa Barbara.

Roesset, J. M. (1998). "Seismic Design of Nuclear Power Plants - Where Are We Now?" *Nuclear Engineering and Design*, 182, 3-15.

Ryan, H. (1994). "Ricker, Ormsby, Klander, Butterworth - A Choice of Wavelets." *Canadian Society of Exploration Geophysicists Recorder*, 19(7), 8-9.

Schnabel, P. B., Lysmer, J., and Seed, H. B. (1972). "SHAKE: A Computer Program for Earthquake Ground Response Analysis for Horizontally Layered Sites." Earthquake Engineering Research Center, University of California, Berkeley, California.

Schnabel, P. B., Lysmer, J., and Seed, H. B. (2009). Computer Program SHAKE2000: A Computer Program for the 1D Analysis of Geotechnical Earthquake Engineering Problems, University of California, Berkeley, California.

Schnabel, P. B., Lysmer, J., and Seed, H. B. (2012). Computer Program SHAKE: A Computer Program for Earthquake Response Analysis of Horizontally Layered Sites, University of California, Berkeley, California.

Seed, H. B., and Idriss, I. M. (1969). "Influence of Soil Conditions on Ground Motions during Earthquakes." *Proceedings of the ASCE, Journal of the Soil Mechanics and Foundations Division*, SM1, 99-137.

Seed, H. B., and Idriss, M. (1970). "Soil Moduli and Damping Factors for Dynamic Response Analysis." Report UCB/EERC 70/10, Earthquake Engineering Research Center, University of California, Berkeley, California.

Somerville, P. G., Smith, R. W., Graves, R. W., and Abrahamson, N. A. (1997). "Modification of Empirical Strong Ground Motion Attenuation Relations to Include the Amplitude and Duration Effects of Rupture Directivity." *Seismological Research Letters*, 68, 199-222.

Stewart, J. P., Fenves, G. L., and Seed, R. B. (1999a). "Seismic Soil-Structure Interaction in Buildings. I: Analytical Aspects." *Journal of Geotechnical and Geoenvironmental Engineering*, 125, GEOBASE, 26-37.

Stewart, J. P., Seed, R. B., and Fenves, G. L. (1999b). "Seismic Soil-Structure Interaction in Buildings. II: Empirical Findings." *Journal of Geotechnical and Geoenvironmental Engineering*, 125, GEOBASE, 38-48.

- Stewart, J. P., and Kwok, A. O. L. (2008). "Nonlinear Seismic Ground Response Analysis: Code Usage Protocols and Verification Against Vertical Array Data." *Proceedings: Geotechnical Engineering and Soil Dynamics IV*, 18-22 May, Sacramento, California.
- Taborda, R. (2010). "Three Dimensional Nonlinear Soil and Site-City Effects in Urban Regions." Ph.D. Dissertation, Carnegie Mellon University.
- Taborda, R., and Bielak, J. (2011). "Large-Scale Earthquake Simulation: Computational Seismology and Complex Engineering Systems." *Computing in Science and Engineering*, 13(4), 14-27.
- Trombetta, N. W., Zupan, J., Bolisetti, C., Puangnak, H., Jones, K. C., Tran, J. K., Bassal, P., Bray, J., Hutchinson, T., Fiegel, G., Kutter, B. L., and Whittaker, A. S. (2011). "Seismic Performance Assessment in Dense Urban Environments: Centrifuge Data Report for NWT01 (Test 4)." Report in preparation, University of California at Davis Center for Geotechnical Modeling, Davis, California.
- Trombetta, N. W. (2013). "Seismic Soil-Foundation Structure Interaction in Urban Environments." Ph.D. Dissertation, University of California, San Diego, California.
- Trombetta, N. W., Mason, H. B., Chen, Z., Hutchinson, T. C., Bray, J. D., and Kutter, B. L. (2013a). "Nonlinear Dynamic Foundation and Frame Structure Response Observed in Geotechnical Centrifuge Experiments." *Soil Dynamics and Earthquake Engineering*, 50, 117-133.
- Trombetta, N. W., Mason, H. B., Hutchinson, T. C., Zupan, J. D., Bray, J. D., and Kutter, B. L. (2013b). "Nonlinear Soil-Foundation-Structure and Structure-Soil-Structure Interaction: Centrifuge Test Observations." *ASCE Journal for Geotechnical and Geoenvironmental Engineering*, In Review.
- Veletsos, A. S., and Wei, Y. T. (1971). "Lateral and Rocking Vibration of Footings." *Journal of the ASCE Soil Mechanics and Foundations Division* 97, SM9, 1227-1248.
- Veletsos, A. S., and Verbic, B. (1973). "Vibration of Viscoelastic Foundations." *Earthquake Engineering and Structural Dynamics*, 2(1), 87-105.
- Veletsos, A. S., and Meek, J. W. (1974). "Dynamic Behavior of Building Foundation Systems." *Earthquake Engineering and Structural Dynamics*, 3(2), 121-138.
- Veletsos, A. S., and Verbic, B. (1974). "Basic Response Functions for Elastic Foundations." *Journal of the ASCE Engineering Mechanics Division*, 100, EM2, 189-205.
- Wolf, J. P. (1985). "Dynamic Soil-Structure Interaction." Prentice Hall, Englewood Cliffs, New Jersey.

- Wong, H. L., and Trifunac, M. D. (1975). "Two-Dimensional, Antiplane, Building-Soil-Building Interaction for Two or More Buildings and for Incident Plane SH Waves." *Bulletin of the Seismological Society of America*, 65(6), 1863-1885.
- Xu, J. (1998). "Three-Dimensional Simulation of Wave Propagation in Inelastic Media on Parallel Computers with Application to Seismic Response." Ph.D. Dissertation, Carnegie Mellon University, Pittsburgh, Pennsylvania.
- Xu, J., Bielak, J., Ghattas, O., and Wang, J. (2003). "Three-Dimensional Nonlinear Seismic Ground Motion Modeling in Basins." *Physics of the Earth and Planetary Interiors*, 137, 81-95.
- Xu, J., Miller, C., Costantino, C., and Hofmayer, C. (2006). "Assessment of Seismic Analysis Methodologies for Deeply Embedded Nuclear Power Plant Structures." U.S. Nuclear Regulatory Commission, Washington, District of Columbia
- Yang, Z., Lu, J., and Elgamal, A. (2004). "A Web-Based Platform for Computer Simulation of Seismic Ground Response." *Advances in Engineering Software*, 35, 249-259.
- Yoshida, N., Kobayashi, S., Suetomi, I., and Muira, K. (2002). "Equivalent Linear Method Considering Frequency Dependent Characteristics of Stiffness and Damping." *Soil Dynamics & Earthquake Engineering*, 22, 205-222.
- Yoshimura, C., Bielak, J., and Hisada, Y. (2003). "Domain Reduction Method for Three-Dimensional Earthquake Modeling in Localized Regions, Part-II: Verification and Examples." *Bulletin of the Seismological Society of America*, 93(2), 825-840.
- Youngs, R. R. (2004). "Software Validation Report for SHAKE04." Geomatrix Consultants, Oakland, California.

APPENDIX A

RESULTS OF SITE-RESPONSE ANALYSES

Results of the site-response analyses performed using SHAKE, DEEPSOIL and LS-DYNA are presented in this appendix. The analysis models and procedures are described in Section 4. Responses are presented in the form of acceleration response spectra, acceleration response histories, stress-strain hysteresis loops of the soil layers, and the peak acceleration and peak strain profiles. The outcrop motion at the base, which is used to calculate the input shear forces for the soil profile, is also included in the acceleration response spectra for comparison. Acceleration amplification spectra from the base to the surface of the soil profile are presented for each ground motion. The acceleration response spectra, response histories and the stress strain loops are calculated at three different depths in the soil profile, at the depths indicated in each figure. Since the acceleration responses are calculated at the interfaces of the soil layers, and stress-strain loops are calculated at the mid-points of the soil layers, the depths at which the corresponding data are presented are slightly different. In the following pages, the results for site E1, site E2, site W1 and site W2 are presented in Figure A-1 to Figure A-13, Figure A-14 to Figure A-26, Figure A-27 to Figure A-52, and Figure A-53 to Figure A-78, respectively. The results for each site begin with the stress-strain loops for all ground motions, followed by the peak acceleration and peak strain profiles, acceleration response spectra, acceleration response histories and the spectral amplifications at the surface.

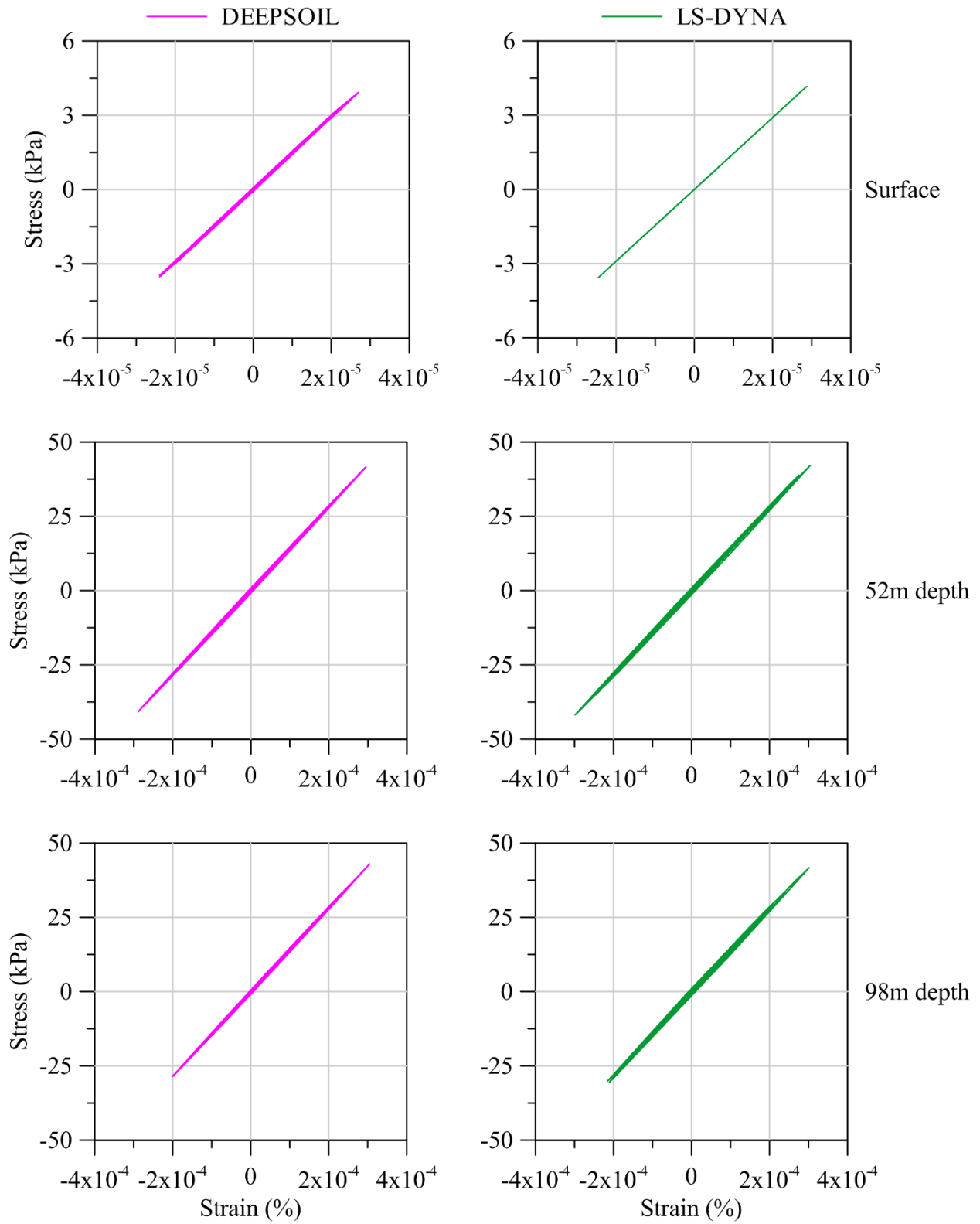


Figure A-1: Stress-strain loops at three different depths for site E1 subjected to ground motion EO1

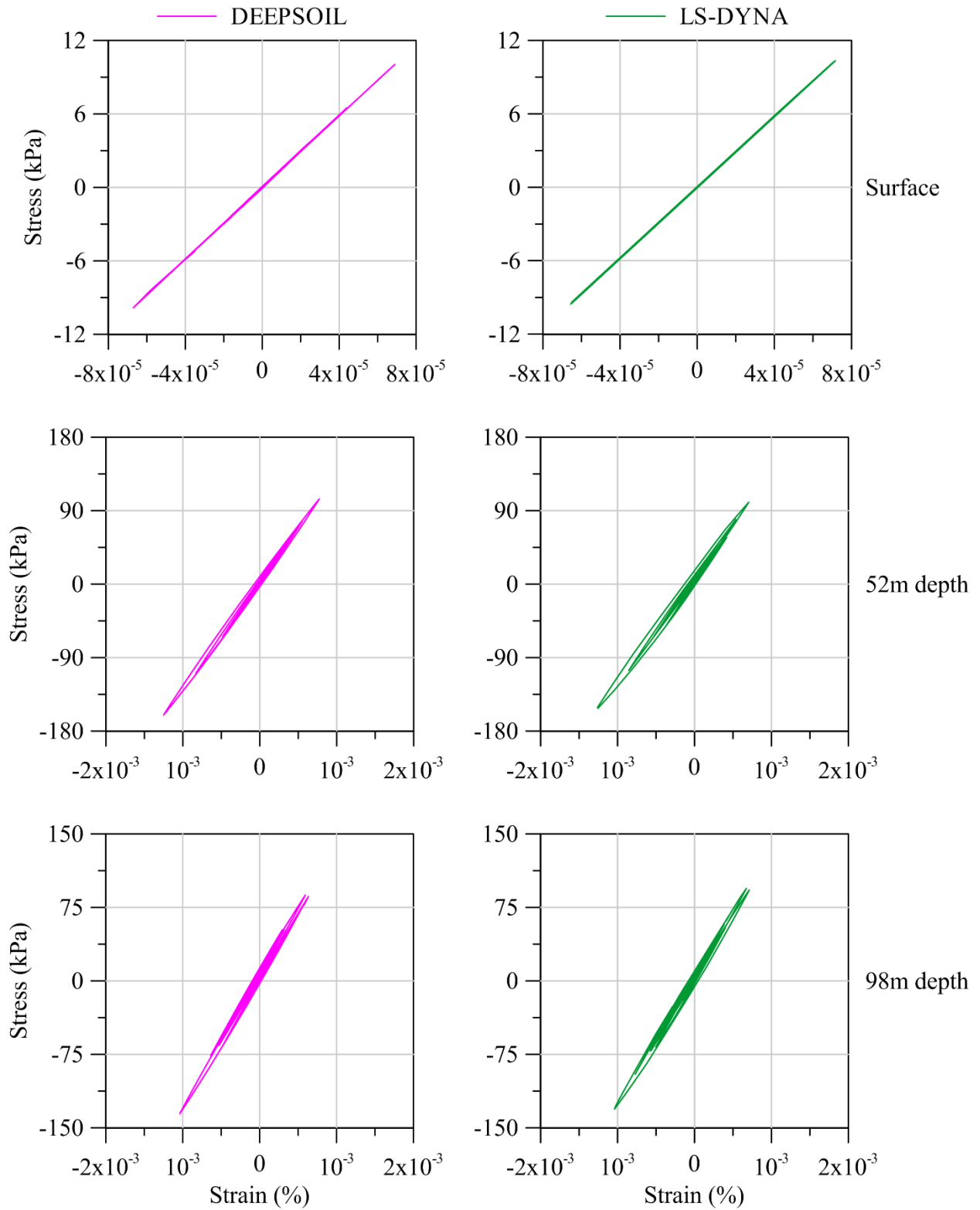


Figure A-2: Stress-strain loops at three different depths for site E1 subjected to ground motion EO2

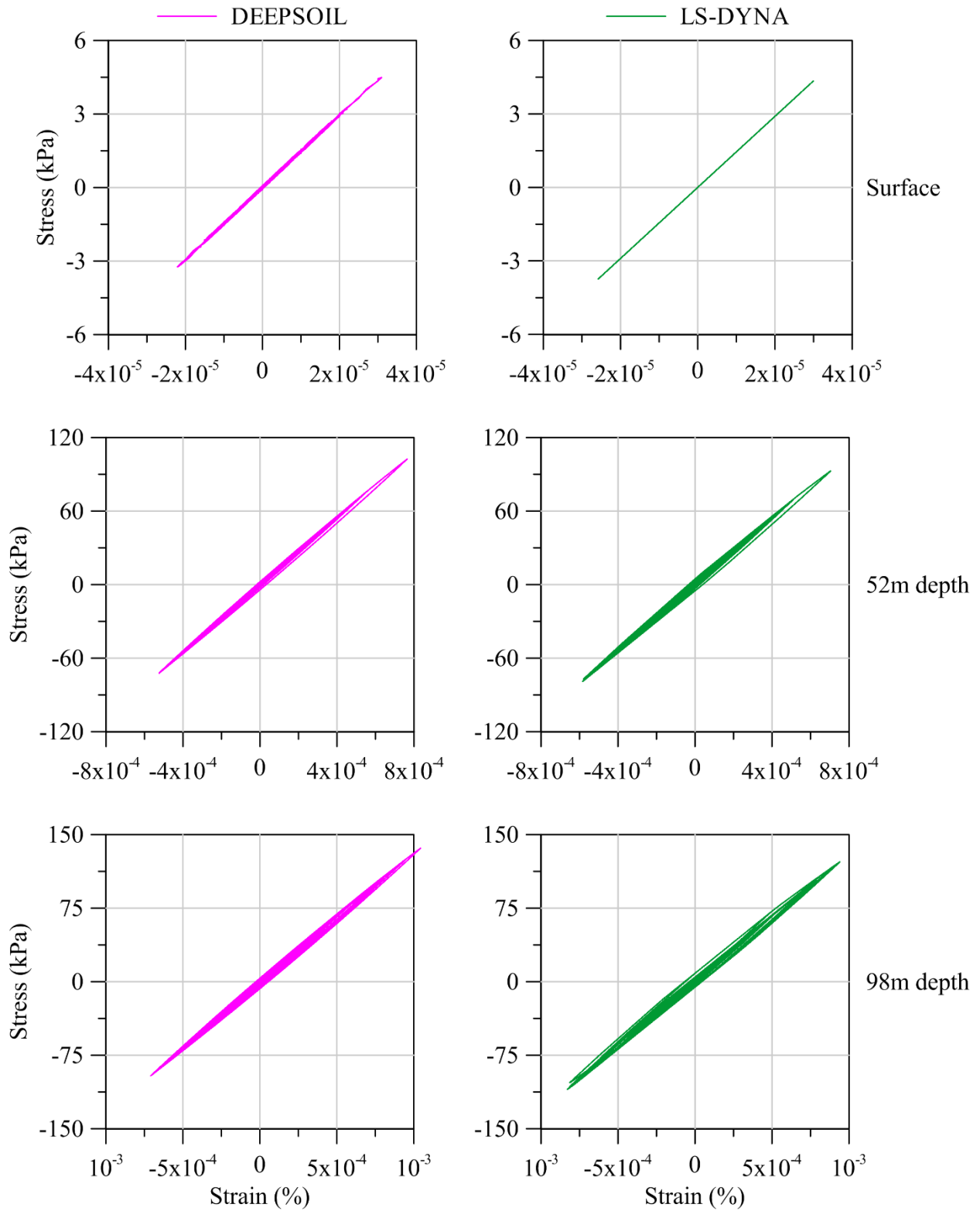


Figure A-3: Stress-strain loops at three different depths for site E1 subjected to ground motion EO3

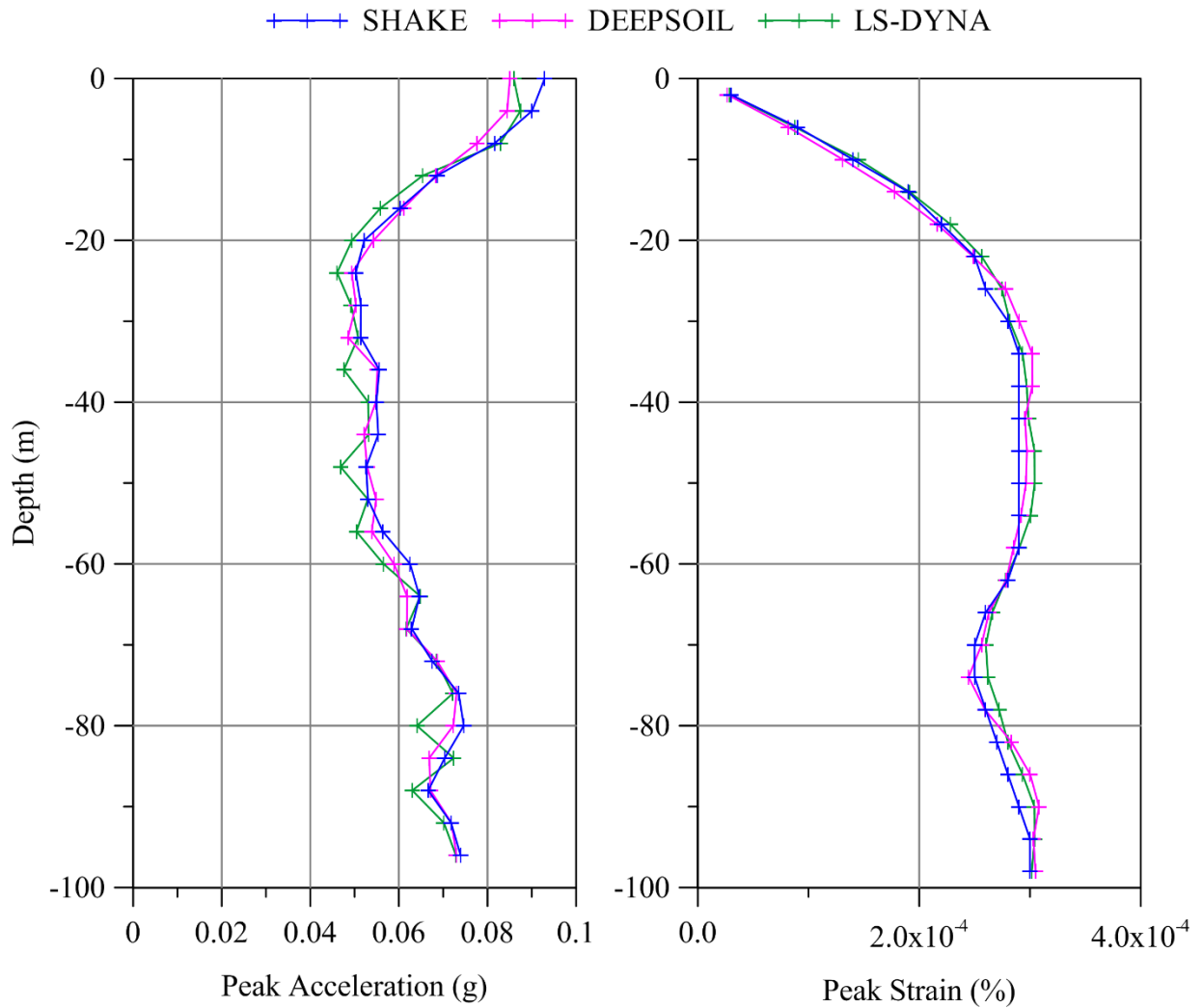


Figure A-4: Peak acceleration and peak strain profiles for site E1 subjected to ground motion EO1

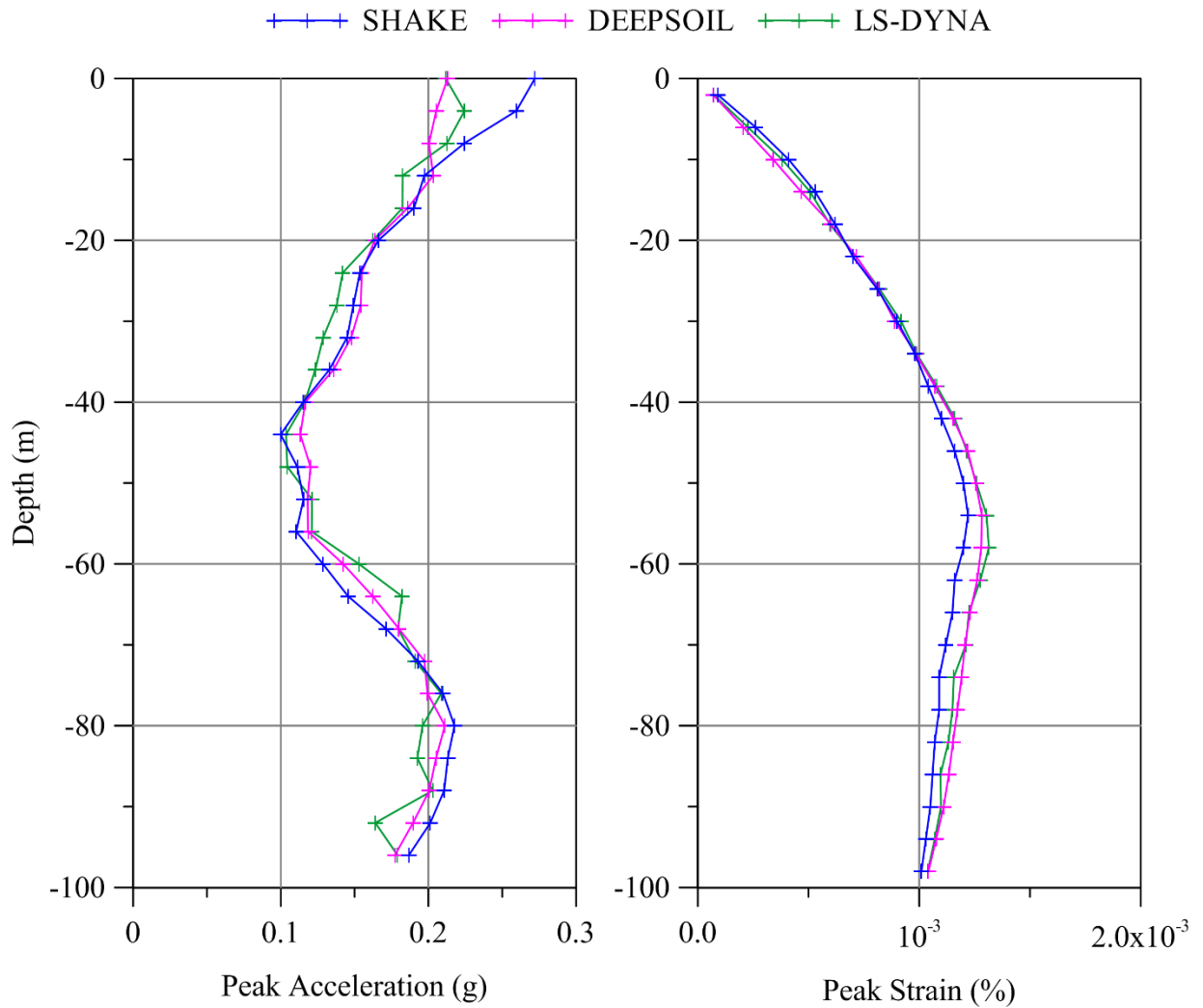


Figure A-5: Peak acceleration and peak strain profiles for site E1 subjected to ground motion EO2

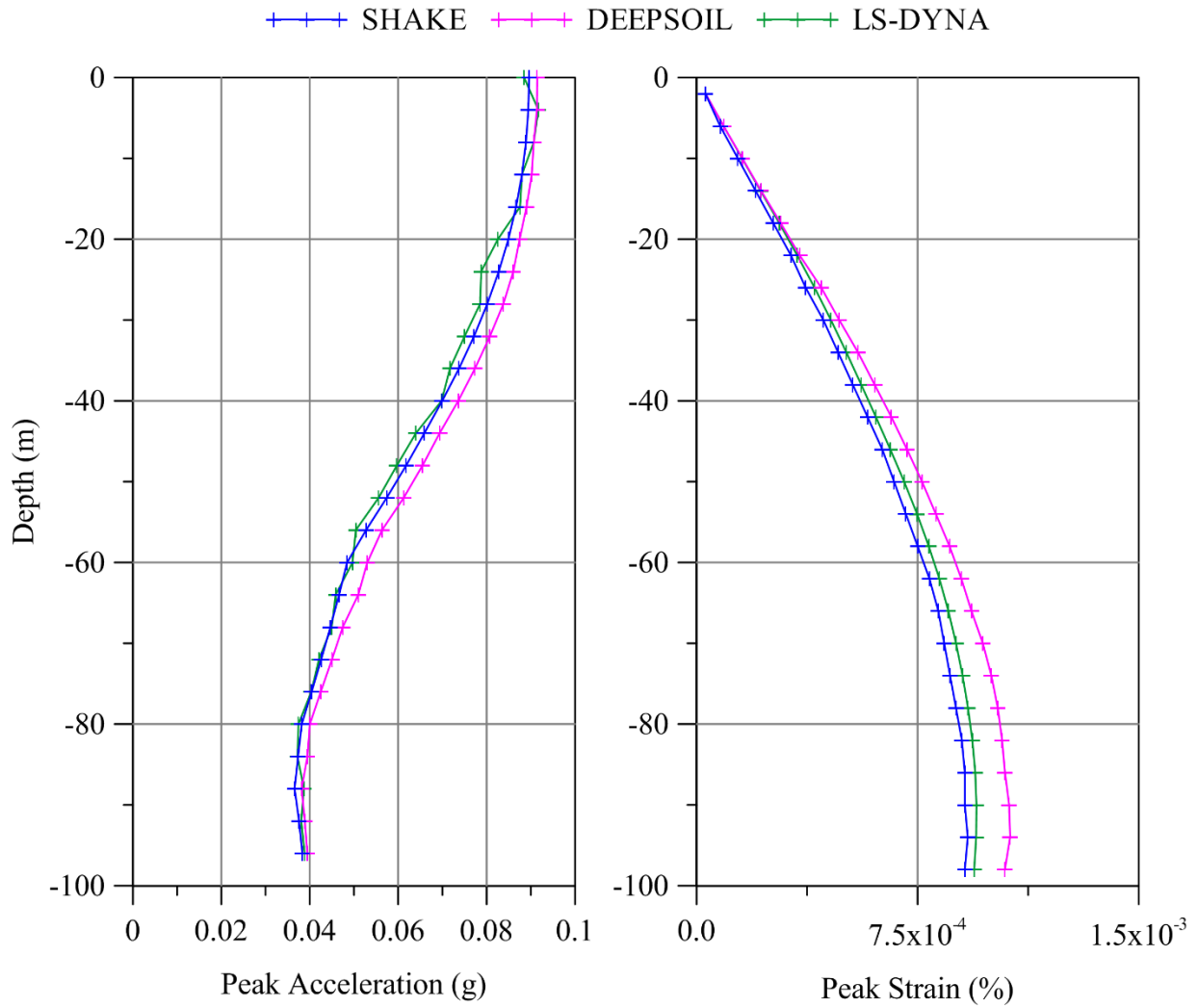


Figure A-6: Peak acceleration and peak strain profiles for site E1 subjected to ground motion EO3

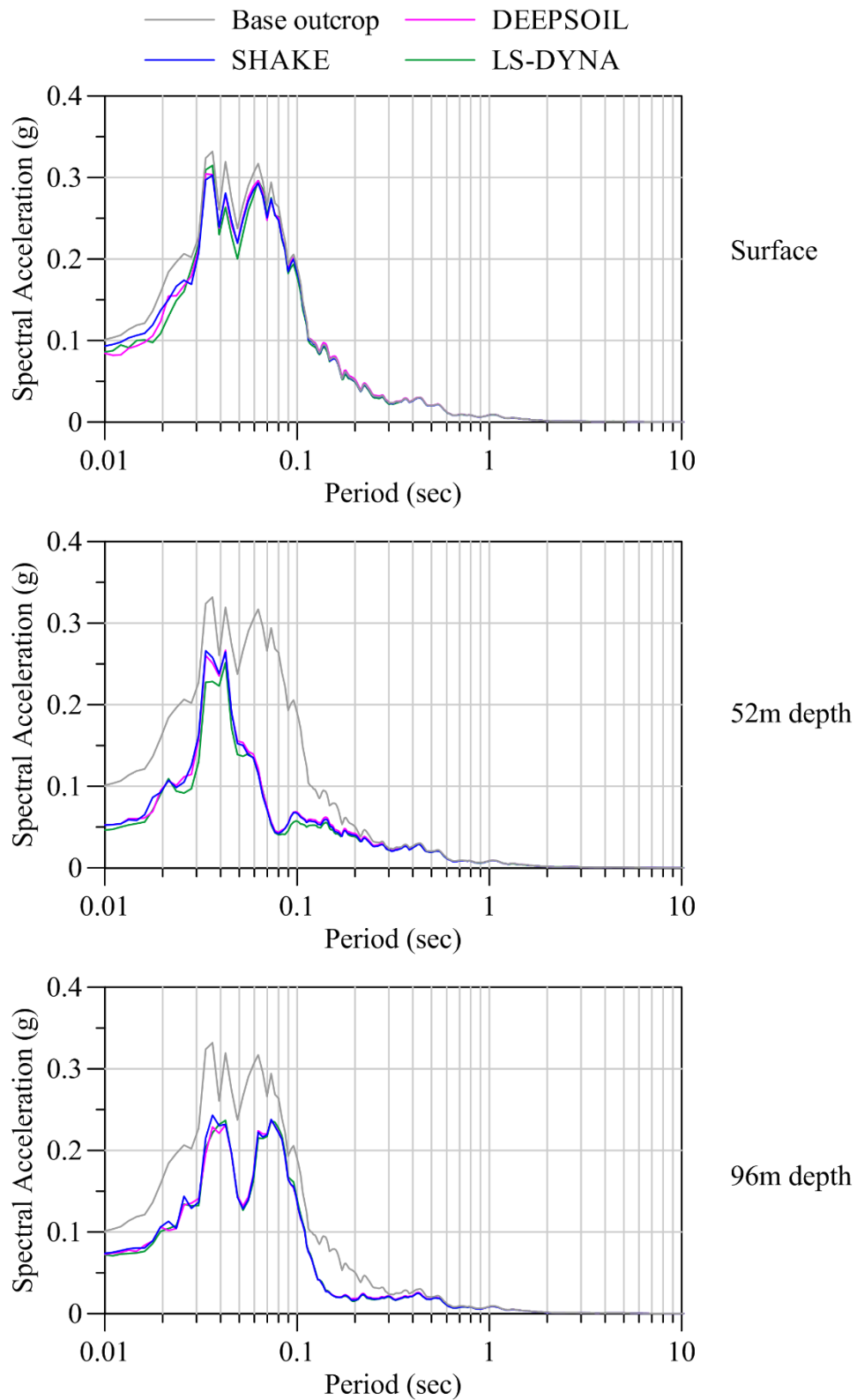


Figure A-7: Acceleration response spectra of the base outcrop motion, and accelerations at three different depths for site E1 subjected to ground motion EO1

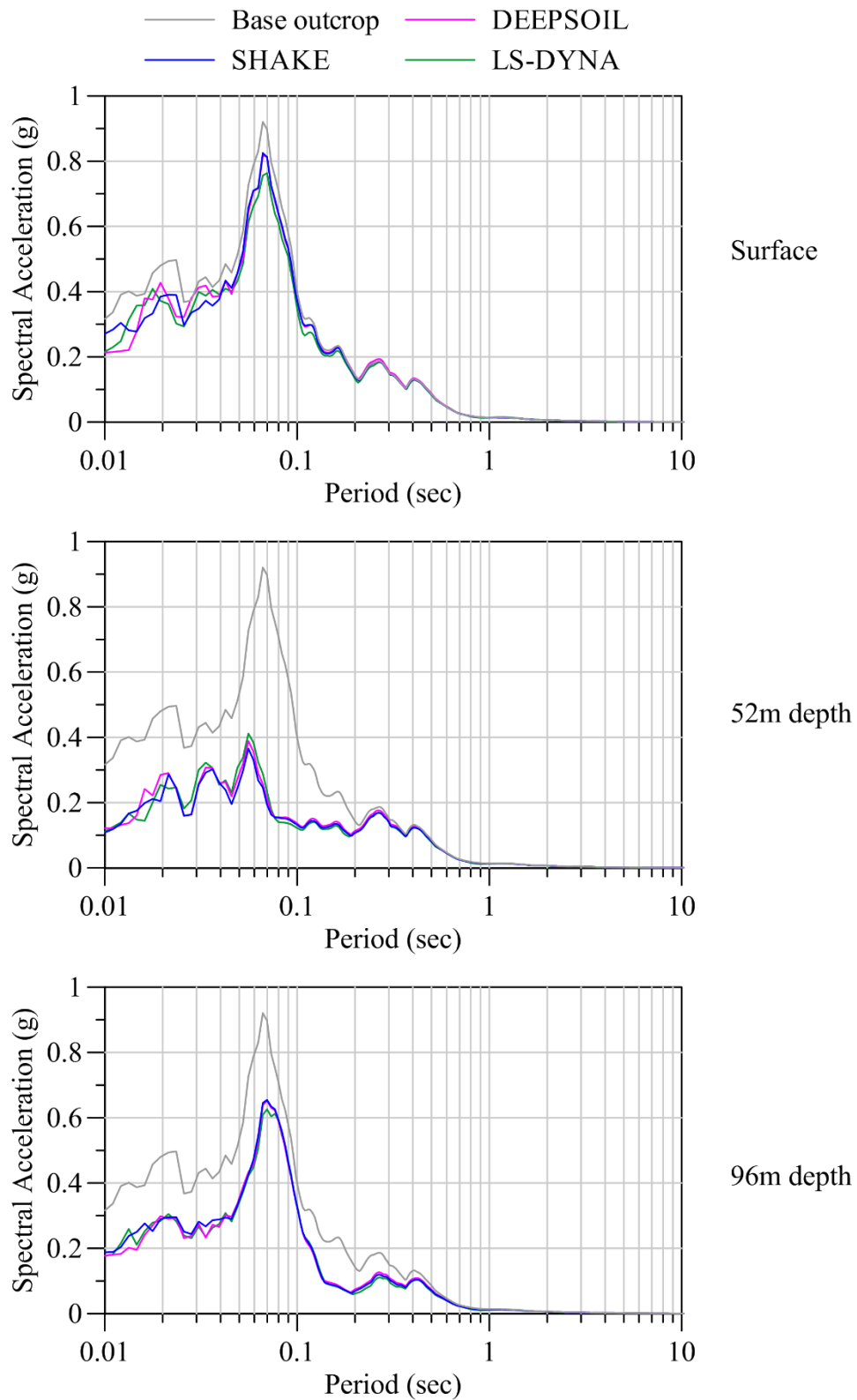


Figure A-8: Acceleration response spectra of the base outcrop motion, and accelerations at three different depths for site E1 subjected to ground motion EO2

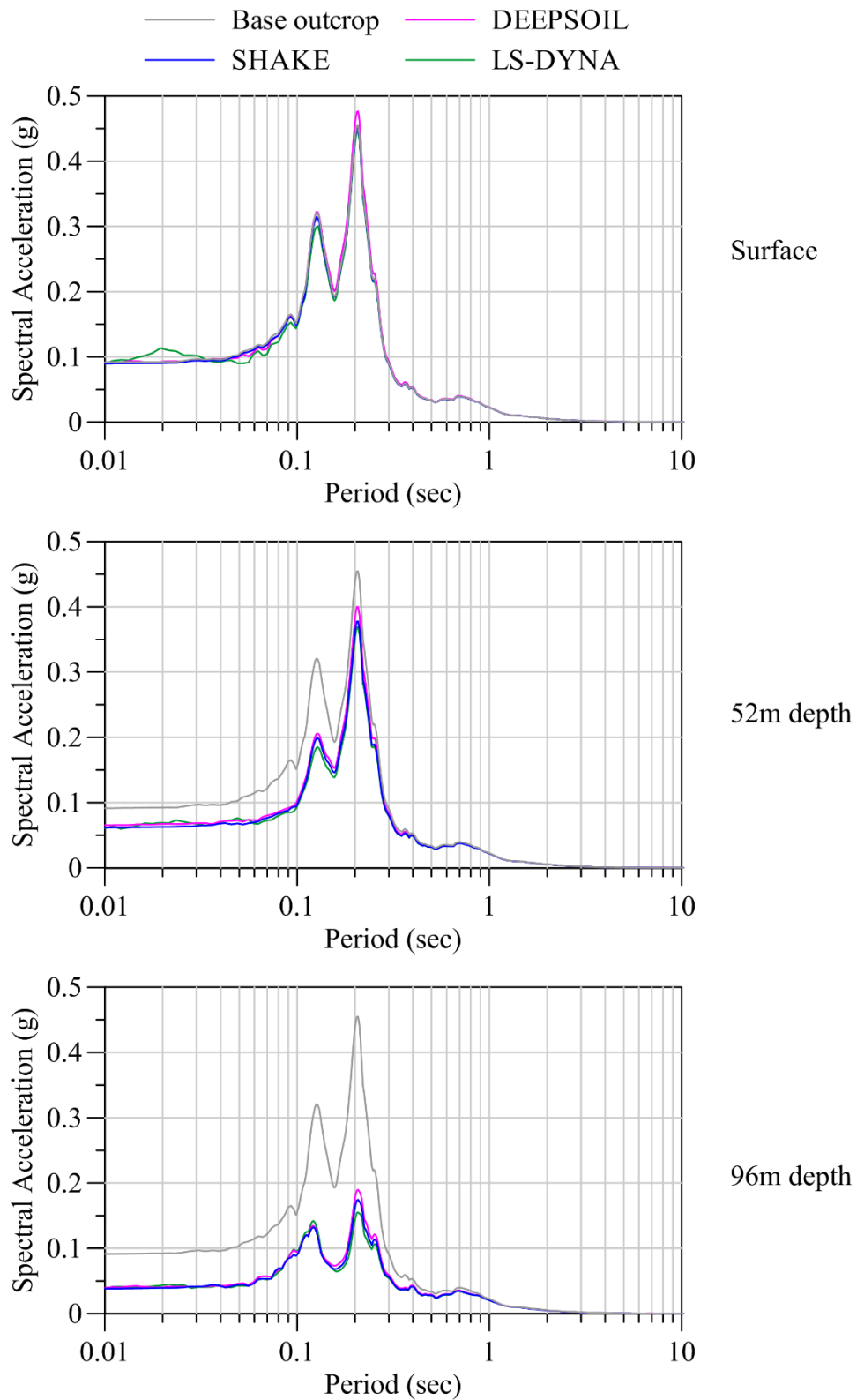


Figure A-9: Acceleration response spectra of the base outcrop motion, and accelerations at three different depths for site E1 subjected to ground motion EO3

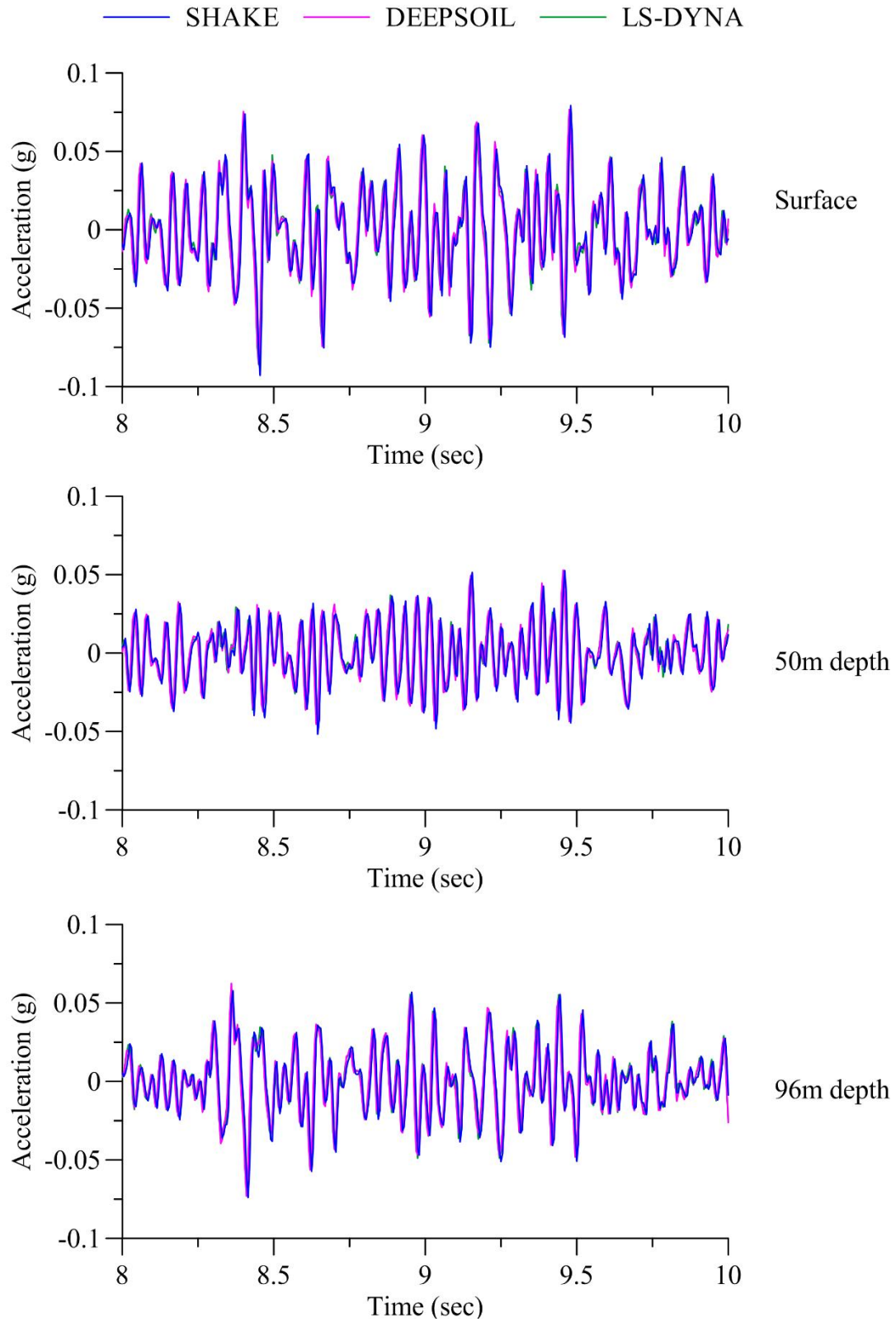


Figure A-10: Acceleration response histories at three different depths for site E1 subjected to ground motion EO1

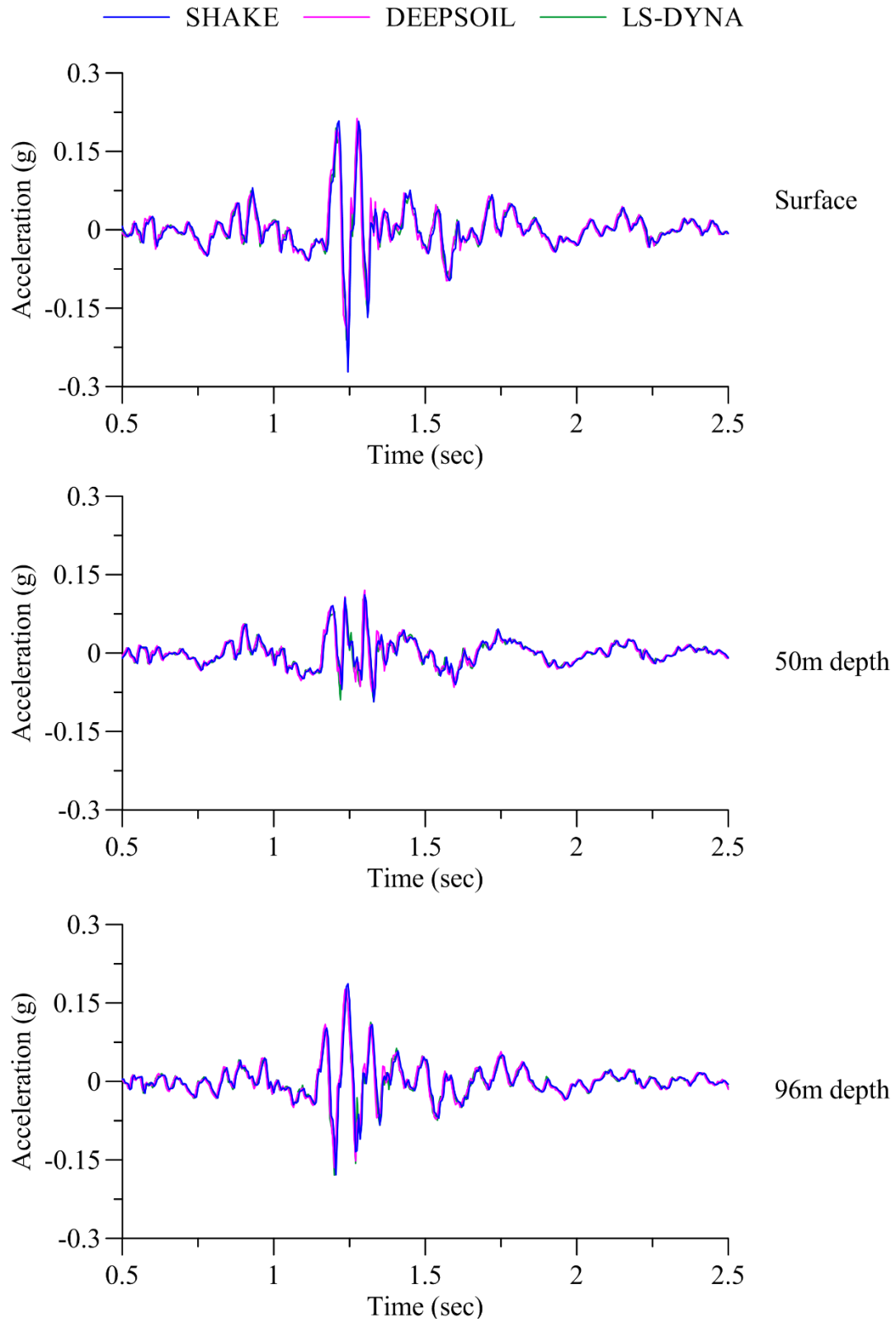


Figure A-11: Acceleration response histories at three different depths for site E1 subjected to ground motion EO2

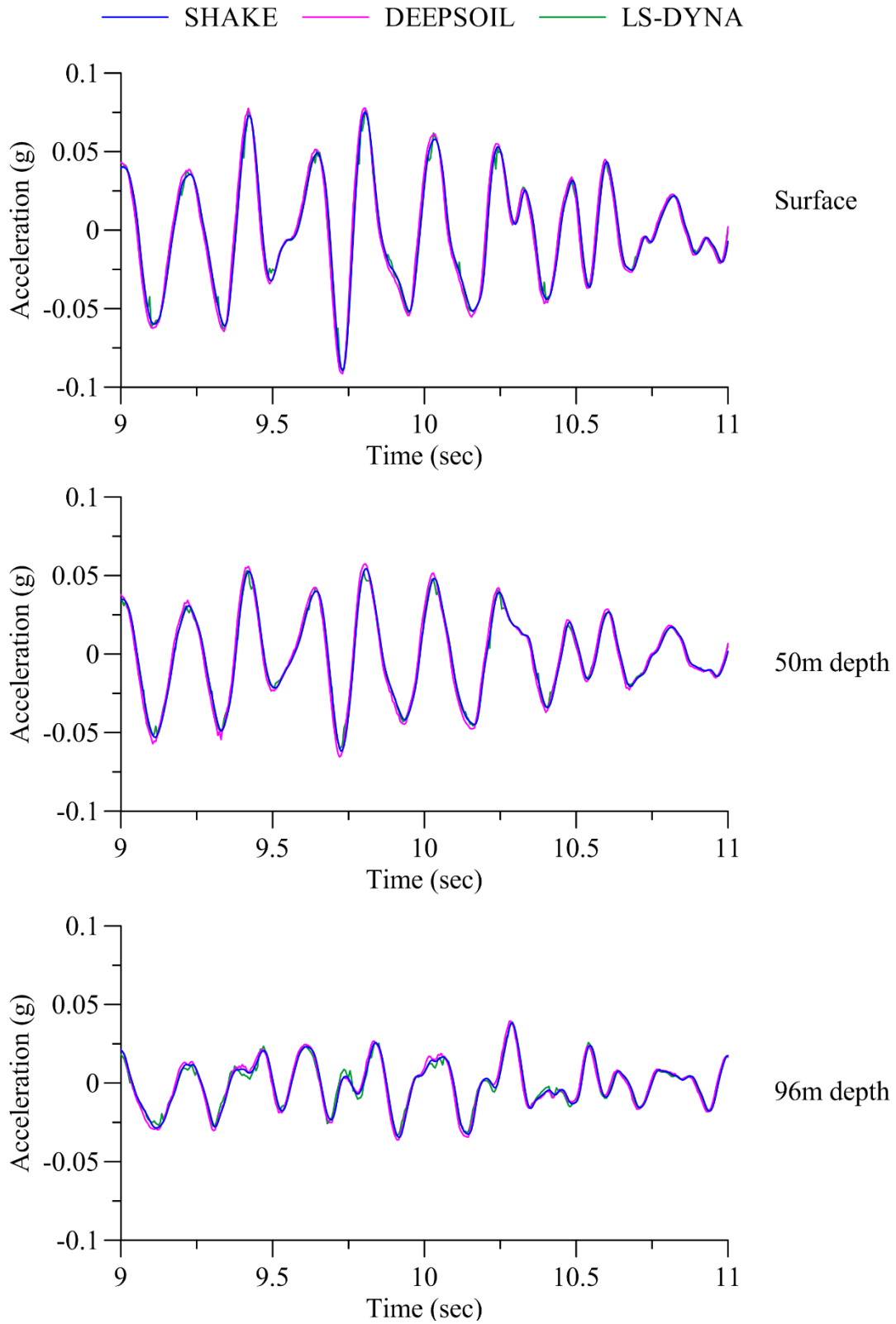


Figure A-12: Acceleration response histories at three different depths for site E1 subjected to ground motion EO3

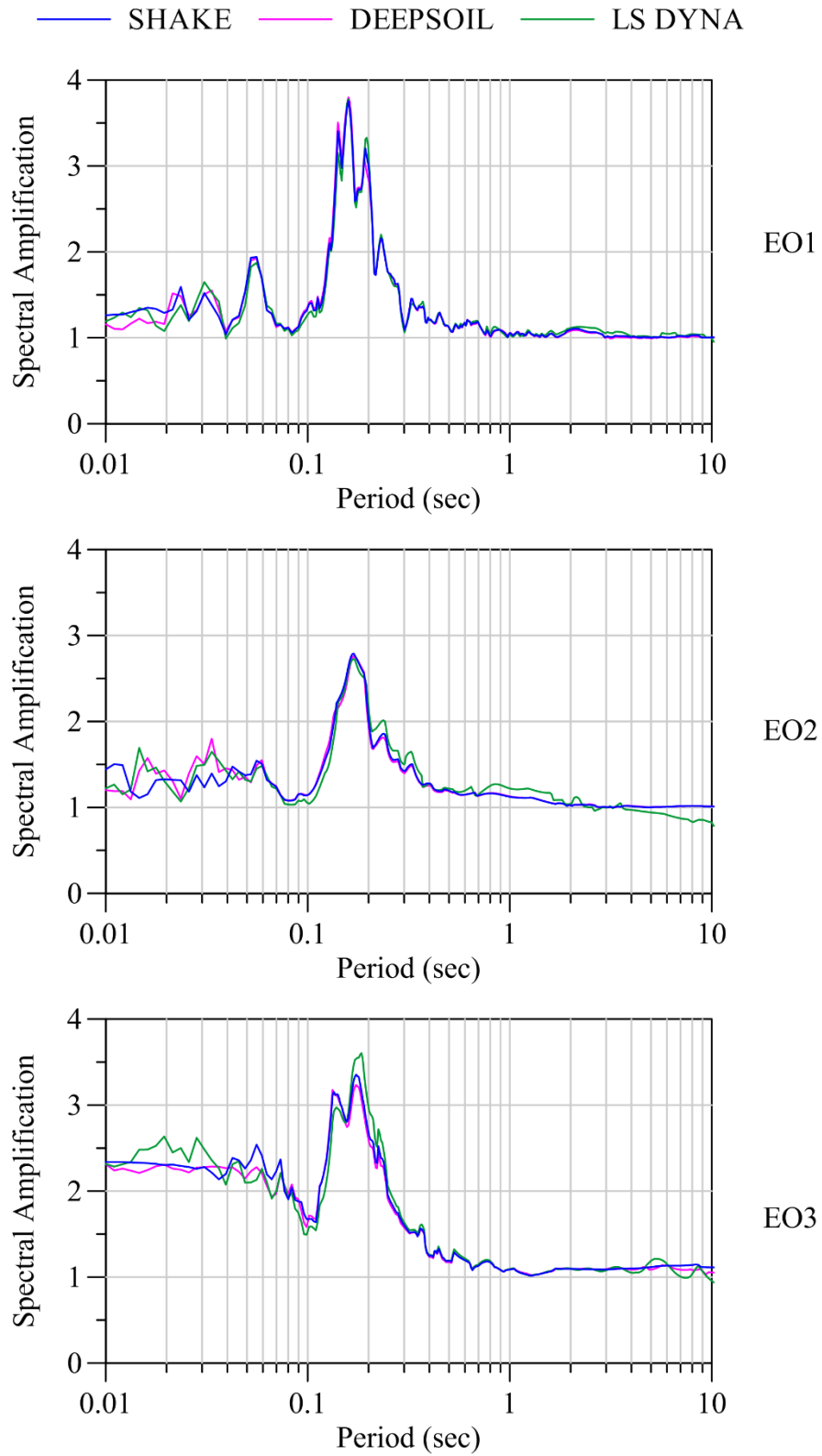


Figure A-13: Spectral amplification of accelerations from the base to the surface of site E1 for ground motions EO1, EO2 and EO3

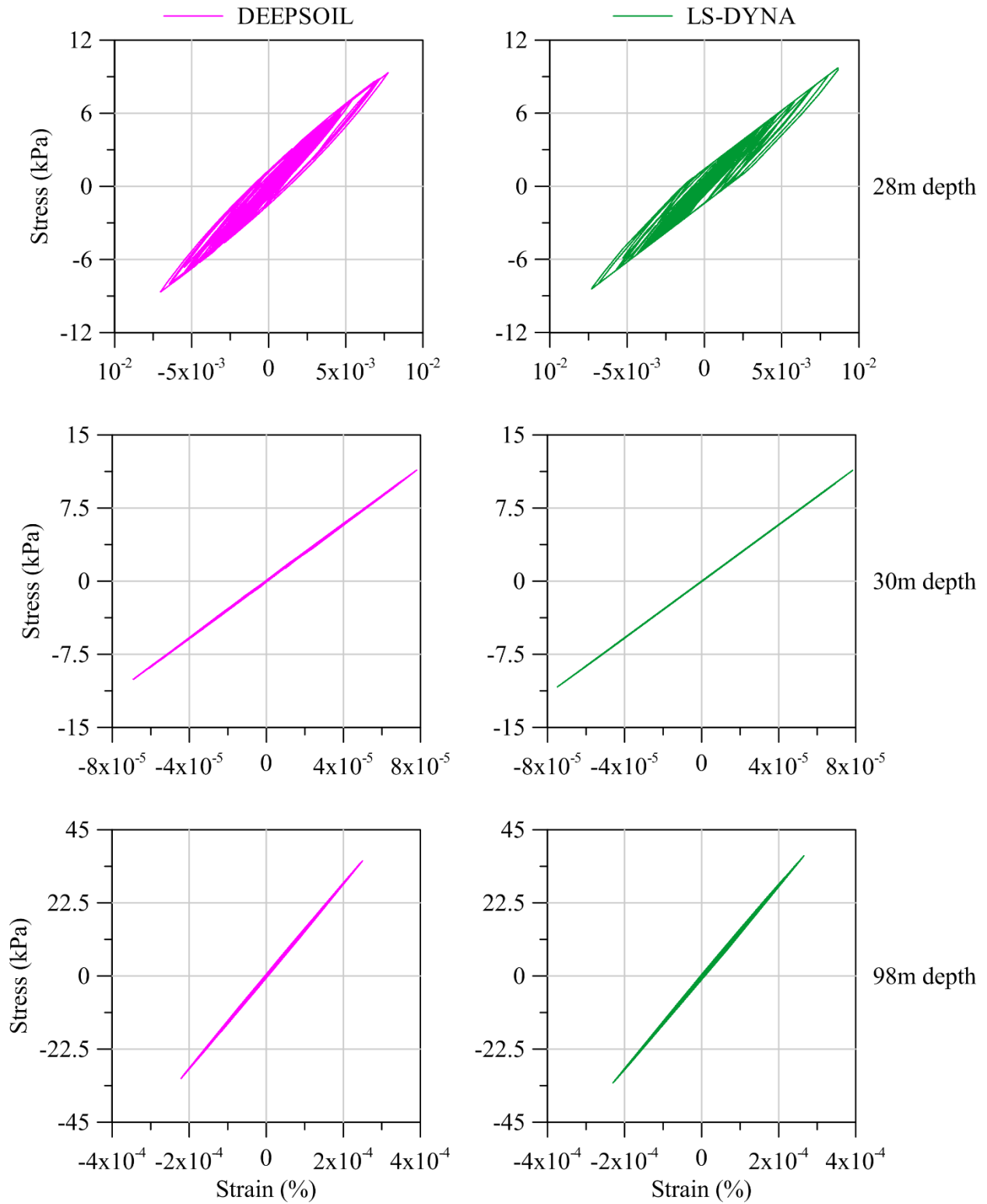


Figure A-14: Stress-strain loops at three different depths for site E2 subjected to ground motion

EO1

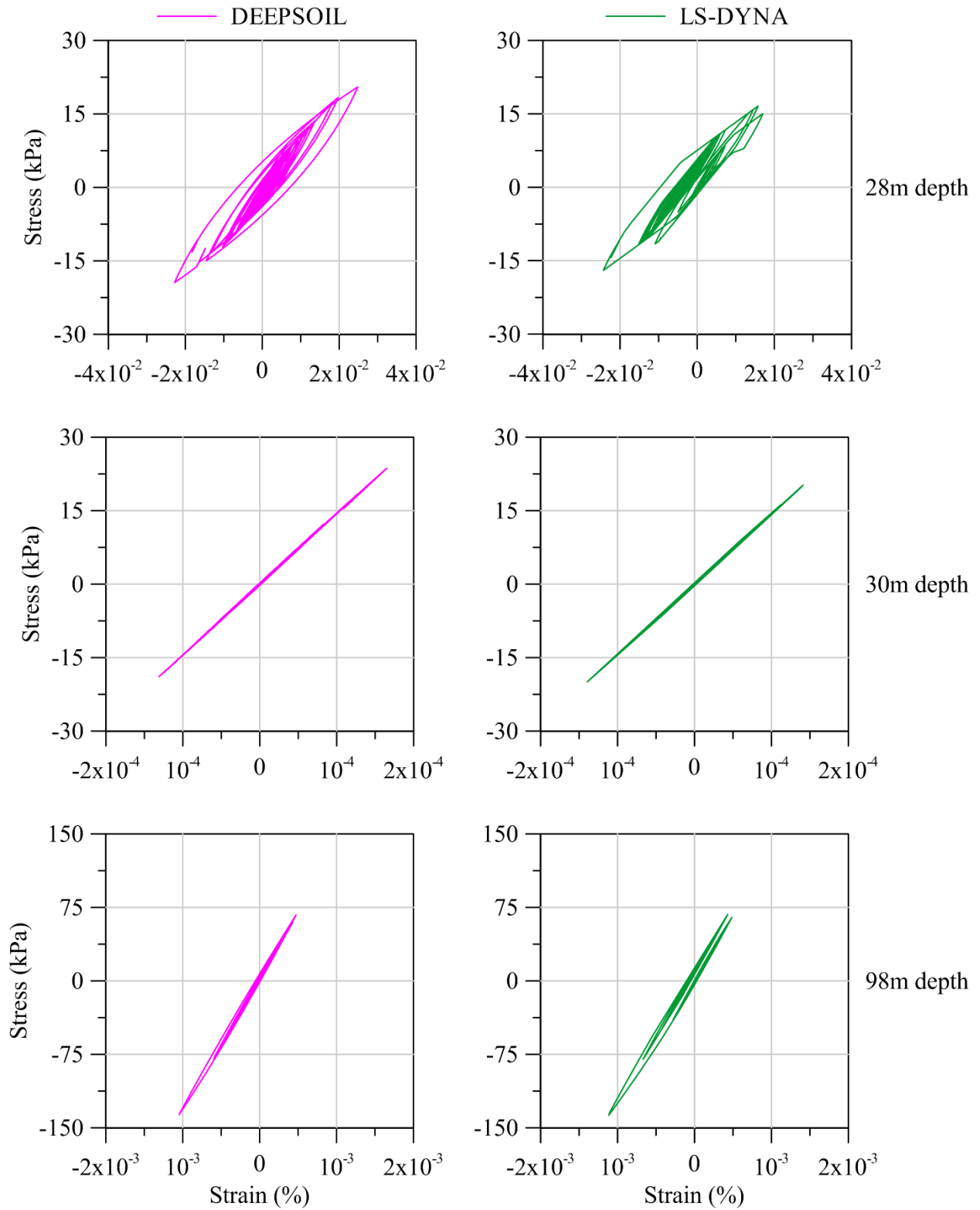


Figure A-15: Stress-strain loops at three different depths for site E2 subjected to ground motion EO2

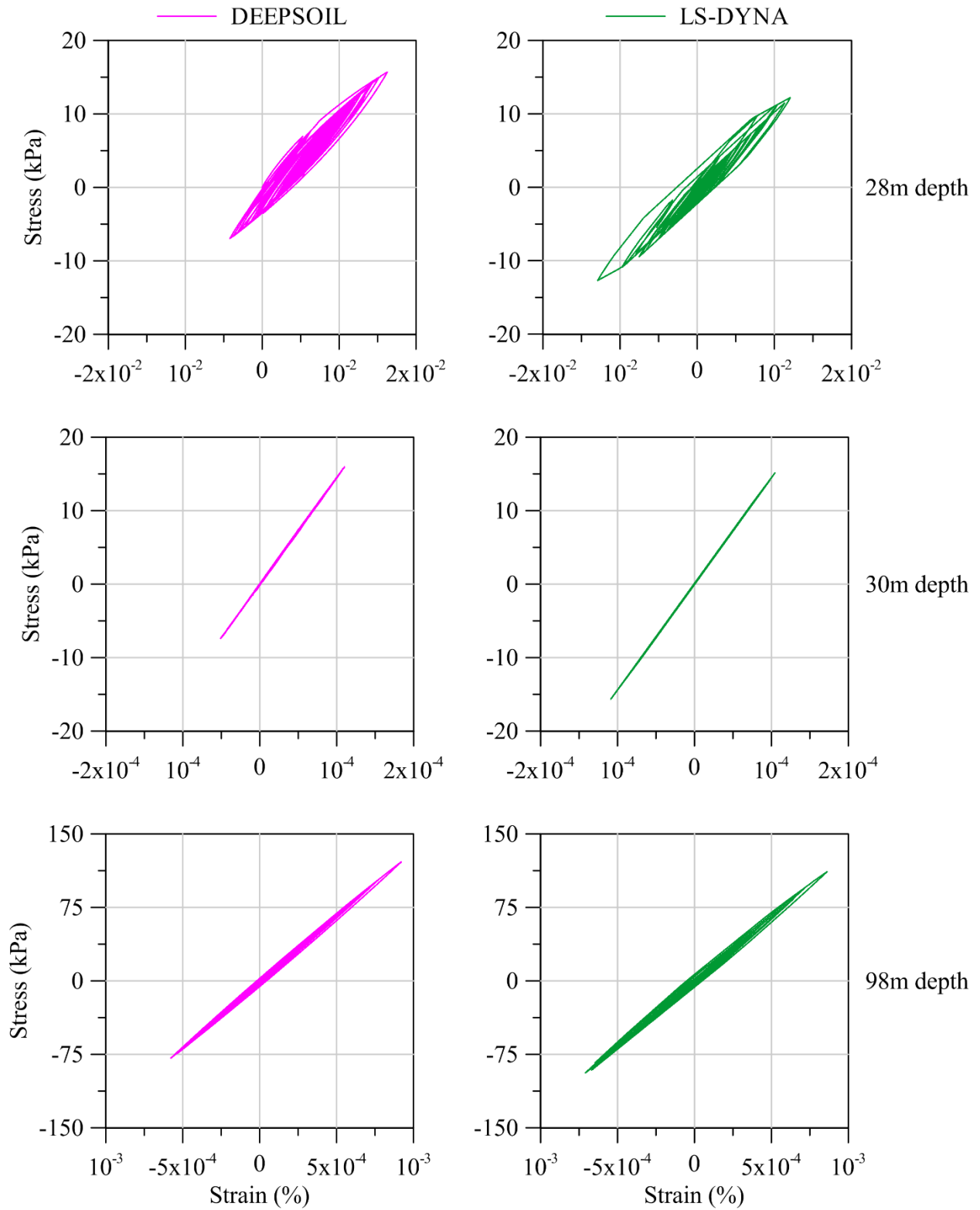


Figure A-16: Stress-strain loops at three different depths for site E2 subjected to ground motion EO3

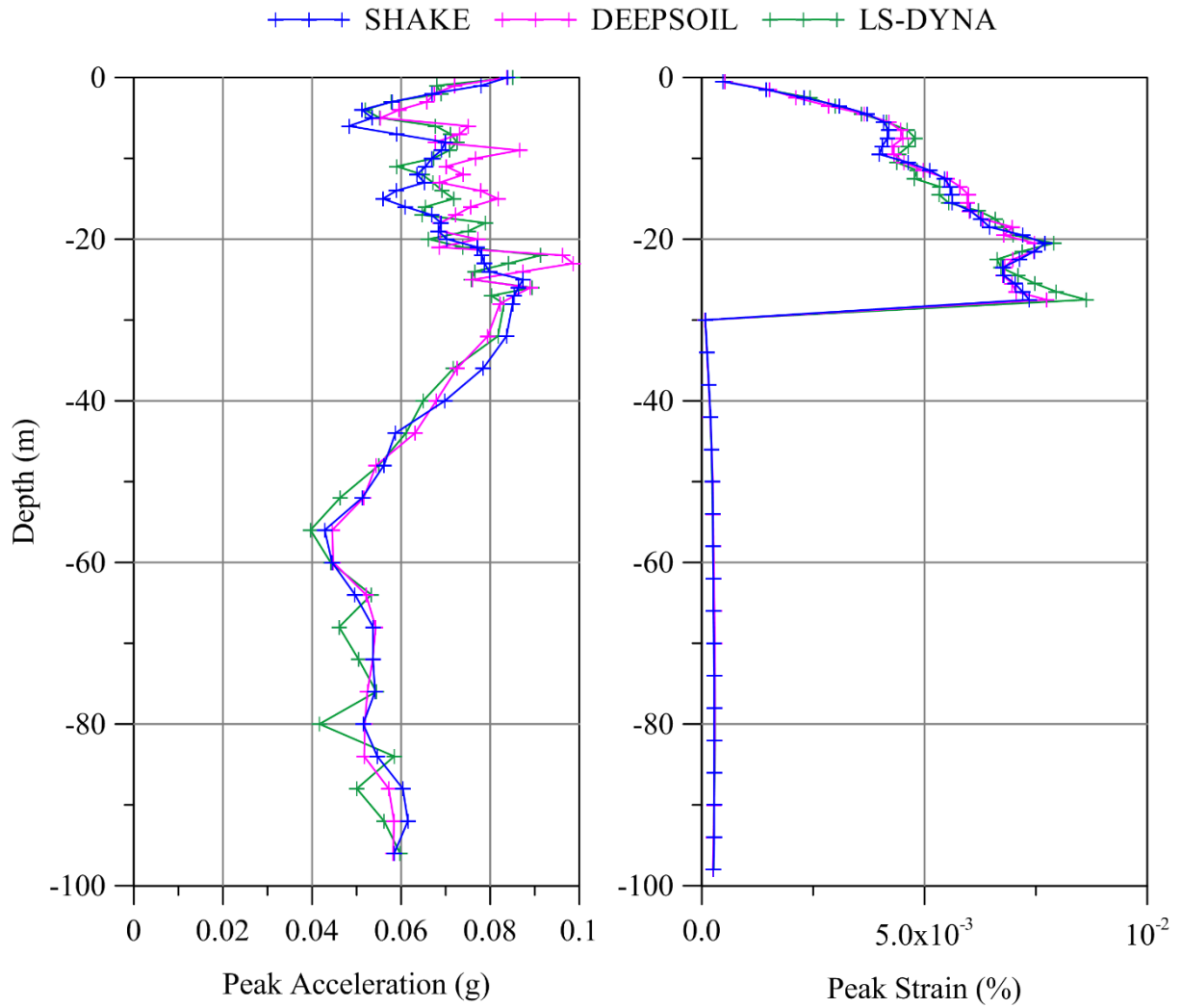


Figure A-17: Peak acceleration and peak strain profiles for site E2 subjected to ground motion EO1

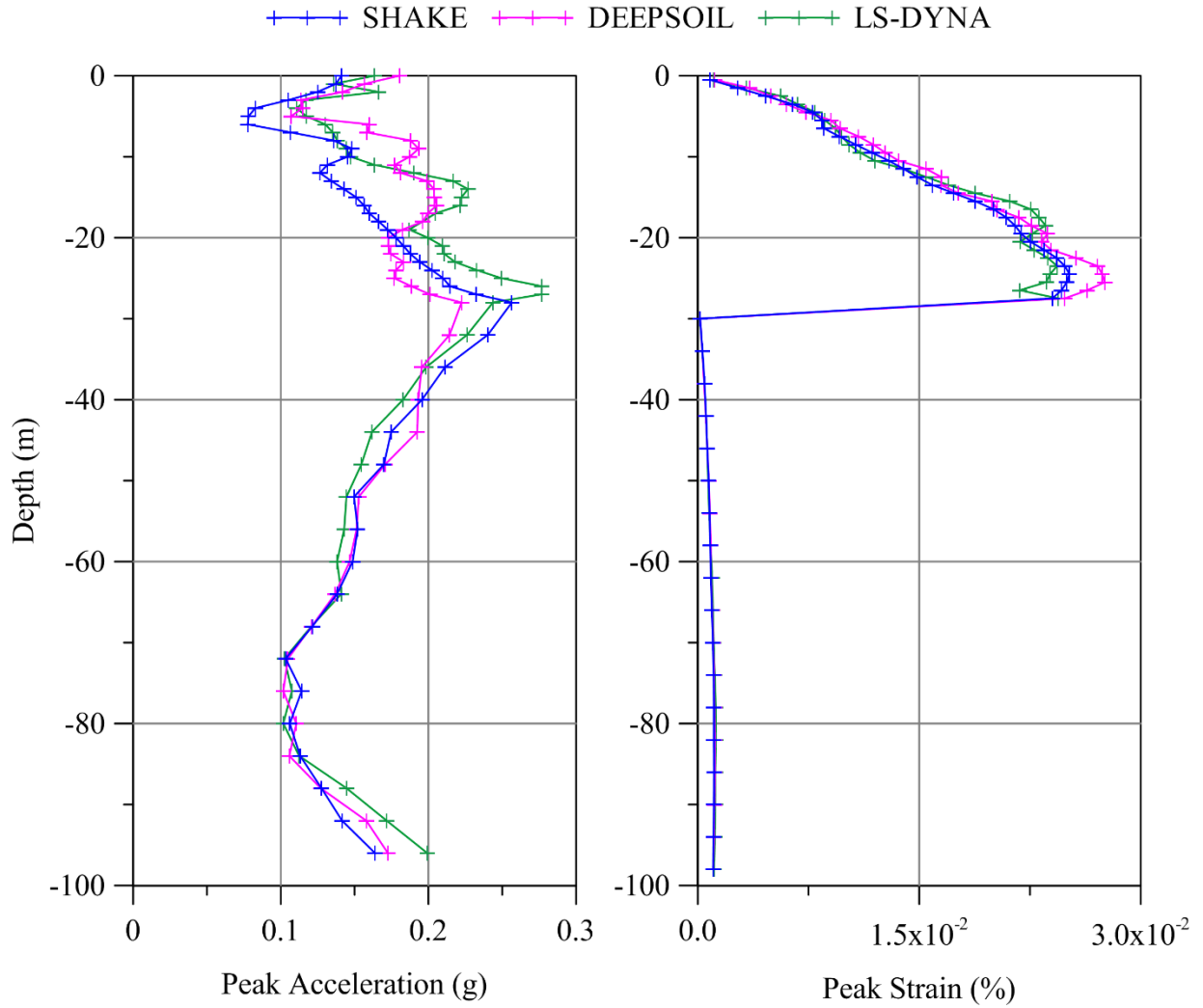


Figure A-18: Peak acceleration and peak strain profiles for site E2 subjected to ground motion EO2

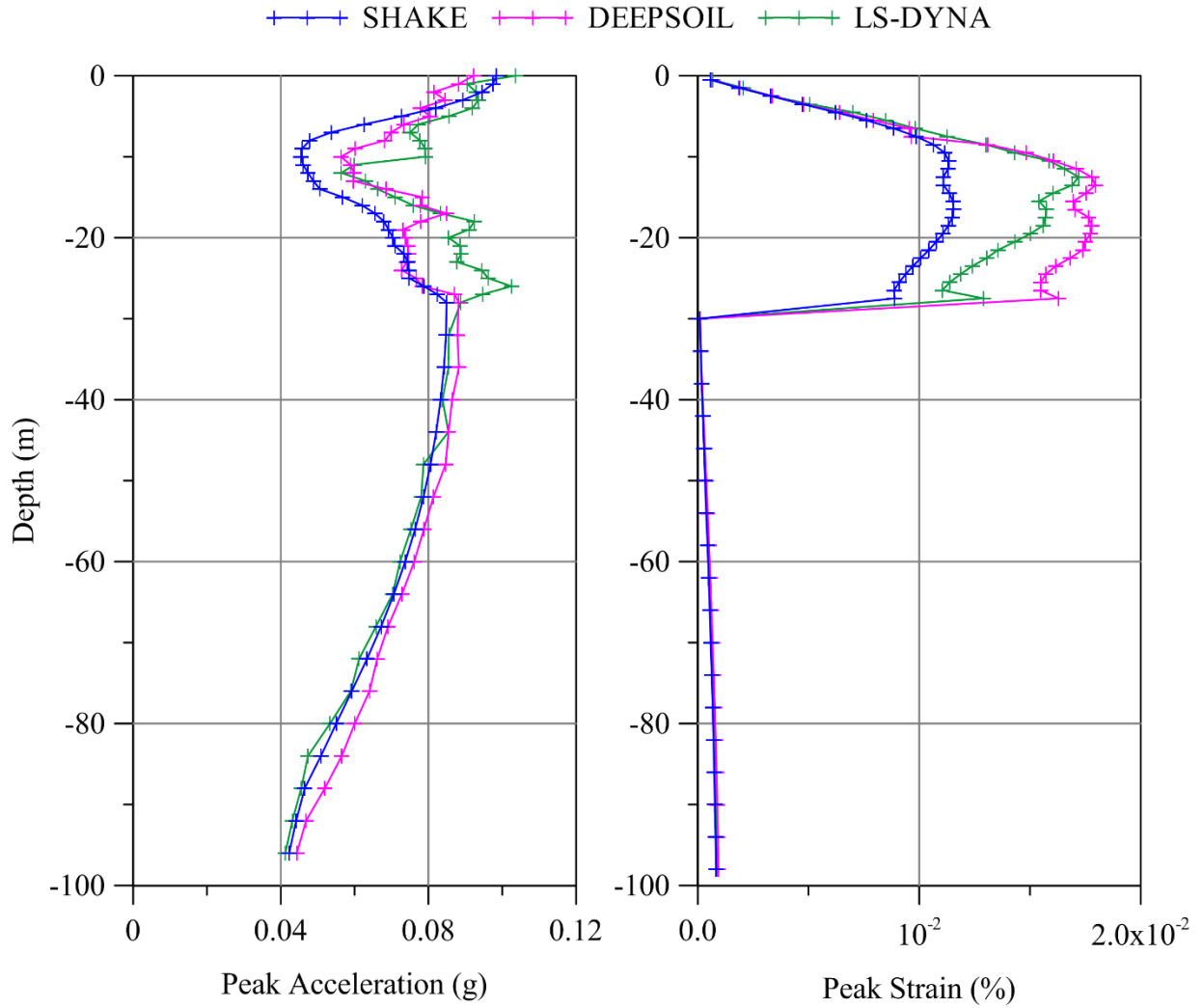


Figure A-19: Peak acceleration and peak strain profiles for site E2 subjected to ground motion EO3

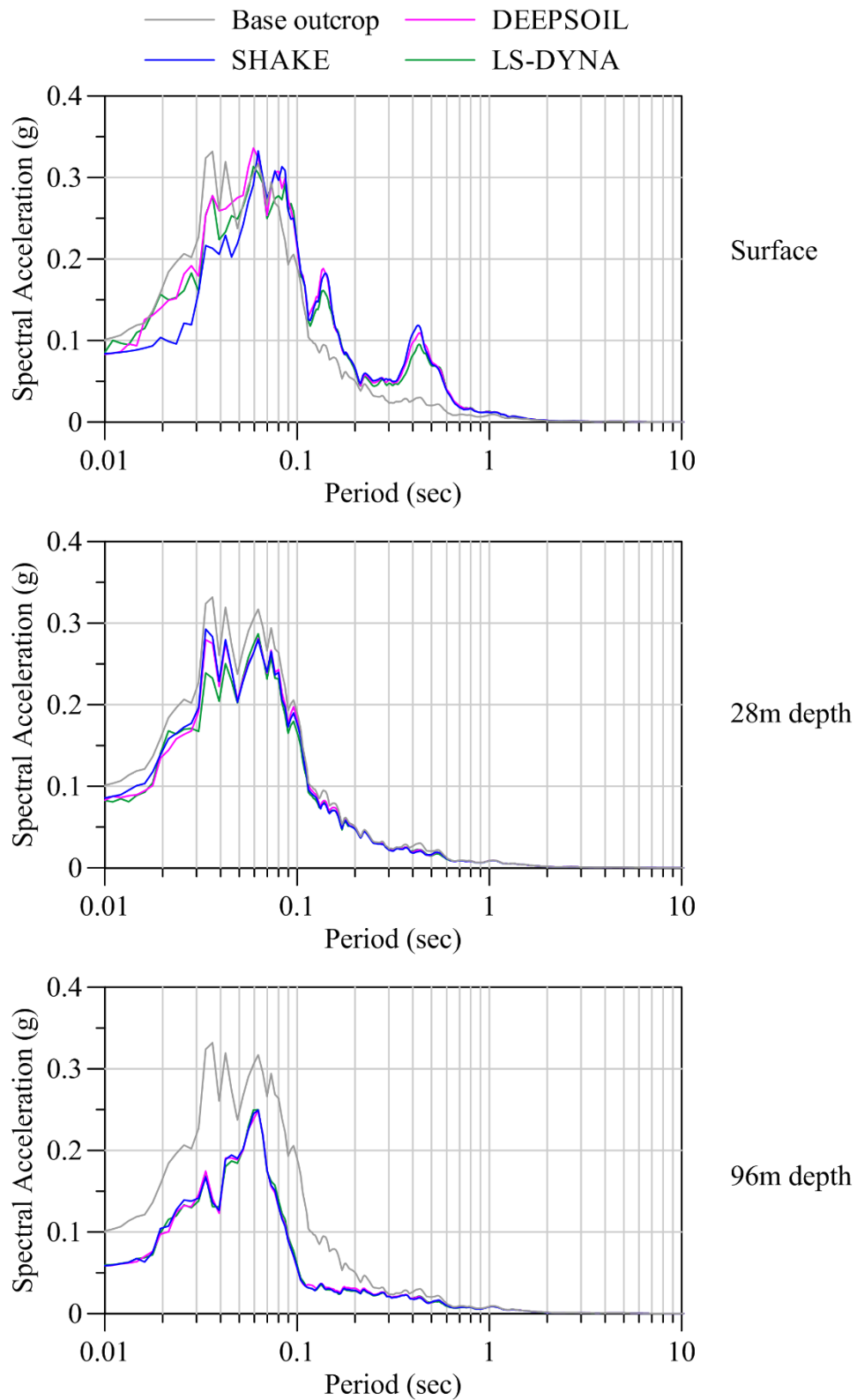


Figure A-20: Acceleration response spectra of the base outcrop motion, and accelerations at three different depths for site E2 subjected to ground motion EO1

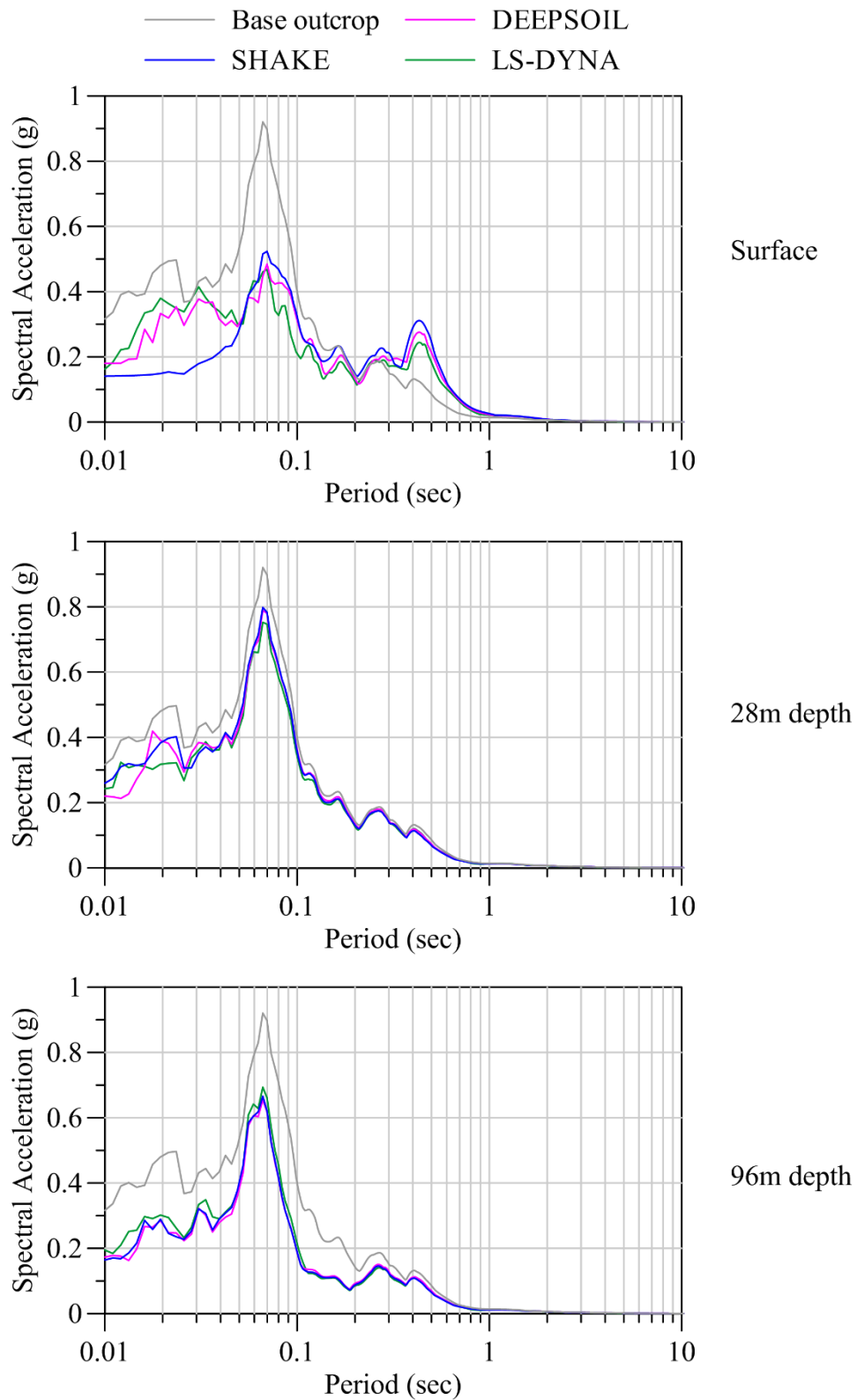


Figure A-21: Acceleration response spectra of the base outcrop motion, and accelerations at three different depths for site E2 subjected to ground motion EO2

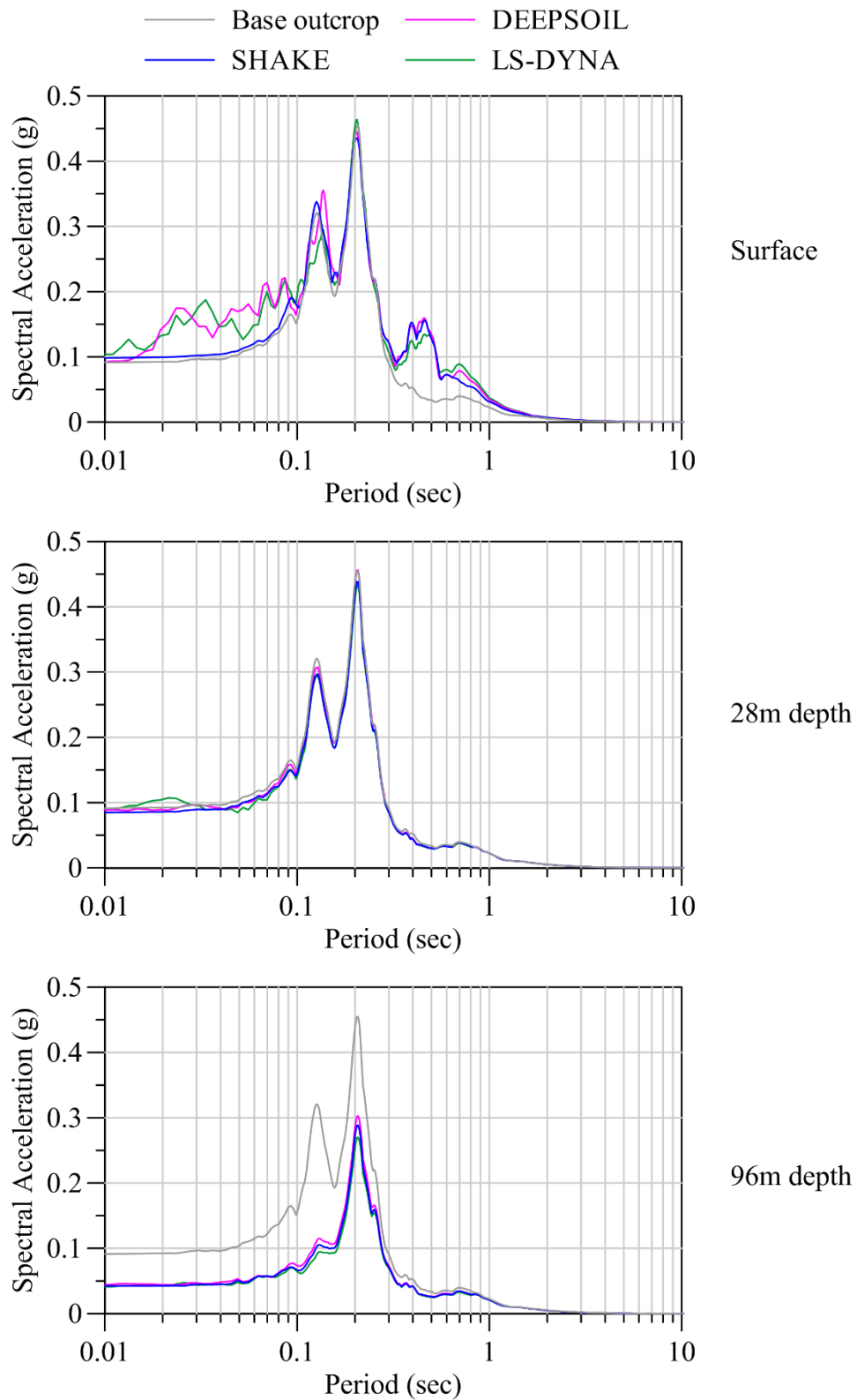


Figure A-22: Acceleration response spectra of the base outcrop motion, and accelerations at three different depths for site E2 subjected to ground motion EO3

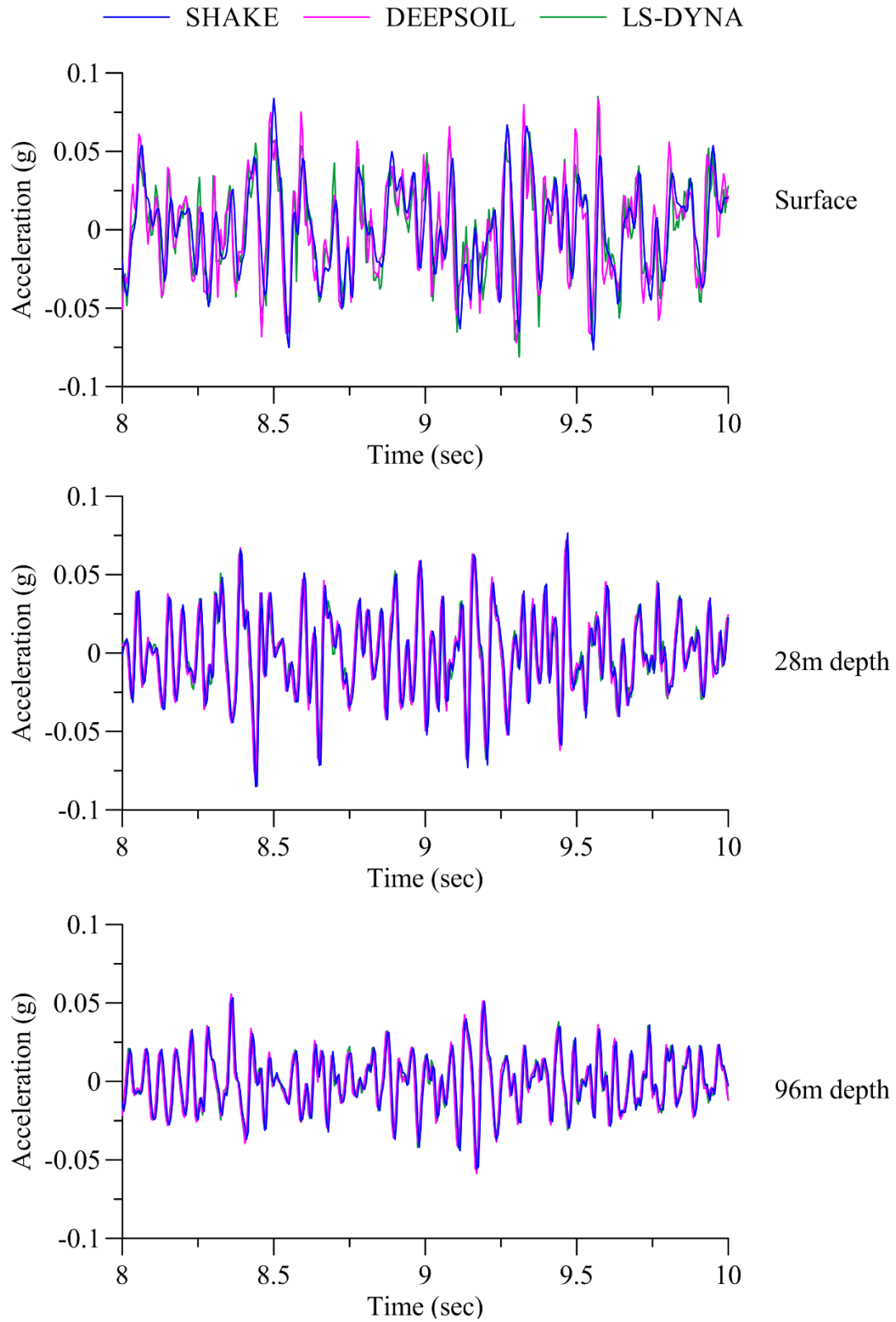


Figure A-23: Acceleration response histories at three different depths for site E2 subjected to ground motion EO1

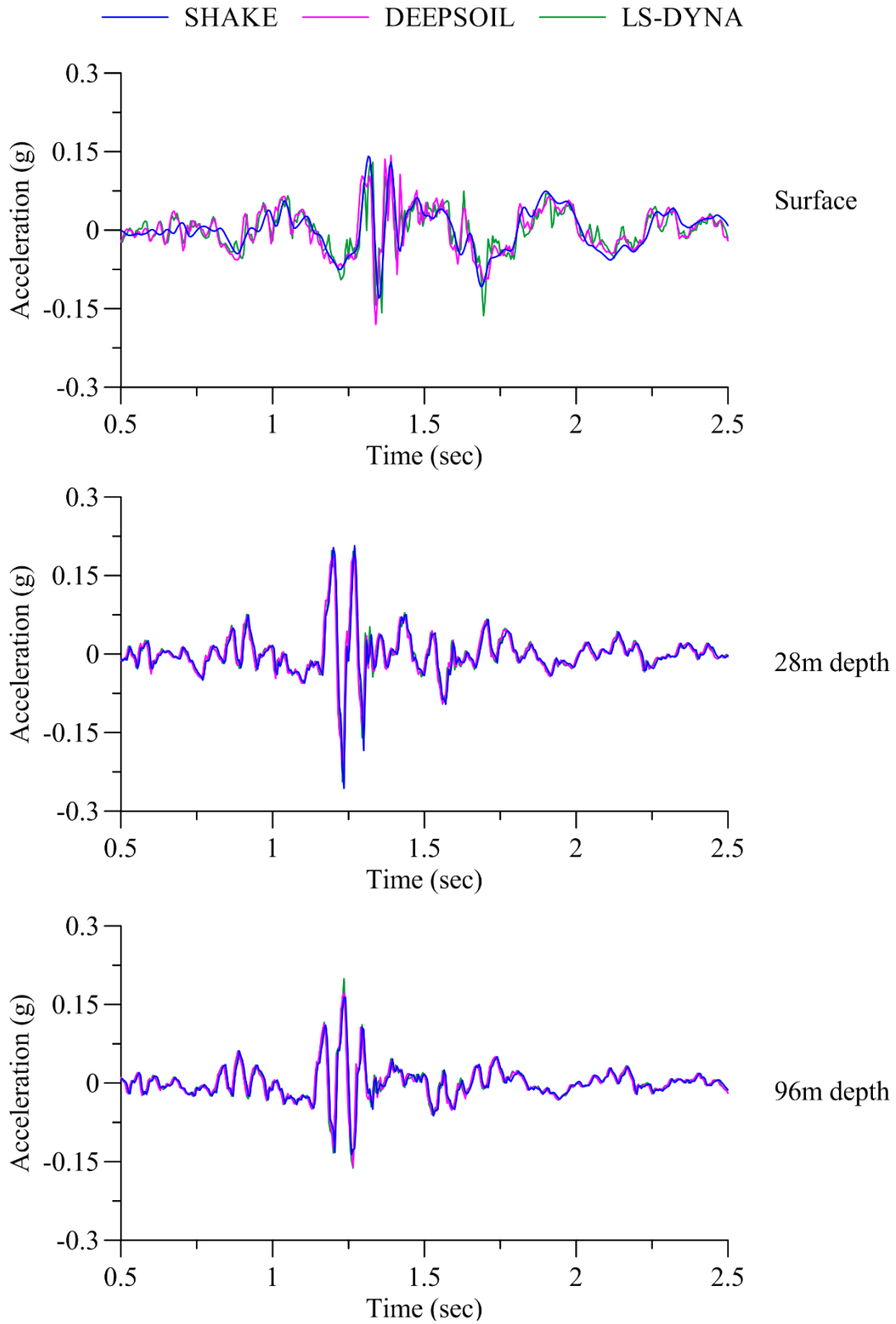


Figure A-24: Acceleration response histories at three different depths for site E2 subjected to ground motion EO2

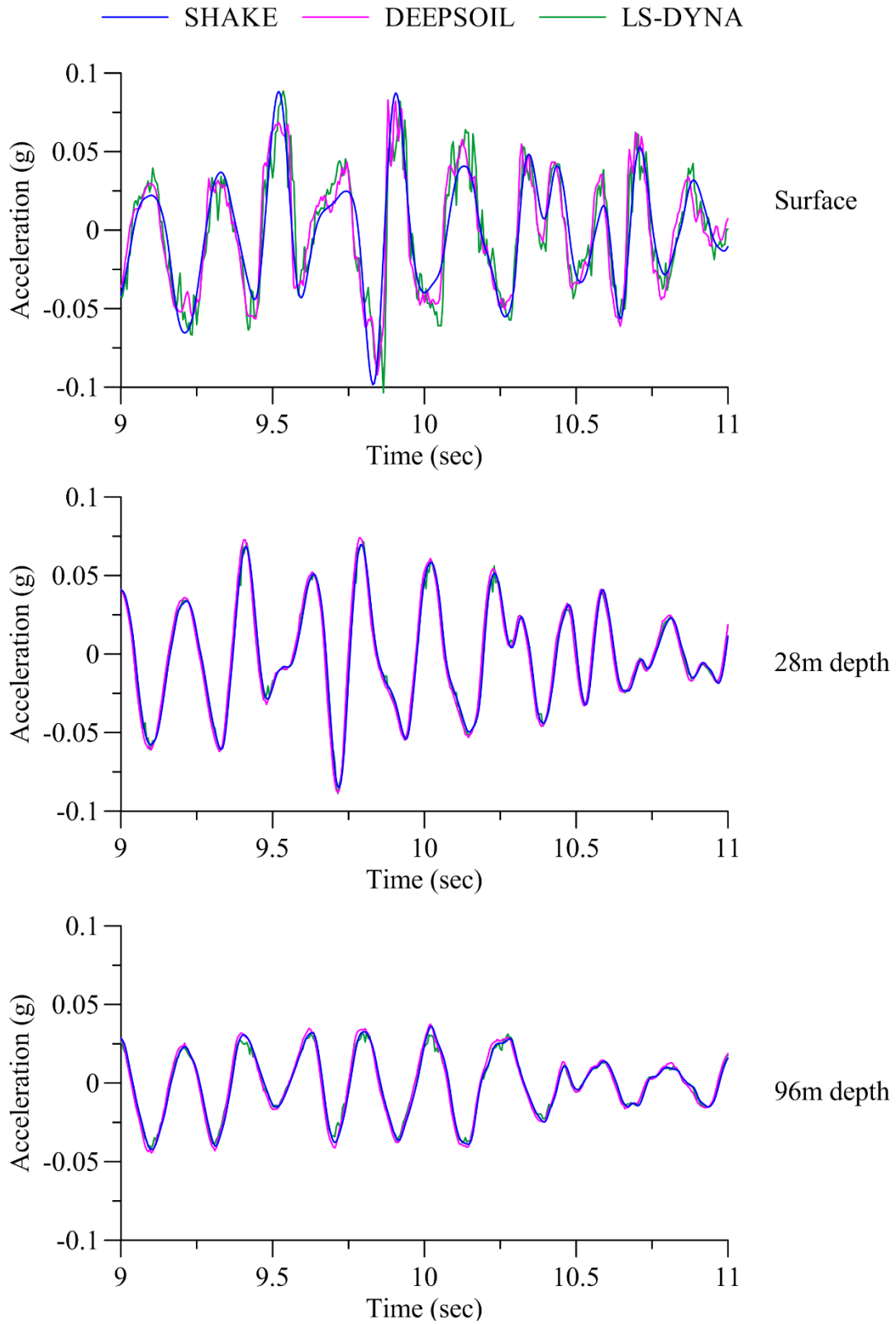


Figure A-25: Acceleration response histories at three different depths for site E2 subjected to ground motion EO3

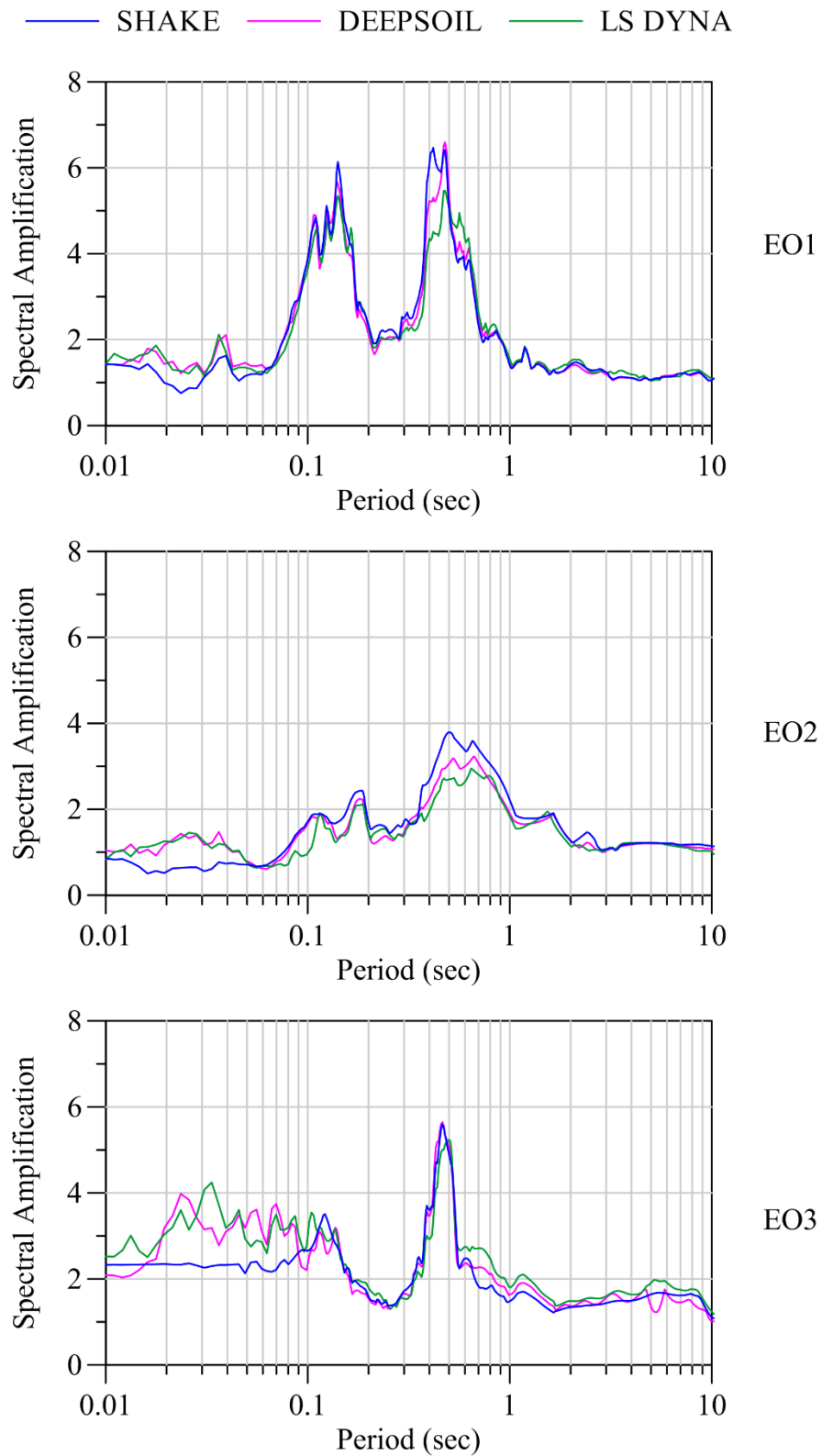


Figure A-26: Spectral amplification of accelerations in site E2 from the base to the surface for ground motions EO1, EO2 and EO3

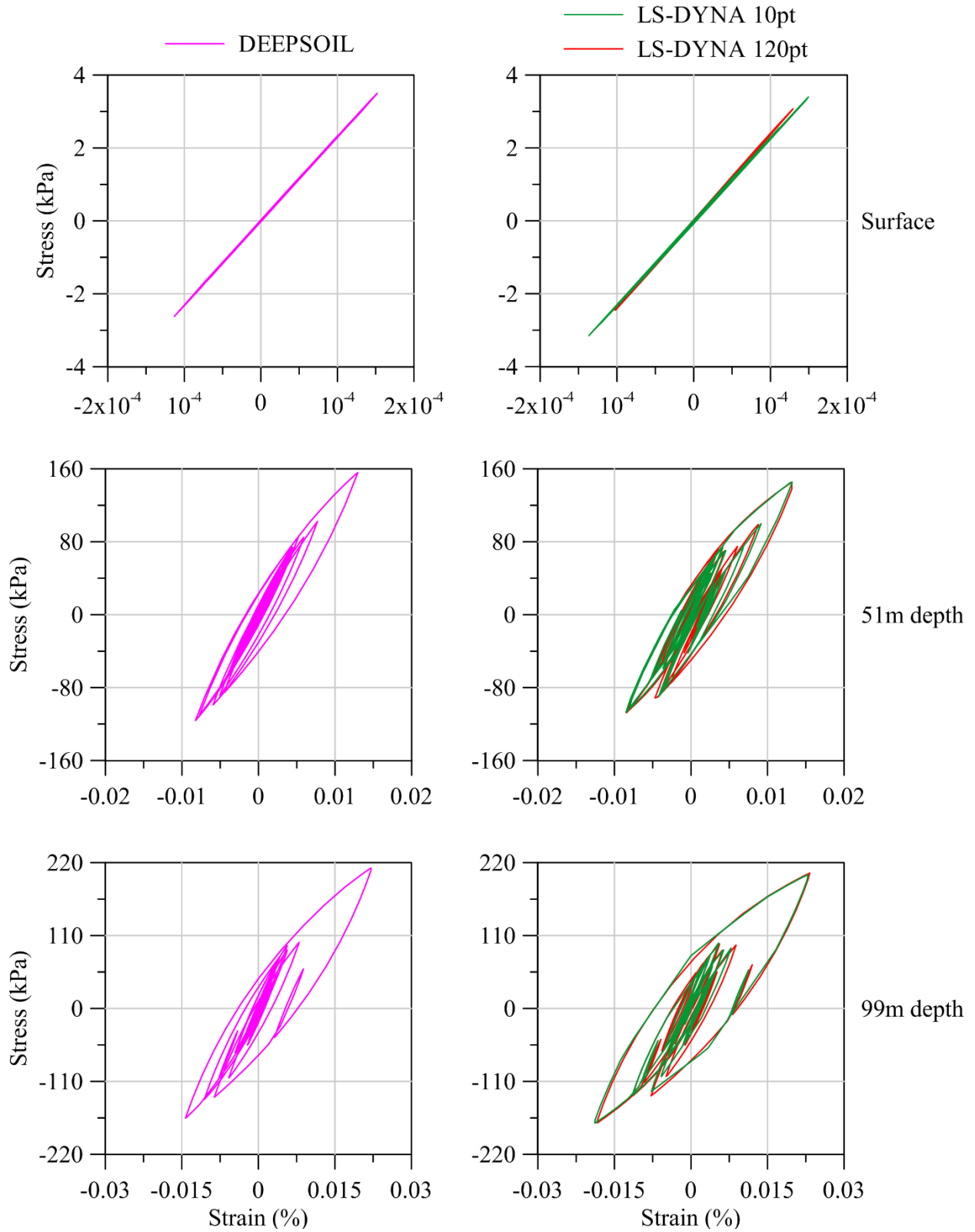


Figure A-27: Stress-strain loops at three different depths for site W1 subjected to ground motion

W01

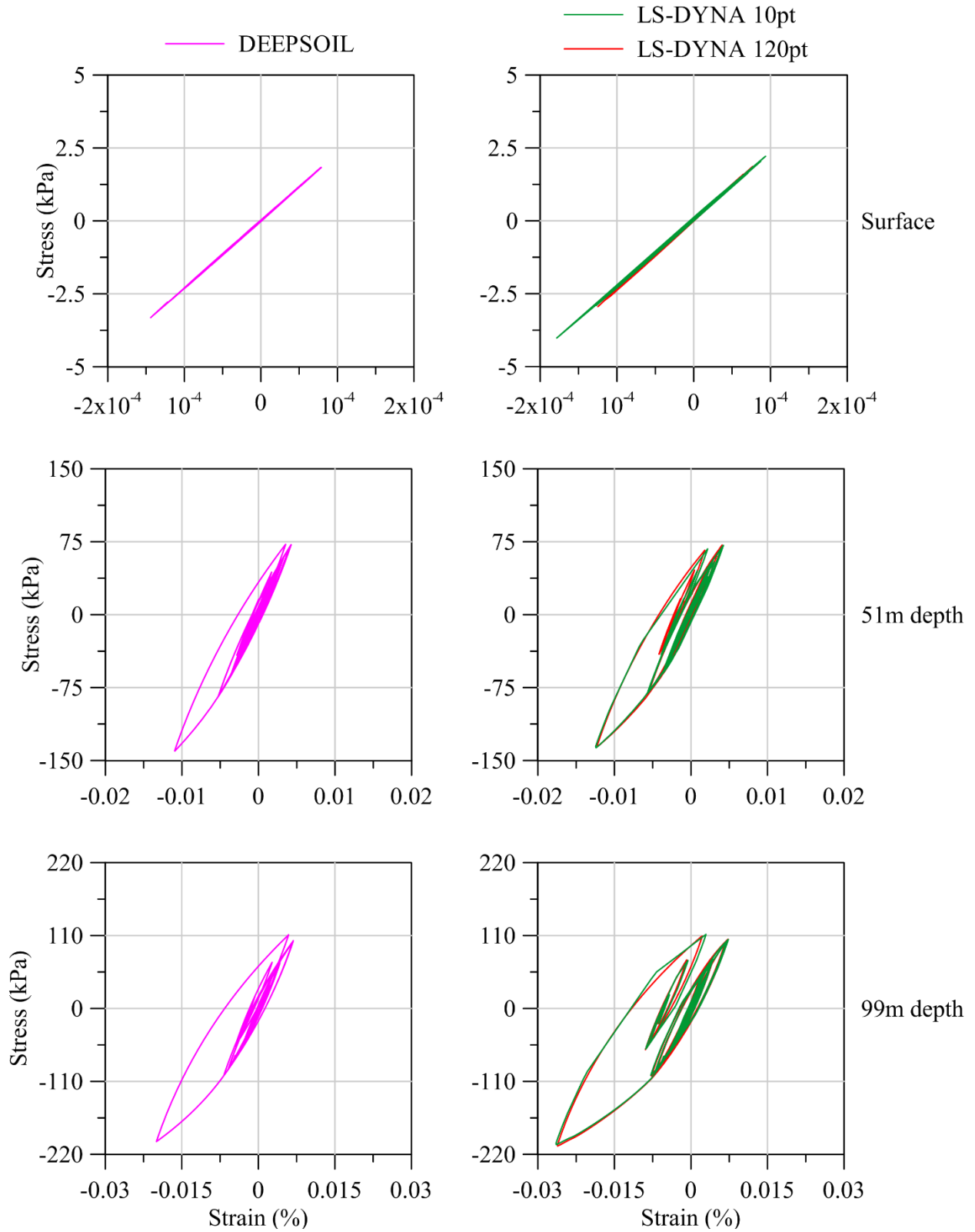


Figure A-28: Stress-strain loops at three different depths for site W1 subjected to ground motion

WO2

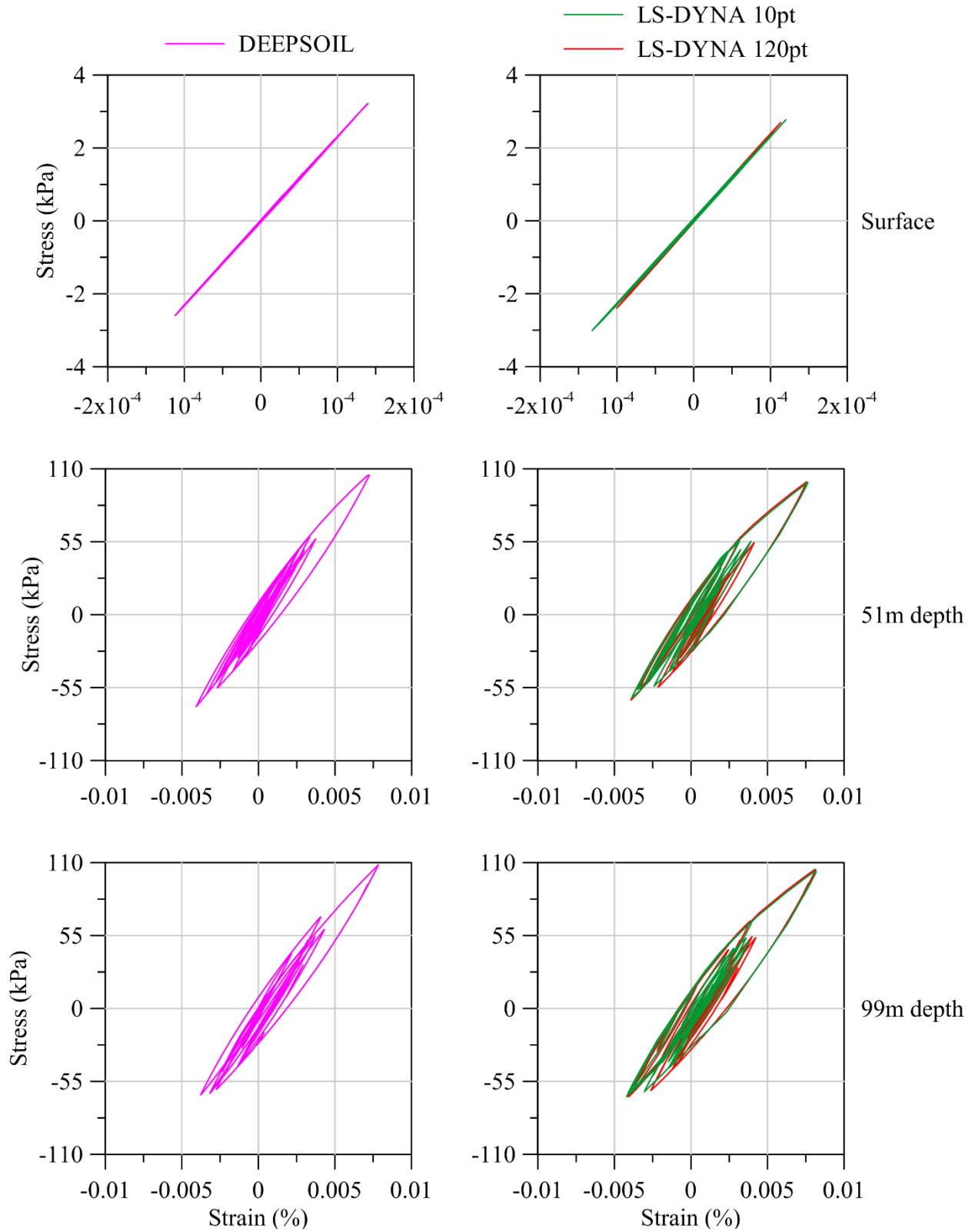
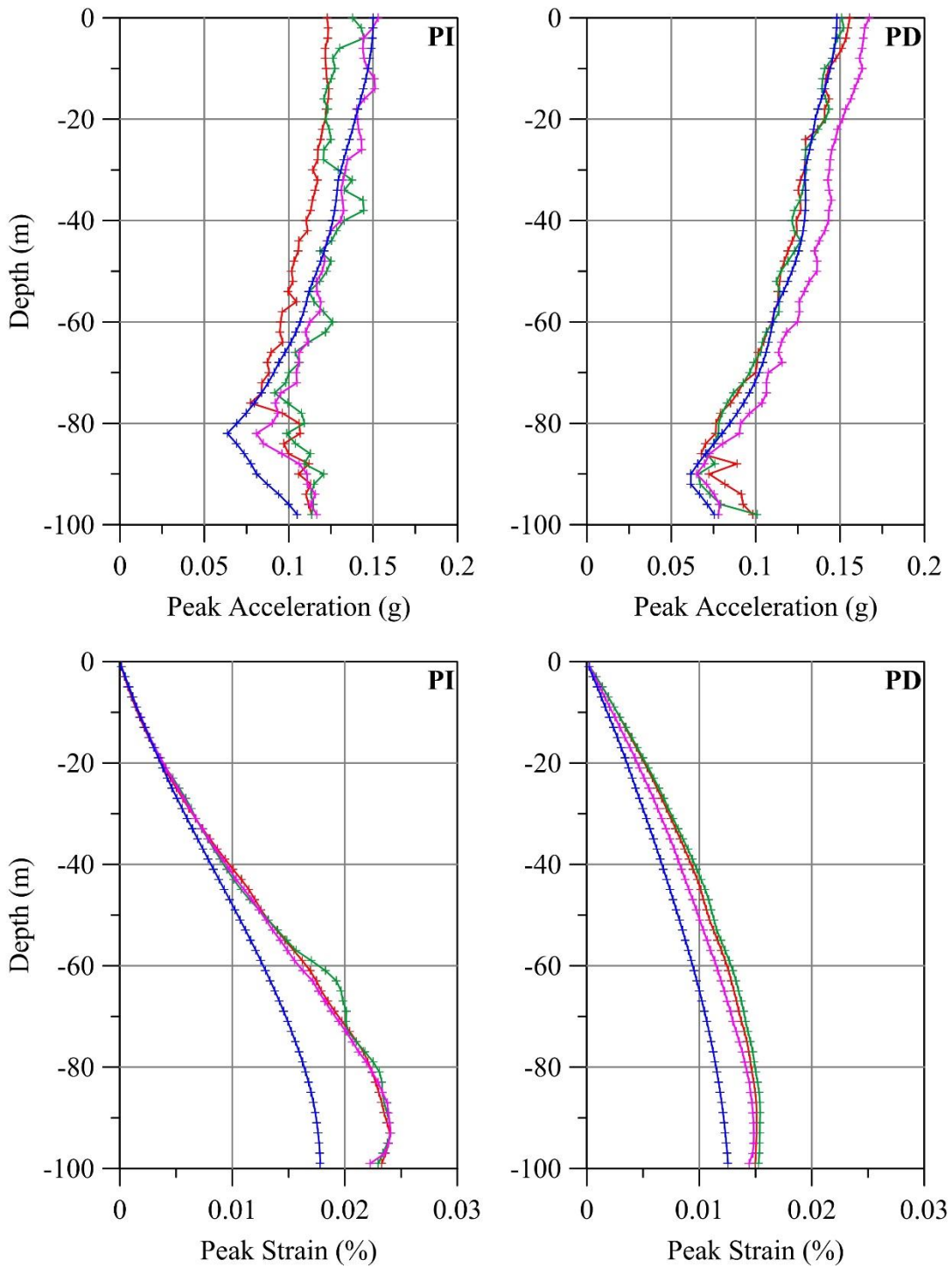


Figure A-29: Stress-strain loops at three different depths for site W1 subjected to ground motion

W03

+ + SHAKE
 + + DEEPSOIL
 + + LS-DYNA 10pt
 + + LS-DYNA 120pt



**Figure A-30: Peak acceleration and peak strain profiles for site W1 subjected to ground motion
 WO1**

+ + SHAKE
 + + DEEPSOIL
 + + LS-DYNA 10pt
 + + LS-DYNA 120pt

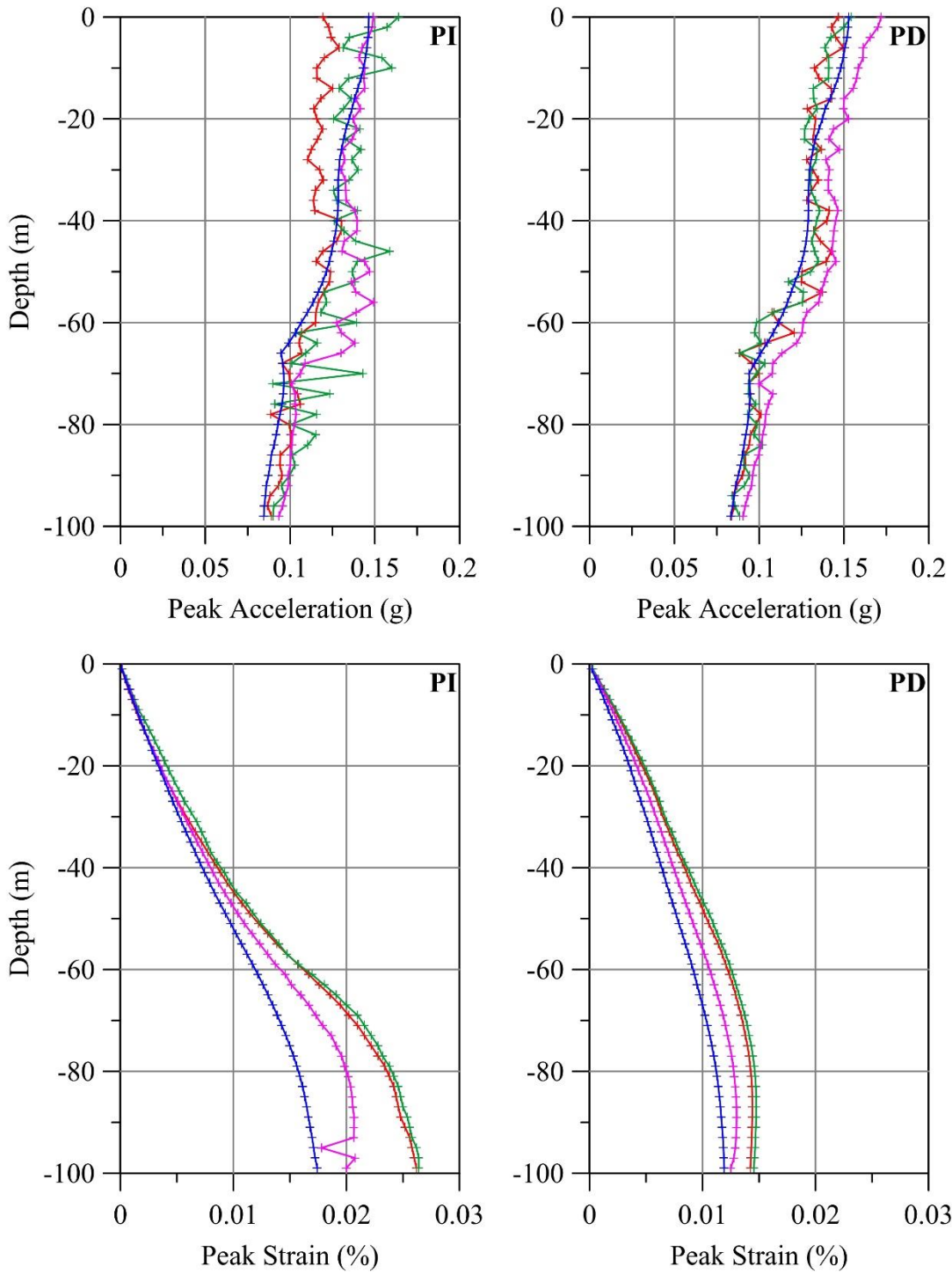


Figure A-31: Peak acceleration and peak strain profiles for site W1 subjected to ground motion

WO2

+ + SHAKE
 + + DEEPSOIL
 + + LS-DYNA 10pt
 + + LS-DYNA 120pt

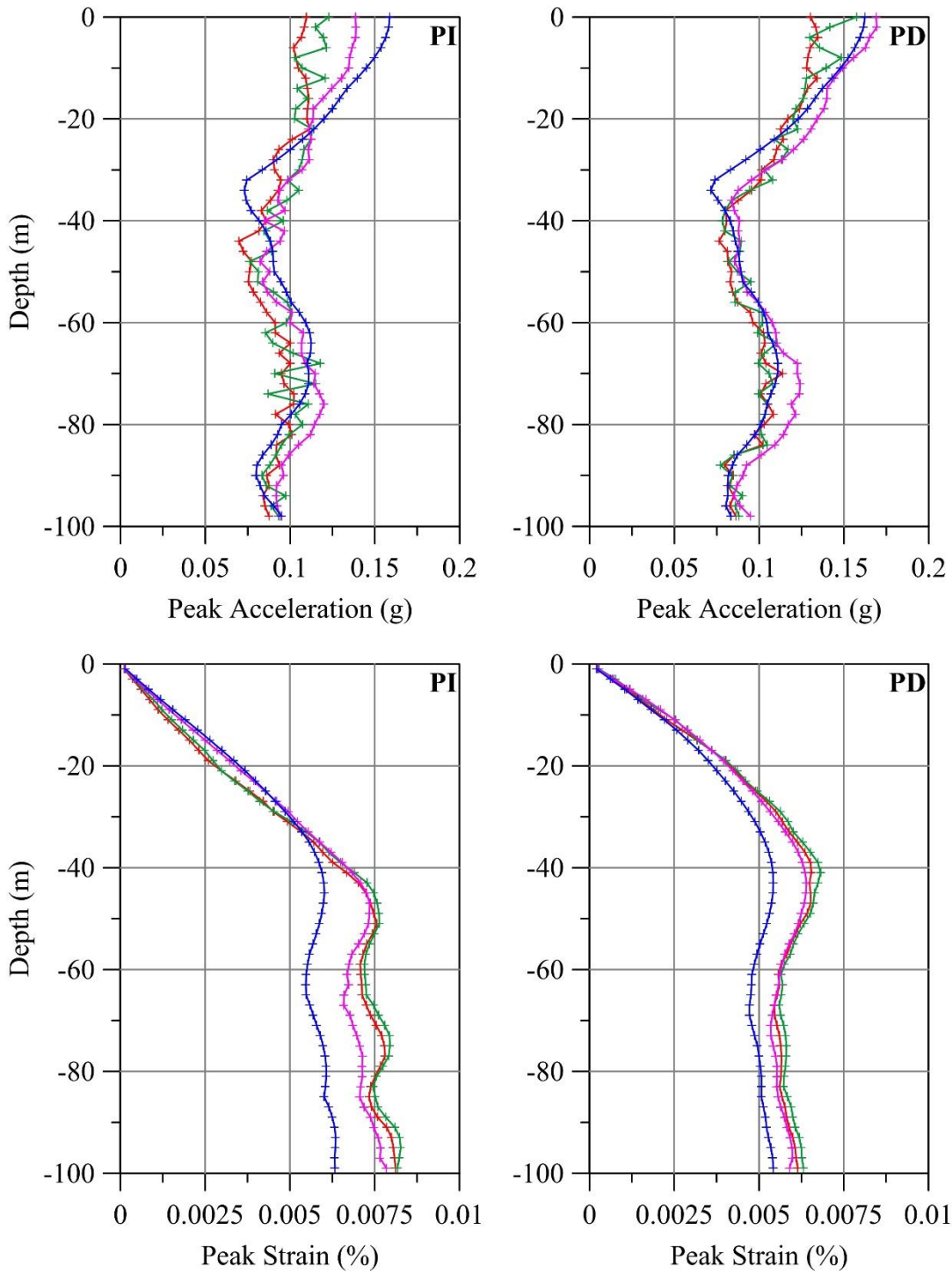


Figure A-32: Peak acceleration and peak strain profiles for site W1 subjected to ground motion

WO3

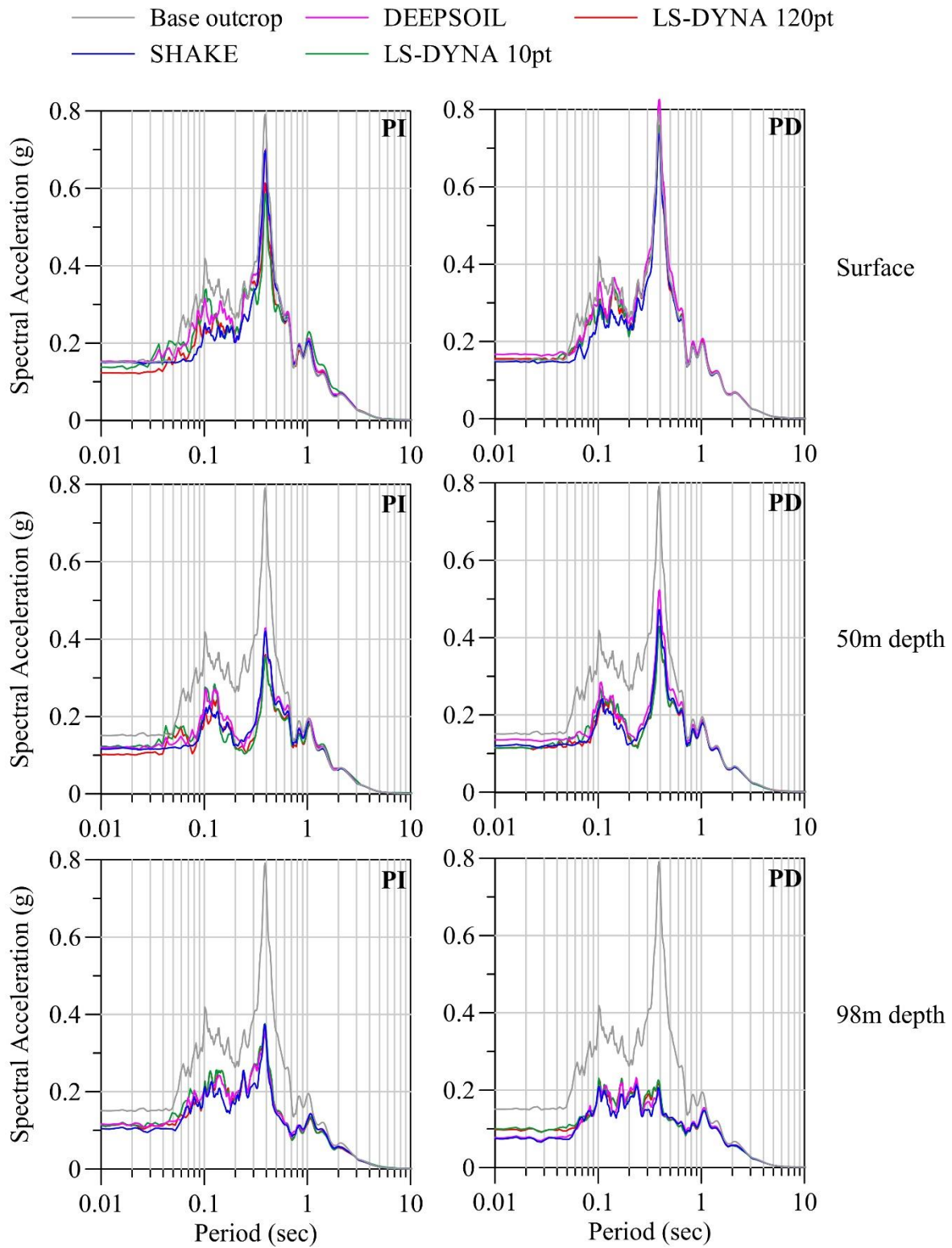


Figure A-33: Acceleration response spectra of the base outcrop motion, and accelerations at three different depths for site W1 subjected to ground motion WO1

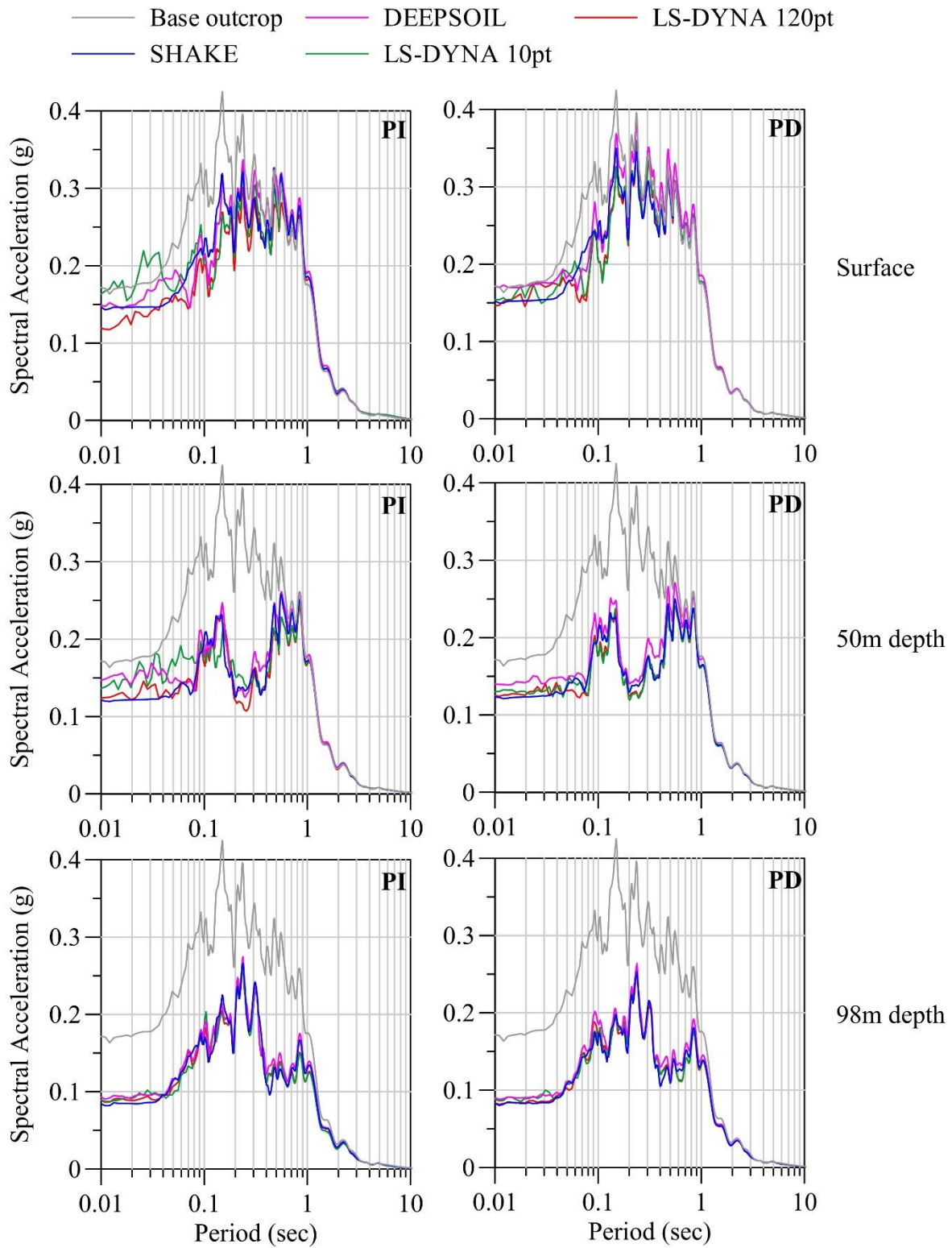


Figure A-34: Acceleration response spectra of the base outcrop motion, and accelerations at three different depths for site W1 subjected to ground motion WO2

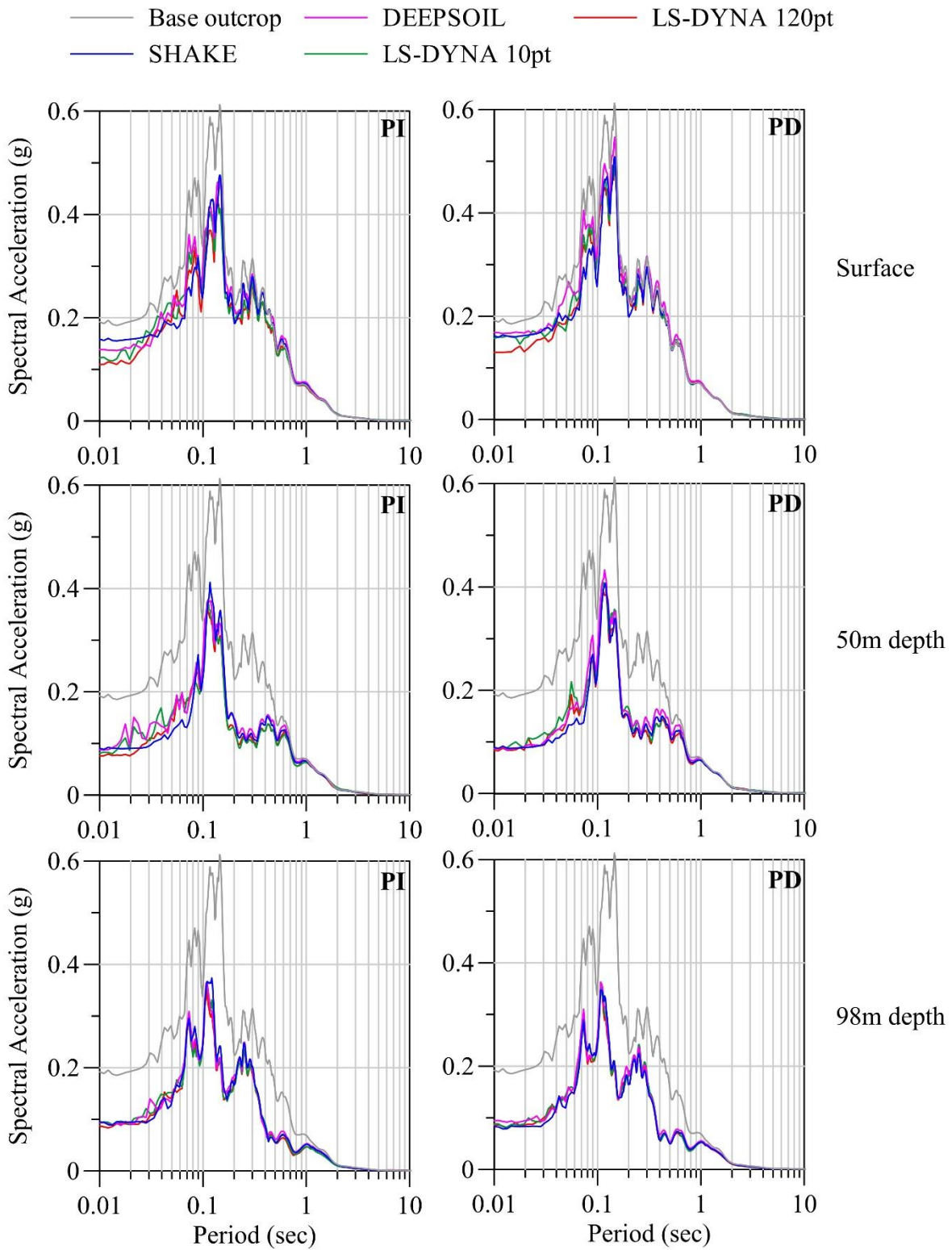


Figure A-35: Acceleration response spectra of the base outcrop motion, and accelerations at three different depths for site W1 subjected to ground motion WO3

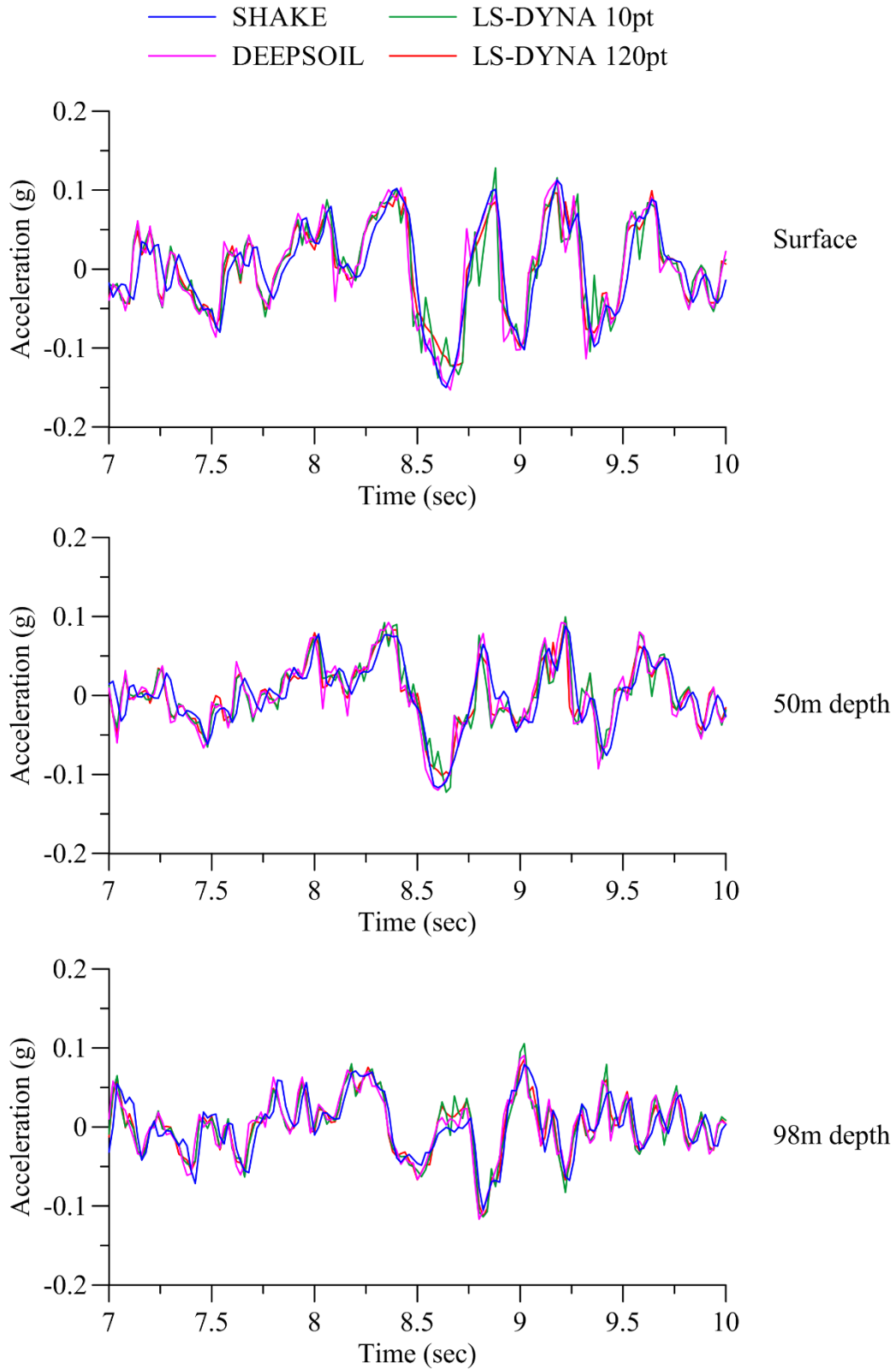


Figure A-36: Acceleration response histories at three different depths for site W1 subjected to ground motion WO1

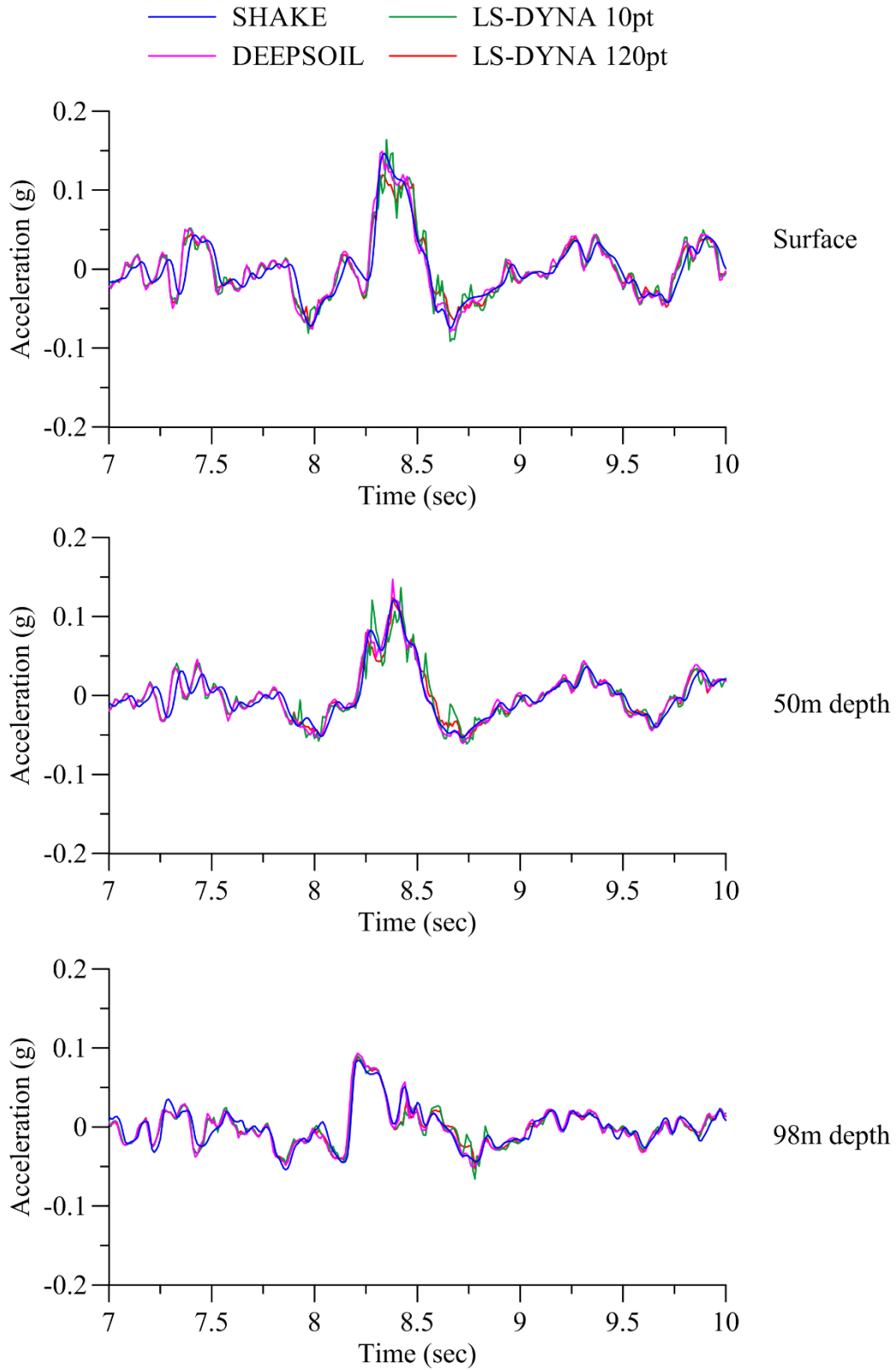


Figure A-37: Acceleration response histories at three different depths for site W1 subjected to ground motion WO2

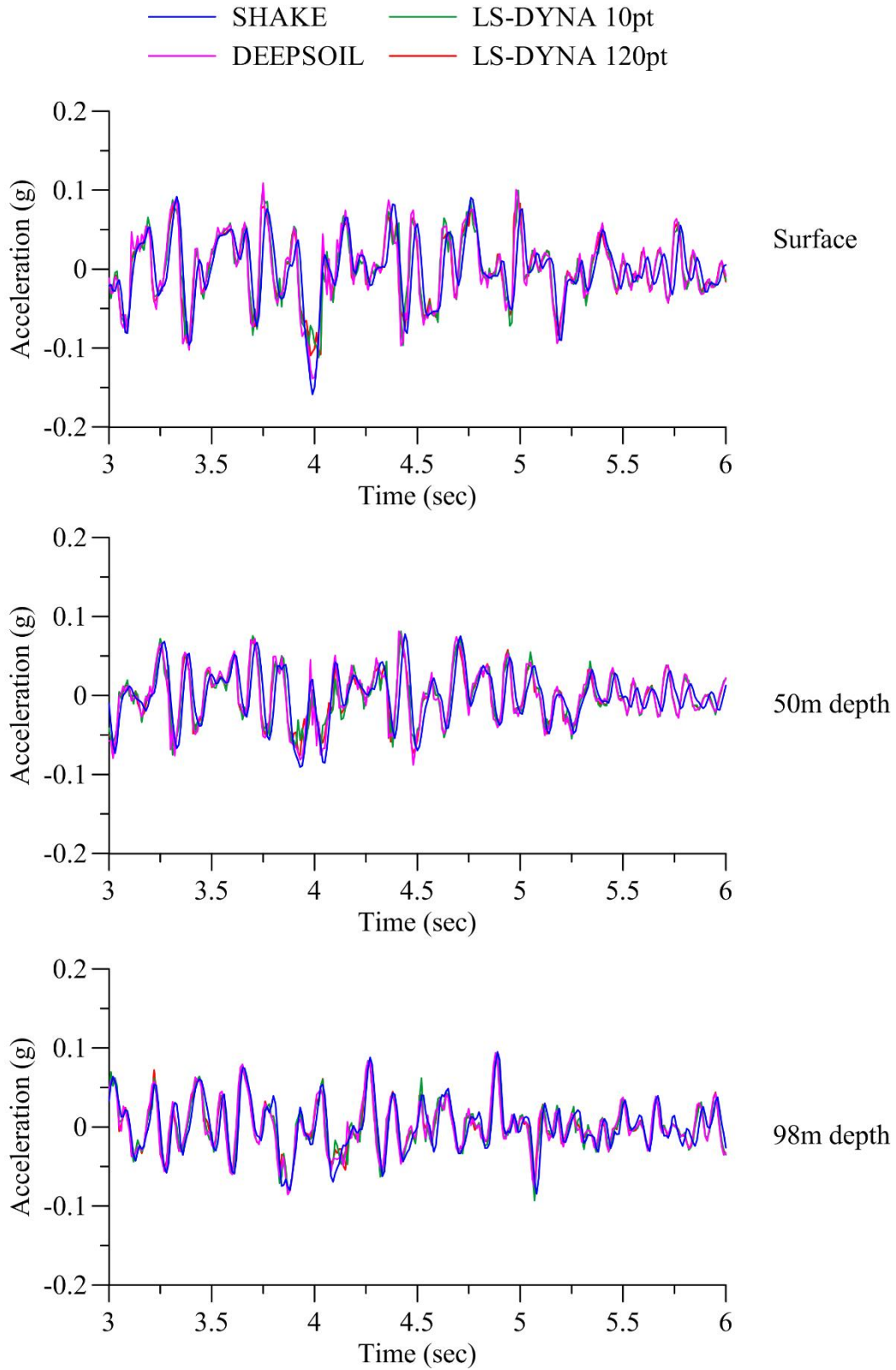


Figure A-38: Acceleration response histories at three different depths for site W1 subjected to ground motion WO3

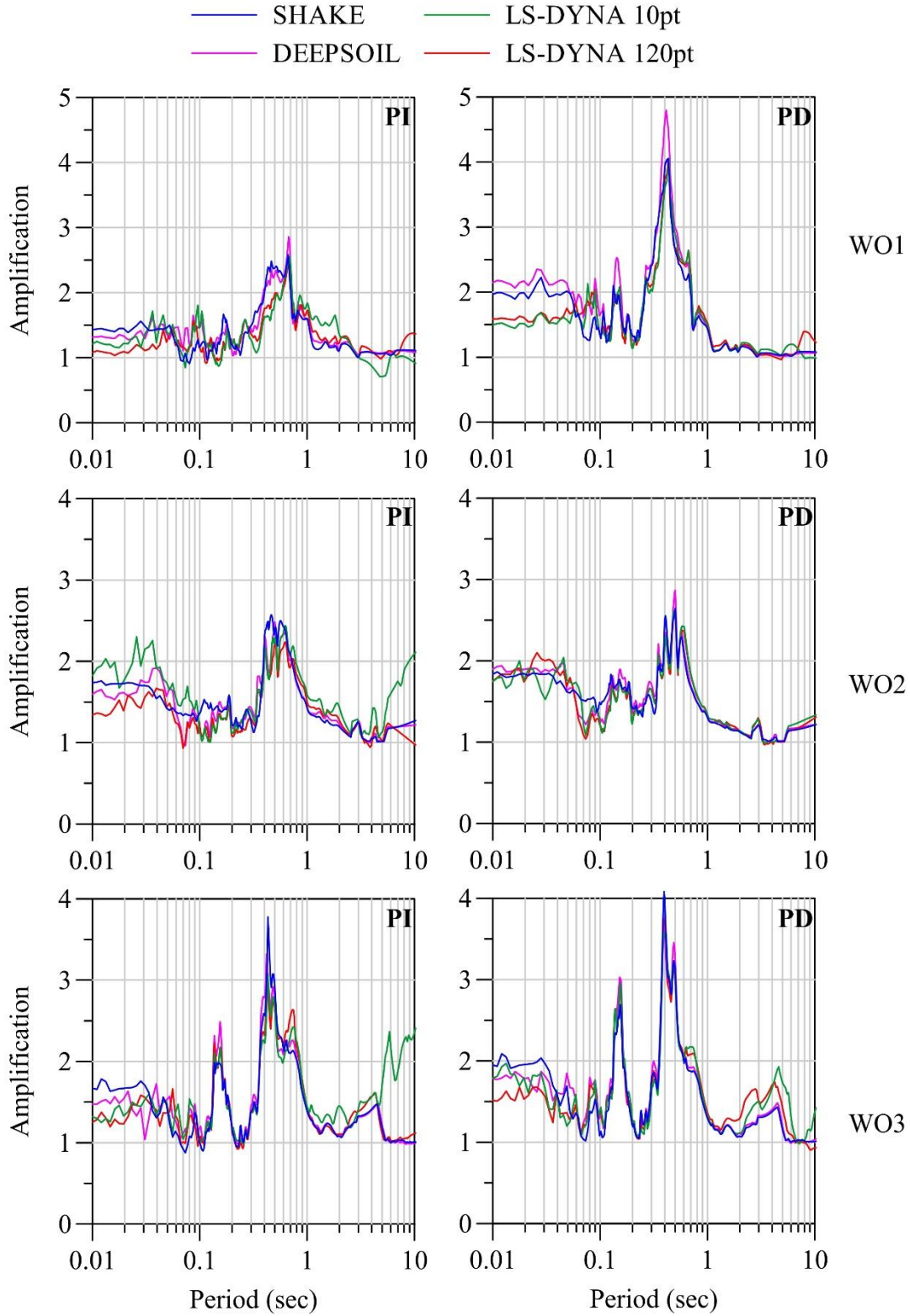


Figure A-39: Spectral amplification of accelerations in site W1 from the base to the surface for ground motions WO1, WO2 and WO3

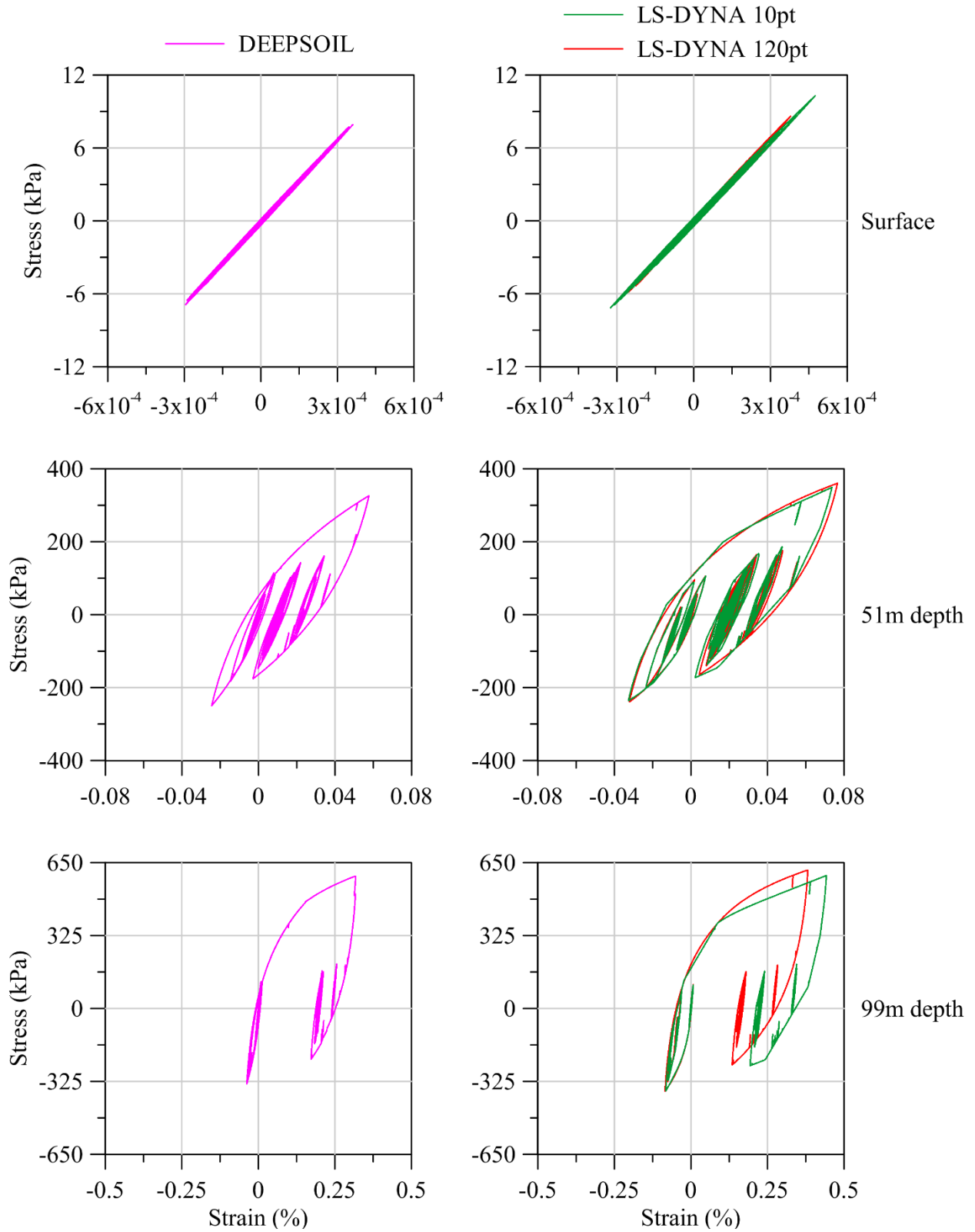


Figure A-40: Stress-strain loops at three different depths for site W1 subjected to ground motion

WP1

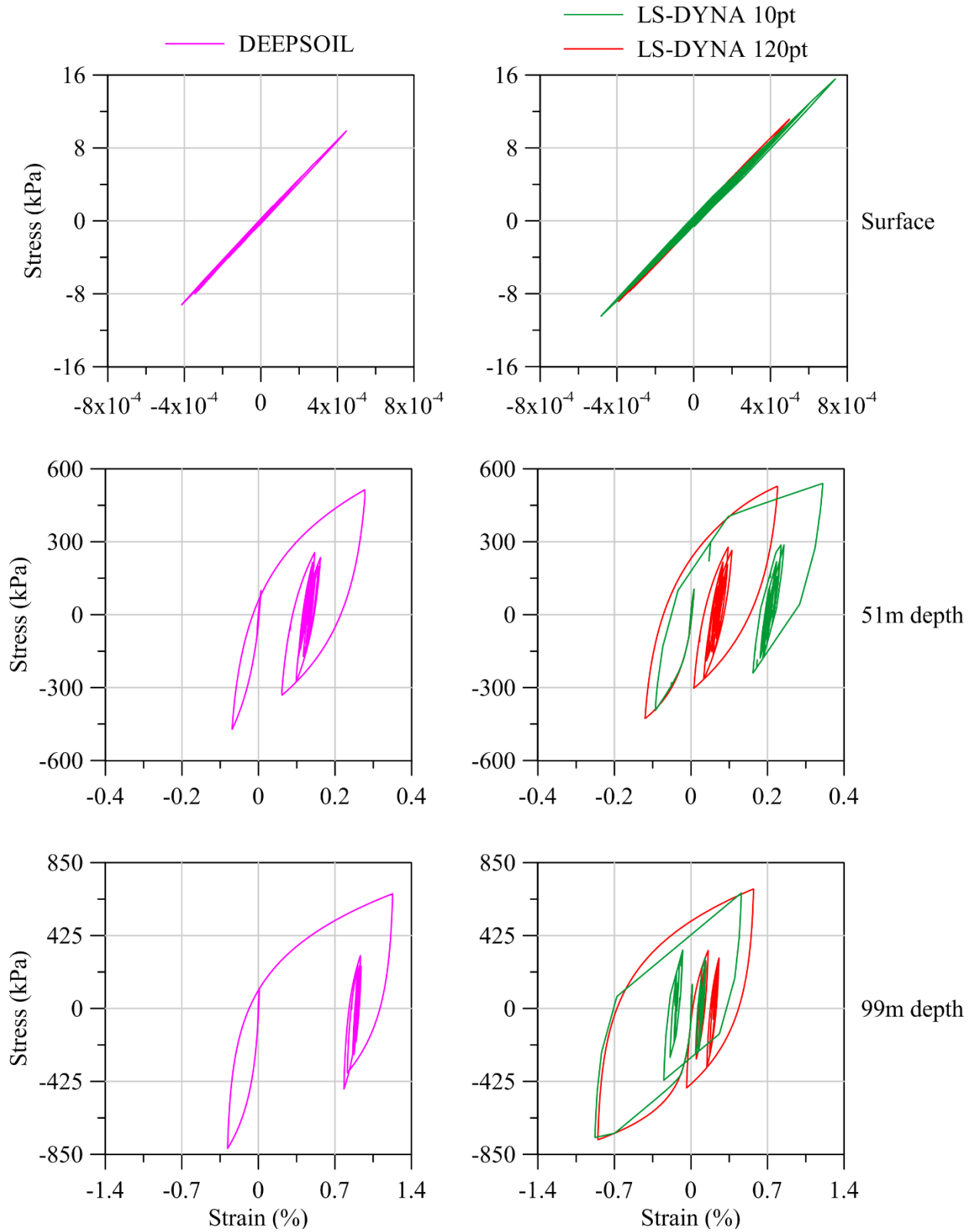


Figure A-41: Stress-strain loops at three different depths for site W1 subjected to ground motion

WP2

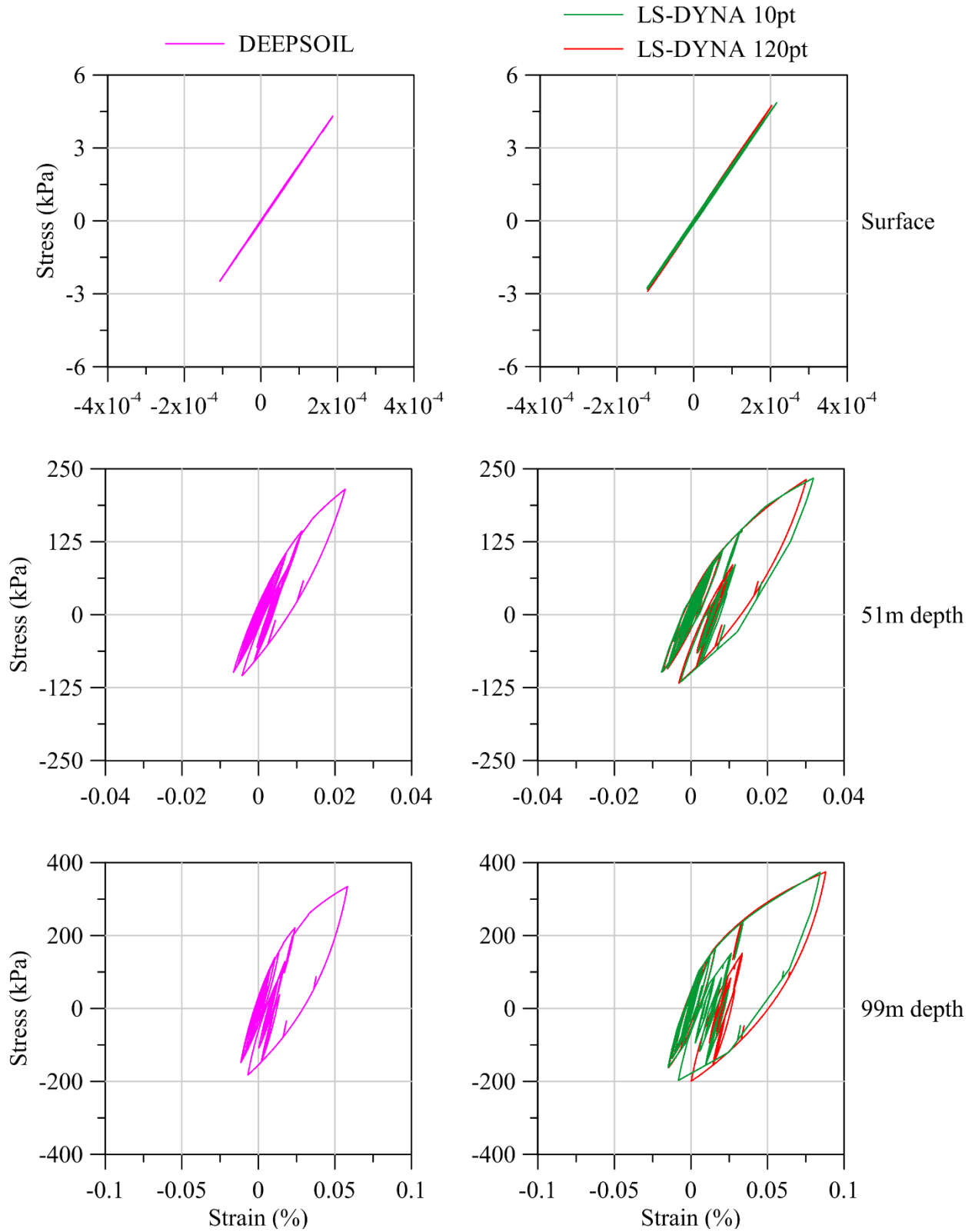
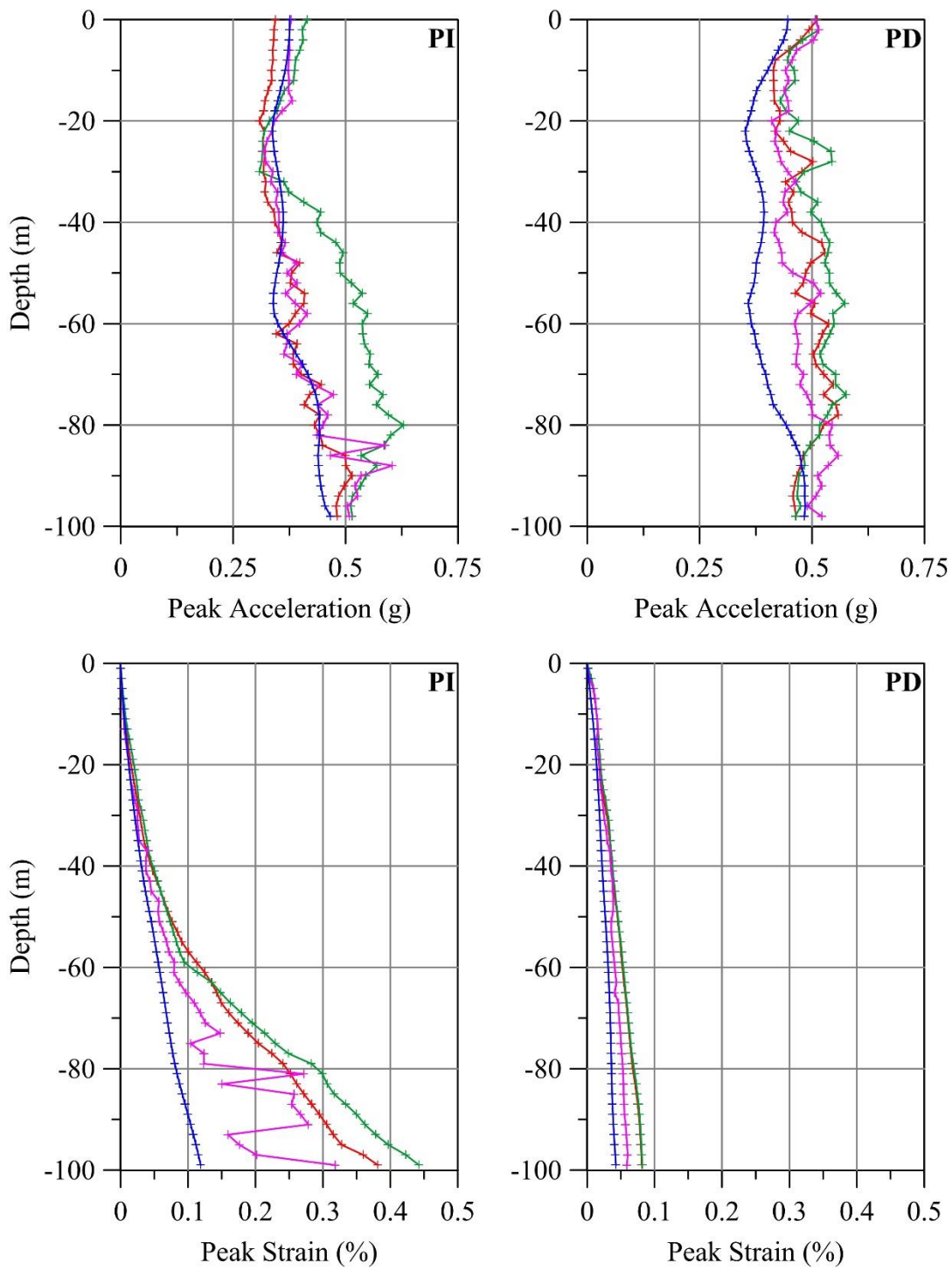


Figure A-42: Stress-strain loops at three different depths for site W1 subjected to ground motion

WP3

+ + SHAKE
 + + DEEPSOIL
 + + LS-DYNA 10pt
 + + LS-DYNA 120pt



**Figure A-43: Peak acceleration and peak strain profiles for site W1 subjected to ground motion
 WP1**

+ + SHAKE
 + + DEEPSOIL
 + + LS-DYNA 10pt
 + + LS-DYNA 120pt

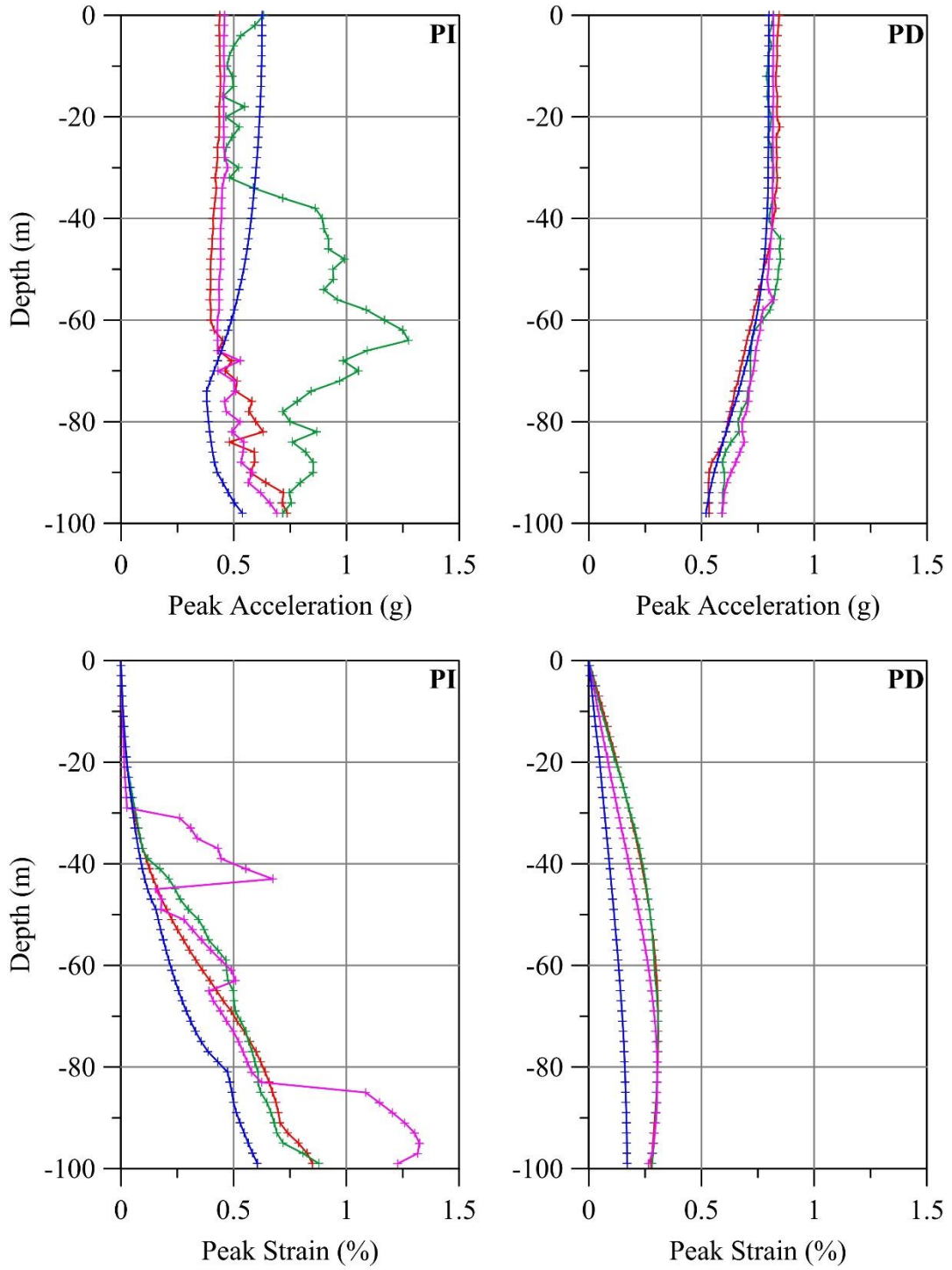


Figure A-44: Peak acceleration and peak strain profiles for site W1 subjected to ground motion WP2

+ + + SHAKE
 + + + DEEPSOIL
 + + + LS-DYNA 10pt
 + + + LS-DYNA 120pt

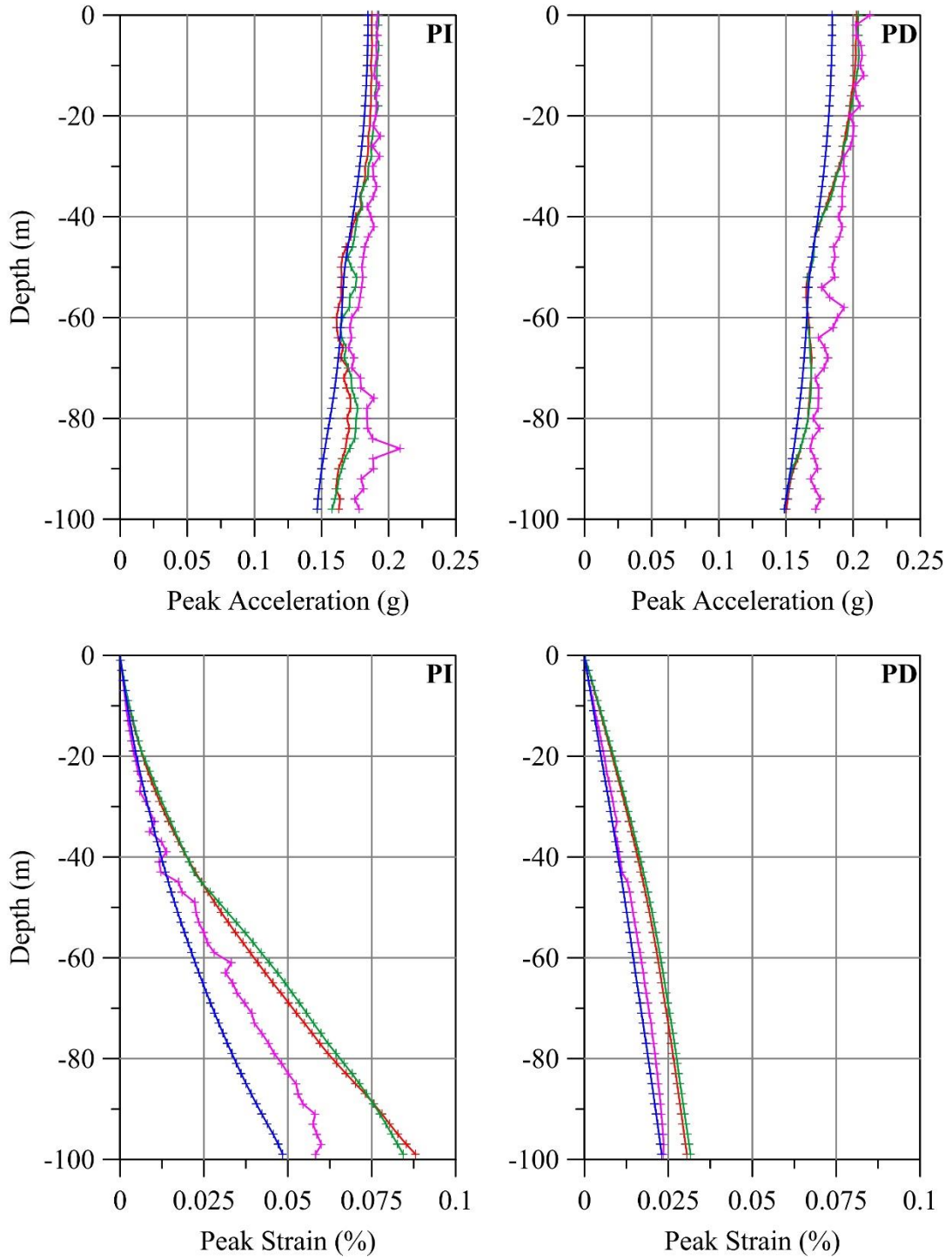


Figure A-45: Peak acceleration and peak strain profiles for site W1 subjected to ground motion WP3

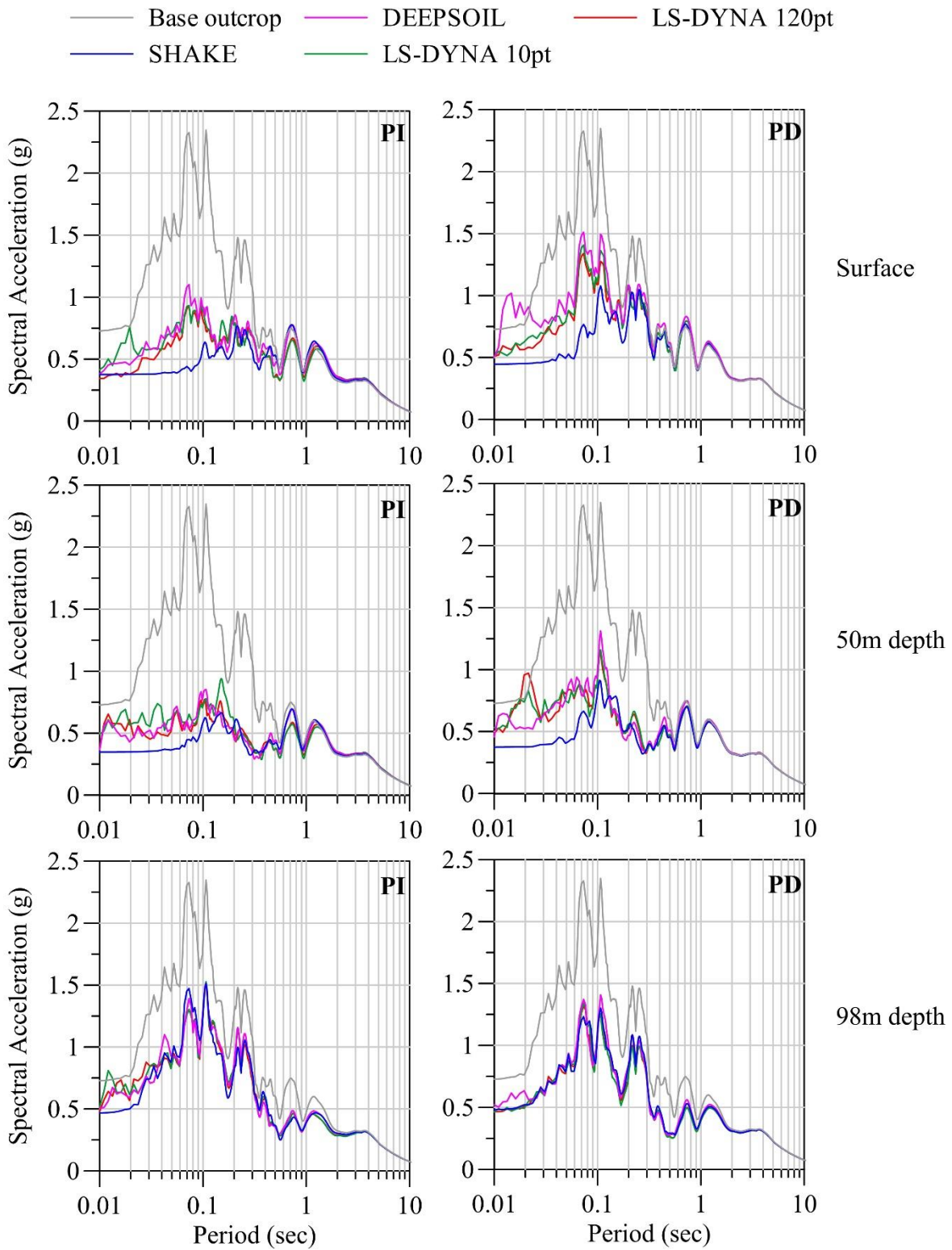


Figure A-46: Acceleration response spectra of the base outcrop motion, and accelerations at three different depths for site W1 subjected to ground motion WP1

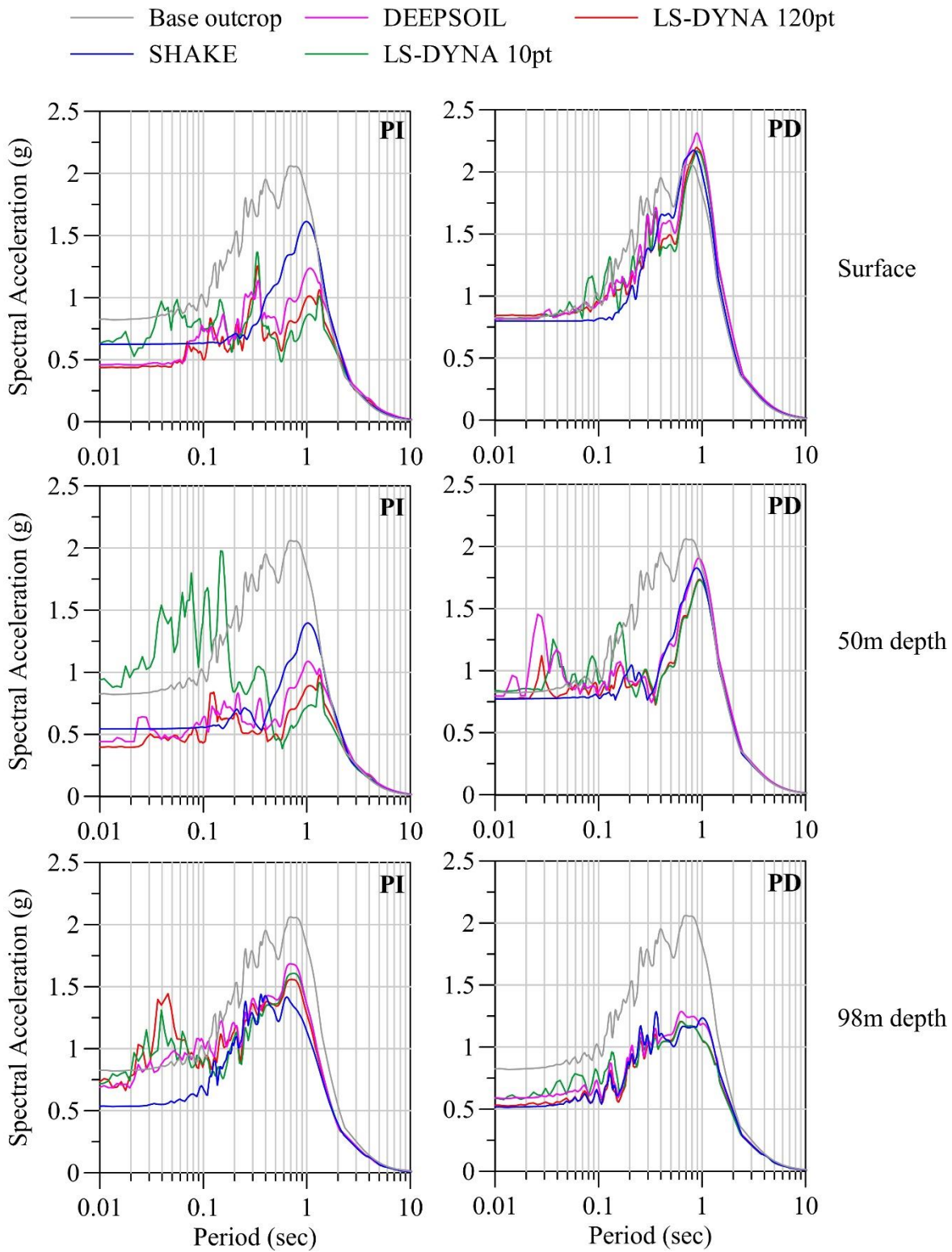


Figure A-47: Acceleration response spectra of the base outcrop motion, and accelerations at three different depths for site W1 subjected to ground motion WP2

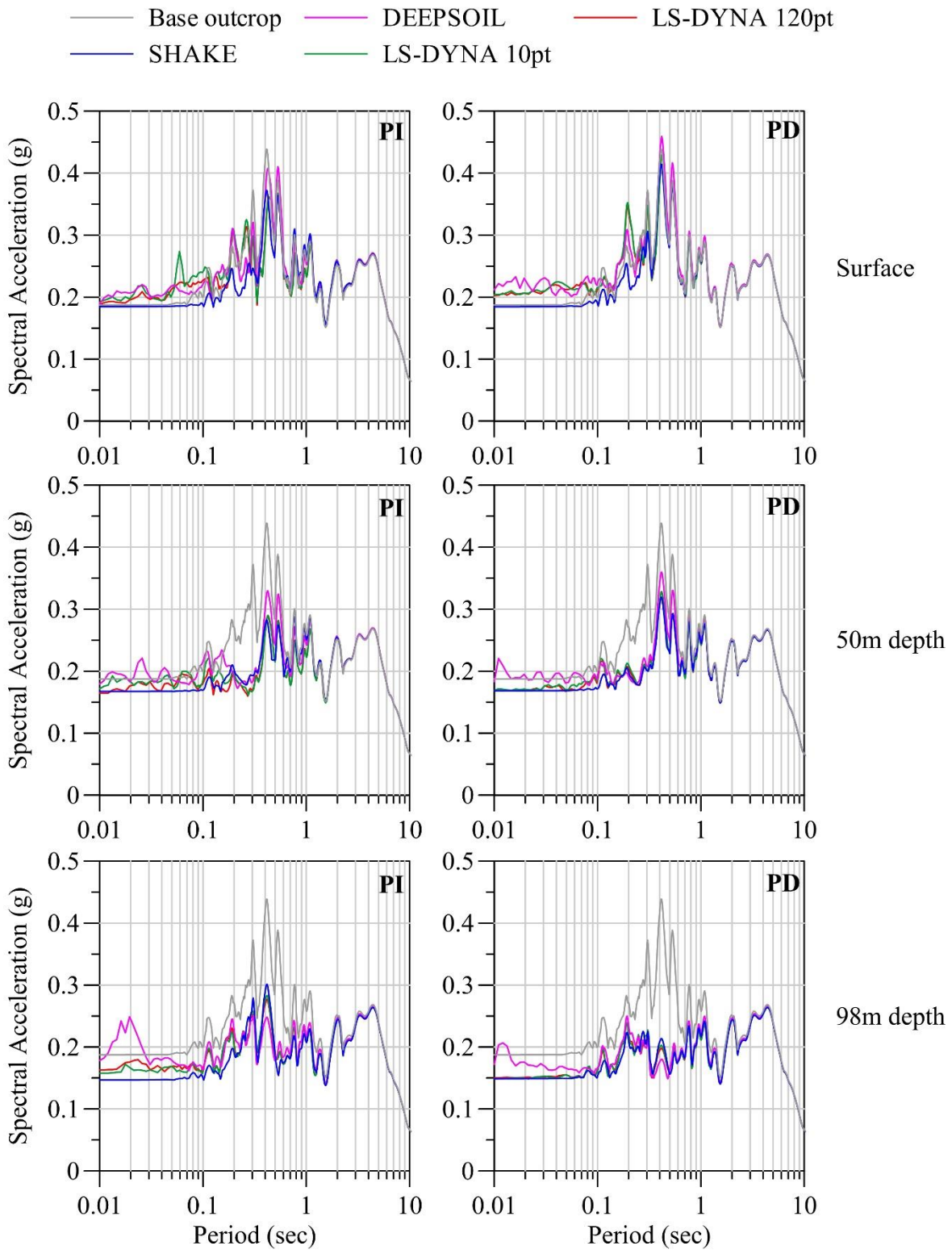


Figure A-48: Acceleration response spectra of the base outcrop motion, and accelerations at three different depths for site W1 subjected to ground motion WP3

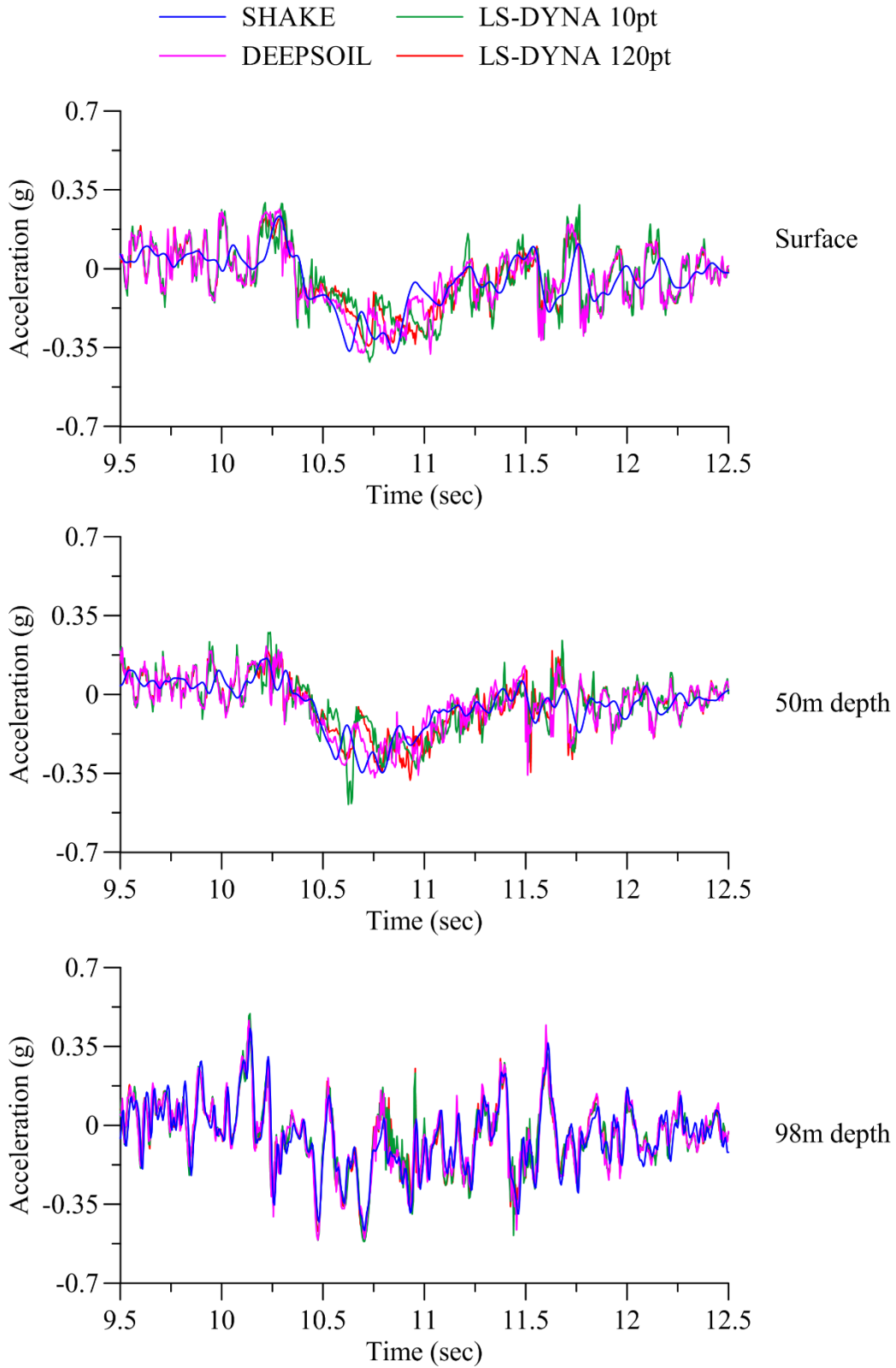


Figure A-49: Acceleration response histories at three different depths for site W1 subjected to ground motion WP1

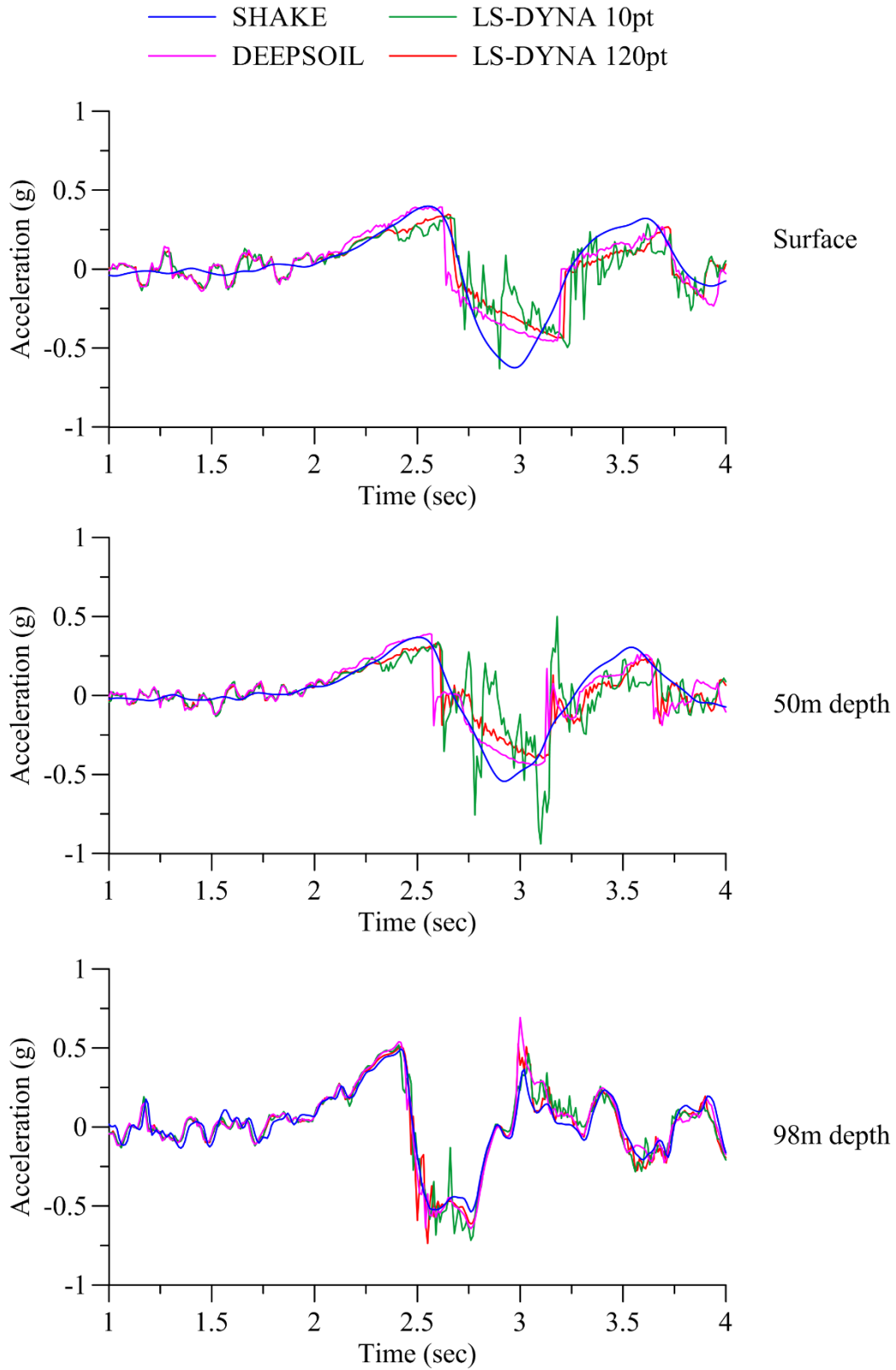


Figure A-50: Acceleration response histories at three different depths for site W1 subjected to ground motion WP2

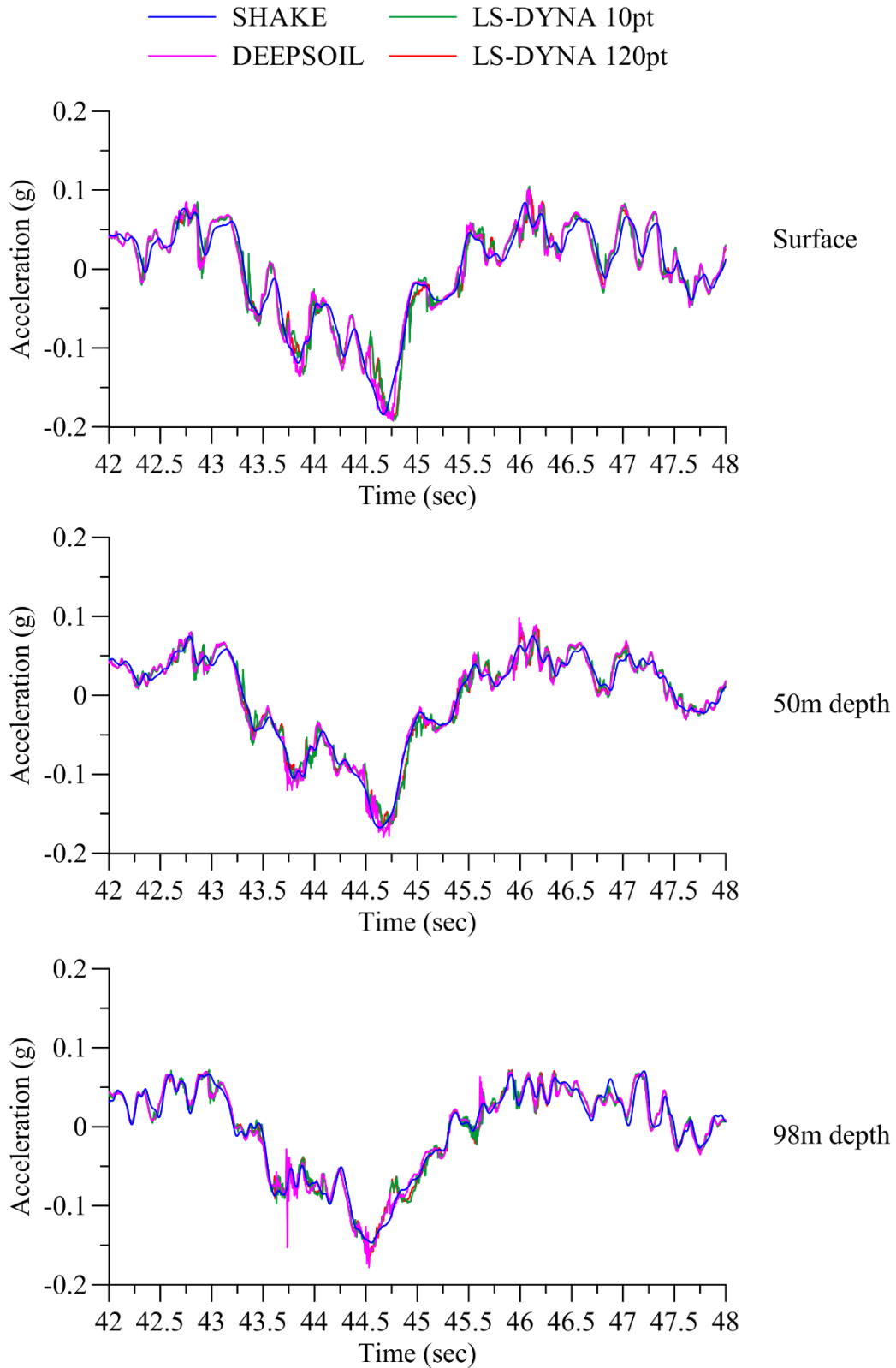


Figure A-51: Acceleration response histories at three different depths for site W1 subjected to ground motion WP3

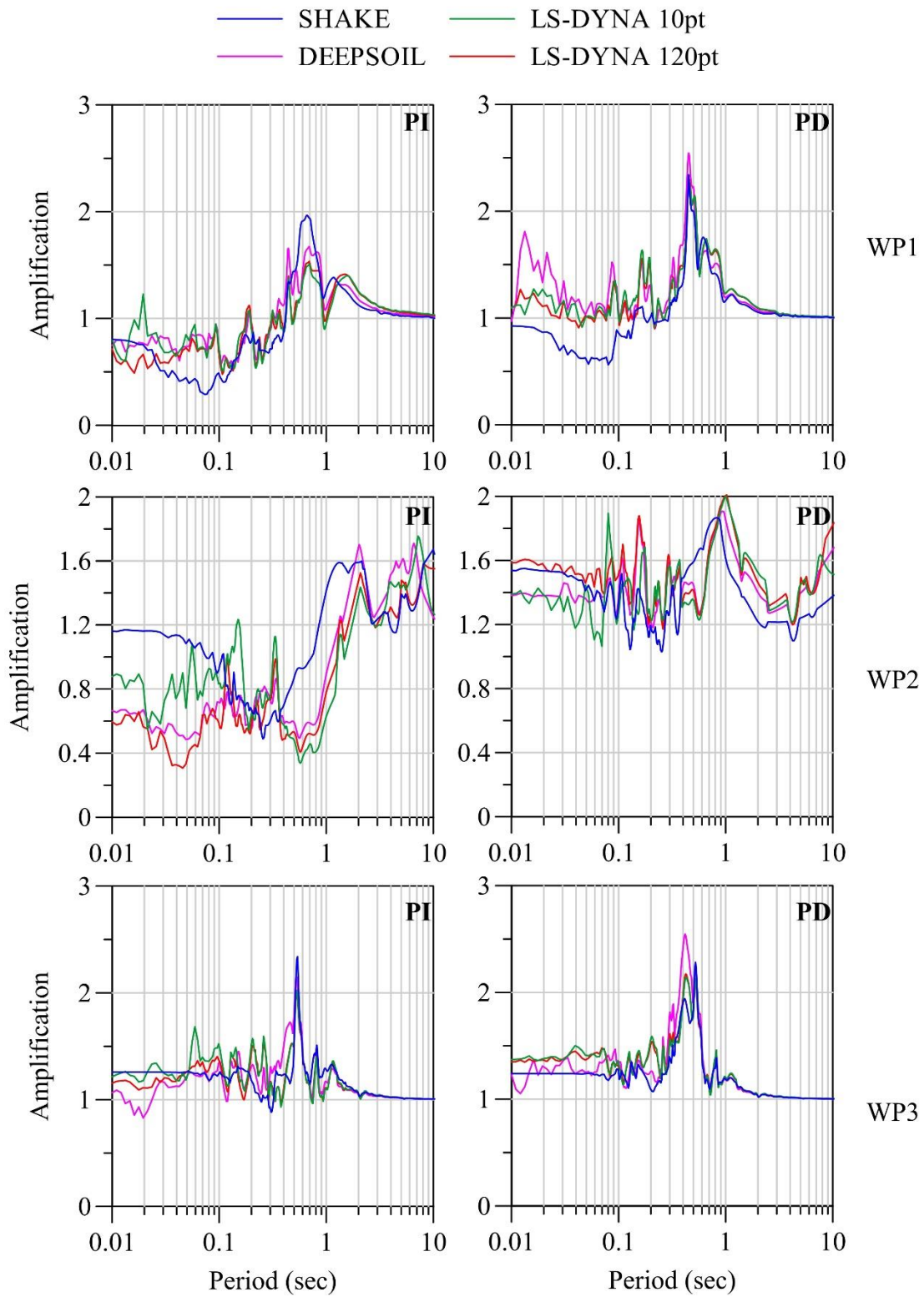


Figure A-52: Spectral amplification of accelerations in site W1 from the base to the surface for ground motions WP1, WP2 and WP3

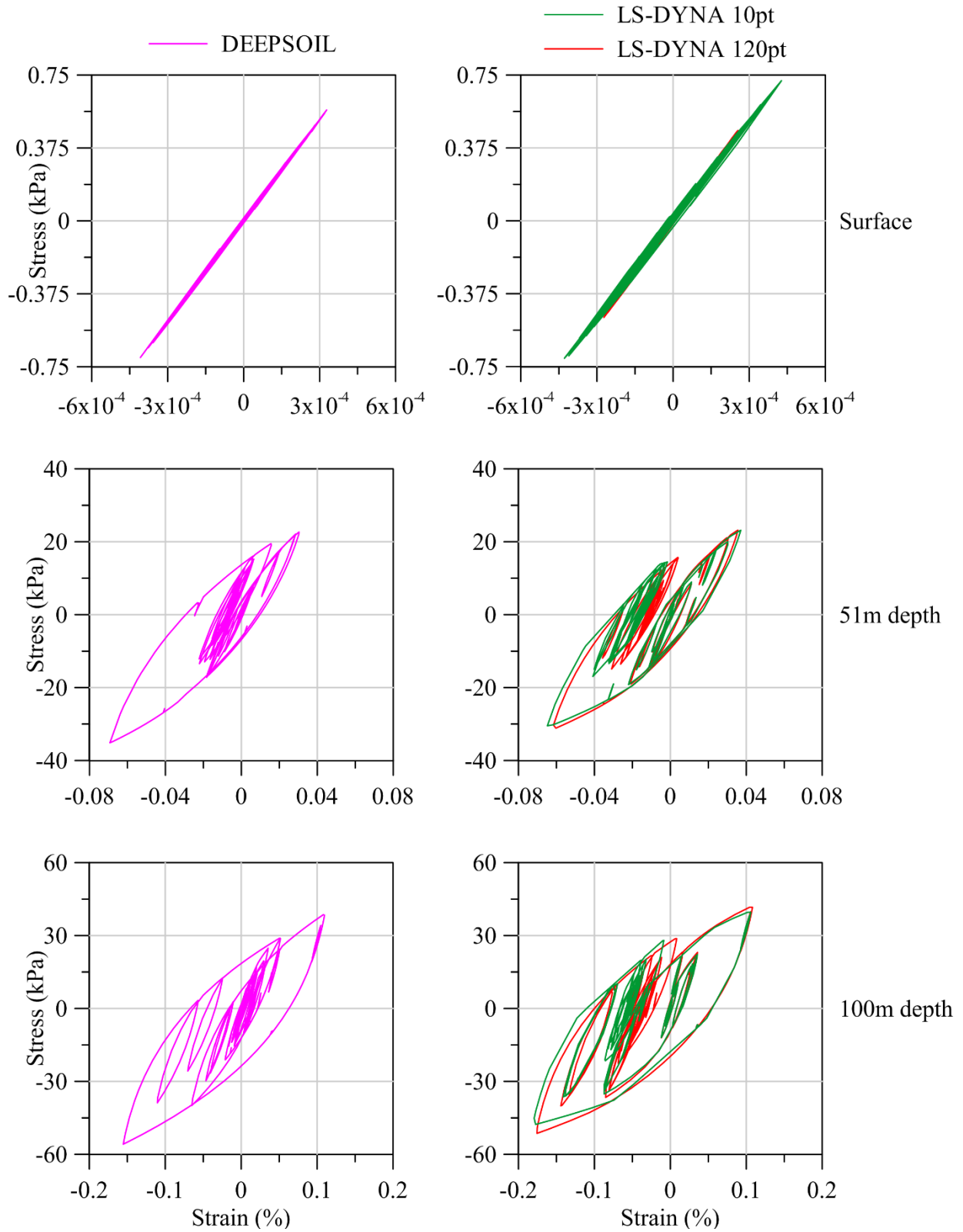


Figure A-53: Stress-strain loops at three different depths for site W2 subjected to ground motion

W01

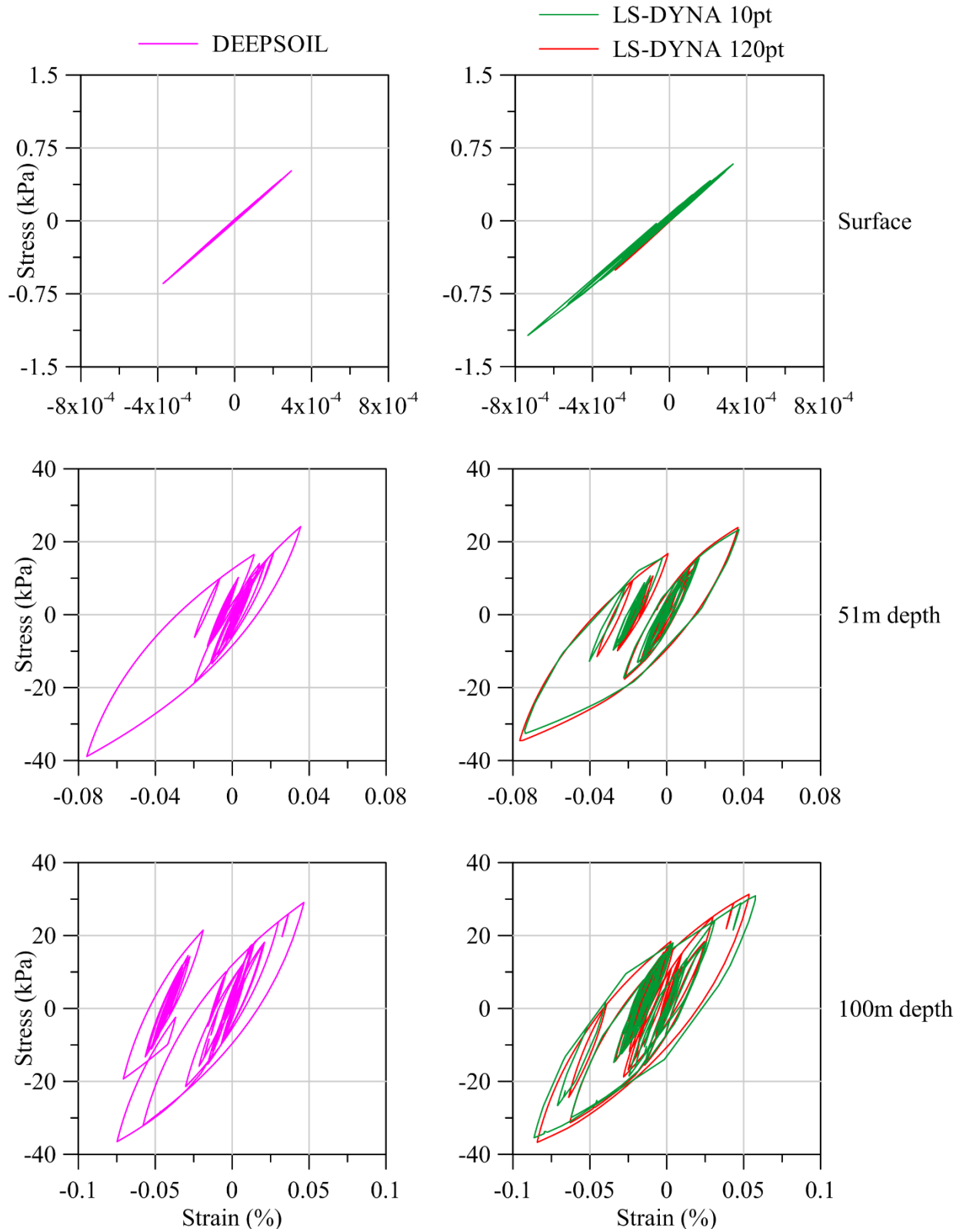


Figure A-54: Stress-strain loops at three different depths for site W2 subjected to ground motion

WO2

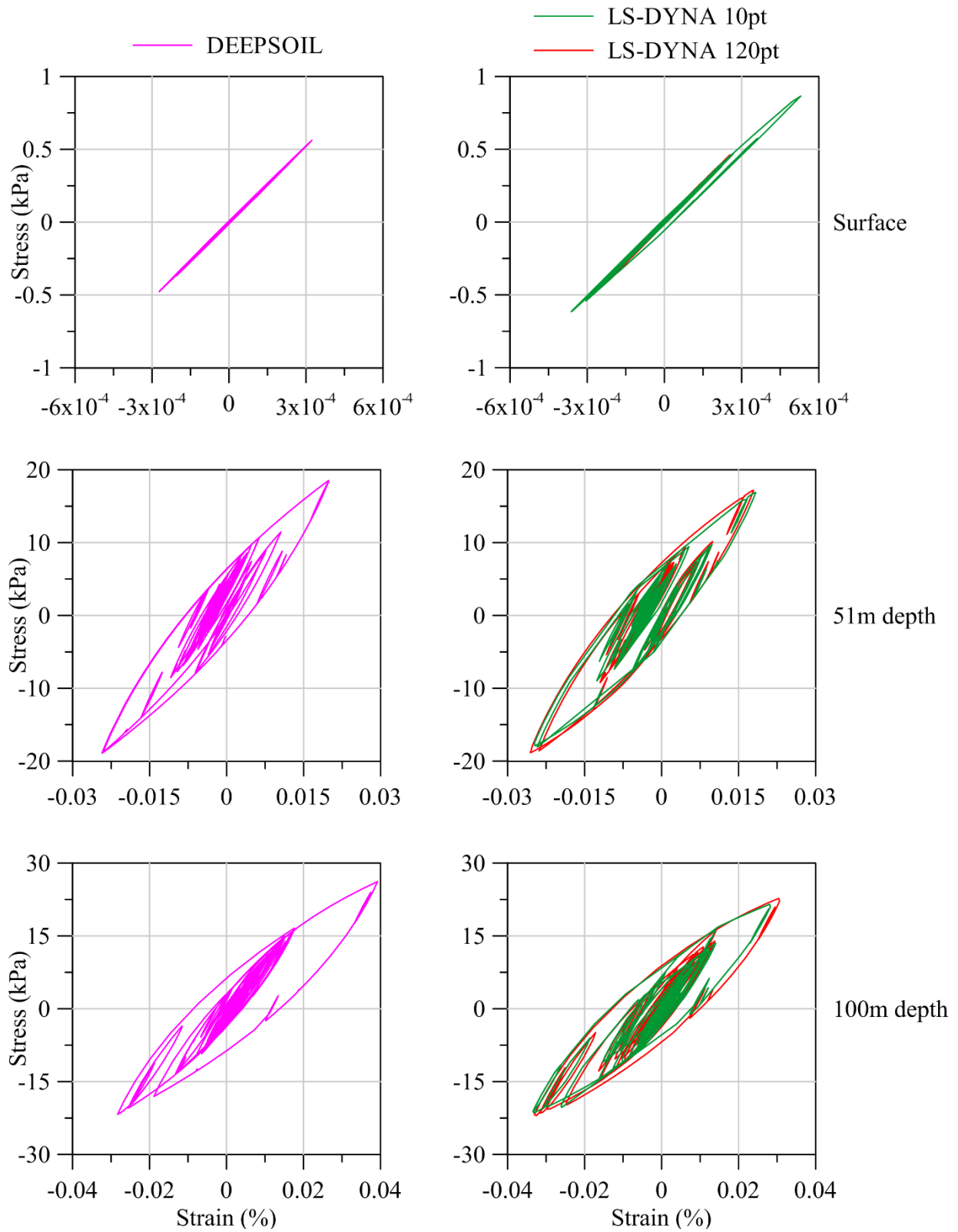


Figure A-55: Stress-strain loops at three different depths for site W2 subjected to ground motion

WO3

+ + SHAKE
 + + DEEPSOIL
 + + LS-DYNA 10pt
 + + LS-DYNA 120pt

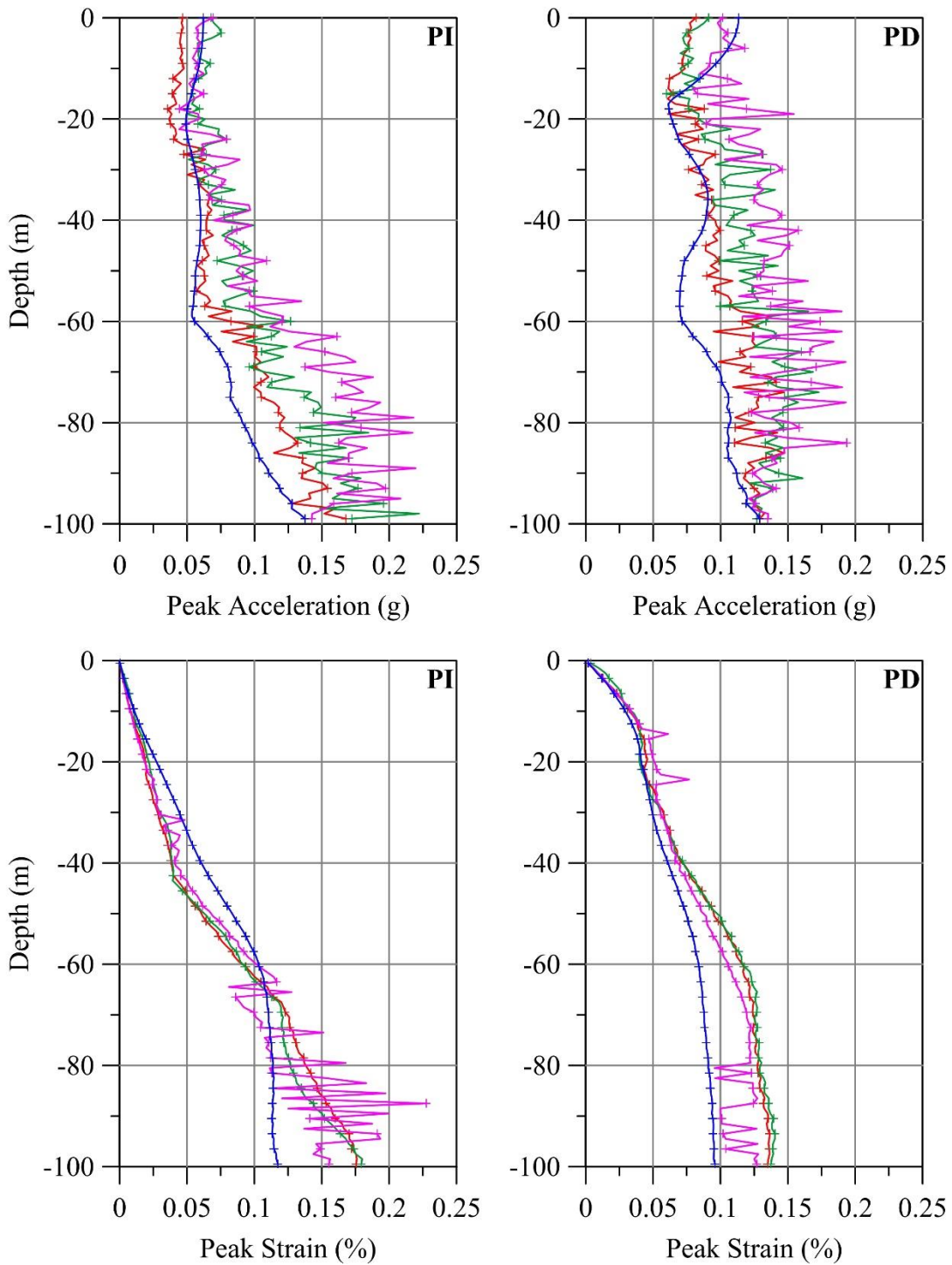


Figure A-56: Peak acceleration and peak strain profiles for site W2 subjected to ground motion

WO1

+ + SHAKE
 + + DEEPSOIL
 + + LS-DYNA 10pt
 + + LS-DYNA 120pt

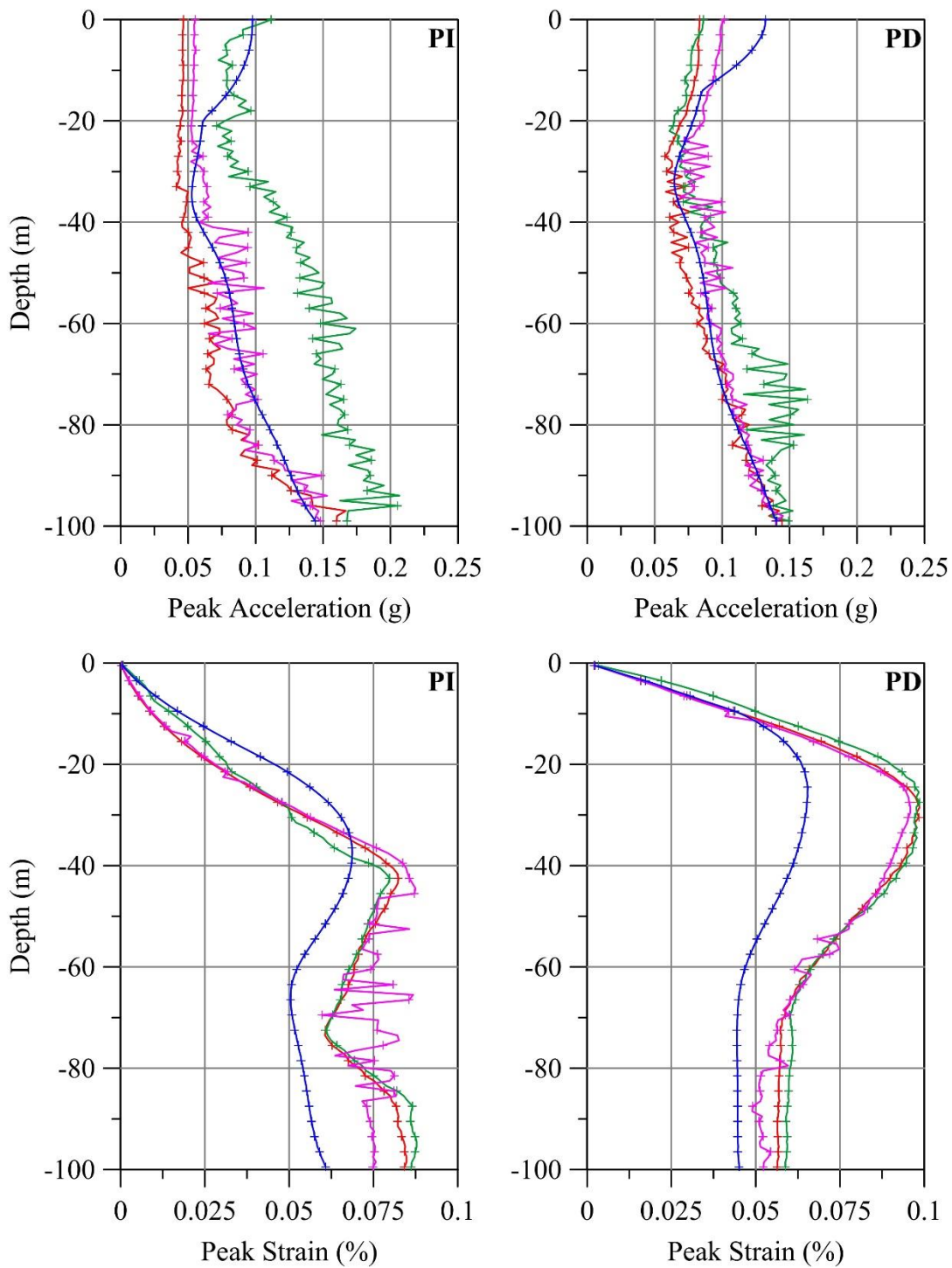


Figure A-57: Peak acceleration and peak strain profiles for site W2 subjected to ground motion

WO2

+ + SHAKE
 + + DEEPSOIL
 + + LS-DYNA 10pt
 + + LS-DYNA 120pt

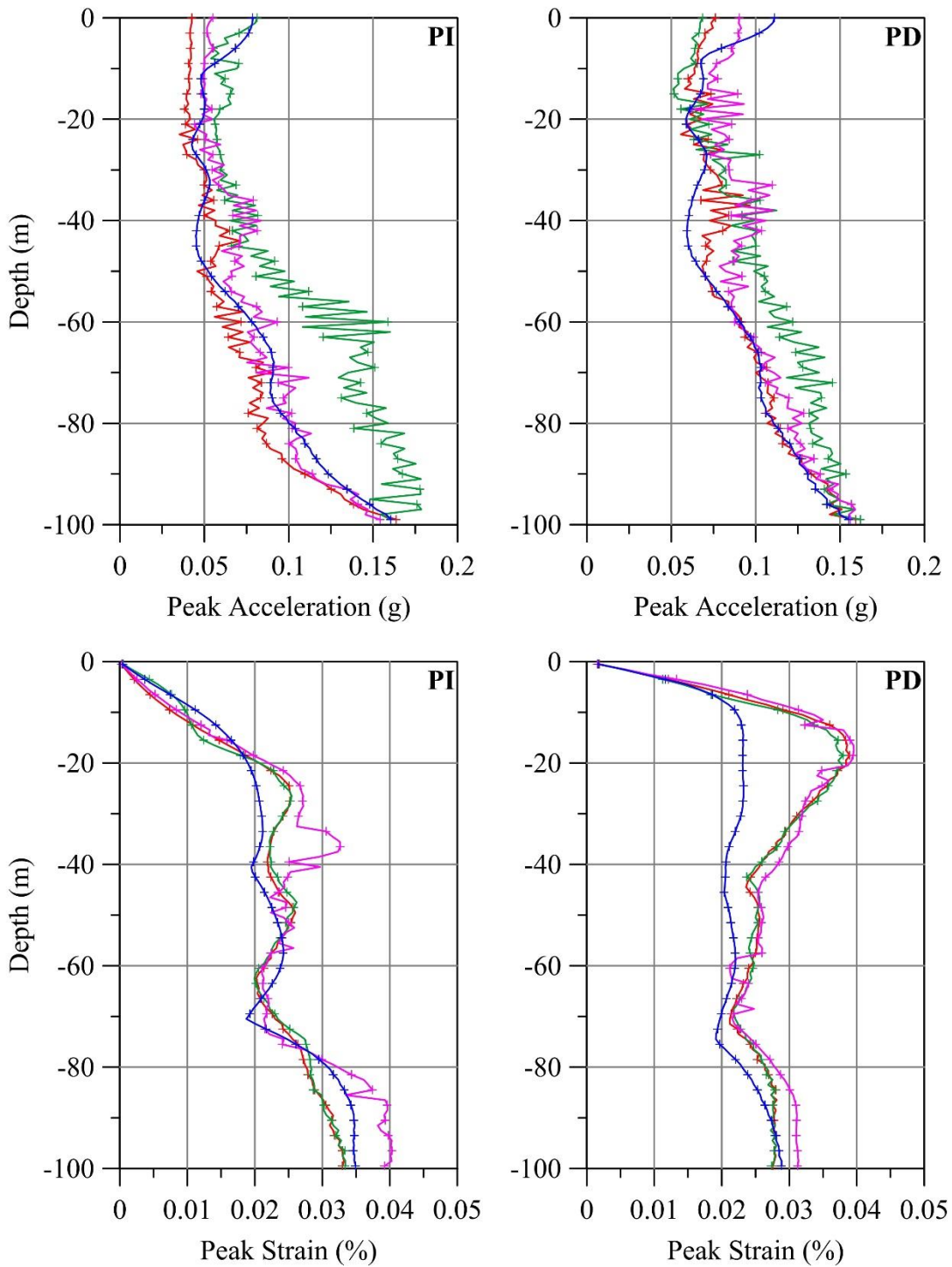


Figure A-58: Peak acceleration and peak strain profiles for site W2 subjected to ground motion

WO3

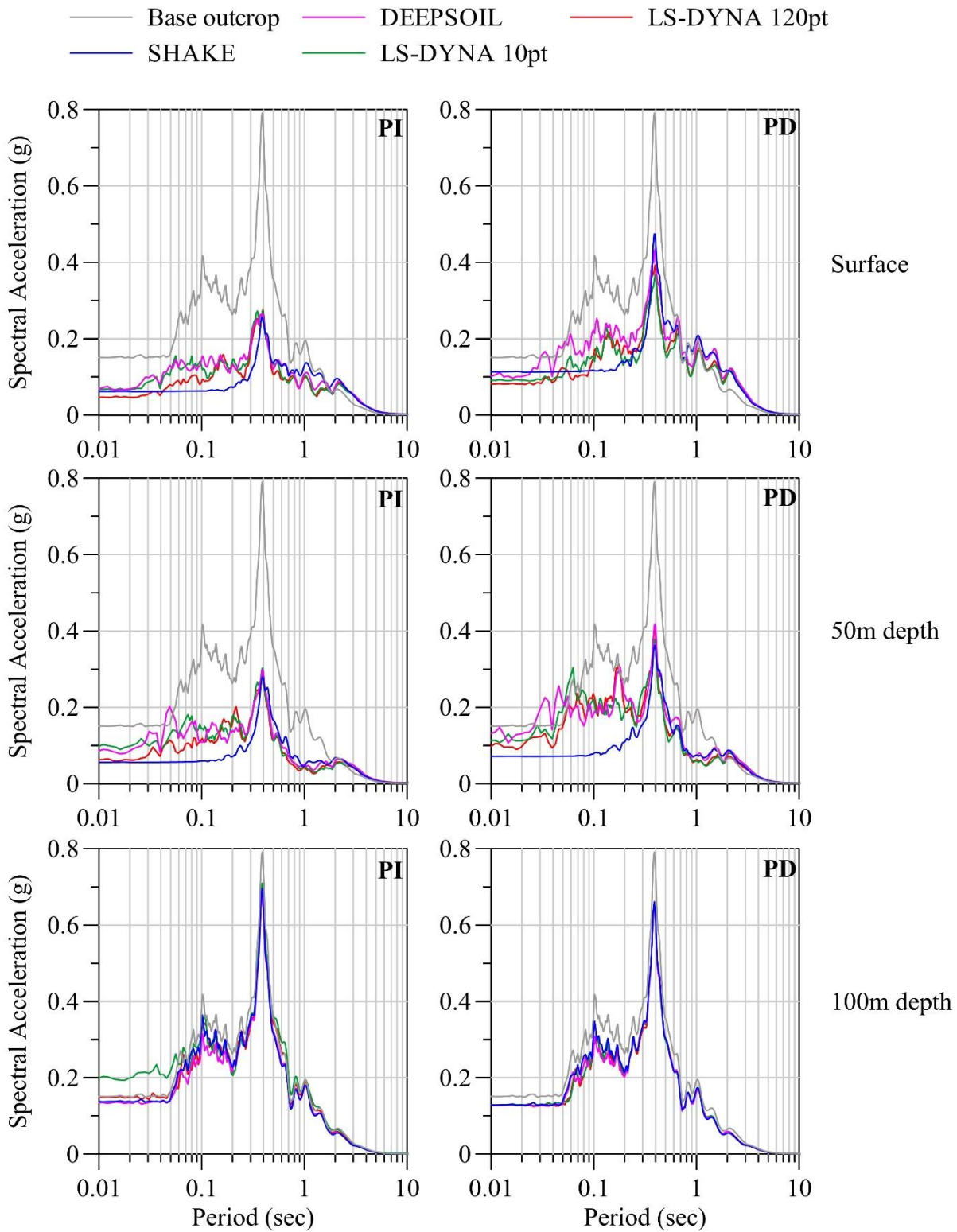


Figure A-59: Acceleration response spectra of the base outcrop motion, and accelerations at three different depths for site W2 subjected to ground motion WO1

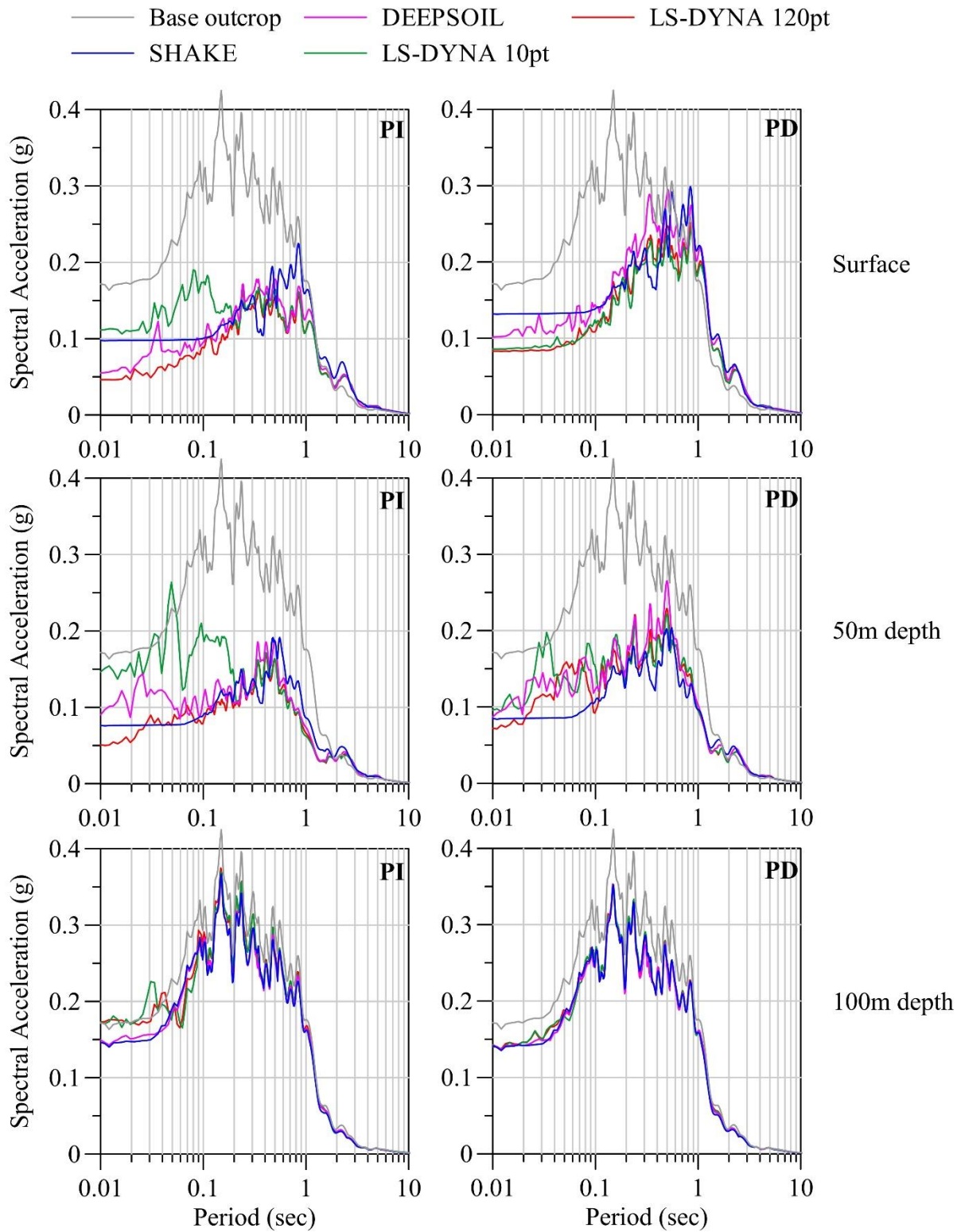


Figure A-60: Acceleration response spectra of the base outcrop motion, and accelerations at three different depths for site W2 subjected to ground motion WO2

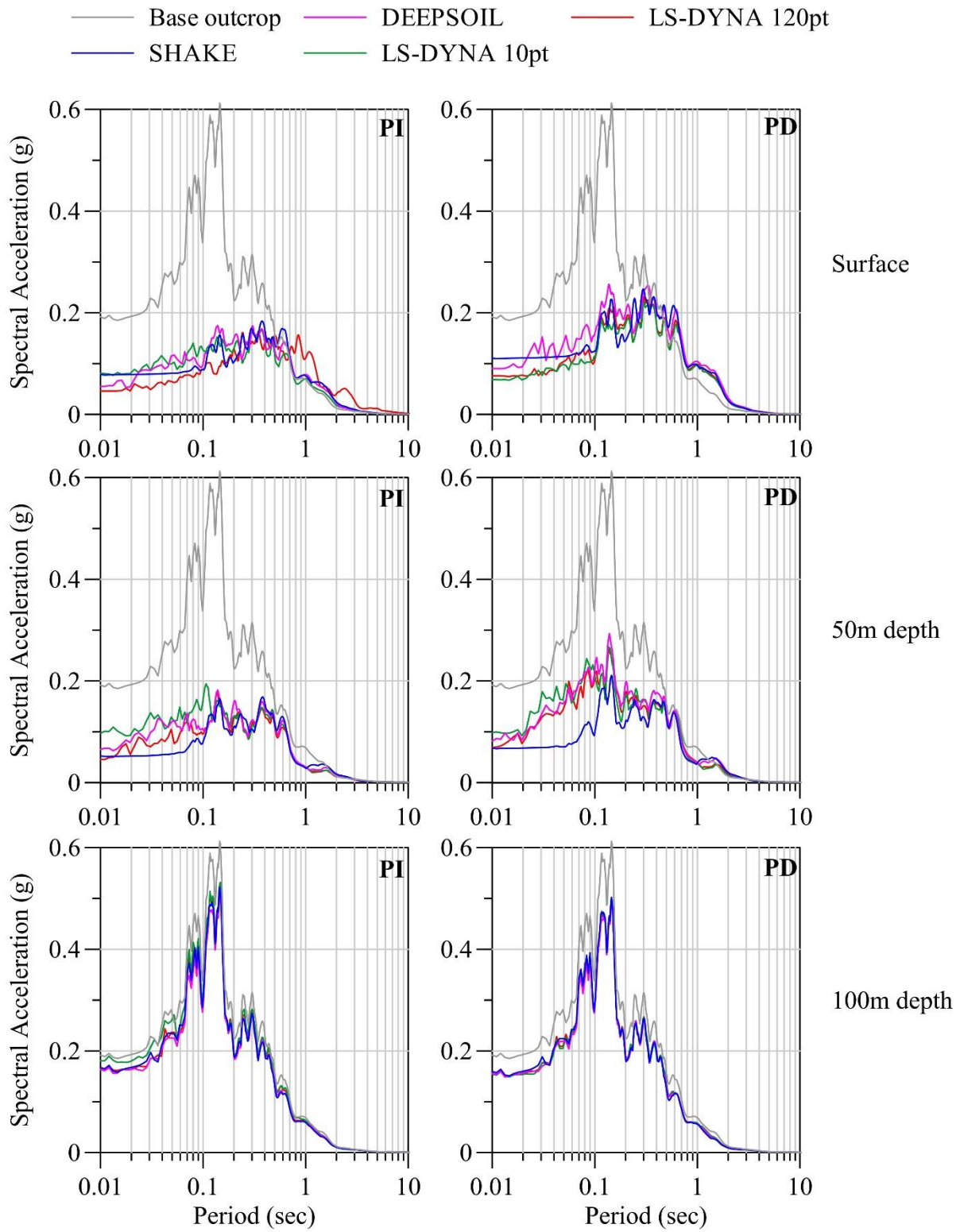


Figure A-61: Acceleration response spectra of the base outcrop motion, and accelerations at three different depths for site W2 subjected to ground motion WO3

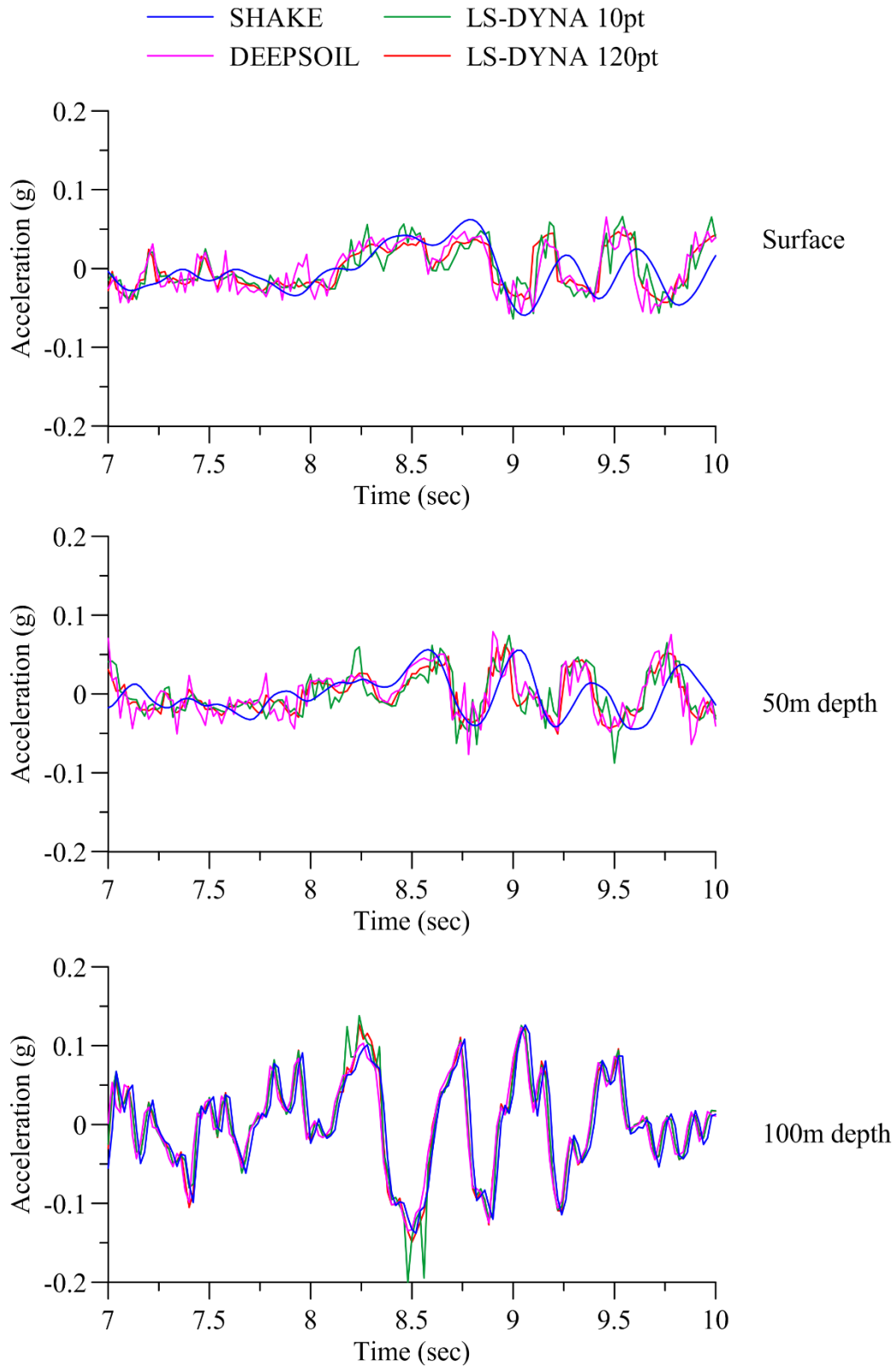


Figure A-62: Acceleration response histories at three different depths for site W2 subjected to ground motion WO1

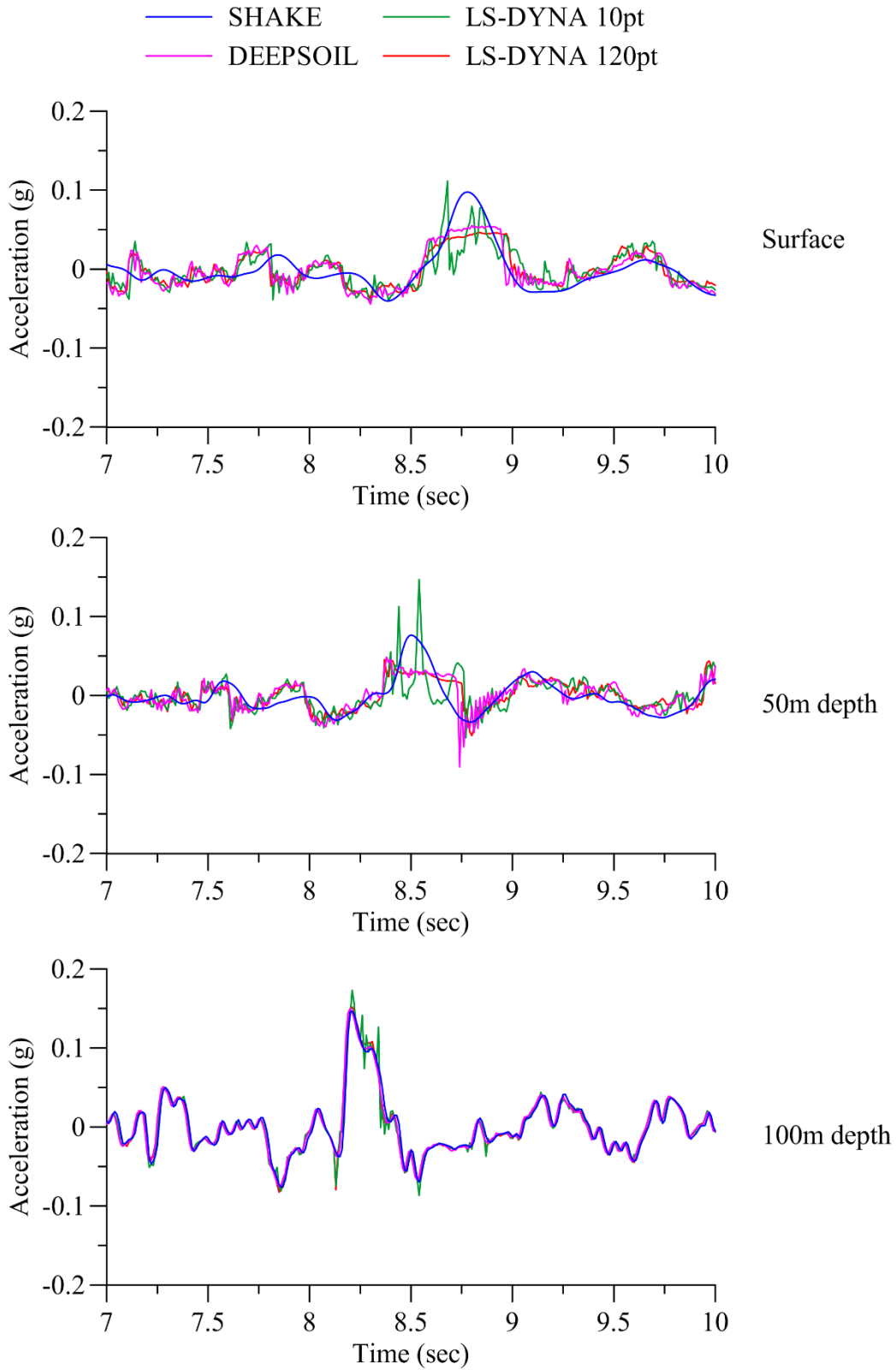


Figure A-63: Acceleration response histories at three different depths for site W2 subjected to ground motion WO2

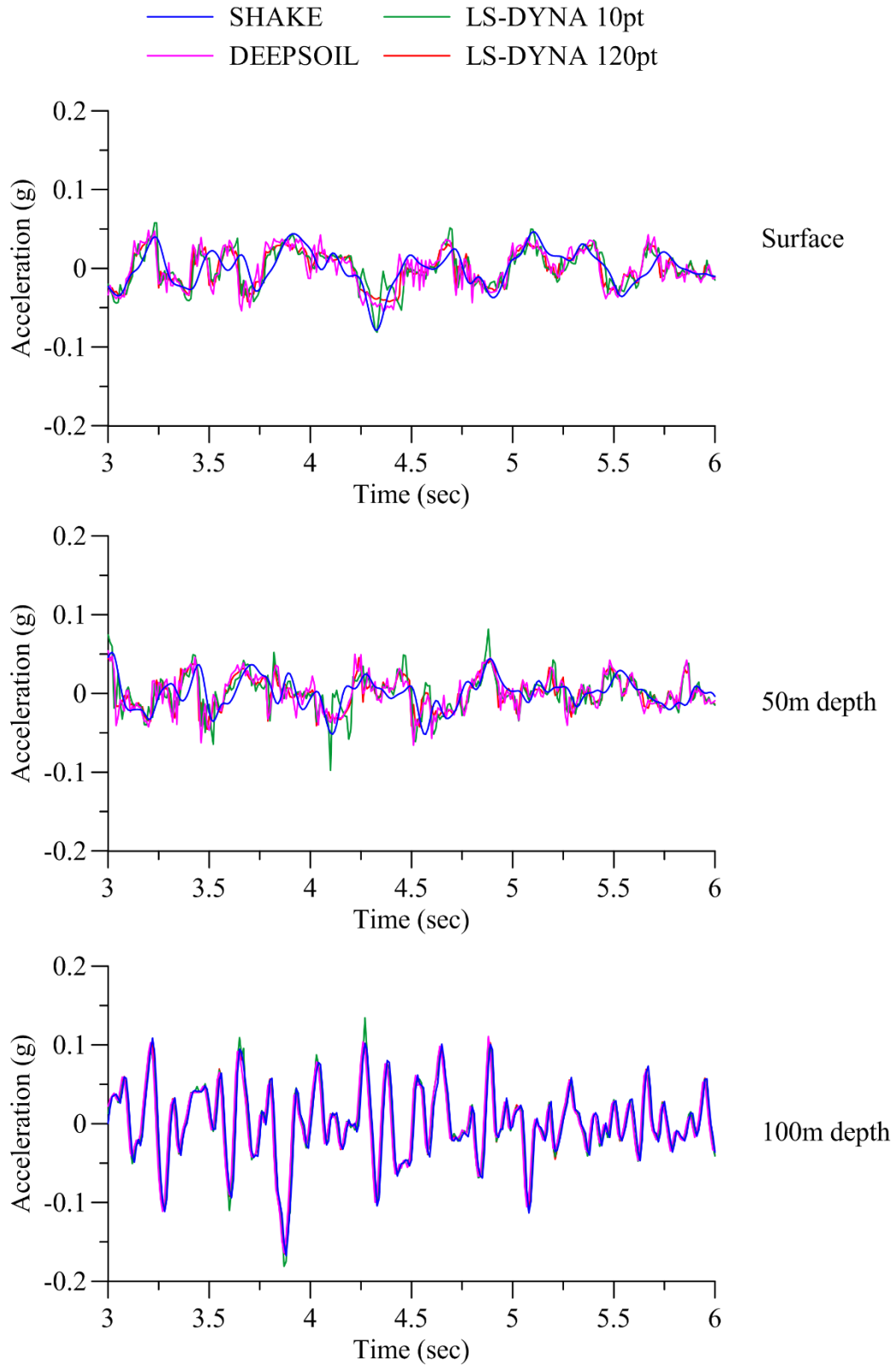


Figure A-64: Acceleration response histories at three different depths for site W2 subjected to ground motion WO3

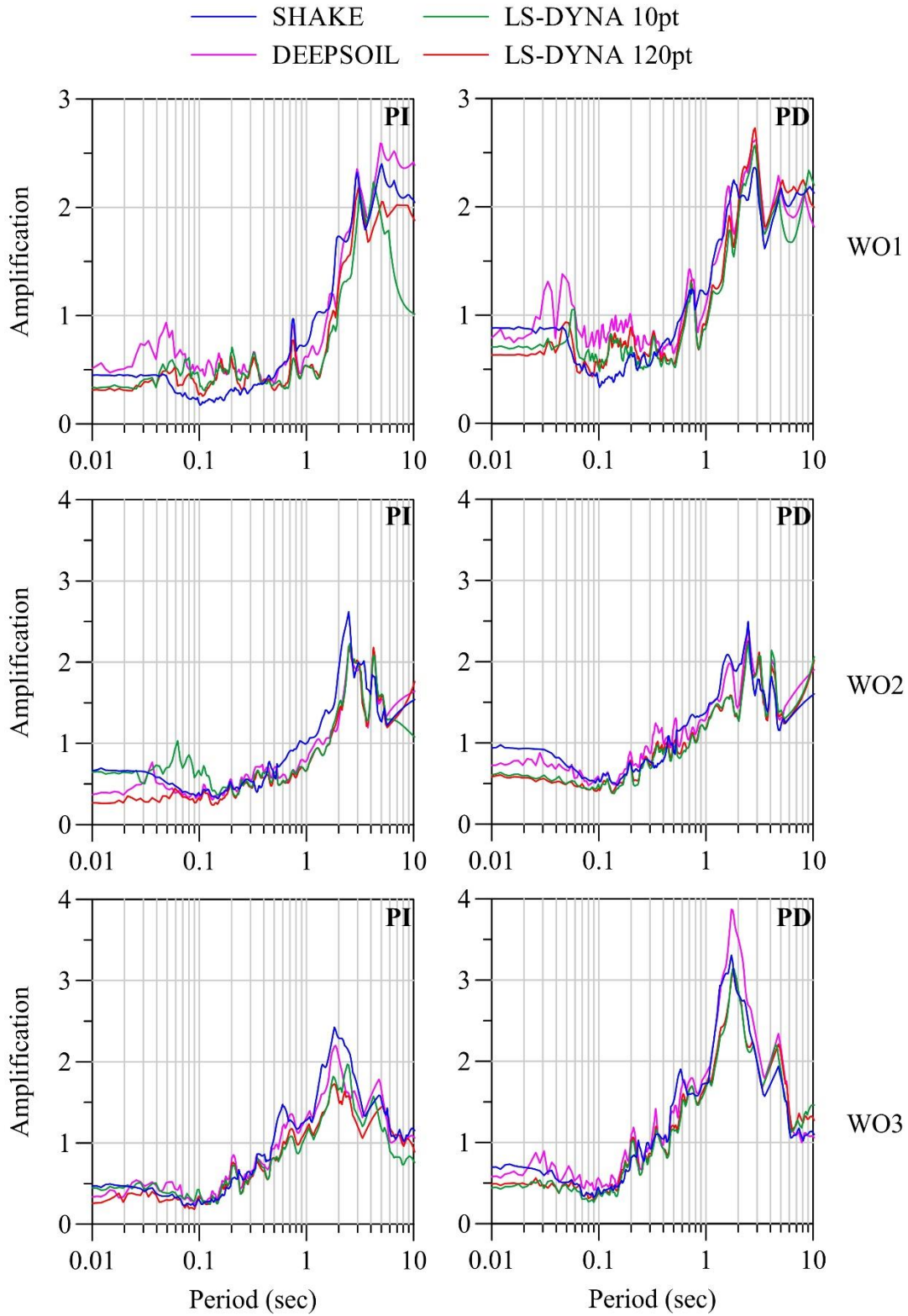


Figure A-65: Spectral amplification of accelerations in site W2 from the base to the surface for ground motions WO1, WO2 and WO3

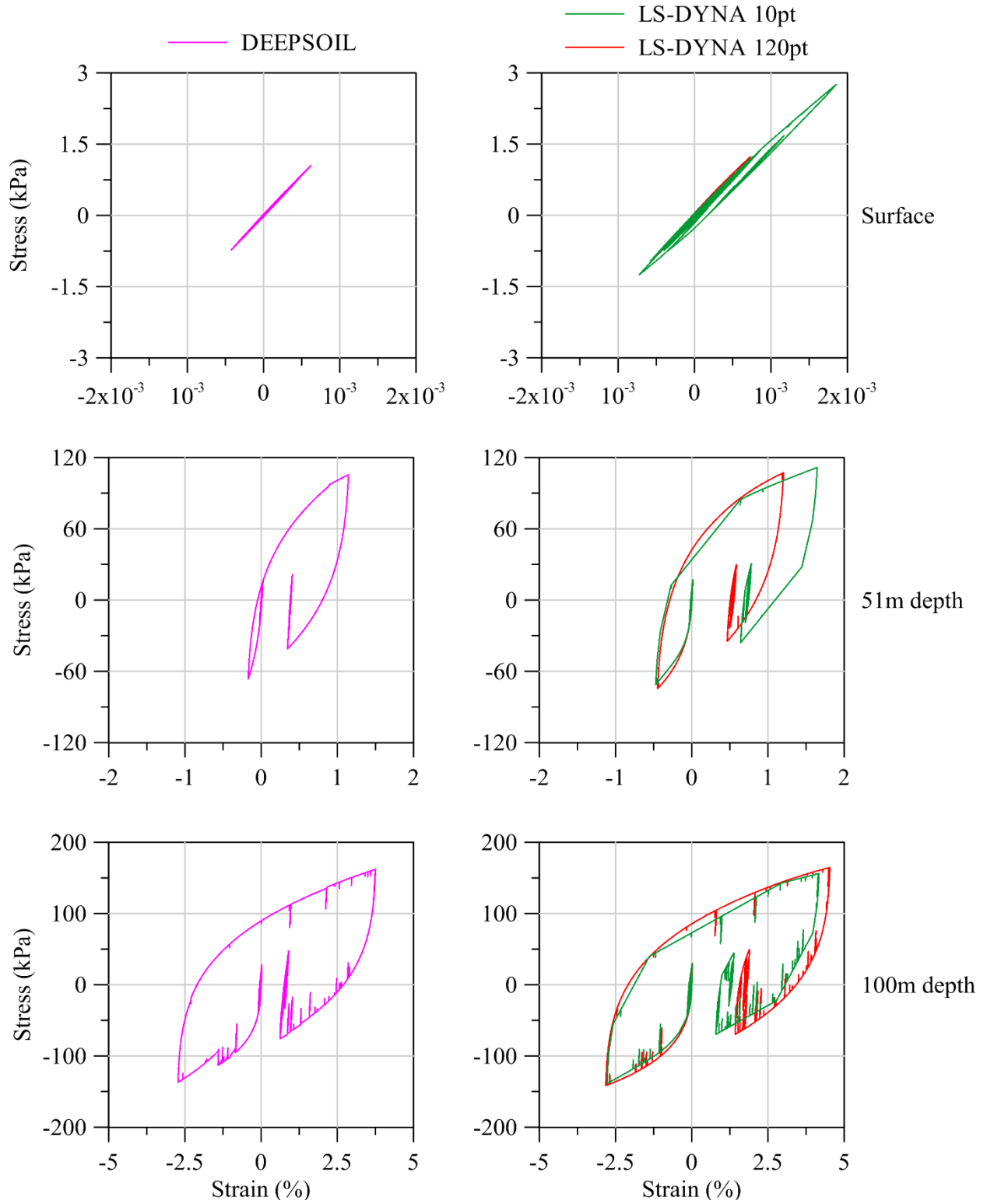


Figure A-66: Stress-strain loops at three different depths for site W2 subjected to ground motion WP1

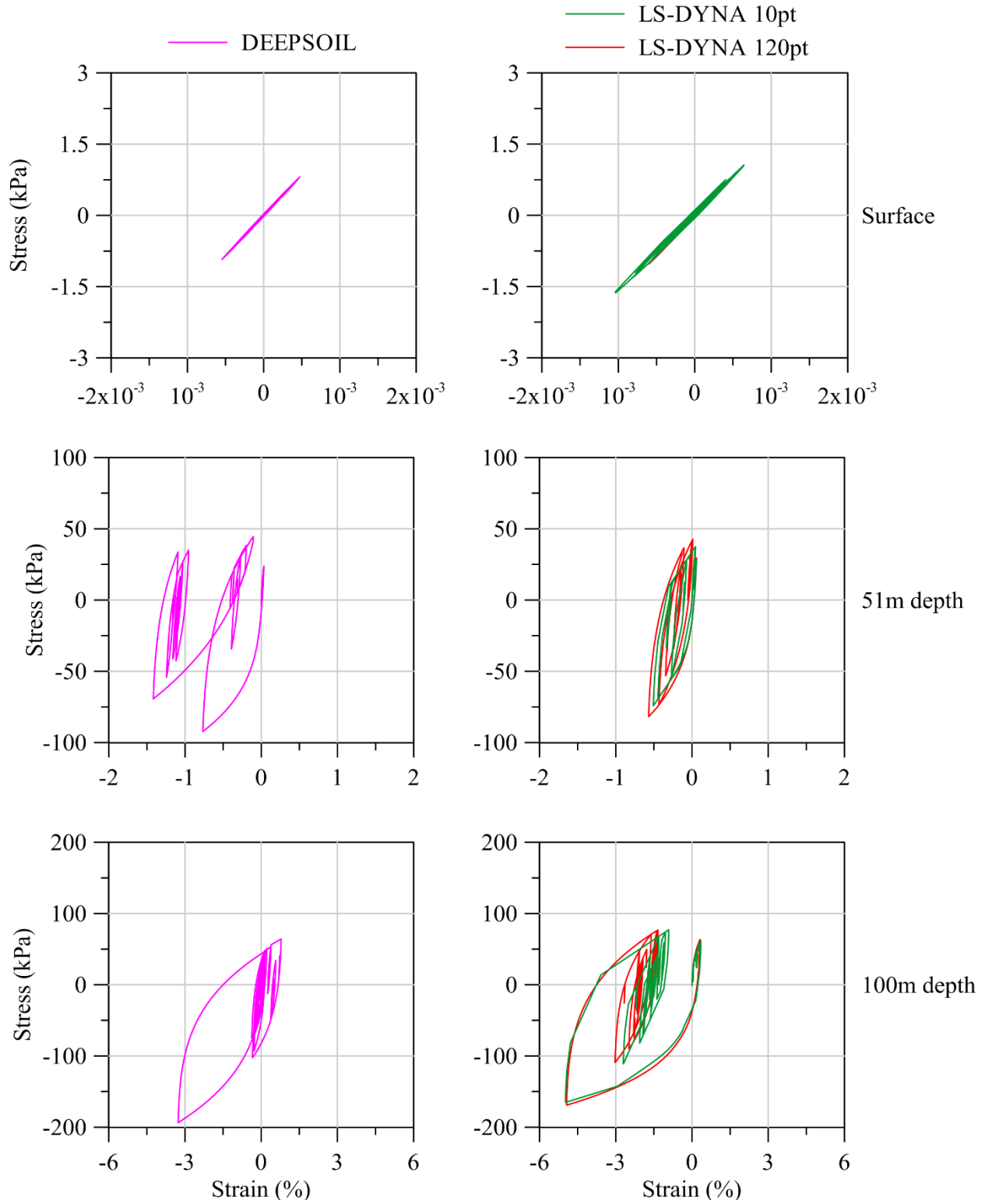


Figure A-67: Stress-strain loops at three different depths for site W2 subjected to ground motion WP2

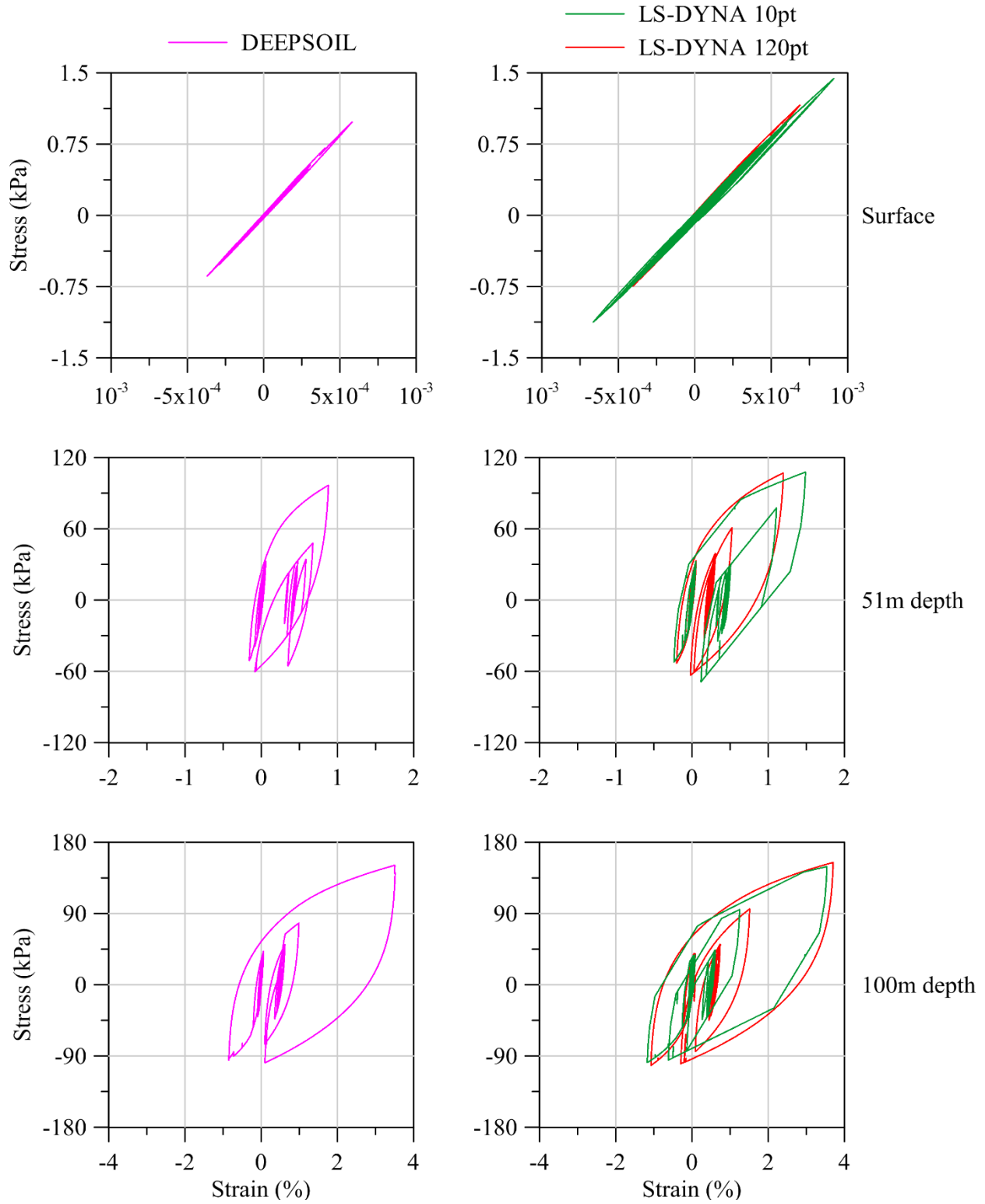


Figure A-68: Stress-strain loops at three different depths for site W2 subjected to ground motion WP3

+ + SHAKE
 + + DEEPSOIL
 + + LS-DYNA 10pt
 + + LS-DYNA 120pt

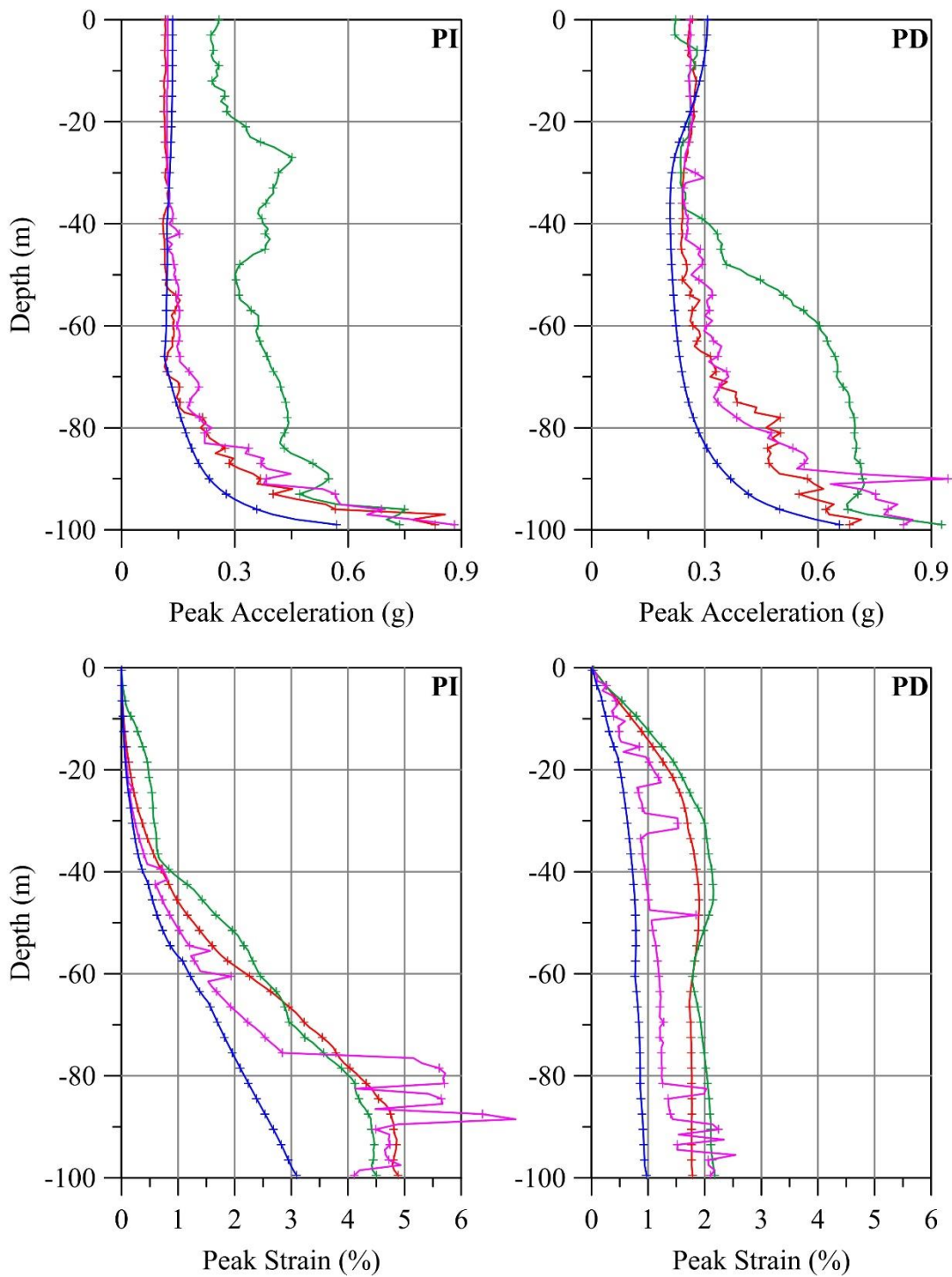


Figure A-69: Peak acceleration and peak strain profiles for site W2 subjected to ground motion

WP1

—+— SHAKE
 —+— DEEPSOIL
 —+— LS-DYNA 10pt
 —+— LS-DYNA 120pt

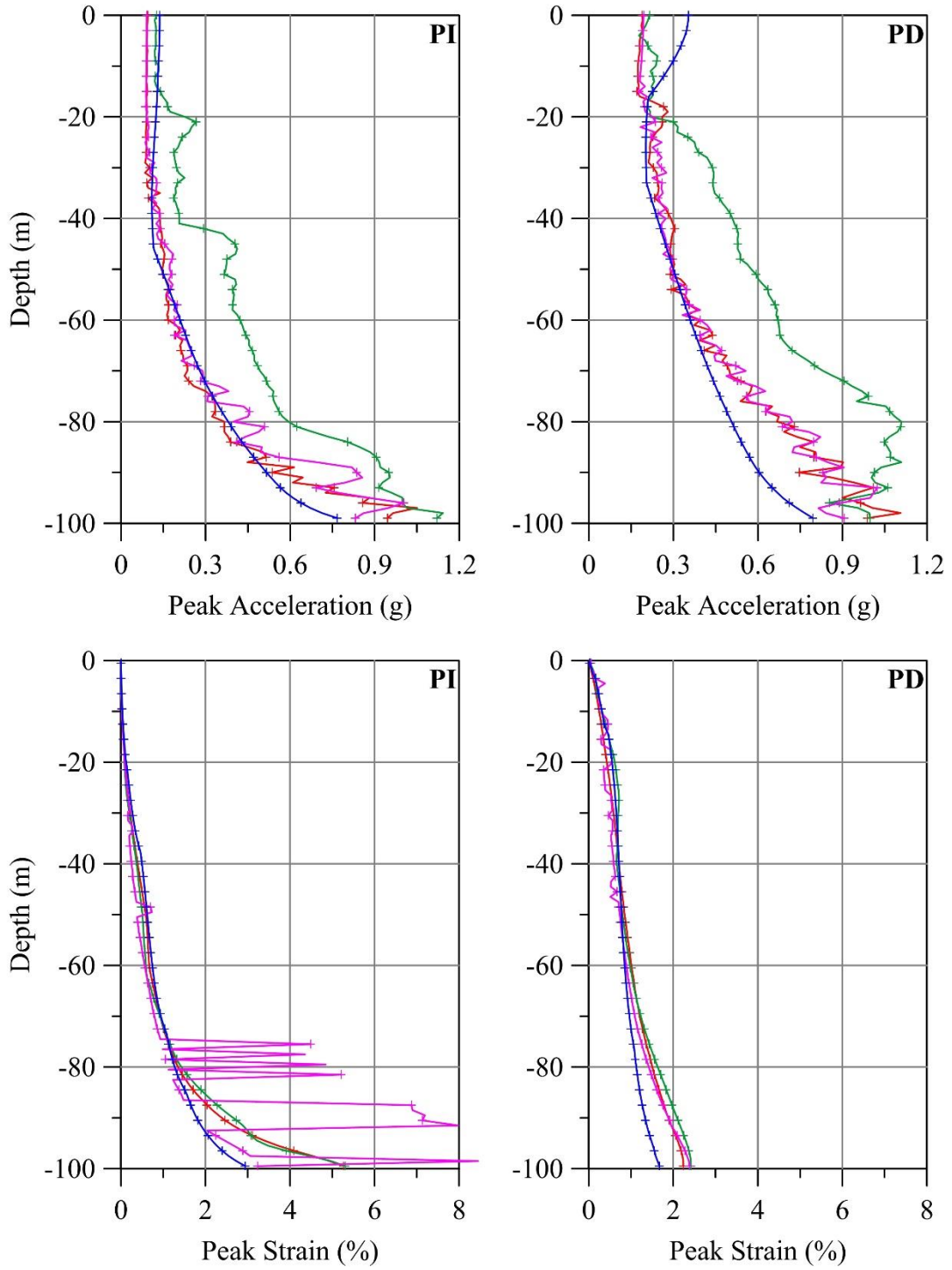


Figure A-70: Peak acceleration and peak strain profiles for site W2 subjected to ground motion WP2

—+— SHAKE
 —+— DEEPSOIL
 —+— LS-DYNA 10pt
 —+— LS-DYNA 120pt

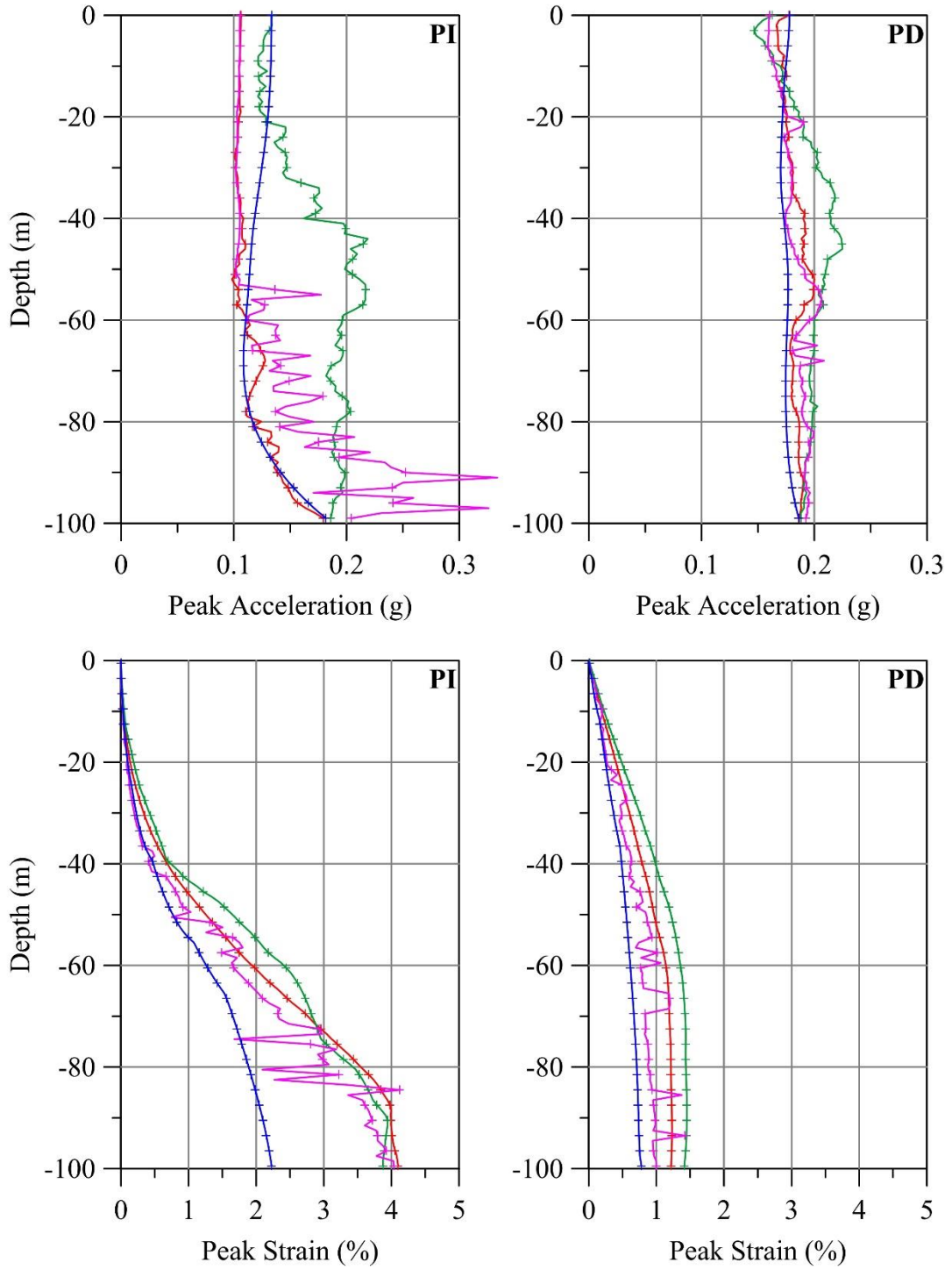


Figure A-71: Peak acceleration and peak strain profiles for site W2 subjected to ground motion WP3

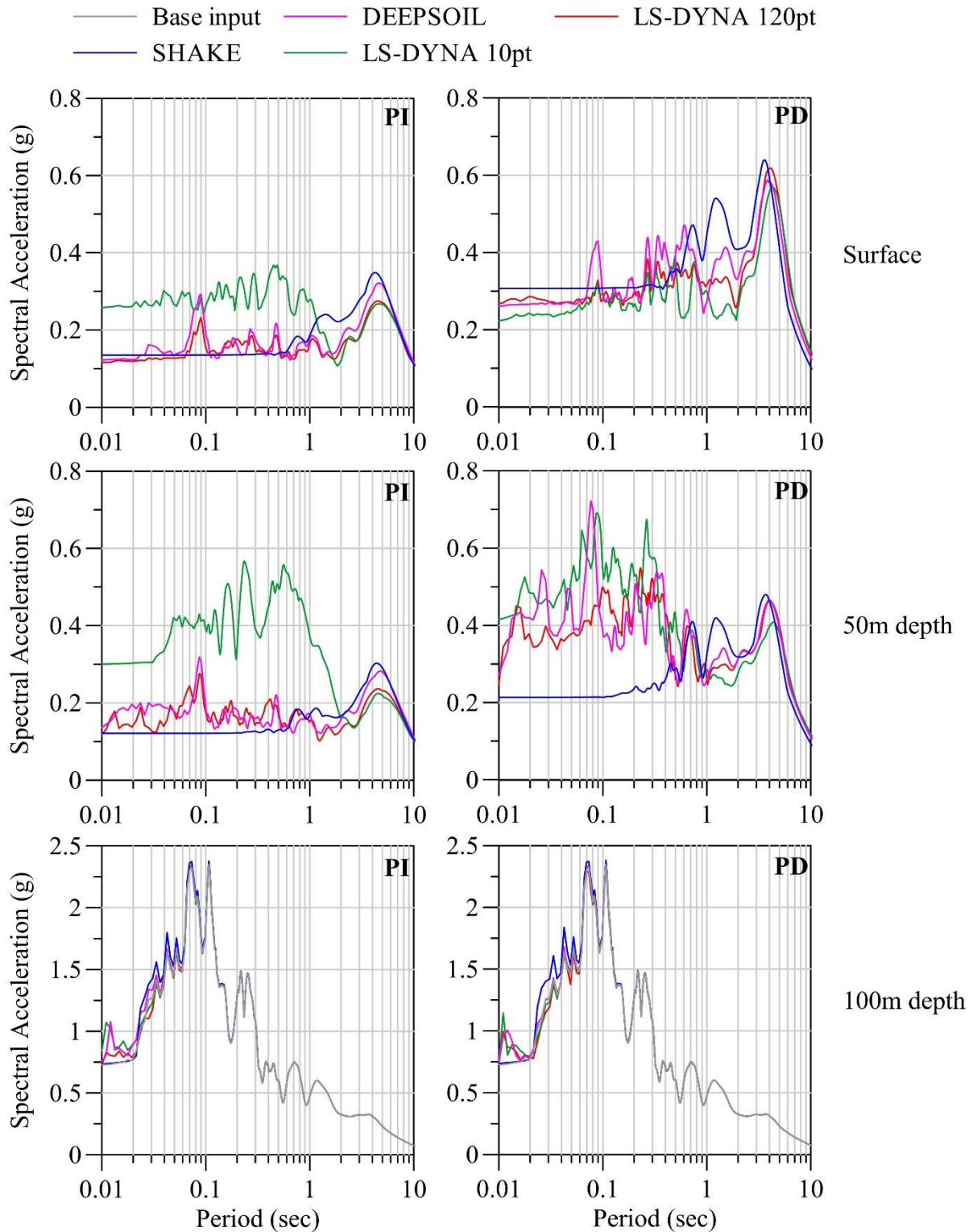


Figure A-72: Acceleration response spectra of the input motion, and accelerations at three different depths for site W2 subjected to ground motion WP1

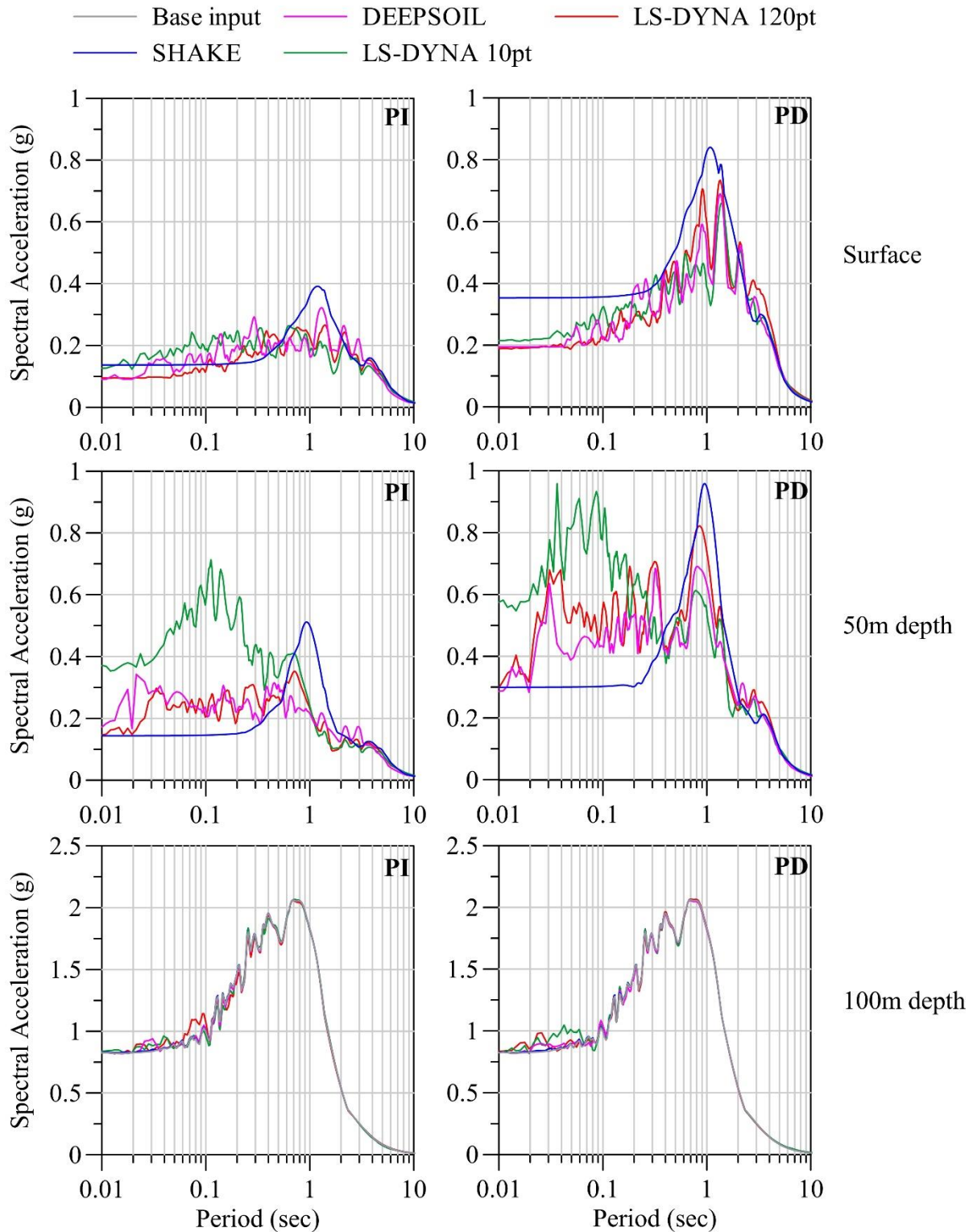


Figure A-73: Acceleration response spectra of the input motion, and accelerations at three different depths for site W2 subjected to ground motion WP2

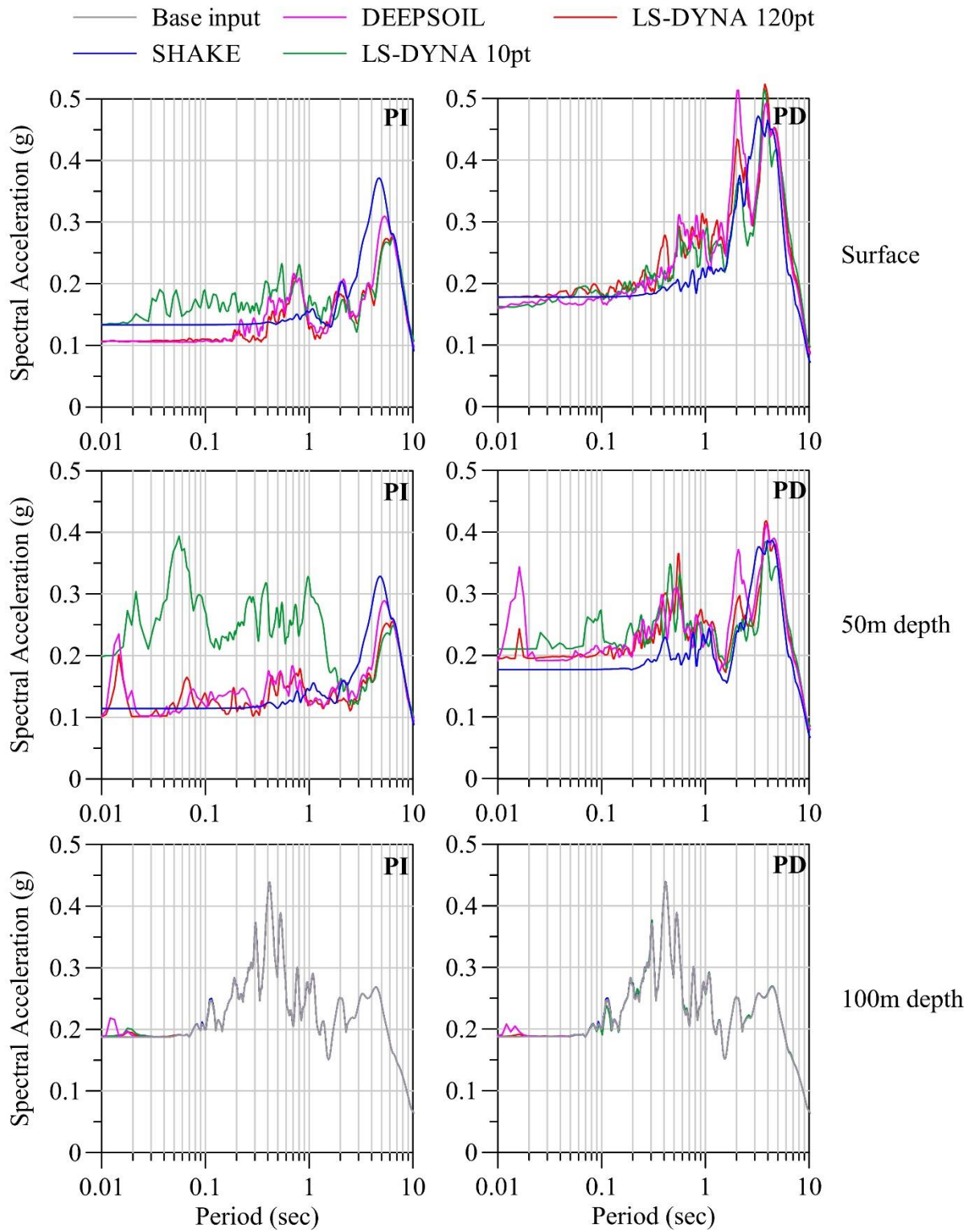


Figure A-74: Acceleration response spectra of the input motion, and accelerations at three different depths for site W2 subjected to ground motion WP3

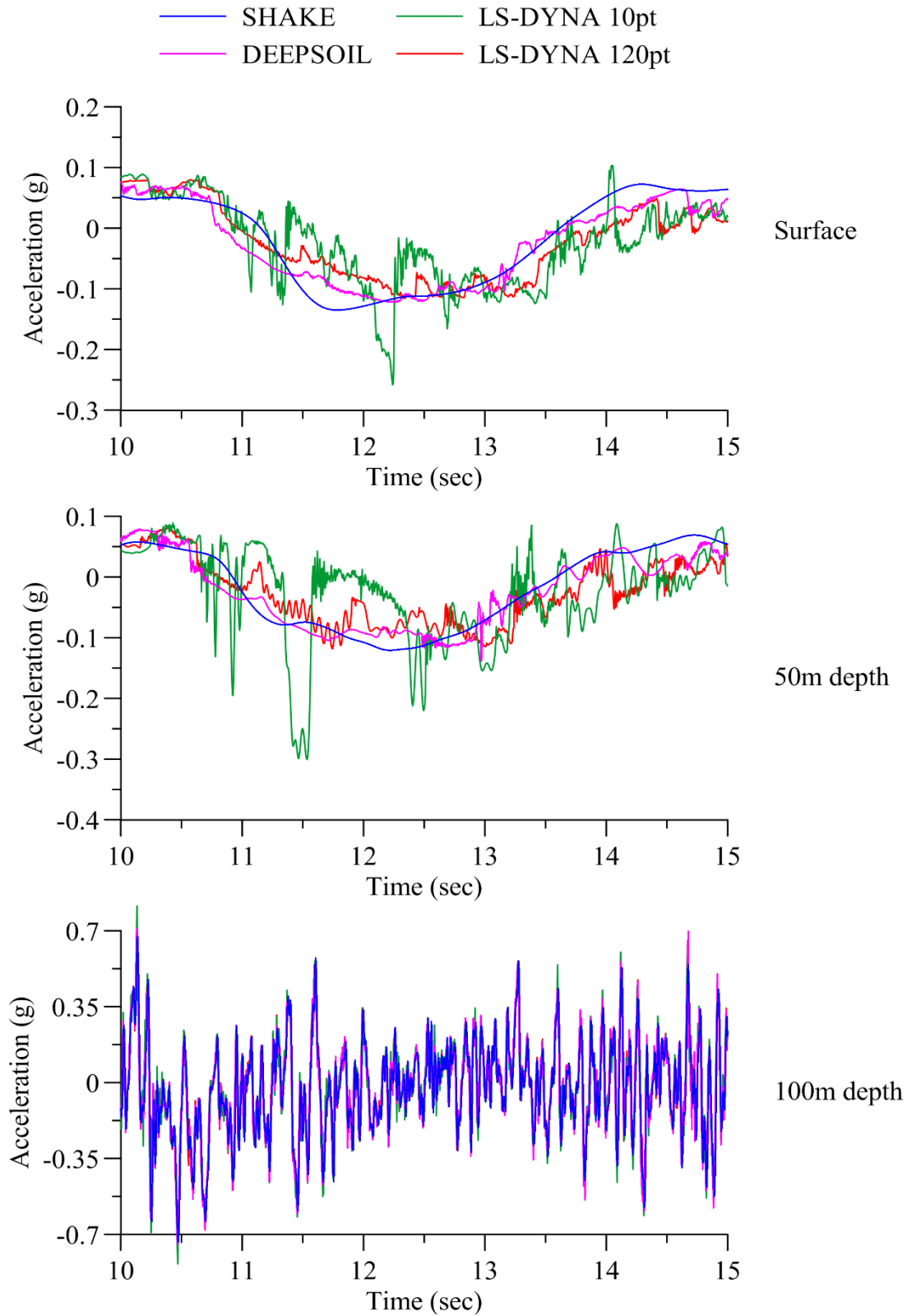


Figure A-75: Acceleration response histories at three different depths for site W2 subjected to ground motion WP1 (unequal scales used for clarity)

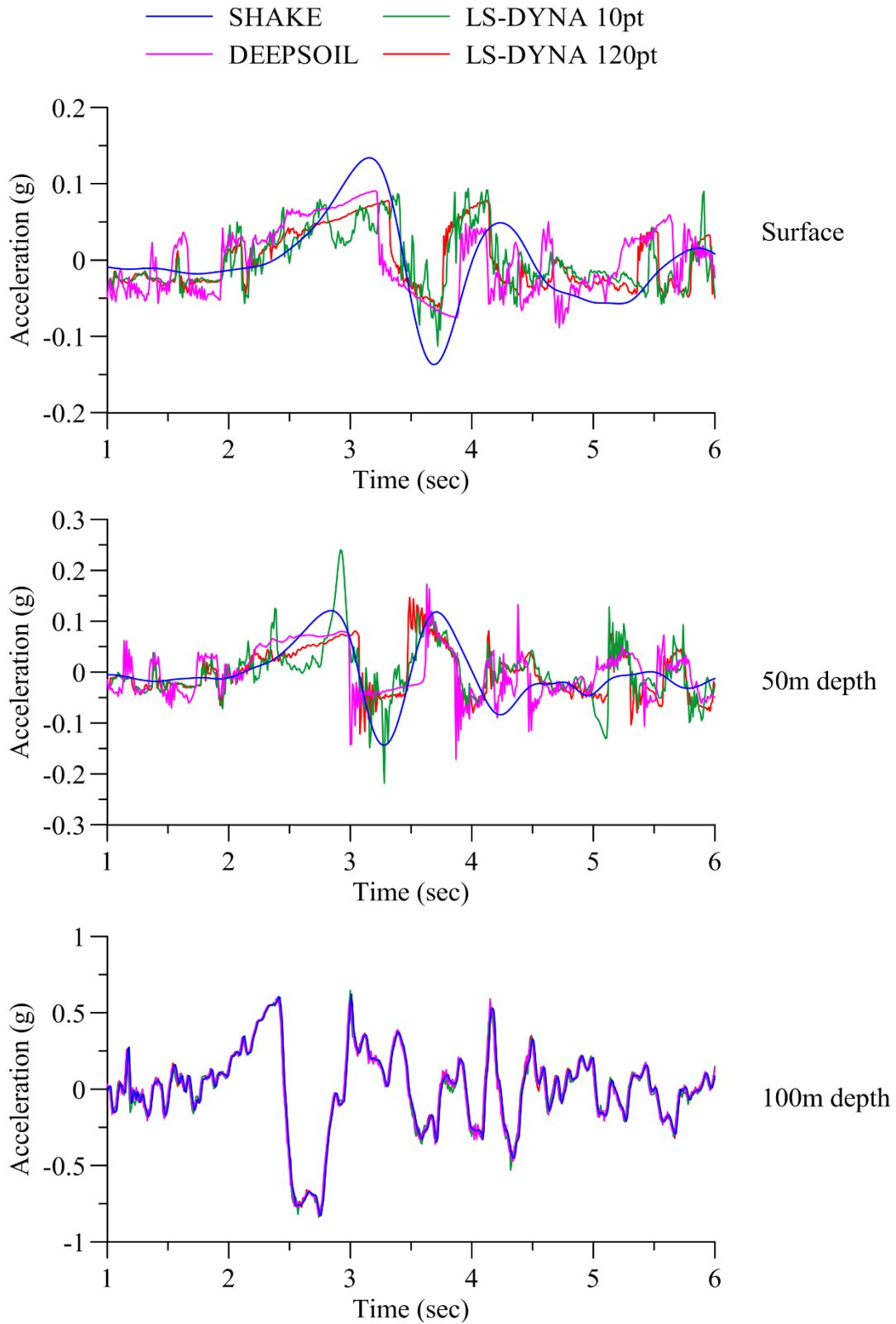


Figure A-76: Acceleration response histories at three different depths for site W2 subjected to ground motion WP2 (unequal scales used for clarity)

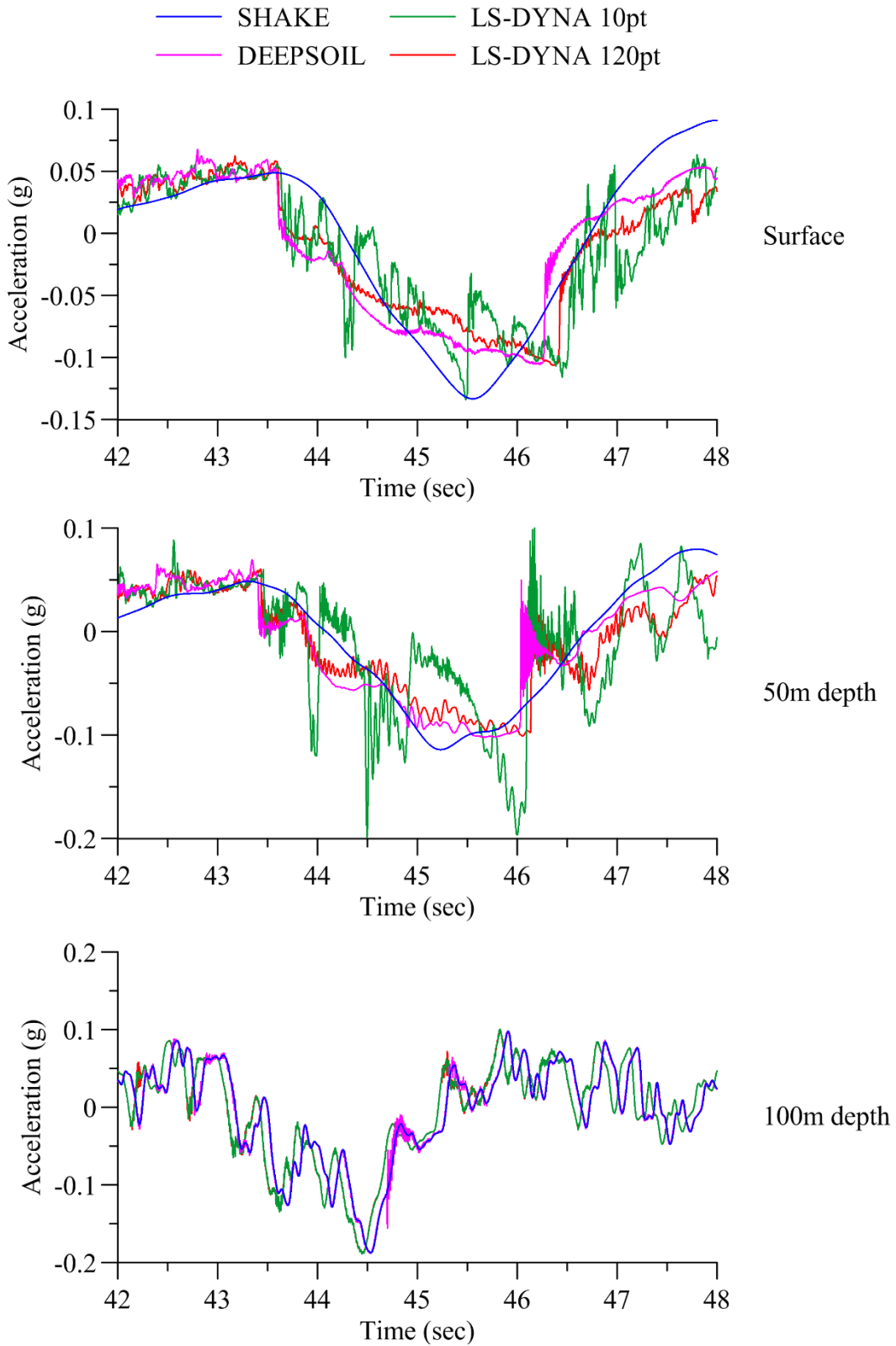


Figure A-77: Acceleration response histories at three different depths for site W2 subjected to ground motion WP3

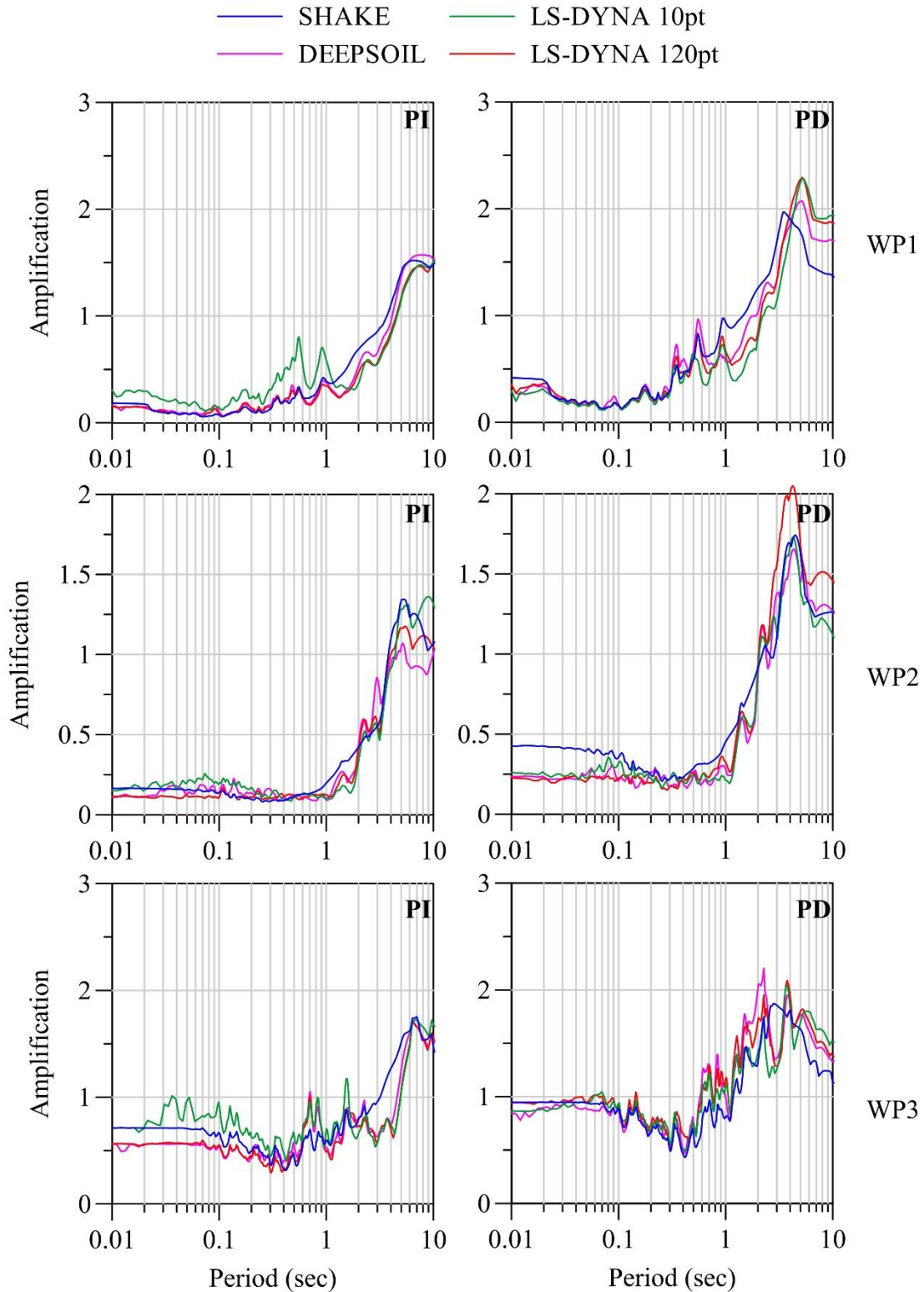


Figure A-78: Spectral amplification of accelerations in site W2 from the base to the surface for ground motions WP1, WP2 and WP3

APPENDIX B THE ORMSBY WAVELET

Earthquake ground motions comprise a spectrum of frequencies. The contribution of each frequency to the total energy carried by the ground motion is different, and most ground motions have a dominant frequency range. These dominant frequencies depend on several factors, such as the site where the ground motion is recorded, directivity of the earthquake, etc. Typical ground motions therefore may not have a considerable contribution from all the frequencies that are relevant to a dynamic system, and may result in overlooking some of the frequencies.

In order to examine and investigate the response of a complex dynamic system, such as a soil-foundation-structure system, it is desirable to use an input ground motion that has a considerable contribution from all frequencies in the desired range. The Ormsby wavelet (Ryan, 1994) provides a convenient alternative to real ground motions for understanding the response of complex dynamic systems. The Ormsby wavelet is a wavelet that features a Fourier transform with a constant magnitude in a specified frequency range. This wavelet is defined by the expression (Ryan, 1994)

$$f(t) = \left[\frac{\pi f_4^2}{f_4 - f_3} [\text{sinc}(\pi f_4(t - t_s))]^2 - \frac{\pi f_3^2}{f_4 - f_3} [\text{sinc}(\pi f_3(t - t_s))]^2 \right] - \left[\frac{\pi f_2^2}{f_2 - f_1} [\text{sinc}(\pi f_2(t - t_s))]^2 - \frac{\pi f_1^2}{f_2 - f_1} [\text{sinc}(\pi f_1(t - t_s))]^2 \right] \quad (\text{B-1})$$

where, f_1 and f_2 define the lower frequency band, f_3 and f_4 define the upper frequency band, t_s is the time of the maximum amplitude, $f(t)$ is the amplitude of the wave at time t , and $\text{sinc}(x)$ is defined by

$$\text{sinc}(x) = \frac{\sin(x)}{x} \quad (\text{B-2})$$

Figure B-1 presents a sample Ormsby wavelet with the frequency parameters, f_1 , f_2 , f_3 and f_4 , equal to 0 Hz, 0.2 Hz, 20 Hz and 25 Hz, respectively, the time of maximum amplitude equal to 2 sec, and normalized to a maximum amplitude of 1. Figure B-2 presents the Fourier transform of this wavelet. The Fourier amplitude of this wavelet increases linearly from f_1 to f_2 , remains constant from f_2 to f_3 , and decreases linearly from f_3 to f_4 . Figure B-3 presents the 1% damped acceleration response spectrum for this wavelet.

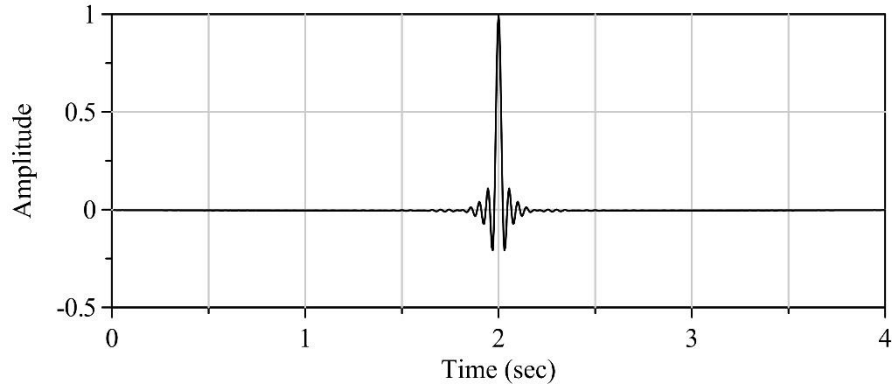


Figure B-1: Time series of an Ormsby wavelet

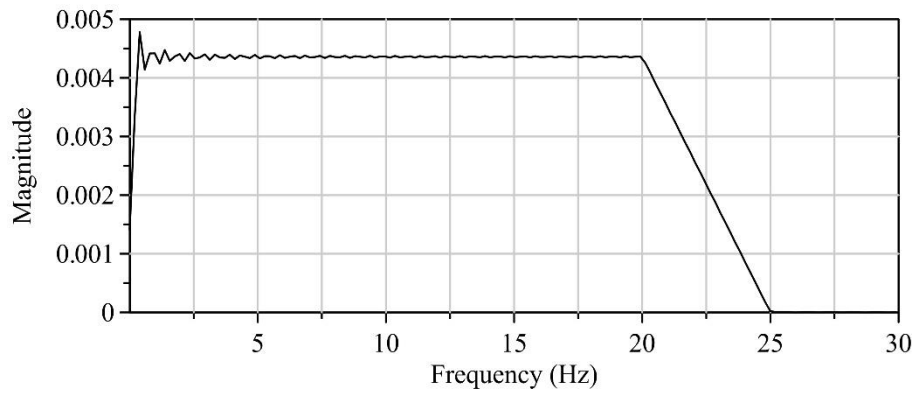


Figure B-2: Fourier transform of an Ormsby wavelet

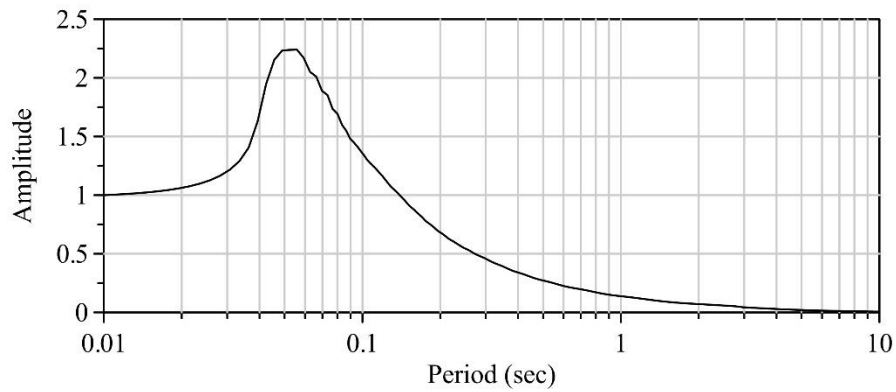


Figure B-3: 1% damped acceleration response spectrum of an Ormsby wavelet

MCEER Technical Reports

MCEER publishes technical reports on a variety of subjects written by authors funded through MCEER. These reports are available from both MCEER Publications and the National Technical Information Service (NTIS). Requests for reports should be directed to MCEER Publications, MCEER, University at Buffalo, State University of New York, 133A Ketter Hall, Buffalo, New York 14260. Reports can also be requested through NTIS, P.O. Box 1425, Springfield, Virginia 22151. NTIS accession numbers are shown in parenthesis, if available.

- NCEER-87-0001 "First-Year Program in Research, Education and Technology Transfer," 3/5/87, (PB88-134275, A04, MF-A01).
- NCEER-87-0002 "Experimental Evaluation of Instantaneous Optimal Algorithms for Structural Control," by R.C. Lin, T.T. Soong and A.M. Reinhorn, 4/20/87, (PB88-134341, A04, MF-A01).
- NCEER-87-0003 "Experimentation Using the Earthquake Simulation Facilities at University at Buffalo," by A.M. Reinhorn and R.L. Ketter, not available.
- NCEER-87-0004 "The System Characteristics and Performance of a Shaking Table," by J.S. Hwang, K.C. Chang and G.C. Lee, 6/1/87, (PB88-134259, A03, MF-A01). This report is available only through NTIS (see address given above).
- NCEER-87-0005 "A Finite Element Formulation for Nonlinear Viscoplastic Material Using a Q Model," by O. Gyebi and G. Dasgupta, 11/2/87, (PB88-213764, A08, MF-A01).
- NCEER-87-0006 "Symbolic Manipulation Program (SMP) - Algebraic Codes for Two and Three Dimensional Finite Element Formulations," by X. Lee and G. Dasgupta, 11/9/87, (PB88-218522, A05, MF-A01).
- NCEER-87-0007 "Instantaneous Optimal Control Laws for Tall Buildings Under Seismic Excitations," by J.N. Yang, A. Akbarpour and P. Ghaemmaghami, 6/10/87, (PB88-134333, A06, MF-A01). This report is only available through NTIS (see address given above).
- NCEER-87-0008 "IDARC: Inelastic Damage Analysis of Reinforced Concrete Frame - Shear-Wall Structures," by Y.J. Park, A.M. Reinhorn and S.K. Kunnath, 7/20/87, (PB88-134325, A09, MF-A01). This report is only available through NTIS (see address given above).
- NCEER-87-0009 "Liquefaction Potential for New York State: A Preliminary Report on Sites in Manhattan and Buffalo," by M. Budhu, V. Vijayakumar, R.F. Giese and L. Baumgras, 8/31/87, (PB88-163704, A03, MF-A01). This report is available only through NTIS (see address given above).
- NCEER-87-0010 "Vertical and Torsional Vibration of Foundations in Inhomogeneous Media," by A.S. Veletsos and K.W. Dotson, 6/1/87, (PB88-134291, A03, MF-A01). This report is only available through NTIS (see address given above).
- NCEER-87-0011 "Seismic Probabilistic Risk Assessment and Seismic Margins Studies for Nuclear Power Plants," by Howard H.M. Hwang, 6/15/87, (PB88-134267, A03, MF-A01). This report is only available through NTIS (see address given above).
- NCEER-87-0012 "Parametric Studies of Frequency Response of Secondary Systems Under Ground-Acceleration Excitations," by Y. Yong and Y.K. Lin, 6/10/87, (PB88-134309, A03, MF-A01). This report is only available through NTIS (see address given above).
- NCEER-87-0013 "Frequency Response of Secondary Systems Under Seismic Excitation," by J.A. HoLung, J. Cai and Y.K. Lin, 7/31/87, (PB88-134317, A05, MF-A01). This report is only available through NTIS (see address given above).
- NCEER-87-0014 "Modelling Earthquake Ground Motions in Seismically Active Regions Using Parametric Time Series Methods," by G.W. Ellis and A.S. Cakmak, 8/25/87, (PB88-134283, A08, MF-A01). This report is only available through NTIS (see address given above).
- NCEER-87-0015 "Detection and Assessment of Seismic Structural Damage," by E. DiPasquale and A.S. Cakmak, 8/25/87, (PB88-163712, A05, MF-A01). This report is only available through NTIS (see address given above).

- NCEER-87-0016 "Pipeline Experiment at Parkfield, California," by J. Isenberg and E. Richardson, 9/15/87, (PB88-163720, A03, MF-A01). This report is available only through NTIS (see address given above).
- NCEER-87-0017 "Digital Simulation of Seismic Ground Motion," by M. Shinozuka, G. Deodatis and T. Harada, 8/31/87, (PB88-155197, A04, MF-A01). This report is available only through NTIS (see address given above).
- NCEER-87-0018 "Practical Considerations for Structural Control: System Uncertainty, System Time Delay and Truncation of Small Control Forces," J.N. Yang and A. Akbarpour, 8/10/87, (PB88-163738, A08, MF-A01). This report is only available through NTIS (see address given above).
- NCEER-87-0019 "Modal Analysis of Nonclassically Damped Structural Systems Using Canonical Transformation," by J.N. Yang, S. Sarkani and F.X. Long, 9/27/87, (PB88-187851, A04, MF-A01).
- NCEER-87-0020 "A Nonstationary Solution in Random Vibration Theory," by J.R. Red-Horse and P.D. Spanos, 11/3/87, (PB88-163746, A03, MF-A01).
- NCEER-87-0021 "Horizontal Impedances for Radially Inhomogeneous Viscoelastic Soil Layers," by A.S. Veletsos and K.W. Dotson, 10/15/87, (PB88-150859, A04, MF-A01).
- NCEER-87-0022 "Seismic Damage Assessment of Reinforced Concrete Members," by Y.S. Chung, C. Meyer and M. Shinozuka, 10/9/87, (PB88-150867, A05, MF-A01). This report is available only through NTIS (see address given above).
- NCEER-87-0023 "Active Structural Control in Civil Engineering," by T.T. Soong, 11/11/87, (PB88-187778, A03, MF-A01).
- NCEER-87-0024 "Vertical and Torsional Impedances for Radially Inhomogeneous Viscoelastic Soil Layers," by K.W. Dotson and A.S. Veletsos, 12/87, (PB88-187786, A03, MF-A01).
- NCEER-87-0025 "Proceedings from the Symposium on Seismic Hazards, Ground Motions, Soil-Liquefaction and Engineering Practice in Eastern North America," October 20-22, 1987, edited by K.H. Jacob, 12/87, (PB88-188115, A23, MF-A01). This report is available only through NTIS (see address given above).
- NCEER-87-0026 "Report on the Whittier-Narrows, California, Earthquake of October 1, 1987," by J. Pantelic and A. Reinhorn, 11/87, (PB88-187752, A03, MF-A01). This report is available only through NTIS (see address given above).
- NCEER-87-0027 "Design of a Modular Program for Transient Nonlinear Analysis of Large 3-D Building Structures," by S. Srivastav and J.F. Abel, 12/30/87, (PB88-187950, A05, MF-A01). This report is only available through NTIS (see address given above).
- NCEER-87-0028 "Second-Year Program in Research, Education and Technology Transfer," 3/8/88, (PB88-219480, A04, MF-A01).
- NCEER-88-0001 "Workshop on Seismic Computer Analysis and Design of Buildings With Interactive Graphics," by W. McGuire, J.F. Abel and C.H. Conley, 1/18/88, (PB88-187760, A03, MF-A01). This report is only available through NTIS (see address given above).
- NCEER-88-0002 "Optimal Control of Nonlinear Flexible Structures," by J.N. Yang, F.X. Long and D. Wong, 1/22/88, (PB88-213772, A06, MF-A01).
- NCEER-88-0003 "Substructuring Techniques in the Time Domain for Primary-Secondary Structural Systems," by G.D. Manolis and G. Juhn, 2/10/88, (PB88-213780, A04, MF-A01).
- NCEER-88-0004 "Iterative Seismic Analysis of Primary-Secondary Systems," by A. Singhal, L.D. Lutes and P.D. Spanos, 2/23/88, (PB88-213798, A04, MF-A01).
- NCEER-88-0005 "Stochastic Finite Element Expansion for Random Media," by P.D. Spanos and R. Ghanem, 3/14/88, (PB88-213806, A03, MF-A01).

- NCEER-88-0006 "Combining Structural Optimization and Structural Control," by F.Y. Cheng and C.P. Pantelides, 1/10/88, (PB88-213814, A05, MF-A01).
- NCEER-88-0007 "Seismic Performance Assessment of Code-Designed Structures," by H.H-M. Hwang, J-W. Jaw and H-J. Shau, 3/20/88, (PB88-219423, A04, MF-A01). This report is only available through NTIS (see address given above).
- NCEER-88-0008 "Reliability Analysis of Code-Designed Structures Under Natural Hazards," by H.H-M. Hwang, H. Ushiba and M. Shinozuka, 2/29/88, (PB88-229471, A07, MF-A01). This report is only available through NTIS (see address given above).
- NCEER-88-0009 "Seismic Fragility Analysis of Shear Wall Structures," by J-W Jaw and H.H-M. Hwang, 4/30/88, (PB89-102867, A04, MF-A01).
- NCEER-88-0010 "Base Isolation of a Multi-Story Building Under a Harmonic Ground Motion - A Comparison of Performances of Various Systems," by F-G Fan, G. Ahmadi and I.G. Tadjbakhsh, 5/18/88, (PB89-122238, A06, MF-A01). This report is only available through NTIS (see address given above).
- NCEER-88-0011 "Seismic Floor Response Spectra for a Combined System by Green's Functions," by F.M. Lavelle, L.A. Bergman and P.D. Spanos, 5/1/88, (PB89-102875, A03, MF-A01).
- NCEER-88-0012 "A New Solution Technique for Randomly Excited Hysteretic Structures," by G.Q. Cai and Y.K. Lin, 5/16/88, (PB89-102883, A03, MF-A01).
- NCEER-88-0013 "A Study of Radiation Damping and Soil-Structure Interaction Effects in the Centrifuge," by K. Weissman, supervised by J.H. Prevost, 5/24/88, (PB89-144703, A06, MF-A01).
- NCEER-88-0014 "Parameter Identification and Implementation of a Kinematic Plasticity Model for Frictional Soils," by J.H. Prevost and D.V. Griffiths, not available.
- NCEER-88-0015 "Two- and Three- Dimensional Dynamic Finite Element Analyses of the Long Valley Dam," by D.V. Griffiths and J.H. Prevost, 6/17/88, (PB89-144711, A04, MF-A01).
- NCEER-88-0016 "Damage Assessment of Reinforced Concrete Structures in Eastern United States," by A.M. Reinhorn, M.J. Seidel, S.K. Kunnath and Y.J. Park, 6/15/88, (PB89-122220, A04, MF-A01). This report is only available through NTIS (see address given above).
- NCEER-88-0017 "Dynamic Compliance of Vertically Loaded Strip Foundations in Multilayered Viscoelastic Soils," by S. Ahmad and A.S.M. Israil, 6/17/88, (PB89-102891, A04, MF-A01).
- NCEER-88-0018 "An Experimental Study of Seismic Structural Response With Added Viscoelastic Dampers," by R.C. Lin, Z. Liang, T.T. Soong and R.H. Zhang, 6/30/88, (PB89-122212, A05, MF-A01). This report is available only through NTIS (see address given above).
- NCEER-88-0019 "Experimental Investigation of Primary - Secondary System Interaction," by G.D. Manolis, G. Juhn and A.M. Reinhorn, 5/27/88, (PB89-122204, A04, MF-A01).
- NCEER-88-0020 "A Response Spectrum Approach For Analysis of Nonclassically Damped Structures," by J.N. Yang, S. Sarkani and F.X. Long, 4/22/88, (PB89-102909, A04, MF-A01).
- NCEER-88-0021 "Seismic Interaction of Structures and Soils: Stochastic Approach," by A.S. Veletsos and A.M. Prasad, 7/21/88, (PB89-122196, A04, MF-A01). This report is only available through NTIS (see address given above).
- NCEER-88-0022 "Identification of the Serviceability Limit State and Detection of Seismic Structural Damage," by E. DiPasquale and A.S. Cakmak, 6/15/88, (PB89-122188, A05, MF-A01). This report is available only through NTIS (see address given above).
- NCEER-88-0023 "Multi-Hazard Risk Analysis: Case of a Simple Offshore Structure," by B.K. Bhartia and E.H. Vanmarcke, 7/21/88, (PB89-145213, A05, MF-A01).

- NCEER-88-0024 "Automated Seismic Design of Reinforced Concrete Buildings," by Y.S. Chung, C. Meyer and M. Shinozuka, 7/5/88, (PB89-122170, A06, MF-A01). This report is available only through NTIS (see address given above).
- NCEER-88-0025 "Experimental Study of Active Control of MDOF Structures Under Seismic Excitations," by L.L. Chung, R.C. Lin, T.T. Soong and A.M. Reinhorn, 7/10/88, (PB89-122600, A04, MF-A01).
- NCEER-88-0026 "Earthquake Simulation Tests of a Low-Rise Metal Structure," by J.S. Hwang, K.C. Chang, G.C. Lee and R.L. Ketter, 8/1/88, (PB89-102917, A04, MF-A01).
- NCEER-88-0027 "Systems Study of Urban Response and Reconstruction Due to Catastrophic Earthquakes," by F. Kozin and H.K. Zhou, 9/22/88, (PB90-162348, A04, MF-A01).
- NCEER-88-0028 "Seismic Fragility Analysis of Plane Frame Structures," by H.H-M. Hwang and Y.K. Low, 7/31/88, (PB89-131445, A06, MF-A01).
- NCEER-88-0029 "Response Analysis of Stochastic Structures," by A. Kardara, C. Bucher and M. Shinozuka, 9/22/88, (PB89-174429, A04, MF-A01).
- NCEER-88-0030 "Nonnormal Accelerations Due to Yielding in a Primary Structure," by D.C.K. Chen and L.D. Lutes, 9/19/88, (PB89-131437, A04, MF-A01).
- NCEER-88-0031 "Design Approaches for Soil-Structure Interaction," by A.S. Veletsos, A.M. Prasad and Y. Tang, 12/30/88, (PB89-174437, A03, MF-A01). This report is available only through NTIS (see address given above).
- NCEER-88-0032 "A Re-evaluation of Design Spectra for Seismic Damage Control," by C.J. Turkstra and A.G. Tallin, 11/7/88, (PB89-145221, A05, MF-A01).
- NCEER-88-0033 "The Behavior and Design of Noncontact Lap Splices Subjected to Repeated Inelastic Tensile Loading," by V.E. Sagan, P. Gergely and R.N. White, 12/8/88, (PB89-163737, A08, MF-A01).
- NCEER-88-0034 "Seismic Response of Pile Foundations," by S.M. Mamoon, P.K. Banerjee and S. Ahmad, 11/1/88, (PB89-145239, A04, MF-A01).
- NCEER-88-0035 "Modeling of R/C Building Structures With Flexible Floor Diaphragms (IDARC2)," by A.M. Reinhorn, S.K. Kunnath and N. Panahshahi, 9/7/88, (PB89-207153, A07, MF-A01).
- NCEER-88-0036 "Solution of the Dam-Reservoir Interaction Problem Using a Combination of FEM, BEM with Particular Integrals, Modal Analysis, and Substructuring," by C-S. Tsai, G.C. Lee and R.L. Ketter, 12/31/88, (PB89-207146, A04, MF-A01).
- NCEER-88-0037 "Optimal Placement of Actuators for Structural Control," by F.Y. Cheng and C.P. Pantelides, 8/15/88, (PB89-162846, A05, MF-A01).
- NCEER-88-0038 "Teflon Bearings in Aseismic Base Isolation: Experimental Studies and Mathematical Modeling," by A. Mokha, M.C. Constantinou and A.M. Reinhorn, 12/5/88, (PB89-218457, A10, MF-A01). This report is available only through NTIS (see address given above).
- NCEER-88-0039 "Seismic Behavior of Flat Slab High-Rise Buildings in the New York City Area," by P. Weidlinger and M. Ettouney, 10/15/88, (PB90-145681, A04, MF-A01).
- NCEER-88-0040 "Evaluation of the Earthquake Resistance of Existing Buildings in New York City," by P. Weidlinger and M. Ettouney, 10/15/88, not available.
- NCEER-88-0041 "Small-Scale Modeling Techniques for Reinforced Concrete Structures Subjected to Seismic Loads," by W. Kim, A. El-Attar and R.N. White, 11/22/88, (PB89-189625, A05, MF-A01).
- NCEER-88-0042 "Modeling Strong Ground Motion from Multiple Event Earthquakes," by G.W. Ellis and A.S. Cakmak, 10/15/88, (PB89-174445, A03, MF-A01).

- NCEER-88-0043 "Nonstationary Models of Seismic Ground Acceleration," by M. Grigoriu, S.E. Ruiz and E. Rosenblueth, 7/15/88, (PB89-189617, A04, MF-A01).
- NCEER-88-0044 "SARCF User's Guide: Seismic Analysis of Reinforced Concrete Frames," by Y.S. Chung, C. Meyer and M. Shinozuka, 11/9/88, (PB89-174452, A08, MF-A01).
- NCEER-88-0045 "First Expert Panel Meeting on Disaster Research and Planning," edited by J. Pantelic and J. Stoyke, 9/15/88, (PB89-174460, A05, MF-A01).
- NCEER-88-0046 "Preliminary Studies of the Effect of Degrading Infill Walls on the Nonlinear Seismic Response of Steel Frames," by C.Z. Chrysostomou, P. Gergely and J.F. Abel, 12/19/88, (PB89-208383, A05, MF-A01).
- NCEER-88-0047 "Reinforced Concrete Frame Component Testing Facility - Design, Construction, Instrumentation and Operation," by S.P. Pessiki, C. Conley, T. Bond, P. Gergely and R.N. White, 12/16/88, (PB89-174478, A04, MF-A01).
- NCEER-89-0001 "Effects of Protective Cushion and Soil Compliancy on the Response of Equipment Within a Seismically Excited Building," by J.A. HoLung, 2/16/89, (PB89-207179, A04, MF-A01).
- NCEER-89-0002 "Statistical Evaluation of Response Modification Factors for Reinforced Concrete Structures," by H.H-M. Hwang and J-W. Jaw, 2/17/89, (PB89-207187, A05, MF-A01).
- NCEER-89-0003 "Hysteretic Columns Under Random Excitation," by G-Q. Cai and Y.K. Lin, 1/9/89, (PB89-196513, A03, MF-A01).
- NCEER-89-0004 "Experimental Study of 'Elephant Foot Bulge' Instability of Thin-Walled Metal Tanks," by Z-H. Jia and R.L. Ketter, 2/22/89, (PB89-207195, A03, MF-A01).
- NCEER-89-0005 "Experiment on Performance of Buried Pipelines Across San Andreas Fault," by J. Isenberg, E. Richardson and T.D. O'Rourke, 3/10/89, (PB89-218440, A04, MF-A01). This report is available only through NTIS (see address given above).
- NCEER-89-0006 "A Knowledge-Based Approach to Structural Design of Earthquake-Resistant Buildings," by M. Subramani, P. Gergely, C.H. Conley, J.F. Abel and A.H. Zaghaw, 1/15/89, (PB89-218465, A06, MF-A01).
- NCEER-89-0007 "Liquefaction Hazards and Their Effects on Buried Pipelines," by T.D. O'Rourke and P.A. Lane, 2/1/89, (PB89-218481, A09, MF-A01).
- NCEER-89-0008 "Fundamentals of System Identification in Structural Dynamics," by H. Imai, C-B. Yun, O. Maruyama and M. Shinozuka, 1/26/89, (PB89-207211, A04, MF-A01).
- NCEER-89-0009 "Effects of the 1985 Michoacan Earthquake on Water Systems and Other Buried Lifelines in Mexico," by A.G. Ayala and M.J. O'Rourke, 3/8/89, (PB89-207229, A06, MF-A01).
- NCEER-89-R010 "NCEER Bibliography of Earthquake Education Materials," by K.E.K. Ross, Second Revision, 9/1/89, (PB90-125352, A05, MF-A01). This report is replaced by NCEER-92-0018.
- NCEER-89-0011 "Inelastic Three-Dimensional Response Analysis of Reinforced Concrete Building Structures (IDARC-3D), Part I - Modeling," by S.K. Kunnath and A.M. Reinhorn, 4/17/89, (PB90-114612, A07, MF-A01). This report is available only through NTIS (see address given above).
- NCEER-89-0012 "Recommended Modifications to ATC-14," by C.D. Poland and J.O. Malley, 4/12/89, (PB90-108648, A15, MF-A01).
- NCEER-89-0013 "Repair and Strengthening of Beam-to-Column Connections Subjected to Earthquake Loading," by M. Corazao and A.J. Durrani, 2/28/89, (PB90-109885, A06, MF-A01).
- NCEER-89-0014 "Program EXKAL2 for Identification of Structural Dynamic Systems," by O. Maruyama, C-B. Yun, M. Hoshiya and M. Shinozuka, 5/19/89, (PB90-109877, A09, MF-A01).

- NCEER-89-0015 "Response of Frames With Bolted Semi-Rigid Connections, Part I - Experimental Study and Analytical Predictions," by P.J. DiCorso, A.M. Reinhorn, J.R. Dickerson, J.B. Radzimirski and W.L. Harper, 6/1/89, not available.
- NCEER-89-0016 "ARMA Monte Carlo Simulation in Probabilistic Structural Analysis," by P.D. Spanos and M.P. Mignolet, 7/10/89, (PB90-109893, A03, MF-A01).
- NCEER-89-P017 "Preliminary Proceedings from the Conference on Disaster Preparedness - The Place of Earthquake Education in Our Schools," Edited by K.E.K. Ross, 6/23/89, (PB90-108606, A03, MF-A01).
- NCEER-89-0017 "Proceedings from the Conference on Disaster Preparedness - The Place of Earthquake Education in Our Schools," Edited by K.E.K. Ross, 12/31/89, (PB90-207895, A012, MF-A02). This report is available only through NTIS (see address given above).
- NCEER-89-0018 "Multidimensional Models of Hysteretic Material Behavior for Vibration Analysis of Shape Memory Energy Absorbing Devices, by E.J. Graesser and F.A. Cozzarelli, 6/7/89, (PB90-164146, A04, MF-A01).
- NCEER-89-0019 "Nonlinear Dynamic Analysis of Three-Dimensional Base Isolated Structures (3D-BASIS)," by S. Nagarajaiah, A.M. Reinhorn and M.C. Constantinou, 8/3/89, (PB90-161936, A06, MF-A01). This report has been replaced by NCEER-93-0011.
- NCEER-89-0020 "Structural Control Considering Time-Rate of Control Forces and Control Rate Constraints," by F.Y. Cheng and C.P. Pantelides, 8/3/89, (PB90-120445, A04, MF-A01).
- NCEER-89-0021 "Subsurface Conditions of Memphis and Shelby County," by K.W. Ng, T-S. Chang and H-H.M. Hwang, 7/26/89, (PB90-120437, A03, MF-A01).
- NCEER-89-0022 "Seismic Wave Propagation Effects on Straight Jointed Buried Pipelines," by K. Elhmadi and M.J. O'Rourke, 8/24/89, (PB90-162322, A10, MF-A02).
- NCEER-89-0023 "Workshop on Serviceability Analysis of Water Delivery Systems," edited by M. Grigoriu, 3/6/89, (PB90-127424, A03, MF-A01).
- NCEER-89-0024 "Shaking Table Study of a 1/5 Scale Steel Frame Composed of Tapered Members," by K.C. Chang, J.S. Hwang and G.C. Lee, 9/18/89, (PB90-160169, A04, MF-A01).
- NCEER-89-0025 "DYNA1D: A Computer Program for Nonlinear Seismic Site Response Analysis - Technical Documentation," by Jean H. Prevost, 9/14/89, (PB90-161944, A07, MF-A01). This report is available only through NTIS (see address given above).
- NCEER-89-0026 "1:4 Scale Model Studies of Active Tendon Systems and Active Mass Dampers for Aseismic Protection," by A.M. Reinhorn, T.T. Soong, R.C. Lin, Y.P. Yang, Y. Fukao, H. Abe and M. Nakai, 9/15/89, (PB90-173246, A10, MF-A02). This report is available only through NTIS (see address given above).
- NCEER-89-0027 "Scattering of Waves by Inclusions in a Nonhomogeneous Elastic Half Space Solved by Boundary Element Methods," by P.K. Hadley, A. Askar and A.S. Cakmak, 6/15/89, (PB90-145699, A07, MF-A01).
- NCEER-89-0028 "Statistical Evaluation of Deflection Amplification Factors for Reinforced Concrete Structures," by H.H.M. Hwang, J-W. Jaw and A.L. Ch'ng, 8/31/89, (PB90-164633, A05, MF-A01).
- NCEER-89-0029 "Bedrock Accelerations in Memphis Area Due to Large New Madrid Earthquakes," by H.H.M. Hwang, C.H.S. Chen and G. Yu, 11/7/89, (PB90-162330, A04, MF-A01).
- NCEER-89-0030 "Seismic Behavior and Response Sensitivity of Secondary Structural Systems," by Y.Q. Chen and T.T. Soong, 10/23/89, (PB90-164658, A08, MF-A01).
- NCEER-89-0031 "Random Vibration and Reliability Analysis of Primary-Secondary Structural Systems," by Y. Ibrahim, M. Grigoriu and T.T. Soong, 11/10/89, (PB90-161951, A04, MF-A01).

- NCEER-89-0032 "Proceedings from the Second U.S. - Japan Workshop on Liquefaction, Large Ground Deformation and Their Effects on Lifelines, September 26-29, 1989," Edited by T.D. O'Rourke and M. Hamada, 12/1/89, (PB90-209388, A22, MF-A03).
- NCEER-89-0033 "Deterministic Model for Seismic Damage Evaluation of Reinforced Concrete Structures," by J.M. Bracci, A.M. Reinhorn, J.B. Mander and S.K. Kunnath, 9/27/89, (PB91-108803, A06, MF-A01).
- NCEER-89-0034 "On the Relation Between Local and Global Damage Indices," by E. DiPasquale and A.S. Cakmak, 8/15/89, (PB90-173865, A05, MF-A01).
- NCEER-89-0035 "Cyclic Undrained Behavior of Nonplastic and Low Plasticity Silts," by A.J. Walker and H.E. Stewart, 7/26/89, (PB90-183518, A10, MF-A01).
- NCEER-89-0036 "Liquefaction Potential of Surficial Deposits in the City of Buffalo, New York," by M. Budhu, R. Giese and L. Baumgrass, 1/17/89, (PB90-208455, A04, MF-A01).
- NCEER-89-0037 "A Deterministic Assessment of Effects of Ground Motion Incoherence," by A.S. Veletsos and Y. Tang, 7/15/89, (PB90-164294, A03, MF-A01).
- NCEER-89-0038 "Workshop on Ground Motion Parameters for Seismic Hazard Mapping," July 17-18, 1989, edited by R.V. Whitman, 12/1/89, (PB90-173923, A04, MF-A01).
- NCEER-89-0039 "Seismic Effects on Elevated Transit Lines of the New York City Transit Authority," by C.J. Costantino, C.A. Miller and E. Heymsfield, 12/26/89, (PB90-207887, A06, MF-A01).
- NCEER-89-0040 "Centrifugal Modeling of Dynamic Soil-Structure Interaction," by K. Weissman, Supervised by J.H. Prevost, 5/10/89, (PB90-207879, A07, MF-A01).
- NCEER-89-0041 "Linearized Identification of Buildings With Cores for Seismic Vulnerability Assessment," by I-K. Ho and A.E. Aktan, 11/1/89, (PB90-251943, A07, MF-A01).
- NCEER-90-0001 "Geotechnical and Lifeline Aspects of the October 17, 1989 Loma Prieta Earthquake in San Francisco," by T.D. O'Rourke, H.E. Stewart, F.T. Blackburn and T.S. Dickerman, 1/90, (PB90-208596, A05, MF-A01).
- NCEER-90-0002 "Nonnormal Secondary Response Due to Yielding in a Primary Structure," by D.C.K. Chen and L.D. Lutes, 2/28/90, (PB90-251976, A07, MF-A01).
- NCEER-90-0003 "Earthquake Education Materials for Grades K-12," by K.E.K. Ross, 4/16/90, (PB91-251984, A05, MF-A05). This report has been replaced by NCEER-92-0018.
- NCEER-90-0004 "Catalog of Strong Motion Stations in Eastern North America," by R.W. Busby, 4/3/90, (PB90-251984, A05, MF-A01).
- NCEER-90-0005 "NCEER Strong-Motion Data Base: A User Manual for the GeoBase Release (Version 1.0 for the Sun3)," by P. Friberg and K. Jacob, 3/31/90 (PB90-258062, A04, MF-A01).
- NCEER-90-0006 "Seismic Hazard Along a Crude Oil Pipeline in the Event of an 1811-1812 Type New Madrid Earthquake," by H.H.M. Hwang and C-H.S. Chen, 4/16/90, (PB90-258054, A04, MF-A01).
- NCEER-90-0007 "Site-Specific Response Spectra for Memphis Sheahan Pumping Station," by H.H.M. Hwang and C.S. Lee, 5/15/90, (PB91-108811, A05, MF-A01).
- NCEER-90-0008 "Pilot Study on Seismic Vulnerability of Crude Oil Transmission Systems," by T. Ariman, R. Dobry, M. Grigoriu, F. Kozin, M. O'Rourke, T. O'Rourke and M. Shinozuka, 5/25/90, (PB91-108837, A06, MF-A01).
- NCEER-90-0009 "A Program to Generate Site Dependent Time Histories: EQGEN," by G.W. Ellis, M. Srinivasan and A.S. Cakmak, 1/30/90, (PB91-108829, A04, MF-A01).
- NCEER-90-0010 "Active Isolation for Seismic Protection of Operating Rooms," by M.E. Talbott, Supervised by M. Shinozuka, 6/8/9, (PB91-110205, A05, MF-A01).

- NCEER-90-0011 "Program LINEARID for Identification of Linear Structural Dynamic Systems," by C-B. Yun and M. Shinozuka, 6/25/90, (PB91-110312, A08, MF-A01).
- NCEER-90-0012 "Two-Dimensional Two-Phase Elasto-Plastic Seismic Response of Earth Dams," by A.N. Yiagos, Supervised by J.H. Prevost, 6/20/90, (PB91-110197, A13, MF-A02).
- NCEER-90-0013 "Secondary Systems in Base-Isolated Structures: Experimental Investigation, Stochastic Response and Stochastic Sensitivity," by G.D. Manolis, G. Juhn, M.C. Constantinou and A.M. Reinhorn, 7/1/90, (PB91-110320, A08, MF-A01).
- NCEER-90-0014 "Seismic Behavior of Lightly-Reinforced Concrete Column and Beam-Column Joint Details," by S.P. Pessiki, C.H. Conley, P. Gergely and R.N. White, 8/22/90, (PB91-108795, A11, MF-A02).
- NCEER-90-0015 "Two Hybrid Control Systems for Building Structures Under Strong Earthquakes," by J.N. Yang and A. Daniellians, 6/29/90, (PB91-125393, A04, MF-A01).
- NCEER-90-0016 "Instantaneous Optimal Control with Acceleration and Velocity Feedback," by J.N. Yang and Z. Li, 6/29/90, (PB91-125401, A03, MF-A01).
- NCEER-90-0017 "Reconnaissance Report on the Northern Iran Earthquake of June 21, 1990," by M. Mehrain, 10/4/90, (PB91-125377, A03, MF-A01).
- NCEER-90-0018 "Evaluation of Liquefaction Potential in Memphis and Shelby County," by T.S. Chang, P.S. Tang, C.S. Lee and H. Hwang, 8/10/90, (PB91-125427, A09, MF-A01).
- NCEER-90-0019 "Experimental and Analytical Study of a Combined Sliding Disc Bearing and Helical Steel Spring Isolation System," by M.C. Constantinou, A.S. Mokha and A.M. Reinhorn, 10/4/90, (PB91-125385, A06, MF-A01). This report is available only through NTIS (see address given above).
- NCEER-90-0020 "Experimental Study and Analytical Prediction of Earthquake Response of a Sliding Isolation System with a Spherical Surface," by A.S. Mokha, M.C. Constantinou and A.M. Reinhorn, 10/11/90, (PB91-125419, A05, MF-A01).
- NCEER-90-0021 "Dynamic Interaction Factors for Floating Pile Groups," by G. Gazetas, K. Fan, A. Kaynia and E. Kausel, 9/10/90, (PB91-170381, A05, MF-A01).
- NCEER-90-0022 "Evaluation of Seismic Damage Indices for Reinforced Concrete Structures," by S. Rodriguez-Gomez and A.S. Cakmak, 9/30/90, PB91-171322, A06, MF-A01).
- NCEER-90-0023 "Study of Site Response at a Selected Memphis Site," by H. Desai, S. Ahmad, E.S. Gazetas and M.R. Oh, 10/11/90, (PB91-196857, A03, MF-A01).
- NCEER-90-0024 "A User's Guide to Strongmo: Version 1.0 of NCEER's Strong-Motion Data Access Tool for PCs and Terminals," by P.A. Friberg and C.A.T. Susch, 11/15/90, (PB91-171272, A03, MF-A01).
- NCEER-90-0025 "A Three-Dimensional Analytical Study of Spatial Variability of Seismic Ground Motions," by L-L. Hong and A.H.-S. Ang, 10/30/90, (PB91-170399, A09, MF-A01).
- NCEER-90-0026 "MUMOID User's Guide - A Program for the Identification of Modal Parameters," by S. Rodriguez-Gomez and E. DiPasquale, 9/30/90, (PB91-171298, A04, MF-A01).
- NCEER-90-0027 "SARCF-II User's Guide - Seismic Analysis of Reinforced Concrete Frames," by S. Rodriguez-Gomez, Y.S. Chung and C. Meyer, 9/30/90, (PB91-171280, A05, MF-A01).
- NCEER-90-0028 "Viscous Dampers: Testing, Modeling and Application in Vibration and Seismic Isolation," by N. Makris and M.C. Constantinou, 12/20/90 (PB91-190561, A06, MF-A01).
- NCEER-90-0029 "Soil Effects on Earthquake Ground Motions in the Memphis Area," by H. Hwang, C.S. Lee, K.W. Ng and T.S. Chang, 8/2/90, (PB91-190751, A05, MF-A01).

- NCEER-91-0001 "Proceedings from the Third Japan-U.S. Workshop on Earthquake Resistant Design of Lifeline Facilities and Countermeasures for Soil Liquefaction, December 17-19, 1990," edited by T.D. O'Rourke and M. Hamada, 2/1/91, (PB91-179259, A99, MF-A04).
- NCEER-91-0002 "Physical Space Solutions of Non-Proportionally Damped Systems," by M. Tong, Z. Liang and G.C. Lee, 1/15/91, (PB91-179242, A04, MF-A01).
- NCEER-91-0003 "Seismic Response of Single Piles and Pile Groups," by K. Fan and G. Gazetas, 1/10/91, (PB92-174994, A04, MF-A01).
- NCEER-91-0004 "Damping of Structures: Part I - Theory of Complex Damping," by Z. Liang and G. Lee, 10/10/91, (PB92-197235, A12, MF-A03).
- NCEER-91-0005 "3D-BASIS - Nonlinear Dynamic Analysis of Three Dimensional Base Isolated Structures: Part II," by S. Nagarajaiah, A.M. Reinhorn and M.C. Constantinou, 2/28/91, (PB91-190553, A07, MF-A01). This report has been replaced by NCEER-93-0011.
- NCEER-91-0006 "A Multidimensional Hysteretic Model for Plasticity Deforming Metals in Energy Absorbing Devices," by E.J. Graesser and F.A. Cozzarelli, 4/9/91, (PB92-108364, A04, MF-A01).
- NCEER-91-0007 "A Framework for Customizable Knowledge-Based Expert Systems with an Application to a KBES for Evaluating the Seismic Resistance of Existing Buildings," by E.G. Ibarra-Anaya and S.J. Fennes, 4/9/91, (PB91-210930, A08, MF-A01).
- NCEER-91-0008 "Nonlinear Analysis of Steel Frames with Semi-Rigid Connections Using the Capacity Spectrum Method," by G.G. Deierlein, S-H. Hsieh, Y-J. Shen and J.F. Abel, 7/2/91, (PB92-113828, A05, MF-A01).
- NCEER-91-0009 "Earthquake Education Materials for Grades K-12," by K.E.K. Ross, 4/30/91, (PB91-212142, A06, MF-A01). This report has been replaced by NCEER-92-0018.
- NCEER-91-0010 "Phase Wave Velocities and Displacement Phase Differences in a Harmonically Oscillating Pile," by N. Makris and G. Gazetas, 7/8/91, (PB92-108356, A04, MF-A01).
- NCEER-91-0011 "Dynamic Characteristics of a Full-Size Five-Story Steel Structure and a 2/5 Scale Model," by K.C. Chang, G.C. Yao, G.C. Lee, D.S. Hao and Y.C. Yeh, 7/2/91, (PB93-116648, A06, MF-A02).
- NCEER-91-0012 "Seismic Response of a 2/5 Scale Steel Structure with Added Viscoelastic Dampers," by K.C. Chang, T.T. Soong, S-T. Oh and M.L. Lai, 5/17/91, (PB92-110816, A05, MF-A01).
- NCEER-91-0013 "Earthquake Response of Retaining Walls; Full-Scale Testing and Computational Modeling," by S. Alampalli and A-W.M. Elgamal, 6/20/91, not available.
- NCEER-91-0014 "3D-BASIS-M: Nonlinear Dynamic Analysis of Multiple Building Base Isolated Structures," by P.C. Tsopelas, S. Nagarajaiah, M.C. Constantinou and A.M. Reinhorn, 5/28/91, (PB92-113885, A09, MF-A02).
- NCEER-91-0015 "Evaluation of SEAOC Design Requirements for Sliding Isolated Structures," by D. Theodossiou and M.C. Constantinou, 6/10/91, (PB92-114602, A11, MF-A03).
- NCEER-91-0016 "Closed-Loop Modal Testing of a 27-Story Reinforced Concrete Flat Plate-Core Building," by H.R. Somaprasad, T. Toksoy, H. Yoshiyuki and A.E. Aktan, 7/15/91, (PB92-129980, A07, MF-A02).
- NCEER-91-0017 "Shake Table Test of a 1/6 Scale Two-Story Lightly Reinforced Concrete Building," by A.G. El-Attar, R.N. White and P. Gergely, 2/28/91, (PB92-222447, A06, MF-A02).
- NCEER-91-0018 "Shake Table Test of a 1/8 Scale Three-Story Lightly Reinforced Concrete Building," by A.G. El-Attar, R.N. White and P. Gergely, 2/28/91, (PB93-116630, A08, MF-A02).
- NCEER-91-0019 "Transfer Functions for Rigid Rectangular Foundations," by A.S. Veletsos, A.M. Prasad and W.H. Wu, 7/31/91, not available.

- NCEER-91-0020 "Hybrid Control of Seismic-Excited Nonlinear and Inelastic Structural Systems," by J.N. Yang, Z. Li and A. Daniellians, 8/1/91, (PB92-143171, A06, MF-A02).
- NCEER-91-0021 "The NCEER-91 Earthquake Catalog: Improved Intensity-Based Magnitudes and Recurrence Relations for U.S. Earthquakes East of New Madrid," by L. Seeber and J.G. Armbruster, 8/28/91, (PB92-176742, A06, MF-A02).
- NCEER-91-0022 "Proceedings from the Implementation of Earthquake Planning and Education in Schools: The Need for Change - The Roles of the Changemakers," by K.E.K. Ross and F. Winslow, 7/23/91, (PB92-129998, A12, MF-A03).
- NCEER-91-0023 "A Study of Reliability-Based Criteria for Seismic Design of Reinforced Concrete Frame Buildings," by H.H.M. Hwang and H-M. Hsu, 8/10/91, (PB92-140235, A09, MF-A02).
- NCEER-91-0024 "Experimental Verification of a Number of Structural System Identification Algorithms," by R.G. Ghanem, H. Gavin and M. Shinozuka, 9/18/91, (PB92-176577, A18, MF-A04).
- NCEER-91-0025 "Probabilistic Evaluation of Liquefaction Potential," by H.H.M. Hwang and C.S. Lee," 11/25/91, (PB92-143429, A05, MF-A01).
- NCEER-91-0026 "Instantaneous Optimal Control for Linear, Nonlinear and Hysteretic Structures - Stable Controllers," by J.N. Yang and Z. Li, 11/15/91, (PB92-163807, A04, MF-A01).
- NCEER-91-0027 "Experimental and Theoretical Study of a Sliding Isolation System for Bridges," by M.C. Constantinou, A. Kartoum, A.M. Reinhorn and P. Bradford, 11/15/91, (PB92-176973, A10, MF-A03).
- NCEER-92-0001 "Case Studies of Liquefaction and Lifeline Performance During Past Earthquakes, Volume 1: Japanese Case Studies," Edited by M. Hamada and T. O'Rourke, 2/17/92, (PB92-197243, A18, MF-A04).
- NCEER-92-0002 "Case Studies of Liquefaction and Lifeline Performance During Past Earthquakes, Volume 2: United States Case Studies," Edited by T. O'Rourke and M. Hamada, 2/17/92, (PB92-197250, A20, MF-A04).
- NCEER-92-0003 "Issues in Earthquake Education," Edited by K. Ross, 2/3/92, (PB92-222389, A07, MF-A02).
- NCEER-92-0004 "Proceedings from the First U.S. - Japan Workshop on Earthquake Protective Systems for Bridges," Edited by I.G. Buckle, 2/4/92, (PB94-142239, A99, MF-A06).
- NCEER-92-0005 "Seismic Ground Motion from a Haskell-Type Source in a Multiple-Layered Half-Space," A.P. Theoharis, G. Deodatis and M. Shinozuka, 1/2/92, not available.
- NCEER-92-0006 "Proceedings from the Site Effects Workshop," Edited by R. Whitman, 2/29/92, (PB92-197201, A04, MF-A01).
- NCEER-92-0007 "Engineering Evaluation of Permanent Ground Deformations Due to Seismically-Induced Liquefaction," by M.H. Baziar, R. Dobry and A-W.M. Elgamel, 3/24/92, (PB92-222421, A13, MF-A03).
- NCEER-92-0008 "A Procedure for the Seismic Evaluation of Buildings in the Central and Eastern United States," by C.D. Poland and J.O. Malley, 4/2/92, (PB92-222439, A20, MF-A04).
- NCEER-92-0009 "Experimental and Analytical Study of a Hybrid Isolation System Using Friction Controllable Sliding Bearings," by M.Q. Feng, S. Fujii and M. Shinozuka, 5/15/92, (PB93-150282, A06, MF-A02).
- NCEER-92-0010 "Seismic Resistance of Slab-Column Connections in Existing Non-Ductile Flat-Plate Buildings," by A.J. Durrani and Y. Du, 5/18/92, (PB93-116812, A06, MF-A02).
- NCEER-92-0011 "The Hysteretic and Dynamic Behavior of Brick Masonry Walls Upgraded by Ferrocement Coatings Under Cyclic Loading and Strong Simulated Ground Motion," by H. Lee and S.P. Prawel, 5/11/92, not available.
- NCEER-92-0012 "Study of Wire Rope Systems for Seismic Protection of Equipment in Buildings," by G.F. Demetriades, M.C. Constantinou and A.M. Reinhorn, 5/20/92, (PB93-116655, A08, MF-A02).

- NCEER-92-0013 "Shape Memory Structural Dampers: Material Properties, Design and Seismic Testing," by P.R. Witting and F.A. Cozzarelli, 5/26/92, (PB93-116663, A05, MF-A01).
- NCEER-92-0014 "Longitudinal Permanent Ground Deformation Effects on Buried Continuous Pipelines," by M.J. O'Rourke, and C. Nordberg, 6/15/92, (PB93-116671, A08, MF-A02).
- NCEER-92-0015 "A Simulation Method for Stationary Gaussian Random Functions Based on the Sampling Theorem," by M. Grigoriu and S. Balopoulou, 6/11/92, (PB93-127496, A05, MF-A01).
- NCEER-92-0016 "Gravity-Load-Designed Reinforced Concrete Buildings: Seismic Evaluation of Existing Construction and Detailing Strategies for Improved Seismic Resistance," by G.W. Hoffmann, S.K. Kunnath, A.M. Reinhorn and J.B. Mander, 7/15/92, (PB94-142007, A08, MF-A02).
- NCEER-92-0017 "Observations on Water System and Pipeline Performance in the Limón Area of Costa Rica Due to the April 22, 1991 Earthquake," by M. O'Rourke and D. Ballantyne, 6/30/92, (PB93-126811, A06, MF-A02).
- NCEER-92-0018 "Fourth Edition of Earthquake Education Materials for Grades K-12," Edited by K.E.K. Ross, 8/10/92, (PB93-114023, A07, MF-A02).
- NCEER-92-0019 "Proceedings from the Fourth Japan-U.S. Workshop on Earthquake Resistant Design of Lifeline Facilities and Countermeasures for Soil Liquefaction," Edited by M. Hamada and T.D. O'Rourke, 8/12/92, (PB93-163939, A99, MF-E11).
- NCEER-92-0020 "Active Bracing System: A Full Scale Implementation of Active Control," by A.M. Reinhorn, T.T. Soong, R.C. Lin, M.A. Riley, Y.P. Wang, S. Aizawa and M. Higashino, 8/14/92, (PB93-127512, A06, MF-A02).
- NCEER-92-0021 "Empirical Analysis of Horizontal Ground Displacement Generated by Liquefaction-Induced Lateral Spreads," by S.F. Bartlett and T.L. Youd, 8/17/92, (PB93-188241, A06, MF-A02).
- NCEER-92-0022 "IDARC Version 3.0: Inelastic Damage Analysis of Reinforced Concrete Structures," by S.K. Kunnath, A.M. Reinhorn and R.F. Lobo, 8/31/92, (PB93-227502, A07, MF-A02).
- NCEER-92-0023 "A Semi-Empirical Analysis of Strong-Motion Peaks in Terms of Seismic Source, Propagation Path and Local Site Conditions, by M. Kamiyama, M.J. O'Rourke and R. Flores-Berrones, 9/9/92, (PB93-150266, A08, MF-A02).
- NCEER-92-0024 "Seismic Behavior of Reinforced Concrete Frame Structures with Nonductile Details, Part I: Summary of Experimental Findings of Full Scale Beam-Column Joint Tests," by A. Beres, R.N. White and P. Gergely, 9/30/92, (PB93-227783, A05, MF-A01).
- NCEER-92-0025 "Experimental Results of Repaired and Retrofitted Beam-Column Joint Tests in Lightly Reinforced Concrete Frame Buildings," by A. Beres, S. El-Borgi, R.N. White and P. Gergely, 10/29/92, (PB93-227791, A05, MF-A01).
- NCEER-92-0026 "A Generalization of Optimal Control Theory: Linear and Nonlinear Structures," by J.N. Yang, Z. Li and S. Vongchavalitkul, 11/2/92, (PB93-188621, A05, MF-A01).
- NCEER-92-0027 "Seismic Resistance of Reinforced Concrete Frame Structures Designed Only for Gravity Loads: Part I - Design and Properties of a One-Third Scale Model Structure," by J.M. Bracci, A.M. Reinhorn and J.B. Mander, 12/1/92, (PB94-104502, A08, MF-A02).
- NCEER-92-0028 "Seismic Resistance of Reinforced Concrete Frame Structures Designed Only for Gravity Loads: Part II - Experimental Performance of Subassemblages," by L.E. Aycaardi, J.B. Mander and A.M. Reinhorn, 12/1/92, (PB94-104510, A08, MF-A02).
- NCEER-92-0029 "Seismic Resistance of Reinforced Concrete Frame Structures Designed Only for Gravity Loads: Part III - Experimental Performance and Analytical Study of a Structural Model," by J.M. Bracci, A.M. Reinhorn and J.B. Mander, 12/1/92, (PB93-227528, A09, MF-A01).

- NCEER-92-0030 "Evaluation of Seismic Retrofit of Reinforced Concrete Frame Structures: Part I - Experimental Performance of Retrofitted Subassemblages," by D. Choudhuri, J.B. Mander and A.M. Reinhorn, 12/8/92, (PB93-198307, A07, MF-A02).
- NCEER-92-0031 "Evaluation of Seismic Retrofit of Reinforced Concrete Frame Structures: Part II - Experimental Performance and Analytical Study of a Retrofitted Structural Model," by J.M. Bracci, A.M. Reinhorn and J.B. Mander, 12/8/92, (PB93-198315, A09, MF-A03).
- NCEER-92-0032 "Experimental and Analytical Investigation of Seismic Response of Structures with Supplemental Fluid Viscous Dampers," by M.C. Constantinou and M.D. Symans, 12/21/92, (PB93-191435, A10, MF-A03). This report is available only through NTIS (see address given above).
- NCEER-92-0033 "Reconnaissance Report on the Cairo, Egypt Earthquake of October 12, 1992," by M. Khater, 12/23/92, (PB93-188621, A03, MF-A01).
- NCEER-92-0034 "Low-Level Dynamic Characteristics of Four Tall Flat-Plate Buildings in New York City," by H. Gavin, S. Yuan, J. Grossman, E. Pekelis and K. Jacob, 12/28/92, (PB93-188217, A07, MF-A02).
- NCEER-93-0001 "An Experimental Study on the Seismic Performance of Brick-Infilled Steel Frames With and Without Retrofit," by J.B. Mander, B. Nair, K. Wojtkowski and J. Ma, 1/29/93, (PB93-227510, A07, MF-A02).
- NCEER-93-0002 "Social Accounting for Disaster Preparedness and Recovery Planning," by S. Cole, E. Pantoja and V. Razak, 2/22/93, (PB94-142114, A12, MF-A03).
- NCEER-93-0003 "Assessment of 1991 NEHRP Provisions for Nonstructural Components and Recommended Revisions," by T.T. Soong, G. Chen, Z. Wu, R-H. Zhang and M. Grigoriu, 3/1/93, (PB93-188639, A06, MF-A02).
- NCEER-93-0004 "Evaluation of Static and Response Spectrum Analysis Procedures of SEAOC/UBC for Seismic Isolated Structures," by C.W. Winters and M.C. Constantinou, 3/23/93, (PB93-198299, A10, MF-A03).
- NCEER-93-0005 "Earthquakes in the Northeast - Are We Ignoring the Hazard? A Workshop on Earthquake Science and Safety for Educators," edited by K.E.K. Ross, 4/2/93, (PB94-103066, A09, MF-A02).
- NCEER-93-0006 "Inelastic Response of Reinforced Concrete Structures with Viscoelastic Braces," by R.F. Lobo, J.M. Bracci, K.L. Shen, A.M. Reinhorn and T.T. Soong, 4/5/93, (PB93-227486, A05, MF-A02).
- NCEER-93-0007 "Seismic Testing of Installation Methods for Computers and Data Processing Equipment," by K. Kosar, T.T. Soong, K.L. Shen, J.A. HoLung and Y.K. Lin, 4/12/93, (PB93-198299, A07, MF-A02).
- NCEER-93-0008 "Retrofit of Reinforced Concrete Frames Using Added Dampers," by A. Reinhorn, M. Constantinou and C. Li, not available.
- NCEER-93-0009 "Seismic Behavior and Design Guidelines for Steel Frame Structures with Added Viscoelastic Dampers," by K.C. Chang, M.L. Lai, T.T. Soong, D.S. Hao and Y.C. Yeh, 5/1/93, (PB94-141959, A07, MF-A02).
- NCEER-93-0010 "Seismic Performance of Shear-Critical Reinforced Concrete Bridge Piers," by J.B. Mander, S.M. Waheed, M.T.A. Chaudhary and S.S. Chen, 5/12/93, (PB93-227494, A08, MF-A02).
- NCEER-93-0011 "3D-BASIS-TABS: Computer Program for Nonlinear Dynamic Analysis of Three Dimensional Base Isolated Structures," by S. Nagarajaiah, C. Li, A.M. Reinhorn and M.C. Constantinou, 8/2/93, (PB94-141819, A09, MF-A02).
- NCEER-93-0012 "Effects of Hydrocarbon Spills from an Oil Pipeline Break on Ground Water," by O.J. Helweg and H.H.M. Hwang, 8/3/93, (PB94-141942, A06, MF-A02).
- NCEER-93-0013 "Simplified Procedures for Seismic Design of Nonstructural Components and Assessment of Current Code Provisions," by M.P. Singh, L.E. Suarez, E.E. Matheu and G.O. Maldonado, 8/4/93, (PB94-141827, A09, MF-A02).
- NCEER-93-0014 "An Energy Approach to Seismic Analysis and Design of Secondary Systems," by G. Chen and T.T. Soong, 8/6/93, (PB94-142767, A11, MF-A03).

- NCEER-93-0015 "Proceedings from School Sites: Becoming Prepared for Earthquakes - Commemorating the Third Anniversary of the Loma Prieta Earthquake," Edited by F.E. Winslow and K.E.K. Ross, 8/16/93, (PB94-154275, A16, MF-A02).
- NCEER-93-0016 "Reconnaissance Report of Damage to Historic Monuments in Cairo, Egypt Following the October 12, 1992 Dahshur Earthquake," by D. Sykora, D. Look, G. Croci, E. Karaesmen and E. Karaesmen, 8/19/93, (PB94-142221, A08, MF-A02).
- NCEER-93-0017 "The Island of Guam Earthquake of August 8, 1993," by S.W. Swan and S.K. Harris, 9/30/93, (PB94-141843, A04, MF-A01).
- NCEER-93-0018 "Engineering Aspects of the October 12, 1992 Egyptian Earthquake," by A.W. Elgamal, M. Amer, K. Adalier and A. Abul-Fadl, 10/7/93, (PB94-141983, A05, MF-A01).
- NCEER-93-0019 "Development of an Earthquake Motion Simulator and its Application in Dynamic Centrifuge Testing," by I. Krstelj, Supervised by J.H. Prevost, 10/23/93, (PB94-181773, A-10, MF-A03).
- NCEER-93-0020 "NCEER-Taisei Corporation Research Program on Sliding Seismic Isolation Systems for Bridges: Experimental and Analytical Study of a Friction Pendulum System (FPS)," by M.C. Constantinou, P. Tsopelas, Y-S. Kim and S. Okamoto, 11/1/93, (PB94-142775, A08, MF-A02).
- NCEER-93-0021 "Finite Element Modeling of Elastomeric Seismic Isolation Bearings," by L.J. Billings, Supervised by R. Shepherd, 11/8/93, not available.
- NCEER-93-0022 "Seismic Vulnerability of Equipment in Critical Facilities: Life-Safety and Operational Consequences," by K. Porter, G.S. Johnson, M.M. Zadeh, C. Scawthorn and S. Eder, 11/24/93, (PB94-181765, A16, MF-A03).
- NCEER-93-0023 "Hokkaido Nansei-oki, Japan Earthquake of July 12, 1993, by P.I. Yanev and C.R. Scawthorn, 12/23/93, (PB94-181500, A07, MF-A01).
- NCEER-94-0001 "An Evaluation of Seismic Serviceability of Water Supply Networks with Application to the San Francisco Auxiliary Water Supply System," by I. Markov, Supervised by M. Grigoriu and T. O'Rourke, 1/21/94, (PB94-204013, A07, MF-A02).
- NCEER-94-0002 "NCEER-Taisei Corporation Research Program on Sliding Seismic Isolation Systems for Bridges: Experimental and Analytical Study of Systems Consisting of Sliding Bearings, Rubber Restoring Force Devices and Fluid Dampers," Volumes I and II, by P. Tsopelas, S. Okamoto, M.C. Constantinou, D. Ozaki and S. Fujii, 2/4/94, (PB94-181740, A09, MF-A02 and PB94-181757, A12, MF-A03).
- NCEER-94-0003 "A Markov Model for Local and Global Damage Indices in Seismic Analysis," by S. Rahman and M. Grigoriu, 2/18/94, (PB94-206000, A12, MF-A03).
- NCEER-94-0004 "Proceedings from the NCEER Workshop on Seismic Response of Masonry Infills," edited by D.P. Abrams, 3/1/94, (PB94-180783, A07, MF-A02).
- NCEER-94-0005 "The Northridge, California Earthquake of January 17, 1994: General Reconnaissance Report," edited by J.D. Goltz, 3/11/94, (PB94-193943, A10, MF-A03).
- NCEER-94-0006 "Seismic Energy Based Fatigue Damage Analysis of Bridge Columns: Part I - Evaluation of Seismic Capacity," by G.A. Chang and J.B. Mander, 3/14/94, (PB94-219185, A11, MF-A03).
- NCEER-94-0007 "Seismic Isolation of Multi-Story Frame Structures Using Spherical Sliding Isolation Systems," by T.M. Al-Hussaini, V.A. Zayas and M.C. Constantinou, 3/17/94, (PB94-193745, A09, MF-A02).
- NCEER-94-0008 "The Northridge, California Earthquake of January 17, 1994: Performance of Highway Bridges," edited by I.G. Buckle, 3/24/94, (PB94-193851, A06, MF-A02).
- NCEER-94-0009 "Proceedings of the Third U.S.-Japan Workshop on Earthquake Protective Systems for Bridges," edited by I.G. Buckle and I. Friedland, 3/31/94, (PB94-195815, A99, MF-A06).

- NCEER-94-0010 "3D-BASIS-ME: Computer Program for Nonlinear Dynamic Analysis of Seismically Isolated Single and Multiple Structures and Liquid Storage Tanks," by P.C. Tsopelas, M.C. Constantinou and A.M. Reinhorn, 4/12/94, (PB94-204922, A09, MF-A02).
- NCEER-94-0011 "The Northridge, California Earthquake of January 17, 1994: Performance of Gas Transmission Pipelines," by T.D. O'Rourke and M.C. Palmer, 5/16/94, (PB94-204989, A05, MF-A01).
- NCEER-94-0012 "Feasibility Study of Replacement Procedures and Earthquake Performance Related to Gas Transmission Pipelines," by T.D. O'Rourke and M.C. Palmer, 5/25/94, (PB94-206638, A09, MF-A02).
- NCEER-94-0013 "Seismic Energy Based Fatigue Damage Analysis of Bridge Columns: Part II - Evaluation of Seismic Demand," by G.A. Chang and J.B. Mander, 6/1/94, (PB95-18106, A08, MF-A02).
- NCEER-94-0014 "NCEER-Taisei Corporation Research Program on Sliding Seismic Isolation Systems for Bridges: Experimental and Analytical Study of a System Consisting of Sliding Bearings and Fluid Restoring Force/Damping Devices," by P. Tsopelas and M.C. Constantinou, 6/13/94, (PB94-219144, A10, MF-A03).
- NCEER-94-0015 "Generation of Hazard-Consistent Fragility Curves for Seismic Loss Estimation Studies," by H. Hwang and J-R. Huo, 6/14/94, (PB95-181996, A09, MF-A02).
- NCEER-94-0016 "Seismic Study of Building Frames with Added Energy-Absorbing Devices," by W.S. Pong, C.S. Tsai and G.C. Lee, 6/20/94, (PB94-219136, A10, A03).
- NCEER-94-0017 "Sliding Mode Control for Seismic-Excited Linear and Nonlinear Civil Engineering Structures," by J. Yang, J. Wu, A. Agrawal and Z. Li, 6/21/94, (PB95-138483, A06, MF-A02).
- NCEER-94-0018 "3D-BASIS-TABS Version 2.0: Computer Program for Nonlinear Dynamic Analysis of Three Dimensional Base Isolated Structures," by A.M. Reinhorn, S. Nagarajaiah, M.C. Constantinou, P. Tsopelas and R. Li, 6/22/94, (PB95-182176, A08, MF-A02).
- NCEER-94-0019 "Proceedings of the International Workshop on Civil Infrastructure Systems: Application of Intelligent Systems and Advanced Materials on Bridge Systems," Edited by G.C. Lee and K.C. Chang, 7/18/94, (PB95-252474, A20, MF-A04).
- NCEER-94-0020 "Study of Seismic Isolation Systems for Computer Floors," by V. Lambrou and M.C. Constantinou, 7/19/94, (PB95-138533, A10, MF-A03).
- NCEER-94-0021 "Proceedings of the U.S.-Italian Workshop on Guidelines for Seismic Evaluation and Rehabilitation of Unreinforced Masonry Buildings," Edited by D.P. Abrams and G.M. Calvi, 7/20/94, (PB95-138749, A13, MF-A03).
- NCEER-94-0022 "NCEER-Taisei Corporation Research Program on Sliding Seismic Isolation Systems for Bridges: Experimental and Analytical Study of a System Consisting of Lubricated PTFE Sliding Bearings and Mild Steel Dampers," by P. Tsopelas and M.C. Constantinou, 7/22/94, (PB95-182184, A08, MF-A02).
- NCEER-94-0023 "Development of Reliability-Based Design Criteria for Buildings Under Seismic Load," by Y.K. Wen, H. Hwang and M. Shinozuka, 8/1/94, (PB95-211934, A08, MF-A02).
- NCEER-94-0024 "Experimental Verification of Acceleration Feedback Control Strategies for an Active Tendon System," by S.J. Dyke, B.F. Spencer, Jr., P. Quast, M.K. Sain, D.C. Kaspari, Jr. and T.T. Soong, 8/29/94, (PB95-212320, A05, MF-A01).
- NCEER-94-0025 "Seismic Retrofitting Manual for Highway Bridges," Edited by I.G. Buckle and I.F. Friedland, published by the Federal Highway Administration (PB95-212676, A15, MF-A03).
- NCEER-94-0026 "Proceedings from the Fifth U.S.-Japan Workshop on Earthquake Resistant Design of Lifeline Facilities and Countermeasures Against Soil Liquefaction," Edited by T.D. O'Rourke and M. Hamada, 11/7/94, (PB95-220802, A99, MF-E08).

- NCEER-95-0001 “Experimental and Analytical Investigation of Seismic Retrofit of Structures with Supplemental Damping: Part 1 - Fluid Viscous Damping Devices,” by A.M. Reinhorn, C. Li and M.C. Constantinou, 1/3/95, (PB95-266599, A09, MF-A02).
- NCEER-95-0002 “Experimental and Analytical Study of Low-Cycle Fatigue Behavior of Semi-Rigid Top-And-Seat Angle Connections,” by G. Pekcan, J.B. Mander and S.S. Chen, 1/5/95, (PB95-220042, A07, MF-A02).
- NCEER-95-0003 “NCEER-ATC Joint Study on Fragility of Buildings,” by T. Anagnos, C. Rojahn and A.S. Kiremidjian, 1/20/95, (PB95-220026, A06, MF-A02).
- NCEER-95-0004 “Nonlinear Control Algorithms for Peak Response Reduction,” by Z. Wu, T.T. Soong, V. Gattulli and R.C. Lin, 2/16/95, (PB95-220349, A05, MF-A01).
- NCEER-95-0005 “Pipeline Replacement Feasibility Study: A Methodology for Minimizing Seismic and Corrosion Risks to Underground Natural Gas Pipelines,” by R.T. Eguchi, H.A. Seligson and D.G. Honegger, 3/2/95, (PB95-252326, A06, MF-A02).
- NCEER-95-0006 “Evaluation of Seismic Performance of an 11-Story Frame Building During the 1994 Northridge Earthquake,” by F. Naeim, R. DiSulio, K. Benuska, A. Reinhorn and C. Li, not available.
- NCEER-95-0007 “Prioritization of Bridges for Seismic Retrofitting,” by N. Basöz and A.S. Kiremidjian, 4/24/95, (PB95-252300, A08, MF-A02).
- NCEER-95-0008 “Method for Developing Motion Damage Relationships for Reinforced Concrete Frames,” by A. Singhal and A.S. Kiremidjian, 5/11/95, (PB95-266607, A06, MF-A02).
- NCEER-95-0009 “Experimental and Analytical Investigation of Seismic Retrofit of Structures with Supplemental Damping: Part II - Friction Devices,” by C. Li and A.M. Reinhorn, 7/6/95, (PB96-128087, A11, MF-A03).
- NCEER-95-0010 “Experimental Performance and Analytical Study of a Non-Ductile Reinforced Concrete Frame Structure Retrofitted with Elastomeric Spring Dampers,” by G. Pekcan, J.B. Mander and S.S. Chen, 7/14/95, (PB96-137161, A08, MF-A02).
- NCEER-95-0011 “Development and Experimental Study of Semi-Active Fluid Damping Devices for Seismic Protection of Structures,” by M.D. Symans and M.C. Constantinou, 8/3/95, (PB96-136940, A23, MF-A04).
- NCEER-95-0012 “Real-Time Structural Parameter Modification (RSPM): Development of Innervated Structures,” by Z. Liang, M. Tong and G.C. Lee, 4/11/95, (PB96-137153, A06, MF-A01).
- NCEER-95-0013 “Experimental and Analytical Investigation of Seismic Retrofit of Structures with Supplemental Damping: Part III - Viscous Damping Walls,” by A.M. Reinhorn and C. Li, 10/1/95, (PB96-176409, A11, MF-A03).
- NCEER-95-0014 “Seismic Fragility Analysis of Equipment and Structures in a Memphis Electric Substation,” by J-R. Huo and H.H.M. Hwang, 8/10/95, (PB96-128087, A09, MF-A02).
- NCEER-95-0015 “The Hanshin-Awaji Earthquake of January 17, 1995: Performance of Lifelines,” Edited by M. Shinozuka, 11/3/95, (PB96-176383, A15, MF-A03).
- NCEER-95-0016 “Highway Culvert Performance During Earthquakes,” by T.L. Youd and C.J. Beckman, available as NCEER-96-0015.
- NCEER-95-0017 “The Hanshin-Awaji Earthquake of January 17, 1995: Performance of Highway Bridges,” Edited by I.G. Buckle, 12/1/95, not available.
- NCEER-95-0018 “Modeling of Masonry Infill Panels for Structural Analysis,” by A.M. Reinhorn, A. Madan, R.E. Valles, Y. Reichmann and J.B. Mander, 12/8/95, (PB97-110886, MF-A01, A06).
- NCEER-95-0019 “Optimal Polynomial Control for Linear and Nonlinear Structures,” by A.K. Agrawal and J.N. Yang, 12/11/95, (PB96-168737, A07, MF-A02).

- NCEER-95-0020 "Retrofit of Non-Ductile Reinforced Concrete Frames Using Friction Dampers," by R.S. Rao, P. Gergely and R.N. White, 12/22/95, (PB97-133508, A10, MF-A02).
- NCEER-95-0021 "Parametric Results for Seismic Response of Pile-Supported Bridge Bents," by G. Mylonakis, A. Nikolaou and G. Gazetas, 12/22/95, (PB97-100242, A12, MF-A03).
- NCEER-95-0022 "Kinematic Bending Moments in Seismically Stressed Piles," by A. Nikolaou, G. Mylonakis and G. Gazetas, 12/23/95, (PB97-113914, MF-A03, A13).
- NCEER-96-0001 "Dynamic Response of Unreinforced Masonry Buildings with Flexible Diaphragms," by A.C. Costley and D.P. Abrams, 10/10/96, (PB97-133573, MF-A03, A15).
- NCEER-96-0002 "State of the Art Review: Foundations and Retaining Structures," by I. Po Lam, not available.
- NCEER-96-0003 "Ductility of Rectangular Reinforced Concrete Bridge Columns with Moderate Confinement," by N. Wehbe, M. Saiidi, D. Sanders and B. Douglas, 11/7/96, (PB97-133557, A06, MF-A02).
- NCEER-96-0004 "Proceedings of the Long-Span Bridge Seismic Research Workshop," edited by I.G. Buckle and I.M. Friedland, not available.
- NCEER-96-0005 "Establish Representative Pier Types for Comprehensive Study: Eastern United States," by J. Kulicki and Z. Prucz, 5/28/96, (PB98-119217, A07, MF-A02).
- NCEER-96-0006 "Establish Representative Pier Types for Comprehensive Study: Western United States," by R. Imbsen, R.A. Schamber and T.A. Osterkamp, 5/28/96, (PB98-118607, A07, MF-A02).
- NCEER-96-0007 "Nonlinear Control Techniques for Dynamical Systems with Uncertain Parameters," by R.G. Ghanem and M.I. Bujakov, 5/27/96, (PB97-100259, A17, MF-A03).
- NCEER-96-0008 "Seismic Evaluation of a 30-Year Old Non-Ductile Highway Bridge Pier and Its Retrofit," by J.B. Mander, B. Mahmoodzadegan, S. Bhadra and S.S. Chen, 5/31/96, (PB97-110902, MF-A03, A10).
- NCEER-96-0009 "Seismic Performance of a Model Reinforced Concrete Bridge Pier Before and After Retrofit," by J.B. Mander, J.H. Kim and C.A. Ligozio, 5/31/96, (PB97-110910, MF-A02, A10).
- NCEER-96-0010 "IDARC2D Version 4.0: A Computer Program for the Inelastic Damage Analysis of Buildings," by R.E. Valles, A.M. Reinhorn, S.K. Kunnath, C. Li and A. Madan, 6/3/96, (PB97-100234, A17, MF-A03).
- NCEER-96-0011 "Estimation of the Economic Impact of Multiple Lifeline Disruption: Memphis Light, Gas and Water Division Case Study," by S.E. Chang, H.A. Seligson and R.T. Eguchi, 8/16/96, (PB97-133490, A11, MF-A03).
- NCEER-96-0012 "Proceedings from the Sixth Japan-U.S. Workshop on Earthquake Resistant Design of Lifeline Facilities and Countermeasures Against Soil Liquefaction, Edited by M. Hamada and T. O'Rourke, 9/11/96, (PB97-133581, A99, MF-A06).
- NCEER-96-0013 "Chemical Hazards, Mitigation and Preparedness in Areas of High Seismic Risk: A Methodology for Estimating the Risk of Post-Earthquake Hazardous Materials Release," by H.A. Seligson, R.T. Eguchi, K.J. Tierney and K. Richmond, 11/7/96, (PB97-133565, MF-A02, A08).
- NCEER-96-0014 "Response of Steel Bridge Bearings to Reversed Cyclic Loading," by J.B. Mander, D-K. Kim, S.S. Chen and G.J. Premus, 11/13/96, (PB97-140735, A12, MF-A03).
- NCEER-96-0015 "Highway Culvert Performance During Past Earthquakes," by T.L. Youd and C.J. Beckman, 11/25/96, (PB97-133532, A06, MF-A01).
- NCEER-97-0001 "Evaluation, Prevention and Mitigation of Pounding Effects in Building Structures," by R.E. Valles and A.M. Reinhorn, 2/20/97, (PB97-159552, A14, MF-A03).
- NCEER-97-0002 "Seismic Design Criteria for Bridges and Other Highway Structures," by C. Rojahn, R. Mayes, D.G. Anderson, J. Clark, J.H. Hom, R.V. Nutt and M.J. O'Rourke, 4/30/97, (PB97-194658, A06, MF-A03).

- NCEER-97-0003 "Proceedings of the U.S.-Italian Workshop on Seismic Evaluation and Retrofit," Edited by D.P. Abrams and G.M. Calvi, 3/19/97, (PB97-194666, A13, MF-A03).
- NCEER-97-0004 "Investigation of Seismic Response of Buildings with Linear and Nonlinear Fluid Viscous Dampers," by A.A. Seleemah and M.C. Constantinou, 5/21/97, (PB98-109002, A15, MF-A03).
- NCEER-97-0005 "Proceedings of the Workshop on Earthquake Engineering Frontiers in Transportation Facilities," edited by G.C. Lee and I.M. Friedland, 8/29/97, (PB98-128911, A25, MR-A04).
- NCEER-97-0006 "Cumulative Seismic Damage of Reinforced Concrete Bridge Piers," by S.K. Kunnath, A. El-Bahy, A. Taylor and W. Stone, 9/2/97, (PB98-108814, A11, MF-A03).
- NCEER-97-0007 "Structural Details to Accommodate Seismic Movements of Highway Bridges and Retaining Walls," by R.A. Imbsen, R.A. Schamber, E. Thorkildsen, A. Kartoum, B.T. Martin, T.N. Rosser and J.M. Kulicki, 9/3/97, (PB98-108996, A09, MF-A02).
- NCEER-97-0008 "A Method for Earthquake Motion-Damage Relationships with Application to Reinforced Concrete Frames," by A. Singhal and A.S. Kiremidjian, 9/10/97, (PB98-108988, A13, MF-A03).
- NCEER-97-0009 "Seismic Analysis and Design of Bridge Abutments Considering Sliding and Rotation," by K. Fishman and R. Richards, Jr., 9/15/97, (PB98-108897, A06, MF-A02).
- NCEER-97-0010 "Proceedings of the FHWA/NCEER Workshop on the National Representation of Seismic Ground Motion for New and Existing Highway Facilities," edited by I.M. Friedland, M.S. Power and R.L. Mayes, 9/22/97, (PB98-128903, A21, MF-A04).
- NCEER-97-0011 "Seismic Analysis for Design or Retrofit of Gravity Bridge Abutments," by K.L. Fishman, R. Richards, Jr. and R.C. Divito, 10/2/97, (PB98-128937, A08, MF-A02).
- NCEER-97-0012 "Evaluation of Simplified Methods of Analysis for Yielding Structures," by P. Tsopelas, M.C. Constantinou, C.A. Kircher and A.S. Whittaker, 10/31/97, (PB98-128929, A10, MF-A03).
- NCEER-97-0013 "Seismic Design of Bridge Columns Based on Control and Repairability of Damage," by C-T. Cheng and J.B. Mander, 12/8/97, (PB98-144249, A11, MF-A03).
- NCEER-97-0014 "Seismic Resistance of Bridge Piers Based on Damage Avoidance Design," by J.B. Mander and C-T. Cheng, 12/10/97, (PB98-144223, A09, MF-A02).
- NCEER-97-0015 "Seismic Response of Nominally Symmetric Systems with Strength Uncertainty," by S. Balopoulou and M. Grigoriu, 12/23/97, (PB98-153422, A11, MF-A03).
- NCEER-97-0016 "Evaluation of Seismic Retrofit Methods for Reinforced Concrete Bridge Columns," by T.J. Wipf, F.W. Klaiber and F.M. Russo, 12/28/97, (PB98-144215, A12, MF-A03).
- NCEER-97-0017 "Seismic Fragility of Existing Conventional Reinforced Concrete Highway Bridges," by C.L. Mullen and A.S. Cakmak, 12/30/97, (PB98-153406, A08, MF-A02).
- NCEER-97-0018 "Loss Assessment of Memphis Buildings," edited by D.P. Abrams and M. Shinozuka, 12/31/97, (PB98-144231, A13, MF-A03).
- NCEER-97-0019 "Seismic Evaluation of Frames with Infill Walls Using Quasi-static Experiments," by K.M. Mosalam, R.N. White and P. Gergely, 12/31/97, (PB98-153455, A07, MF-A02).
- NCEER-97-0020 "Seismic Evaluation of Frames with Infill Walls Using Pseudo-dynamic Experiments," by K.M. Mosalam, R.N. White and P. Gergely, 12/31/97, (PB98-153430, A07, MF-A02).
- NCEER-97-0021 "Computational Strategies for Frames with Infill Walls: Discrete and Smeared Crack Analyses and Seismic Fragility," by K.M. Mosalam, R.N. White and P. Gergely, 12/31/97, (PB98-153414, A10, MF-A02).

- NCEER-97-0022 "Proceedings of the NCEER Workshop on Evaluation of Liquefaction Resistance of Soils," edited by T.L. Youd and I.M. Idriss, 12/31/97, (PB98-155617, A15, MF-A03).
- MCEER-98-0001 "Extraction of Nonlinear Hysteretic Properties of Seismically Isolated Bridges from Quick-Release Field Tests," by Q. Chen, B.M. Douglas, E.M. Maragakis and I.G. Buckle, 5/26/98, (PB99-118838, A06, MF-A01).
- MCEER-98-0002 "Methodologies for Evaluating the Importance of Highway Bridges," by A. Thomas, S. Eshenaur and J. Kulicki, 5/29/98, (PB99-118846, A10, MF-A02).
- MCEER-98-0003 "Capacity Design of Bridge Piers and the Analysis of Overstrength," by J.B. Mander, A. Dutta and P. Goel, 6/1/98, (PB99-118853, A09, MF-A02).
- MCEER-98-0004 "Evaluation of Bridge Damage Data from the Loma Prieta and Northridge, California Earthquakes," by N. Basoz and A. Kiremidjian, 6/2/98, (PB99-118861, A15, MF-A03).
- MCEER-98-0005 "Screening Guide for Rapid Assessment of Liquefaction Hazard at Highway Bridge Sites," by T. L. Youd, 6/16/98, (PB99-118879, A06, not available on microfiche).
- MCEER-98-0006 "Structural Steel and Steel/Concrete Interface Details for Bridges," by P. Ritchie, N. Kauh and J. Kulicki, 7/13/98, (PB99-118945, A06, MF-A01).
- MCEER-98-0007 "Capacity Design and Fatigue Analysis of Confined Concrete Columns," by A. Dutta and J.B. Mander, 7/14/98, (PB99-118960, A14, MF-A03).
- MCEER-98-0008 "Proceedings of the Workshop on Performance Criteria for Telecommunication Services Under Earthquake Conditions," edited by A.J. Schiff, 7/15/98, (PB99-118952, A08, MF-A02).
- MCEER-98-0009 "Fatigue Analysis of Unconfined Concrete Columns," by J.B. Mander, A. Dutta and J.H. Kim, 9/12/98, (PB99-123655, A10, MF-A02).
- MCEER-98-0010 "Centrifuge Modeling of Cyclic Lateral Response of Pile-Cap Systems and Seat-Type Abutments in Dry Sands," by A.D. Gadre and R. Dobry, 10/2/98, (PB99-123606, A13, MF-A03).
- MCEER-98-0011 "IDARC-BRIDGE: A Computational Platform for Seismic Damage Assessment of Bridge Structures," by A.M. Reinhorn, V. Simeonov, G. Mylonakis and Y. Reichman, 10/2/98, (PB99-162919, A15, MF-A03).
- MCEER-98-0012 "Experimental Investigation of the Dynamic Response of Two Bridges Before and After Retrofitting with Elastomeric Bearings," by D.A. Wendichansky, S.S. Chen and J.B. Mander, 10/2/98, (PB99-162927, A15, MF-A03).
- MCEER-98-0013 "Design Procedures for Hinge Restrainers and Hinge Sear Width for Multiple-Frame Bridges," by R. Des Roches and G.L. Fenves, 11/3/98, (PB99-140477, A13, MF-A03).
- MCEER-98-0014 "Response Modification Factors for Seismically Isolated Bridges," by M.C. Constantinou and J.K. Quarshie, 11/3/98, (PB99-140485, A14, MF-A03).
- MCEER-98-0015 "Proceedings of the U.S.-Italy Workshop on Seismic Protective Systems for Bridges," edited by I.M. Friedland and M.C. Constantinou, 11/3/98, (PB2000-101711, A22, MF-A04).
- MCEER-98-0016 "Appropriate Seismic Reliability for Critical Equipment Systems: Recommendations Based on Regional Analysis of Financial and Life Loss," by K. Porter, C. Scawthorn, C. Taylor and N. Blais, 11/10/98, (PB99-157265, A08, MF-A02).
- MCEER-98-0017 "Proceedings of the U.S. Japan Joint Seminar on Civil Infrastructure Systems Research," edited by M. Shinozuka and A. Rose, 11/12/98, (PB99-156713, A16, MF-A03).
- MCEER-98-0018 "Modeling of Pile Footings and Drilled Shafts for Seismic Design," by I. PoLam, M. Kapuskar and D. Chaudhuri, 12/21/98, (PB99-157257, A09, MF-A02).

- MCEER-99-0001 "Seismic Evaluation of a Masonry Infilled Reinforced Concrete Frame by Pseudodynamic Testing," by S.G. Buonopane and R.N. White, 2/16/99, (PB99-162851, A09, MF-A02).
- MCEER-99-0002 "Response History Analysis of Structures with Seismic Isolation and Energy Dissipation Systems: Verification Examples for Program SAP2000," by J. Scheller and M.C. Constantinou, 2/22/99, (PB99-162869, A08, MF-A02).
- MCEER-99-0003 "Experimental Study on the Seismic Design and Retrofit of Bridge Columns Including Axial Load Effects," by A. Dutta, T. Kokorina and J.B. Mander, 2/22/99, (PB99-162877, A09, MF-A02).
- MCEER-99-0004 "Experimental Study of Bridge Elastomeric and Other Isolation and Energy Dissipation Systems with Emphasis on Uplift Prevention and High Velocity Near-source Seismic Excitation," by A. Kasalanati and M. C. Constantinou, 2/26/99, (PB99-162885, A12, MF-A03).
- MCEER-99-0005 "Truss Modeling of Reinforced Concrete Shear-flexure Behavior," by J.H. Kim and J.B. Mander, 3/8/99, (PB99-163693, A12, MF-A03).
- MCEER-99-0006 "Experimental Investigation and Computational Modeling of Seismic Response of a 1:4 Scale Model Steel Structure with a Load Balancing Supplemental Damping System," by G. Pekcan, J.B. Mander and S.S. Chen, 4/2/99, (PB99-162893, A11, MF-A03).
- MCEER-99-0007 "Effect of Vertical Ground Motions on the Structural Response of Highway Bridges," by M.R. Button, C.J. Cronin and R.L. Mayes, 4/10/99, (PB2000-101411, A10, MF-A03).
- MCEER-99-0008 "Seismic Reliability Assessment of Critical Facilities: A Handbook, Supporting Documentation, and Model Code Provisions," by G.S. Johnson, R.E. Sheppard, M.D. Quilici, S.J. Eder and C.R. Scawthorn, 4/12/99, (PB2000-101701, A18, MF-A04).
- MCEER-99-0009 "Impact Assessment of Selected MCEER Highway Project Research on the Seismic Design of Highway Structures," by C. Rojahn, R. Mayes, D.G. Anderson, J.H. Clark, D'Appolonia Engineering, S. Gloyd and R.V. Nutt, 4/14/99, (PB99-162901, A10, MF-A02).
- MCEER-99-0010 "Site Factors and Site Categories in Seismic Codes," by R. Dobry, R. Ramos and M.S. Power, 7/19/99, (PB2000-101705, A08, MF-A02).
- MCEER-99-0011 "Restrainer Design Procedures for Multi-Span Simply-Supported Bridges," by M.J. Randall, M. Saiidi, E. Maragakis and T. Isakovic, 7/20/99, (PB2000-101702, A10, MF-A02).
- MCEER-99-0012 "Property Modification Factors for Seismic Isolation Bearings," by M.C. Constantinou, P. Tsopelas, A. Kasalanati and E. Wolff, 7/20/99, (PB2000-103387, A11, MF-A03).
- MCEER-99-0013 "Critical Seismic Issues for Existing Steel Bridges," by P. Ritchie, N. Kauh and J. Kulicki, 7/20/99, (PB2000-101697, A09, MF-A02).
- MCEER-99-0014 "Nonstructural Damage Database," by A. Kao, T.T. Soong and A. Vender, 7/24/99, (PB2000-101407, A06, MF-A01).
- MCEER-99-0015 "Guide to Remedial Measures for Liquefaction Mitigation at Existing Highway Bridge Sites," by H.G. Cooke and J. K. Mitchell, 7/26/99, (PB2000-101703, A11, MF-A03).
- MCEER-99-0016 "Proceedings of the MCEER Workshop on Ground Motion Methodologies for the Eastern United States," edited by N. Abrahamson and A. Becker, 8/11/99, (PB2000-103385, A07, MF-A02).
- MCEER-99-0017 "Quindío, Colombia Earthquake of January 25, 1999: Reconnaissance Report," by A.P. Asfura and P.J. Flores, 10/4/99, (PB2000-106893, A06, MF-A01).
- MCEER-99-0018 "Hysteretic Models for Cyclic Behavior of Deteriorating Inelastic Structures," by M.V. Sivaselvan and A.M. Reinhorn, 11/5/99, (PB2000-103386, A08, MF-A02).

- MCEER-99-0019 "Proceedings of the 7th U.S.- Japan Workshop on Earthquake Resistant Design of Lifeline Facilities and Countermeasures Against Soil Liquefaction," edited by T.D. O'Rourke, J.P. Bardet and M. Hamada, 11/19/99, (PB2000-103354, A99, MF-A06).
- MCEER-99-0020 "Development of Measurement Capability for Micro-Vibration Evaluations with Application to Chip Fabrication Facilities," by G.C. Lee, Z. Liang, J.W. Song, J.D. Shen and W.C. Liu, 12/1/99, (PB2000-105993, A08, MF-A02).
- MCEER-99-0021 "Design and Retrofit Methodology for Building Structures with Supplemental Energy Dissipating Systems," by G. Pekcan, J.B. Mander and S.S. Chen, 12/31/99, (PB2000-105994, A11, MF-A03).
- MCEER-00-0001 "The Marmara, Turkey Earthquake of August 17, 1999: Reconnaissance Report," edited by C. Scawthorn; with major contributions by M. Bruneau, R. Eguchi, T. Holzer, G. Johnson, J. Mander, J. Mitchell, W. Mitchell, A. Papageorgiou, C. Scaethorn, and G. Webb, 3/23/00, (PB2000-106200, A11, MF-A03).
- MCEER-00-0002 "Proceedings of the MCEER Workshop for Seismic Hazard Mitigation of Health Care Facilities," edited by G.C. Lee, M. Ettouney, M. Grigoriu, J. Hauer and J. Nigg, 3/29/00, (PB2000-106892, A08, MF-A02).
- MCEER-00-0003 "The Chi-Chi, Taiwan Earthquake of September 21, 1999: Reconnaissance Report," edited by G.C. Lee and C.H. Loh, with major contributions by G.C. Lee, M. Bruneau, I.G. Buckle, S.E. Chang, P.J. Flores, T.D. O'Rourke, M. Shinozuka, T.T. Soong, C-H. Loh, K-C. Chang, Z-J. Chen, J-S. Hwang, M-L. Lin, G-Y. Liu, K-C. Tsai, G.C. Yao and C-L. Yen, 4/30/00, (PB2001-100980, A10, MF-A02).
- MCEER-00-0004 "Seismic Retrofit of End-Sway Frames of Steel Deck-Truss Bridges with a Supplemental Tendon System: Experimental and Analytical Investigation," by G. Pekcan, J.B. Mander and S.S. Chen, 7/1/00, (PB2001-100982, A10, MF-A02).
- MCEER-00-0005 "Sliding Fragility of Unrestrained Equipment in Critical Facilities," by W.H. Chong and T.T. Soong, 7/5/00, (PB2001-100983, A08, MF-A02).
- MCEER-00-0006 "Seismic Response of Reinforced Concrete Bridge Pier Walls in the Weak Direction," by N. Abo-Shadi, M. Saiidi and D. Sanders, 7/17/00, (PB2001-100981, A17, MF-A03).
- MCEER-00-0007 "Low-Cycle Fatigue Behavior of Longitudinal Reinforcement in Reinforced Concrete Bridge Columns," by J. Brown and S.K. Kunnath, 7/23/00, (PB2001-104392, A08, MF-A02).
- MCEER-00-0008 "Soil Structure Interaction of Bridges for Seismic Analysis," I. PoLam and H. Law, 9/25/00, (PB2001-105397, A08, MF-A02).
- MCEER-00-0009 "Proceedings of the First MCEER Workshop on Mitigation of Earthquake Disaster by Advanced Technologies (MEDAT-1), edited by M. Shinozuka, D.J. Inman and T.D. O'Rourke, 11/10/00, (PB2001-105399, A14, MF-A03).
- MCEER-00-0010 "Development and Evaluation of Simplified Procedures for Analysis and Design of Buildings with Passive Energy Dissipation Systems, Revision 01," by O.M. Ramirez, M.C. Constantinou, C.A. Kircher, A.S. Whittaker, M.W. Johnson, J.D. Gomez and C. Chrysostomou, 11/16/01, (PB2001-105523, A23, MF-A04).
- MCEER-00-0011 "Dynamic Soil-Foundation-Structure Interaction Analyses of Large Caissons," by C-Y. Chang, C-M. Mok, Z-L. Wang, R. Settgast, F. Waggoner, M.A. Ketchum, H.M. Gonnermann and C-C. Chin, 12/30/00, (PB2001-104373, A07, MF-A02).
- MCEER-00-0012 "Experimental Evaluation of Seismic Performance of Bridge Restrainers," by A.G. Vlassis, E.M. Maragakis and M. Saiid Saiidi, 12/30/00, (PB2001-104354, A09, MF-A02).
- MCEER-00-0013 "Effect of Spatial Variation of Ground Motion on Highway Structures," by M. Shinozuka, V. Saxena and G. Deodatis, 12/31/00, (PB2001-108755, A13, MF-A03).
- MCEER-00-0014 "A Risk-Based Methodology for Assessing the Seismic Performance of Highway Systems," by S.D. Werner, C.E. Taylor, J.E. Moore, II, J.S. Walton and S. Cho, 12/31/00, (PB2001-108756, A14, MF-A03).

- MCEER-01-0001 "Experimental Investigation of P-Delta Effects to Collapse During Earthquakes," by D. Vian and M. Bruneau, 6/25/01, (PB2002-100534, A17, MF-A03).
- MCEER-01-0002 "Proceedings of the Second MCEER Workshop on Mitigation of Earthquake Disaster by Advanced Technologies (MEDAT-2)," edited by M. Bruneau and D.J. Inman, 7/23/01, (PB2002-100434, A16, MF-A03).
- MCEER-01-0003 "Sensitivity Analysis of Dynamic Systems Subjected to Seismic Loads," by C. Roth and M. Grigoriu, 9/18/01, (PB2003-100884, A12, MF-A03).
- MCEER-01-0004 "Overcoming Obstacles to Implementing Earthquake Hazard Mitigation Policies: Stage 1 Report," by D.J. Alesch and W.J. Petak, 12/17/01, (PB2002-107949, A07, MF-A02).
- MCEER-01-0005 "Updating Real-Time Earthquake Loss Estimates: Methods, Problems and Insights," by C.E. Taylor, S.E. Chang and R.T. Eguchi, 12/17/01, (PB2002-107948, A05, MF-A01).
- MCEER-01-0006 "Experimental Investigation and Retrofit of Steel Pile Foundations and Pile Bents Under Cyclic Lateral Loadings," by A. Shama, J. Mander, B. Blabac and S. Chen, 12/31/01, (PB2002-107950, A13, MF-A03).
- MCEER-02-0001 "Assessment of Performance of Bolu Viaduct in the 1999 Duzce Earthquake in Turkey" by P.C. Roussis, M.C. Constantinou, M. Erdik, E. Durukal and M. Dicleli, 5/8/02, (PB2003-100883, A08, MF-A02).
- MCEER-02-0002 "Seismic Behavior of Rail Counterweight Systems of Elevators in Buildings," by M.P. Singh, Rildova and L.E. Suarez, 5/27/02. (PB2003-100882, A11, MF-A03).
- MCEER-02-0003 "Development of Analysis and Design Procedures for Spread Footings," by G. Mylonakis, G. Gazetas, S. Nikolaou and A. Chauncey, 10/02/02, (PB2004-101636, A13, MF-A03, CD-A13).
- MCEER-02-0004 "Bare-Earth Algorithms for Use with SAR and LIDAR Digital Elevation Models," by C.K. Huyck, R.T. Eguchi and B. Houshmand, 10/16/02, (PB2004-101637, A07, CD-A07).
- MCEER-02-0005 "Review of Energy Dissipation of Compression Members in Concentrically Braced Frames," by K.Lee and M. Bruneau, 10/18/02, (PB2004-101638, A10, CD-A10).
- MCEER-03-0001 "Experimental Investigation of Light-Gauge Steel Plate Shear Walls for the Seismic Retrofit of Buildings" by J. Berman and M. Bruneau, 5/2/03, (PB2004-101622, A10, MF-A03, CD-A10).
- MCEER-03-0002 "Statistical Analysis of Fragility Curves," by M. Shinozuka, M.Q. Feng, H. Kim, T. Uzawa and T. Ueda, 6/16/03, (PB2004-101849, A09, CD-A09).
- MCEER-03-0003 "Proceedings of the Eighth U.S.-Japan Workshop on Earthquake Resistant Design of Lifeline Facilities and Countermeasures Against Liquefaction," edited by M. Hamada, J.P. Bardet and T.D. O'Rourke, 6/30/03, (PB2004-104386, A99, CD-A99).
- MCEER-03-0004 "Proceedings of the PRC-US Workshop on Seismic Analysis and Design of Special Bridges," edited by L.C. Fan and G.C. Lee, 7/15/03, (PB2004-104387, A14, CD-A14).
- MCEER-03-0005 "Urban Disaster Recovery: A Framework and Simulation Model," by S.B. Miles and S.E. Chang, 7/25/03, (PB2004-104388, A07, CD-A07).
- MCEER-03-0006 "Behavior of Underground Piping Joints Due to Static and Dynamic Loading," by R.D. Meis, M. Maragakis and R. Siddharthan, 11/17/03, (PB2005-102194, A13, MF-A03, CD-A00).
- MCEER-04-0001 "Experimental Study of Seismic Isolation Systems with Emphasis on Secondary System Response and Verification of Accuracy of Dynamic Response History Analysis Methods," by E. Wolff and M. Constantinou, 1/16/04 (PB2005-102195, A99, MF-E08, CD-A00).
- MCEER-04-0002 "Tension, Compression and Cyclic Testing of Engineered Cementitious Composite Materials," by K. Kesner and S.L. Billington, 3/1/04, (PB2005-102196, A08, CD-A08).

- MCEER-04-0003 "Cyclic Testing of Braces Laterally Restrained by Steel Studs to Enhance Performance During Earthquakes," by O.C. Celik, J.W. Berman and M. Bruneau, 3/16/04, (PB2005-102197, A13, MF-A03, CD-A00).
- MCEER-04-0004 "Methodologies for Post Earthquake Building Damage Detection Using SAR and Optical Remote Sensing: Application to the August 17, 1999 Marmara, Turkey Earthquake," by C.K. Huyck, B.J. Adams, S. Cho, R.T. Eguchi, B. Mansouri and B. Houshmand, 6/15/04, (PB2005-104888, A10, CD-A00).
- MCEER-04-0005 "Nonlinear Structural Analysis Towards Collapse Simulation: A Dynamical Systems Approach," by M.V. Sivaselvan and A.M. Reinhorn, 6/16/04, (PB2005-104889, A11, MF-A03, CD-A00).
- MCEER-04-0006 "Proceedings of the Second PRC-US Workshop on Seismic Analysis and Design of Special Bridges," edited by G.C. Lee and L.C. Fan, 6/25/04, (PB2005-104890, A16, CD-A00).
- MCEER-04-0007 "Seismic Vulnerability Evaluation of Axially Loaded Steel Built-up Laced Members," by K. Lee and M. Bruneau, 6/30/04, (PB2005-104891, A16, CD-A00).
- MCEER-04-0008 "Evaluation of Accuracy of Simplified Methods of Analysis and Design of Buildings with Damping Systems for Near-Fault and for Soft-Soil Seismic Motions," by E.A. Pavlou and M.C. Constantinou, 8/16/04, (PB2005-104892, A08, MF-A02, CD-A00).
- MCEER-04-0009 "Assessment of Geotechnical Issues in Acute Care Facilities in California," by M. Lew, T.D. O'Rourke, R. Dobry and M. Koch, 9/15/04, (PB2005-104893, A08, CD-A00).
- MCEER-04-0010 "Scissor-Jack-Damper Energy Dissipation System," by A.N. Sigaher-Boyle and M.C. Constantinou, 12/1/04 (PB2005-108221).
- MCEER-04-0011 "Seismic Retrofit of Bridge Steel Truss Piers Using a Controlled Rocking Approach," by M. Pollino and M. Bruneau, 12/20/04 (PB2006-105795).
- MCEER-05-0001 "Experimental and Analytical Studies of Structures Seismically Isolated with an Uplift-Restraint Isolation System," by P.C. Roussis and M.C. Constantinou, 1/10/05 (PB2005-108222).
- MCEER-05-0002 "A Versatile Experimentation Model for Study of Structures Near Collapse Applied to Seismic Evaluation of Irregular Structures," by D. Kusumastuti, A.M. Reinhorn and A. Rutenberg, 3/31/05 (PB2006-101523).
- MCEER-05-0003 "Proceedings of the Third PRC-US Workshop on Seismic Analysis and Design of Special Bridges," edited by L.C. Fan and G.C. Lee, 4/20/05, (PB2006-105796).
- MCEER-05-0004 "Approaches for the Seismic Retrofit of Braced Steel Bridge Piers and Proof-of-Concept Testing of an Eccentrically Braced Frame with Tubular Link," by J.W. Berman and M. Bruneau, 4/21/05 (PB2006-101524).
- MCEER-05-0005 "Simulation of Strong Ground Motions for Seismic Fragility Evaluation of Nonstructural Components in Hospitals," by A. Wanitkorkul and A. Filiatrault, 5/26/05 (PB2006-500027).
- MCEER-05-0006 "Seismic Safety in California Hospitals: Assessing an Attempt to Accelerate the Replacement or Seismic Retrofit of Older Hospital Facilities," by D.J. Alesch, L.A. Arendt and W.J. Petak, 6/6/05 (PB2006-105794).
- MCEER-05-0007 "Development of Seismic Strengthening and Retrofit Strategies for Critical Facilities Using Engineered Cementitious Composite Materials," by K. Kesner and S.L. Billington, 8/29/05 (PB2006-111701).
- MCEER-05-0008 "Experimental and Analytical Studies of Base Isolation Systems for Seismic Protection of Power Transformers," by N. Murota, M.Q. Feng and G-Y. Liu, 9/30/05 (PB2006-111702).
- MCEER-05-0009 "3D-BASIS-ME-MB: Computer Program for Nonlinear Dynamic Analysis of Seismically Isolated Structures," by P.C. Tsopelas, P.C. Roussis, M.C. Constantinou, R. Buchanan and A.M. Reinhorn, 10/3/05 (PB2006-111703).
- MCEER-05-0010 "Steel Plate Shear Walls for Seismic Design and Retrofit of Building Structures," by D. Vian and M. Bruneau, 12/15/05 (PB2006-111704).

- MCEER-05-0011 "The Performance-Based Design Paradigm," by M.J. Astrella and A. Whittaker, 12/15/05 (PB2006-111705).
- MCEER-06-0001 "Seismic Fragility of Suspended Ceiling Systems," H. Badillo-Almaraz, A.S. Whittaker, A.M. Reinhorn and G.P. Cimellaro, 2/4/06 (PB2006-111706).
- MCEER-06-0002 "Multi-Dimensional Fragility of Structures," by G.P. Cimellaro, A.M. Reinhorn and M. Bruneau, 3/1/06 (PB2007-106974, A09, MF-A02, CD A00).
- MCEER-06-0003 "Built-Up Shear Links as Energy Dissipators for Seismic Protection of Bridges," by P. Dusicka, A.M. Itani and I.G. Buckle, 3/15/06 (PB2006-111708).
- MCEER-06-0004 "Analytical Investigation of the Structural Fuse Concept," by R.E. Vargas and M. Bruneau, 3/16/06 (PB2006-111709).
- MCEER-06-0005 "Experimental Investigation of the Structural Fuse Concept," by R.E. Vargas and M. Bruneau, 3/17/06 (PB2006-111710).
- MCEER-06-0006 "Further Development of Tubular Eccentrically Braced Frame Links for the Seismic Retrofit of Braced Steel Truss Bridge Piers," by J.W. Berman and M. Bruneau, 3/27/06 (PB2007-105147).
- MCEER-06-0007 "REDARS Validation Report," by S. Cho, C.K. Huyck, S. Ghosh and R.T. Eguchi, 8/8/06 (PB2007-106983).
- MCEER-06-0008 "Review of Current NDE Technologies for Post-Earthquake Assessment of Retrofitted Bridge Columns," by J.W. Song, Z. Liang and G.C. Lee, 8/21/06 (PB2007-106984).
- MCEER-06-0009 "Liquefaction Remediation in Silty Soils Using Dynamic Compaction and Stone Columns," by S. Thevanayagam, G.R. Martin, R. Nashed, T. Shenthan, T. Kanagalingam and N. Ecemis, 8/28/06 (PB2007-106985).
- MCEER-06-0010 "Conceptual Design and Experimental Investigation of Polymer Matrix Composite Infill Panels for Seismic Retrofitting," by W. Jung, M. Chiewanichakorn and A.J. Aref, 9/21/06 (PB2007-106986).
- MCEER-06-0011 "A Study of the Coupled Horizontal-Vertical Behavior of Elastomeric and Lead-Rubber Seismic Isolation Bearings," by G.P. Warn and A.S. Whittaker, 9/22/06 (PB2007-108679).
- MCEER-06-0012 "Proceedings of the Fourth PRC-US Workshop on Seismic Analysis and Design of Special Bridges: Advancing Bridge Technologies in Research, Design, Construction and Preservation," Edited by L.C. Fan, G.C. Lee and L. Ziang, 10/12/06 (PB2007-109042).
- MCEER-06-0013 "Cyclic Response and Low Cycle Fatigue Characteristics of Plate Steels," by P. Dusicka, A.M. Itani and I.G. Buckle, 11/1/06 06 (PB2007-106987).
- MCEER-06-0014 "Proceedings of the Second US-Taiwan Bridge Engineering Workshop," edited by W.P. Yen, J. Shen, J-Y. Chen and M. Wang, 11/15/06 (PB2008-500041).
- MCEER-06-0015 "User Manual and Technical Documentation for the REDARSTM Import Wizard," by S. Cho, S. Ghosh, C.K. Huyck and S.D. Werner, 11/30/06 (PB2007-114766).
- MCEER-06-0016 "Hazard Mitigation Strategy and Monitoring Technologies for Urban and Infrastructure Public Buildings: Proceedings of the China-US Workshops," edited by X.Y. Zhou, A.L. Zhang, G.C. Lee and M. Tong, 12/12/06 (PB2008-500018).
- MCEER-07-0001 "Static and Kinetic Coefficients of Friction for Rigid Blocks," by C. Kafali, S. Fathali, M. Grigoriu and A.S. Whittaker, 3/20/07 (PB2007-114767).
- MCEER-07-0002 "Hazard Mitigation Investment Decision Making: Organizational Response to Legislative Mandate," by L.A. Arendt, D.J. Alesch and W.J. Petak, 4/9/07 (PB2007-114768).
- MCEER-07-0003 "Seismic Behavior of Bidirectional-Resistant Ductile End Diaphragms with Unbonded Braces in Straight or Skewed Steel Bridges," by O. Celik and M. Bruneau, 4/11/07 (PB2008-105141).

- MCEER-07-0004 "Modeling Pile Behavior in Large Pile Groups Under Lateral Loading," by A.M. Dodds and G.R. Martin, 4/16/07(PB2008-105142).
- MCEER-07-0005 "Experimental Investigation of Blast Performance of Seismically Resistant Concrete-Filled Steel Tube Bridge Piers," by S. Fujikura, M. Bruneau and D. Lopez-Garcia, 4/20/07 (PB2008-105143).
- MCEER-07-0006 "Seismic Analysis of Conventional and Isolated Liquefied Natural Gas Tanks Using Mechanical Analogs," by I.P. Christovasilis and A.S. Whittaker, 5/1/07, not available.
- MCEER-07-0007 "Experimental Seismic Performance Evaluation of Isolation/Restraint Systems for Mechanical Equipment – Part 1: Heavy Equipment Study," by S. Fathali and A. Filiatrault, 6/6/07 (PB2008-105144).
- MCEER-07-0008 "Seismic Vulnerability of Timber Bridges and Timber Substructures," by A.A. Sharma, J.B. Mander, I.M. Friedland and D.R. Allicock, 6/7/07 (PB2008-105145).
- MCEER-07-0009 "Experimental and Analytical Study of the XY-Friction Pendulum (XY-FP) Bearing for Bridge Applications," by C.C. Marin-Artieda, A.S. Whittaker and M.C. Constantinou, 6/7/07 (PB2008-105191).
- MCEER-07-0010 "Proceedings of the PRC-US Earthquake Engineering Forum for Young Researchers," Edited by G.C. Lee and X.Z. Qi, 6/8/07 (PB2008-500058).
- MCEER-07-0011 "Design Recommendations for Perforated Steel Plate Shear Walls," by R. Purba and M. Bruneau, 6/18/07, (PB2008-105192).
- MCEER-07-0012 "Performance of Seismic Isolation Hardware Under Service and Seismic Loading," by M.C. Constantinou, A.S. Whittaker, Y. Kalpakidis, D.M. Fenz and G.P. Warn, 8/27/07, (PB2008-105193).
- MCEER-07-0013 "Experimental Evaluation of the Seismic Performance of Hospital Piping Subassemblies," by E.R. Goodwin, E. Maragakis and A.M. Itani, 9/4/07, (PB2008-105194).
- MCEER-07-0014 "A Simulation Model of Urban Disaster Recovery and Resilience: Implementation for the 1994 Northridge Earthquake," by S. Miles and S.E. Chang, 9/7/07, (PB2008-106426).
- MCEER-07-0015 "Statistical and Mechanistic Fragility Analysis of Concrete Bridges," by M. Shinozuka, S. Banerjee and S-H. Kim, 9/10/07, (PB2008-106427).
- MCEER-07-0016 "Three-Dimensional Modeling of Inelastic Buckling in Frame Structures," by M. Schachter and AM. Reinhorn, 9/13/07, (PB2008-108125).
- MCEER-07-0017 "Modeling of Seismic Wave Scattering on Pile Groups and Caissons," by I. Po Lam, H. Law and C.T. Yang, 9/17/07 (PB2008-108150).
- MCEER-07-0018 "Bridge Foundations: Modeling Large Pile Groups and Caissons for Seismic Design," by I. Po Lam, H. Law and G.R. Martin (Coordinating Author), 12/1/07 (PB2008-111190).
- MCEER-07-0019 "Principles and Performance of Roller Seismic Isolation Bearings for Highway Bridges," by G.C. Lee, Y.C. Ou, Z. Liang, T.C. Niu and J. Song, 12/10/07 (PB2009-110466).
- MCEER-07-0020 "Centrifuge Modeling of Permeability and Pinning Reinforcement Effects on Pile Response to Lateral Spreading," by L.L. Gonzalez-Lagos, T. Abdoun and R. Dobry, 12/10/07 (PB2008-111191).
- MCEER-07-0021 "Damage to the Highway System from the Pisco, Perú Earthquake of August 15, 2007," by J.S. O'Connor, L. Mesa and M. Nykamp, 12/10/07, (PB2008-108126).
- MCEER-07-0022 "Experimental Seismic Performance Evaluation of Isolation/Restraint Systems for Mechanical Equipment – Part 2: Light Equipment Study," by S. Fathali and A. Filiatrault, 12/13/07 (PB2008-111192).
- MCEER-07-0023 "Fragility Considerations in Highway Bridge Design," by M. Shinozuka, S. Banerjee and S.H. Kim, 12/14/07 (PB2008-111193).

- MCEER-07-0024 "Performance Estimates for Seismically Isolated Bridges," by G.P. Warn and A.S. Whittaker, 12/30/07 (PB2008-112230).
- MCEER-08-0001 "Seismic Performance of Steel Girder Bridge Superstructures with Conventional Cross Frames," by L.P. Carden, A.M. Itani and I.G. Buckle, 1/7/08, (PB2008-112231).
- MCEER-08-0002 "Seismic Performance of Steel Girder Bridge Superstructures with Ductile End Cross Frames with Seismic Isolators," by L.P. Carden, A.M. Itani and I.G. Buckle, 1/7/08 (PB2008-112232).
- MCEER-08-0003 "Analytical and Experimental Investigation of a Controlled Rocking Approach for Seismic Protection of Bridge Steel Truss Piers," by M. Pollino and M. Bruneau, 1/21/08 (PB2008-112233).
- MCEER-08-0004 "Linking Lifeline Infrastructure Performance and Community Disaster Resilience: Models and Multi-Stakeholder Processes," by S.E. Chang, C. Pasion, K. Tatebe and R. Ahmad, 3/3/08 (PB2008-112234).
- MCEER-08-0005 "Modal Analysis of Generally Damped Linear Structures Subjected to Seismic Excitations," by J. Song, Y-L. Chu, Z. Liang and G.C. Lee, 3/4/08 (PB2009-102311).
- MCEER-08-0006 "System Performance Under Multi-Hazard Environments," by C. Kafali and M. Grigoriu, 3/4/08 (PB2008-112235).
- MCEER-08-0007 "Mechanical Behavior of Multi-Spherical Sliding Bearings," by D.M. Fenz and M.C. Constantinou, 3/6/08 (PB2008-112236).
- MCEER-08-0008 "Post-Earthquake Restoration of the Los Angeles Water Supply System," by T.H.P. Tabucchi and R.A. Davidson, 3/7/08 (PB2008-112237).
- MCEER-08-0009 "Fragility Analysis of Water Supply Systems," by A. Jacobson and M. Grigoriu, 3/10/08 (PB2009-105545).
- MCEER-08-0010 "Experimental Investigation of Full-Scale Two-Story Steel Plate Shear Walls with Reduced Beam Section Connections," by B. Qu, M. Bruneau, C-H. Lin and K-C. Tsai, 3/17/08 (PB2009-106368).
- MCEER-08-0011 "Seismic Evaluation and Rehabilitation of Critical Components of Electrical Power Systems," S. Ersoy, B. Feizi, A. Ashrafi and M. Ala Saadeghvaziri, 3/17/08 (PB2009-105546).
- MCEER-08-0012 "Seismic Behavior and Design of Boundary Frame Members of Steel Plate Shear Walls," by B. Qu and M. Bruneau, 4/26/08 . (PB2009-106744).
- MCEER-08-0013 "Development and Appraisal of a Numerical Cyclic Loading Protocol for Quantifying Building System Performance," by A. Filiatrault, A. Wanitkorkul and M. Constantinou, 4/27/08 (PB2009-107906).
- MCEER-08-0014 "Structural and Nonstructural Earthquake Design: The Challenge of Integrating Specialty Areas in Designing Complex, Critical Facilities," by W.J. Petak and D.J. Alesch, 4/30/08 (PB2009-107907).
- MCEER-08-0015 "Seismic Performance Evaluation of Water Systems," by Y. Wang and T.D. O'Rourke, 5/5/08 (PB2009-107908).
- MCEER-08-0016 "Seismic Response Modeling of Water Supply Systems," by P. Shi and T.D. O'Rourke, 5/5/08 (PB2009-107910).
- MCEER-08-0017 "Numerical and Experimental Studies of Self-Centering Post-Tensioned Steel Frames," by D. Wang and A. Filiatrault, 5/12/08 (PB2009-110479).
- MCEER-08-0018 "Development, Implementation and Verification of Dynamic Analysis Models for Multi-Spherical Sliding Bearings," by D.M. Fenz and M.C. Constantinou, 8/15/08 (PB2009-107911).
- MCEER-08-0019 "Performance Assessment of Conventional and Base Isolated Nuclear Power Plants for Earthquake Blast Loadings," by Y.N. Huang, A.S. Whittaker and N. Luco, 10/28/08 (PB2009-107912).

- MCEER-08-0020 “Remote Sensing for Resilient Multi-Hazard Disaster Response – Volume I: Introduction to Damage Assessment Methodologies,” by B.J. Adams and R.T. Eguchi, 11/17/08 (PB2010-102695).
- MCEER-08-0021 “Remote Sensing for Resilient Multi-Hazard Disaster Response – Volume II: Counting the Number of Collapsed Buildings Using an Object-Oriented Analysis: Case Study of the 2003 Bam Earthquake,” by L. Gusella, C.K. Huyck and B.J. Adams, 11/17/08 (PB2010-100925).
- MCEER-08-0022 “Remote Sensing for Resilient Multi-Hazard Disaster Response – Volume III: Multi-Sensor Image Fusion Techniques for Robust Neighborhood-Scale Urban Damage Assessment,” by B.J. Adams and A. McMillan, 11/17/08 (PB2010-100926).
- MCEER-08-0023 “Remote Sensing for Resilient Multi-Hazard Disaster Response – Volume IV: A Study of Multi-Temporal and Multi-Resolution SAR Imagery for Post-Katrina Flood Monitoring in New Orleans,” by A. McMillan, J.G. Morley, B.J. Adams and S. Chesworth, 11/17/08 (PB2010-100927).
- MCEER-08-0024 “Remote Sensing for Resilient Multi-Hazard Disaster Response – Volume V: Integration of Remote Sensing Imagery and VIEWS™ Field Data for Post-Hurricane Charley Building Damage Assessment,” by J.A. Womble, K. Mehta and B.J. Adams, 11/17/08 (PB2009-115532).
- MCEER-08-0025 “Building Inventory Compilation for Disaster Management: Application of Remote Sensing and Statistical Modeling,” by P. Sarabandi, A.S. Kiremidjian, R.T. Eguchi and B. J. Adams, 11/20/08 (PB2009-110484).
- MCEER-08-0026 “New Experimental Capabilities and Loading Protocols for Seismic Qualification and Fragility Assessment of Nonstructural Systems,” by R. Retamales, G. Mosqueda, A. Filiatrault and A. Reinhorn, 11/24/08 (PB2009-110485).
- MCEER-08-0027 “Effects of Heating and Load History on the Behavior of Lead-Rubber Bearings,” by I.V. Kalpakidis and M.C. Constantinou, 12/1/08 (PB2009-115533).
- MCEER-08-0028 “Experimental and Analytical Investigation of Blast Performance of Seismically Resistant Bridge Piers,” by S.Fujikura and M. Bruneau, 12/8/08 (PB2009-115534).
- MCEER-08-0029 “Evolutionary Methodology for Aseismic Decision Support,” by Y. Hu and G. Dargush, 12/15/08.
- MCEER-08-0030 “Development of a Steel Plate Shear Wall Bridge Pier System Conceived from a Multi-Hazard Perspective,” by D. Keller and M. Bruneau, 12/19/08 (PB2010-102696).
- MCEER-09-0001 “Modal Analysis of Arbitrarily Damped Three-Dimensional Linear Structures Subjected to Seismic Excitations,” by Y.L. Chu, J. Song and G.C. Lee, 1/31/09 (PB2010-100922).
- MCEER-09-0002 “Air-Blast Effects on Structural Shapes,” by G. Ballantyne, A.S. Whittaker, A.J. Aref and G.F. Dargush, 2/2/09 (PB2010-102697).
- MCEER-09-0003 “Water Supply Performance During Earthquakes and Extreme Events,” by A.L. Bonneau and T.D. O’Rourke, 2/16/09 (PB2010-100923).
- MCEER-09-0004 “Generalized Linear (Mixed) Models of Post-Earthquake Ignitions,” by R.A. Davidson, 7/20/09 (PB2010-102698).
- MCEER-09-0005 “Seismic Testing of a Full-Scale Two-Story Light-Frame Wood Building: NEESWood Benchmark Test,” by I.P. Christovasilis, A. Filiatrault and A. Wanitkorkul, 7/22/09 (PB2012-102401).
- MCEER-09-0006 “IDARC2D Version 7.0: A Program for the Inelastic Damage Analysis of Structures,” by A.M. Reinhorn, H. Roh, M. Sivaselvan, S.K. Kunnath, R.E. Valles, A. Madan, C. Li, R. Lobo and Y.J. Park, 7/28/09 (PB2010-103199).
- MCEER-09-0007 “Enhancements to Hospital Resiliency: Improving Emergency Planning for and Response to Hurricanes,” by D.B. Hess and L.A. Arendt, 7/30/09 (PB2010-100924).

- MCEER-09-0008 "Assessment of Base-Isolated Nuclear Structures for Design and Beyond-Design Basis Earthquake Shaking," by Y.N. Huang, A.S. Whittaker, R.P. Kennedy and R.L. Mayes, 8/20/09 (PB2010-102699).
- MCEER-09-0009 "Quantification of Disaster Resilience of Health Care Facilities," by G.P. Cimellaro, C. Fumo, A.M. Reinhorn and M. Bruneau, 9/14/09 (PB2010-105384).
- MCEER-09-0010 "Performance-Based Assessment and Design of Squat Reinforced Concrete Shear Walls," by C.K. Gulec and A.S. Whittaker, 9/15/09 (PB2010-102700).
- MCEER-09-0011 "Proceedings of the Fourth US-Taiwan Bridge Engineering Workshop," edited by W.P. Yen, J.J. Shen, T.M. Lee and R.B. Zheng, 10/27/09 (PB2010-500009).
- MCEER-09-0012 "Proceedings of the Special International Workshop on Seismic Connection Details for Segmental Bridge Construction," edited by W. Phillip Yen and George C. Lee, 12/21/09 (PB2012-102402).
- MCEER-10-0001 "Direct Displacement Procedure for Performance-Based Seismic Design of Multistory Woodframe Structures," by W. Pang and D. Rosowsky, 4/26/10 (PB2012-102403).
- MCEER-10-0002 "Simplified Direct Displacement Design of Six-Story NEESWood Capstone Building and Pre-Test Seismic Performance Assessment," by W. Pang, D. Rosowsky, J. van de Lindt and S. Pei, 5/28/10 (PB2012-102404).
- MCEER-10-0003 "Integration of Seismic Protection Systems in Performance-Based Seismic Design of Woodframed Structures," by J.K. Shinde and M.D. Symans, 6/18/10 (PB2012-102405).
- MCEER-10-0004 "Modeling and Seismic Evaluation of Nonstructural Components: Testing Frame for Experimental Evaluation of Suspended Ceiling Systems," by A.M. Reinhorn, K.P. Ryu and G. Maddaloni, 6/30/10 (PB2012-102406).
- MCEER-10-0005 "Analytical Development and Experimental Validation of a Structural-Fuse Bridge Pier Concept," by S. El-Bahey and M. Bruneau, 10/1/10 (PB2012-102407).
- MCEER-10-0006 "A Framework for Defining and Measuring Resilience at the Community Scale: The PEOPLES Resilience Framework," by C.S. Renschler, A.E. Frazier, L.A. Arendt, G.P. Cimellaro, A.M. Reinhorn and M. Bruneau, 10/8/10 (PB2012-102408).
- MCEER-10-0007 "Impact of Horizontal Boundary Elements Design on Seismic Behavior of Steel Plate Shear Walls," by R. Purba and M. Bruneau, 11/14/10 (PB2012-102409).
- MCEER-10-0008 "Seismic Testing of a Full-Scale Mid-Rise Building: The NEESWood Capstone Test," by S. Pei, J.W. van de Lindt, S.E. Pryor, H. Shimizu, H. Isoda and D.R. Rammer, 12/1/10 (PB2012-102410).
- MCEER-10-0009 "Modeling the Effects of Detonations of High Explosives to Inform Blast-Resistant Design," by P. Sherkar, A.S. Whittaker and A.J. Aref, 12/1/10 (PB2012-102411).
- MCEER-10-0010 "L'Aquila Earthquake of April 6, 2009 in Italy: Rebuilding a Resilient City to Withstand Multiple Hazards," by G.P. Cimellaro, I.P. Christovasilis, A.M. Reinhorn, A. De Stefano and T. Kirova, 12/29/10.
- MCEER-11-0001 "Numerical and Experimental Investigation of the Seismic Response of Light-Frame Wood Structures," by I.P. Christovasilis and A. Filiatrault, 8/8/11 (PB2012-102412).
- MCEER-11-0002 "Seismic Design and Analysis of a Precast Segmental Concrete Bridge Model," by M. Anagnostopoulou, A. Filiatrault and A. Aref, 9/15/11.
- MCEER-11-0003 "Proceedings of the Workshop on Improving Earthquake Response of Substation Equipment," Edited by A.M. Reinhorn, 9/19/11 (PB2012-102413).
- MCEER-11-0004 "LRFD-Based Analysis and Design Procedures for Bridge Bearings and Seismic Isolators," by M.C. Constantinou, I. Kalpakidis, A. Filiatrault and R.A. Ecker Lay, 9/26/11.

- MCEER-11-0005 “Experimental Seismic Evaluation, Model Parameterization, and Effects of Cold-Formed Steel-Framed Gypsum Partition Walls on the Seismic Performance of an Essential Facility,” by R. Davies, R. Retamales, G. Mosqueda and A. Filiatrault, 10/12/11.
- MCEER-11-0006 “Modeling and Seismic Performance Evaluation of High Voltage Transformers and Bushings,” by A.M. Reinhorn, K. Oikonomou, H. Roh, A. Schiff and L. Kempner, Jr., 10/3/11.
- MCEER-11-0007 “Extreme Load Combinations: A Survey of State Bridge Engineers,” by G.C. Lee, Z. Liang, J.J. Shen and J.S. O’Connor, 10/14/11.
- MCEER-12-0001 “Simplified Analysis Procedures in Support of Performance Based Seismic Design,” by Y.N. Huang and A.S. Whittaker.
- MCEER-12-0002 “Seismic Protection of Electrical Transformer Bushing Systems by Stiffening Techniques,” by M. Koliou, A. Filiatrault, A.M. Reinhorn and N. Oliveto, 6/1/12.
- MCEER-12-0003 “Post-Earthquake Bridge Inspection Guidelines,” by J.S. O’Connor and S. Alampalli, 6/8/12.
- MCEER-12-0004 “Integrated Design Methodology for Isolated Floor Systems in Single-Degree-of-Freedom Structural Fuse Systems,” by S. Cui, M. Bruneau and M.C. Constantinou, 6/13/12.
- MCEER-12-0005 “Characterizing the Rotational Components of Earthquake Ground Motion,” by D. Basu, A.S. Whittaker and M.C. Constantinou, 6/15/12.
- MCEER-12-0006 “Bayesian Fragility for Nonstructural Systems,” by C.H. Lee and M.D. Grigoriu, 9/12/12.
- MCEER-12-0007 “A Numerical Model for Capturing the In-Plane Seismic Response of Interior Metal Stud Partition Walls,” by R.L. Wood and T.C. Hutchinson, 9/12/12.
- MCEER-12-0008 “Assessment of Floor Accelerations in Yielding Buildings,” by J.D. Wieser, G. Pekcan, A.E. Zaghi, A.M. Itani and E. Maragakis, 10/5/12.
- MCEER-13-0001 “Experimental Seismic Study of Pressurized Fire Sprinkler Piping Systems,” by Y. Tian, A. Filiatrault and G. Mosqueda, 4/8/13.
- MCEER-13-0002 “Enhancing Resource Coordination for Multi-Modal Evacuation Planning,” by D.B. Hess, B.W. Conley and C.M. Farrell, 2/8/13.
- MCEER-13-0003 “Seismic Response of Base Isolated Buildings Considering Pounding to Moat Walls,” by A. Masroor and G. Mosqueda, 2/26/13.
- MCEER-13-0004 “Seismic Response Control of Structures Using a Novel Adaptive Passive Negative Stiffness Device,” by D.T.R. Pasala, A.A. Sarlis, S. Nagarajaiah, A.M. Reinhorn, M.C. Constantinou and D.P. Taylor, 6/10/13.
- MCEER-13-0005 “Negative Stiffness Device for Seismic Protection of Structures,” by A.A. Sarlis, D.T.R. Pasala, M.C. Constantinou, A.M. Reinhorn, S. Nagarajaiah and D.P. Taylor, 6/12/13.
- MCEER-13-0006 “Emilia Earthquake of May 20, 2012 in Northern Italy: Rebuilding a Resilient Community to Withstand Multiple Hazards,” by G.P. Cimellaro, M. Chiriatti, A.M. Reinhorn and L. Tirca, June 30, 2013.
- MCEER-13-0007 “Precast Concrete Segmental Components and Systems for Accelerated Bridge Construction in Seismic Regions,” by A.J. Aref, G.C. Lee, Y.C. Ou and P. Sideris, with contributions from K.C. Chang, S. Chen, A. Filiatrault and Y. Zhou, June 13, 2013.
- MCEER-13-0008 “A Study of U.S. Bridge Failures (1980-2012),” by G.C. Lee, S.B. Mohan, C. Huang and B.N. Fard, June 15, 2013.
- MCEER-13-0009 “Development of a Database Framework for Modeling Damaged Bridges,” by G.C. Lee, J.C. Qi and C. Huang, June 16, 2013.

- MCEER-13-0010 “Model of Triple Friction Pendulum Bearing for General Geometric and Frictional Parameters and for Uplift Conditions,” by A.A. Sarlis and M.C. Constantinou, July 1, 2013.
- MCEER-13-0011 “Shake Table Testing of Triple Friction Pendulum Isolators under Extreme Conditions,” by A.A. Sarlis, M.C. Constantinou and A.M. Reinhorn, July 2, 2013.
- MCEER-13-0012 “Theoretical Framework for the Development of MH-LRFD,” by G.C. Lee (coordinating author), H.A. Capers, Jr., C. Huang, J.M. Kulicki, Z. Liang, T. Murphy, J.J.D. Shen, M. Shinozuka and P.W.H. Yen, July 31, 2013.
- MCEER-13-0013 “Seismic Protection of Highway Bridges with Negative Stiffness Devices,” by N.K.A. Attary, M.D. Symans, S. Nagarajaiah, A.M. Reinhorn, M.C. Constantinou, A.A. Sarlis, D.T.R. Pasala, and D.P. Taylor, September 3, 2014.
- MCEER-14-0001 “Simplified Seismic Collapse Capacity-Based Evaluation and Design of Frame Buildings with and without Supplemental Damping Systems,” by M. Hamidia, A. Filiatrault, and A. Aref, May 19, 2014.
- MCEER-14-0002 “Comprehensive Analytical Seismic Fragility of Fire Sprinkler Piping Systems,” by Siavash Soroushian, Emmanuel “Manos” Maragakis, Arash E. Zaghi, Alicia Echevarria, Yuan Tian and Andre Filiatrault, August 26, 2014.
- MCEER-14-0003 “Hybrid Simulation of the Seismic Response of a Steel Moment Frame Building Structure through Collapse,” by M. Del Carpio Ramos, G. Mosqueda and D.G. Lignos, October 30, 2014.
- MCEER-14-0005 “Seismic Performance of Steel Plate Shear Walls Considering Various Design Approaches,” by R. Purba and M. Bruneau, October 31, 2014.
- MCEER-14-0006 “Air-Blast Effects on Civil Structures,” by Jinwon Shin, Andrew S. Whittaker, Amjad J. Aref and David Cormie, October 30, 2014.
- MCEER-14-0007 “Seismic Performance Evaluation of Precast Girders with Field-Cast Ultra High Performance Concrete (UHPC) Connections,” by G.C. Lee, C. Huang, J. Song, and J. S. O’Connor, July 31, 2014.
- MCEER-14-0008 “Post-Earthquake Fire Resistance of Ductile Concrete-Filled Double-Skin Tube Columns,” by Reza Imani, Gilberto Mosqueda and Michel Bruneau, December 1, 2014.
- MCEER-14-0009 “Cyclic Inelastic Behavior of Concrete Filled Sandwich Panel Walls Subjected to In-Plane Flexure,” by Y. Alzeni and M. Bruneau, December 19, 2014.
- MCEER-14-0010 “Analytical and Experimental Investigation of Self-Centering Steel Plate Shear Walls,” by D.M. Dowden and M. Bruneau, December 19, 2014.
- MCEER-15-0001 “Seismic Analysis of Multi-story Unreinforced Masonry Buildings with Flexible Diaphragms,” by J. Aleman, G. Mosqueda and A.S. Whittaker, June 12, 2015.
- MCEER-15-0002 “Site Response, Soil-Structure Interaction and Structure-Soil-Structure Interaction for Performance Assessment of Buildings and Nuclear Structures,” by C. Bolisetti and A.S. Whittaker, June 15, 2015.



EARTHQUAKE ENGINEERING TO EXTREME EVENTS

University at Buffalo, The State University of New York

133A Ketter Hall ■ Buffalo, New York 14260-4300

Phone: (716) 645-3391 ■ Fax: (716) 645-3399

Email: mceer@buffalo.edu ■ Web: <http://mceer.buffalo.edu>



University at Buffalo *The State University of New York*

ISSN 1520-295X